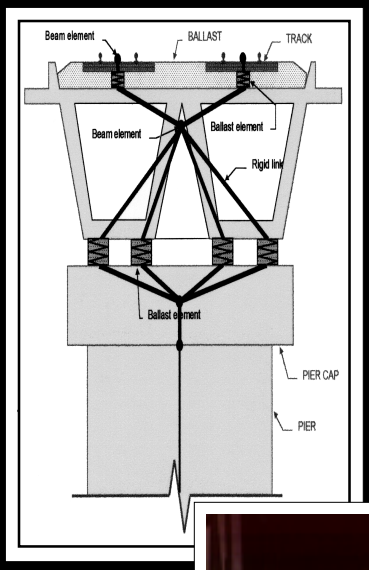
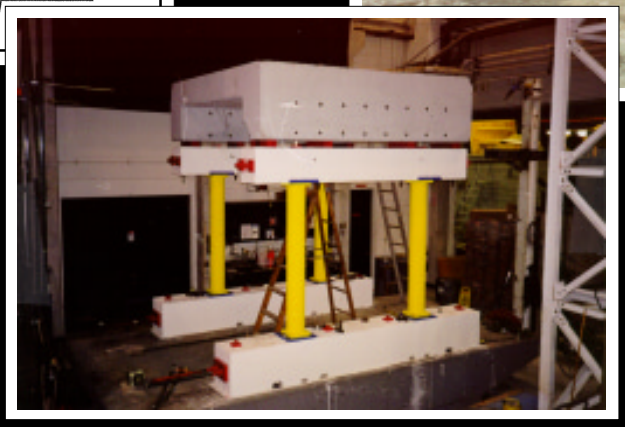
Proceedings of the U.S.-Italy Workshop on Seismic Protective Systems for Bridges







Edited by

Ian M. Friedland
Multidisciplinary Center for Earthquake Engineering Research
University at Buffalo, State University of New York
Red Jacket Quadrangle
Buffalo, New York 14261

Michael C. Constantinou
University at Buffalo, State University of New York
Department of Civil, Structural and Environmental Engineering
Ketler Hall
Buffalo, New York 14260

MCEER
MULTIDISCIPLINARY CENTER FOR EARTHQUAKE ENGINEERING RESEARCH
A National Center of Excellence in Advanced Technology Applications

ISSN 1520-295X

Technical Report MCEER-98-0015
November 3, 1998
This workshop was held at Columbia University and was supported by the Federal Highway Administration under contract number DTFH61-92-C-00106.

FEDERAL HIGHWAY ADMINISTRATION

NOTICE

This report was jointly prepared by the University of Southern California, The Pennsylvania State University and the Multidisciplinary Center for Earthquake Engineering Research (MCEER) through a contract from the Federal Highway Administration. Neither MCEER, associates of MCEER, its sponsors, the University of Southern California, The Pennsylvania State University, nor any person acting on their behalf:

a. makes any warranty, express or implied, with respect to the use of any information, apparatus, method, or process disclosed in this report or that such use may not infringe upon privately owned rights; or

b. assumes any liabilities of whatsoever kind with respect to the use of, or the damage resulting from the use of, any information, apparatus, method, or process disclosed in this report.

Any opinions, findings, and conclusions or recommendations expressed in this publication are those of the author(s) and do not necessarily reflect the views of MCEER, the Federal Highway Administration.



Proceedings of the U.S.-Italy Workshop on Seismic Protective Systems for Bridges

held at
Columbia University
New York City, NY
April 27-28, 1998

Edited by I.M. Friedland[1] and M.C. Constantinou[2]

Publication Date: November 3, 1998

Technical Report MCEER-98-0015

organized by I.M. Friedland and M.C. Constantinou
under NCEER Highway Project Task Number 106-F-5.3.3
and Raimondo Betti, Columbia University; Paolo Emilio Pinto, Università di Roma "La Sapienza;" and Gian Michele Calvi, Università Degli Studi di Pavia

This workshop was sponsored by the U.S. Federal Highway Administration
(contract number DTFH61-92-C-00106) and
the National Group for Defense
Against Earthquakes of the Italian National Research Council

1 Assistant Director for Bridges and Highways, Multidisciplinary Center for Earthquake Engineering Research
2 Professor, Department of Civil, Structural and Environmental Engineering, University at Buffalo, State University of New York

MULTIDISCIPLINARY CENTER FOR EARTHQUAKE ENGINEERING RESEARCH
University at Buffalo, State University of New York
Red Jacket Quadrangle, Buffalo, NY 14261

In Memory of Dr. William N. Patten

Dr. William Neff Patten, an internationally recognized leader in the field of structural control, passed away on November 23, 1998. He was a professor in the School of Aerospace and Mechanical Engineering and the Director of the Center for Structural Control at the University of Oklahoma. From 1980 until the time of his death, Dr. Patten had been conducting experimental work on the development of motion mitigation systems for structures. He had recently succeeded in having a semi-active intelligent stiffener demonstrated on an in-service interstate highway bridge, the first full-scale demonstration of a semi-active control system for bridges (and structures) in the U.S. In recognition of his efforts, *Engineering News Record* named him as one of their "Top 25 Newsmakers: Leaders Cited for Achievements that Served the Industry in 1996" (January 1997 issue). In addition, he recently received a four-year award through FHWA's TEA-21 program for research, development, and field testing of an intelligent stiffener for bridge stress reduction.

He was a finalist for the Civil Engineering Research Foundation Charles Pankow Award for Innovation, 1997; a finalist for the NOVA Award presented by the Construction Innovation Forum, 1997; and he was awarded the Oklahoma Society of Professional Engineers' Outstanding Engineering Achievement Award for 1998. Dr. Patten held three patents in the semi-active structural control area, and had published over 55 articles on that subject.

Dr. Patten received his B.S. from the University of Maryland and his M.S. and Ph.D. degrees from Virginia Polytechnic Institute, all in Mechanical Engineering. He served his country as a Combat Engineer in the U.S. Army, 9th Infantry Division in Vietnam and was awarded a Bronze Star and an Army Commendation Medal with First Oak Leaf Cluster. He was a member of ASME, ASCE and the American Society of Automotive Engineers.

On a personal note, we at MCEER and the University at Buffalo regarded Dr. Patten to be an outstanding engineering scholar. He belonged to a small group of engineering researchers with expertise in experimental verifications and strong analytical abilities. His background enabled him to develop new types of hardware as well as adapt or modify existing equipment. Moreover, he was able to find appropriate applications for his work in these new technologies.

He was a quiet man, intelligent and confident, who was a dedicated and effective teacher. His contributions will be greatly missed.

Michael C. Constantinou and Ian M. Friedland, Editors

Preface

This report presents the proceedings of the U.S.-Italy Workshop on Seismic Protective Systems for Bridges, which was held at Columbia University in New York City, New York on April 27 and 28, 1998. The workshop was attended by 12 Italian and 27 U.S. participants. It was organized by the Multidisciplinary Center for Earthquake Engineering Research (MCEER), which is headquartered at the State University of New York at Buffalo, in Buffalo, NY. Financial sponsorship on the U.S. side was through the MCEER Highway Project, which is sponsored by the U.S. Federal Highway Administration; similar sponsorship for the Italian side was provided by the National Group for Defense Against Earthquakes (GNDT) of the Italian National Research Council (CNR). Columbia University, New York City was a co-sponsor of the workshop and provided important logistical and operational support.

The workshop consisted of presentations of 13 U.S. and 11 Italian papers which focused on research and the application of seismic protective systems for bridges, and the state-of-the-art and practice in bridge seismic isolation and energy dissipation in the two countries. Presentations were also made on the related subjects of: active control systems applications; the use of other advanced technologies for improving the seismic performance of bridges including the use of composites and rocking-column concepts; and the development of bridge fragility curves applicable to the performance of bridges with protective systems. Presentations were brief but intended to provide an overview of recent developments in each country. Discussions were held on each major topic as well as the following subjects: (a) comparison of and the differences between design philosophies and practice in each country, and (b) written guidelines, standards, and codes of practice currently in use in the two countries.

It was recognized that both Italy and the U.S. are at the forefront in the development and application of seismic protective systems for bridges. Participants, and particularly the invited observers from state transportation agencies and the bridge engineering community, were pleased to learn of these developments and recent applications. However, there was common agreement that information and knowledge related to the design, installation, and long-term operation and maintenance of bridge seismic protective systems has not been effectively disseminated to the practicing bridge engineering community. The result is that bridge owning agencies are not currently in a position to make informed decisions regarding the relative merits or performance objectives for seismic protective system hardware, and the agencies are required to rely almost solely on the expertise of hardware vendors and fabricators. It was noted that this has slowed the acceptance of seismic protective systems in day-to-day bridge design and reconstruction practice in the U.S.

Due to rapid advancements currently being made in the development and application of seismic protective systems technologies, it was agreed that a continuing dialog and exchange of information between the U.S. and Italy on seismic protective systems for bridges should continue, and that a second workshop should be organized in Italy in the near future. While this first workshop provided a common basis of comparison for workshop participants, the second workshop should concentrate on specific applications and topics of direct use to practitioners, including design philosophy and standardization of practice and codes.

The workshop was preceded by a tour of interesting bridge rehabilitation projects around the New York City area on April 26, 1998. The tour was arranged and hosted by Dr. Bojidar Yanev, Assistant Commissioner of the New York City Department of Transportation.

The U.S. Steering Committee for the workshop consisted of:

Dr. Michael Constantinou, State University of New York at Buffalo, chair
Dr. Frieder Seible, University of California at San Diego
Mr. Tom Post, California Department of Transportation,
Mr. Ian M. Friedland, Multidisciplinary Center for Earthquake Engineering Research

The Italian-side organizers and Steering Committee consisted of:

Dr. Paolo E. Pinto, Università di Roma "La Sapienza"
Dr. Gian Michele Calvi, Università Degli Studi di Pavia.

Appreciation is extended to Dr. Raimondo Betti of Columbia University for his help and efforts in organizing and making arrangements for the use of the facilities provided by Columbia University.



Participants of the U.S.-Italy Workshop on Seismic Protective Systems for Bridges

Table of Contents

Session I	Italian and European Guidelines for Seismic Design of Isolated Bridges *Franco Braga, Gian Michele Calvi and Paolo E. Pinto*	3
	Seismic Protective Systems for Bridges in the United States: State-of-the Art and State-of-Practice *Michael C. Constantinou and Andrew S. Whittaker*	13
Session II	The 1997 AASHTO Seismic Isolation Guide Specification *John F. Stanton*	31
	Development of the European Standard on Antiseismic Devices *Agostino Marioni and Renzo Medeot*	47
	Caltrans Bridge Research and Applications of New Technologies *Dorie E. Mellon and Thomas J. Post*	57
	The Analysis and Design of Elastomeric Bearings for Application in Bridges *James M. Kelly*	73
	A Methodology for the Design of Energy Dissipation Devices for the Seismic Protection of Bridges *Vincenzo Ciampi*	89
Session III	Energy Dissipation as a Technological Answer to Highly Demanding Design Problems *Renzo Medeot*	107
	Seismic Isolation of Railway Bridges *Mauro Dolce, Domenico Liberatore, Corrado Bonuccelli and Giuseppe Traini*	127
	Applications of Isolation Bearings to Bridges *Manouchehr Karshenas and Iraj I. Kaspar*	147
	Seismic Bearings for Large Span Bridges *Roy A. Imbsen*	157
	Design of the Caltrans Seismic Response Modification Device (SRMD) Test Facility *Gianmario Benzoni and Frieder Seible*	173

Session IV	Design Criteria for Seismic Isolation Devices *Rosario Ceravolo, Alessandro De Stefano and Giuseppe Mancini*	191
	Sensitivity of Response of Isolated Bridges to Modeling and Design Parameters - A Case Study *Andrei M. Reinhorn, Vassil K. Simeonov, Grant DeRue and Michael C. Constantinou*	213
	Effects of Multi-support Excitation on Isolated Bridges *Giorgio Monti and Paolo E. Pinto*	225
	Development of Bridge Fragility Curves *Masanobu Shinozuka*	249
	Testing of Bridges with Isolation/Dissipation Devices at the ELSA Laboratory *Artur V. Pinto, Paolo Negro and Fabio Taucer*	257
Session V	The Use of Advanced Composites in Seismic Retrofitting *Frieder Seible*	283
	Stress Reduction System of Medium Span Bridges Using Semiactive Controls *William Neff Patten, Jinghui Sun and Guangjun Li*	299
	SMA Devices for Seismic Isolation of Bridges: Design and Experimental Behaviour *Mauro Dolce and Roberto Marnetto*	313
	Rocking Columns: An Effective Means of Seismically Isolating a Bridge *John B. Mander, R. Contreras and R. Garcia*	335
Session VI	Modeling of Elastomeric Devices in the Dynamic Linear and Nonlinear Range *Antonello De Luca and Giuseppe Faella*	351
	Modeling and Characterization of Seismic Isolation Bearings *Gregory L. Fenves, Wei-Hsi Huang, Andrew S. Whittaker, Peter W. Clark and Stephen A. Mahin*	371

High Damping Elastomeric Bearings (HDEB): Experimental Tests and Preliminary Results 387
Franco Braga

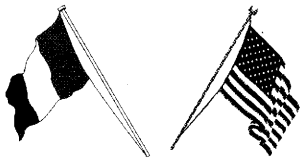
Optimal Design of Isolated Bridges and Isolation Systems for Existing Bridges 407
Gian Michele Calvi and Alberto Pavese

Appendix A

Workshop Agenda A-3

U.S. Participants A-7

Italian Participants A-11



Session I

Italian and European Guidelines for Seismic Design of Isolated Bridges
Franco Braga, Gian Michele Calvi and Paolo E. Pinto

Seismic Protective Systems for Bridges in the United States: State-of-the Art and State-of-Practice
Michael C. Constantinou and Andrew S. Whittaker

Italian and European Guidelines for Seismic Design of Isolated Bridges

Franco Braga, Gian Michele Calvi and Paolo E. Pinto

Department of Structures, Soil Mechanics, Applied Geology - University of Basilicata - Italy
Department of Structural Mechanics, University of Pavia - Italy
Department of Structural and Geotechnical Engineering - University of Rome 'La Sapienza' - Italy

Abstract

In the past few years official Guidelines have been issued in Europe and in Italy to regulate the design of (passively) isolated bridges. Explicity covered is the use of elastomeric and elasto-plastic elements. The design philosophy aims at ensuring adequate protection with respect to two Limit-States or Performance Levels: the first one being the limit of fully elastic response, the second one being a state where the structure is still undamaged while the isolating elements are close to their ultimate deformation. Capacity design measures are adopted to ensure the protection of the structural parts even for larger-than-anticipated seismic events. Detailed requirements on the behaviour of the isolating elements so that they can reliably fulfil their protective role are given. Modelling, methods of analysis and verification criteria complete the content of the Guidelines. Aspects requiring improved definition are discussed in the conclusions of the paper.

Introduction

Seismic isolation of bridges has been introduced officially in Europe for the first time with the issuance of the Eurocode 8 - Part 2: Bridges (EC8/2,(1)), in late 1994. Actual diffusion of this document within EU member countries started in 1995. At present it is being applied experimentally in a number of countries, before being submitted to a formal enquiry to be completed by 1998. Revision of the 1994 draft is planned for the year 2000.

In Italy, practice has been much in advance with respect to the progress of the norms. Apart from two bridges, originally designed in the mid seventies with isolating/dissipating devices, the bulk of the 150 or so existing isolated bridges has been either designed ex novo or retrofitted in the course of the eighties and early nineties.

Design was then based on ad hoc specifications commissioned to experts by the Client, which in the majority of the cases has been the State-owned company Autostrade. Only in 1991 the Guidelines for Seismic Design of Bridges with Isolating/Dissipating Devices were published by Autostrade (2). The general features of this document are in line with the performance-based philosophy of the Eurocodes (3 performance levels are considered), and several aspects related to the definition of the seismic action (elastic response spectrum, site effects, etc.) are the same or similar to those of Eurocode 8 - Part 1 (General and Buildings), version 1988, (3).

Although still conceptually valid and up-to-date, the Autostrade document is now for internal use only, since an official national document has been issued in 1996 by the Ministry of Public Works (MPW-96, (4), again in the form of Guidelines.

The MPW-96 norm has been written in full awareness of both the Autostrade (1991) and of the EC8/2 (1994) documents: while it conforms with their (common) general philosophy, it incorporates additionally the progresses made in the more recent times, in particular for what concerns the formulation of the requirements and of the criteria for acceptance of the mechanical devices.

This last document will therefore be considered as representative of the present european view on the subject and summarized in the following presentation. Account will also be given, however, of a few points of a certain significance on which different choices were made in the other two documents.

General Requirements

Isolated bridges are required to possess adequate reliability with respect to two response levels, or Limit-States, conventionally denominated as Damage Limit State (DLS) and Ultimate Limit State (ULS).

The average return periods for the exceedance of these two levels are indicated as no less than 150 and 500 years, respectively.

The DLS is defined as one of fully elastic response for both the structure and the devices.

At the ULS, only the isolating devices may reach their ultimate capacity, while all structural parts including deck, piers, abutments and foundations must not yield or enter inelastic range.

A third level of action is considered in the Autostrade (1991) document; in this level the PGA is increased by a factor 1,4 with respect to the second level (no return period attached). For this action a ductility demand of up to 1,5 is admitted for the piers, while damages can take place in the devices, though they should maintain their bearing capacity for vertical loads.

An increase of the PGA by a factor of 1,4 would represent a shift of the return period from about

500 to about 1000 years, for the most seismic regions of Italy.

Consideration of this third level of verification, however, has not been retained in MPW-96: the capacity design provisions associated with the ULS verifications were deemed adequate to cover the risks due to higher intensity events.

Additionally, it is worth mentioning that in EC8/2 an explicit distinction is made between bridges which are *fully* or *partially* isolated. The latter category is described as one in which isolation is not provided in all of the piers. The requirement in this case is that the deck should remain elastic, while inelastic ductile response develops both in the isolating devices and in some of the piers.

Design of these bridges requires mandatorily non-linear time-history analyses. Further, a capacity design rule is given in order to ensure that yielding of the selected piers does not impair inelastic action in the devices. For this purpose, the flexural strength of the yielding piers must be somewhat larger than that corresponding to the yielding of the devices. Obviously, inelastic piers must be designed and detailed for fully ductile behaviour, in accordance with the provisions of EC8/1-2-3.

Partially isolated bridges are not mentioned neither in the Autostrade (1991), nor in the MPW-96 Guidelines: since both are guidance documents one might consider this typology as not excluded in principle, although this option appears not to have been implemented in practice thus far.

Seismic Action

The basic model of the action in MPW-96 is the same as that of the Eurocode 8. The generic horizontal component of the free-field motion is described by means of its 5% damping elastic response spectrum. The shape of the spectrum, which is independent of the intensity and has to be scaled by the two values of the PGA appropriate for the verification of the DLS and the ULS, respectively, is made up of a linear ascending ramp from $T = 0$ to $T = T_B$, where the flat, constant spectral acceleration portion begins. At the corner period $T = T_C$ a constant spectral velocity branch starts, ending at $T = T_D$, followed by are indefinite constant spectral displacement portion.

The values of the corner periods separating the three portions of the spectrum depend on the soil conditions, except for T_D which is assumed as constant and equal to $T_D = 3{,}0$ secs.

The transformation of the spectral ordinates for damping values different from $\zeta = 5\%$ is obtained through the factor: $\eta = (7/2 + \zeta)^{1/2}$, which need not to be less than 0,7.

Three reference soil site conditions are defined: A, B, C, ordered for decreasing values of the mechanical properties of the soil.

Soil type C consists of deposits of cohesive or non-cohesive materials, in the latter case with or without interposed layers of softer cohesive soils, characterized by values of V_S increasing rather continuously with depth, starting from $V_S \geq 150$ m/sec at 20 m. It is not allowed to build isolated

structures on soil sites of lesser quality than type C.

The standard spectrum given by MPW-96 can be replaced by site-specific spectra obtained through ad hoc studies. The ordinates of the latter spectra, however, cannot be less than those of the standard tri-partite spectrum, at the periods of interest for the isolated system.

Indications are given in MPW-96 for the use of spectrum compatible (either standard or site-specific) accelerograms. No less than 4 of them are required, and their average spectral ordinates should match the target spectrum with a 90% approximation in the range $T_{fb} \div 1{,}2\ T_i$ (T_{fb}, $T_i \equiv$ period of the non-isolated and of the isolated structure, respectively), and with a 80% approximation elsewhere.

In the general case, the structure has to be analyzed for the three translational components of ground motion, assumed as independent from each other. In case of linear behaviour, the results from the three separate analyses can be combined according to the expression:

$$E_x + 0{,}3\ E_y + 0{,}3\ E_z$$

with implicit rotation of the indexes.

When the analysis is non-linear, the three components have to be applied simultaneously, and the response values to be used for the design are the average values of the maximum response under each of the triplets of independent input components (the average values plus one standard deviation for the design of the isolators).

Soil structure interaction Consideration of this effect is mandatory when soil deformability is such as to contribute 30% or more to the total deformation of the structure at the deck level.

Spatial variability of the input MPW-96 does not place much emphasis on this phenomenon. The only explicit provision consists in adding a contribution to the maximum distortion of the devices, to account for the relative movement at the foundation level. This contribution is estimated as: $d_r = x \cdot V_g/V_p$, where x is the distance between two consecutive piers, V_g is the peak ground and V_p is the body waves velocity.

This simplified approach is at variance with the approach of EC8/2, where consideration of spatial variability is made mandatory for bridges crossing heterogeneous media or having a length in excess of 600 m, and models of different degrees of sophistication are provided in one of the Annexes.

Requirements on the isolators

Detailed requirements on the mechanical properties of the isolators are contained in MPW-96. These are in line with the corresponding ones recently elaborated as european pre-standard by the

CEN Technical Committee 167 which are described in full in a separate contribution to this Workshop.

For the sake of self-consistency of this presentation, a short and essentially descriptive outline of the main requirements is given in the following.

MPW-96 addresses explicity only two-types of devices: elastomeric bearings and elasto-plastic devices. Use of systems other than these two types (as for ex. friction or roller bearings, oleodynamic units, etc.) is not excluded but the proof of their adequacy is left to the producer/designer.

Elastomeric bearings

The behaviour of these isolating elements is characterized by means of two quantities: the equivalent elastic stiffness: k_e, and the equivalent viscous damping coefficient: ζ.

The definition of k_e for a cycle of amplitude d is: $k_e = 2\ W_e/d^2$ (W_e is the elastic strain energy), and its value is calculated from the expression:

$$k_e = G_{din} \cdot A/t_e$$

G_{din} being the dynamic shear modulus at amplitude d, and A and t_e the area in plan and the total height of the bearing, respectively.

The equivalent damping is the ratio between the energy dissipated in one cycle of amplitude d (W_d) and 4π times the elastic energy W_e.

Both k_e and ζ must possess uniform and stable properties with respect to production variability, ageing, temperature effect, variation of the vertical load, cyclic horizontal loading. With respect to the two last mentioned effects it is required that:

a) under the variation of the vertical load due to the dynamic action, both k_e and ζ should not vary by more than 10% with respect to their design values. In the design process, both the minimum and the maximum values of k_e and ζ shall be used, unless the difference in percent between maximum and minimum is less than 20%;

b) denoting by d_2 the maximum design displacement of the bearings, they should be capable of sustaining 10 cycles at 1,25 d_2 without showing negative strain hardening, nor a variation (in any cycle) of k_e and ζ larger than 15% with respect the initial cycle.

Qualification tests include:

a) determination of the vertical stiffness of the bearing, to be measured as the secant stiffness between the deformations corresponding to 30% and 100% of the maximum design vertical load.

b) determination of the static shear modulus G, to be measured as the secant modulus between the shear deformations of $\gamma = 0{,}30$ and $\gamma = 0{,}60$, respectively.

c) determination of the dynamic shear modulus G_{din} and of ζ through sinusoidal tests at 0,5 Hz for $\gamma = 1$, as well as for $\gamma = 0{,}05$, 0,5, 0,7, 2,0. G_{din} for $\gamma = 1$ must fall within the range 0,40÷1,40 MPa. Other tests are required for creep effects, ageing (60 years), stability under shear and compression ($\gamma = 1{,}8$, 1,5 V_{max}, 0,5 V_{min}), and bond resistance between elastomer and steel plates at extreme deformations ($\gamma > 2{,}5$).

Elasto-plastic devices

Usually these devices are not meant for supporting vertical loads, for which separate bearings must be provided. The devices are designed to remain fully elastic (and rather stiff laterally) for the DLS event, while they are expected to dissipate large amounts of energy for events of higher intensity. Their behaviour under monotonically increasing lateral loads is idealized as bilinear, and characterized by two points: the yield threshold (F_1, d_1), and the point corresponding to the maximum displacement (F_2, d_2).

Rules are given for the determination of these two points, based on tests both static and dynamic. The second branch, in particular, is determined from the hysteretic curve of the fifth cycle in a dynamic test, to be described in the following.

Stability of the dissipative behaviour is an essential feature of these devices, hence a stringent test must be passed: 10 loading, unloading and reloading cycles at 1,5 d_2, without showing strain softening and without variations of the stiffness of more than 5%.

Additionally, in order to ensure stability of the hysteretic response of the devices, all parts of them not meant to be dissipative must possess an adequate overstrength.

Qualification tests include:

a) cyclic static tests, with 10 full cycles at $\pm d_2$.

b) cyclic dynamic tests, with at least 5 cycles at $\pm d_2$ with a frequency of 0,5 Hz.

Tests are also foreseen for the bearings operating in parallel with the dissipating devices: static and dynamic friction coefficient and effect of ageing on friction values.

Modelling of the bridge and methods of analysis

The general requirement concerning the structural model is that it should be able to describe accurately the dynamic response of the bridge, with special attention to the stiffness of the concrete parts, the constitutive behaviour of the isolators, the effects of friction, the action of the bumpers, etc.

More specifically, different stiffnesses must in general be used for the deck and for the piers, and, for the latter, the stiffnesses might be different for the DLS and for the ULS.

Inclusion of soil deformability and of soil structure interaction effects has been discussed already. When elastomeric devices are adopted, their behaviour can be modeled as viscoelastic, with an equivalent stiffness and an equivalent damping evaluated as explained above, provided that the weighted modal damping at ULS for all modes does not exceed 10%.

When this is not the case, the actual behaviour of the isolator as obtained from the tests must be introduced and, consequently, a time-history analysis must be performed.

This requirement applies in all cases when elasto-plastic dissipators are used.

The constitutive law adopted must reproduce the experimental curves as closely as feasible and, in particular:
- shall give the same forces at the displacements $\pm d_2$
- shall have the same pattern of stiffness variation in the unloading and reloading branches
- shall yield the same amount of dissipated energy in the cycle at $\pm d_2$

Two methods of analysis are possible: modal analysis with response spectrum, time-history analysis with spectrum-compatible accelerograms. Equivalent static analysis is not allowed.

This exclusion is also present in the Guidelines of Autostrade, while EC8/2 is a little more permissive. In EC8/2 a so-called "Fundamental mode method" is in fact included, to be used when bridge configuration is such that response is dominated by a single, and simple, mode, and provided other criteria regarding the isolation system are also met.

For what concerns the geometric conditions, the static approach is allowed for straight bridges in the longitudinal direction, provided the effective mass of all piers is less than 1/5 of the tributary mass of the deck, and for the transverse direction if the bridge is nearly symmetric, or the spans are simply supported on the piers.

This last condition appears as out of place (apart from is dubious validity, unless it is meant for single span bridges) since for long isolated bridges a degree of continuity of the deck is a necessary requirement.

When the fundamental mode method is applied, the total mass of the bridge is assumed to participate in it.

From the side of the isolation system, the limitations for the use of the static method are:
- the secant stiffness at d_2 must not be less than 50% of the stiffness at 0.2 d_2.
- the effective damping is not larger than 10%
- the forces developed by the isolators when displacement increases from 0,5 d_2 to d_2 are not less than 2,5% of the total gravity load above the isolators.

In comparison with other codes, the limit set by both EC8/2 and MPW-96 to the equivalent global damping value: 10%, in order that an elastic analysis (dynamic or static) can be performed, is

significantly more severe. This limit comes from judgement and from a limited number of numerical investigations. Qualitatively, it is based on the consideration that in the case of bridges is more difficult than in the case of buildings to achieve a situation where all devices work simultaneously with the same displacement, and hence with the same damping, and this makes the determination of a single overall value more uncertain. Numerical tests (on typical bridges) made by using some of the expressions internationally proposed for the equivalent damping have given differences on the maximum of the response of up to more than 100%, among them and between each of them and the exact values obtained through non-linear analysis.

This aspect is believed to be worth of further careful investigations.

Verifications

Damage Limit State

Compliance with DLS in deemed to be automatically satisfied for the structural parts of the bridge, once they satisfy the verifications for the ULS.

For the isolation devices, the damage is related to the residual displacements. For example, for elastomeric bearings it is required that the permanent displacement does not exceed 2% of the design displacement d_2.

Ultimate Limit State

For the structure under the effects of the seismic load combination, the requirements of MPW-96 are as follows:

- the deck should be checked for the limit state of yielding using the same material factors ($\gamma_S = 1,15$ for steel, $\gamma_C = 1,4$ for concrete) adopted for the ordinary variable load combinations;
- the piers and the abutments, together with their foundations, should be checked for the limit-state as above, but with the action effects deriving from the analysis amplified by a capacity design factor of 1,35.

The capacity design approach adopted by EC8/2 is more pervasive than that of MPW-96: it requires all structural parts above and below the isolation interface (i.e., including both deck and piers) to be checked for the action effects deriving from the analysis multiplied by one overstrength factor $\gamma_{oi} = 1,10\ K_{max}/K_{min}$, where K_{max} and K_{min} are the maximum and the minimum stiffness of the isolators at the design displacement, as obtained from the qualification tests.

The verifications required for the elastomeric bearings by both MPW-96 and EC8/2 are of course consistent with the rules given on the draft document of CEN TC 167-SC1 on antiseismic devices. Actually some of the rules presently contained in EC8/2 will be later transferred into the Standard

prepared by CEN TC 167-SC1, once this Standard will be finalized.

In brief, these verifications reduce to:

- the force on the isolator should always be compressive;
- the steel plates should have sufficient thickness in order not to yield in tension;
- the total shear deformation (i.e., the sum of that induced by the vertical load, by the angular rotation and by the seismic action, including in this latter the contribution of the rigid body relative displacements between piers) should non exceed $\gamma^*/1,4$ where γ^* is the maximum shear reached during the bond tests;
- the ratio between the vertical force and the total shear deformation should be such as to avoid instability of the bearing.

The verifications required for the mechanical elasto-plastic devices include checking that they are never subjected to tensile forces, and that all parts of the devices not intended for energy dissipation remain below yielding, with a safety factor $\gamma \geq 1,5$.

For the rest, design dictates the performances of the dissipators, and these performances are subjected to the qualification and acceptance tests previously described.

Conclusive Remarks

The gap which existed in Europe between reality (i.e. actual application of seismic isolation to bridges) and availability of normative documents to regulate the process, has almost vanished by now.

Present practice concentrates exclusively on passive isolation and, more specifically for italian bridges, on the use of metallic elasto-plastic devices, although a spectrum of other systems have been used and are in production (elastomeric or lead-rubber bearings, oleodynamic dampers of various types, etc.), or are under study (ex. Shape Memory Alloy).

From the point of view of the design for isolation two aspects, already well identified in the past, remain open for improvements. One is a realistic definition of the expected ground displacements at the various supports. The importance of the point is too obvious to be underlined, since both the effectiveness and the integrity of the devices are dependent on it.

From the few analytical studies available it would seem that, depending on site conditions, rather large margins with respect to design displacements should be provided, to avoid possible disruption of the devices.

The second aspect, which is connected with the first one, refers to the most appropriate type of analysis for isolated bridges.

The question is: in the face of such large uncertainties on the input, how much accuracy (and hence sophistication) is warranted in the method of analysis?

The answer cannot be a simple one and valid for all situations. One of the tasks for the future could be that of identifying and classifying soil situations of increasing complexity and/or uncertainty, and of associating to each of these an appropriate analytical approach.

References

1. EUROCODE 8 *Design Provisions for Earthquake Resistance of Structures.* ENV 1998-2-BRIDGES. Comité Européen de Normalisation (CEN), Brussels, 1994

2. *Guidelines for Seismic Design of Bridges with Isolating/Dissipating Devices.* AUTOSTRADE, Roma, 1991

3. EUROCODE 8 *Design Provision for Earthquake Resistance of Structures. ENV 1998-1-2-3 Seismic Actions and General Requirements, General and Specific Rules for Buildings of Various Materials.* Comité Européen de Normalisation (CEN), Brussels, 1988

4. *Guidelines for the Design, Construction and Approval of Seismically Isolated Structures.* Ministry of Public Works, Italy, 1996

SEISMIC PROTECTIVE SYSTEMS FOR BRIDGES IN THE UNITED STATES: STATE-OF-THE-ART AND STATE-OF-PRACTICE

Michael C. Constantinou
Department of Civil, Structural and Environmental Engineering,
University at Buffalo State University of New York
Buffalo, NY 14260

Andrew S. Whittaker
Pacific Earthquake Engineering Research Center
University of California at Berkeley
Richmond, CA 94804-4698

ABSTRACT

The use of seismic isolation and passive energy dissipation hardware for bridge applications has gained widespread acceptance in all seismic regions in the United States. Much research and the development of guidelines has accompanied the marked upswing in isolation-related construction. This review paper presents information on the state of the art and state of practice of seismic protective systems for bridges in the United States. Current and recently completed research and studies on system and component behavior are summarized, and the impact of this work on the newly revised AASHTO *Guide Specification for Seismic Isolation of Bridges* is identified.

INTRODUCTION

The field of seismic protective systems includes seismic isolation and passive, semi-active, and active energy dissipation systems. Use of these relatively new technologies has burgeoned in the past few years due to significant analytical and experimental research work, development and promulgation of design guidelines, and the specification of enhanced performance objectives for bridge structures. The focus of the design professional community to date has been seismic isolation and passive energy dissipation systems as evinced by the scope of newly prepared guide specifications and the types of hardware either implemented or under consideration at the time of this writing. As such, only seismic isolation and passive energy dissipation systems are discussed in this paper.

Seismic protective systems is too broad a subject to discuss in detail in this paper. The detailed bibliography found at the end of this manuscript should provide the reader with access to much additional and supporting information to that outlined below. Another resource for the reader is a protective systems database at the University of California at Berkeley, which was developed with funding from the California Department of Transportation (Caltrans). The database, entitled PROSYS, has been developed and implemented in the World Wide Web. The address for the site is **http:///www.eerc.berkeley.edu/prosys.html**. The database contains a brief introduction to the

various types of protective systems devices and technologies, a summary of key applications of protective systems, an interactive database of tests on individual devices or groups of devices, and an interactive database on tests of systems incorporating earthquake protective systems.

The purpose of this paper is twofold: (1) to provide the reader with an overview of the state of the art in the United States and (2) to describe the state of practice of seismic protective systems, in the United States. Greater emphasis is placed on the first topic. The state of the art in the field of seismic protective systems for bridge applications is presented by a discussion of the seminal, newly completed, and current experimental and analytical research work in the United States. Studies ranging from large-scale earthquake-simulator experiments to analytical studies of friction at the microscopic level are described. The state of practice of seismic protective systems is presented through a brief discussion of key applications of protective systems technology in regions of low-to-moderate and high seismic hazard.

In mid-1997, AASHTO released a draft copy of the *Guide Specifications for Seismic Isolation Design*. This draft document will soon replace the 1991 Specification. The key changes to the Specification are described at the end of this paper.

STATE OF THE ART: EXPERIMENTAL RESEARCH

Experimental work on seismic isolation and energy dissipation systems has been primarily conducted at the University of California at Berkeley and at the University of Buffalo. These two universities have undertaken large-scale earthquake-simulator testing of bridges and buildings equipped with seismic isolation and energy dissipation systems; have tested an array of protective systems hardware; and have generated much experimental data. The tests have confirmed the efficacy of seismic protective systems, provided data for the development and checking of analytical models, and facilitated the application of different hardware.

Significant experimental work has also been conducted at the University of Washington on structural elastomeric and sliding bearings. This research program has substantially impacted newly developed design procedures and specifications for seismic isolation bearings.

Before discussing the research work at Berkeley, Buffalo, and Washington, it is instructive to describe two important ongoing experimental projects on seismic protective systems. The first project is the Caltrans/Federal Highway Administration (FHWA) program for the full-scale performance testing of seismic isolation and energy dissipation hardware. This program, which is briefly described in Mellon and Post [1], will involve dynamic testing of a variety of seismic isolation and energy dissipation devices with the objective of establishing key behavioral and performance characteristics for a small subset of protective systems hardware. The second project is the construction of the Caltrans Seismic Response Modification Device Test Facility at the University of California at San Diego (Seible and Benzoni [2]). This test facility, which is expected to be operational in 1998, will be capable of subjecting isolation bearings to axial loads of up to 12,000 kips (53 MN) and multidirectional horizontal motions of up to ±48 in. (±1.2m) peak displacement and 70 in/s (1.8 m/s) peak velocity.

University of California at Berkeley

Research on seismic isolation systems began at the University of California at Berkeley in 1976. The research concentrated on the development of natural rubber bearings for isolating buildings. This work culminated in the development of the high-damping elastomeric bearings. Numerous earthquake-simulator studies and component tests were conducted. Kelly [3] provides a partial list of the publications related to this work. While the majority of these studies have concentrated on the application of seismic isolation of buildings with an emphasis on elastomeric systems, the research data have been widely used to promote the use of the technology by the design professional community for bridge and building applications.

The first experimental studies on isolated bridges were conducted in the early 1980s by Kelly and Buckle (Kelly et al. [4]) using a 427 kN (96 kip) model isolated with low damping elastomeric bearings and lead-rubber bearings. Significant new information regarding the benefits of damping in the isolation system on the reduction of displacements across the isolation interface and the stability of elastomeric bearings at large displacements or shear strains were the key products of this research (Buckle and Kelly [5]).

In 1994, Gilani et al. [6] conducted field testing and dynamic analysis of a four-span seismically isolated viaduct in Walnut Creek, California. The viaduct was the first new bridge in California to be seismically isolated. The primary objectives of the study were to determine the dynamic properties of the viaduct by snap-back and ambient vibration testing; to assess the contributions of different components of the viaduct, including the foundation, to the dynamic properties of the viaduct; and to correlate the results of the finite element analysis with the measured response of the viaduct.

Recently, the University of California at Berkeley began a coordinated experimental and analytical research program with funding from the California Department of Transportation (Caltrans). The key objectives of the research program are (1) to develop an improved understanding of the response of seismically isolated single- and double-span bridges to tridirectional earthquake shaking and (2) to speed the implementation of seismic protective systems by working with expert Caltrans engineers to develop performance specifications for isolation systems. The project is divided into five key tasks, three of which include an experimental component:

- *Isolation Components and Systems.* (1) Testing and response correlation of a rigid block model supported on four seismic isolation bearings to displacement orbits and tridirectional earthquake histories (including near-field motions). Three types of bearings will be tested: high damping elastomeric, lead-rubber, and friction pendulum. See Fenves et al. [7] for more information. (2) Component testing of previously tested elastomeric bearings to systematically evaluate the relationship between scragged and unscragged properties, the relation between the scagged properties as calculated from the original testing and proposed testing (aging tests), and the relation between scragged properties at different temperatures. The data from these tests will be used to help validate the values for λ identified in the draft *AASHTO Guide Specification for Seismic Isolation Design.*

- *Energy Dissipation Systems*. (1) Testing of controllable fluid dampers in a damper test machine. (2) Earthquake-simulator testing of hybrid isolation systems composed of elastomeric bearings and fluid viscous dampers to assess the efficacy of such systems for near-field earthquake shaking.

- *Earthquake Simulator Studies*. Two models (rigid block model and bridge-deck model) have been designed to investigate important issues associated with the implementation of seismic protective systems in bridges. In addition to the earthquake-history testing noted above, the rigid block model will be used to investigate abutment-to-deck connections. The bridge-deck model will be used to assess the effects of mass eccentricity, skewed supports, and substructure flexibility.

University at Buffalo, State University of New York

Experimental research in seismic isolation systems began at the University at Buffalo in 1987 with the establishment of the National Center for Earthquake Engineering Research. The research initially concentrated on the use of sliding isolation systems for building structures, progressively moved toward bridge structures and the use of energy dissipation systems, and recently culminated in earthquake-simulator testing of elastomeric bridge isolation systems using near-field earthquake histories. Highlights of the research effort to date include

- Testing of sliding interfaces to determine frictional properties under dynamic conditions (Mokha et al. [8, 9, 10]), including tests under triaxial dynamic loading (Mokha et al. [11]).

- Earthquake-simulator testing of building structures with sliding isolation systems (Constantinou et al. [12], Mokha et al. [13], including tests in which bearing uplift was induced (Al-Husseini et al. [14]).

- Extensive testing of various sliding interfaces to establish the effects of temperature, load dwell, cumulative travel, and artificial aging on frictional properties (Constantinou et al. [15]). This effort led to the development of the property-modification factors, which have been incorporated into the 1997 *AASHTO Guide Specification for Seismic Isolation Design* [16].

- Field testing of an isolated bridge and component testing of its isolation bearings, including low temperature testing (Wendichansky [17], Kim et al. [18]).

- Testing of prestressed seismic isolation bearings to control uplift (Kasalanati [19]).

- Earthquake-simulator testing of seismic isolation systems.

Seismic isolation systems for bridges were first studied at the University at Buffalo in 1991. At that time, a sliding isolation system supporting a 227 kN rigid deck model was tested on the Buffalo earthquake simulator (Constantinou et al. [20, 21]). Work at Buffalo continued in a joint research effort with Taisei Corporation of Japan with the construction of a 160 kN bridge which included piers of varying stiffness. As part of the joint research project, a variety of isolation systems were including the friction pendulum bearing (Constantinou et al. [22]; Tsopelas et al.

[23]), sliding isolation systems with elastomeric restoring force devices and fluid dampers (Tsopelas et al. [24, 25]), pressurized fluid devices (Tsopelas and Constantinou [26]), and lubricated sliding bearings with yielding steel devices (Tsopelas and Constantinou [27, 28]). The testing included motions compatible with the Level 2 Japanese bridge-design spectra, motions compatible with the Caltrans 0.6g spectra, and historic earthquake histories with high peak accelerations and velocities. Two key observations from these studies were (1) hysteretic or viscous damping can be effectively used to reduce displacements in isolated bridges, and (2) isolation systems with minimal restoring force can develop significant permanent displacements if subjected to multiple earthquake histories. Data from these tests were used to help develop procedures for implementing hybrid isolation systems in bridges and to modify existing design criteria for conventional isolation systems in the 1997 *AASHTO Guide Specifications for Seismic Isolation Design* [16].

The testing programs described above were conducted prior to the 1994 Northridge, California, and the 1995 Hyogo-ken Nanbu (Kobe), Japan, earthquakes. These earthquakes generated a large number of earthquake histories with near-field characteristics that include high peak ground accelerations and velocities. Near-field effects immediately became an important consideration for the design of seismic isolation systems close to major faults. An experimental study of elastomeric isolation systems for bridges has been recently completed in which emphasis was placed on earthquake histories with near-field characteristics. Kasalanati [19] reports the results of tests of high damping elastomeric systems and elastomeric systems with added linear and nonlinear viscous dampers.

University of Washington

For the last fifteen years, the University of Washington has undertaken experimental and analytical studies on structural bridge bearings. Although the experimental work primarily addressed non-seismic applications, the data have been used to modify design procedures for bearings in both the AASHTO Standard Specifications and the 1997 *AASHTO Guide Specifications for Seismic Isolation Design.* The work started with a comprehensive review of the state of knowledge on elastomeric bearings (Stanton and Roeder [29]). In 1987, Roeder et al. [30] published a report on the performance of elastomeric bearings. This report presented experimental data on a number of important subjects including:

- Service-level behavior and failure modes under compression
- Effect of combined compression and rotation on the behavior and failure modes of structural bearings
- Mechanical properties of bearings in combined compression and shear
- Buckling of structural bearings
- Fatigue life of elastomeric structural bearings

Using these data, Roeder et al. [31] developed more rational design procedures for elastomeric bearings by explicit consideration of fatigue. Elements of these experimentally based procedures

have been incorporated in the 1997 *AASHTO Guide Specifications for Seismic Isolation Design* [16].

Recently, researchers at the University of Washington have focused on sliding bearings. In conjunction with Queen's University in Canada, extensive tests on sliding bearings were undertaken to assess the effects of a variety of conditions, including those of temperature and contamination, on frictional properties (Campbell et al. [32], Stanton et al. [33]). Data from this testing program have been used to develop property-modification factors for seismic isolation bearings [15].

STATE OF THE ART: ANALYTICAL RESEARCH

Analysis of Elastomeric Bearings

Significant information is available on the behavior of elastomeric bearings, and Kelly and his research associates have undertaken much of this work (see Kelly [3, 34]). Explicit expressions have been developed for compression, rotation, and stability of elastomeric bearings. Other analytical work of interest includes the analysis of compression, rotation, and stability of elastomeric bearings by researchers at the University of Washington [29, 30] and the analysis of annular elastomeric bearings (Constantinou et al. [35]).

Modeling of Seismic Isolation and Energy Dissipation Hardware

Mathematical models of varying sophistication have been to describe the mechanical behavior of seismic isolation and energy dissipation hardware, specifically:

- Models have been developed to describe the behavior of hardware based on simple physical models, which are calibrated using test data. Typically, these models are based on simple plasticity or visco-plasticity models. Examples are models for the behavior of sliding bearings (Constantinou et al. [22, 36], Mokha et al. [11]), and models for elastomeric bearings (Tsopelas et al. [37], Kikuchi and Aiken [38]). Models for the behavior of fluid viscous dampers have been developed in which the behavior is typically represented by linear or nonlinear viscous models and other viscoelastic fluid models (Soong and Dargush [39], Constantinou et al. [40]).

- More advanced models have been developed which, while still requiring some calibration with test data, are strongly based on fundamental principles. Examples of more advanced models are those for fluidic devices (see Tsopelas and Constantinou [26], Symans and Constantinou [41], and Makris et al. [42]).

- Continuum mechanics has been used to develop mathematical models for seismic isolation and energy dissipation devices; examples of such models are given by Makris et al. [43, 44, 45]).

Computer Code for the Analysis of Protective Systems

A number of general-purpose computer programs have been marketed that are capable of response-history analysis of seismically isolated structures. Of these programs, ABAQUS [46] and ANSYS [47] likely have the most advanced capabilities. Other computer codes, such as DRAIN-2D [48] and ANSR [49], have more limited capabilities. Starting in the early 1990s, the 3D-BASIS family of computer programs (Nagarajaiah et al. [50, 51], Tsopelas et al. [37]), developed specifically for the analysis of seismically isolated buildings and bridges, was released. The 3D-BASIS programs have seen widespread use by the research and design professional communities in the United States.

In 1997, SAP2000 [52] and IDARC-BRIDGE [53] were released; both have extensive nonlinear analysis capabilities and a suite of elements for modeling seismic isolation and energy dissipation devices.

Heat Transfer and Temperature Rise in Protective Systems Hardware

Seismic isolation bearings and energy dissipation devices dissipate energy by heat. Because it is not currently possible to test protective systems hardware at realistic frequencies, displacements, and velocities, either scale-models of prototype hardware are tested dynamically or prototype hardware is tested pseudo-statically. Neither approach will correctly capture the flow of heat through a bearing or damper or the increase in temperature in a prototype device. Such issues are likely important for lead-rubber bearings of unusual proportions, sliding bearings, fluid viscous dampers, and viscoelastic dampers. Analytical solutions for the temperature increase in sliding bearings and fluid viscous dampers have been developed in the past 12 months (Makris et al. [42] and Constantinou et al. [15]).

Property-Modification Factors

Analysis and design of protective systems for bridges is routinely based on assumed mechanical properties for the seismic isolation bearings and passive energy dissipation devices. Such properties typically form the basis for the prototype and production hardware acceptance criteria. Little attention is routinely given to change in material properties with either repeated cycling or aging. Examples of change due to repeated cycling include scragged versus unscragged values of effective stiffness for elastomeric bearings and breakaway versus dynamic coefficient of friction for sliding bearings.

The 1991 *AASHTO Guide Specifications for Seismic Isolation Design* [54] did not take into account the fact that material properties of selected isolation and damping systems vary as a function of strain history and age. This shortcoming was rectified in the 1997 *Guide Specifications* [16] by the introduction of property-modification (or) factors. The values assigned to these factors, although preliminary and mutable at the time of this writing, provide the design professional with a broad understanding of how mechanical properties can change with strain history and time. The 1997 *Guide Specifications* requires the design professional to perform analysis using bounding values of isolator properties (defined through individual values of which are assigned to environmental conditions, aging, history of loading, etc.). Background information on this rational approach to design of protective systems, and the data

used to establish the values of these factors in the 1997 *Guide Specifications* are presented in Constantinou et al. [15]. More information on values for to account for the effects of strain history and aging will be a product of the on-going studies at the University of California at Berkeley.

Response Modification Factors

Response modification factors, in one form or another, have been used for the design of conventional buildings and bridges for more than 35 years. Such factors are intended to account for the reserve strength, ductility, and energy dissipation capacity in well-detailed structural components (Whittaker et al. [55]).

In a bridge (or building) incorporating protective systems hardware, the design objective is generally to eliminate damage to structural components in the design earthquake. For the design of superstructures in seismically isolated buildings, building codes specify values for the response modification factor that range between one quarter and one third of the value assigned to the identical framing in a conventional building. Building substructures are designed for the forces delivered by the isolators in the design earthquake. This seemingly simplistic approach is intended to essentially eliminate inelastic response in the substructure and superstructure of an isolated building. A similar philosophy has been adopted in the 1997 *Guide Specifications for Seismic Isolation Design.*

Much lower and more appropriate values for response modification factors (or R factors) have been assigned to isolated bridge substructures. The use of the lower values assigned to R in the 1997 *Guide Specifications* should ensure elastic or near-elastic response in the substructure of an isolated bridge. The values assigned to R for isolated bridges were partly established by analysis (see Quarshie [56]). Although the studies of Quarshie generally support the values assigned to R in the *Guide Specifications*, Quarshie recommended that the ductility-based component of R should be set equal to 1.0 and that any reduction in design force be based solely on the estimated reserve strength (beyond nominal ultimate strength) of the substructure. Additional information on the response of isolated bridges with yielding substructures (associated with a value of R much greater than 1.0) will be a product of the studies at Berkeley.

GUIDELINES FOR THE IMPLEMENTATION OF PROTECTIVE SYSTEMS IN THE UNITED STATES

The 1991 *AASHTO Guide Specifications for Seismic Isolation Design* [54] provided significant impetus for the application of seismic isolation to bridges in the United States. The *1991 Guide Specifications* [54] were heavily based on the 1991 *Uniform Building Code* regulations for the design of seismic isolation systems for buildings [57]. Both the 1991 *Uniform Building Code* and the 1991 *Guide Specifications* mandate that the isolation system exhibit a significant restoring force to both avoid large cumulative permanent displacements under repeated earthquake shaking, and to reduce the sensitivity of its displacement response to the characteristics of the earthquake shaking. The key revisions in the 1997 *Guide Specifications* were (1) the introduction of property-modification factors as outlined above, (2) reduction of values assigned to the response modification factor, (3) modifications to the methods of analysis of protective systems

and guidelines for the analysis of hybrid isolation systems including passive viscous damping devices, and (4) changes to the requirements for post-yield stiffness and restoring force in individual seismic isolators.

STATE-OF-PRACTICE IN THE UNITED STATES

Seismic isolation is a now a mature bridge-engineering technology with more than 100 completed applications in the United States. A partial listing of these projects can be found at the following web site: **http://www.eerc.berkeley.edu/prosys**. An inventory of recent Caltrans applications can be found in Mellon and Post [1].

Both highway and rail bridges have been isolated for new and retrofit construction with elastomeric or sliding bearings. Most of the more recent applications have made use of either lead-rubber or friction-pendulum seismic isolation bearings. The lead-rubber and friction-pendulum seismic isolation bearings have been widely used for bridge applications because both types of isolators offer high stiffness at small displacements to resist operational loads (e.g., braking and centrifugal forces) and substantial energy dissipation (damping).

Many of the applications identified in the *PROSYS* database are for retrofit construction in regions of low to moderate seismic risk such as the midwestern and eastern regions of the United States. In these regions there is much work under way to replace components of aging bridge construction, including road decks and bridge bearings. Simultaneously, new requirements for the seismic resistance of bridge construction have been introduced. Seismic isolation has proven to be a cost effective means by which a) to replace aged steel bridge bearings with new bearings capable of sustaining increased axial loads, thermally induced displacements, and rotations as well as moderate earthquake-induced displacements and (b) to limit the forces imposed on the substructure during earthquake shaking to avoid the need to substantially strengthen piers, pile caps, and piles. Three such examples of retrofit construction are located in Missouri and Illinois:

I-70 Rehabilitation of the Poplar St. Bridge

- 349 lead-rubber seismic isolation bearings supplied to isolate 5370 feet of new (replacement) multi-girder steel bridge construction on 51 multi-column bents
- 30 tapered steel pin seismic isolation bearings supplied to retrofit 15 fly-over ramps

I-70 Rehabilitation at the MLK Third Street Viaduct

- 131 lead-rubber seismic isolation bearings supplied to retrofit a multi-span bridge; axial loads range between 60 and 1800 kips per bearing

US 40/I-64 Double-Deck Approach Structure to the Poplar St. Bridge

- 788 seismic isolation bearings (type unknown at the time of this writing) supplied for retrofit construction; axial loads range between 50 and 1220 kips per bearing

For each of these three projects, the design of the seismic isolation system was based on the draft AASHTO *Guide Specifications for Isolation Bearings*. The key design objectives in each case were (1) to share the earthquake-induced loads between all bents, (2) to increase the fundamental period of the bridge to reduce earthquake-acceleration demands on the substructure, and (3) to add substantial energy dissipation at the level of the bridge bearings to reduce both the relative displacements between adjacent segments of the bridge deck and the displacements across the isolation interface. All three objectives were achieved by replacing the existing steel fixed and expansion bearings with *flexible* seismic isolation bearings. Figure 1 shows such an application. A lead-rubber bearing can be seen in the foreground of this figure; an older steel bridge bearing can be seen in the background.

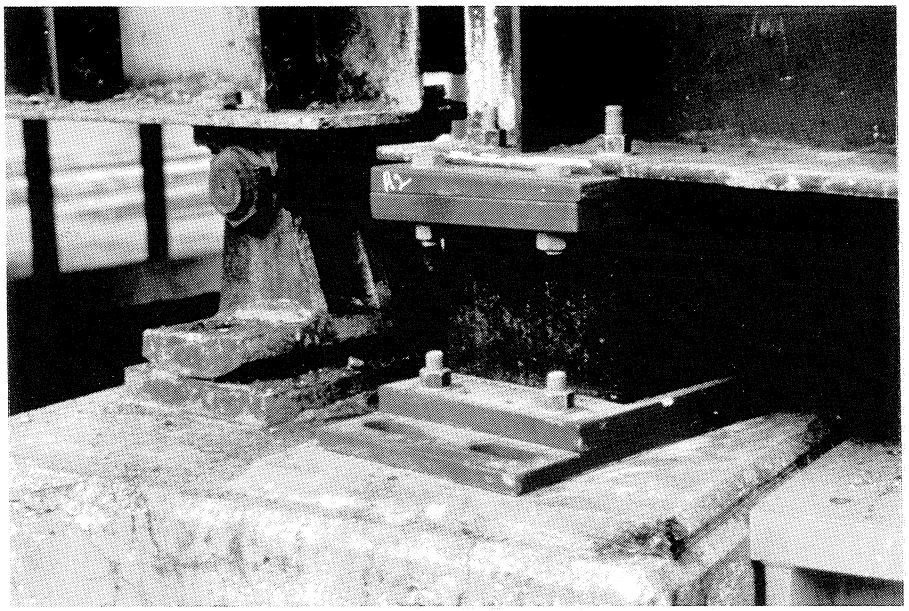


Figure 1. Seismic retrofit of an existing bridge using lead-rubber bearings (Photograph courtesy of Dynamic Isolation Systems, Inc.)

Many of the toll bridges in the San Francisco Bay Area are being retrofitted with protective systems hardware in order to minimize damage to their superstructures and substructures during maximum capable earthquake shaking. In different applications, elastomeric, lead-rubber, and friction-pendulum seismic isolation bearings are being used. Fluid viscous dampers are proposed for some of the projects. More information is presented in Mellon and Post [1]. For these projects the earthquake-induced displacement demands are appreciably higher than those used for the retrofit of the bridges in Missouri and Illinois: requiring the use of dampers to reduce displacements in some cases, and the construction of isolation bearings of unprecedented sizes in many cases.

The research programs at Buffalo and Berkeley have focused on the application of seismic isolation and damping systems to one- and two-span bridges. The authors hope that information from these research projects will speed the application of protective systems hardware to new

single- and double-span bridges: a genre of bridge construction that has yet to substantially benefit from seismic isolation and energy dissipation hardware.

ACKNOWLEDGEMENTS

Numerous individuals made significant contributions to this manuscript, including Dr. Panos Tsopelas (University at Buffalo); Drs. Peter Clark, Gregory Fenves, Stephen Mahin, and Nicos Makris (University of California at Berkeley); Ms. Dorie Mellon (Caltrans); Ms. Joyce Lem (ABKJ, Inc.); Mr. Mark Capron (Sverdrup); Mr. Greg Orsolini (DeLeuw Cather) and Dr. Tim Ingham (TYLI). Dr. Ron Mayes (DIS, Inc.), Mr. Bob Schneider (Taylor Devices), Mr. Byron West (SEP), and Mr. Tom Zemanek (Enidine) provided information on completed and in-progress construction projects using seismic protective systems. Ms. Janine Hannel edited the manuscript. All of these contributions are gratefully acknowledged.

REFERENCES

(1) Mellon, D. E. and Post, T. J. (1998), "Caltrans Bridge Research and Application of New Technologies", Proc. US-Italy Workshop on Seismic Protective Systems for Bridges, New York, New York.

(2) Seible, F. and Benzoni, G. (1998), "Caltrans SRMD", Proc. US-Italy Workshop on Seismic Protective Systems for Bridges, New York, New York.

(3) Kelly, J. M. (1993), *Earthquake-Resistant Design with Rubber*, Springer-Verlag, London, UK.

(4) Kelly, J.M., Buckle, I.G. and Tsai H-C. (1986), "Earthquake Simulator Testing of a Base-Isolated Bridge Deck", Report UCB/EERC-85/09, Earthquake Engineering Research Center, University of California, Berkeley, CA.

(5) Buckle, I.G. and Kelly, J.M. (1986), "Properties of Slender Elastomeric Isolation Bearings During Shake Table Studies of a Large-Scale Model Bridge Deck", Proc. 2nd World Congress on Joints and Bearings, ACI, SP-94-15, Volume 1, p. 247-267.

(6) Gilani, A.S., Mahin, S.A., Fenves, G.L., Aiken, I.D., and Chavez, J.W. (1995), "Field Testing of Bridge Design and Retrofit Concepts", Report UCB/EERC-95/14, Earthquake Engineering Research Center, University of California, Berkeley, CA.

(7) Fenves, G. L., Huang, W-H, Whittaker, A.S., Clark, P.W., and Mahin, S.A. (1998), "Modeling and Characterization of Seismic Isolation Bearings", Proc. US-Italy Workshop on Seismic Protective Systems for Bridges, New York, New York.

(8) Mokha, A., Constantinou, M. C. and Reinhorn, A. M. (1988), "Teflon Bearings in Aseismic Base Isolation: Experimental Studies and Mathematical Modeling", Report NCEER-88-0038, National Center for Earthquake Engineering Research, Buffalo, NY.

(9) Mokha, A., Constantinou, M. and Reinhorn, A. (1990), "Teflon Bearings in Base Isolation. I: Testing", J. Structural Engng., ASCE, Vol. 116, No. 2, 438-454.

(10) Mokha, A., Constantinou, M. C. and Reinhorn, A. M. (1991), "Further Results on Frictional Properties of Teflon Bearings", J. Structural Engineering, ASCE, Vol. 117, No. 2, 622-626.

(11) Mokha, A., Constantinou, M. C. and Reinhorn, A. M. (1993), "Verification of Friction Model of Teflon Bearings Under Triaxial Load", J. Structural Engineering, ASCE, Vol. 119, No. 1, 240-261.

(12) Constantinou, M. C., Mokha, A. and Reinhorn, A. M. (1991), "Study of Sliding Bearing and Helical-Steel-Spring Isolation System", J. Structural Engineering, ASCE, Vol. 117, No. 4, 1257-1275.

(13) Mokha, A., Constantinou, M. C., Reinhorn, A. M. And Zayas, V. A. (1991), "Experimental Study of Friction-Pendulum Isolation System", J. Structural Engineering, ASCE, Vol. 117, No. 4, 1201-1217.

(14) Al-Hussaini, T. M., Zayas, V. A. and Constantinou, M. C. (1994), "Seismic Isolation of Multistory Frame Structures Using Spherical Sliding Isolation Systems", Report NCEER-94-0007, National Center for Earthquake Engineering Research, Buffalo, NY.

(15) Constantinou, M. C., Tsopelas, P. and Kasalanati A. (1998), "Property Modification Factors for Seismic Isolation Bearings", Final Report on Task 106-F-4.2.1(a), NCEER Highway Project, to appear as Technical Report of the National Center for Earthquake Engineering Research, Buffalo, NY.

(16) American Association of State Highway and Transportation Officials (1997), "Guide Specifications for Seismic Isolation Design".

(17) Wendichansky, D. A. (1996), "Experimental Investigation of the Dynamic Response of Two Bridges Before and After Retrofitting with Elastomeric Bearings", Ph.D. Dissertation, Department of Civil Engineering, State University of New York at Buffalo.

(18) Kim, D. K., Mander, J. B. and Chen S. S. (1996), "Temperature and Strain Rate Effects on the Seismic Performance of Elastomeric and Lead-Rubber Bearings", Proc. The Fourth World Congress on Joint Sealing and Bearing Systems for Concrete Structures, ACI, SP-164-18.

(19) Kasalanati, A. (1998), "Experimental Study of Bridge Elastomeric and Other Isolation and Energy Dissipation Systems with Emphasis on Uplift Prevention and High Velocity Near-Source Seismic Excitation", Ph.D. Dissertation, Department of Civil Engineering, State University of New York at Buffalo.

(20) Constantinou, M. C., Kartoum, A., Reinhorn, A. M. and Bradford P. (1991), "Experimental and Theoretical Study of a Sliding Isolation System for Bridges", Report NCEER-91-0027, National Center for Earthquake Engineering Research, Buffalo, NY.

(21) Constantinou, M. C., Kartoum, A., Reinhorn, A. M. and Bradford P. (1992), "Sliding Isolation System for Bridges: Experimental Study", Earthquake Spectra, EERI, Vol. 8, No. 3, 321-344.

(22) Constantinou, M. C., Tsopelas, P., Kim, Y-S. and Okamoto, S. (1993), " NCEER-Taisei Corporation Research Program on Sliding Seismic Isolation Systems for Bridges: Experimental and Analytical Study of a Friction Pendulum System (FPS), Report NCEER-93-0020, National Center for Earthquake Engineering Research, Buffalo, NY.

(23) Tsopelas, P., Constantinou, M. C., Kim, Y-S. and Okamoto, S. (1996), "Experimental Study of FPS System in Bridge Seismic Isolation", Earthquake Engineering and Structural Dynamics, Vol. 25, 65-78.

(24) Tsopelas, P., Okamoto, S., Constantinou, M. C., Ozaki, D. and Fujii, S. (1994), "NCEER-Taisei Corporation Research Program on Sliding Seismic Isolation Systems for Bridges: Experimental and Analytical Study of Systems Consisting of Sliding Bearings, Rubber Restoring Force Devices and Fluid Dampers", Report NCEER-94-0002, National Center for Earthquake Engineering Research, Buffalo, NY.

(25) Tsopelas, P., Constantinou, M. C., Okamoto, S., Fujii, S. and Ozaki, D. (1996), "Experimental Study of Bridge Seismic Sliding Isolation Systems", Engineering Structures, Vol. 18, No. 4, 301-310.

(26) Tsopelas, P. and Constantinou, M. C. (1994) "NCEER-TAISEI Corporation Research Program on Sliding Seismic Isolation Systems for Bridges-Experimental and Analytical Study of Systems Consisting of Sliding Bearings and Fluid Restoring Force/Damping Devices." Report No. NCEER 94-0014. National Center for Earthquake Engineering Research, Buffalo, NY.

(27) Tsopelas, P. and Constantinou, M. C. (1994) "NCEER-TAISEI Corporation Research Program on Sliding Seismic Isolation Systems for Bridges-Experimental and Analytical Study of Systems Consisting of Lubricated PTFE Sliding Bearings and Mild Steel Dampers." Report No. NCEER 94-0022, National Center for Earthquake Engineering Research, Buffalo, NY.

(28) Tsopelas, P. and Constantinou, M. C. (1997) "Study of Elastoplastic Bridge Seismic Isolation System." Journal of Structural Engineering, ASCE, Vol. 123, No 4, 489-498.

(29) Stanton, J. F. and Roeder, C. W. (1982), "Elastomeric Bearings Design, Construction, and Materials", NCHRCP Report 248, Transportation Research Board, Washington, D.C.

(30) Roeder, C. W., Stanton, J. F. and Taylor A. W. (1987), "Performance of Elastomeric Bearings", NCHRCP Report 298, Transportation Research Board, Washington, D.C.

(31) Roeder, C. W., Stanton, J. F. and Taylor A. W (1990), "Fatigue of Steel-Reinforced Elastomeric Bearings" Journal of Structural Engineering, ASCE, Vol. 116, No 2, 407-426.

(32) Campbell, T. I., Pucchio, J. B., Roeder, C. W. and Stanton, J. F. (1991), "Frictional Characteristics of PTFE Used in Slide Surfaces of Bridge Bearings", Proc. 3rd World Congress on Joint Sealing and Bearing Systems for Concrete Structures, Toronto, Ontario, Canada, Vol. 2 of Preprints (published by the National Center for Earthquake Engineering Research, Buffalo, NY), 847-870.

(33) Stanton, J. F., Roeder, C. W. and Campbell, T. I. (1993), "High Load Multi-Rotational Bridge Bearings", Final Report. National Cooperative Highway Research Program, NCHRP 10-20A, Transportation Research Board, Washington, D.C.

(34) Kelly, J. M. (1998), "Analysis and Design of Elastomeric Bearings for Application in Bridges", Proc. US-Italy Workshop on Seismic Protective Systems for Bridges, New York, New York.

(35) Constantinou, M. C., Kartoum, A. and Kelly, J. M. (1992), "Analysis of Compression of Hollow Circular Elastomeric Bearings", Engineering Structures, Vol. 14, No. 2, 103-111.

(36) Constantinou, M., Mokha, A. and Reinhorn, A. (1990), "Teflon Bearings in Base Isolation. II: Modeling", J. Structural Engng., ASCE, Vol. 116, No. 2, 455-474.

(37) Tsopelas, P., Constantinou, M.C. and Reinhorn, A.M. (1994) "3D-BASIS-ME: Computer Program for Nonlinear Dynamic Analysis of Seismically Isolated Single and Multiple Structures and Liquid Storage Tanks." Report No. NCEER 94-0010, National Center for Earthquake Engineering Research, Buffalo, NY.

(38) Kikuchi, M. and Aiken, I. D. (1997) "Analytical Hysteresis Model for Elastomeric Seismic Isolation Bearings", Earthquake Engineering and Structural Dynamics, Vol. 26, No. 2, 215-231.

(39) Soong, T. T. and Dargush, G. F. (1996), *Passive Energy Dissipation Systems in Structural Engineering*, J. Wiley & Sons, London, UK.

(40) Constantinou, M. C., Soong, T. T. and Dargush, G. F. (1997), *Passive Energy Dissipation Systems for Structural Design and Retrofit*, Monograph, National Center for Earthquake Engineering Research, Buffalo, NY.

(41) Symans, M. D. And Constantinou, M. C. (1998) "Experimental Testing and Analytical Modeling of Semi-Active Fluid Dampers for Seismic Protection", Journal of Intelligent Material Systems and Structures, (to appear).

(42) Makris, N., Roussos, Y., Whittaker, A. and Kelly, J. (1997) "Viscous Heating of Fluid Dampers During Seismic and Wind Excitations: Analytical Solutions and Design Formulae", Report UCB/EERC-97/11, Earthquake Engineering Research Center, University of California, Berkeley, CA.

(43) Makris, N., Constantinou, M. C. and Dargush, G. F. (1993) "Analytical Modeling of Viscoelastic Fluid Dampers", J. Structural Engng., ASCE, Vol. 119, No. 11, 3310-3325.

(44) Makris, N., Dargush, G. F. and Constantinou, M. C. (1993) "Dynamic Analysis of Generalized Viscoelastic Fluids", J. Engineering Mechanics., ASCE, Vol. 119, No. 8, 1663-1679.

(45) Makris, N., Dargush, G. F. and Constantinou, M. C. (1995) " Dynamic Analysis of Viscoelastic-Fluid Dampers", J. Engineering Mechanics., ASCE, Vol. 121, No. 10, 1114-1121.

(46) ABAQUS, Hibbit, Karlsson & Sorensen, Inc., Pawtucket, Rhode Island, 1989.

(47) ANSYS, Swanson Analysis Systems, Inc. Houston, Pennsylvania, 1987.

(48) Kannan, A. M. and Powell, G. H. (1973) "DRAIN-2D - A General Purpose Program for Dynamic Analysis of Inelastic Plane Structures with Users Guide" Report No. UBC/EERC-73/22, Earthquake Engineering Research Center, University of California, Berkeley, CA.

(49) Mondkar, D. P. and Powell, G. H. (1975) "ANSR – General Purpose Program for Analysis of Nonlinear Structural Response", Report No. UBC/EERC-75/37, Earthquake Engineering Research Center, University of California, Berkley, CA.

(50) Nagarajaiah, S., Reinhorn, A. M. and Constantinou M. C. (1991) "3D-BASIS Nonlinear Dynamic Analysis of Three-Dimensional Base Isolated Structures: Part II" Report No. NCEER 91-0005, National Center for Earthquake Engineering Research, Buffalo, NY.

(51) Nagarajaiah, S., Li, C., Reinhorn, A. M. and Constantinou M. C. (1993) "3D-BASIS-TABS: Computer Program for Nonlinear Dynamic Analysis of Three Dimensional Base Isolated Structures." Report No. NCEER 93-0011, National Center for Earthquake Engineering Research, Buffalo, NY.

(52) CSI, *SAP2000*, Computers and Structures, Inc., Berkeley, CA.

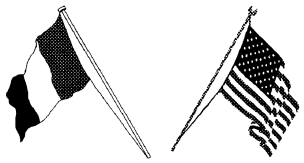
(53) Reinhorn, A. M., Simeonov, V., DeRue, G. and Constantinou M. C. (1998), "Sensitivity of Inelastic Seismic Response of Base Isolated Bridges", Proc. US-Italy Workshop on Seismic Protective Systems for Bridges, New York, New York.

(54) American Association of State Highway and Transportation Officials (1991), "Guide Specifications for Seismic Isolation Design", Washington, D.C.

(55) Whittaker, A.S., Uang, C.M., and Bertero, V.V., "An Experimental Study of the Behavior of Dual Steel Systems", Report UCB/EERC-88/14, Earthquake Engineering Research Center, University of California, Berkeley, CA.

(56) Quarshie, J. (1998) "Response Modification Factors for Seismically Isolated Bridges", Ph.D. Dissertation, Department of Civil Engineering, State University of New York at Buffalo.

(57) International Conference of Building Officials (1991). Uniform Building Code, Earthquake Regulations for Seismic-Isolated Structures. Whittier, CA.



Session II

The 1997 AASHTO Seismic Isolation Guide Specification
John F. Stanton

Development of the European Standard on Antiseismic Devices
Agostino Marioni and Renzo Medeot

Caltrans Bridge Research and Applications of New Technologies
Dorie E. Mellon and Thomas J. Post

The Analysis and Design of Elastomeric Bearings for Application in Bridges
James M. Kelly

A Methodology for the Design of Energy Dissipation Devices for the Seismic Protection of Bridges
Vincenzo Ciampi

THE 1997 AASHTO SEISMIC ISOLATION GUIDE SPECIFICATION

John F. Stanton. PE,
Professor of Civil Engineering
University of Washington,
Seattle WA 98195

ABSTRACT

AASHTO published its first Seismic Isolation Guide Specification in 1991. In 1995, the need for updating the original document became obvious, and the newly-formed Seismic Committee T-3 was charged with the task of the updating. A special Task force was appointed to do the job, and the work was completed by February 1997. The new Guide Specification has been balloted by AASHTO and has been accepted. This paper discusses some of the issues addressed by the new document.

BACKGROUND

In 1991, AASHTO produced its first Seismic Isolation Guide Specification for Bridges (Guide, 1991). Although Guide Specifications are advisory rather than mandatory, its introduction was an important event because it provided a mantle of legitimacy for a fledgling industry. The previous absence of such a document had acted as a deterrent to the use of seismic isolation in bridges.

In 1991, elastomeric bearings were the predominant isolation hardware, and this fact was reflected in the provisions of the specifications. By 1995, other bearing types, and sliding bearings in particular, had been developed to become viable isolators. The new T-3 Seismic Technical Committee of AASHTO was then charged with updating the Guide Specification to incorporate the current state of the industry. To perform this task the T-3 Committee formed a volunteer Task Group consisting of three state bridge engineers, three industry representatives, three university professors and one representative from the Federal Highway Administration. (Membership is detailed in Appendix A). The Task Group essentially re-wrote the Guide Specification by considering the current state of practice and research. The group's communal activity was limited to eight two-day meetings between October 1995 and February 1997.

OVERVIEW OF THE NEW GUIDE SPECIFICATIONS

The New Guide Specifications are intended to be read in conjunction with the AASHTO Standard Specifications for Highway Bridges (1996). Where conflicts occur, the Guide Specification controls. The primary differences lie in the areas of Seismic Design (Division 1-A of the Standard Specifications) and detailed design of bearings. The Guide Specifications address the following broad topics:

- Ground Motion selection.
- Analysis issues. These include permissible methods of analysis, force reduction factors, etc.
- General Design Requirements. These include clearances, minimum lateral restoring force, stability, non-seismic forces, etc.)
- Test Requirements for isolation systems
- Special design requirements for elastomeric bearings
- Special design requirements for sliding bearings
- Special design requirements for other bearings

Although every section was extensively reviewed and discussed, major differences from the previous specifications occur in the following areas:

- Analysis changed to include substructure properties.
- R Factors lowered to ensure elastic response in the substructure
- Minimum stiffness requirements changed

- Detailed requirements added for specific systems.
- Bounding values added for properties to be used for design.

DETAILED DISCUSSION OF SPECIFIC ISSUES

Permissible Methods of Analysis.

The Guide Specifications permit four methods of analysis. Non-linear Time History (NLTH) analysis is the most sophisticated and accounts explicitly for the nonlinear physical properties of the isolator system. It also requires the selection or generation of a suite of at least three suitable ground motions, each of which consists of two orthogonal horizontal components. Rules are given for scaling the amplitudes of the motions so that their spectra are consistent in magnitude with the design spectrum in the AASHTO Standard Specifications that is used for seismic design of fixed-based systems. Frequency scaling to achieve a closer match with the design spectrum across a range of periods is optional. Using it offers a modest advantage in that the amplitudes of the scaled ground motions, and thus the design forces and displacements, are likely to decrease slightly.

The other three methods, namely Multi-Mode Spectral analysis, Single-Mode Spectral analysis and Uniform Load method are all based on the assumption that the system can be modeled with sufficient accuracy by a linear system with visco-elastic damping. The equivalent linear stiffness is taken as the secant stiffness at maximum force and displacement and the equivalent damping is derived from the energy dissipated per cycle. The advantage of the assumption is that it permits relatively simple analysis and avoids potential disagreements over the selection of the ground motions, because a prescribed spectrum is used. The disadvantages lie in the lack of fidelity with which the true response is captured. For example, two systems with the same maximum force and displacement and the same hysteresis loop area, such as those illustrated in Fig. 1, will have the same equivalent elastic properties and hence the same predicted response. NLTH analysis would likely show slightly different responses for the two.

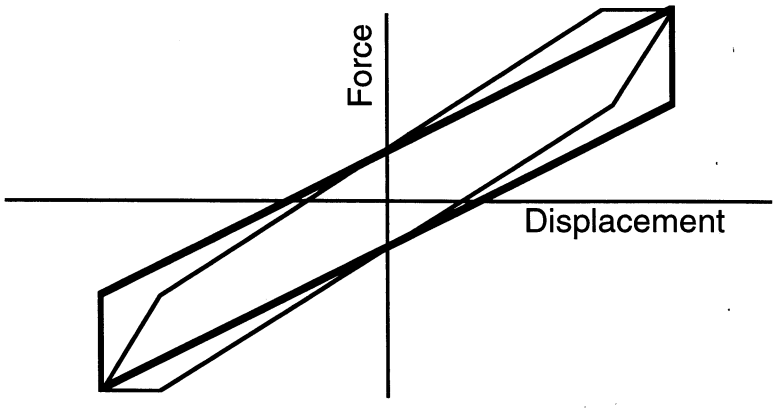


Figure 1. - Nonlinear Systems with the same Equivalent Linear Properties.

The equivalent linearization is justified because the errors in response prediction are believed to be smaller than the uncertainties in the ground motion. Equivalent linear methods are not permitted for systems with over 30% damping, or when the equivalent linear period exceeds 3 seconds. However, systems with more than 30% equivalent damping may be analyzed using linear methods provided that no more than a maximum of 30% damping is used in the computations. The latter may be a relatively attractive option because the difference in response between, say, 30% and 40% damping is relatively small.

Uniform Load Method

The usual goal of an isolation design is the reduction of forces in the structure or its foundations. This can be achieved by using a long-period isolation system, but the cost is large displacements at the isolator interface. These can be relieved to some extent by an increase in damping, but a fundamental linkage remains between forces and displacements, whereby smaller forces mean larger displacements. The designer may choose among different force/displacement combinations to find one that is acceptable. This philosophy differs from that of fixed-base designs, wherein the designer starts with a structure that has essentially unchangeable stiffness properties, and computes the resulting forces and displacements.

It is thus slightly confusing to present the design of the isolation system in terms of a design force, which is the same form as is used for fixed-base designs, namely

$$F = C_s W \tag{1}$$

where

$$C_s = \frac{K_{eff}\, d}{W} \tag{2}$$

since this leads to the self-evident

$$F = K_{eff}\, d \tag{3}$$

where

C_s = Elastic seismic response coefficient.
d = Total deck displacement relative to ground.
F = Statically equivalent seismic force
K_{eff} = Effective linear stiffness of combined isolation and substructure systems.
W = Total vertical load for design of the seismic isolation system.

However the design equations are used in the form of Eqn. 1 in order to maintain consistency with the Standard Specifications. A more useful relationship can be obtained by using the estimated displacement

$$d = \frac{10\ A\ S_i\ T_{eff}}{B} \tag{4}$$

which is an approximation to the true value of

$$d = \frac{g\ A\ S_i\ T_{eff}}{4\ \pi^2 B} \tag{5}$$

where

A = Ground acceleration coefficient.
B = Constant related to damping coefficient
= 1.0 for 5% damping
> 1.0 for > 5% damping
g = acceleration due to gravity
K_{eff} = Effective linear stiffness of combined isolation and substructure systems.
S_i = Soil coefficient
T_{eff} = Effective Period
W = Total vertical load for design of the seismic isolation system.

Since

$$T_{eff} = 2\pi \sqrt{\frac{W}{g\ K_{eff}}} \tag{6}$$

Equations 1-5 can be combined to eliminate T_{eff} and give

$$\frac{F}{W} * d = \left(\frac{g}{4\ \pi^2}\right)\left(\frac{A\ S_i}{B}\right)^2 \tag{7}$$

For a given earthquake input, damping level and soil type, the right hand side of Eqn. 7 is a constant. The left hand side is the base shear coefficient, F/W, multiplied by the maximum displacement, d. Thus the equation shows that the force is inversely proportional to the displacement and a decrease in one must be accompanied by a concomitant increase in the other. In other words, there is no free lunch.

Eqn. 5 is derived from the assumption that the period of the isolation system lies in the constant velocity part of the response spectrum, in which

$$S_a = \frac{g\ A\ S_i}{B\ T} \tag{8}$$

But, for all elastic systems

$$S_d \approx \frac{1}{\omega^2} S_a = \frac{T^2}{4\pi^2} S_a \tag{9}$$

Thus

$$S_d \approx \left(\frac{T^2}{4\pi^2}\right)\left(\frac{g\ A\ S_i}{B\ T}\right) = \frac{g\ A\ S_i\ T}{4\ \pi^2 B} = \frac{9.79 A\ S_i\ T}{B}$$

which is rounded to

$$S_d \approx \frac{10\ A\ S_i\ T}{B} \tag{10}$$

Here, T is taken to be T_{eff}, and S_d is called d in the Guide Specifications, so

$$d \approx \frac{10\ A\ S_i\ T_{eff}}{B} \tag{11}$$

Directionality of response.

In both fixed-base and isolation designs, the primary seismic problems in bridges are assumed to be in the transverse direction. This is so because longitudinal motion is usually inhibited by impacts with, and subsequent resistance of, the abutments. Despite the existence of wording that requires consideration of motion in two orthogonal horizontal directions, the underlying thinking is most readily applied to the transverse motions of right bridges. Combinations, such as SRSS or the AASHTO "30% rule", of independently computed responses to orthogonal input motions are typically not satisfactory if abutment impacts occur, as is the case for a heavily skewed bridge (Maragakis 1989, Bjornson et al. 1998). In these cases, a NLTH analysis is the most realistic option. This issue is one in which further study is warranted.

Acceleration Coefficient.

In order to maintain consistency with AASHTO documents, the acceleration coefficient is to be taken from the maps in the Standard Specifications. The largest value of 0.80g is found in both Southern California and Alaska. The maps, drawn in 1990, are supposedly based on a 10% probability of exceedence in 50 years, which corresponds to a 475 year return period, and is referred to here as the 10/50 event. This single level of seismic input may be acceptable for fixed-base designs, but it presents two problems in seismically isolated structures. They are based on the fact that, for an isolation system to function correctly and to lead to the intended forces and displacements, the clearance around the isolated structure must be large enough and the substructure must not yield. These two conditions must be fulfilled even in the maximum credible event (MCE) which is often taken to be 10% exceedence in 250 years, or a 10/250 event. Isolation designs should therefore be based on this 10/250 event, lest they malfunction at the very time that they are most needed.

Unfortunately the ratio between the 10/50 event and the 10/250 event is not uniform across seismic zones: it lies between approximately 1.05 and 1.5 and between 1.5 and 2.75 in severe and moderate seismic zones respectively. The argument may be expressed in words rather than numbers: in severe seismic regions earthquakes occur so frequently that the largest earthquake to be expected in a 50 year time window is close to the maximum credible event, whereas this is not true of lower seismic zones, in which earthquakes occur much less frequently.

The result is that a 10/250 event cannot be obtained from a 10/50 map by using a single scale factor. However, the maps in the most recent NEHRP

Provisions (NEHRP 1997) represent the latest USGS maps for both 500 and 2400 year return periods (approximately 10/50 and 10/250 events). The NEHRP 2400 year map appears to be close to the AASHTO 475 year map. For this reason the AASHTO 10/50 map was accepted for use in isolation design, although clearly the Guide Specifications must change as more data becomes available and the maps continue to evolve.

Response Modification Factors

In the Standard Specifications, inelastic response is calculated by dividing the elastic forces by a Response Modification Factor (RMF). Different values pertain to different components of the structure, in accordance with their relative ductility capacities and with the difficulty of inspection and post-earthquake repair. Thus the RMF for a foundation is half the RMF for the connecting substructure. This means that the foundations should theoretically be twice as strong as the substructure, and thus should still behave elastically when the substructure has reached its maximum resistance, including all increases due to strain hardening, etc.

In an isolated system, the forces that are calculated using equivalent linear properties will occur during an earthquake. Thus an RMF of 1.0 is appropriate for the isolation system itself. For the substructure and foundations, the Isolation Guide Specifications dictate RMF values of half of those in the Standard Specifications, which range from 2 to 5, but not less than 1.5. The goal is to ensure that the responses of the substructure and foundation remain essentially elastic when the isolation system experiences its maximum force. The resulting RMFs therefore vary from 1.5 to 2.5. This provision is based on the fact that the ductility component of this RMF is approximately 1.0, and the remainder is composed of strength beyond theoretical first yield that is derived from redundancy, material overstrength, strain hardening, etc., that is commonly available in structures.

Variation in isolator properties.

The properties of isolators inevitably vary due to manufacturing differences, aging, wear, temperature, etc. These variations may alter the effective period or damping of the system, either of which will influence the response. Thus the Guide Specifications require that, regardless of the method of analysis used, the analysis be conducted twice, once with the maximum probable properties and then with the minimum probable values. The goal is to obtain safe, or conservative, estimates of both the maximum force and displacement. In general, the maximum force and displacement will be obtained by using the maximum and minimum stiffness respectively.

Values for the probable maximum and minimum properties are needed. Ideally, these would be based on a statistical analysis of the relevant property variations, but in most cases the necessary data is not available at present. Thus estimates are based on the best available data and the judgment of professionals in

the field. The Guide Specification defines the minimum and maximum properties to the nominal one by a series of System Property Modification factors, λ_{max} and λ_{min}. Different λ_{max} values are associated with different aspects of the system, such as wear or temperature, and they are then combined. The same is true for λ_{min}. At present, all of the λ_{min} values are taken as 1.0, because the differences from the nominal properties values are expected to be small enough to make a negligible difference in response. Negligible is defined for these purposes as ± 15%. The λ_{max} values are to be established by system characterization tests that are approved by the Engineer. In the absence of such tests, provisional values are defined in Appendix A. It is expected that individual suppliers will determine whether the benefits to be gained from conducting such tests justify their cost.

The issue of System Modification Factors prompted significant debate within the Committee. On the one hand, the buyer of the system should be protected by ensuring that the system will perform as designed within a reasonable tolerance. On the other, an excess of "conservative" factors could lead to maximum predicted forces and displacements which are both so much larger than the nominal values that isolation may be ruled out as a viable option. A funding source for the extensive testing program needed to generate the necessary data was not immediately apparent.

Minimum stiffness for design.

The Guide Specifications require that isolation system possess a restoring force that exceeds a minimum threshold value. The goal is to ensure a re-centering capability and to avoid the possibility of lateral offsets due to slight errors in leveling. The latter could occur if the bearing is installed slightly out of level. The requirements are expresses in terms of the stiffness of the "spring-like" component of the restoring force, i.e.. excluding friction and viscous forces, but they do not need to be satisfied if a constant restoring force system is used.

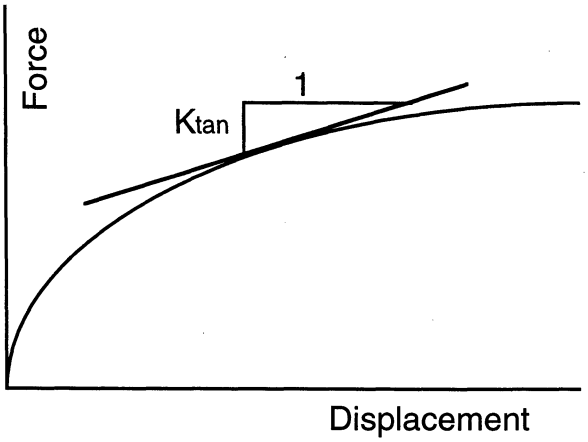


Figure 2. - Tangent stiffness criterion

Two criteria are specified. The first, illustrated in fig. 2, requires that the period associated with the tangent stiffness at any point on the force-deflection curve be less than 6 seconds. In the absence of dissipative forces, this implies a maximum lateral displacement, Δ, due to inaccurate leveling of

$$\Delta = 352\ \theta \text{ inches} \tag{12}$$

where θ = angle of inclination of the bearing. The intention of this first criterion is to avoid systems with a very low stiffness that could lead to large residual displacements. The second criterion, illustrated in fig. 3, is that the restoring force at the design displacement, d_i, be greater than the restoring force at $0.5d_i$ by an amount greater than W/80, where W is the vertical load. This criterion was carried over from the previous Guide Specifications and implies a period of

$$T = 2.02\sqrt{d_i} \tag{13}$$

where d_i is expressed in inches. It controls when d_i>9". Otherwise the first criterion controls.

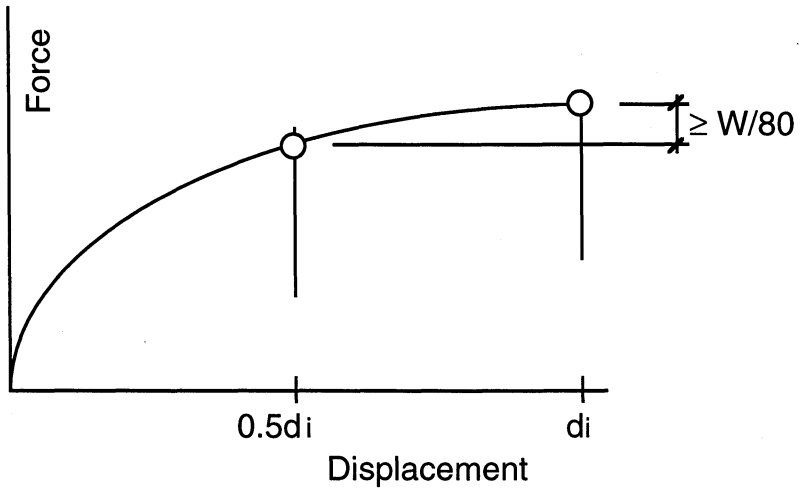


Figure 3. - Secant stiffness criterion.

Test requirements

The Guide Specifications require three types of testing to be conducted, each at a different time. First, System Characterization Tests must be conducted that demonstrate that the system possesses the properties that are used in design. They include such issues as low-temperature performance and wear tests. These tests should be conducted before isolators for a specific job are designed. They are expected to be conducted once for each new type of isolator developed and do not form part of a job-specific quality control program. The objective of these tests is to

ensure a threshold level of confidence in the competence of manufacturers wishing to enter the market.

Prototype Tests are required for every job, unless results from similarly sized isolator units used on a previous job are already available. The purpose is to verify that the principles demonstrated by the System Characterization Tests are valid at the scale and geometry of, and with the precise materials used in, the isolators for the job in question. From the results of these tests the adequacy of the system is determined.

Quality Control Tests are required of every job. Separate test requirements are given for elastomeric and for sliding isolators that reflect the important characteristics of each type. Every bearing must at least pass a short compressive test to 1.5 times maximum dead + live load and must then be tested in combined compressive force plus shear deformation.

DESIGN EXAMPLE - CONCRETE BOX GIRDER BRIDGE

In this section, the design methodology of the new Guide Specification is illustrated by example.

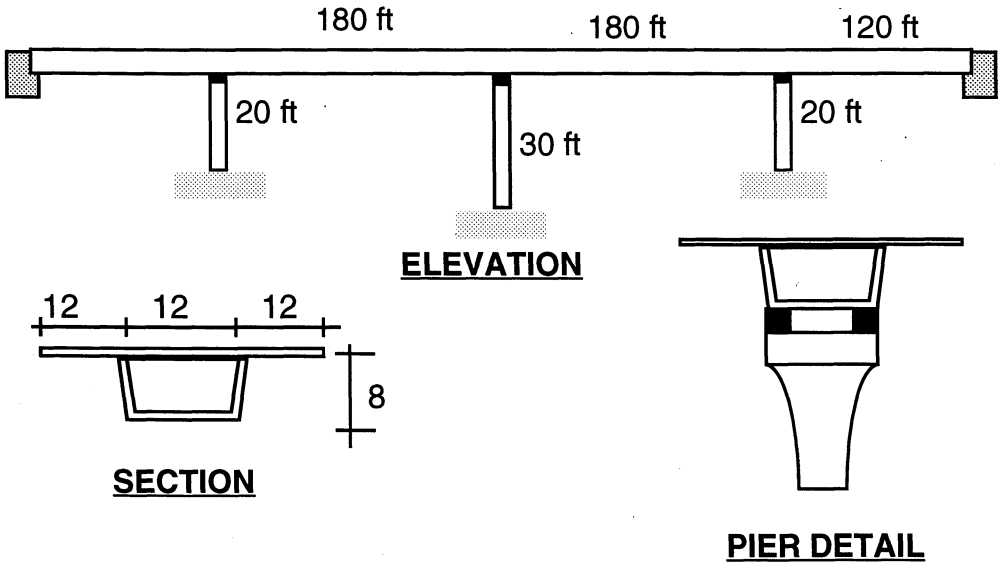


Figure 4. - Box Girder Bridge Geometry

A prestressed concrete box girder bridge carries two lanes over four spans of 120 ft, 180 ft, 180 ft and 120 ft as shown. Expansion joints occur only at the abutments. The piers are single column bents, oval in cross-section and flared at the

top to form a piercap. The structure is in San Diego, California, and the soil profile corresponds to AASHTO profile II.

Use the AASHTO Guide Specification for Seismic Isolation Design to establish a preliminary design for a suitable isolation system.

Data:
A = ground acceleration coefficient for San Diego = 0.4
S_i = site coefficient based on soil profile II = 1.5
Bridge deck weight = 9 kips/ft
Use R = 50% of 3.0 = 1.5 for column design.

Preliminary Design:
Maximum tributary mass occurs at column 3, and is
9 k/ft * 180 ft = 1620 kips.

The Guide Specifications (1997) give the following equations for the "Uniform Load Method", which may be used here as a starting point for the design. More sophisticated analysis may be conducted later.

$$F = C_s W \tag{13}$$

$$C_s = \frac{K_{eff}\, d}{W} \tag{14}$$

$$C_s = \frac{A\, S_i}{T_{eff}\, B} \tag{15}$$

$$d = T_{eff}\, \frac{10\, A\, S_i}{B} \tag{16}$$

$$T_{eff} = 2\pi \sqrt{\frac{W}{K_{eff}\, g}} \tag{17}$$

where
F = seismic force acting on the structure above the isolation interface.
W = weight of the structure above the isolation interface.
K_{eff} = effective stiffness of the isolation system (including column stiffness) at maximum displacement.
T_{eff} = effective period corresponding to K_{eff}.
g = acceleration due to gravity.

Table 1. Possible combinations of force and displacement

Design :	A	B	C	D	E
T_{eff}	0.5	1	2	3	4
d	2	4	8	12	16
F_{max}	1324	662.1	331.0	220.7	165.5

Table 1 shows possible combinations of seismic force and displacement. It was prepared using equations (13) though (17). B was assumed to be 1.5, corresponding to 20% damping. For a first trial bearing, select 8" displacement and a corresponding T_{eff} = 2.0 seconds (Design C in table 1). Assume two bearings per piercap, so each carries 1620/2 = 810 kips.

Elastomeric Bearing Solution.

In elastomeric bearings, the critical characteristic is shear strain in the elastomer. Compression and rotation both cause bulging which leads to shear strain. Shear deformations also lead to shear strain. Shear strains can be calculated as:

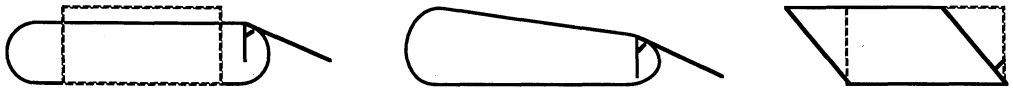


Figure 5. - Shear strains in elastomeric bearings.

$$\gamma_c = \sigma/(GS) \tag{18}$$

$$\gamma_r = \frac{B^2\Theta}{2t_i T_r} \tag{19}$$

$$\gamma_s = d/T_r \tag{20}$$

Where

G = elastomer shear modulus

S = shape factor = $\frac{\text{plan area}}{\text{perimeter area}}$ of an elastomer layer.

B = plan dimension perpendicular to rotation axis

Θ = rotation on bearing (including construction tolerance)

t_i = elastomer layer thickness

T_r = total elastomer thickness = Σt_i.

d= horizontal (i.e. shear) displacement.

The Guide Specifications give two alternate equations for γ_c, which are intended to take into account the compressibility of the rubber. Equation (18) is a simple approximate alternative to both that is adequate for the present purposes.

Relevant AASHTO design criteria for the bearing are:

$\gamma_c < 2.5$ (limits compressive stress) (21)

$\gamma_c + \gamma_{s,eq} + 0.5\gamma_r < 5.5$ (limits total shear strain) (22)

In general a high shape factor (i.e. rubber layers that are thin compared with their plan dimensions) permit carriage of high compression stresses, but induce high strains due to rotation. A shape factor in the range 8-12 is usually a good compromise.

The controlling criteria are:

- K_{eff} must be satisfied
- Shear strain due to compression must be within the AASHTO limit of 2.5. (equation 21).
- Total shear strain in the elastomer must be within the AASHTO limit. (equation 22).
- Shear strain due to shear deformation should be limited to about 2.0 under normal circumstances, and up to approximately 2.75 in extreme circumstances. (This is a practical limit to avoid delamination of the elastomer from the plates. It is not an AASHTO requirement).

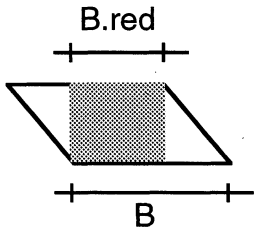


Figure 6. - Reduced area of elastomeric bearings.

When the bearing deforms in shear, the area common to top and bottom plates is reduced and is called the "reduced area". AASHTO is not totally clear whether these "reduced" dimensions should be used for all calculations. Reduced dimensions are assumed here.

Table 2. Possible bearing dimensions.

Bearing Design no:	1	2	3	4
W = width (in)	25	25	25	25
B = length (in)	24.2	26.5	29.6	33.9
n = no. of layers	6.97	6.18	5.43	4.72
t = layer thickness	0.614	0.760	0.966	1.27
T = total rubber thickness	4.29	4.69	5.24	6.00

Table 2 shows dimensions for possible bearings, derived assuming that an appropriate limit is met in all cases and G=100 psi. The most economical solution is probably given by the smallest, most highly stressed bearing. Thus try a bearing that is 25" x 25", which is at the extreme end of the feasible range in the table.

B_{red} = 25 - 8" = 17"
A_{red} = 17 * 25 = 425 in^2
σ = 810 kips/425 in^2 = 1.91 ksi

In order to limit γ_c, try 8 layers of elastomer each 0.5" thick. Then:

$$S = \frac{BL}{2t_i\,(B+L)} = \frac{17 * 25}{2 * 0.5 * (17 + 25)} = 10.1$$

$\gamma_c = \sigma/(GS)$ $=1.91/(0.1\text{ ksi} * 10.1) = 1.88 < 2.5$ OK

$$\gamma_r = \frac{B_{red}^2\Theta}{2t_i\,T_r} = \frac{17^2 * 0.01}{2 * 0.5 * 4.0} = 0.72$$

$\gamma_s = d/T_r$ $= 8"/4" = 2.0$ OK

$\gamma_c + \gamma_{s,eq} + 0.5\gamma_r = 1.88 + 2.0 + 0.5 * 0.72 = 4.24 < 5.5$ OK

The fraction of critical damping is given by

$$\beta = \frac{1}{2\pi}\,\frac{\text{Hysteresis loop area}}{K_{eff}\,d^2}$$

The loop area is

$$\text{Area} = 4Q_d * (d - Q_d/K_u)$$

where

Q_d = yield strength of bearing (taken at zero displacement). It is typically supplied by either a lead plug, high damping rubber characteristics or an external yielding metal device.

K_u = unloading stiffness (assumed infinite here).

In this case, Q_d must be 0.065W, = 52.65 kips, and K_d, the post-yield stiffness, must be 14.1 kips/in, in order to provide 20% damping.

Summary of Elastomeric Bearing:

2 bearings per pier
Bearing size 25"x25", 8 layers of elastomer @ 0.5" thick each
Elastomer: G = 100 psi
Shear device (lead plug or external device), yield force = 56 kips.

Sliding Bearing Solution.

Assume:

Coefficient of friction Teflon-stainless steel = 7% (at earthquake sliding speeds).
Compressive load per bearing = 810 kips as before.

$$Q_d = \mu P = 0.07 * 810 \text{ kips} = 56.7 \text{ kips}$$

An elastic restoring force is needed in addition to the frictional resistance. For a maximum force in each bearing of 165.5 kips (0.5*331 kips from Table 1) at d = 8"

$$F_{tot} = 165.5 \text{ kips} = Q_d + K_d\, d$$

$$K_d = \frac{165.5 - 56.7}{8} = 13.6 \text{ k/in}$$

This may be supplied in a number of ways, such as:

- steel springs with their axes oriented horizontally,
- an elastomeric bearing which carries no axial load but resists shear deformations. (The size will be similar to that calculated above)
- a spherical surface on the stainless steel slider. (The FPS system).

Example: spherical surface:

For a non-dissipative system,

$$R = W/K_d = 810 \text{ kips}/(13.6 \text{ k/in}) = 60"$$

where

W = weight of isolated structure
R = radius of spherical surface

Hysteresis loop area = 4 * (8" * 56.7 kips) = 1814.4 in-kips

$$\text{Damping ratio} = \frac{\text{loop area}}{2\pi\, k_{eff}\, d_i^2} = \frac{1814.4}{2\pi\, (165.5/8)\, 8^2} = 0.22 = 22\%$$

Install to ± 0.005 radians. Then static eccentricity = Rθ = 60"*0.005 = 0.3"
Residual drift after earthquake = μ_{eff} * R = 0.03*60 = 1.8", if μ_{eff} is the effective coefficient of friction that exists after the earthquake.

Summary of sliding bearing solution:

Spherical surface radius = 70"
Displacement capacity = 8"
Friction coefficient = 0.07 at earthquake sliding speeds.

REFERENCES

Guide Specifications for Seismic Isolation Design (1991). AASHTO, Washington DC. 20 pp.

Guide Specifications for Seismic Isolation Design (1995), 2nd edition. AASHTO, Washington DC. 92 pp.

Standard Specifications for Highway Bridges, 16th ed. (1996) AASHTO, Washington DC. 92 pp.

"NEHRP Recommended Provisions for Seismic Regulations for Buildings". FEMA. Washington, DC, 1997.

Bjornsson, S., Eberhard, M.O. and Stanton, J.F. (1997) "Seismic Behavior of Skew Bridges". Report no. SGEM 97-01, Structural and Geotechnical Engineering and Mechanics Program, Department of Civil Engineering, University of Washington, Seattle, WA.

Maragakis, E. (1985) "Model for the Rigid Body Motions of Skew Bridges". PhD Thesis, California Institute of Technology, Pasadena, CA.

APPENDIX A - TASK GROUP MEMBERSHIP

State Agency Representatives:
Mr. James Roberts, CALTRANS. (Chair).
Mr. Roberto Lacalle, CALTRANS. (Working Chair).
Mr. Li-Hong Sheng, CALTRANS. (Co-Chair).
Mr. Ralph Anderson, Illinois DOT.
Mr. Myint Lwin, Washington State DOT.

Industry Representatives:
Mr. Paul Bradford, R.J. Watson Inc.
Dr. Ronald Mayes, Dynamic Isolation Systems.
Dr. Victor Zayas, Earthquake Protection Systems.

University Representatives:
Prof. Michael Constantinou, SUNY Buffalo.
Prof. James Kelly, UC, Berkeley.
Prof. John Stanton, University of Washington.

DEVELOPMENT OF THE EUROPEAN STANDARD ON ANTISEISMIC DEVICES

Agostino Marioni and Renzo Medeot

Abstract

In recent years, the European techno-scientific community has been called upon to make great efforts to draft new building codes: the so called EUROCODES . Each of the latter, has required in turn the drafting of Standards on the design and manufacturing requirements of specific devices such as structural bearings, pre-stressing systems, etc.

Within this framework, Sub-Committee TC 167 – SC 1 – ANTISEISMIC DEVICES was constituted. The scope of this sub-committee is to proceed with the standardization of antiseismic devices for use in structures erected in seismic areas in accordance with EUROCODE 8.

Antiseismic devices include shock-transmitters, isolators, hydraulic dampers, etc. As it is well known, antiseismic devices were developed within the last two decades; above all, in relation to the dissemination of the "Seismic Isolation" concept, but they have found valid employment in other seismic strategies.

The paper illustrates the structure of the European Standard, the criteria adopted in its drafting, the procedures to follow for its approval, and some of the aspects which render this document innovative.

1. Introduction

An increasing number of congresses and symposia as well as other professional meetings give testimony to the significant strides made by seismic engineering during the last quarter century. Progress, has mainly been the result of newly developed design strategies taking hold (e.g. base isolation) and the awareness that energy dissipation can be a useful tool in the hands of the design engineer to control the response of structures struck by an earthquake. In other words, earthquakes are being increasingly perceived as phenomena involving the transimssion of mechanical energy instead of being interpreted only in terms of resulting forces.

Notwithstanding, the newly conceived design strategies (the software) could not have found useful application without a parallel development of mechanical devices (the hardware) needed for their implementation.

Thus, many research laboratories and certain pioneering industries have decided to invest important resources in this field, inventing and improving a series of devices that exploit well known physical phenomena for the seismic protection of structures.

As it is often the case when technological growth in a given field reaches important levels of development as well as a reasonable degree of maturity, a need spontaneously arises to establish

ground rules that define principles of general validity. Said rules ultimately come to nest in documents of increasing importance like recommendations, guidelines and standards.

Within the spirit of the above, in March, 1992, the Italian Standardization Institute (UNI) forwarded to the European Committee on Standardization (CEN) a formal request calling for the creation of a Technical Committee charged with drafting a norm to cover antiseismic hardware. In order to facilitate and accelerate the decision-making process, the request called for the formation of a Technical Sub-committee within the existing Technical Committee TC-167 tasked with drafting the European Standard on Structural Bearings.

Within the framwork of existing procedures, CEN launched an inquiry among the member nations with a July, 1992 deadline. Fourteen of them responded to the inquiry with 11 votes in favour and 3 against. In September 1992, the Bureau Technique Secteur 1 (BTS1) as the competent body in construction within CEN, responded favorably to the UNI request upon examination of the inquiry results.

After having paid due bureaucratic tribute, and appointed the experts panel from the countries interested in the drafting of the Standard, the first meeting of the officially nominated CEN7TC167-SC1 finally convened in Vienna in October, 1993. This occasion saw the creation of a work program with fixed target dates, the election of a Chairman, the Secretary and the installation of six Working Groups, each with an appointed "Convener".

2. The Developing Process Of European Standards

CEN is the European organisation authorised to issue EN Norms. It embraces 18 EC and EFTA countries whose voting power is illustrated in table 1. Each member country participates in CEN activities through its national standard agencies (UNI for Italy, DIN for Germany. etc.).

CEN appoints Technical Committees (TC's) for the development of the standards (the TC 167 is one of them) and each nation has the right to send three delegates to the TC. The TC in turn can set up special subcommittees (SC) and working groups (WG) that may call experts for the preparation of the standards.

The necessary steps to reach an approved and in force European norm (EN) are the following:

1. The WG's prepare drafts of the standard or standard parts
2. The TC revise the drafts and, when completed approves them by simple majority of the nations represented at the meeting. The approval process is not so easy and quick for the following main reasons:
   - Each TC meeting require 20 to 30 people of different European country to meet. The meetings and the agenda shall be announced well in advance (two months notice) and all the papers to be discussed shall be distributed at least 30 days before. Therefore it is practically impossible to do more than one or two meetings per year.
   - Generally every nation tries to include in the standard products locally manufactured and in some case there are conflicts of scientific knowledge or approach and even conflicts of interests.

- All the documents prepared by the WG shall be revised in order to check the harmonisation of the various parts of the standard and to verify the fulfilment of the CEN rules for the drafting and presentation of European Standards (PNE-Rules).
- Last but not least all the work performed by the TC delegates and experts is made on a voluntary base and therefore sometimes not very quickly. Only the secretariat task, performed by UNI is financed partly by the Italian association of bearings manufacturers ACEDIS and partly by CEN funds

3. Generally the documents are approved in English. Once approved they shall be translated into the two other official languages (the 3 official languages are: English, French and German). The official translations are performed by the national standard organisations (respectively BSI, AFNOR and DIN)
4. The documents in the three official languages are sent to the 18 CEN nations for the Public Enquiry. The nations have got 6 months to call the internal commission and to submit comments to the TC
5. The TC, directly or through its working groups shall examine and answer to all comments received and redraft the standard incorporating all the accepted comments. Then the standard shall be approved again by the TC.
6. The documents are sent again for the official translation and distributed to all nations
7. Formal vote is made by weighted votes according to table 1
8. After positive voting the EN shall be implemented in all CEN nations
   - by giving the status of a national standard, either by publication of an identical text or by endorsement and
   - by withdrawing any conflicting national standards

In year 1994 TC 167 set up a special sub-committee called SC1. SC 1 is presided by Dr. Ing. Renzo Medeot and was established in order to develop a standard on Antiseismic Devices. These include all kinds of structural devices utilised for the protection of structures like bridges, civil buildings, industrial buildings and plants from the damaging effects of earthquakes. Also the new created SC 1 has an internal structure subdivided in WG's for the draft of the various parts of the standard but on its activity will more exhaustively refer Dr. Medeot himself.

The updated structure of TC 167 and SC1 with the convenors and tasks of all working groups is given in table 2.

3. General Criteria For A Good Standard

A Standard, given its nature, is in principle a document that limits user's freedom (i.e. manufacturers design engineers, etc.) and favours the present to detriment of future. However, in order to be a good Standard, it cannot impair technological progress within its area of applicability by favouring what is in existence over what might be developed in the future. So as to avoid such an eventuality, CEN established few rules. The three most important of these rules are:

a) Requirements should be expressed in terms of performance as much as possible;
b) Only those characteristics which can be verified by a given method shall be included in the Standard; and

c) The Standard must represent an objective state-of-the-art and thus must not exclude any system whose validity has been proven through successful application.

Point (a) above regards a long held controversy as to whether it might be possible to draft a Standard that can be purely performance oriented. Unfortunately, the answer has to be negative. Nonetheless, it is always possible to find an equitable compromise between "product oriented" and "performance oriented" requirements that can result in full observance of criteria (b) and (c). The application of the above cited criteria favours progress in as much as it promotes loyall competition through clear and fair rules that protect the interest of the community.

For some types of devices, certain classes (or level) of performance are specified, especially in terms of the tolerances applicable to the most important parameters.

4. Structure Of The Standard On Antiseismic Devices

Before defining the structure of the Standard, in the same manner as other scientific fields (e:g: Biology) there was an attempt to create a "systematic" of present seismic hardware, that is to say, to group existing devices on the basis of the functions they perform, the common principles governing their functioning, the types of materials used, etc. Thus, the starting point was the creation of divisions of a general character and then moving toward increasingly detailed subdivisions.

The first division has been set between those systems only capable of transmitting horizontal forces to those capable of transmitting vertical loads as well. The latter are usually referred to as isolators whereas the former are simply called seismic devices.

Both isolators and seismic devices, have then been subdivided into four groups on the basis of the functions performed and the principles governing their functioning. In the case of seisnmic devices, said groups are, in order of increasing dissipating capacity:

1. Rigid Connection Devices
2. Linear Devices
3. Non-Linear Devices
4. Viscous Devices (Dampers)

Rigid Connection Devices have then been subdivided into:

- Sacrificial Restraints (i.e. devices which are rigid under service loads and fail at the occurrence of an earthquake)
- Shock-transmitters (i.e. devices which accommodate slow movements without appreciable resistance and become rigid at the occurrence of an earthquake)

The subdivisions within the other groups have followed the same fashion. It is interesting to note the criteria selected to distinguish linear devices from Non-linear Devices, that also represents a case of harmonization with EC8.

In order to understand what follows, one must remember that, in Europe, as an alternative to isolators, seismic devices (obviously to the exclusion of rigid devices) are used in conjunction to traditional free moving bearings to create "isolating systems". For a deeper understanding of the subject, refer to reference [1].

Now, returning to the distinction between Linear and Non-linear Devices, *Eurocode 8* has furnished a decisive contribution inasmuch as it lists a series of criteria (Part 2, § 7.3.3) to be fulfilled in order to conduct multimodal response spectrum analysis (sometimes referred to as multimodal linear analysis) and more precisely:

b.1. The effective stiffness of the isolating system at the design displacement (d_d) is at least 50% of the effective stiffness at 0.2 d_d.

b.2. The effective damping of the isolation system does not exceed 10%.

b.3. The force-displacement characteristics of the isolation system are not strongly dependent of the rate of loading and of the vertical and bi-directional load.

b.4. The isolation system produces a restoring force such that its increase between 0.5 d_d and d_d is at least 0.025 of the total gravity load above the isolators.

The same criteria have been adopted to define Linear Devices. Thus, linear devices become the hardware typically used in structures designed and verified by linear analysis. Such a choice is a good example of coordination between the Standard and the Eurocode.

Much attention has been focused on the definition of the various types of devices. In effect, the CEN rules require that "the definitions shall be unambiguous and as concise as possible".

As an example, examine the following:

> "Viscous devices are those devices whose reaction does not depend on the amount of displacement incurred, but rather, depends on the rate of its application according to the following equation:
>
> $$F = C \times v^n$$
>
> Sometimes referred to as constitutive law."

In the above equation, v is the velocity, and n varies from 0 to 2, depending on the type of device.

The structure of the *European Standard on Antiseismic Devices* has been modified several times and in its definitive version is articulated in six Parts, to wit:

Part 1 General Design Rules and Requirements
Part 2 Rigid Connection Devices
Part 3 Linear Devices

Part 4 Non-linear Devices
Part 5 Viscous Devices (or Dampers)
Part 6 Isolators

In other words, evaluation of conformity is seen as a purely technical matter closely linked with a specific product and the way it is produced which can be standardized for the benefit of comparability.

The clause on evaluation of conformity develops criteria for type-testing, production control and tests to be conducted. It clearly distinguishes between:

- initial product testing
- tests to be conducted by the first party (manufacturer) as a part of production control at the factory
- tests conducted by second or third parties, if any, to confirm ongoing conformity (surveillance tests).

It should be noted that, in addition to the above, individual Parts also contain clauses governing the testing of various types of devices (i.e. test methods, equipment and procedures) as well as conformity evaluation criteria geared to the specific type of device.

Each Part comprises several clauses, Sub-clauses, etc. It is of interest to analyse the Clauses in Part 1; that is, those that concern subjects of general validity:

1) Scope
2) Normative References
3) Symbols, Definitions and Abbreviations
4) General Design Rules
5) Use of Structural Bearings in Seismic Areas
6) Combination of Antiseismic Devices
7) Functional Requirements
8) Protection
9) Evaluation of Conformity
10) Marking and Labeling
11) Transport, Storage and Installation
12) Maintenance and Replacement

Some comments on the more important clauses:

Scope: This is a required clause at the beginning of every CEN Standard to define its subject as well as the aspects in unambiguously and thereby indicate the limits of its applicability. In our case, this clause is as follows:

"This European Standard deals with the design and manufacturing requirements for antiseismic devices used in structures in seismic areas in accordance with the EC 8".

General Design Rules: Earthquakes are random phenomena and consequent uncertainties and unexpected behaviour are mitigated through the adoption of precautionary measures in the design stage.

Ultimate and *Serviceability Limit States* are specified in the design of seismic devices (this rule is common to all European Standards).

Use of Structural Bearings in Seismic Areas: The *European Standard on Structural Bearings* does not cover their use under dynamic actions. The *Standard on Antiseismic Devices* covers this gap through the provision of certain important requirements to be met (*e.g.*, the increase in coefficient of friction for sliding bearings).

Combination of Antiseismic Devices: Combining pre-existing devices generates "hybrids" that, may show interesting new characteristics. However, something quite to the contrary could also occur. Thus, general rules are furnished to avoid any such eventuality.

Evaluation of Conformity: This clause is not to be confused with "attestation of conformity". The difference between the two is explained as follows:

"**evaluation**" is the answer to the question: "*How can conformity be ensured*?"

whereas,

"**attestation**" is the answer to the question: "*Who is going to certify conformity, and under what prerequisites and conditions*?"

As it may be appreciated from the above, in addition to bureaucratic "red-tape", "technological democracy" also exacts its "pound-of-flesh" but, in exchange, it affords fair treatment and equal opportunity to all.

5. Conclusions

The long period of time allocated by the Work Program for the completion of the European Standard on Antiseismic Devices is justified not only by the observance of procedures and regulations established by CEN, but also by the vast entity of the material treated as well as the fact that important processes of development are presently in progress.

In effect, the Standard aims to cover all manner of Seismic Hardware in existence and leave a door open to future progress. This principally derives from the fact that the Standard is highly performance-oriented and this feature also constitutes per se a guarantee of equity between the various systems that may be used as alternatives.

The wealth represented by alternative systems available ensures a freedom of choice to the design engineer insofar as the design strategy deemed most appropriate.

This freedom of choice is further amplified by the fact that several classes (or levels) of performance have been defined for each type of device. As a matter of principle, the existence of classes of performance also offers a great advantage, that of being able to optimize a project from a standpoint of economy.

In addition to the Information Annexes which usually accompany the various Parts of this Standard, in order to give useful comments and explanations to the reader, the members of the Technical Committee are pledged to draft a Guideline, or better yet, a sort of "User's Handbook" with further suggestions and selection criteria.

This presentation of the *European Standard on Antiseismic Devices* has also given this author an opportunity to illustrate the procedures adopted in Europe to draft and approve norms.

CEN has established very stringent rules regarding the structure and contents of a Standard as well how it is presented. However, this set of rules is far from being a handicap. In fact, it actually constitutes a most useful tool that facilitates the work of those who endeavor to draft a Standard.

This author, in his capacity as Chairman, desires to express his appreciation to all the expert members of TC 167-SC1 for the work performed to date as well as the contributions they will be called upon to provide before final approval of the Standard.

7. References

Marioni, A. - The European Standard for Structural Bearings, *Fourth World Congress on Joints and Bearings*, Sacramento, CA – Sept. 1996

Medeot, R. - The European Approach to Seismic Isolation of Bridges, *Fourth World Congress on Joints and Bearings*, Sacramento, CA – Sept. 1996

TABLE 1 - The CEN Members And Their Voting Power

Member country	Weighting	Member country	Weighting
France	10	Switzerland	5
Germany	10		
Italy	10	Austria	4
United Kingdom	10	Sweden	4
Spain	8	Denmark	3
		Finland	3
Belgium	5	Ireland	3
Greece	5	Norway	3
Netherlands	5	Czechia	3
Portugal	5	Luxembourg	2
		Iceland	1

TABLE 2 - CEN TC 167 Structure

CEN TC 167 – Structural bearings	Chairman : A. Marioni (I)

CEN TC 167/SC1 – Antiseismic Devices	Chairman : R. Medeot (I)

• WG 11	Parts 1,7	Convenor: C. Nuti (I)
• WG 12	Parts 2,6	Convenor: G. Wolff (A)
• WG 13	Parts 3,4 (viscous dampers)	Convenor: K. Reinsch (D)
• WG 14	Part 4 (metal springs)	Convenor: K. Reinsch (D)
• WG 15	Part 4 (elastomeric springs) Part 6 (elastomeric bearings)	Convenor: C. Coladant (F)
• WG 16	Part 5,4 (non linear devices)	Convenor: M. Dolce (I)

CALTRANS BRIDGE RESEARCH AND APPLICATIONS OF NEW TECHNOLOGIES

By
Dorie Mellon, P.E.
California Department of Transportation
Office of Structure Design
and
Thomas Post, P.E., J.D.
California Department of Transportation
Office of Earthquake Engineering

ABSTRACT

Since the first application of isolation technology by Caltrans on the Sierra Point Overhead Bridge in 1985, the State of California has exercised limited use of new technologies such as seismic isolation and energy dissipation in bridge applications. However, in recent years, the unusual and complex design issues presented by the California Toll Bridge Retrofit Program have produced several large scale retrofit projects employing isolation, damping, and lock-up devices. These existing and proposed applications as well as related research, including the Seismic Response Modification Device (SRMD) Testing Program at the University of California, San Diego and the "Caltrans/FHWA Testing at ETEC", will be presented. In addition to the above mentioned technologies, this paper will cover Caltrans' research and trial installations of alternative column casing such as composites and wire wrap for bridge column retrofit.

INTRODUCTION

Over the past several years, Caltrans has sought to improve the seismic performance of its bridges. While the major effort in this area has been the improvement of structural details to provide more ductile behavior, new systems and materials have also be used. The use of new, non-traditional systems and materials has increased, along with their acceptance in California as cost-effective and less intrusive alternatives for certain types of projects.

Isolation systems, damping systems and advanced composite materials have been either used or will be used in seismic retrofit projects on California highway bridges. While the first projects to use these systems were done to experiment with the applicability of the systems to bridge retrofit, subsequent use of these systems arose because in some cases, the more common retrofitting methods were either much more expensive or because they were too intrusive, as in the case of retrofitting of historical structures, where adding steel jacketing or replacing superstructure elements is undesirable from an aesthetic or historical perspective. Additionally, isolators and dampers can be used to tune the response of the structure in ways traditional retrofits cannot.

Acceptance of these systems has been promoted by extensive testing programs organized by manufacturers, researchers and government which have not only utilized laboratory testing but also field demonstrations. Also, on the case of isolation systems, some field installations have experienced earthquake loadings.

BACKGROUND

The 1971 Sylmar Earthquake in Southern California was the watershed event for seismic design of highway bridges in the United States. Prior to that event, seismic loadings were dealt with by assuming they were a lateral load equivalent to a percentage of the dead load. Sylmar indicated that the loadings can be substantially higher and that improved structural details were needed not only for added strength but also to provide increased ductility.

The typical highway structure in today's California inventory consists mainly of concrete box girder structures as it did also in the 1970's. The increased efforts in developing better analytical tools as well as improved reinforcing details which rose out of the Sylmar Earthquake have led to more reliable structures being built. However, there was also a need to improve the existing structures and raise their resistance to seismic damage. Thus began a retrofit program to enhance the seismic survivability of highway structures.

The first phase targeted superstructure hinges. Prior to 1971, the typical California highway bridge hinge did not have the resisting elements needed to keep large earthquake displacements from unseating the supported span and leading to a collapse mechanism. Therefore, the retrofit program for hinges was to add steel restrainer cables inside the cells of the box girders or on either side of the girder webs in the case of steel girder structures.

The second phase of the retrofit program involved improving the performance of the substructure elements, mainly the columns and foundations. Typically, the retrofit for a concrete column is to place a steel casing around the outside of column, as the column reinforcement details prior to 1971 provided little in the way of ductility. The main reinforcing bars were tied together with #4 bars at a spacing of 12 inches. While this did provide some shear resistance and confinement for the column, its primary intent was to facilitate the hoisting of the column cage into place. It certainly did not give the ductile behavior associated with a continuous spiral of rebar placed around the main bars.

Additionally, the main column bars typically were not continuous into the footing. Starter bars extended out of the footing to which the main column bars were then lap spliced. This lap splice, combined with little confinement capacity would lead to the pulling apart of the lap splice during severe shaking. In the case of bridges with only a single column in each bent, the formation of a hinge at the columns base could lead to collapse.

The steel casing helps to provide the confinement and shear capacity lacking in the pre-1971 columns. Based primarily on research originated in New Zealand, the steel casing acts as a pressure vessel and confines the column during the violent shaking from an earthquake. Thus, the load carrying capacity of the column is maintained and a collapse is avoided. The casing is typically composed of two steel plate shells placed around the column and the welded together.

The foundations would also require retrofitting as they had been designed for gravity loads and not for the uplift potential associated with seismic loadings. In those footings deficiencies include a lack of reinforcing steel at the top of the footing and very light reinforcement in the piles. Therefore, additional piles would typically be placed around the perimeter of the existing footing and a top mat of reinforcement placed atop the existing footing with new concrete cast over the new elements.

Composite materials have been used as an alternative to steel plate casings while isolation and damping systems approach the seismic retrofit issue from a different perspective than the more typical retrofit described above. Rather than modifying the structure to withstand full seismic loading, isolation and

damping systems seek to remove seismic energy from the system and reduce the demands on the existing structural elements.

EARLY ISOLATION PROJECTS (1985-1994)

The first Caltrans application of isolation technology was the seismic retrofit of the Sierra Point Bridge in 1985. Lead-rubber bearings were placed at the top of the piers to reduce shear transfer from the superstructure. This retrofit prevented the need to modify the old piers. Isolation as a seismic retrofit strategy for bridges was brand new to California. As a result, Caltrans considered this project experimental. Two more structures were retrofitted in the same manner in 1987 (the Eel River Bridge) and in 1988 (the All American Canal Bridge). These projects (see table 1) were developed with a specific bearing type and manufacturer in mind. Due to the novelty of these designs, engineers at Caltrans used design software provided by the bearing vendor and also relied on the vendor for assistance in developing the contract specifications. Since these retrofit contracts had an experimental designation, the isolation bearings were a proprietary "sole source" bid item. As a result, the plans and specifications were developed without extensive detail on the isolation items.

Table 1
Caltrans owned bridges with isolation and damping applications (non-toll structures)

Bridge Name	Bridge Number	Year of Installation	Type of Project	Type of Device	Approx. Load (kips)	Approx Displacement (inches)
Sierra Point	35-0130	1985	retrofit	LRB	INA	+/- 7
Eel River	4-16R/L	1987	retrofit	LRB	INA	+/- 10
All American Canal	58-0195R/L	1988	retrofit	LRB	INA	+/- 13
Temporary Viaduct/Olympic Blvd OC	28-TEMP 28-312K	1993 1999*	new	LRB	DL+LL 800	+/- 9
Alemany Interchange	37-0070	1994	retrofit	LRB	DL+LL 300	+/- 11
Rte 242/I-680 Separation	28-0040F	1994	retrofit	LRB	DL 400	+/- 11
Bayshore Blvd	34-0103	1994	retrofit	LRB	DL+LL 480	+/- 7
3 Mile Slough*	24-0121	1998*	retrofit	LRB	DL+LL 620	+/- 14
Rio Vista*	23-0024	2000*	retrofit	LRB Viscous Dampers	DL+LL 740 154	+/- 18 10 total stroke
Rio Hondo	53-2637	1997	retrofit	FPS	DL+LL 1400	+/- 12
91/5 HOV Conn. Sep.*	55-0833F	1998*	new	Viscous Dampers	250	16 total stroke

LRB = lead-core rubber isolation bearing
FPS = Friction Pendulum System
INA= information not available
*= project still in bid or construction phase

The first test of isolation as a retrofit strategy occurred during the Petrolia earthquake of April 25-26, 1992. The Eel River Bridge which was located 14 miles from the epicenter, experienced significant movement with limited spalling (as expected) at the joints. This performance demonstrated the validity of base isolation as "a solution for older, hard to repair piers". [1]

The next series of isolation projects came 5 to 6 years later with the isolation of a new structure in 1993 (Temporary Viaduct) and the seismic retrofit of three existing bridges in 1994 (Alemany Interchange, Rte 242/I-680 Separation, and Bayshore Blvd), (see table 1). The isolation of 4 spans of the Temporary Viaduct in the 680/24 interchange in Walnut Creek was the first application of isolation technology to a new structure. Bearings which were installed in the temporary structure will be reused when the 4 isolated spans of the Temporary Viaduct are relocated to create the 4 span isolated permanent structure of the Olympic Boulevard Overcrossing. On this job the emphasis shifted from protecting a vulnerable substructure in an older bridge to cost savings in building a smaller substructure due to reduced seismic shear forces in a new structure. The Walnut Creek project was also unique in that it was the first Caltrans isolation design which allowed for competition in the selection of the bearing manufacturer. The first bearings chosen by the bridge contractor to be installed in the Temporary Viaduct were not familiar to Caltrans (in fact they had never been built). As it turned out, these bearings required an exhaustive and time demanding process of reviewing several submittals of working drawings and calculations. The bearings were unable to meet the performance criteria set forth in the plans and specifications and, ultimately, the bearings were rejected. Upon rejection of the original bearings another bearing manufacturer was brought in to provide the isolators, and the project was allowed to continue on schedule.

CHANGES IN DESIGN AND TESTING METHODS

In the mid 1990's, the California bridge design community saw a sharp rise in the number of isolation bearings types and manufacturers. Isolation options now included lead rubber bearings, high damping rubber bearings, flat and spherical sliding bearings, and roller bearings. In addition, energy dissipation devices in the form of viscous and friction dampers and elasto-plastic devices were being introduced as individual elements or as part of the isolation device. The supporting device information that vendors brought to Caltrans was highly diverse. At one end of the spectrum a manufacturer would present testing results from respected institutions, lists of prior applications, supporting calculations, and suggested design methods. On the other end of the spectrum, a salesman would come in with nothing more than an "isolation concept" which had yet to be built. The common thread to this information was that it came from the manufacturers themselves and therefore, must be considered bias.

In order to use isolation in their designs, bridge engineers needed to have access to design methods and performance data that was independent of vendors. The isolation bearing selection process in the Temporary Viaduct project, as well as other isolation projects, called attention to the need of developing a more comprehensive specification that would allow for competition among bearing manufacturers while ensuring the quality and intent of the design. Changes were needed in two areas; design and specifications. These changes began to occur in 1994 and 1995 when committees were formed for the Caltrans/FHWA testing program at ETEC and the T3-AASHTO Isolation Guide Specification task force, respectively.

CALTRANS/FHWA TESTING AT ETEC

The creation of the Caltrans/FHWA Testing at ETEC (Energy Technology Engineer Center) was an attempt to allow a design engineer to take advantage of the attractive technology of isolation and energy dissipation by using unbiased data. The three major objectives of the Caltrans/FHWA testing at ETEC are as follows:

> "1. Implement a program of testing, focusing on full scale dynamic tests, sufficient to characterize the fundamental properties and performance characteristics of the devices evaluated.
> 2. Provide guidance regarding the selection, design and use of seismic isolation and energy dissipating devices for different levels of performance.
> 3. Feed the development of suggested guide specifications for the use of isolation and energy dissipating devices in new bridge construction projects and retrofit applications." [2]

While the results of this testing program have yet to be released, it is apparent that while the devices showed generally good performance, manufacturers are not able to accurately predict the performance of their products. This point emphasizes the need for thorough testing of a device prior to its installation in a structure.

1997 AASHTO GUIDE SPECIFICATION FOR SEISMIC ISOLATION

The 1991 AASHTO Guide Specification for Seismic Isolation covered elastomeric bearings to a limited degree and was of little assistance to a designer faced with the many bearing options of the mid nineties. In 1995 the AASHTO Subcommittee on Bridges and Structures formed a new Technical Committee, T-3 Seismic Design, chaired by James Roberts (Caltrans' Chief Bridge Engineer). This committee was charged with assisting in the development of a comprehensive Guide Specification for Design of Seismic Isolation Bearings. A task force made up of representatives of state bridge engineers, the FHWA, the isolation industry, and academia was created to develop an unbiased specification for Seismic Isolation Bearings. The 1997 AASHTO Guide Specification for Seismic Isolation was adopted in the fall ballot of 1997 and printing of this document is anticipated for the fall of 1998.[3] This guide specification covers a variety of isolation systems including those with additional damping elements. Topics covered include isolation design, materials, manufacturing methods, testing, and adjustment factors for the aging of bearings.

PROTECTIVE SYSTEMS RESEARCH PROJECT AT UCB

Another source of independent data on isolation and damping was proposed by the Earthquake Engineering Research Center (EERC) of the University of California, Berkeley in 1994. The proposal was for a research project which would provide information on the subject of isolation and damping pertinent to the bridges of California. This proposal, the Caltrans-EERC Research Program in Seismic Protective Systems, was approved by Caltrans in 1995, but due to administrative and funding delays is just now in full swing. This program, which involves both isolation bearings and dampers, will test devices individually and as a system.

Bearings of high damping rubber, sliding, and lead core-rubber types will be tested under bi-directional controlled displacement. Measured responses of these isolators will be compared to mathematical models to determine which model(s) offer the best correlation. Some older elastomeric bearings will be tested to investigate change in properties due to aging.

Energy dissipation devices being tested may include viscous, friction, and lead extrusion dampers. These devices will be tested individually in a testing apparatus developed for the Golden Gate Bridge retrofit

project. If analysis indicates favorable performance, the dampers will be added to an isolated structure for shake table testing of hybrid systems.

Other areas of investigation include isolation of flexible structures and response of an isolated structure subject to deck-abutment impact. Ground motions for the shake table tests have been specifically for this project.

Another interesting product of this research program is a database of isolation and energy dissipation systems (entitled PROSYS) which includes key applications and research. The database is available, in its unfinished form, on the World Wide Web at http://www.eerc.berkeley.edu/prosys.html.

It is anticipated that the results of this research will contribute in the areas of education, appropriate application, design, and specification development for projects utilizing seismic protective systems.

TOLL BRIDGE RETROFIT PROGRAM

After the Loma Prieta earthquake of 1989, Caltrans was directed to commence with the retrofit design contracts for several California toll structures [4]. By the mid 1990's the retrofit strategies for these structures were being finalized. These bridges presented some unique challenges to the design engineer which precluded many traditional retrofit strategies. The Loma Prieta and Northridge earthquakes had resulted in much higher input ground motions. Performance criteria after retrofit had changed from a "no-collapse" to "open to traffic almost immediately after a major event". These heavily traveled bridges were required to stay open with minimal lane closures during construction and their historic significance prevented designs which significantly altered their appearance. Early analysis showed that due to the method and materials of original construction and age of these structures, up to 90% of superstructure members required retrofit. The associated cost was astounding. With conventional methods of retrofit exhausted, the toll bridges brought an entirely new level of attention to isolation and damping technologies.

Upon closer investigation (using the software product ADINA), it was determined that isolation and damping technologies could effectively address some of the demanding design criteria of the toll structures while providing a significant cost savings over conventional retrofit methods. In the case of the retrofit of the east spans of the San Francisco-Oakland Bay Bridge, the number of superstructure members requiring retrofit dropped from 90 to 15 percent. However, utilizing these technologies in unique structures with such demanding design conditions came at a price. Previous applications had been limited to structures with relatively stiff piers in favorable soil conditions. Isolation bearings were designed with periods below 3 seconds and displacement was limited to under 12 inches and shear strains were around 100%. In addition, the heaviest load to be placed on a single bearing on a state owned project was 800 kips. The retrofit strategies of the east spans of the San Francisco-Oakland Bay Bridge (now slated for demolition and replacement), the Benicia-Martinez Bridge, the Coronado and other toll bridges called for unprecedented performance by isolation and damping devices (see Table 2). These designs called for isolator loads up to 12,000 kips with total displacements capacities of up to 98 inches. Design periods for some isolators were well in excess of 3 seconds and shear strains in elastomeric bearings exceed 200%. Performance requirements for viscous dampers on these projects went a high as 84 inches of total stroke and 450 kips in axial load.

Table 2
Caltrans owned toll-bridges with isolation, damping and lock-up device applications

Bridge Name	Type of Device	approx. max. load (kips)	design displacement (inches)
Benicia-Martinez	Friction Pendulum Bearing	5100	+/- 49
Coronado*	Elastomeric Bearing Viscous Dampers	2300 400	+/- 27 20 total stroke
West Spans of the SFOBB	Uni-directional FPS bearings Viscous Dampers	4500 450	+/- 18 36 total stroke
Vincent Thomas	Viscous Dampers	200	52 total stroke
Richmond-San Rafael	Elastomeric Bearings Viscous Dampers	2200 225	+/- 30 84 total stroke
Carquinez	Lock-up Devices	3500	12 total stroke

SFOBB = San Francisco-Oakland Bay Bridge * Proposed application, design still in progress

FULL SCALE INDIVIDUAL BEARING AND DAMPER TESTING

The unprecedented performance criteria of these proposed devices immediately raised questions of feasibility, longevity and wear, prototype and production testing, and the ability to characterize the performance of these devices as part of the seismic response of the retrofit bridge. Lively debate ensued amongst Caltrans engineers, design consultants, the Toll Bridge Peer Review Panel, the Seismic Advisory Board, and academia. It was decided that the proposed applications of these devices would be acceptable, but only on the condition that adequate testing was conducted on full scale specimens. In addition, future testing of aged bearings was required to monitor the change of properties over time. Since a testing apparatus capable of testing the toll bridge devices did not exist, Caltrans embarked on the development of a dedicated testing facility, with a testing program, to support the design and application of isolators and dampers in the Toll Bridge Retrofit Program. [5]

The testing program developed is divided into three phases. Phase 1 testing addresses performance characterization of full sized specimens at slow speeds, a uni-directional displacement path, and static axial loading. This testing includes testing similar to the prototype testing called for in the AASHTO guide specification and a 10,000 cycle wear test. Phase 2 testing will investigate performance characterization of full scale specimens at real time and displacement histories. The tests in this phase will include 6 degrees of freedom (displacement and rotational), high velocities, sinusoidal and time history input. Phase 3 testing deals with the elusive issue of longevity. Since longevity of a device is of paramount importance to the actual design application, isolation and damping devices from toll structures will be removed and tested every 5-10 years. The full-scale 6 degree of freedom dynamic testing apparatus and supporting facility (entitled the "Seismic Response Modification Device Test System) for this testing program is currently under construction at the Powell Structural Research Laboratories on the University of California, San Diego campus. The first specimens to be tested there are the prototype isolation bearings for the retrofit of the Benicia-Martinez toll bridge. Six Friction Pendulum bearings are currently being manufactured by Earthquake Protection Systems, Inc. and are scheduled for prototype testing in San Diego in the fall of 1998. The largest of these bearings are 151 inches across, 22 inches high, and weighs 50,000

pounds. The maximum design load is approximately 5000 kips and the maximum required displacement is plus or minus 53.5 inches. After completion of prototype and production testing, two of the Benicia-Martinez prototype bearings will undergo dynamic characterization in Phase 2 testing. Phase 3 testing will be conducted 5 to 10 years after bearing installation. Plans for testing the dampers, isolators, and lock-up devices of the other toll bridge retrofit projects will be formed once the construction contracts have been awarded.

The goals of the program are to provide a dedicated facility for the testing of full scale seismic response modification devices, to characterize full size specimens, directly monitor long term performance of devices, verify modeling elements used in analysis, and enhance the future understanding and application of these devices. Although the price of this facility and testing program is high (15 million dollars), the cost is justified due to the significant savings realized by using this technology in the toll bridge retrofits.

SCALED TESTING OF ISOLATION SYSTEM

Another research program directly resulting from the Toll Bridge Retrofit Program is the "Seismic Isolation Retrofit of Long Span Bridges Isolation System Proof-of-Concept Studies". This project, which will be conducted at the EERC, arose from engineers interest in a comparison of measured vs. predicted response of a long span isolated structure. This study will investigate the performance of a moderately flexible superstructure which is supported by flexible piers. Superstructure types represented will be single and two level truss spans and box girder spans. Types of isolators include Friction Pendulum System, flat sliders with attached restoring springs, lead rubber bearings, and high damping rubber bearings. Shake table tests will investigate the following:

- response of earthquake ground motions
- torsional response due to mass and stiffness eccentricities
- effects of vertical EQ shaking and overturning
- effects of high frequency vertical EQ shaking
- influence of substructure flexibility
- influence of superstructure flexibility
- effects of wind-load restraints
- permanent displacement
- comparison of measured vs. predicted response

This project, which will begin next year, will attempt to characterize the response of various isolation systems and validate the analytical models used on the toll structure retrofit projects

RECENT ISOLATION AND DAMPING BRIIDGE INSTALLATIONS

Although the new technology applications of the toll bridges have attracted significant attention, Caltrans has also applied dampers and isolators to structures of more moderate size and demands. These consist of 3 isolation retrofits and one application of dampers in a new structure (see table 1). Although not as glamorous as the toll projects, these bridges better represent the type of structures that will be equipped with isolation and energy dissipation devices in the future.

The Three Mile Slough Bridge is a 734 foot steel truss with a 183 foot center lift span. A non-isolated retrofit strategy considered for this structure involved supplemental piers to accommodate seismic forces. This strategy was not only extremely costly due to construction in the water, it was determined that the addition of piers would exacerbate scour to the foundation. The final solution called for the installation of

either lead-core rubber or elasto-plastic isolation bearings at both abutments and top of piers. This project is currently under construction and the lead-rubber bearings selected by the contractor will be installed imminently.

The Rio Vista bridge retrofit (also known as the Sacramento River Bridge) uses both isolation and damping as tools in its design strategy. The 2500 foot long steel lift span will be installed with lead rubber bearings at the piers and viscous dampers at the base of the tower legs of the lift span. Viscous dampers were shown in analysis to be highly effective in damping energy due to tower rocking while providing a 50 to 60% reduction in displacement. Several kinds of isolators were considered during analysis including high-damping rubber bearings, Friction Pendulum System bearings, and lead-core rubber bearings. Ultimately, lead-core rubber bearings were chosen for the design. Extensive nonlinear analysis (using SAP90, DRAIN-2DX & 3DX, and ABACUS) was conducted with site specific time histories and spectra. [6] This project is due to go out to bid in the summer of 1998 pending identification of funding.

The retrofit of the Rio Hondo bridge uses isolation to reduce shear input to a weak substructure. This project allowed for two types of isolation systems. The first alternative called for Friction Pendulum Bearings to be placed at top of pier and abutments. The second alternative called for lead-core rubber bearings at the top of pier and flat sliders plus elastomeric springs at the abutments. This design is the first to install seismic isolation joints in an isolated structure. These joints have been designed by Caltrans to accommodate movement during a seismic event without damage. The software package SADSAP was used to perform the nonlinear time history analysis with site specific time histories and ARS curves.[7]

The 91/5 HOV Connector Separation is the first use of dampers in a Caltrans owned structure. Viscous dampers were employed in this continuous, two span, cast in place, prestressed concrete, box-girder bridge design in order to enhance the structures seismic performance. The dampers allowed for both abutments to work together and result in reduced demands to the columns. Non-linear time history analysis was conducted using SADSAP. Since site specific time data was not available, several California earthquake time histories were used in the analysis.[8] Competition among pre-qualified manufactures was allowed in this project and installation of the dampers is anticipated by the end of 1998. Plans are being considered for the instrumentation of this structure to monitor performance of the dampers.

These projects represent a growing awareness of isolation and damping as tools in retrofit and design strategies. Designers are using more sophisticated methods of analysis and considering a greater variety of types of devices. Significant changes in specifications in the area of pre-qualification and performance requirements are allowing for competition among device suppliers while giving designers a higher level of confidence in the quality of devices that will ultimately be installed in their project (a balance that is very difficult to maintain). This is an iterative process in which many lessons are learned with each project. Performance requirements, design methods and contract specifications are constantly evolving. The completion of the several ongoing research projects mentioned in this paper as well as the publishing of the revised AASHTO guide specification for seismic isolation design should make huge contributions to future damping and isolation projects.

COMPOSITE MATERIALS

Caltrans has made use of composite materials as an alternative to steel plate column casings to provide ductile behavior under seismic loading. Both glass and carbon fiber systems have been used with both machine application and hand lay-up.

TESTING

Caltrans has established a testing program for composite column casing systems to pre-qualify them for use on its projects. The testing program consists of coupon testing for material durability and material properties and large scale column testing to determine structural performance of the casing.

For purposes of pre-qualification, a composite column casing system consists of the unique physical form of the system; the materials system, including the fiber material, physical form of the fiber material, resin, primer, and adhesive as applicable; the installation process; the system supplier; the materials supplier; and the installer. The supplier also provides a proposed design procedure and a construction specification.

The coupon testing program for composites is concerned with confirming the structural and material properties of the composite system and with getting a perspective on material durability issues. To that end, the following composite properties are tested:

Ultimate Tensile Strength of the primary material, Strain to Failure, Modulus, Density/Specific Gravity, Mass per Unit Length, Sizing Content, Fabric Construction, Tensile Strength of the composite, Strain at failure, Mass per unit area, Thickness, Resin Content, Mass %Volatiles,
Mass %Fiber Content, Volume % fibers, Glass Transition Temperature,
Gel Time @ Curing Temperature, Cure Time @ Curing temperature, drape, and Interlaminar Shear Strength.

And for resins and adhesives:

Tensile Strength, Strain at Failure, Modulus, Mixing Ratio by volume and mass, Glass Transition Temperature, Infrared or HPLC Curves,
Temperature/Time/Gel Time Curve(Component A, Component B),
Temperature/Time/% Cure Curve, DTA, DCS, or DMA Curves,
and Lap Shear Strength.

Testing is also performed on ring samples to determine hoop strain at failure, hoop modulus at failure and maximum stress at failure. Maximum hoop stress at failure and secant hoop modulus shall be calculated using the following equations:

$$\text{Hoop Stress (s)} = \frac{P_f(r_o^2 + r_i^2)}{(r_o^2 - r_i^2)}$$

$$\text{Secant Modulus } (E_{hoop}) = \frac{2r_i^2}{r_o^2 - r_i^2)} S_{0.1\leftrightarrow 0.6}$$

Where P_f is the failure pressure, r_i and r_o are the inside and outside diameters of the ring, respectively, and $S_{0.1\leftrightarrow 0.6}$ is the slope of the pressure-hoop strain between 0.1% and 0.6% strains.

DURABILITY TESTING

The following describes the durability test being performed as part of the Caltrans program.

A. Water Resistance

Panels shall be exposed to a condition maintained at 100% relative humidity and 100 +/- 2°F. (Apparatus as described in ASTM D 2247 or ASTM E 104 is satisfactory.) Specimens shall be tested at intervals of 1000, 3000, and 10,000 hours exposure. Specimens should be tested as soon as possible after removal from the water.

B. Ultraviolet Resistance

Panels shall be subjected to exposure in equipment meeting the requirements of ASTM G 53, using FS 40 UV-B bulbs. One cycle shall be four (4) hours at 140°F and four (4) hours of condensate exposure at 104°F. After 100 cycles the specimens shall be removed and tested as above.

C. Temperature Resistance

Panels shall be subjected to a continuous temperature of 140°F for 1000 and 3000 hours before testing. Specimens shall be allowed to return to ambient temperatures prior to testing.

D. Salt Water Resistance

Panels shall be totally immersed at 75 +/- 3°F in an artificial sea water solution prepared according to ASTM D 1141, omitting heavy metal reagents, for intervals of 1000, 3000, and 10,000 hours prior to testing. The artificial sea water shall be regularly monitored and changed or refreshed as needed. Specimens should be tested as soon as possible after removal from the salt water.

E. Fuel Resistance

Panels shall be immersed for four (4) hours in diesel motor fuel prior to testing. Specimens should be tested as soon as possible following removal from the diesel fuel.

F. Alkali Resistance

Panels shall be immersed in a saturated solution of calcium carbonate (pH 9.5) at 75 +/- 3°F for intervals of 1000, 3000, and 10,000 hours prior to testing. The pH of the solution shall be monitored at regular intervals and the solution changed as needed.

G. Freeze-Thaw Resistance

Panels shall be subjected to freeze-thaw cycling by exposure for 24 hours under A, above, followed by 24 hours at 0°F. Panels shall be subjected to twenty (20) freeze-thaw cycles, and shall be allowed to return to ambient temperature prior to specimen preparation and testing.

LARGE SCALE SYSTEM TESTING

The other major component of the composite testing program is the large scale testing of the composite casing on a column and subjected to simulated earthquake displacements.

All composite column casing systems shall satisfy reduced scale cyclic column testing to verify casing's constructability and effectiveness as a seismic retrofit measure. To qualify a system as an alternative column casing for seismic retrofit, a minimum of two types of retrofit enhancements shall be demonstrated and tested. For each shape, cyclic tests shall be conducted to demonstrate the performance of both retrofit enhancements and corresponding non-retrofitted "As-Built" condition. Manufacturers may elect to qualify only one shape (circular or rectangular) by satisfying all tests requirements for either the circular tests or rectangular tests, thus limiting their qualifications to these systems.

For each geometrical shape, and for each corresponding enhancement, a minimum of one retrofitted "As-Built" column and one non-retrofitted column is built and tested. For example, to qualify a system for circular column retrofit applications, the following four test specimens must be constructed and tested:

1. Circular Shear As-Built Column (Non-retrofitted)
2. Circular Lap Splice As-Built Column (Non-retrofitted)
3. Circular Shear Retrofitted Column subjected to double bending load
4. Circular Lap Splice Retrofitted Column subjected to single bending load.

All column details need to conform to the current Caltrans design criteria, with proper scaling factors when applicable, and satisfy the following:

1. Minimum confinement stress of 300 psi in the lap splice and/or plastic hinging zone
2. Maximum material elongation of 0.001 in/in in the lap splice zone and 0.004 in/in in the plastic hinging zone
3. Minimum confinement stress of 150 psi and material elongation of 0.004 must be maintained elsewhere in the column with appropriate transition
4. Minimum displacement ductility for the retrofitted column of 8 to 12 is to be expected.

An expected concrete strength of 5000 psi at the time of testing and Grade 60 reinforcing steel shall be used, although Grade 40 is preferable when available.

The concrete design shall have aggregate no larger than one-half inch. The footing block as well as the loading block of the test columns shall be properly reinforced such that no degradation in these locations is allowed.

The test specimens are as follows:

1. Cross Sections

The cross section of the rectangular test column shall be 24"x 24" with a total of 28 #6 longitudinal bars evenly spaced with #2 ties at 5" spacing. The cross section of the circular test column shall be 24" in diameter with a total of 20 #6 longitudinal bars evenly spaced with #2 ties at 5" spacing.

2. Shear Enhancement Specimen

The shear enhancement test columns has a clear span of 96" shear arm between anchorage blocks and maintains a maximum aspect ratio of 4 in the direction of the test if dimensions are modified.

3. Lap Splice Enhancement Specimen

The lap slice enhancement columns shall have the moment arm of 144".

4. Loading

Test columns shall be subjected to a vertical load (axial) of $0.1f'_cAg$ where concrete strength based on the original design strength of 3250 psi. For example, the column with rectangular section should have a vertical load of 190 kips.

The attached figures illustrate column configuration requirements.

5. Instrumentation

The structure test specimens are instrumented to record strains at various locations during the testing.

6. Loading History

All test columns are subjected to a number of full reversed cycles of loads and displacements. Initial cycles up to 75% of the lateral yielding force shall be carried out under load control. Two fully reversed cycles at 25%, 50% and 75% of the yielding force to verify that both the load and data acquisition system. Subsequent tests beyond 75% yielding force shall carried out under displacement control. Three fully reversed cycles are imposed at each ductility level of 1, 2, 3, 4, 6 and 8. If at the end of the test the column maintain more than 80 percent of the peak lateral strength, a final push with the maximum of full stroke in a single direction is performed.

FIELD TESTING AND PRODUCTION

To date, both carbon and E-glass column casings have been used on Caltrans bridges. The field demonstration work has proven valuable for refining the construction process when using these materials. The San Elijo Lagoon Bridge and parts of the Santa Monica Viaduct have machine applied carbon column casings while the Griffith Park Interchange has E-glass casings which were hand applied. For the most part, the procedures went well, but not without some experimentation and on the job learning by all parties involved.

One project where we did have a difficult lesson was on the Arroyo Seco Bridge in Pasadena. Arroyo Seco is an open spandrel arch bridge. The retrofit called for using either carbon or E-glass column wrapping to minimize the effects on the appearance of the bridge. The successful contractor chose to use carbon and apply it by means of a wrapping machine. Because of the high aspect ratio of the rectangular columns, the machine wrapping performed poorly. As a result, hand applied methods are being reviewed as a substitution.

CONCLUSION

It is anticipated that the completion of the several ongoing research projects mentioned in this paper will provide answers in the areas of performance characterization as well as longevity, wear, and aging. New guidelines on design and performance specification will assist the engineer in the appropriate application of new technologies while recently developed non-linear analysis software will enable the design engineer to perform the sophisticated analysis that may be accompanied with the application of this technology. (However, it must be emphasized that attention to simple rational design methods must always be present.) As California's transportation system grows, so does the need for creative solutions to seismic demand and performance criteria which address public safety, cost, minimum disruption to traffic, and the environment. To date, isolation, energy dissipation, and composite materials have offered some effective solutions to difficult seismic stuctural challenges. While there are still significant questions regarding these new technologies, they present good alternatives for future designs.

REFERENCES

[1] Roberts, J.E., "Sharing California's Seismic Lessons", Modern Steel Construction; July, 1992

[2] "Guidelines for the Testing of Seismic Isolation and Energy Dissipating Devices", CERF REPORT: HITEC 96-02; March, 1996

[3] AASHTO, 1997 Proposed "Draft of Guide Specification for Seismic Isolation Design"; May 15, 1997

[4] Housner, G.W., Penzien, J., Agbabian, M.S., Arnold, C., Dickinson, L.V., Elsesser, E., Idriss, I.M., Jennings, P.C., Podolny,W., Scordelis, A.C., Wallace, R.E., "Competing Against Time, Report to Governor George Deukmejian from The Governor's Board of Inquiry on the Loma Prieta Earthquake"; May 31, 1990.

[5] Mellon, D.E., "Caltrans' Proposed Testing of the Seismic Response Modification Devices for the Toll Bridge Retrofit Program", Proc. of National Seismic Conference On Bridges And Highways, Sacramento CA; July, 1997

[6] Abbas, H.,Singh, S.P., Uzarski,J., "Seismic Evaluation and Retrofit of Sacramento River Bridge at Rio Vista" accepted for the Sixth US National Conference on Earthquake Engineering, Seattle WA; EERI, May, 1998

[7] Delis, E., Tokas, C., Madani, M., Thompson, K., "Analytical Studies for Seismic Isolation in Highway Bridges", Proc. of Structures Congress XV, (2)1471---1478, Portland OR, 1997

[8] Delis, E., Malla, R., Madani.M., Thompson, K., "Energy Dissipation Devices Using Hydraulic Dampers", Proc. of Structures Congress XIV, (2)1188--1196 Chicago IL, 1996

[9] Roberts, J. E., "Composite Construction in California Bridge Seismic Retrofitting" US-Japan Workshop on Seismic Systems for Bridges, Hawaii, July, 1997

[10] Sultan, M, "Evaluating Advanced Composites for Applications in Transportation Structures - a Model Public-Private Partnership"

[11] Post, T, Sultan, M, "California's Program for the Use of Composite Materials for Seismic Retrofit" 13th U.S. - Japan Bridge Engineering Workshop

THE ANALYSIS AND DESIGN OF ELASTOMERIC BEARINGS FOR APPLICATION IN BRIDGES

James M. Kelly
Earthquake Engineering Research Center
University of California
Berkeley, California 94720

ABSTRACT

The use of seismic isolation technology is increasing worldwide, and when elastomeric isolators are used they are designed by simple linear elastic methods that have been verified by laboratory testing and by finite element analysis. As code requirements for isolated structures have evolved, equivalent static design procedures have been replaced by nonlinear dynamic analysis, and it has proved very difficult to accurately model the mechanical characteristics of high-damping rubber isolators. Some of the problems will be discussed here.

INTRODUCTION

Although use of seismic isolation technology is increasing throughout the world and approximate linear design approaches are available, the design process for most projects continues to be based on nonlinear dynamic analyses. For analyses of purely softening isolation systems that exhibit approximately bilinear force-displacement behavior (e.g., lead-plug bearings, friction pendulum bearings, or hybrid systems incorporating sliding surfaces and restoring springs), hysteretic elements (one per bearing) accurately capture the bearing response over the entire range of displacements. From an energy standpoint, hysteretic elements are appropriate for such bearings because the mechanism of energy dissipation is either yielding of lead or coulomb (sliding) friction and closely matches the energy dissipation modeled of the bilinear element.

Bilinear hysteretic elements are also used to model high-damping natural rubber bearings, but in this case the optimum model parameters are typically dependent on the maximum displacement in the bearing, particularly when the rubber is in the moderate strain range where the tangent stiffness is continuously softening. A single bilinear element will not trace precisely the force-displacement response to the maximum displacement, and there is no guarantee that the energy dissipated by the model is equal to that dissipated by a bearing. The dissipation in high-damping rubbers appears to result from a combination of hysteretic and viscous mechanism. A single model for high-damping natural rubber isolators that dissipates the same quantity of energy as observed in dynamic tests of isolators over the complete range of displacement is needed, but is not yet available.

For analyses using very strong ground motions, the model must account for the behavior of rubber at large strains. Properly designed and manufactured elastomeric bearings are unique in that they respond with increasing stiffness at large strains as a result of strain crystallization in the rubber. While most projects designed to date have relied only on softening isolation systems, the trend toward increasing design ground motions will likely lead to the use of softening-stiffening systems that provide acceptable performance over a broader range of input intensities. A purely soft-

ening system optimized for very large ground motions will be relatively stiff under more frequent, moderate ground motions, leading to amplified accelerations over the height of the superstructure. In contrast, a softening-stiffening system can be designed to be sufficiently flexible at moderate levels of input, so that the forces transmitted through the bearings are substantially reduced in anticipated seismic events, while still limiting displacements in severe earthquakes having very low probabilities of occurrence.

A critical aspect in the design of natural rubber bearings is the stability of the bearing in the displaced configuration. The linear theory of bearing buckling provides no guidance in this case. This type of instability is of crucial importance in bearing design since the peak downward load will occur at the same time as the peak horizontal displacement; their combination will be the limit state of the isolator. An approach to the prediction of the occurrence of instability in the deflected state will be given here. The method is intended to predict the critical horizontal displacement at which the bearing exhibits zero incremental horizontal stiffness. Comparison with test results show that the method is conservative, but not excessively so.

MECHANICAL CHARACTERISTICS OF ELASTOMERIC BEARINGS

The mechanical characteristics of multilayered elastomeric bearings have been studied for many decades, and while exact analyses using nonlinear techniques are still quite difficult, simple predictions based on elastic theory have been developed by many researchers and verified by laboratory testing and more recently by finite element analysis. The most important mechanical property of the isolation bearing is, of course, its horizontal stiffness; this is given by

$$K_H = GA/t_r \tag{1}$$

where G is the shear modulus of the elastomer, A is the full cross-sectional area (which may differ from the area of the reinforcing shims), and t_r is the total thickness of the rubber. The maximum horizontal displacement, D, is related to the maximum shear strain, γ, by

$$\gamma = D/t_r \tag{2}$$

The vertical stiffness, K_V, and the bending stiffness—expressed as EI by analogy with beam theory—are also given by a simple linear elastic theory and are needed for designing a bearing.

The vertical frequency of an isolated structure, often an important design criterion, is controlled by the vertical stiffness of the bearings that comprise the system. In order to predict this vertical frequency, the designer need only compute the vertical stiffness of the bearings under a specified dead load, and for this a linear analysis is adequate. The initial response of a bearing under vertical load is very nonlinear and depends on several factors. Normally, bearings have a substantial run-in before the full vertical stiffness is developed. This run-in, which is strongly influenced by the alignment of the reinforcing shims and other aspects of the workmanship in the molding process, cannot be predicted by analysis, but is generally of little importance in predicting the vertical response of a bearing.

Another important bearing property that must be analyzed for design is the buckling behavior of the isolator. In order to conduct this analysis, the response of the compressed bearing to bending

moment is necessary. Referred to as the "bending stiffness", this can be ascertained by an extension of the same analysis that is done to determine the vertical stiffness.

The vertical stiffness of a rubber bearing is given by the formula

$$K_V = E_c A / t_r \tag{3}$$

where A is the cross-sectional area of the bearing (in this case it usually is taken as the area of the shim plates), t_r is the total thickness of rubber in the bearing, and E_c is the instantaneous compression modulus of the rubber-steel composite under the specified level of vertical load. The value of E_c for a single rubber layer is controlled by the shape factor, S, defined as

$$S = \text{loaded area/force-free area}$$

which is a dimensionless measure of the aspect ratio of the single layer of the elastomer. For example, for a circular pad of diameter, ϕ, and thickness, t,

$$S = \phi / 4t \tag{4}$$

and for a square pad of side dimension, b, and thickness, t,

$$S = b / 4t \tag{5}$$

For a single pad in the form of a complete circle of radius R, the compression modulus, E_c, is given by

$$E_c = 6GS^2 \tag{6}$$

and for a square pad with side dimension a, the result is

$$E_c = 6.73GS^2 \tag{7}$$

In some cases bearings are designed with unfilled central holes. The result for a bearing with an inside radius a, and outside radius b is

$$E_c = \lambda 6GS^2 \tag{8}$$

where

$$\lambda = \left\{ b^2 + a^2 - [(b^2 - a^2)/(\ln b/a)] \right\} / (b - a)^2 \tag{9}$$

When $a/b \to 0$, then $\lambda \to 1$, hence, $E_c = 6GS^2$, which is the result for the full circular pad. When $a/b \to 1$, by writing $a/b = 1 - \varepsilon$ and letting $\varepsilon \to 0$, we find that $\lambda \to 2/3$ and $E_c = 4GS^2$, which is the result for the infinite strip. When $a/b > 0.10$, the value of λ is almost two-thirds, indicating that the presence of even a small hole has a large effect on E_c, therefore, in most cases for bearings with central holes, the value of E_c should be taken as $4GS^2$ rather than $6GS^2$.

Under direct compression the constraint provided by the bonded steel shims produces a shear strain in the rubber, which is denoted by γ_c. If the nominal compression strain denoted by ε_c and given by

$$\varepsilon_c = \Delta / t_r$$

where Δ is the vertical displacement, then the result for the maximum shear strain developed at the edges of the pad is $\gamma_c = 6S\varepsilon_c$.

The maximum shear strain due to compression is not the only shear strain quantity of interest to the designer. It is also useful to estimate the average strain in the following manner: because rubber is somewhat strain sensitive, G is often modified according to the strain level, particularly in highly filled rubbers. In compression the shear strain varies widely over the volume of the pad, therefore, the appropriate value of the modulus used to estimate the average strain is based on a calculation of the elastic stored energy in the pad. From this calculation the average shear strain, γ_{ave}, is given by $\gamma_{ave} = \sqrt{6}S\varepsilon_c$ Although a certain degree of trial and error is needed, computations of this kind allow the designer to estimate the appropriate value of G, which can then be used to estimate the vertical stiffness. First we must assume a value of G in order to calculate ε_c and from that calculate γ_{ave}; we then modify G and iterate as necessary. Because the modulus is not very sensitive to strain above about 20%, few iterations are needed.

The bending stiffness of a pad is computed using a similar approach with the same type of displacement assumptions. The pad is assumed loaded by a pure moment, M, and the deformation is assumed to be a rotation of the top and bottom bonded plates. The relative angle between the top and bottom plates is denoted by α, and the radius of curvature, ρ generated by the deformation is related to α by

$$\frac{1}{\rho} = \frac{\alpha}{r}$$

By analogy with beam theory, where

$$M = EI/\rho$$

we write

$$M = (EI)_{eff}\frac{\alpha}{t} \tag{10}$$

For a circular pad of radius R, the result is

$$M = \frac{3\alpha G}{2t^3} \cdot \frac{\pi R^6}{12}$$

Taking the E in EI as $E_c = 6GS^2$, we have the result $\pi R^4/12$ for I, which is one third the beam moment of inertia. The difference is caused by the fact that the pressure distribution varies as a cubic parabola across the pad, whereas in a beam, the bending stress distribution is linear. In the case of a square pad, the effective EI is very close to one-third the beam EI, being

$$(EI)_{eff} = E_c(0.329I) \tag{11}$$

For the circular pad with a central hole, we have

$$(EI)_{eff} = 2GS^2I\frac{(b+a)^2}{b^2-a^2} \tag{12}$$

The shear stresses induced by the bending are given by

$$\gamma_b = 6S\varepsilon_b \tag{13}$$

where $\varepsilon_b = \mathrm{R}\cdot\alpha/t$ is the edge compression strain produced by bending. The average shear strain (in the sense of overall shear strain energy) is given by

$$\gamma_b^{ave} = \frac{\sqrt{2}}{4}S\varepsilon_b \tag{14}$$

When the shape factor of the pad becomes large, the effect of compressibility of the rubber begins to be important. Compressibility can be approximately incorporated in the previous formulae through the ad hoc modification [1]

$$\frac{1}{E_c} = \frac{1}{E_c'} + \frac{1}{K} \tag{15}$$

where $1/E_c'$ is the compression modulus assuming incompressibility behavior, and K is the bulk modulus of the material. More exact formulae have been developed for this effect [2], but the bulk modulus is such a difficult quantity to measure that use of the simple ad hoc formula is good enough for design purposes. The value of K varies quite widely in reference material, ranging from a low of 1000 MPa (145,000 psi) [3] to 2500 MPa (363,000 psi) [4]. The value most commonly used, and which appears to fit laboratory test results on bearings, is 2000 MPa (290,000 psi).

When rewritten for E_c for a circular pad, we have $E_c' = 6GS^2$, thus

$$E_c = \frac{6GS^2K}{6GS^2+K} \tag{16}$$

When S is small, we have

$$E_c = 6GS^2\left(1-\frac{6GS^2}{K}\right)$$

so that for, say, better than 10% accuracy, S is such that

$$6S^2 < K/60G$$

with K = 2000 MPa (290,000 psi) and G = 0.7 MPa (101.5 psi), the $S < 7$.

When S is large and $6GS^2/K$ is much greater than one

$$E_c = K(1 - K/6GS^2)$$

showing that K is an upper bound to E_c and will approximate E_c to better than 10% accuracy if

$$S > (K/0.6G)^{1/2} \approx 70$$

Shape factors of this magnitude are unlikely, but the formulae show that an allowance for compressibility is needed for shape factors above about 10.

MODELING OF ISOLATION BEARINGS BY BILINEAR MODELING

When dynamic analysis is required by code, all isolation bearings are modeled by a bilinear model based on the three parameters, K_1, K_2, and Q, as shown in Figure 1. The elastic stiffness, K_1, is either estimated from available hysteresis loops from elastomeric bearing tests or as a multiple of K_2 for lead-plug bearings and friction pendulum bearings. The characteristic strength, Q, is estimated from the hysteresis loops for the elastomeric bearings. For lead-plug bearings Q is given by the yield stress in the lead and the area of the lead, while in the friction pendulum bearings it is given by the friction coefficient of the sliding surface and the load carried by the bearing. The post-yield stiffness can be accurately estimated or predicted for all three types of bearings.

The effective stiffness, defined as the secant slope of the peak-to-peak values in a hysteresis loop, is given by

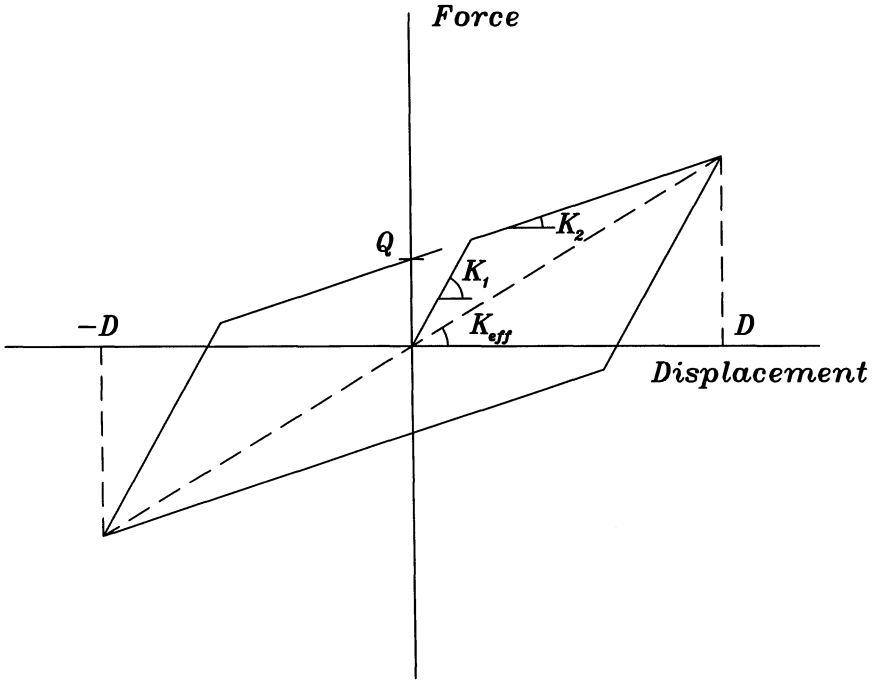


Figure 1 - Parameters for Bilinear Modeling

$$K_{eff} = K_2 + Q/D, \qquad D \geq D_y \tag{17}$$

where D_y is the yield displacement. In terms of the primary parameters,

$$D_y = Q/(K_1 - K_2) \tag{18}$$

and the area of the hysteresis loop (the energy dissipated per cycle), W_D, is

$$W_D = 4Q(D - D_y)$$

The effective damping, β_{eff}, is defined by

$$\beta_{eff} = 4Q(D - D_y)/2\pi K_{eff} D^2 \tag{19}$$

This can be expressed in non-dimensional quantities by defining a non-dimensional displacement

$$y = D/D_y$$

and a non-dimensional characteristic strength

$$a = Q/K_2 D_y$$

whereby the effective damping becomes

$$\beta_{eff} = \frac{2a}{\pi} \cdot \frac{y - 1}{(y + a)y} ; \qquad y \geq 1 \tag{20}$$

For fixed a, $\beta = 0$ at $y = 1$ and tends to zero as $y \to \infty$. The maximum value of β given by $d\beta/dy = 0$ occurs at

$$y = 1 + (1 + a)^{1/2} \tag{21}$$

with

$$\beta_{max} = \frac{2a}{\pi} \cdot \frac{1}{2(1 + a)^{1/2} + (2 + a)} \tag{22}$$

Now $a = Q/K_2 D_y$, thus from Eq. (18), we have $a = (K_1 - K_2)/K_2$.

This leads to the curious result that the maximum value of the effective damping depends only on the ratio of K_1 to K_2. The second slope, K_2, is easy to determine for any type of isolation system, but the first slope, K_1, is usually done by eye and can vary over a wide range. Since the characteristic strength Q can also be accurately determined, the value of K_1 has no influence on the effective stiffness, but obviously has a strong influence on the damping and, in particular, on the maximum value, which can be an important promotional value for a proprietary system.

To illustrate the effect of the selection of K_1 on the damping, consider a system with the same Q

and K_2 values (thus the same effective period at all values of D and the same hysteresis loop), but modeled by different values of K_1. We take Q = 44.5 kN (10 kips) and K_2 = 350 kN (2 kips/in.): $K_1^1 = 51K_2$, $K_1^2 = 21K_2$, $K_1^3 = 6K_2$, and $K_1^4 = 3K_2$.

The values of D_y, a for these are

D_y^1 = 2.5 mm (0.10 in.) $a^1 = 50.0$ D_y^3 = 25.4 mm (1.00 in.) $a^3 = 5.0$

D_y^2 = 6.35 mm (0.25 in.) $a^2 = 20.0$ D_y^4 = 63.5 mm (2.50 in.) $a^4 = 2.0$

The peak values of β and the displacement at which each occurs are as follows:

$\beta_{max}^1 = 0.480$ at D = 20.8 mm (0.82 in.) $\beta_{max}^3 = 0.268$ at D = 87.6 mm (3.45 in.)

$\beta_{max}^2 = 0.410$ at D = 35.6 mm (1.40 in.) $\beta_{max}^4 = 0.170$ at D = 173.5 mm (6.83 in.)

The variation of β with D for the four cases (as shown in Figure 2) illustrates how the damping at small displacements can be very high if K_1 is selected to be large. It also shows that as D becomes large, all β versus D curves tend to become the same. The point is that the same hysteresis curve when modeled by a bilinear model can have a very different pattern of damping values, depending only on how the initial stiffness is selected.

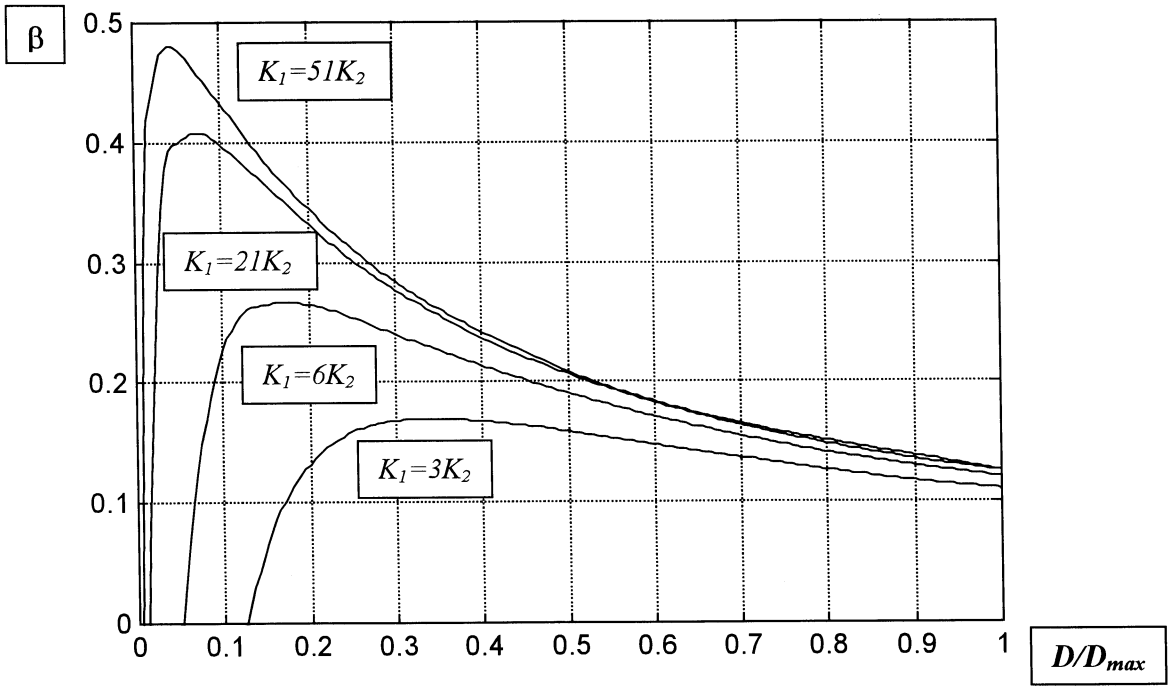


Figure 2 - Effective Damping as a Function of Displacement for Different Choices of K_1

IMPLICATIONS OF BILINEAR MODELING

The most significant implication of the use of bilinear modeling of high-damping rubber bearings is that the damping at small to moderate displacements is underestimated, and this could have an influence on the response of the structure. The kinetic energy imparted to the structure by the ground motion in the initial phase of the event will not be absorbed and could lead to larger than predicted displacements and forces. Since the code requirements for design of isolated structures in near-fault locations are now so severe, it is essential to make a dynamic analysis as accurate as possible.

One approach to improve the modeling of the high-damping bearing is based on the empirical result that the energy dissipated in one cycle is proportional to the displacement to a power close to 1.5, which suggests that basis of a model combining viscous and elastic-plastic elements. This is described in detail in Clark and Kelly [5]. Although it improves the accuracy of the model, it does not accurately represent the material behavior over the complete range of displacement.

BUCKLING AND STABILITY OF ELASTOMERIC ISOLATORS

A multilayered elastomeric bearing can be susceptible to a buckling type of instability similar to that of an ordinary column, but dominated by the low-shear stiffness of a bearing. The previous analysis of the overall deformation of a single pad can be used in a buckling analysis that treats the bearing as a continuous composite system. This analysis considers the bearing to be a beam, and the deformation is assumed to be such that plane sections normal to the undeformed central axis remain plane, but not necessarily normal to the deformed axis.

The theory for the buckling of isolation bearings is an outgrowth of work by Haringx in 1947 on the mechanical characteristics of helical steel springs and rubber rods used for vibration mountings. This work was published in a series of reports, the third of which [6] covers the stability of solid rubber rods. The Haringx theory was later applied by Gent [7] to the problem of the stability of multilayered rubber compression springs, and it is this application that forms the basis for the theory given here.

The method parallels the linear elastic analysis of the Euler buckling of a column. To model the rubber isolator as a continuous beam, it is necessary to introduce certain modifications to the quantities defined in the previous section. Consider the bearing to be a column of length h with a cross-sectional area A, and define the shear stiffness per unit length as $P_S = GA_S$, where A_S is an effective shear area given by

$$A_S = A \cdot h/t_r$$

where h is the total height of the bearing (rubber plus steel), and t_r is, as defined earlier, the total height of rubber. The increase in A is needed to account for the fact that steel does not deform in the composite system. The bending stiffness is similarly modified, so that the $(EI)_{eff}$ for a single pad of thickness t, becomes EI_S, where

$$EI_S = E_C \cdot \frac{1}{3} I \cdot \frac{h}{t_r}$$

In terms of these quantities, the overall horizontal stiffness K_H, (which was GA/t_r) becomes

$$K_H = GA_S/h$$

and the Euler buckling load for a column with no shear deformation is

$$P_E = \pi^2 EI_S/h^2$$

The usual situation for a bearing in an isolation system is shown in Figure 3. The bearing is constrained against rotation at both ends and is free to move sideways at the top. The result for the critical buckling load, P_{crit}, is the solution of the equation

$$P^2 + PP_S - P_S P_E = 0 \tag{23}$$

from which the critical load, $P_{crit,}$ is given by

$$P_{crit} = -P_S + \sqrt{P_S^2 + 4P_S P_E}/2 \tag{24}$$

For most bearings, where S is 5 or greater, $P_E >> P_S$, the critical load can be approximated by

$$P_{crit} = (P_S P_E)^{1/2} \tag{25}$$

Using this expression and recalling the definitions of P_S and P_E we have $P_{crit} = \sqrt{2}\pi GASr/t_r$, where r is the radius of gyration.

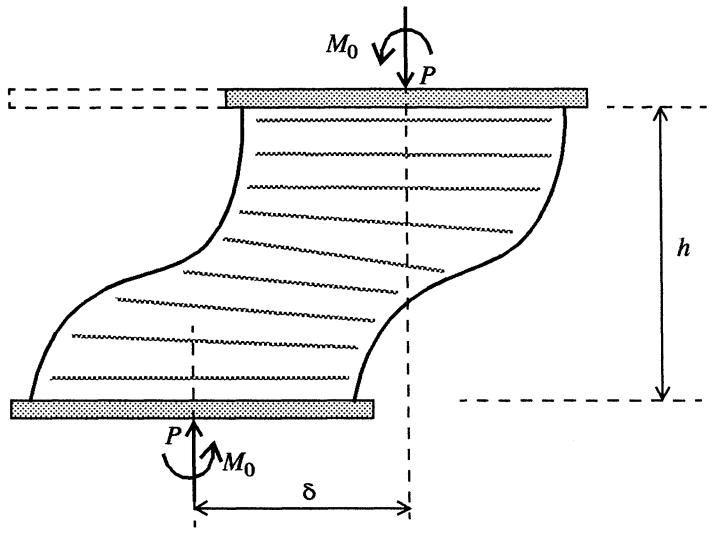


Figure 3 - Boundary conditions for an isolation bearing under a vertical load, P (the bearing buckles with no lateral force constraint, but is prevented from rotating at each end)

The critical pressure, $p_{crit} = P_{crit}/A$, can be expressed in terms of S and the quantity S_2, referred to as the aspect ratio or the second shape factor, defined by $S_2 = \phi/t_r$ or b/t_r. Thus

$$\begin{aligned} p_{crit}/G &= \frac{\pi}{2\sqrt{2}} SS_2 \text{ for a circular bearing} \\ p_{crit}/G &= \frac{\pi}{\sqrt{6}} SS_2 \text{ for a square bearing} \end{aligned} \tag{26}$$

INFLUENCE OF VERTICAL LOAD ON HORIZONTAL STIFFNESS

When the load carried by the bearing is comparable to the buckling load, the horizontal stiffness, K_H, is reduced. The reduction is obtained by using the same linear elastic analysis and is given by

$$K_H = \frac{GA_S}{h}\left[1 - \left(\frac{P}{P_{crit}}\right)^2\right]$$

If the load is less than 0.32 times the buckling load, the accuracy of the usual formula for K_H is better than 10%, and in most projects' design requirements will ensure that this is the case.

The downward displacement, δ_V, of the top of a bearing carrying a vertical load, P, and displaced through a sideways movement D at the top, is also given by the buckling analysis in the form

$$\delta_V = \frac{P_S + P}{P_E}\frac{D^2}{h}$$

In most cases, $P >> P_S$, thus

$$\delta_V = \frac{P}{P_{crit}} \cdot \frac{P_{crit}}{P_E} \cdot \frac{D^2}{h} = \left(\frac{P}{P_{crit}}\right) \cdot \sqrt{\frac{P_S}{P_E}} \cdot \frac{D^2}{h}$$

Now

$$\frac{P_S}{P_E} = \frac{GA_S h^2}{\pi^2 E I_S} = \frac{Ah^2}{2\pi^2 I S^2}$$

In terms of $r = (I/A)^{1/2}$, we have

$$\frac{\delta_V}{h} = \frac{P}{P_{crit}} \cdot \frac{h}{\sqrt{2}\pi r S} \cdot \frac{D^2}{h^2}$$

This downward displacement is in addition to that produced by pure compression of the isolator and is caused by the rotation of the reinforcing steel shims in the center of the bearing. This rotation produces a shear stress caused by the component of the vertical load along the rotated layers,

and the resulting shear strain causes the downward movement of the top of the bearing.

STABILITY UNDER LARGE LATERAL DISPLACEMENT

The buckling analysis for an elastomeric isolator is based on the linear theory that is analogous to the buckling analysis of a column, and as in the case in the usual theory, provides the buckling load or buckling stress in the undisplaced position, but no information on the stability of a bearing the displaced position. In the undisplaced position the instability is an example of a bifurcation process; but in the displaced position, the instability will manifest itself by the loss of positive incremental horizontal stiffness. This type of instability is of crucial importance in bearing design since the peak downward load on an isolator will occur at the same time as the peak horizontal displacement and in combination will be one of the limit states for which the isolator will need to be proportioned.

In principle, a complex nonlinear analysis will be needed to predict the bearing behavior under the combination of peak vertical load and maximum horizontal displacement. A simple hypothesis for an approximation to the limit state when an isolator is loaded in shear and with vertical load is that the area A in the expression for the critical load in the undeformed configuration [Eq. (7)] be replaced by the reduced area A_r; the concentration of the vertical stress due to displacement will not affect the bending resistance, but could reduce the resistance due to shear.

For a square bearing of side dimension B, the reduced area A_r is given by

$$A_r = B(B - D)$$

so that if the hypothesis is correct, the critical displacement, D_{crit}, under a specified load, P, is given by

$$P = \sqrt{GA_r \frac{\pi^2 (EI)_{eff}}{t_r^2}} = (A_r/A)^{1/2} P_{crit}$$

and

$$D_{crit}/B = 1 - (P/P_{crit})^2$$

The overlap area for a square bearing is easy to calculate, but is harder for a circular bearing of radius R. With the notation shown in Figure 4, where θ is the half-angle subtended at the center of the intersection of the top and bottom circles and $\phi = \pi/2 - \theta$, the displacement D and the reduced area A_r are given by

$$D = 2R\cos\theta = 2R\sin\phi$$

and

$$A_r = 2R^2(\theta - \sin\theta\cos\theta) = 2R^2\left(\frac{\pi}{2} - \phi - \sin\phi\cos\phi\right)$$

t is convenient to non-dimensionalize these by defining

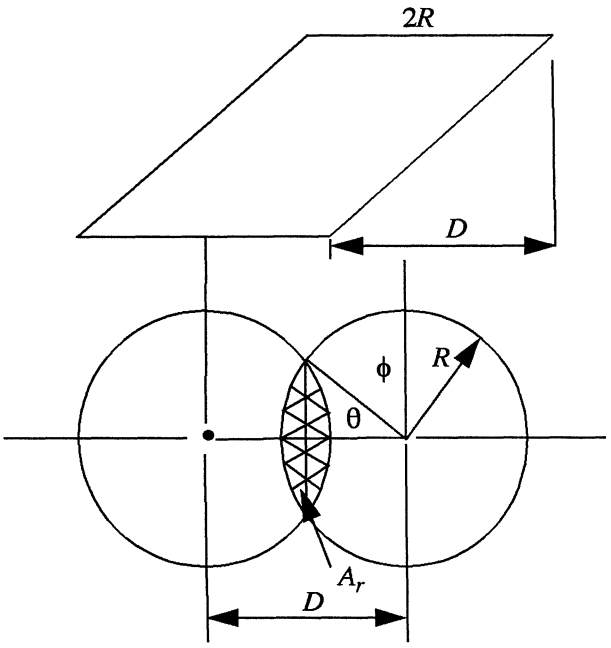


Figure 4 - Notation for reduced area

$$d = D/2R \qquad \text{and} \qquad a = A_r/\pi R^2$$

leading to

$$d = \cos\theta = \sin\phi$$

$$a = \frac{2}{\pi}(\theta - \sin\theta\cos\theta) = 1 - \frac{2}{\pi}\phi - \frac{2}{\pi}\sin\phi\cos\phi$$

The single curve that results from the simultaneous solution of these two equations is given in Table 1. For rapid calculation of the results in the absence of a table or a figure, it is useful to expand the two equations for small values of ϕ corresponding to small d and small displacements or for small values of θ corresponding to small values of a and very large displacements.

When ϕ is small, the first equation can be written as

$$\phi = \sin^{-1}d = d + \frac{d^3}{6} + \frac{3d^5}{40} + \ldots$$

and

$$\sin\phi\cos\phi = \frac{1}{2}\sin 2\phi = \frac{1}{2}\left(2\phi - \frac{8\phi^3}{6} + \frac{32\phi^5}{120} + \ldots\right)$$

Thus

Table 1 - Normalized reduced area

d	θ rads	a	a_a^1*	a_a^2*	p
0.10	1.471	0.873	0.873		0.934
0.20	1.369	0.747	0.747		0.864
0.30	1.266	0.624	0.624		0.790
0.40	1.159	0.505	0.505		0.710
0.50	1.047	0.391	0.391		0.625
0.60	0.927	0.285	0.284		0.534
0.70	0.795	0.188	0.0187		0.434
0.80	0.644	0.1044	0.1005	0.1074	0.323
0.85	0.555	0.0683		0.0697	0.261
0.90	0.451	0.0374		0.0380	0.193
0.95	0.318	0.0136		0.0134	0.117

*Note: $a_a^1 = 1 - \frac{4d}{\pi} + \frac{2}{3\pi}d^3 + \frac{d^5}{10\pi}$ $a_a^2 = \frac{8\sqrt{2}}{3\pi}(1-d)^{3/2}$

$$\phi + \sin\phi\cos\phi = 2\phi - \frac{2}{3}\phi^3 + \frac{2}{15}\phi^5$$

$$= 2\left(d + \frac{d^3}{6} + \frac{3}{40}d^5\right) - \frac{2}{3}d^3\left(1 + \frac{d^6}{6}\right)^3 + \frac{2}{15}d^5$$

$$= 2d - \frac{1}{3}d^3 - \frac{1}{20}d^5$$

leading to the approximation a_a^1 for a in the form

$$a_a^1 = 1 - \frac{4d}{\pi} + \frac{2}{3\pi}d^3 + \frac{d^5}{10\pi}$$

This expansion is accurate to 4% up to $d = 0.80$ and better for values of less than this, as shown in Table 1. Beyond this it is possible to use an expansion for small values of θ, with

$$d = 1 - \theta^2/2 \qquad \theta = \sqrt{2(1-d)}$$

we find a second approximately a_a^2 given by

$$a_a^2 = \frac{2}{\pi}\left[\theta - \frac{1}{2}\left(2\theta - \frac{8}{6}\theta^3\right)\right] = \frac{8\sqrt{2}}{3\pi}(1-d)^{3/2}$$

This is accurate to 3% at $d = 0.80$ and better for values of d larger than that.

For a circular bearing the critical displacement, D_{crit}, is given by $2Rd_{crit}$, where d_{crit} is that value of d that leads to

$$a = (P/P_{crit})^2$$

For small values of the vertical load relative to the undisplaced critical load, the approximation of a by a_a^2 is valid, and leads to

$$\frac{\delta\sqrt{2}}{3\pi}(1-d)^{3/2} = (P/P_{crit})^2$$

giving

$$d = 1 - \frac{1}{2}\left(\frac{3\pi}{4}\right)^{2/3}(P/P_{crit})^{4/3}$$

This is reasonably accurate for those values of d for which a_a^2 was accurate (i.e., $0.8 \le d \le 1.0$ and $0.1 \ge a \ge 0$. Since $a = (P/P_{crit})^2$, this means that it covers the range

$$0 \le (P/P_{crit}) \le 0.3$$

At the other extreme, the approximation

$$a = 1 - 4d/\pi$$

was very good for $d \le 0.5$ and fairly good (10% accurate) for $d \le 0.8$. This leads to

$$d = \frac{\pi}{4}(1-a) = \frac{\pi}{4}[1 - (P/P_{crit})^2]$$

Since $d = 0.5$ means $a = 0.4$, this should be accurate for $0.6 \le p \le 1$.

The exact answer for the value of (P/P_{crit}) that makes a specific value of d critical is obtained in Table 1, and the curve produced by this inverse solution can be compared to the two approximations.

CONCLUSIONS

Although elastomeric isolators have been used for many years in seismic isolation projects, there is still a need to develop more accurate modeling techniques that allow the accurate prediction of structure response under extreme ground motion. Recent developments in code requirements for

the design of isolated structures are leading to very large displacement demands on seismic isolators, which the designers try to control by adding external dampers of various types. More accurate modeling of elastomeric isolators could reduce the design displacement and produce less expensive designs. It is recommended that work on the modeling of elastomeric isolators be considered a high priority for future research funding.

REFERENCES

1. Lindley, P.B. (1966), "Load-Compression Relationships of Rubber Units," *J. Strain Analysis*, I(3):190-195.

2. Kelly, J.M. (1996), *Earthquake-Resistant Design with Rubber*, 2nd. edition, Springer-Verlag, London.

3. Lindley, P.B. (1978), Engineering Design with Natural Rubber, *NR Technical Bulletin*, Malaysian Rubber Producers' Research Association, Brickendonbury, England.

4. Malaysian Rubber Producers' Research Association (1988), Natural Rubber Science and Technology, ed. A.J. Roberts, Oxford University Press, Oxford, England.

5. Clark, P.W. and J.M. Kelly (1996), "Energy-Based Modeling of High-Damping Rubber Isolators for Dynamic Analysis," *Proc.*, ASCE Inter. Conf. and Exposition on Natural Disaster Reduction, Washington, D.C.

6. Haringx, J.A. (1948), "On Highly Compressible Helical Springs and Rubber Rods, and Their Application for Vibration-Free Mounting," III Philips Research Reports, 4:206-220.

7. Gent, A.N. (1964), "Elastic Stability of Rubber Compression Springs," *J. Mech. Engrg.*, 6(4):318-326.

A methodology for the design of energy dissipation devices for the seismic protection of bridges

Vincenzo Ciampi

University of Rome, 'La Sapienza', Italy

Abstract

The present work aims at establishing design criteria for a rational use of the elastic-plastic devices employed for the seismic protection of bridge structures. The proposed target is attained via an energy based approach which is formulated as an optimum problem. An appropriate non dimensional index, related to both dissipated and input energy, is assumed as a measure of the optimum performance of the device, which is constrained to comply with service and ultimate conditions of the structure. Preliminary numerical results, concerning single degree of freedom systems, show that it is possible to construct optimal design graphs that depend on only two constitutive parameters of the device: yield force and elastic stiffness. Further curves are also given which allow to perform an "a posteriori" check of both the relevant structural response quantities and the damage level suffered by the device.

Introduction

The recent years have seen a continuous growth in the development and application of protective systems for earthquake hazard mitigation and guidelines or appendices to seismic codes have begun to be drafted in those countries where passive control systems have been utilized. Moreover, state-of-the-art reports and review papers are now common, as well as dedicated session at Conferences or special Workshops. Despite the above, in the guidelines a conservative tendency can be noted, that is justified not only by the short experience on the actual behavior of the structural systems, but also by the lack of available aids for a safe design, (1). Therefore a general need exists to better (re)consider some problems that have not got to a satisfactory solution yet, and a great effort in the research is spent to try to develop simplified design procedures, often based on optimality concepts, although the complexity of the problem suggests to resort preferably to linear systems or to invoke a linearized behavior (e.g. (9), (12), (16)).

Since a clearly stated design methodology seems to be still lacking, the present work is aimed at providing a general framework for obtaining design graphs when account is to be made for the actual nonlinear behavior of the protection devices. The suggested procedure is illustrated according to an oriented application to typical bridge structures endowed with elastic-plastic energy dissipation devices and the novelty, with respect to similar attempts, should be sought in a different and more comprehensive methodological statement of the problem, rather than in the analysis tools employed and the general results obtained.

In particular, the protection device has been assumed as the key element for the seismic protection and, therefore, the conditions for its maximum exploitation, associated with the minimum values of the structural response, have been sought for. The elastic stiffness, the elastic-plastic stiffness and the conventional yield point of the device have been given the role of design variables, whereas the objective function has been formulated as a particular measure of the ratio between the energy dissipated in the device and the input energy supplied by the earthquake. A two steps numerical optimization is carried out and (i) the conditions for the maximum performance of the device are derived first, according to an unconstrained optimum problem, i.e. without considering functional limitations, (ii) subsequently the bounds for the range of the optimal values of the design parameters are taken into account and calibrated to comply with the service and ultimate conditions of the bridge and the safe operating life of the devices. For the analyses, the seismic action has been defined according to the Eurocode provisions (10) and pseudo-stationary acceleration profiles have been used accordingly. In view of the huge number of numerical analyses to be performed, a preliminary study has been carried out in order to define the minimum number of acceleration time histories needed for a meaningful statistics of the computed quantities.

The reference models

Since the primary target of the work is the formulation of a proper design methodology, it is convenient, initially, to keep the reference models for the structure and the seismic input as simple and standard as possible, yet retaining all the relevant quantities of engineering interest, in order to focus the attention on the procedure in itself, rather than on the generality of the achievable results.

Structural model

A widely used protection scheme for bridge structures, specially in Italy, is that where the deck is disconnected from the substructure, as in the case of simply supported or continuous span bridges, and the protection devices are located at the abutments, or on top of the piers, (Figure 1)

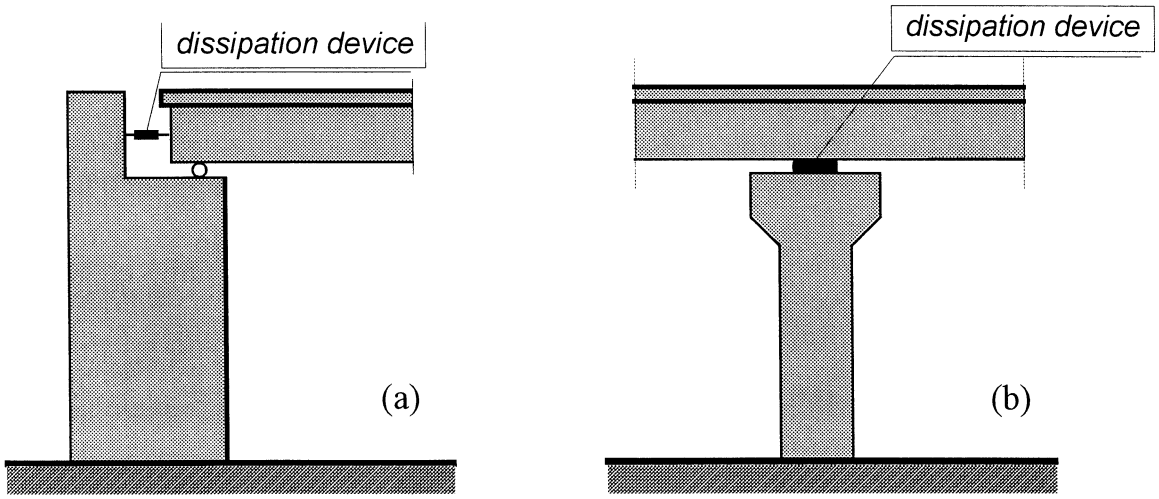


Figure 1

In these cases and when the substructures do not contribute significantly to the overall bridge dynamic behavior, a simple one degree of freedom system, like the one of Figure 2, can be used for studying the bridge protection problem.

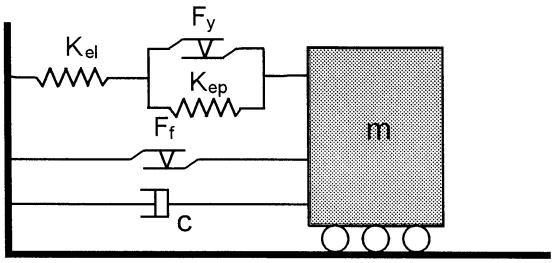


Figure 2

The following related differential equation permits to reproduce the longitudinal bridge motion x induced by the seismic ground displacement x_g:

$$m\ddot{x} + c\dot{x} + F(x) = -m\ddot{x}_g \qquad (1)$$

In equation (1) m is the deck mass, c is the linear damping constant and $F(x)$ is the restoring force, (Figure 3), which sums the force exerted by the device (F_d) and the friction force (F_f) arising from the conventional bearings necessary to transmit the vertical loads to the substructure.

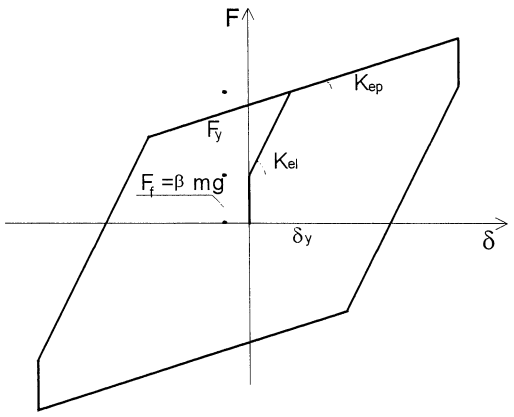


Figure 3

A useful non dimensional form of equation (1) can be obtained by dividing the right and left hand sides by the maximum absolute seismic force $m\ddot{x}_{g,max}$, so that the relevant quantities of the computed structural response can be made independent of the earthquake intensity. This latter is herein referred to as the product Cg where g is the gravity constant and C is the seismic zone index that, according to (10), attains the values $C = 0.15$, 0.25, 0.35, respectively for small, moderate and strong earthquakes. As concerns the restoring force $F_d(x)$, that is the behavior of the energy dissipation device, a standard kinematic hardening behavior, characteristic of elastoplastic type devices, which are the most common in Italy, is assumed; hence the behavior of the entire model can be made dependent upon three sole mechanical parameters of the device: yield force F_y, initial elastic

stiffness K_{el} and secondary or elastoplastic stiffness K_{ep}; which are replaced in turn by the following normalized quantities: $\eta_y = F_y/m\,\ddot{x}_{g,max}$, $T = 2\pi\,(m/K_{el})^{1/2}$ and $\kappa = K_{ep}/K_{el}$, which will assume in the sequel the role of design variables, V_d.

Other important model parameters, whose variation has been investigated, are the viscous damping ratio $\nu = cT/4\pi m$ and the friction coefficient $\beta = F_f/w$, $w=mg$ being the deck weight. Initially, the conventional values ν=5% and β=0, still according to (10), have been considered, then the sensitivity of the results has been checked against a more realistic reduced value for the structural damping ν=2% and β=0, and against simultaneous presence of friction ν=2% and β=2%, where, according to (14), only the average sliding value has been considered disregarding the breakaway, that is the friction peak.

The relevant engineering quantities, which characterize the response of the model, will be expressed accordingly in normalized form; among them of particular interest the maximum relative displacement $\zeta_{max} = x_{max}/m\,\ddot{x}_{g,max}$ between the deck and the substructure, the kinematic ductility $\mu_k = x_{max}/(F_y/K_{el}) = x_{max}/x_y$, or an equivalent measure of the damage sustained by the dissipation device, the maximum force transmitted to the substructure $\eta_{max} = F_{d,max}/m\,\ddot{x}_{g,max} = \eta_y\,(1+\kappa(\mu_k-1))$ and some energy related response quantities.

Ground motion model

A great attention should normally be devoted to the definition and modeling of the seismic action. In fact, the effectiveness of the design of a protective scheme depends strongly on the knowledge level of the earthquake expected at the site. Further, it is generally recognized that acceleration time histories artificially generated are unduly conservative and whenever possible it is preferable to use actual seismic records to characterize the seismic action. However, as long as a detailed seismic zoning, capable to provide expected earthquake magnitude, source distance and site conditions, is lacking, it is preferable to revert to the generation of artificial accelerograms compatible with coded spectra, if some generality of the results is sought. Based on the above consideration, two families of pseudo-stationary accelerograms have been generated by means of the THGE program, (15), using the indications given in (10) for the characterization of the spectrum profiles. Two different profiles have been considered: soil type A and C representative respectively of "stiff" and "soft" soil conditions (Figure 4a). The generated accelerograms have a 20 seconds duration, while the non stationary time behavior is taken into account using the trapezoidal envelope function suggested in ((7),(8)), with initial transient and stationary part of 3 and 12 seconds respectively (fig.4b).

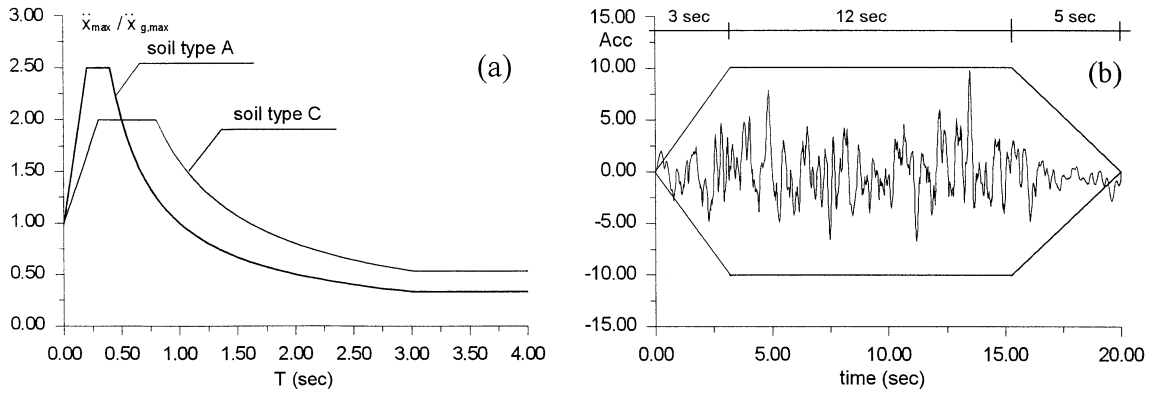


Figure 4

A set of analyses has been carried out in order to define the number of artificially generated accelerograms to be used for a meaningful statistical description of the results; in other words the minimum number of accelerograms, above which both the average value and the standard variation of the peak responses reach a sufficiently stable value. The sensitivity of the results against the number of accelerograms employed is reported in the last section of the paper; since it is shown that a good compromise value is around 10, a set of 10 generated accelerograms, for each soil type, has been used throughout.

Characteristic response quantities

A large set of preliminary numerical investigations has been carried out, aiming at evaluating the dependence of the characteristic response quantities on the device parameters V_d. It is important to stress that by the term response quantities are always meant here the average results obtained over the set of the 10 previously specified accelerograms. The results should indicate: (a) the quantities showing more regular variation and hence candidate to represent the objective function in view of the subsequent optimization analyses, (b) the sensitivity of the model response with respect to the interested variables, (c) the range of engineering interest for the model parameters. The variation of the response quantities against the parameters of the device, η_y, T, and κ, has been computed and, for comparison purposes, these quantities have been grouped into four different homogeneous sets: static, kinematic, damage and energy quantities. The first two classes, representative of the structural behavior, are of interest for the serviceability and limit state of the bridge, and include, among the others, the maximum force transmitted to the substructure, η_{max}, and the maximum relative and residual displacements, ζ_{max} and ζ_{res}; similarly the third class represents the low cycle fatigue of the dissipating device and comprises the kinematic and hysteretic ductility, μ_k and μ_h, and a novel damage index, DF, introduced in (2), (and discussed in a companion paper in this workshop); the fourth class represents the global behavior and comprises, in turn, the relative and absolute input energy, E_{ir} and E_{ia}, (see for example (17)), and the hysteretic energy E_h. The results indicate that: (i) it appears that the response quantities depend on the model parameters in a well behaved fashion, (ii) among the response quantities the energy quantities show the best regularity. As concerns the feasible range of the device parameters, V_d, that is the range outside which the corresponding characteristic structural response quantities would attain values beyond practical interest, it has been found to coincide with the intervals:[$0.03 \leq \eta_y \leq 0.45$; $0.5 \leq T \leq 3.0$ sec; $0 \leq \kappa \leq 0.1$]. The motivations for the adopted bounds are the following: the bounds on T avoid excess of ductility or displacement demand; lower values of η_y are limited by the braking force, whereas higher values result in an anti-economical use of the dissipation device that would not yield significantly; finally values greater than 0.1 for κ would lead to unreasonably large values of the force transmitted to the substructure, in contrast with the protection philosophy.

Optimal design formulation

The set up of effective design criteria is closely related to the pursued targets. In the present case the target is twofold: (i) on the one hand the economy of the structure requires that the effects induced by the seismic action should be kept at a minimum, both in terms of the maximum force η_{max} transmitted to the substructure and in terms of the relative or residual maximum displacements ζ_{max}, ζ_{res}, acceptable for the deck.; (ii) on the other hand the economy of the protection system requires that the performance of the device should be kept at a maximum, consistently with an acceptable damage level.

An appropriate mathematical framework for a comprehensive treatment of the above, in part mutually conflicting, demands corresponds to formulate and solve a multi-objective optimization problem.; and in fact a more direct reference to such an approach is presented in a previous paper, (5). Here the optimal design problem is, more simply, presented as a scalar optimization where the original problem of selecting the design variables V_d , so to get both the maximum exploitation of the device and the simultaneous attainment of minimum values of the structural response control variables, V_c, which comprise both limit and service conditions, has been split into two distinct and sequential phases. First, the range of the V_d values that provide unconstrained maxima for a properly selected objective function, representative of the device performance, is computed; subsequently, an "a posteriori" check is carried out to find out the limitations placed by the control variables V_c on the unconstrained optimal range.

The idea of formulating the design problem of energy dissipation systems as the optimal, (min or max), of some selected scalar functions has been used in several studies, starting from the early ones (11), and has been often associated with the use of energy concepts. Using the experience drawn from previous works on specialized design problems, (4), (6), an objective function has emerged whose maximization leads to satisfactory design for a large class of applications. This function, called here *EDI*, Energy Dissipation Index, is defined as the ratio of the integral over time of the energy dissipated in the dissipation system, to the corresponding integral of the relative energy input by the earthquake:

$$EDI = \frac{\int E_h dt}{\int E_{ir} dt} \tag{2}$$

EDI appears, from the definition, as a function of time, but it is its maximum value over time which is of interest. It may be interpreted as a performance index of the dissipation device, because it represents the portion of the input energy that it is able to dissipate; maximizing this index substantially corresponds to request the dissipation device to dissipate as much as possible of the energy input to the structure by the ground motion; at the same time maximizing *EDI* corresponds also to minimize its complement to 1, which expresses the part of the input energy which is available for damaging the structure.

The choice of *EDI* has been found, (3), to present also other advantages: (i) *EDI* shows very regular behavior both versus time, (being an almost non decreasing function over time which reaches its final maximum value rather rapidly with respect to the duration of the excitation) and with respect to the variation of the structural parameters, (presenting, in the space of the design variables, well defined maxima, which are also relatively independent on the details of the input used); (ii) when basing the design choices on the maximization of *EDI*, all the relevant response parameters, which is important to control, show very satisfactory values, which represent a good compromise with respect to conflicting needs, so that it appears that by maximizing *EDI* a multi-objective optimization problem is indirectly solved. All the considerations anticipated will find an immediate verification in the particular application at hand.

The design variables and the control variables used in the present context are, respectively, the already defined device parameters and a selection of the characteristic response quantities:

$$V_d \equiv [0.03 \leq \eta_y \leq 0.45 \ ; \ 0.5 \leq T \leq 3.0 \text{ sec}; \ 0 \leq \kappa \leq 0.1] \tag{3}$$

$$V_c \equiv [\eta_{max},\ \zeta_{max},\ \zeta_{res},\ \mu_k,\ \mu_h,\ DF,\ E_h,\ E_{ir}] \tag{4}$$

Optimal design graphs

In the present application it has been further verified, and will be shown, by an example, later, that the energy ratio *EDI* is practically independent on the hardening parameter κ. Consequently, it is possible to restrict the search space of the design variables to the (T, η_y) plane so that the graph of the *EDI* function can be easily analyzed through a geometric contour lines representation (Figure 5a). However, for interpretation purposes, it is more instructive to examine the different cross sections of *EDI*, (T=*const* , η_y), where T plays the role of a parameter, as shown in Figure 5b. From inspection of the figure it appears that it is possible to locate a well defined maximum of *EDI* for each cross section *T=const*; it comes out, further, that the location of such a maximum increases in definiteness as T increases and that the intensity of the maximum is almost independent on T.

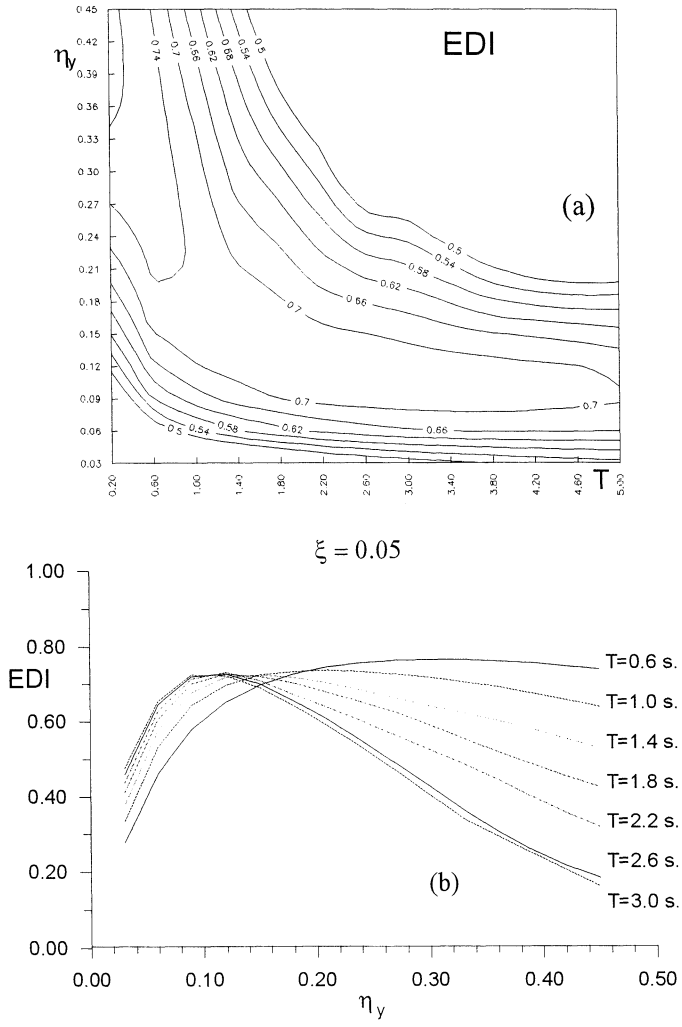


Figure 5 – Representation of the *EDI* surface: a) by contour lines, b) through cross sections drawn for T = *const*.

The anticipated independence of *EDI* on the hardening parameter κ is demonstrated by the observation of Figure 6.

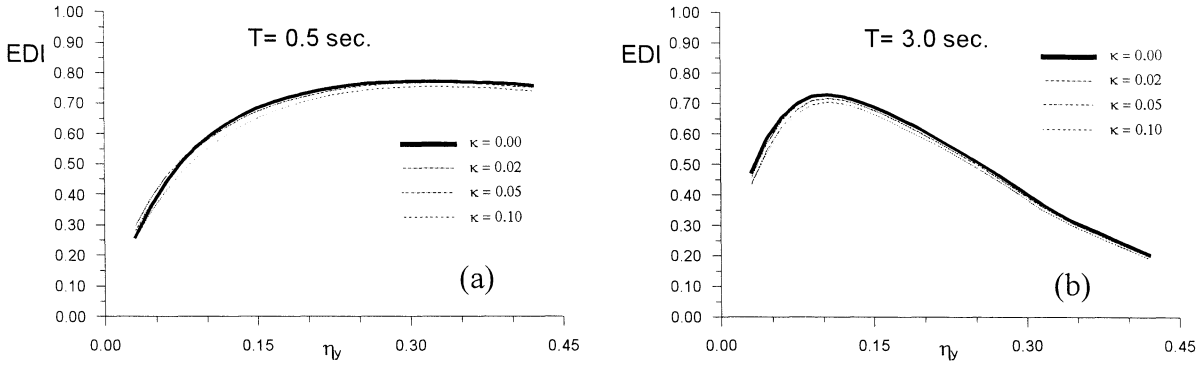


Figure 6 –*EDI* - η_y curves for different values of the elastoplastic stiffness κ.
(a) T = 0.5 sec., (b) T = 3.0 sec. – soil type C, ν = 5%, β = 0%.

The representation given by Figure 5 can also be employed to construct the optimal design curves in the plane (T, η_y); to this end it suffices to draw for each T the corresponding η_y for which *EDI* has a maximum. Such graphs, shown in figure 7 for both soil types A and C, constitute the sought optimal design curves and can also be interpreted as design spectra of the yield force in the dissipation device. It is important to note that these optimal design curves can be used independently of κ and do assure the maximum possible exploitation of the protection devices; in this respect note also that η_y remains approximately constant for $T \geq 1.5$–2 sec..

However the choice of a particular couple of points, T, η_y, along the optimal curves, does not automatically guarantee the satisfaction of other important conditions, related to the limit and service conditions of the bridge. To this end, using the optimal design values, a number of further curves has been constructed in a similar way, involving now the characteristic response quantities included in the control variable set, V_c. These curves are plotted in figures 8-11, superposed to the optimal design curve for comparison purposes. For brevity, only the η_{max}, ζ_{max}, ζ_{res}, μ_k and μ_h variations are shown, and only for the soil type C conditions.

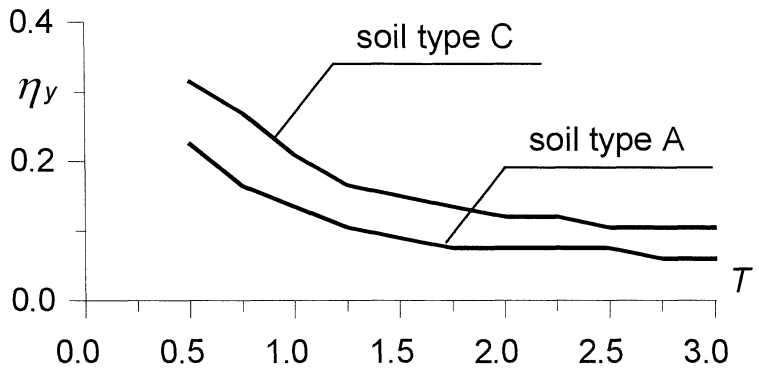


Figure 7 – Optimal design curves for the yield force of the dissipation device

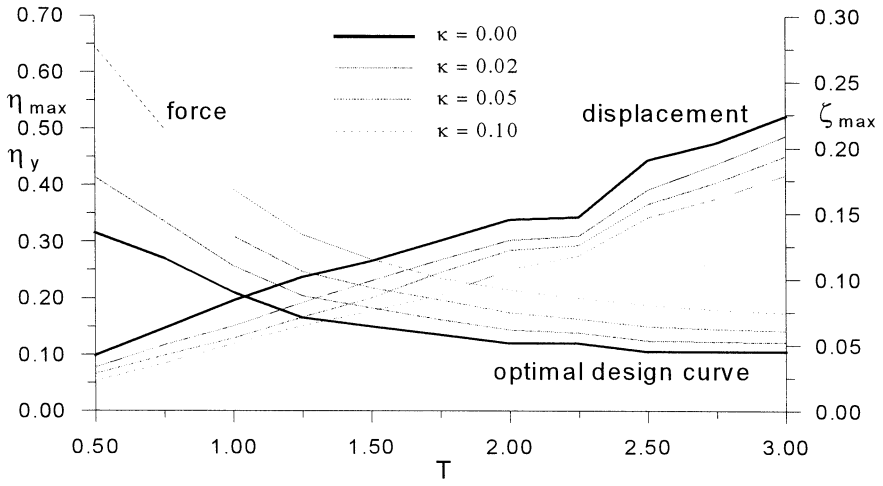


Figure 8

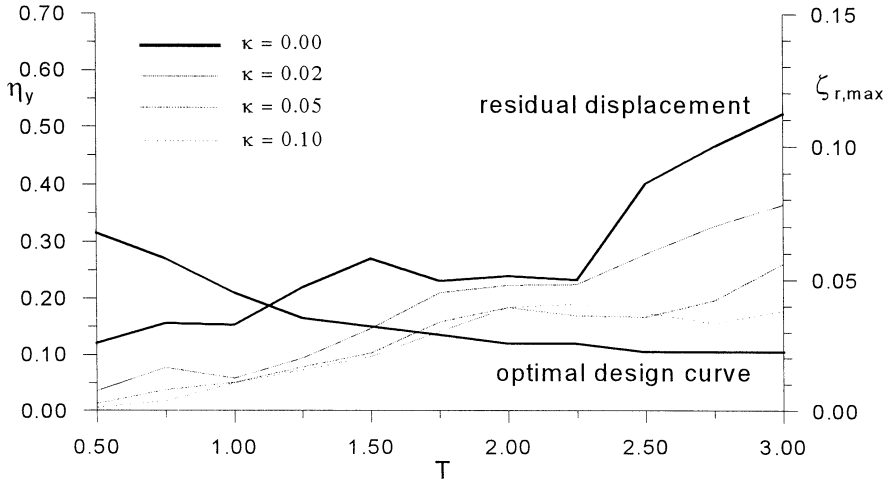


Figure 9

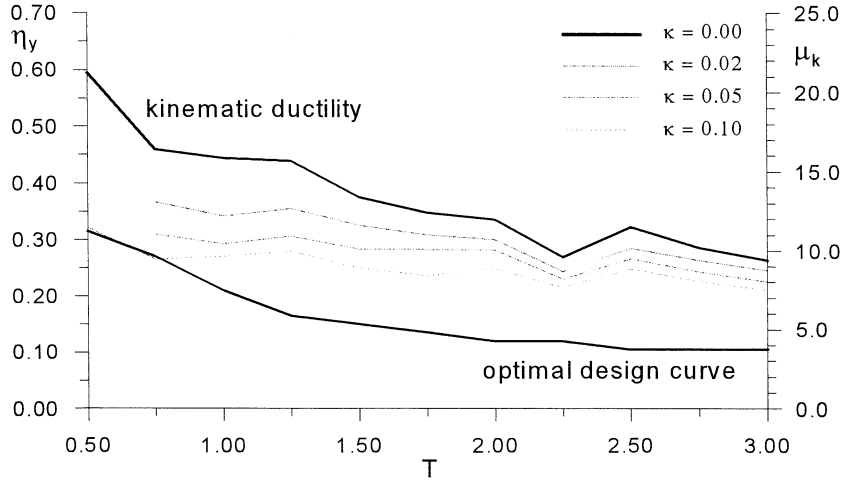


Figure 10

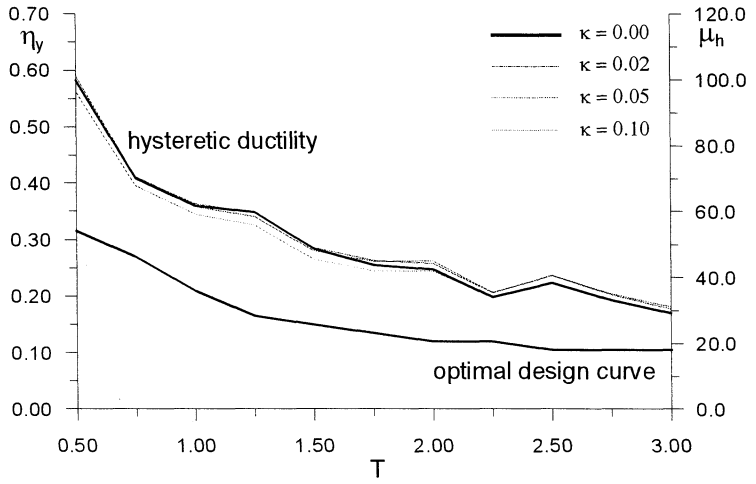


Figure 11

The use of graphs like the ones presented in Figures 8-11 allows for some flexibility in the design. In fact, as concerns the limit state conditions, one can start by fixing the optimal design values V_d of the dissipation device and then check if the limitations imposed by the control variable V_c turn out to be satisfied; otherwise the acceptable limit values for the control variables V_c can be predefined and then the optimal "constrained" design variables V_d derived.

A further flexibility is introduced by considering that the optimal design solutions, as presented through cross sections of the *EDI* surface at constant *T*, although generally well defined, present, specially for lower periods, some flatness, (Figure 5b, 6a). This means that points in the neighbor of the optimal are still good design solutions, that is, the locus of feasible design range can be extended from a curve to an area, if points within a predefined tolerance with respect to the maximum *EDI* are equally well accepted. The construction of the extended design locus, corresponding to a 5% tolerance on the optimal *EDI* values, is presented in Figure 12, while a direct check of the alteration of the response quantities against a modification of the design variables can be performed on graphs like the ones of Figure 13.

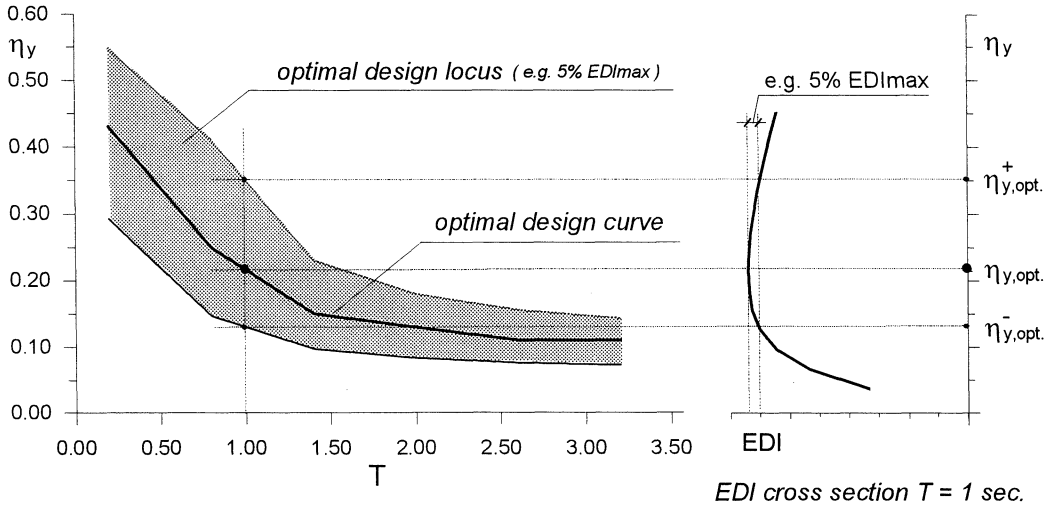


Figure 12

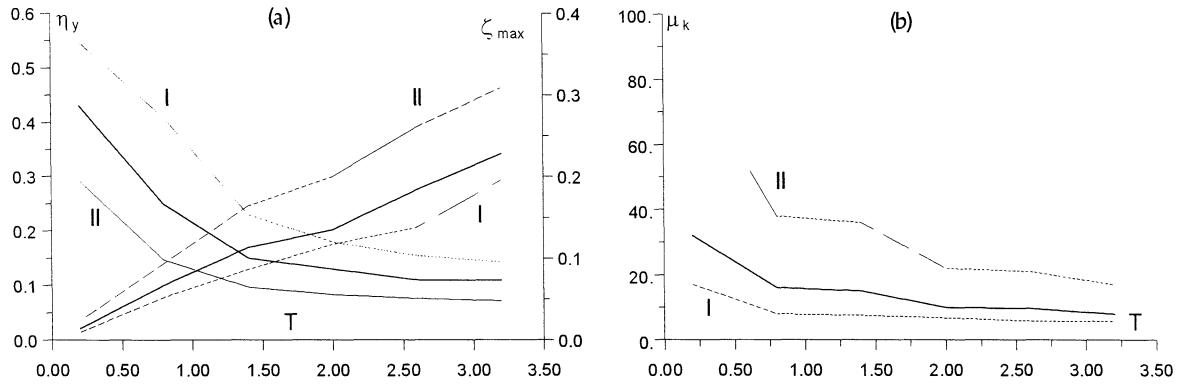


Figure 13

Finally, as concerns the service conditions, let's consider, just as an example, the limitations imposed by the braking force F_b to both the yield force F_{max} and the elastic stiffness K_{el} of the dissipation device. In the plane of Figure 7, the F_b force spectrum is represented by a horizontal straight line, whose position cannot be fixed independently of the seismic zone intensity, because of the adopted normalization, and depends also on the ratio w/L, where w and L are respectively the weight and length of the bridge deck. The limitations played by F_b are therefore case dependent and, generally speaking, it can be only said that, the lower will be C or w/L, the higher will be the restrictions imposed by F_b on the optimal design values.

Comparisons with some Italian design guidelines

An interesting topic is the comparison of the presented design results with the indications of two recently issued Italian guidelines. The first ones have been issued by Autostrade, an Italian company owner of the largest Italian highway network, and are specifically devoted to bridges, (7), (8), the second ones are more recent, more general in scope, since they refer to all types of isolated structures, with a specific section for bridges, and have been authorized by the Consiglio Superiore dei Lavori Pubblici, an Authority of the Italian Ministry of Public Works, (13). These two are, presently, the only instructions available in Italy for the problem under study. Both guidelines share the philosophy of relating the allowed seismic damage to the seismic intensity, according to different damage levels; in both guidelines the lowermost intensity level, (level 1), corresponding to earthquakes from low to moderate, is associated to a peak ground acceleration which is a fraction of the one associated with the higher intensity level, (level 2), corresponding to strong earthquakes. The level 1 intensity results the most demanding for the design of the dissipation device, in both guidelines; in fact, for this case, any damage of the device is excluded, so that a lower bound to the yield force of the device is imposed which practically determines the design.
Just as an example, let's refer to the case of the guidelines issued by Autostrade, where the level 1 earthquake corresponds to a p.g.a. $\ddot{x}_{g,max} = Cg/4$. The comparison between the two design curves (labeled criterion "[*]", from (7), and criterion "[P]", the one herein proposed) is given in Figure 14 where it is possible to note that the optimal design force η_y of the "[P]" case is considerably lower than the corresponding one of the "[*]" case. As a consequence, if the "[P]" criterion would be adopted, then some damage for the device should be accepted, also for moderate earthquakes, (level 1 intensity). It is then interesting to compute the actual damage suffered by the dissipation device for

moderate earthquakes and to compare this latter with the damage suffered for strong earthquake, $\ddot{x}_{g,max} = Cg$ (level 2), in which case also the "[*]" criterion allows damage.

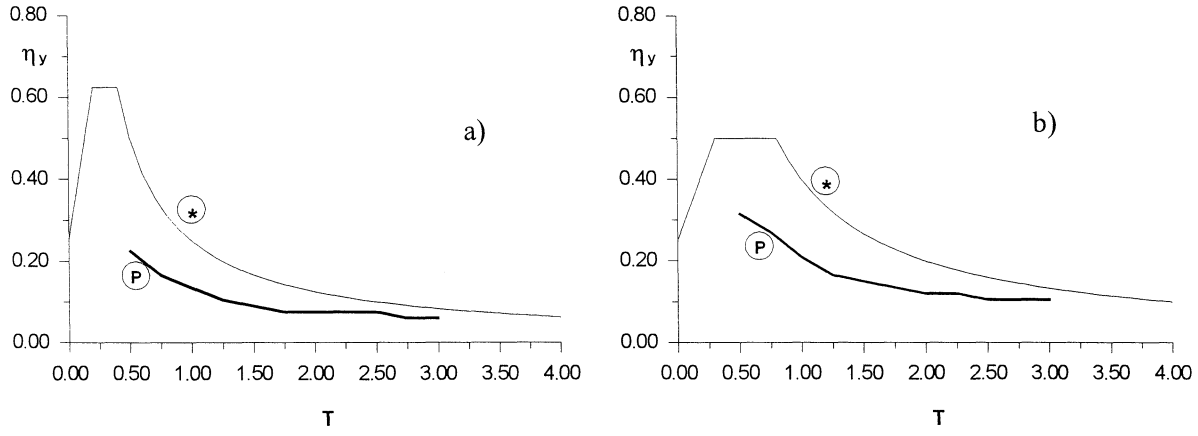


Figure 14 - Design spectra for η_y: [*] lower bound from (7), [P] proposed design graphs; a) soil type A; b) soil type C

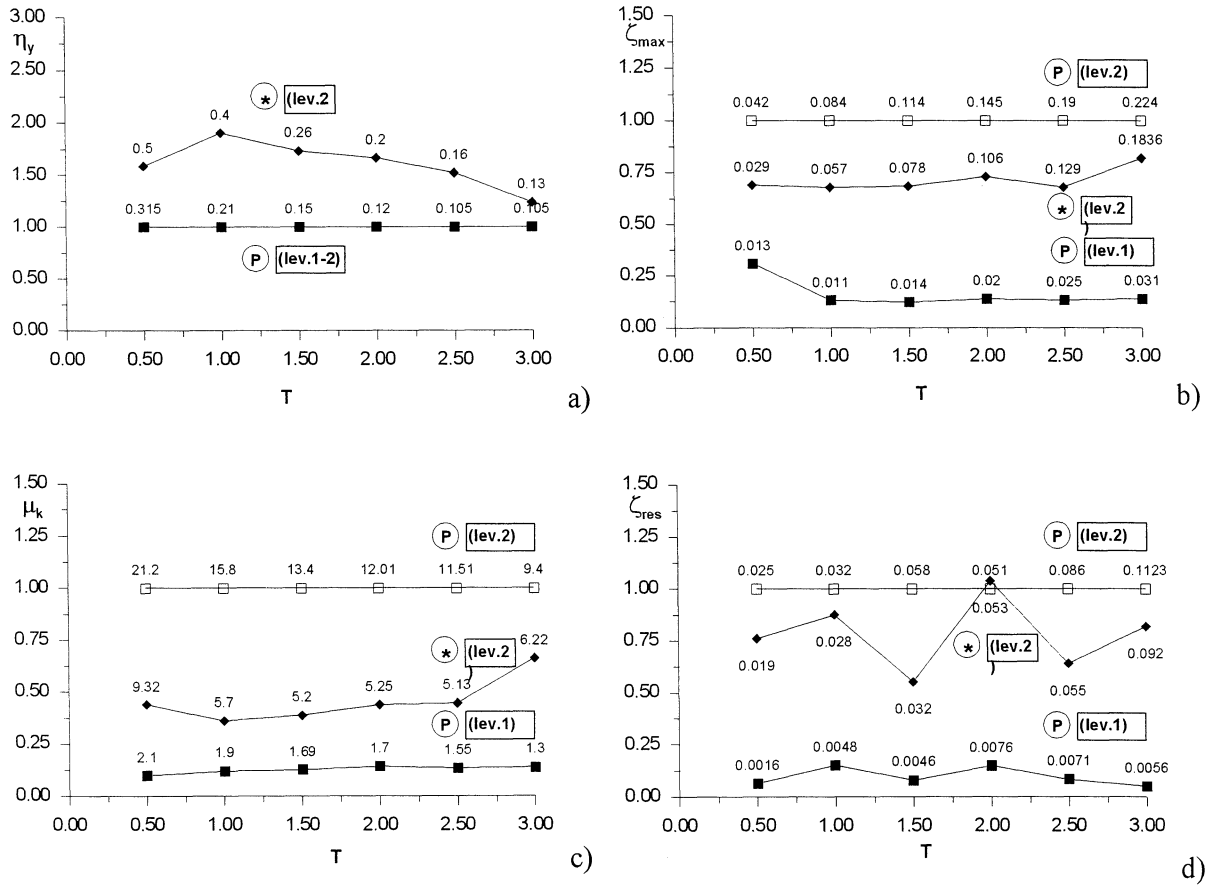


Figure15 – Comparison of the characteristic response quantities computed according to the "[P]" and "[*]" design criteria; (a) η_{max}, (b) ζ_{max}, (c) μ_k, (d) ζ_{res}; (soil type C - ν=5%, β=0%).

The relative differences between the effects of using the two design criteria are shown in Figure 15, where, for a better understanding, the data relative to the "[P]" criterion have been normalized to unity. Given the kinematics ductility μ_k the role of damage measure, Figure 15c shows that, at the design level 1, the dissipation device remains in the elastic range for the "[*]" criterion, whereas it sustains very limited damage for the "[P]" criterion; on the other hand, at the design level 2, the damage associated with the "[P]" criterion is about 2 times greater than the one associated with the "[*]" criterion, as expected, since the proposed optimal design is based on the assumption of maximum exploitation of the dissipation device. In any case, when the absolute values are considered, in place of the relative ones, as also reported, for all response quantities, in Figure 15, it is observed that the maximum value for μ_k is around 20; such a value is completely acceptable, as confirmed by the results found in the literature and by the ones which would be found in association with more sophisticated damage indexes, as the one, DF, proposed in (2). In view of the above, it is hence important to assess the gain expected if the "[P]" criterion is substituted for the "[*]" criterion. To this end, and using the same normalization as before, the relative differences in the response quantities η_{max}, ζ_{max}, ζ_{res} are shown in Figure 15a, 15b, 15d. In the case of strong earthquakes, (level 2), the comparison is favorable to the "[P]" criterion; in fact it shows that for the "[*]" criterion it is necessary to accept an increase of about 50% of the force, against only a 25% reduction of the relative or residual displacements; on the other hand for moderate earthquakes, (level 1), both the device damage and the residual displacements, only present for the "[P]" criterion, are sufficiently small that neither substitution nor re-centering operations are required, so that the operational effectiveness of the protection system is not compromised.

Sensitivity analyses

The two problems of the dependence of the results on the level and type of the additional structural dissipation, other than the one supplied by the installed protection devices, and on the number of accelerograms used in the analyses, have been studied separately. For the first problem, in fact, the conventional damping value $\nu = 5\%$, as given in (8), and used for the basic analyses, might appear oversized; further, if different dissipation sources exist, these latter should be more realistically attributed to the friction provided by the conventional bearings. A further set of design curves has then been constructed, according to the following values: (a) reduced viscous damping ν=2% and (b) reduced viscous damping ν=2% plus friction contribution β=2%. The comparison of the results

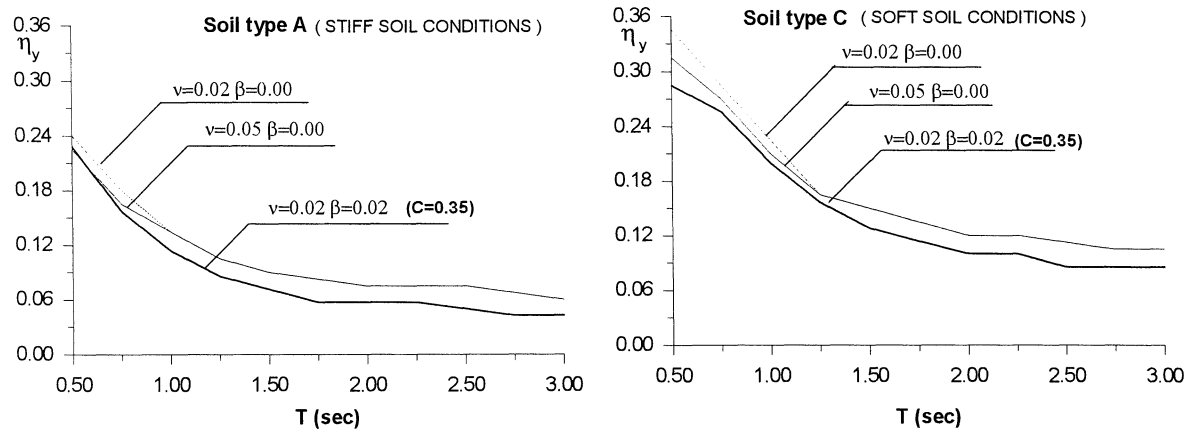


Figure 16

is shown in Figure 16 for the two type of soil conditions. From the figure it can be noted that the the viscous damping reduction has almost negligible effects, and only in the region T<1 sec.; while the

simultaneous presence of friction produces a non negligible reduction of the optimal yield force parameter, as it could be expected since F_f sums up with F_{max}, (Figure 3).
For the second problem, to study the "asymptotic" behavior of the results against the increasing number of accelerograms, an homogeneous sample of 30 acceleration time histories has been generated, which includes the 10 accelerograms used for the numerical optimization. With reference to the example case defined by the following design parameters: η_y=0.2, κ=0, T=1 sec., a number of analyses has been performed, using sets of 5, 10, 15, 20, 25, 30 accelerograms; these sets have been obtained by using different combinations of the 30 generated acceleration time histories. For each analysis the results have been expressed in terms of the ratio between the standard deviation and the mean value of the considered response quantities, and then plotted as a function of the number of accelerograms used within each set. The inspection of the plots, obtained as said above, has led to the conclusion that the results stay almost constant, from sets of 10 accelerograms on. To give an estimate of the reliability of the results reported in the previous paragraphs, the deviations computed for the set of 10 accelerograms used in the numerical optimization, (case A in table 1) are listed together with the average deviations computed for all of the other sets, (case B). From the listed values it can be observed that the spread of the results depend on the considered quantity. In particular, the spread is maximum in the case of the residual displacement ζ_{res}, whereas it turns out to be close to zero for the index *EDI*. This latter result confirms, once more, the effectiveness of such an indicator when it is given the role of the objective function. Finally, by the comparison of the results of case A and B in table 1, it is concluded that the 10 accelerograms used for the numerical optimization constitute a meaningful set in view of the reliability of the results.

Table 1 – Deviation of the results as a function of the number of the accelerograms

case	ζ_{max}	ζ_{res}	E_{ir}	E_h	*EDI*	μ_k	μ_h	*DF*
A	0.26	0.62	0.09	0.09	0.01	0.23	0.14	0.30
B	0.28	0.64	0.10	0.10	0.02	0.29	0.11	0.31

Conclusions

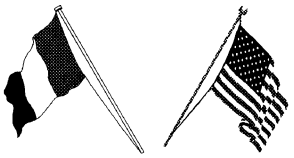
It is has been presented a methodology for the optimal design of energy dissipation devices used for the seismic protection of typical bridge structures. The proposed formulation attempts to solve the problem of searching the conditions of maximum exploitation of the dissipation device, the key element in the protection scheme, yet complying with practical constraints related to both the bridge and device behavior. The formulation is based on an appropriate definition of an energy based performance index for the dissipation device, and on its maximization. The adopted structural model accounts for the nonlinear interaction between bridge deck and substructure and for friction in the bearings, but has been kept as simple as possible, so to focus the attention only on very essential aspects of the problem; single degree of freedom systems, with rigid-elastic-plastic restoring forces, have, hence, been considered. The results of the investigations indicate that it is possible to construct optimal design graphs which allow for a simple selection of the design parameters of the dissipation device, while respecting predefined constraints required by the serviceability and limit states of both the bridge and the device. In spite of the extreme simplicity of the adopted model, the results presented are already capable to provide indications useful for designing the seismic protection of bridges with simply supported decks resting on relatively stiff piers, as compared to the stiffness of

the protection devices. Moreover the methodology has the potential to be generalized to different, more complex, structural protection situations.

References

1. I.G. Buckle, "Future directions in seismic isolation, passive energy dissipation and active control", *Proc. of a Seminar on Seismic Isolation, Passive Energy Dissipation and Active Control*. Report no. ATC-17-1, 1993, pp. 825-830
2. V. Ciampi, M. Arcangeli, S. Perno, , "Characterization of the Low-cycle Fatigue Life of a Class of Energy Dissipating Devices", *Proc. of the 2nd Europ. Conf. on Struct. Dynamics*; EURODYN 93, Trondheim, Norway, Vol.1, 1993, pp. 137-144
3. V. Ciampi, M. De Angelis, "Optimal Design of Passive Control Systems Based on Energy Dissipation for Earthquake Protection of Structures", *Proc. of the 3rd Europ. Conf. on Struct. Dynamics*; EURODYN 96, Florence, Italy, Vol.1, 1996, pp. 525-532
4. V. Ciampi, M. De Angelis, F. Paolacci, "Design of yielding or friction based dissipative bracings for seismic protection of buildings", *Engineering Structures*, Vol.17, 1995, pp. 381-391
5. V. Ciampi, M. De Angelis, C. Valente, "On the optimal design of energy dissipation devices for the seismic protection of bridges" *Proc. of the 11th World Conf. On Earthquake Engineering*, Acapulco, Mexico, 1996
6. M. De Angelis, V. Ciampi, "Effectiveness of dissipative connections on improving the earthquake response of adjacent structures", *Proc. of the 10th European Conf. On Earthquake Engineering*, Vienna 1994, (G. Duma Ed.), Balkema, Rotterdam, 1995, pp. 1891-1896
7. M. Dolce, G. Ducci, "Istruzioni per la progettazione antisismica dei ponti con l'impiego di dispositivi isolatori/dissipatori", *AUTOSTRADE*, Anno XXXIII, n.1, Gennaio-Marzo 1991, pp. 110-123, (in Italian)
8. M. Dolce, G. Ducci, "Seismic Protection Guidelines for Highway Bridges in Italy", *Preprint Third World Congress on Joint Sealing and Bearing Systems for Concrete Structures*, Vol.2 - *Bearings and Isolators*, Toronto, Ontario, Canada, Oct. 27-31, 1991, pp.1321-1338
9. D.J. Dowdell, S. Cherry, "Optimal response control of friction damped structures", *Proc. of the 10th European Conference on Earthquake Engineering*, Vienna 1994, (G. Duma Ed.), Balkema, Rotterdam, 1995, pp. 2051-2056.
10. EC8 - Commission of the European Communities *Eurocode No. 8: Structures in Seismic Regions - Design - Part 1*. Report no. EUR 12266, Brussels, Luxembourg, 1989
11. A. Filiatrault, S. Cherry, "Seismic design spectra for friction damped structures", *ASCE, Journal of Structural Engineering*, Vol. 116, N.5, 1990, pp. 1334-1355
12. J.A. Inaudi, J.M. Kelly, "Optimum damping in linear isolation systems", *Earthquake Engineering and Structural Dynamics*, Vol. 22, 1993, pp. 583-598.
13. "Linee guida per progettazione, esecuzione e collaudo di strutture isolate dal sisma", Pubblicazione autorizzata dal Consiglio Superiore dei Lavori Pubblici, *Ingegneria Sismica*, Anno XIV- n.1 - Gennaio-Aprile 1997, pp. 31-48 (in Italian)
14. A. Mokha, M.C. Constantinou, A.M. Reinhorn, "Further results on frictional properties of teflon bearings" *ASCE, Journal of Structural Engineering*, Vol. 117, N.2, 1991, pp. 622-626
15. A. Preumont, " The generation of spectrum compatible accelerograms for the design of nuclear power plants", *Earthquake Engineering and Structural Dynamics*, Vol. 12, 1984, pp. 481-497
16. R.E. Scholl, "Design criteria for yielding and friction energy dissipators", *Proc. of a Seminar on Seismic Isolation, Passive Energy Dissipation and Active Control*. Report no. ATC-17-1, 1993, pp. 485-495

17. C.M. Uang, V.V. Bertero, "Evaluation of seismic energy in structures", *Earthquake Engineering and Structural Dynamics*, Vol. 19, 1990, pp. 77-90



Session III

Energy Dissipation as a Technological Answer to Highly Demanding Design Problems
Renzo Medeot

Seismic Isolation of Railway Bridges
Mauro Dolce, Domenico Liberatore, Corrado Bonuccelli and Giuseppe Traini

Applications of Isolation Bearings to Bridges
Manouchehr Karshenas and Iraj I. Kaspar

Seismic Bearings for Large Span Bridges
Roy A. Imbsen

Design of the Caltrans Seismic Response Modification Device (SRMD) Test Facility
Gianmario Benzoni and Frieder Seible

ENERGY DISSIPATION AS A TECHNOLOGICAL ANSWER TO HIGHLY DEMANDING DESIGN PROBLEMS

by

Renzo MEDEOT

FIP Industriale - Italy

ABSTRACT

The spontaneous idea that most commonly comes to mind to seismic engineer practitioners is that of interpreting an earthquake in terms of forces and deformations induced upon the structure. Actually, forces and displacements are but a mere manifestation of a seismic attack rather than its very essence. An earthquake is an energy phenomenon against which defense strategies must be organized duly accounting for its intrinsic nature.

The paper illustrates how the use of energy concepts makes it possible to delineate an anti-seismic design strategy that takes into account the type of structure and yields maximum advantage in terms of existing hardware. It also presents a highly demanding retrofit project in which this design approach is used.

1.-INTRODUCTION

What does an earthquake consist of and which are the mechanisms that produce it is known by now to the public at large, thanks to the programs of information disseminated throughout most countries, especially after the occurrence of an important seismic event.

Notwithstanding, not all seismic engineers today have a clear vision as to how such a disastrous natural phenomenon visits damages upon the works constructed by man's creative genius. The most spontaneous idea that comes to mind to seismic engineer practitioners is that of interpreting an earthquake in terms of forces and deformations induced upon the structure. As a consequence, there is a tendency to think only about increasing the strength of the latter.

Actually, forces and displacements are but a mere manifestation of seismic attacks rather than their very essence. Earthquakes are essentially energy phenomena against which defense strategies must be organized duly accounting for their intrinsic nature.

Although Housner already suggested an energy-based design method in 1956, it has been only recently that this approach has gained widespread attention. Akiyama (1985), Uang [1] and Bertero [2] (1988) made a valuable contribution to the development of the theoretical aspects of an energy-based approach.

However, the principles of Physics that govern the effects of dissipation on the control of dynamic phenomena were studied more than two centuries ago. Nonetheless, their practical application has come about much later and within a much different time-frame in several sectors of Engineering.

The sector that was the first to adopt such damping technologies was the military (France, 1897) followed by the automobile industry applications to ensure comfort and stability of motor vehicles.

It took some time before Civil Engineering applications were forthcoming. In effect, it is necessary to arrive at the last quarter of this century to find their first appearance.

One of the factors that may have delayed the application of dissipative systems to Civil Engineering could be the innate diffidence of civil engineers toward mechanical devices ("machines") which, for the purpose of damping, have to be suitably inserted into a structure and properly interact with it.

A second delaying factor could be ascribed to the absence of reliable calculation methods (*i.e.*: modeling and dynamic analysis). That is, appropriate "***software***".

Nonetheless, the delay in development with respect to other engineering fields has been rapidly overcome during the last two decades. Progress has mainly been the result of newly developed design strategies taking hold (*e.g.*: Base Isolation) and the awareness that energy dissipation can be a powerful tool in the hands of the design engineer to control the response of structures struck by windstorms or earthquakes.

In other words, these natural events are being increasingly perceived as phenomena involving the transmission of mechanical energy instead of being interpreted only in terms of forces and displacements resulting from the simple application of mathematical equations.

However, said awareness has mainly concerned the academic world and has spread only to a limited extent amongst civil engineer practitioners.

And the last, but not least, delaying factor might be identified in the lack of mechanical devices capable dissipating energy, *i.e.*: appropriate "***hardware***".

In fact, newly conceived design strategies could not have found useful application without the parallel development of the hardware needed for their implementation.

Thus, several pioneering industries and research laboratories have decided to invest important resources in this field, inventing and perfecting a series of devices that exploit well known Physics phenomena and adapting them to the protection of structures.

2. THE ENERGY APPROACH

In order to gain a better understanding of this paper subject, some general concepts should be called to mind.

As it is known, any resistance criterion adopted in the dimensioning of a structure (*e.g.*: permissible stresses, limit states, etc.) always necessitates the verification that:

$$\textbf{DEMAND} \leq \textbf{CAPACITY} \tag{1}$$

where the terms **DEMAND** and **CAPACITY** assume, from time to time, their appropriate meaning.

Expression (1), sometimes referred to as Design Equation, is valid in Earthquake Engineering even when the energy concepts are applied in the sizing of the structural members.

In effect, let us consider the following energy balance equation (Bertero, [3]):

$$\mathbf{E_i = E_s + E_d} \tag{2}$$

where,

$\mathbf{E_i}$ is the energy input at the foundation of the structure due to ground motion

$\mathbf{E_s}$ represents the stored energy

$\mathbf{E_d}$ is the dissipated energy

The energy $\mathbf{E_s}$ can be stored in two distinct ways, to wit:

$$\mathbf{E_s = E_e + E_k} \tag{3}$$

where,

$\mathbf{E_e}$ is the elastic strain energy
$\mathbf{E_k}$ represents kinetic energy

The energy $\mathbf{E_d}$ can also be dissipated by two distinct mechanisms, and precisely,

$$\mathbf{E_d = E_h + E_v} \tag{4}$$

where,

$\mathbf{E_h}$ is the energy dissipated by hysteretic (or plastic) deformation.
$\mathbf{E_v}$ is the energy dissipated by viscous damping

$\mathbf{E_h}$ is associated with forces that depend only upon deformation (or displacements) while the energy $\mathbf{E_v}$ is associated with the forces **F** that depend only on the velocity **v** through a constitutive law of the type $\mathbf{F = C \times v^n}$ (exponent **n** ranging from 0-2).

By introducing expressions (3) and (4) in equation (2), we obtain the energy balance equation in the following form:

$$\mathbf{E_i = E_e + E_k + E_h + E_v} \tag{5}$$

When one compares the above equation to the Design Equation (1) it becomes clear that $\mathbf{E_i}$ can be interpreted as the Demand while the four terms of the other side of the equation can represent the possible capacities of the structure.

Equation (5) clearly points out the fact that the design engineer must, at the onset of his project, make a good estimate of $\mathbf{E_i}$ for the Design Earthquake.

The second step consists in the analysis of whether it is technically and/or economically feasible to balance the Demand only by means of the elastic behavior $\mathbf{E_s}$ of the structure through an increase in the elastic strength of its structural members or it is instead convenient to resort to the dissipative terms $\mathbf{E_h}$ and $\mathbf{E_v}$.

For a good number of years it was common practice to use, in addition to $\mathbf{E_s}$, only the term $\mathbf{E_h}$ through the inelastic (or plastic) behavior of the structure, *i.e.*: inducing deformations beyond the elastic limit of the structure. This is the so called ***traditional*** or ***conventional*** approach that is still currently used.

It should nonetheless be recalled that this dissipative mechanism results in structural member damage, whose repair can be very costly and can also imply the structure itself being out of service temporarily.

Only in recent years has it been recognized that it is possible to significantly increase $\mathbf{E_h}$ and $\mathbf{E_v}$ as well as control the entire structure through the use of energy dissipating devices inserted at properly determined locations. This is referred to as the ***Passive Energy Dissipation*** approach.

If it is not technically feasible or it is economically disadvantageous to balance the energy input $\mathbf{E_i}$ by $\mathbf{E_s}$ alone or through $\mathbf{E_s + E_d}$, there is still the option to attempt decreasing the energy input $\mathbf{E_i}$ itself. This can be accomplished through the so called ***Seismic Isolation*** approach.

Seismic Isolation was proposed over a century ago [5], but it has found extensive application only during the last two decades. Such delay finds its explanation in the lack of adequate seismic hardware suitable to effectively and reliably implement said Seismic Isolation techniques.

The most rational approach, whenever practically and economically feasible, is the one that resorts to all the terms in equation (2). This is the ***Hybrid Solution*** consisting of the combination of the Seismic Isolation and the Passive Energy Dissipation approaches. Hybrid solutions have gained preference amongst Italian Seismic Engineers.

3. THE SEISMIC HARDWARE

Before setting off to develop a project, the seismic engineer must make certain strategic choices and the same - beyond personal preferences - depend on the type of structure, the seismicity and geological nature of the site, the norms currently in force and other incidental parameters.

In the past, it was *also* necessary to take into account one more limitation; that is to say, the unavailability of suitable seismic hardware that could also prove to be reliable. Such a limiting factor does no longer exist.

Today, seismic engineers can rely upon numerous solutions and relevant types of seismic devices that have already been adopted with success within the last two decades. Said solutions, notwithstanding their large variety, can be roughly grouped into two main types, and precisely:

a. those that provide the ***structural members*** with sufficient flexibility, strength and ductility to absorb and dissipate the energy input; as mentioned earlier, these solutions are called ***"conventional design approaches"***;

b. those that aim at protecting the structure against earthquake damage by limiting the effects of a seismic attack (rather than resisting it) through the use of *seismic devices* properly inserted into the structure; this approach is usually referred to as ***"seismic mitigation"***.

Figure 1. in the next page, schematically illustrates the possible seismic design strategies ("seismic software") and their respective devices ("seismic hardware").

Without going deeply into the matter of selection criteria, which goes beyond the scope of this paper, certain useful concepts are reported below to facilitate understanding Figure 1.

The superior seismic behavior of hyperstatic structures, and bridges in particular, is well known as they call upon all structural members to work together at the critical moment.

However, construction techniques and the risk of occurrence of differential settling on the foundations often suggest the choice of isostatic arrangements for bridges.

The advantages of the two concepts can be maintained through the adoption of **hydraulic shock-transmitters** that create temporary restraints. In point of fact, the latter allow slow displacements (*e.g.*: those due to thermal variations) without appreciable resistance, but prevent those of sudden onset due to an earthquake. As a consequence, the structure remains isostatic under service loads while it becomes hyperstatic during a seismic attack through the creation of temporary restraints.

An interpretation of their function from the standpoint of the energy-based approach is that of increasing the overall capacity of the structure to store energy, both elastic and kinetic (in the sense that they force all the structural members to cooperate by moving jointly).

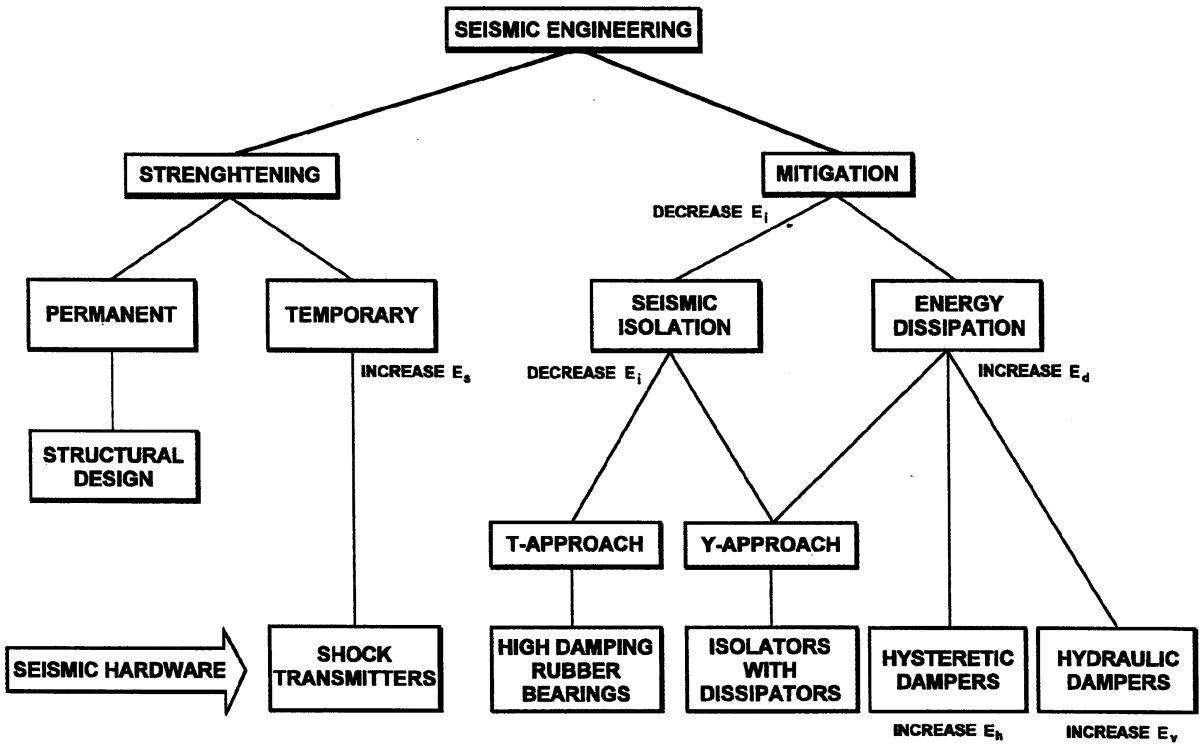


Figure 1. Seismic Design Approaches and the Respective Devices

Conversely, shock-transmitters do not lend any contribution to the dissipation of energy. Figure 1 shows that the alternative to ***Strengthening*** or *Conventional Design Approach* is ***Seismic Mitigation***.

This can be achieved through *Seismic Isolation* or *Energy Dissipation* (better yet, through a combination of both).

As previously stated, Seismic Isolation is a design strategy that aims to reduce the amount of energy input $\mathbf{E_i}$ at structure foundations. Said strategy can be implemented in two ways, both of which rely on "seismic isolators", to wit:

- Through the reduction of the seismic response subsequent to the shift of the fundamental period of the structure (the so called **T-Approach**).

- Through the limitation of the forces transmitted at the base of the structure (the **Y-Approach**). This approach is also characterized by a high level of energy dissipation that permits the control and reduction of relative displacements. [6]

In practical terms, the seismic hardware presently used to implement the T-strategy mainly comprises high-damping rubber bearings. Essentially, these are laminated rubber bearings fabricated from dissipative elastomer. Despite the name (high-damping...) their dissipating capacity is limited, because their equivalent damping ratio does not go beyond 15%.

An interpretation of their function from the standpoint of the energy-based approach is that of considering them reflectors of energy throughout the spectrum, with the exception of the frequencies close to the natural frequency of the structure. However, their dissipating capacity, though modest, nonetheless impedes the accumulation of energy through resonance.

The so called Y-approach in Seismic Isolation is achieved through the use of special Seismic Isolators which must be capable of ensuring the following four functions:

- transmit vertical loads
- provide lateral flexibility
- provide restoring force
- provide significant energy dissipation

Examples of special Seismic Isolators are the **Lead Rubber Bearings**, the **Friction Sliders**, the **Friction Pendulum** and the **Sliders with steel hysteretic dissipators**. Particularly, the latter have been developed by Italian industry. Sliders with steel hysteretic dissipators are so conceived as to maintain - *within the isolator* - a clear separation between the device which transmits vertical loads and provides lateral flexibility (first two functions) and the device that takes care of the horizontal actions (remaining two functions).

Vertical loads are transmitted through traditional sliding bearings of the "free" type (*i.e.*: elastomeric, pot or spherical bearings), while the other two isolator functions are provided through steel hysteretic dissipators. The latter can be of the most diverse geometric shapes, and at least a dozen different types have found practical application.

Several combinations of bearings and steel hysteretic dissipators are possible, and the choice of an optimal combination depends either on the basis of requirements to be fulfilled (*i.e.*: elastic stiffness, post-elastic stiffness, amount of displacement, dissipative efficiency, etc.) or considerations of a practical nature such as overall dimensions, ease of installation, maintenance, etc.

A recent inquiry demonstrates that, in Italy, the sliders with steel hysteretic dissipators have been utilized in over 80% of bridge seismic retrofit projects.

In terms of energy dissipating capability, Lead Rubber Bearings and the Friction Pendulum can easily reach 30% of equivalent damping ratio, while Friction Sliders and Sliders with steel hysteretic dissipators can even come virtually very close to the maximum theoretical value.

However, their dissipating capacity is limited by the need to provide sufficient restoring force. In the special Seismic Isolators, the interpretation of their function according to the energy-based approach is similar to that given for the high-damping rubber bearings. However, they are imperfect reflectors of energy in that they let high frequencies pass through. This is not significant in bridge design, but can constitute a disadvantage in some applications (*e.g*: civil edifices). Given their elevated dissipating capacity, the relative displacements are strongly limited and there is no danger of resonance to the point that, in the structures where they are utilized, it is even difficult to define a natural frequency for them.

If the adoption of Seismic Isolation is not feasible and the structure possesses sufficient flexibility (*i.e.*: appreciable relative displacements occur during an earthquake due to elastic deformation of its structural elements) then both Hysteretic Dampers and Hydraulic Dampers can be validly inserted into the structure to reduce its seismic response.

The interpretation of their function in terms of the energy-based approach is elemental: they serve to dissipate, in the form of heat, the earthquake induced mechanical energy by eliminating

(or at least minimizing) the energy dissipation demands (plastic hinge formation) in the primary structural members.

It should be noted that the amount of energy at play in a structure during a design level seismic attack ranges from 1 to 30 MJ ! (about 1000 -30000 BTU).

The above raises the fundamental question: "Will the seismic device survive the damage produced in itself by the energy it dissipates during an earthquake?".

To date, very few full-scale devices have been tested with an actual seismic input. The reason is quite simple: there are very few testing rigs in the world with adequate power to conduct such an experimental test (requiring between several hundred kW or even more than one MW depending on the size of the device) [9]. In effect, precisely this level of power at play should invite reflection on the part of design engineers when selecting the type of hardware.

It is important to point out that in both new and retrofit seismic project, the selection of the type of seismic hardware must not necessarily fall upon a single type of device. In many cases, the adoption of combinations of devices can accrue significant advantage.

Italian engineers are showing a trend toward increased interest in the adoption of different types of seismic hardware within the confines of a single project.

It can be said that a similar trend is taking hold elsewhere in the world as well. As examples of successful applications of the above in the United States, it is appropriate to mention the combination of High Damping Rubber Bearings with Hydraulic Dampers (Los Angeles City Hall -CA), as well as the combination of Isolators with steel hysteretic dissipators and Shock-transmitters (Marquam Bridge in Portland, OR)

3. THE MARQUAM BRIDGE

The seismic retrofit project of Marquam Bridge is the first example of the application in the United States of high dissipative capacity isolators in combination with shock transmitters developed and vastly applied in bridge seismic engineering in Italy during the last twenty years.

3.1 Description of the Structure

The Marquam Bridge was built in 1963 over the Willamette River (see Fig. 2); it comprises metal trusses carrying two superimposed roadways for a total length of 1,043 ft.

The present static arrangement is of typical "Gerber girder" construction in which the two end-girders have a cantilever beam towards the center of the bridge, upon which the suspended central truss is supported (see Fig. 4).

The two end spans measure 301 feet 6 inches, the central span has a total length of 440 feet - of which 260 feet comprise the central suspended truss. The values indicated for the spans represent the center to center distance between the piers. In plan view, the structure is characterized by a straight longitudinal axis.

The piers are reinforced concrete configured upon a two-uprights transverse framework connected by two beams (see Fig.3). The uprights have a center to center distance of 65 feet.

Their upper section is circular with a diameter of 12 feet while their lower section (below the high water mark) is elliptical (14 feet × 24 feet) with semi-circular ends.

The main axis of the section forms a skewed angle of approximately 20 degrees with the longitudinal axis of the bridge.

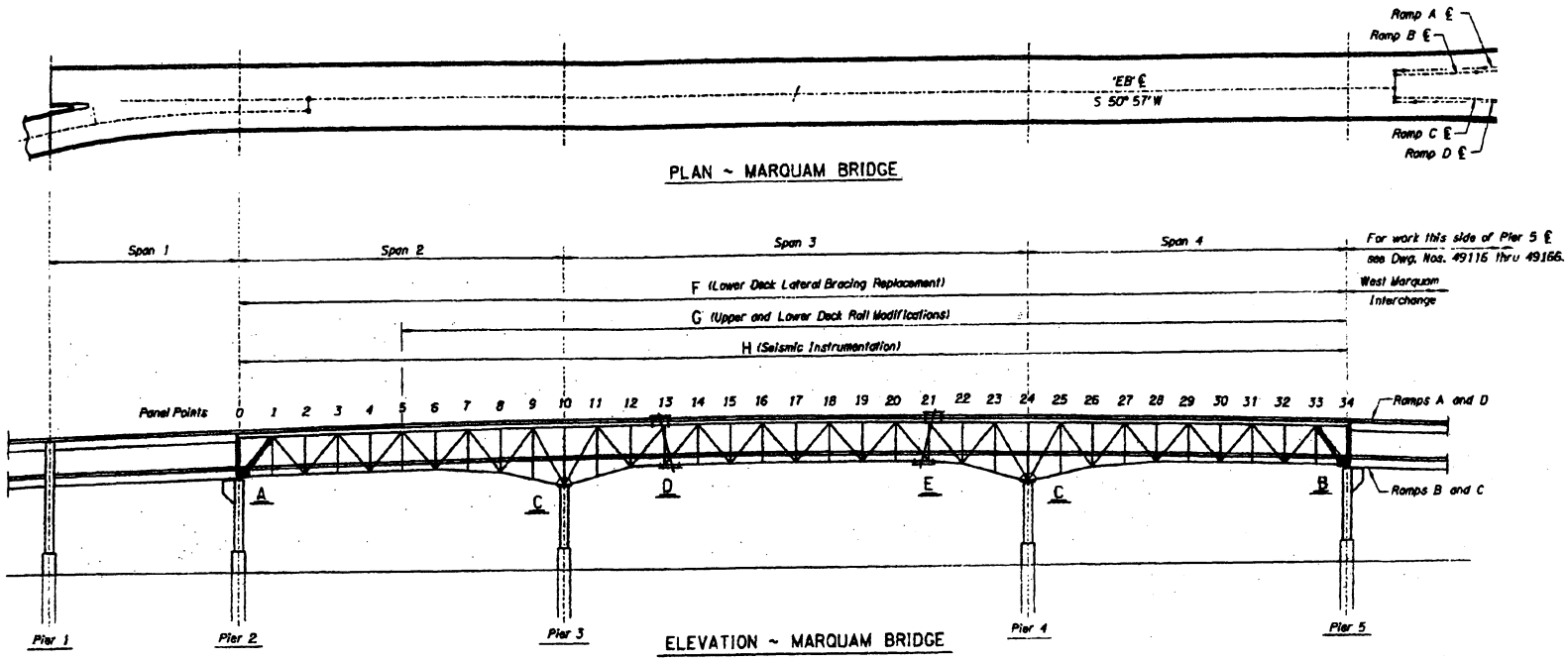


Figure 2. Plan and elevation of Marquam Bridge

The uprights are connected by means of rectangular section struts placed, one each, at the top and where the section of the uprights changes from elliptical to circular.

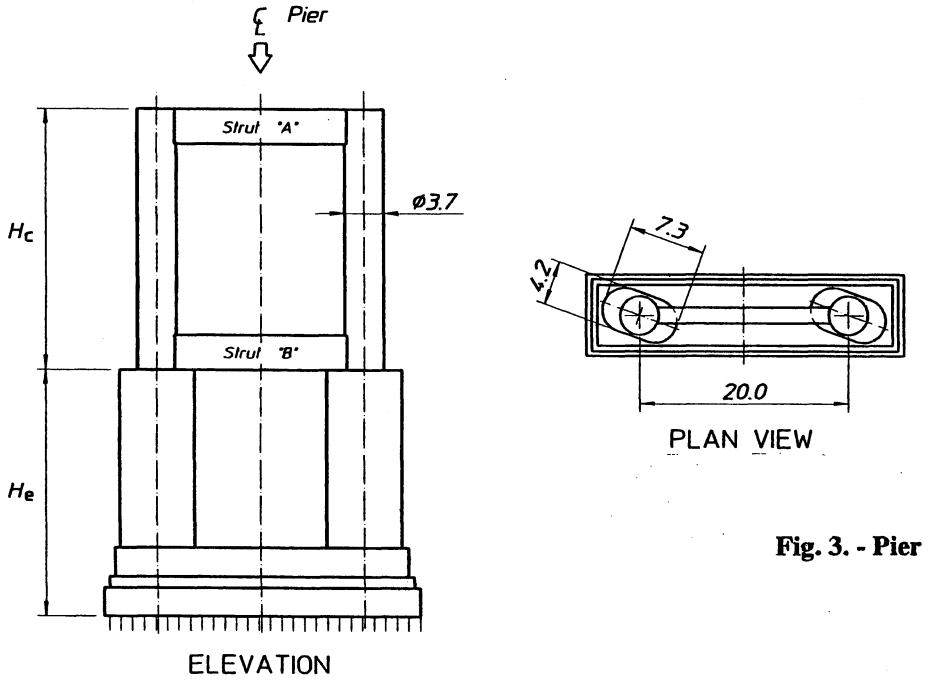


Fig. 3. - Pier

The height of the piers is listed in Table 1 below where H_c indicates the height of the upper circular section and H_e indicates the height of the lower, elliptical section.

Pier (#)	H_c (ft)	H_e (ft)
2	81	54
3	67	57
4	66	60
5	81	46

Table 1. - Height of Piers

3.2 Seismic Requirements

During the preliminary stages of the project, a multi-modal linear analysis using a design spectrum in accordance with the AASHTO standards was conducted on the existing structure by

way of orientation. The results demonstrated that the structure was absolutely incapable of resisting the Design Maximum Expected Earthquake.

It was decided at this time to proceed with a retrofit project for which the following requirements were advanced:

a. to attain the *total seismic protection* for the structure in the event of the Design Maximum Expected Earthquake in both the longitudinal and transverse directions.

b. to avoid the need for strengthening existing structural elements (i.e., piers, trusses, foundations, etc.).

c. to limit the relative displacements to values compatible with the existing gaps (longitudinal deflection not to exceed $\pm$ 5 in.).

"*Total seismic protection*" signifies that the entire structure shall remain within the elastic limits during the most severe expected seismic attack, i.e., any structural damage shall be avoided.

In addition to the observance of existing norms in force, said requirements aimed to minimize the direct cost of the intervention as well as indirect expenditures (*i.e.*: disruption of traffic).

The design engineers tried to satisfy the above mentioned requirements by using the seismic hardware that was then available in the United States, albeit without success.

This author diagnosed that the problem depended on the lack of adequate energy dissipating capacity on the part of the adopted hardware and suggested a relatively simple solution, which consisted of the replacement of the pre-existing vulnerable steel bearings (4 rockers and 4 hinges) by high energy dissipating isolators and the insertion of four shock transmitters at the expansion end of the suspended span.

The results of a step-by-step, non-linear analysis demonstrated the validity of this solution, which was in effect adopted.

Better yet, to the above mentioned objectives, a fourth one was added, to wit:

d. to maintain the existing original "structural system" (i.e., the bearing arrangement on Fig. 4) for the service loads.

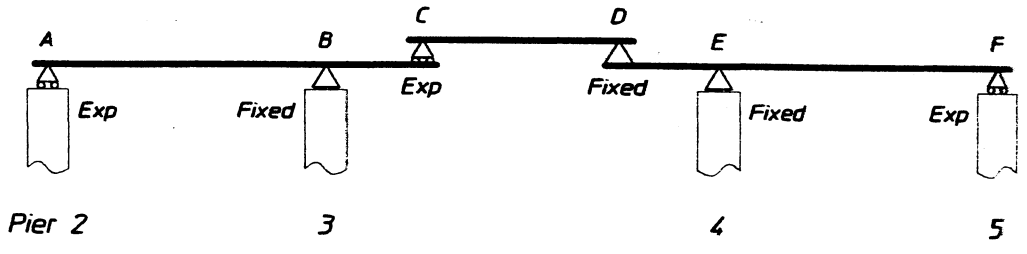


Fig. 4 The Structural System of Marquam Bridge

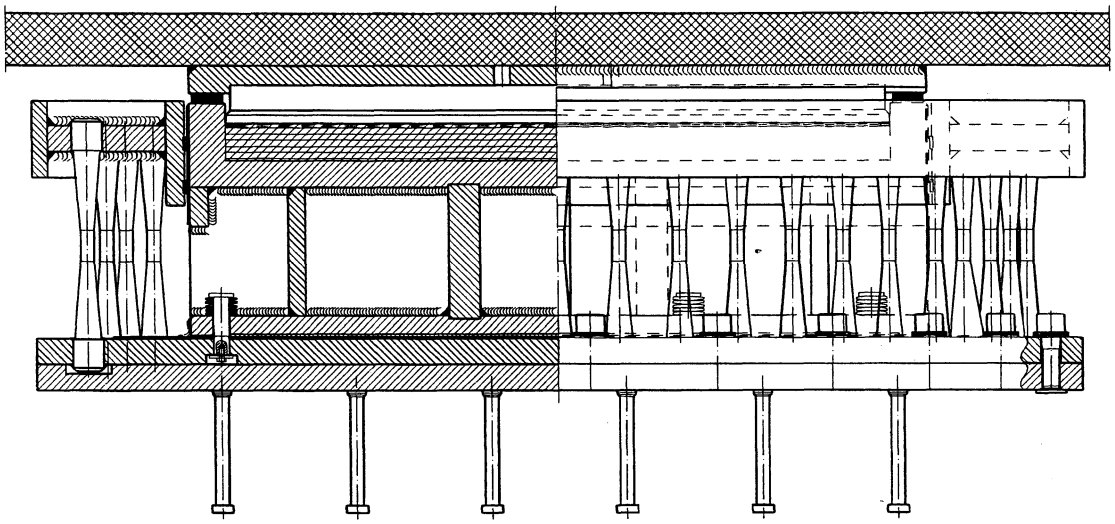


Figure 5. Isolator of the "fixed" type – Model VEP 5200

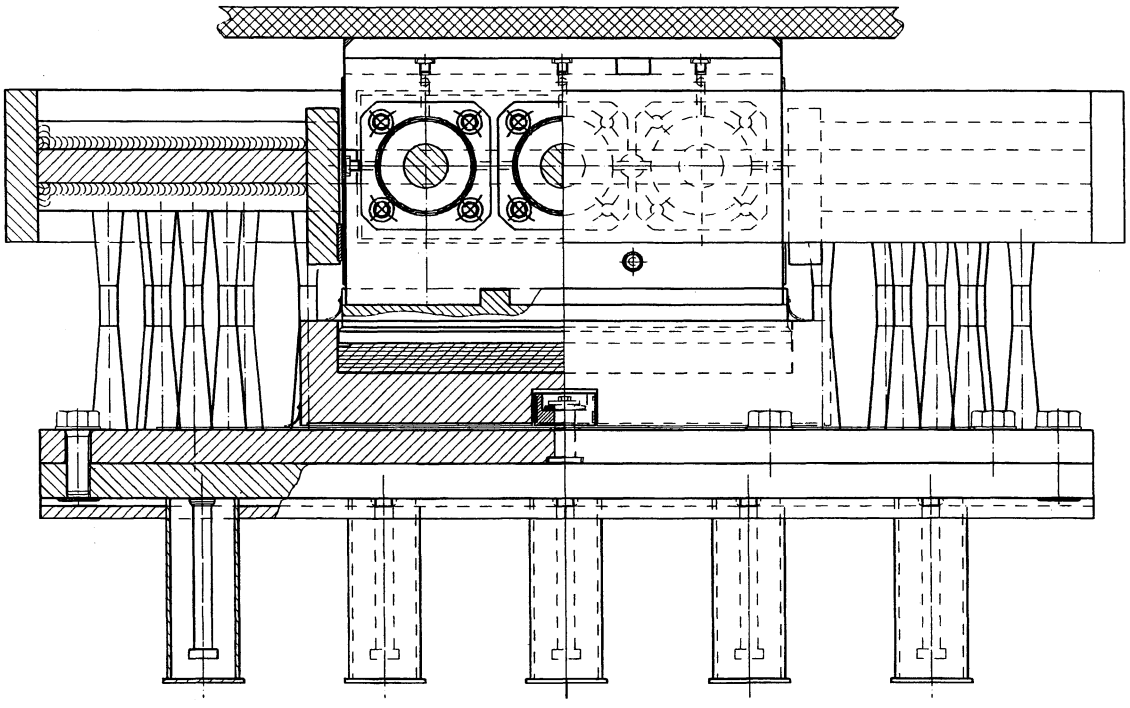


Figure 6. Isolator of the "mobile" type- Model VEP 1400/280-ST

The objective **d** is justified by the remark that the design engineer in the early 60s may have not duly taken into account seismic actions, but most certainly must have conceived and designed the bridge in question properly accounting for service loads and thermal deformations by providing "fixed" and "expansion" points on designated abutments and piers.

However, the reasons that originally induced the design engineer to adopt a certain arrangement over another are almost always unknown.

Thus, unless justifiable reasons require the opposite, it would be appropriate that the bridge's structural conception is not modified by the seismic retrofit intervention, as the bridge must continue to function under the same service loads and thermal deformations.

Finally, leaving things unaltered as much as possible makes life easier for the future engineers who will attempt to improve seismic protection utilizing more advanced devices that technological research will put at their disposal.

3.3 Seismic Hardware and Design Approach

The isolators adopted for this retrofit project essentially comprise (see Figure 5):

- a free sliding pot-bearing that serves to transmit vertical loads and permits the lateral displacements in all directions
- a series of steel hysteretic elements suitable to control the horizontal actions

The isolators installed at the expansion points (Piers 2 and 5) additionally comprise a shock transmitter (Figure 8) which is active between superstructure and steel hysteretic elements thus accommodating thermal deformations without appreciable actions on said elements.

It is worth mentioning that service loads (i.e., wind, braking actions, etc.) and moderate earthquakes do not stress the dissipating elements owing to the use of "sacrificial restrainers" (or shear keys). Said "sacrificial restrainers" impede any displacement in the isolators of the "fixed" type (Piers 3 and 4) and the transverse movements on those of the "mobile" type (Piers 3 and 6). It thus follows that the objective **d** is attained.

In the event of the Design Maximum Expected Earthquake, the following occurs;

- the sacrificial restrainers break away
- the shock-transmitters are activated (i.e., become rigid).

As a consequence, the equivalent bearing system of the bridge becomes the following:

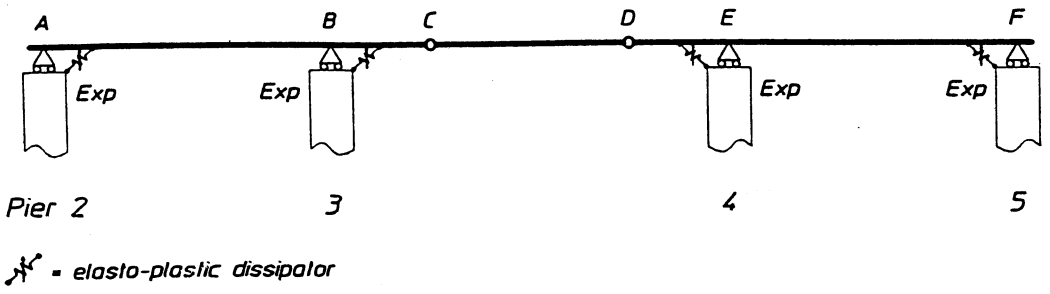


Fig. 7 Equivalent Bearing System during an earthquake attack.

In other words, the structure becomes hyperstatic, multi-span continuous girder type, which has proven to be the most effective when it comes to resisting seismic events.

Upon suitable choice of the dissipating elements' yield threshold, all piers remain within the elastic limits, even in the case of the most severe earthquake.

The high energy dissipating capacity of the hysteretic elements permits maintaining relative displacements within the specified limits of ±5 in.

Tables 2 and 3 list the average of the 4 peak values obtained from the individual step-by-step non linear analyses performed using different accelerograms, in both the longitudinal and transverse directions respectively. The symbols have the following meaning:

s_b = deformation of the bearing (displacement of thrust minus displacement of the pier top)

F_b = force acting on each bearing

$F_{b,max}$ = maximum permissible force for each bearing

s_o = displacement of the pier top

V_0 = total shear force upon the section under strut "A"

M_1 = total bending moment at pier mid-height

M_2 = total bending moment at pier bottom

Pier #	s_b (in)	F_b (kips)	$F_{b,max}$ (kips)	s_o (in)	V_0 (kips)	M_1 (kips×feet)	M_2 (kips×feet)
2	3.9	306	350	3.8	641	46,589	109,075
3	3.3	453	850	4.0	884	59,101	126,150
4	3.4	455	850	4.1	832	55,642	118,717
5	4.5	316	350	3.6	642	47,030	99,434

Table 2. - Longitudinal Dynamic Analysis Peak Values

Pier #	s_b (in)	F_b (kips)	$F_{b,max}$ (kips)	s_o (in)	V_0 (kips)	M_1 (kips×feet)	M_2 (kips×feet)
2	3.2	296	550	2.1	1,157	46,147	103,997
3	4.0	469	1,100	1.5	958	38,640	90,896
4	4.0	467	1,100	1.5	911	37,168	93,840
5	3.5	301	350	2.0	1,094	48,134	99,434

Table 3. - Transverse Dynamic Analysis Peak Values

From the above it must be then concluded that even objectives **a**, **b** and **d** are equally attained to an extent beyond expectations, as the appropriate choice of the yield threshold avoids having to reinforce the piers and foundations and/or widening the existing expansion gaps - with remarkable savings in costs and the execution timetable of the retrofit project.
The Marquam Bridge has regained a new youth. In the comfort of the positive experience matured in Italy, the good results of rigorous analysis and severe laboratory tests, one can reasonably count on this structure's capability to fully carry out its mission for still many decades.

3.4 Testing

Each device type was tested at the FIP Industriale laboratories and the tests were witnessed and certified by experts from the Earthquake Engineering Research Center (EERC) at the University of California at Berkeley.

A detailed report on the results of the testing is beyond the scope of this presentation. The following summarizes the type of test conducted, purpose, testing procedure, acceptance criteria and some significant results thereof.

3.4.1 Shock Transmitters

The rig used for testing the shock transmitters comprised bolted steel members, a double-action actuator and servo valve, a hydraulic power supply and a closed loop electronic control system (see Figure 8 below).

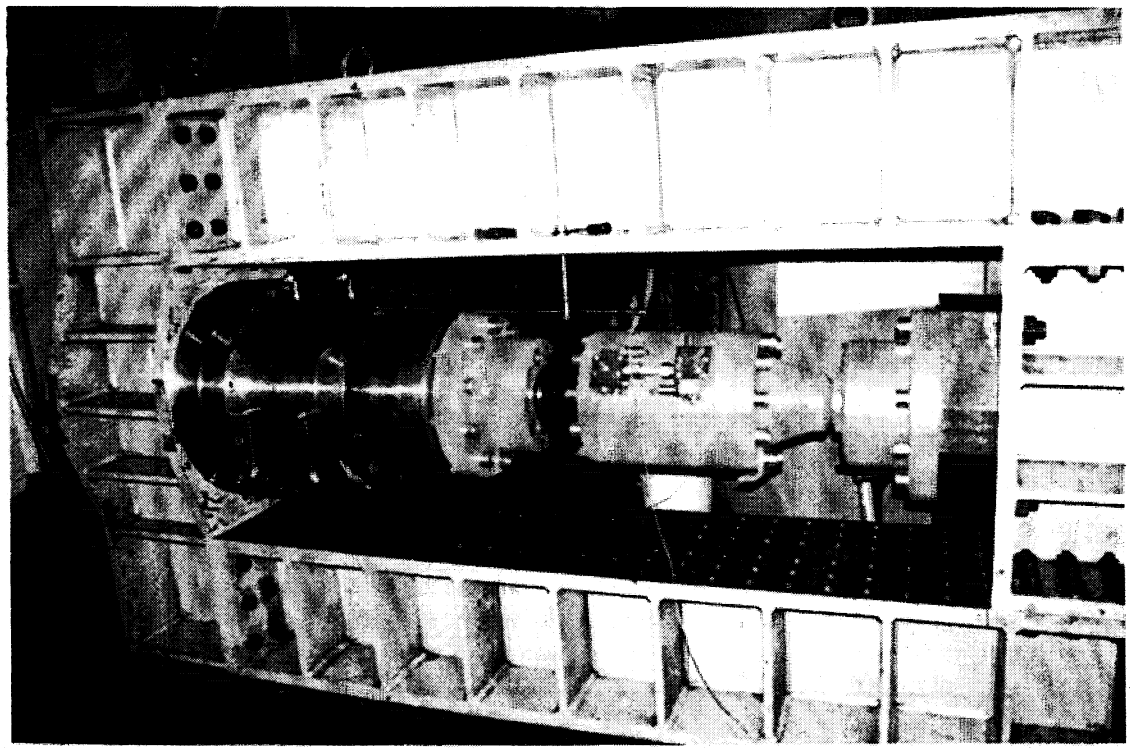


Figure 8 . Shock Transmitter Test Set-up

Impressed Deflection Test

The objectives of the test were to evaluate devices force resistance at low (i.e., thermal) velocity as well as to verify their axial displacement capacity.

Testing Procedure: The device shall have an impressed deflection ranging from 0 to 2.75 in. to 0 to –2.75 in. to 0 within one hour. A continuous plot of the load and deflection shall be recorded to permit evaluation of the device.

Acceptance Criteria: During the impressed deflection cycle, the device shall develop no more force than 40 kips.

Results: The measured maximum response was 21.3 kips.

Simulated Dynamic Force Transfer Test

The test objective was to evaluate the stiffness of the device for impulse forces and constant forces.

Testing Procedure: The device shall have a force of 440 kips applied in less than 0,5 seconds and the force sustained for 5 seconds. Then the force shall be inverted to –440 kips for 0,5 seconds and sustained for 5 seconds.

Acceptance Criteria: The deflection during loading from 0 to 440 kips and from 0 to –440 kips shall be no greater than 0.25 in. The deflection during the sustained portions shall not exceed 0.25 in.

Results: The measured displacements ranged from 0.13 to 0.25 in.

Note: applied forces were in excess of the specified values

The same tests were conducted on the ST shock transmitters unit installed in the "movable" type of bearings at the expansion points (Piers 2 and 5).

The maximum response force required by the specifications was 20 kips in the displacement range of + 1.75 to – 1.75 in. The measured maximum force was 6.3 kips.

The specifications of the Simulated Dynamic Force Transfer Test required for this device that forces equal to + 375 kips and – 375 kips be applied to the shock-transmission device, with deflections no greater than 0.30 in. The measured maximum deflections were equal to 0.24 in.

3.4.2 Friction Test

The rig used to test the PTFE discs included one horizontal actuator to impose the specified displacements and a hydraulic jack to impose the required axial force on the disc.

The objective of the test was to provide a correction factor for the effect of velocity on the coefficient of friction in the Simulated Dynamic Load Test of sliding isolators.

Test Conditions:

Disc diameter	3 in
Contact pressure	2,300 psi
Pre-load time	1 hour
Sliding distance	± 1.5 in
Reference thermal speed	4 in/min
Conventional seismic speed	5 in/sec
Number of cycles (each test)	10

The results are the following:

$$\mu_{static} = 0.003$$
$$\mu_{dynamic} = 0.009$$

From the above, a factor equal to 3 was used to correct the PTFE friction contribution to hysteresis loops of the Simulated Dynamic Load Test.

3.4.3 Seismic Isolators

The system used for testing the Seismic Isolators was composed of the FIP reaction block (rated at 9,000 metric ton.) with horizontal and vertical servo-controlled actuators, a hydraulic power supply, and a closed loop electronic control system.

Vertical Static Load Test

The objective of the Vertical Static Load Test was to verify the load capacity of the seismic isolators in the presence of the maximum rotation.

Testing Procedure: A load equal to 150 percent of the design capacity of the tested device shall be applied for a period of one hour. The device shall be in rotated position during the test. Rotation shall be 0,015 radians or the design rotation, whichever is greater

Acceptance Criterion: The tested device shall show no indication of failure or other defects such as weld cracking, plate distortions, extrusion of the elastomer or bearing material, or displacement of the elastomer seal while under load or subsequently upon disassembly and inspection.

Test Results: No evidence of weld cracking, plate distortion, extrusion of the elastomer and/or the bearing material or displacement of the elastomer seal was observed at any stage during or after the test.

Note: VEP 5200, with its 5,200 kips load capacity, claims to be the largest high damping isolator installed to date.

Lateral Static Load Test

The primary objective of the lateral static load test was to evaluate the behavior of the seismic isolators prior to the failure of the service load restrainers.

Testing Procedure: The devices shall be vertically loaded at the design dead load during lateral static testing. The devices shall be loaded laterally for 10 complete cycles of loading from 0 to F_1 to 0 to $-F_1$ to 0. The value of F_1 for each device shall be the lowest value from Table 4. The cycles of loading shall be at a uniform rate. A continuous plot of the lateral load and deflection shall be recorded.

The deflection shall be measured on the first portion of the fifth cycle and be within the range specified in Table 4 (parameter s_1).

After the cycle load testing, the devices shall be loaded laterally to load restrainer failure while maintaining the vertical dead load. Failure is defined to be the total fracture of the service load restrainers.

Acceptance criteria: Deflections shall be within the range specified in Tab. 4 (parameter s_1) and the lateral load at failure (Break away load) shall be within the range specified for parameter F_1.

Test Results: Table 4 below lists the results of the tests.

Type of Bearing	**s_1 (in)**	**Maximum Displacement (in)**	**F_1 (kips)**	**Break awayLoad (kips)**
VEP 1400/280-ST	0 - 0.20	0.08	170 - 230	197
VEP 5200	0 -0.20	0.04	360 - 460	436

Table 4. - Target Parameters and Results of the Lateral Static Load Test.

Simulated Dynamic Load Test

The objective of the test was to evaluate the hysteretic performance of the devices.

Testing Procedure: The devices shall be vertically loaded at the design dead load during simulated dynamic testing. The devices shall be loaded laterally for 15 complete cycles of loading from 0 to 5.0 in. to 0 to –5.0 in. to 0. The cycles of loading shall be at a uniform rate.

The value of the peak force shall be measured on the first portion of the fifth cycle. The energy dissipated in one hysteretic loop shall be computed for the fifth cycle.

A continuous plot of the lateral load and deflection shall be recorded to permit an evaluation of the elasto-plastic and hysteretic performance of the device.

Acceptance Criteria: Peak force and hysteretic energy dissipation at the fifth cycle shall be within the respective ranges of the parameters F_2 and EDC.

Test Results: The results of the tests are listed in Table 5 below.

Type of Isolator	F_2 (kips)	Measured Peak Force (kips) *5th cycle*	*15th cycle*	EDC (kips× in)	Hysteretic Energy (kips× in) *5th cycle*	*15th cycle*
VEP 1400/280-ST	265 - 360	360	320	3,850	4,880	4,360
VEP 5200	530 - 715	660	580	6,200	8,120	7,000

Table 5. - Target Parameters and Results of Simulated Dynamic Load Test.

The hysteretic loops of VEP 1400/280-ST and VEP 5200 devices are shown in Figures 15 and 16 respectively.

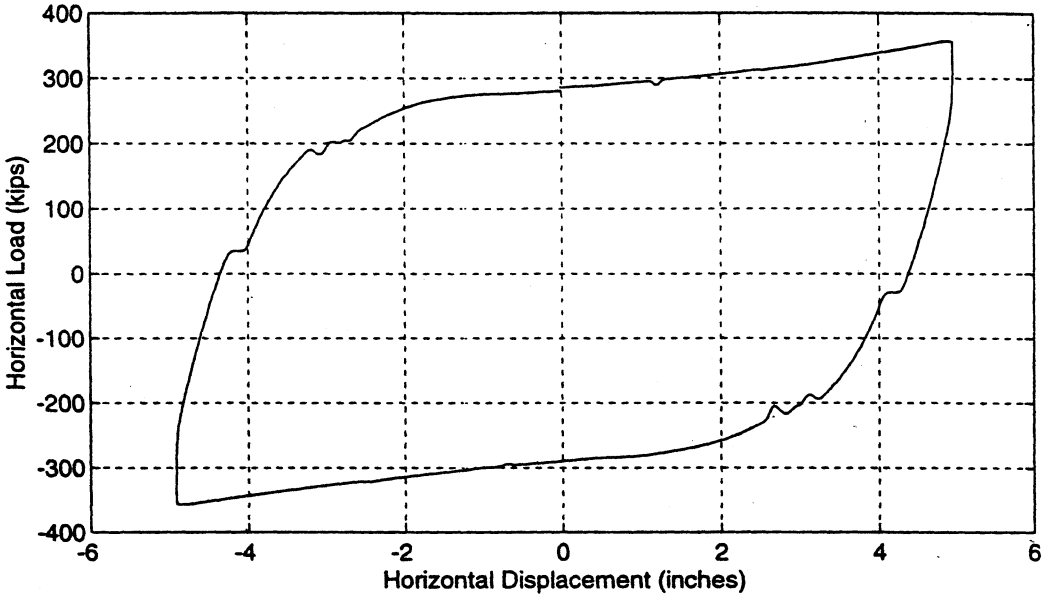


Fig. 15 : Hysteretic Loop of VEP 1400/280-ST at 5th cycle

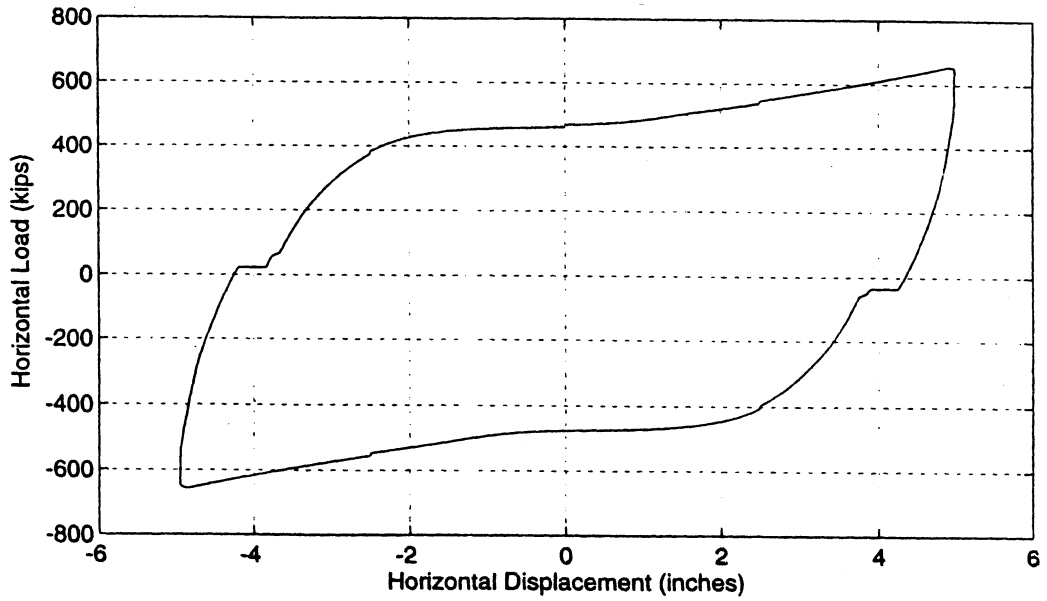


Fig. 16 : Hysteretic Loop of VEP 5200 at 5th cycle

4. CONCLUSIONS

Earthquake Engineering has witnessed significant development during the course of the last two decades. The result has been reached owing to the parallel development of new design strategies (the "seismic software") and the perfection of suitable mechanical devices to implement said strategies (the "seismic hardware").

The seismic design of a bridge cannot be a simple application of mathematical equations, but requires the understanding of the phenomena involved and the preparation of a "plan of defense", *i.e.*: a specific design strategy.

The use of an energy approach, and particularly the use of an energy balance equation, offers a promising rational basis for defining the design strategy, as well as deriving maximum advantage from the type of structure under study and the existing seismic hardware.

In terms of the state-of-the art in technical-scientific knowledge, the most promising strategy is the combination of controlling the energy input through Seismic Isolation and increasing energy dissipation through the insertion of appropriate dissipative seismic devices in the structure.

Although basic concepts and general guidelines for retrofit of structures have been formulated, the proper strategy for a given facility is a unique problem requiring a customized solution.

The Marquam Bridge Retrofit Project represents the first case of application in the United States of isolators with steel hysteretic dampers in combination with shock transmitters.

The proper selection of the retrofit strategy and the seismic hardware has allowed to achieve all the objectives with a minimum of effort; that is to say, with contained cost and, above all, without having to resort to the strengthening of the substructure.

ACKNOWLEDGEMENTS

This application has not consisted in the simple acceptance and use of existing seismic devices, but rather, their adaptation to the American reality and its particular set of applicable rules and is thus the end result of a long cooperative effort of almost three years between US and Italian design engineers
The author wishes to express in particular his sincere gratitude for the active and fruitful cooperation rendered by Mr. Steve Starkey, Mr. Phil Rabb, and the rest of the Engineering Staff, Bridge Division, at the Oregon Department of Transportation.

6. REFERENCES

[1] Uang, C. M., "Use of Energy as a Design Criterion in Earthquake-resistant Design", *UCB/ERC-88/18,* University of California at Berkeley, 1988.

[2] Bertero, V.V., "Earthquake Hazard Reduction: Technical Capability - U.S. Perspective", *Proc. 2nd Japan-US Workshop on Urban EQ Hazards Reduction,* Shimizu: Tokai University, 1988.

[3] Bertero, V. V., "Seismic Upgrading of Existing Structures", *Tenth World Conference on Earthquake Engineering,* Madrid, Spain, July 1992.

[4] Dowrick, D. J., *Earthquake-resistant Design for Engineers and Architects,* John Wiley & Sons, LTD, 1987.

[5] Kelly, J.M., "Seismic Base Isolation", Join Sealing and Bearing Systems for Concrete Structures, Vol. 1 – Pub. ACI (1982)

[6] Medeot, R., and Albajar, L., "The Evolution of Seismic Devices for Bridges in Italy", *Tenth World Conference on Earthquake Engineering,* Madrid, Spain, July 1992.

[7] Medeot, R., "The European Approach on Seismic Isolation of Bridges", *Fourth World Congress on Joints and Bearings,* Sacramento, California, September 1996.

[8] Medeot, R., "Dampers Developed for Seismic Engineering Suitable for Use in Wind Engineering", *2nd European and African Conference on Wind Engineering,* Genoa, Italy, June 1997.

[9] Medeot, R., "Some Thoughts on Seismic Hardware Testing", *International Joints and Bearings Research Council Newsletter,* February, 1996.

Seismic Isolation of Railway Bridges

Mauro Dolce[(1)], Domenico Liberatore[(1)], Corrado Bonuccelli[(1)] and Giuseppe Traini[(2)]

[(1)]USB-DiSGG (Dipartimento di Strutture, Geotecnica, Geologia applicata all'ingegneria, Università della Basilicata), Potenza, Italy

[(2)]ITALFERR SIS-TAV S.p.A., Via Marsala 53, 00100 – Roma, Italy

Abstract

Railway bridges are peculiar structural systems, where the structure interacts with tracks and vehicles in a complicated manner, involving strongly nonlinear effects. The interaction effects under earthquakes are particularly difficult to be understood and evaluated. Peculiar aspects, such as the nonlinear behavior of track-bridge interface (ballast), the dynamic behavior of train vehicles, the unilateral contact constraint between wheel and rail, between rail and deck as well as in the deck bearings, have to be taken into account. They need a full three-dimensional analysis, taking into account all the nonlinear phenomena occurring in both the structure and the track.

A very accurate nonlinear dynamic analysis program (BRIE) was previously implemented by the authors, to study the seismic response of railway bridges. A peculiar behavior was detected for conventional bridges, due to the vehicle-track-bridge interaction, with important implications regarding serviceability. The observation of such results suggests that seismic isolation could turn out to be effective in reducing not only structural damage, but also the risk of service loss, although very few applications are presently made all over the world.

In this paper the seismic behavior of a railway bridge equipped with seismic isolation/dissipation devices is investigated. It is a typical bridge of the new Italian high speed railway line under construction. Reference is made to only one type of devices, having elasto-plastic behaviour, while the parameters characterizing the response of such devices (threshold force, post-yield stiffness) is varied. Although only one case is analyzed, and a more comprehensive study is needed, the actual advantages coming from seismic isolation in comparison with conventional design of railway bridges are highlighted and some indications on the optimal choice of the behavioral parameters are obtained.

Introduction

Up to now, the seismic vulnerability of railway bridges has not been acknowledged enough, because

of the high strength and stiffness asked for by the serviceability and ultimate limit states requirements. In fact the high values of the braking/acceleration forces induce large reactions in the supports. Moreover, to limit the danger of track buckling and ballast de-consolidation, high stiffness of supports is required (1,2). These requirements, along with some additional provisions for durability, make railway bridges intrinsically safe against horizontal forces, as long as collapse is concerned under usual design earthquakes. However this favourable conditions do not longer hold when very strong earthquakes are considered, as the recent January '95 Kobe Earthquake proved, and when serviceability conditions, especially related to the interactions between bridge, track and vehicles, are considered.

Railway serviceability, in fact, is not only related to structural damage or collapse, but even to permanent track displacements due to vibrations and relative displacements in dynamically excited bridges. Moreover structural vibrations induce tilting moment in train vehicles, either still or moving, possibly causing their tilting up and compromising the runability of bridges during earthquakes.

Evaluating the complex train-track-bridge phenomena occurring in a railway bridge under seismic actions is not, however, an easy task. A very detailed modelling of the bridge and of the track is required, taking into account the strong nonlinear behaviour of piers, bearings and track ballast, including unilateral contacts, as well as of the train vehicles, with their complex damping systems and the possible uplift of wheels.

The computer programs for the nonlinear analyses of bridges do not normally address this type of problems, as they cannot account for the interaction between bridge, track and train. For the above reasons, a new software package BRIE (Bridge-Railway Interactions under Earthquakes) was devised and implemented by the authors (3). BRIE is a three-dimensional nonlinear finite element program, which models accurately R/C structural elements (piers and abutments), track, track-deck connection (ballast or direct fastening), train vehicles, wheel-rail unilateral contact constraint. It can also model accurately the characteristics of bearings, taking into account friction and unilateral constraint, and of passive control devices, such as elasto-plastic or visco-elastic isolators and dampers. Finally synchronous or non-synchronous seismic motions, as well as soil structure interaction, can be considered. The analysis is carried out by applying static actions first (vertical dead and live loads, temperature variations) and then earthquake.

A parametric analysis was carried out, to study the seismic behaviour of the most common types of bridge of the Italian new high speed lines. All these bridges were designed according to the current railway seismic code (4), relying their collapse safety on the strength and ductility capacity of the piers, with no special provision related to the serviceability requirements. The results, which are not published yet, highlighted some dangerous phenomena, such as the transverse rocking of decks, causing uplift of bearings and of rail, the high rail compressive stresses, causing buckling and permanent lateral displacements, lateral tilting up of vehicles. Most of these problems could apparently take benefit from seismic isolation systems, at the interface between decks and piers or abutments.

The aim of the present paper is to show the results of a preliminary investigation on the effectiveness of seismic isolation systems in improving the performance of railway bridges under earthquakes. The same accurateness in modelling applied to the previous investigation on conventional railway bridges is used, in order to detect the important phenomena related to serviceability.

Only one bridge was considered, selected among the typical structural types and layout of the high speed lines under construction in Italy. It is a five span simply supported deck bridge. No train was considered in this preliminary investigation. An elasto-plastic isolation system was selected, being the

simplest and, at the same time, suitable for railway requirements, which are high initial stiffness and high strength in relation to braking/acceleration forces. A direct comparison with the results obtained for conventional bridges permit to appreciate and quantify the advantage of seismic isolation with respect to conventional design.

Characteristics of the Bridge and of the Isolation System

In Figure 1 the static scheme of the bridge selected for the present study is reported. It is a double track simply supported deck bridge, with five 33.60 m long spans and 11.60 m tall piers. The bearing system of each bridge deck is made of 2 fixed (internal) bearings and 2 movable multidirectional (external) bearings at the left end, three multidirectional and one unidirectional (internal) bearing at the right end, as shown in Figure 2.

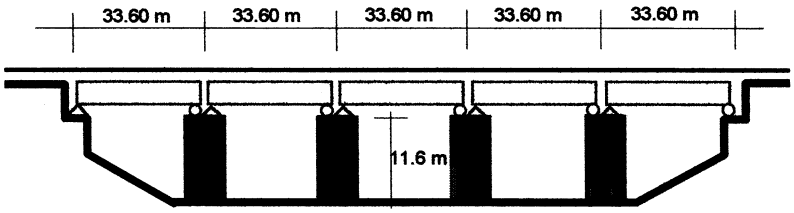


Figure 1. Scheme of the 5 span railway bridge

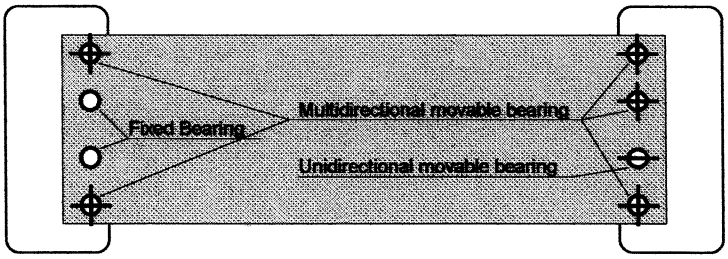


Figure 2. Arrangement of the bearing system.

The isolation system is conceived so as to substitute the longitudinal and lateral constraints of the conventional bridge, given by the fixed and unidirectional bearings, with elasto-plastic constraints. It is therefore made of four multidirectional bearings on each end of a deck, with additional elasto-plastic energy dissipation elements or devices acting in the same direction as the fixed or unidirectional bearings of the conventional structure, as shown in Figure 5.

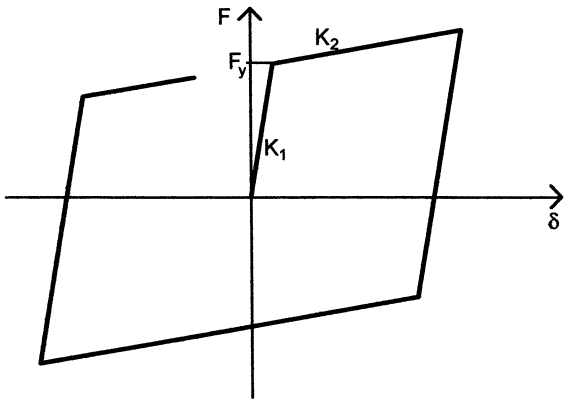


Figure 3. Elasto-plastic behavior of the isolation devices.

Elasto-plastic devices or bearings embodying elasto-plastic steel elements have been widely used in highway bridges (6) in Italy. An example of these devices and the relevant experimental results can be found in (7). The assumed elasto-plastic law is shown in Figure 3. The characterising quantities are: the yielding force F_y, the initial stiffness K_1, the post-elastic stiffness K_2.

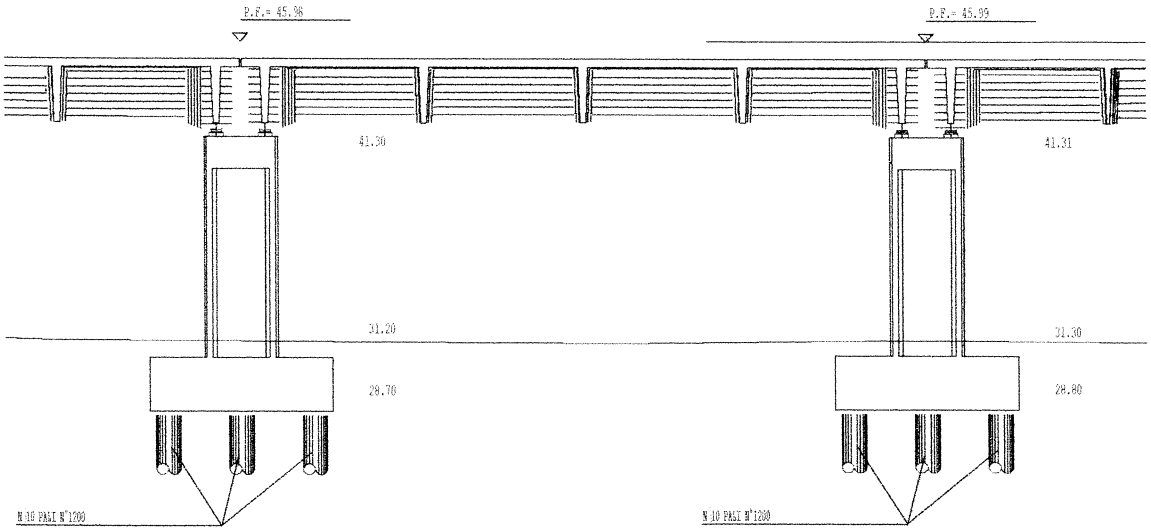


Figure 4. Typical span configuration.

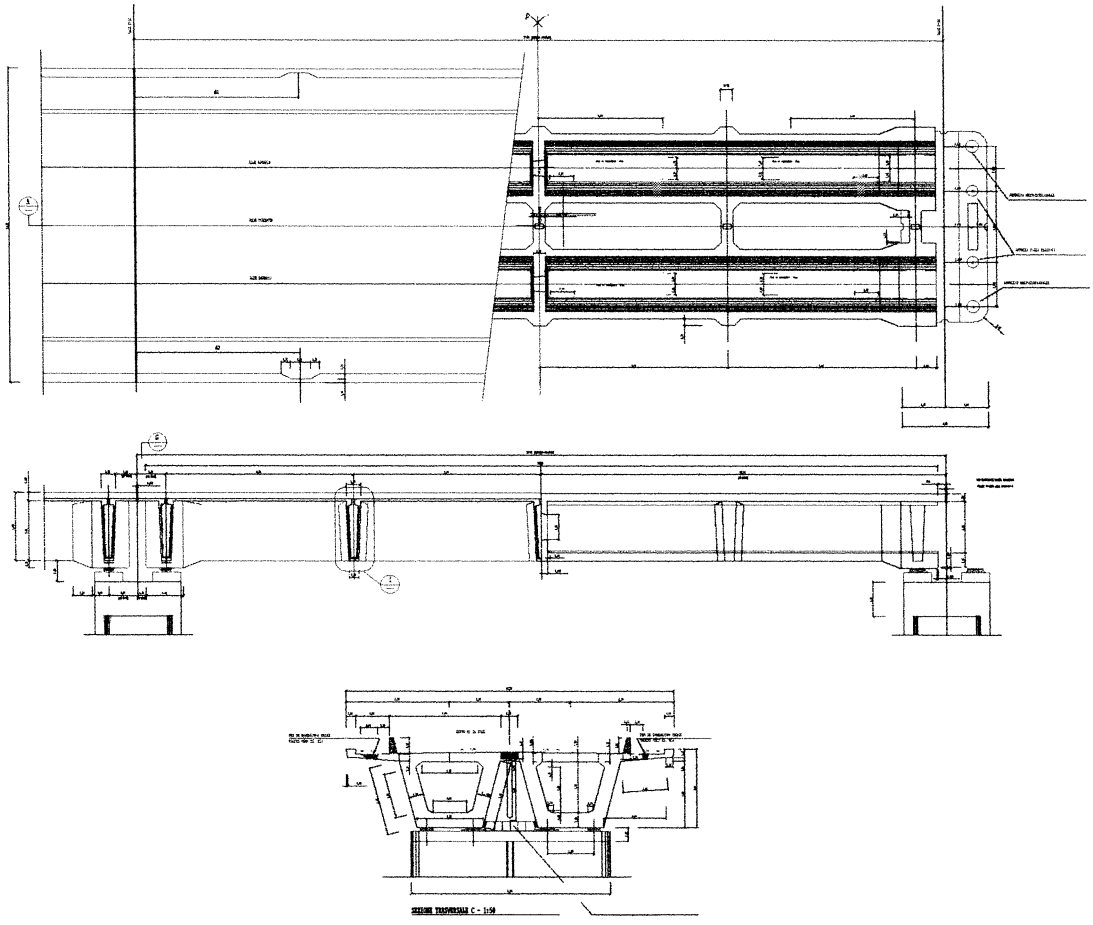


Figure 5. Geometrical characteristics of the deck.

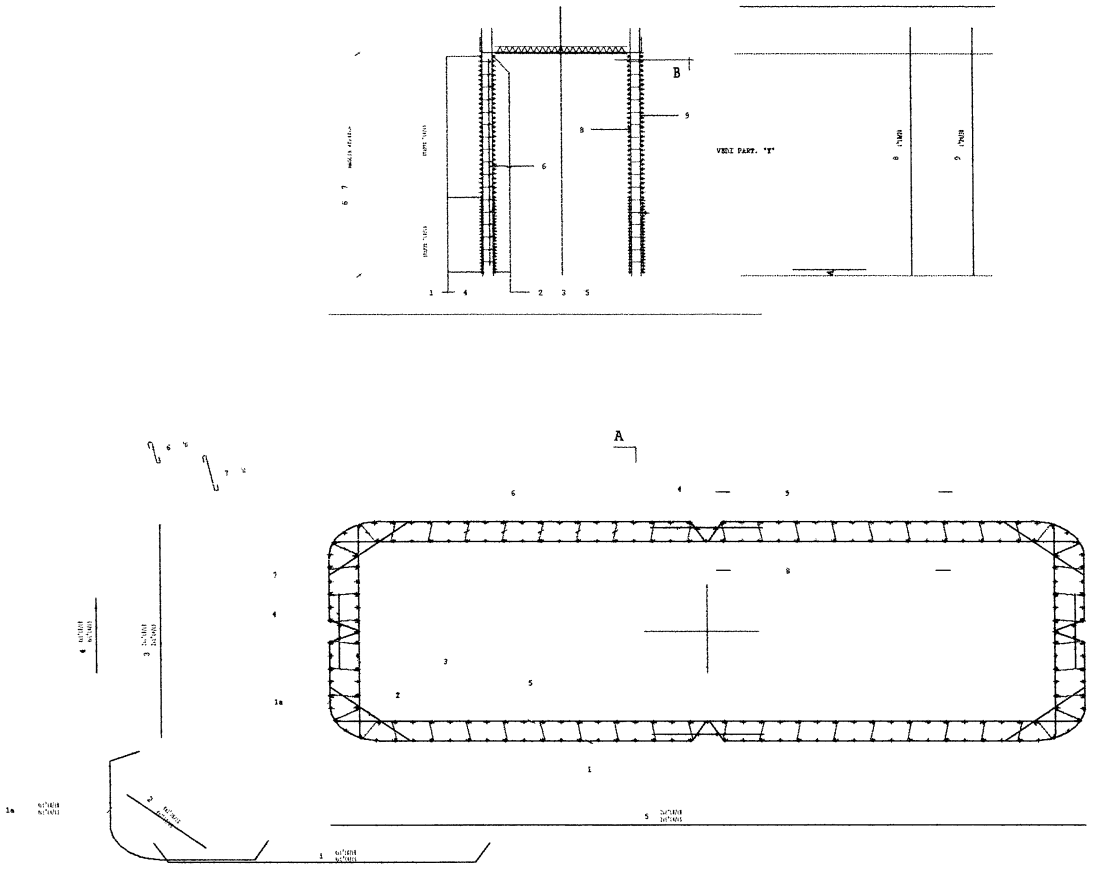


Figure 6. Details of the pier reinforcements.

In figs. 4, 5, 6 the design drawings show the main characteristics of the bridge. It is designed for the 2nd Seismic Category of the Italian code. The relevant reduced spectrum has 0.07g maximum spectral acceleration. The safety coefficient for steel strength is about 1.7. Although the design forces are not high, the design procedure leads to a considerable overstrength of piers, due to both the high safety coefficient on steel strength and the minimum reinforcement requirements.

To evaluate the seismic response of this bridge, it was subjected to two synchronous 3D actions of different intensities. In one case the horizontal components and the vertical component have 0.28g and 0.187g PGA respectively, while, in the other case, 0.40g and 0.267g were assumed respectively. The three components are independent and generated to fit the EC8 type B spectrum (8), with 10 secs. duration.

		F_y = 1700 KN	F_y = 2550 KN	F_y = 3400 KN
a/g = 0.28	K_2/K_1 = 0.00	1	2	3
	K_2/K_1 = 0.01	4	5	6
	K_2/K_1 = 0.05	7	8	9
a/g = 0.40	K_2/K_1 = 0.00	10	11	12
	K_2/K_1 = 0.01	13	14	15
	K_2/K_1 = 0.05	16	17	18
a/g = 0.28	NO ISOLATION	19		
a/g = 0.40	NO ISOLATION	20		

Table 1 – Cases considered and number of analysis.

In order to investigate the effectiveness of the elasto-plastic isolation system when varying some of its fundamental parameters, 9 different cases have been considered, each of them being analysed for the two above said earthquake intensities, as shown in table 1. The basic design of the isolation system is referred to the serviceability conditions under service loads, i.e. to the requirements of high stiffness and no permanent displacements under the maximum longitudinal braking/acceleration forces. Since the bridge has two tracks, braking forces on one track and acceleration forces on the other must be considered. The total longitudinal force due to service loads is 1700 KN, which is about 13% of the dead load – including track and ballast – of a deck. This is assumed to be the yielding force F_y in the elasto-plastic cycle, while the corresponding displacement is assumed to be 1 mm, i.e. the initial stiffness K_1 is equal to 1700 KN/mm. In the parametric analysis, the yielding force has been varied by assuming values equal to 1.0, 1.5 and 2.0 times the basic value. For the post-elastic to initial stiffness ratio, K_2/K_1, three values have been considered, i.e. 0.00, 0.01, 0.05, which are typical values for the existing devices. Considering two intensity levels, a total of 18 analyses have been carried out on the bridge with the isolation system.

Model and Analysis

The model has been set up to be analysed by the special purpose program BRIE (3), with reference to its library of finite elements. However some simplification have been made, with respect to the full capabilities of BRIE, in order to speed up the analyses and reduce the number of parameters affecting the results, e.g. no train is present on the bridge, synchronous earthquake motions, fixed abutment and no soil structure interaction are assumed.

In this paragraph the modelling criteria for track, deck, bearing and isolation devices, piers, abutment and foundations are described, along with the analysis procedure.

Although the track is made of two rails connected by sleepers, it is modelled as a unique elastic beam, positioned along the track axis line and discretised into *Elastic Beam Elements*, as shown in Figure 7. These elements are connected to the deck or to the soil through the rigid links of the *Ballast Spring Elements*,. The lateral stiffening effect of sleepers is taken into account by suitably calibrating the stiffness of the ballast rotational springs. Large displacements are considered in the beam elements, so that rail buckling is also accounted for in the analyses.

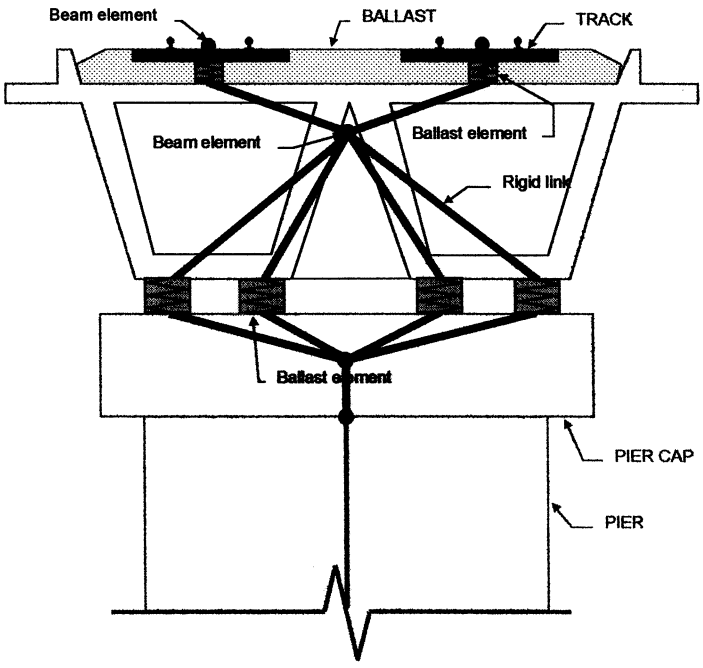


Figure 7. Track-bridge system model.

The *ballast spring element* is made of three translational and three rotational springs, with different elastic or nonlinear characteristics. The springs are connected to the two nodes through rigid links. The directions of the springs and of the rigid links are parallel to the axes of the local reference

system *r-s-t*, as shown in Figure 8. The springs can be either linear or non linear.

Two different behaviours of nonlinear springs are defined, according to their direction. The spring acting in the r-direction has the behaviour shown in Figure 9 (left), where the initial stiffness in tension and in compression are different, thus allowing unilateral constraints to be simulated. The other two translational and all the three rotational springs follow an elastic perfectly plastic hysteretic law, whose elastic stiffness and plastic force depend, at any moment, on the stress state of the first spring, according to Figure 9 (right). Different elasto-plastic characteristics can be assigned to the various springs of a same element. An initial different cohesive strength could be eventually assigned to each spring, which is annihilated as soon as one of the springs reach the failure value.

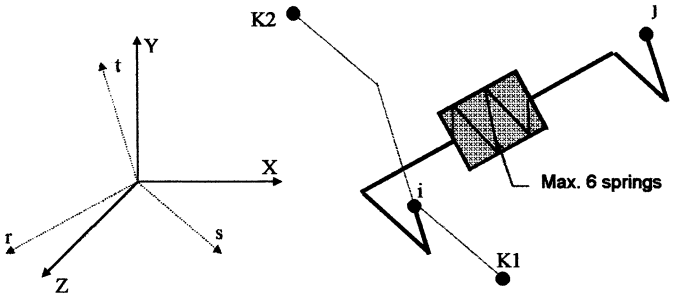


Figure 8. Ballast spring element.

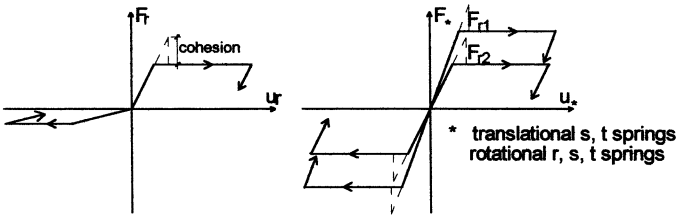


Figure 9. Force-displacement law of the springs of the ballast element.

To model the ballast, the r-axis of the first translational spring is vertically directed, while the horizontal s-axis and t-axis are longitudinally and transversely directed respectively. The stiffness and strength of the horizontal springs thus depend on the force in the vertical spring, and then on the load acting on the track.

Although especially conceived to model the ballast behaviour, the *ballast spring element* can be used in a wider range of situations, to get a more or less refined simulation of different behaviours. In the present investigation it is also used to model bearings.

The *beam elements* modelling tracks are aligned along the track axis lines. The springs of the *ballast element* are positioned as shown in figs. 7 and 10.

The deck is modeled with elastic *beam elements*, as nonlinear effects are not expected in simply supported pre-stressed concrete deck bridges. *Beam elements* are aligned along the centroidal axis of the deck and are connected to the track axis through the rigid links of the *ballast element*, as shown in figs. 7, 10.

The discretization length of the tracks

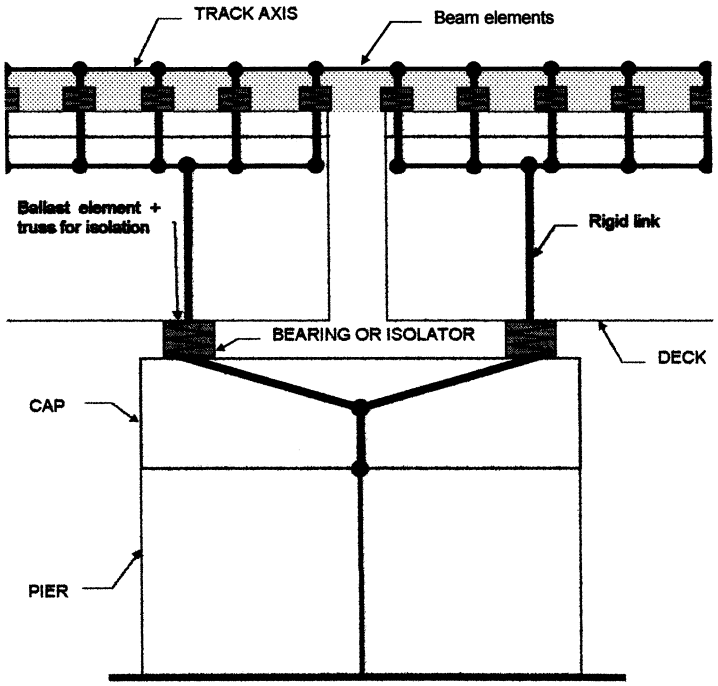


Figure 10. Longitudinal view of the track-bridge system.

and the deck is 1.00 m, resulting in 290 *beam elements* and 291 *ballast spring elements* to model each track and 170 *beam elements* to model the deck.

Bearings are modelled with *ballast spring elements*. Elastic springs are used for conventional bearings, assigning respectively high and almost zero stiffness, to model "fixed" and "movable" conditions, in the horizontal directions. Nonlinear springs in the r-direction are used to model the unilateral constraint in the vertical direction.

The isolation system is modelled using *ballast spring elements*, for the multi-directional movable bearings, and *elasto-plastic truss elements* along the selected directions, for the elasto-plastic elements or devices.

R/C piers are modelled with nonlinear *fibre beam elements* and *elastic beam elements*, as shown in Figure 11. *Fibre beam elements* are used to accurately simulate the inelastic flexural behaviour of R/C columns, taking into account axial force variations. The cross section of each element is discretised into concrete and steel fibres. In the longitudinal direction each element can be subdivided into sub-elements of different lengths, as shown in Figure 12. The stress-strain constitutive laws are multi-linear hysteretic for both materials. The stress state is evaluated at the mid-length of each sub-element. The cross sections of the element are assumed to remain plane, according to the Navier hypothesis. The element is assumed to remain elastic in shear and torsion. The shear stiffness is halved, to account for shear cracking. No shear failure is expected, owing to the design shear reinforcement.

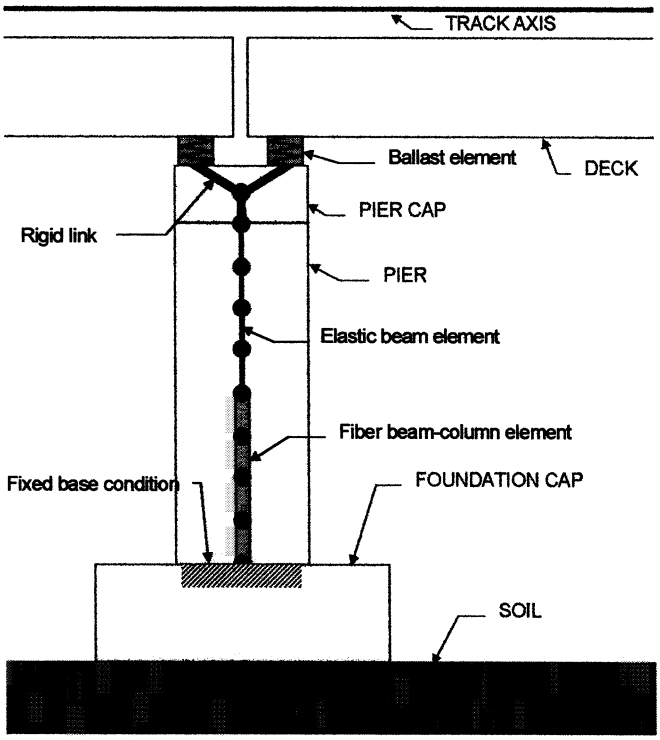


Figure 11. Typical discretization of a cap-pier-foundation system.

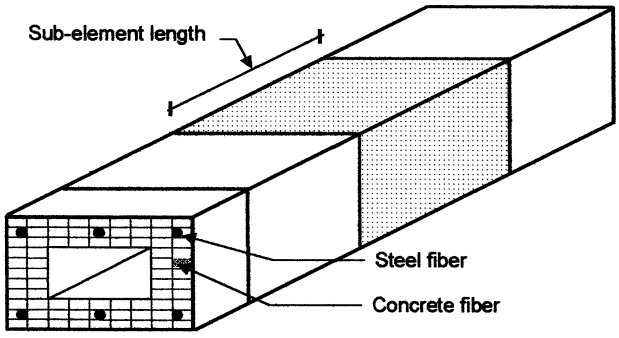


Figure 12. Fiber beam-column element

Since the *fibre beam element* is very time consuming, it is used to model only the lower part of piers, possibly subjected to yielding, while the upper part, which is expected to remain elastic, is simulated by elastic beam elements. 4 *fibre elements*, with only one sub-element each, and 4 *elastic beam elements* are used to model each pier, according to Figure 11. The cross section is discretised into 28 concrete fibres and 32 steel fibres. The strengths of concrete and steel are assumed to be 35 and 430 MPa, respectively.

Although abutments and backfill could be modelled by BRIE using nonlinear fibre beam elements

and nonlinear springs, respectively, in the present investigation, abutments are considered fixed for simplicity. Analogously, pier foundations are assumed infinitely stiff, thus neglecting any soil-structure interaction effects.

Static and thermal loads are applied before starting the seismic dynamic analysis, to initialise the stress state of elements. Dead loads are applied to the structure without track, to avoid fictitious stresses (3), while train loads and thermal actions are applied to the complete track-structure system.

Seismic actions are applied by prescribing three different displacement history components to the pier bases. For simplicity, synchronous motion is assumed.

The total number of degrees of freedom of the above described model is about 5000, with 21 bandwidth. The integration time step is 0.01 sec., resulting in 1000 total number of steps.

The dynamic equations of motion are solved in the time domain through step-by-step time integration, making use of the Newmark method and the classical Newton-Raphson equilibrium iteration procedure. The use of equilibrium iterations permits to use a relatively large time step. In order to save computer time, as well as computer storage, the sky-line representation of the stiffness matrix is used, together with an efficient bandwidth optimiser, which has been purposely conceived to exploit the usual layout of track-bridge models.

Results

The results of the simulation analyses are presented in two different types of diagrams, giving respectively the extreme values of the main response quantities of all the cases and the detailed behaviour (time histories) of one of the bridges with seismic isolation compared to the bridge without isolation.

In the first type of diagrams, the envelope values attained by the most significant response quantities are reported as a function of the yielding force of the isolation system. Six curves and two horizontal straight lines are provided in each diagram. The curves give the maximum and minimum values for the three considered stiffness ratios, while the ordinate of the straight lines give the corresponding maximum and minimum envelope values relevant to the conventional bridge.

In the second type of diagram, a selection of the most representative time histories of stresses and displacements, as well as the moment – curvature cycles of piers and the force-displacement curves of isolators, will be presented for case 14 (F_y = **2550 kN**, $K_2/K_1 = 0.01$, $a/g = 0.40$) and case 20 (no seismic isolation, $a/g = 0.40$). They will help to understand the dynamic behaviour of the different structural systems. The comments are especially addressed to the differences of the response between the structural systems with and without isolation, while, for a deeper understanding of the behaviour of the conventional bridge and of its interaction with the track, the reader must refer to (3).

In figs. 13 and 14 there are reported the envelope values of the displacements of the pier caps relative to the ground and the time histories of the displacements of piers 1 and 2, for case 14 and case 20. In figs. 15 and 16, the envelope values of the longitudinal and transverse base shears and of the axial force and the time histories of piers 1 and 2 for cases14 and 20 are reported. In fig. 17 there are shown the moment-curvature cycles at the base of piers 1 and 2 of cases 14 and 20. The response of piers 3 and 4 are very similar to that of piers 2 and 1 respectively and are not reported. In fig. 18 there are shown the envelope values of the vertical acceleration at the midspan of the decks.

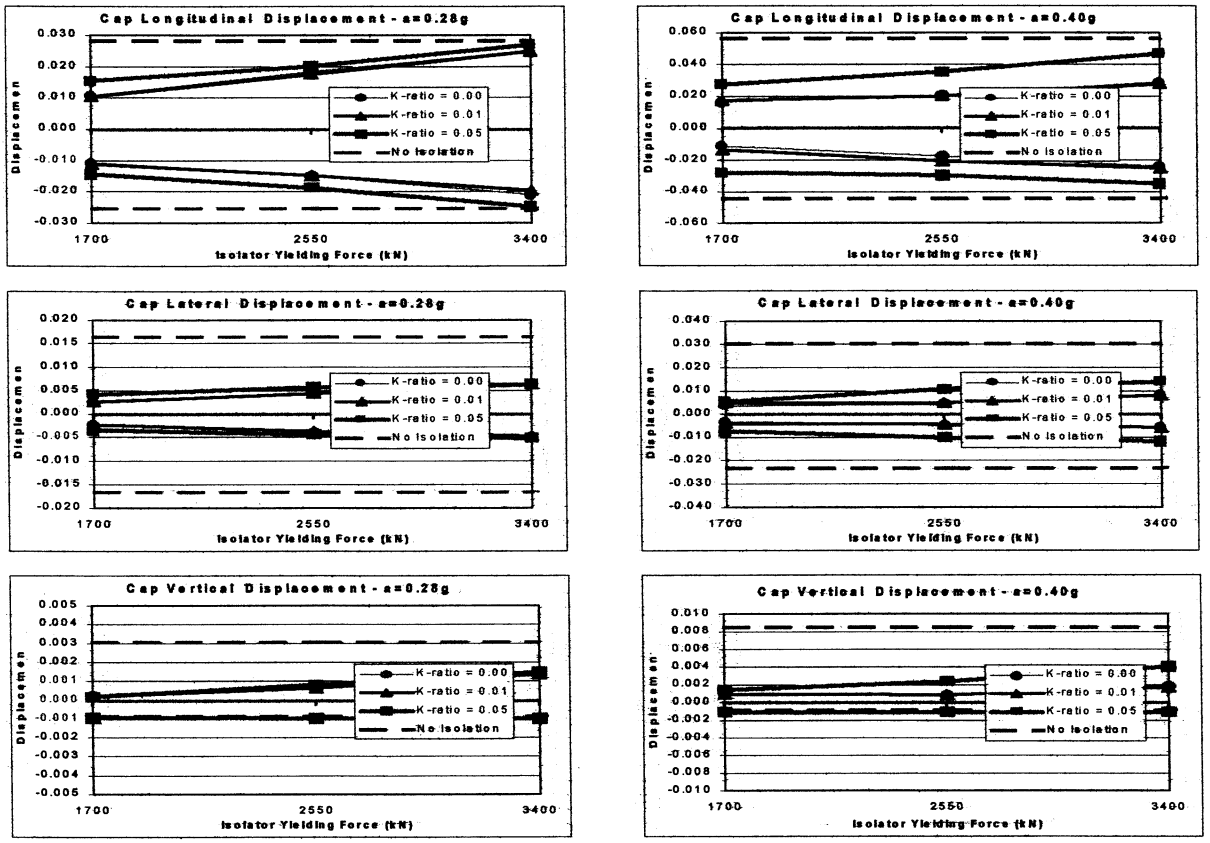


Figure 13. Envelope values of the longitudinal, lateral and vertical displacements of pier caps

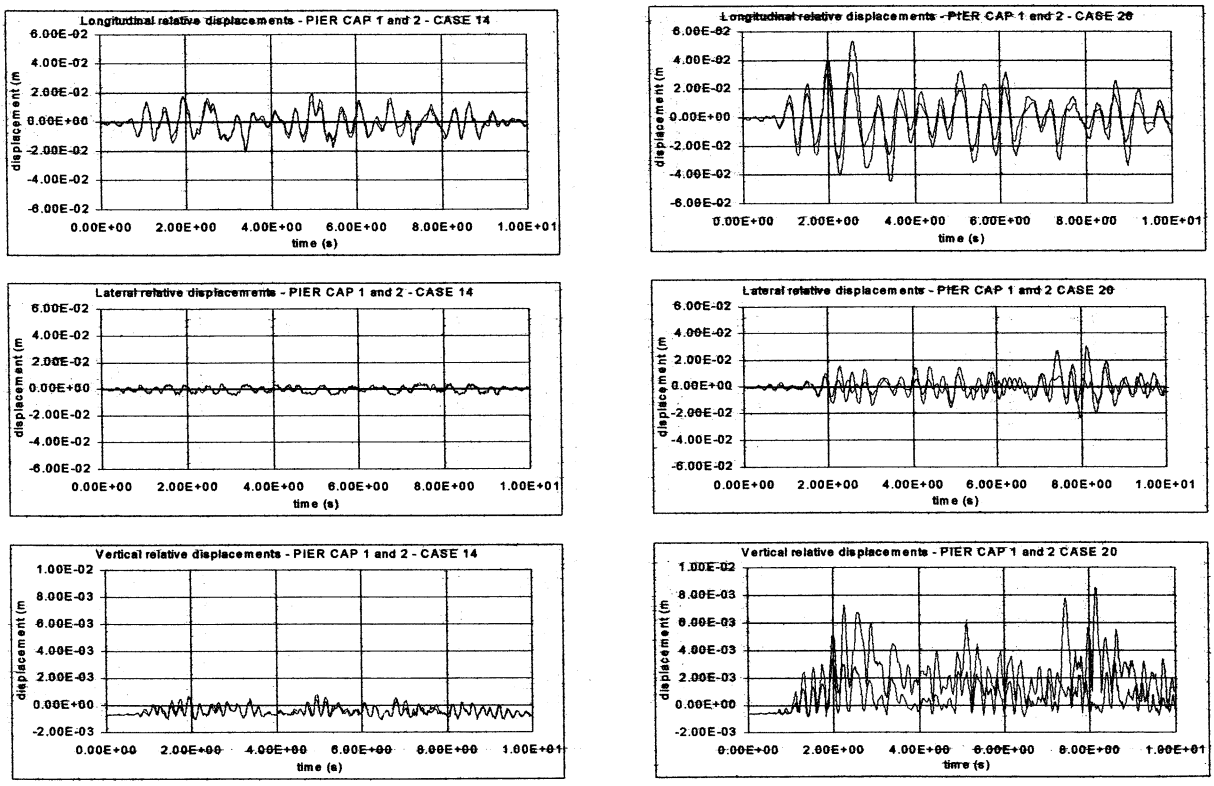


Figure 14. Time histories of the displacements of pier caps 1 and 2 for cases 14 and 20.

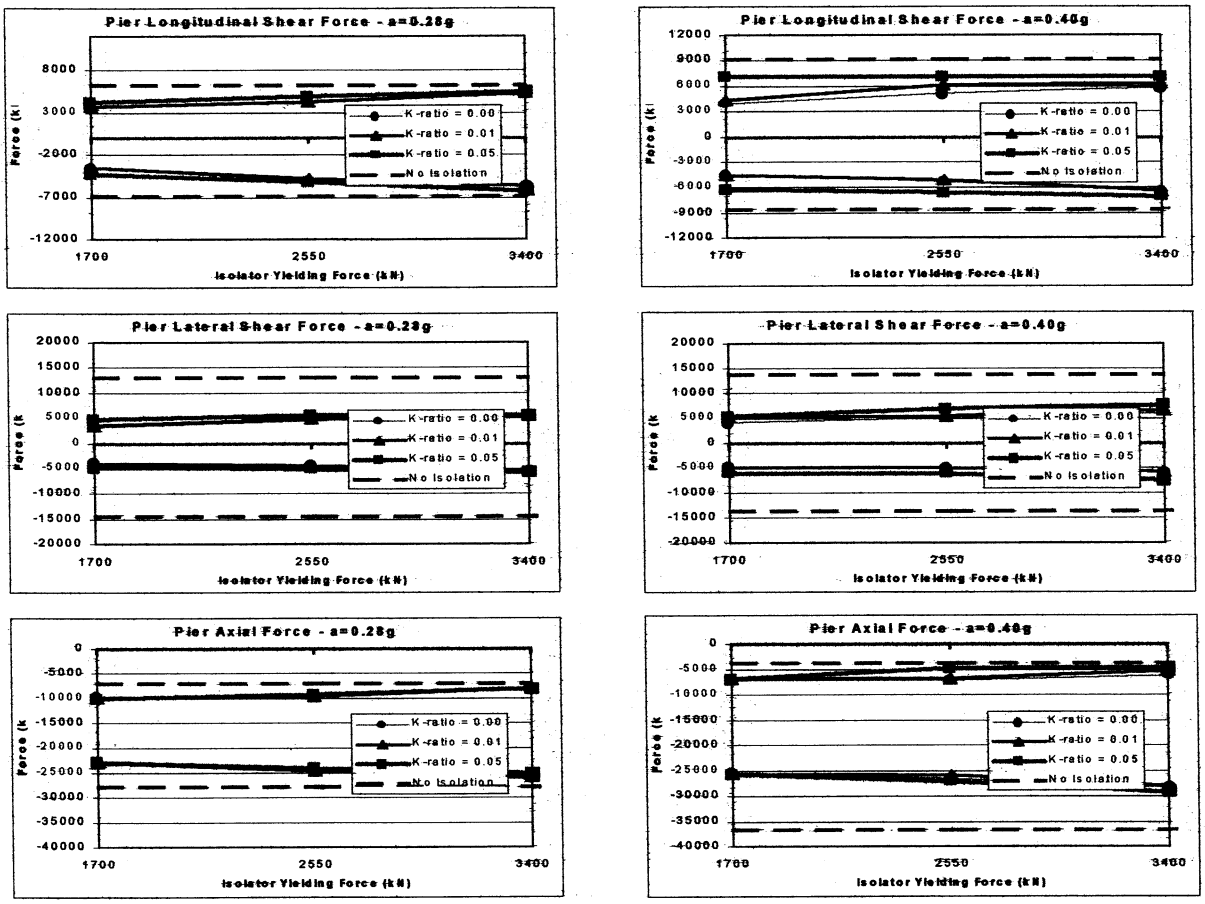


Figure 15. Envelope values of the shear and axial forces in the piers.

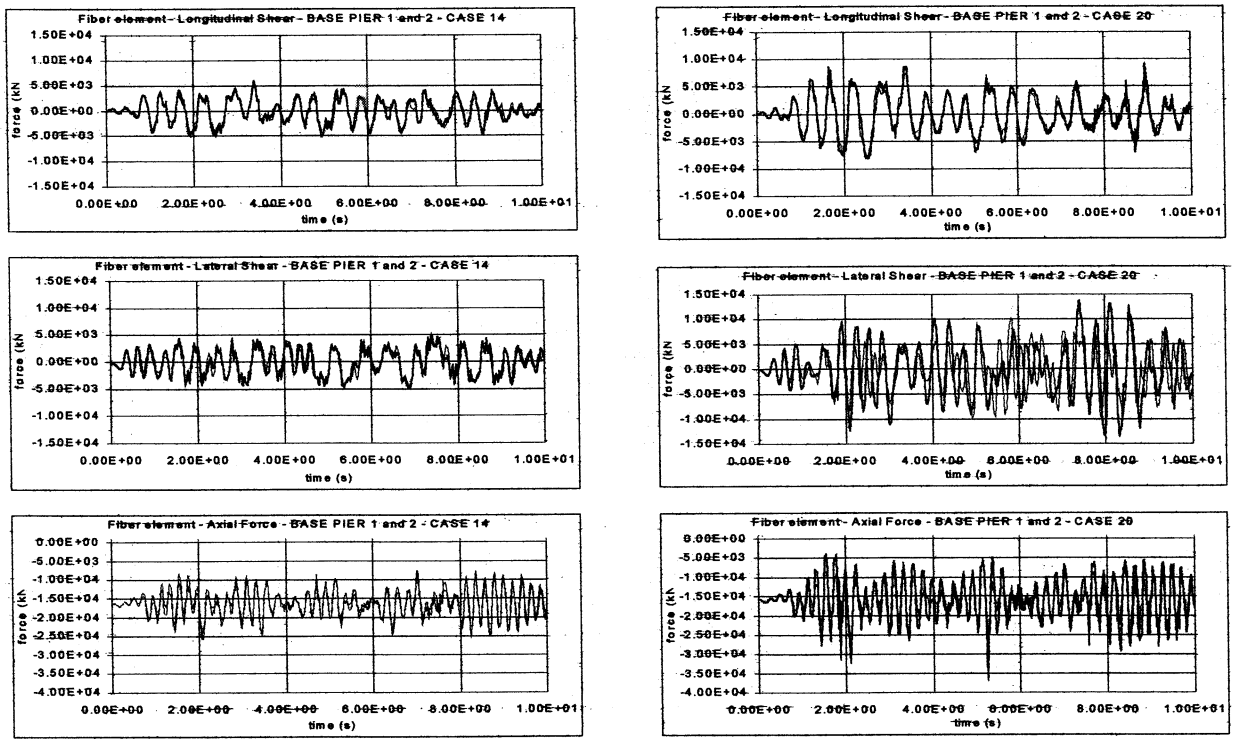
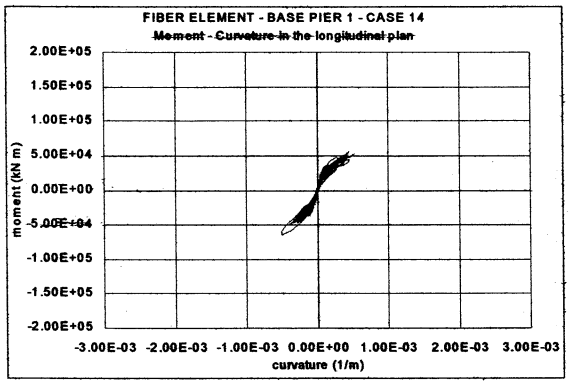
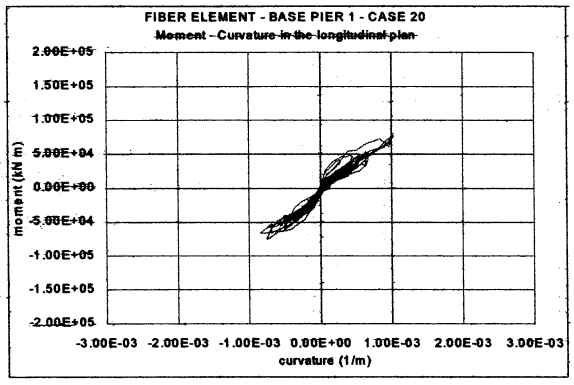
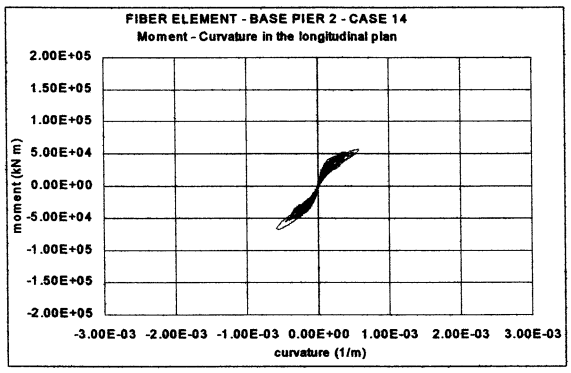
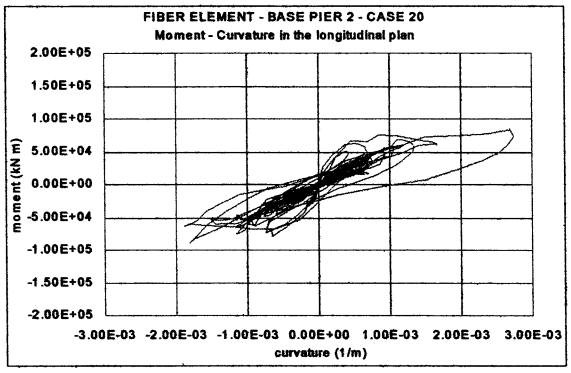


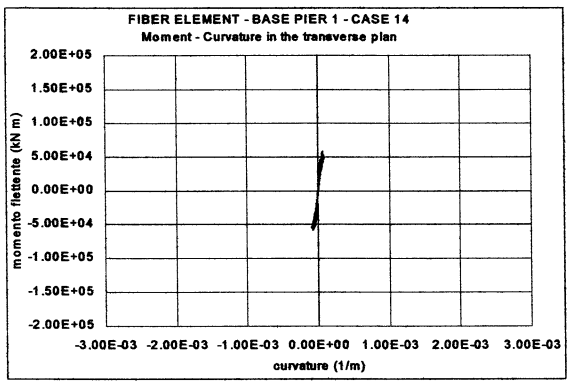
Figure 16. Time histories of the shear and axial forces in piers 1 and 2, for cases 14 and 20.

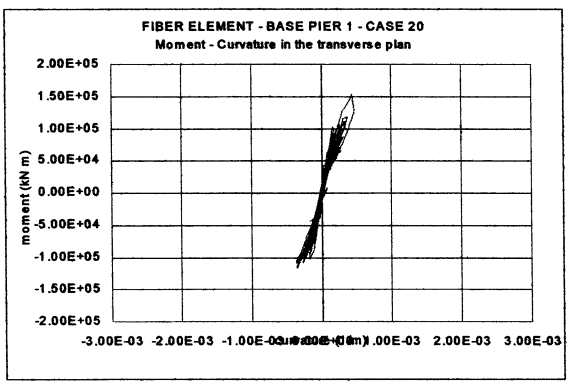


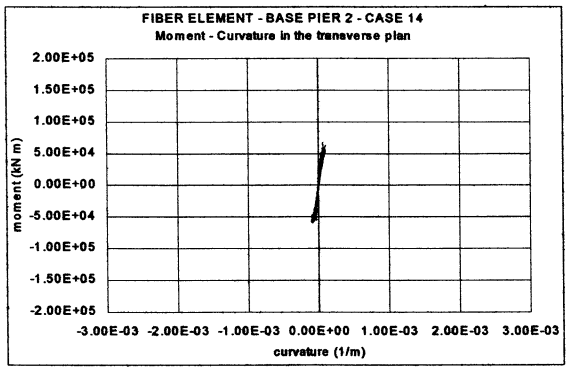












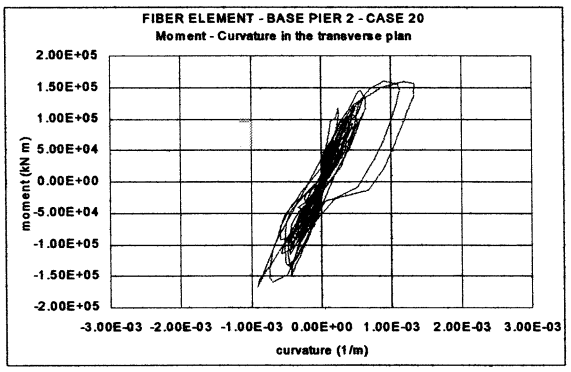


Figure 17. Moment-curvature cycles of piers 1 and 2, for cases 14 and 20.

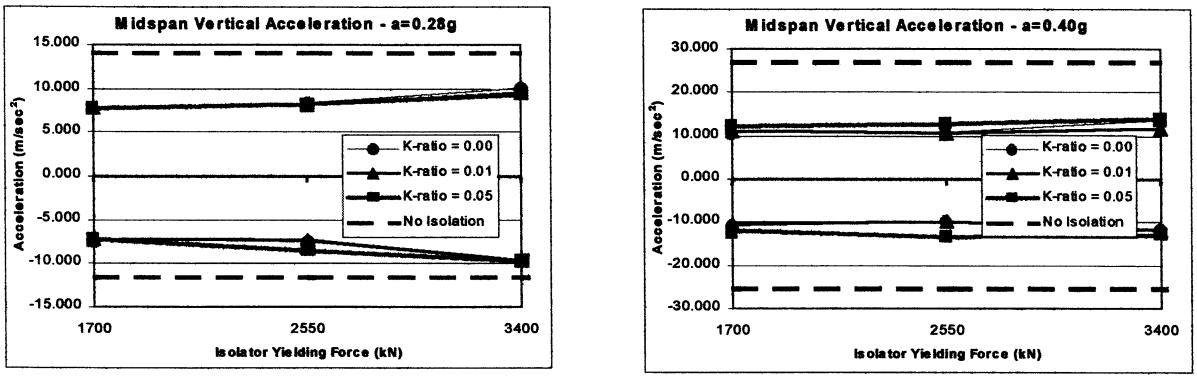


Figure 18. Envelope values of the vertical acceleration at the midspan of the decks.

For all the aforementioned quantities, the response of the isolated bridge is considerably better than the response of the conventional bridge, thus proving the great benefits obtainable with seismic isolation. This is undoubtedly to be ascribed to the considerable reduction of the shear transmitted to the pier in the isolated bridges, thanks to the cut of force operated by the isolation system. The shear at the pier bases of an isolated bridge, in fact, is equal to the yielding force, plus the effects of the eventual post-elastic hardening, plus the contribution of the pier mass, while in the conventional bridge the shear at the pier bases is only limited by their flexural strength.

An impressive beneficial effect is obtained for the vertical displacement at the top of the piers. This displacement is due to the flexural concrete cracking, which lengthen the geometrical axis of the pier (3,5). This effect can be very dangerous as it gives rise to large vertical accelerations in the deck (Figure 17), in this case being magnified by resonance of deck (3), and, consequently, large variations of the pier axial forces. It also contributes to the large variation of the vertical reactions of bearings, up to their uplift, as well as to the uplift rails and of vehicle wheels. The dramatic reduction of the pier curvature (Figure 16) in the isolated bridge reduces considerably the elongation of the pier axis, and then the above said effects.

A further general observation is relevant to the uniform response of the piers (see figs. 14, 16, 17) in the isolated bridge, owing to the equalising effect of the isolation system, while in the conventional bridge the intermediate piers are much more stressed than the external ones.

The moment-curvature diagrams (Figure 17) show that no yielding occurs in the isolated bridge, while concrete cracking is evident in the longitudinal direction and only incipient in the transverse direction. On the contrary in the conventional bridge, yielding occurs in pier 2 and curvatures are 5-10 times greater than in the isolated bridge. The almost equal maximum moments in the piers and in the two directions is also a clear consequence of the cut of force in the two directions operated by the isolation system.

The axial forces at the base of the piers (see figs. 15 and 16) show a large variation, with respect to its initial static value (15700 kN). This is mainly a consequence of the large vertical accelerations induced in the deck by the cyclic elongation of the piers. For the above explained reasons, this effect, as well as the axial force variation, is strongly reduced in the isolated bridge cases.

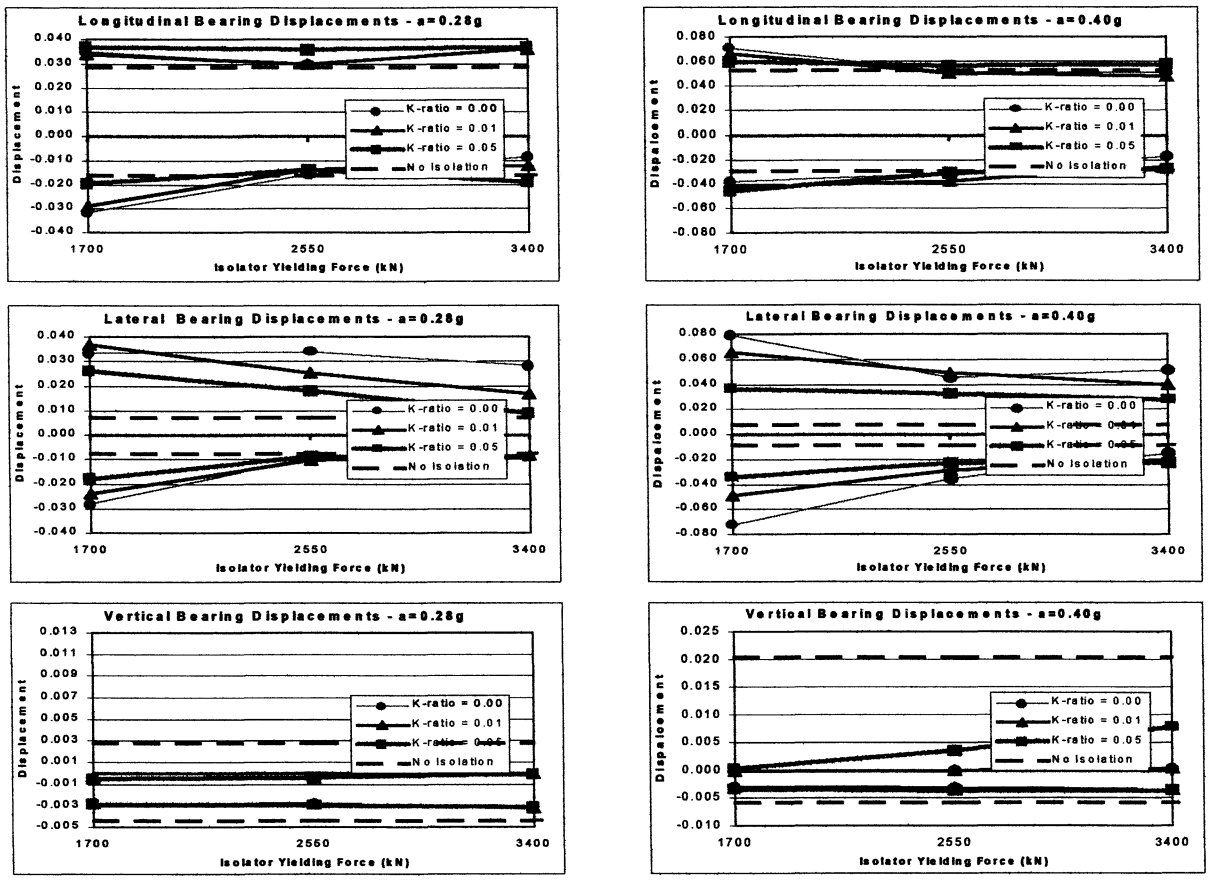


Figure 19. Envelope values of the displacements of the bearings.

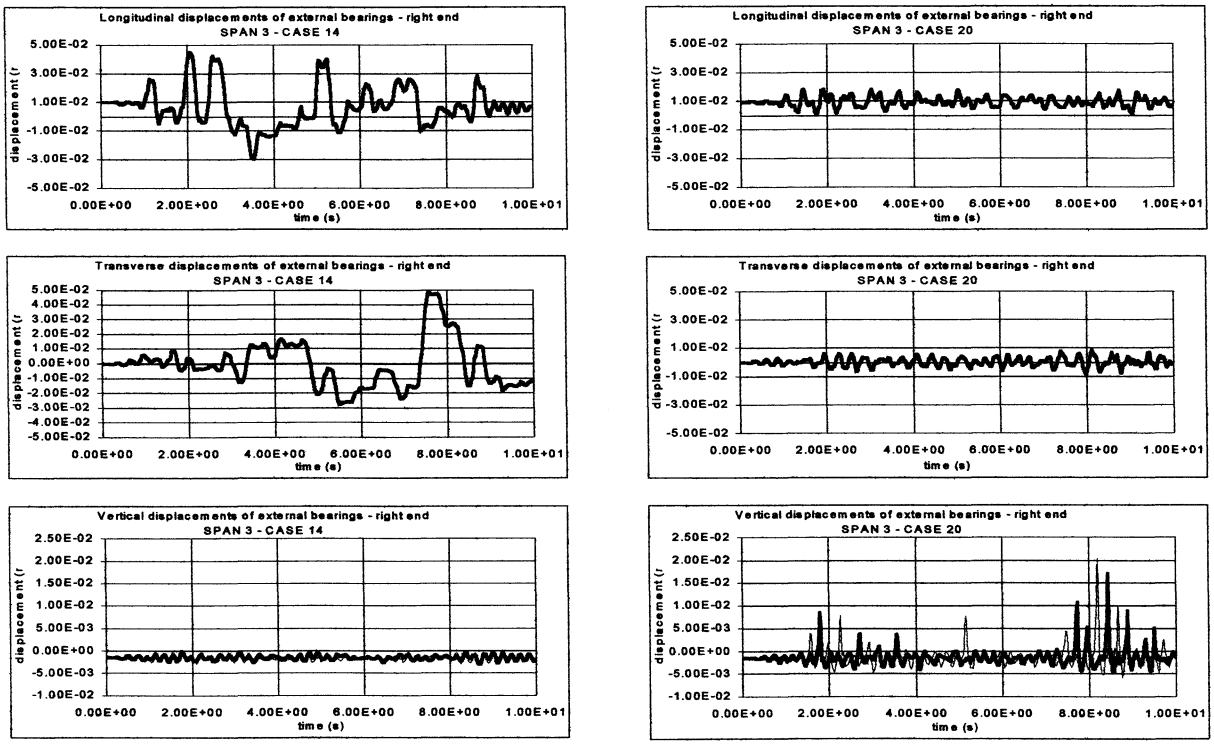


Figure 20. Time histories of the displacements of the bearings of cases 14 and 20.

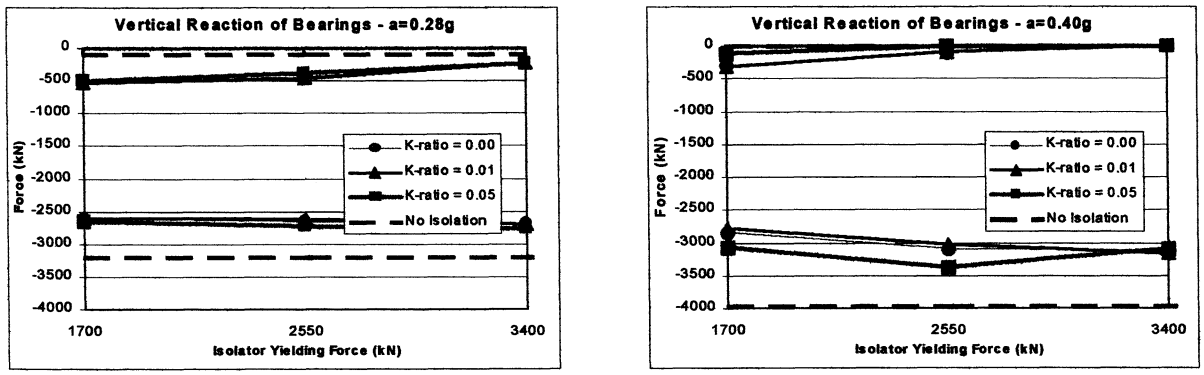


Figure 21. Envelope values of the vertical reactions in the bearings.

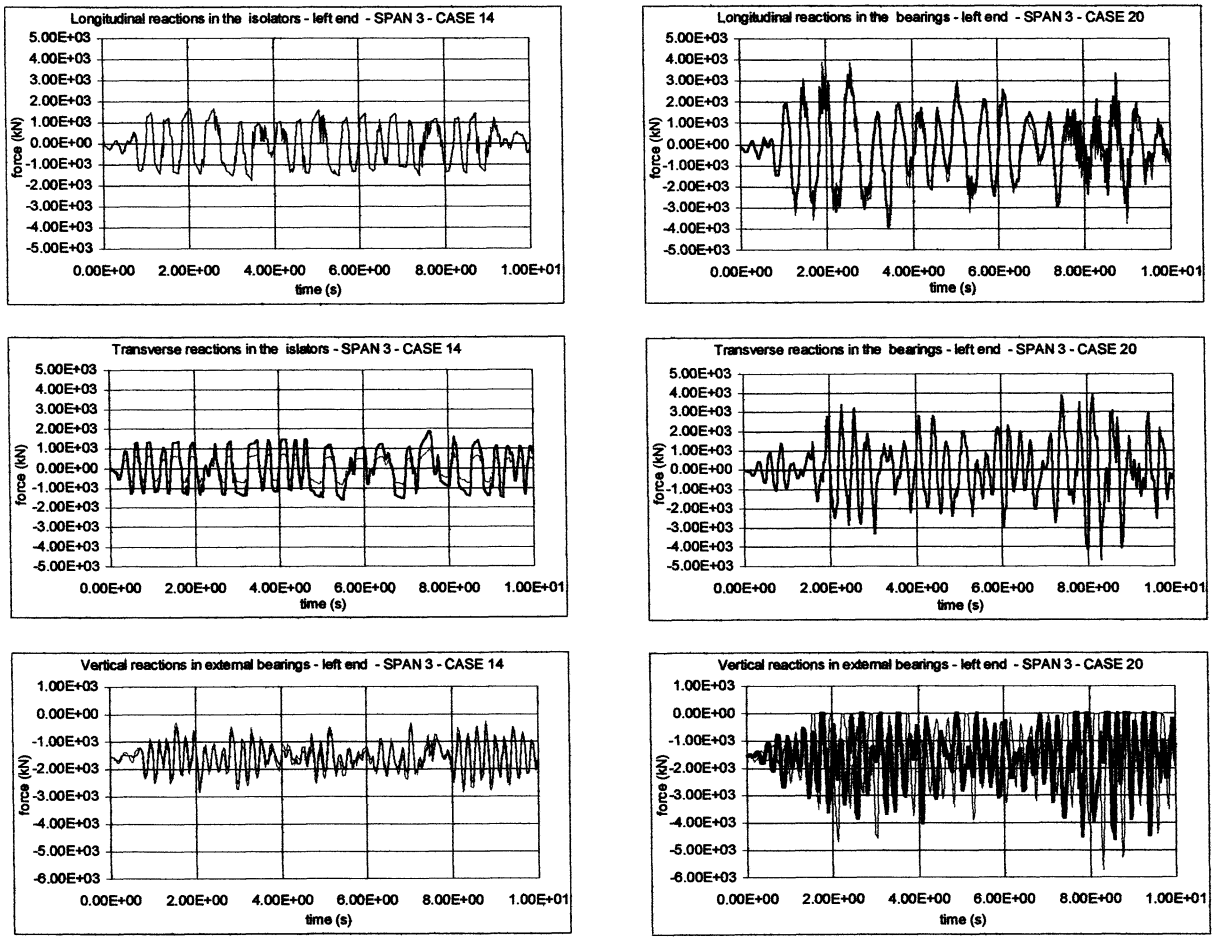


Figure 22. Time histories of the reactions of the bearings in the conventional bridge (case 20) and of the isolators for the isolated bridge (case 14).

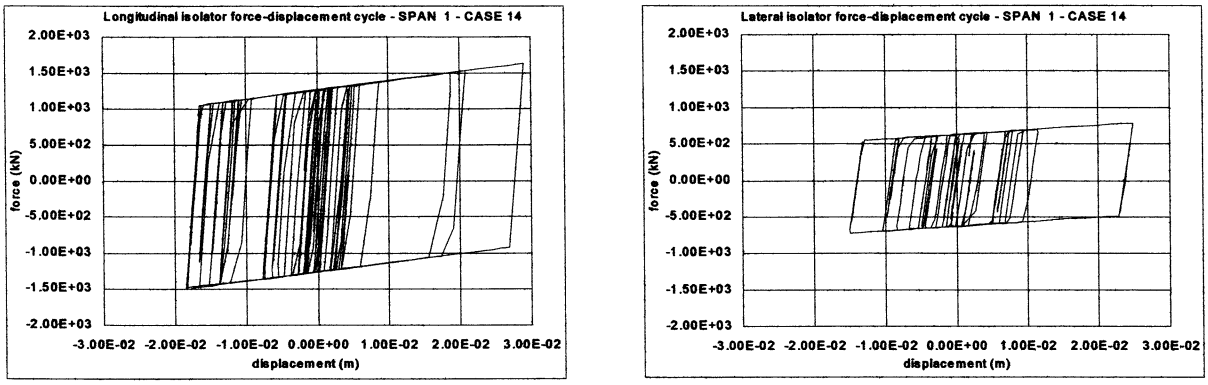


Figure 23. Force-displacement cycles of two isolators of case 14.

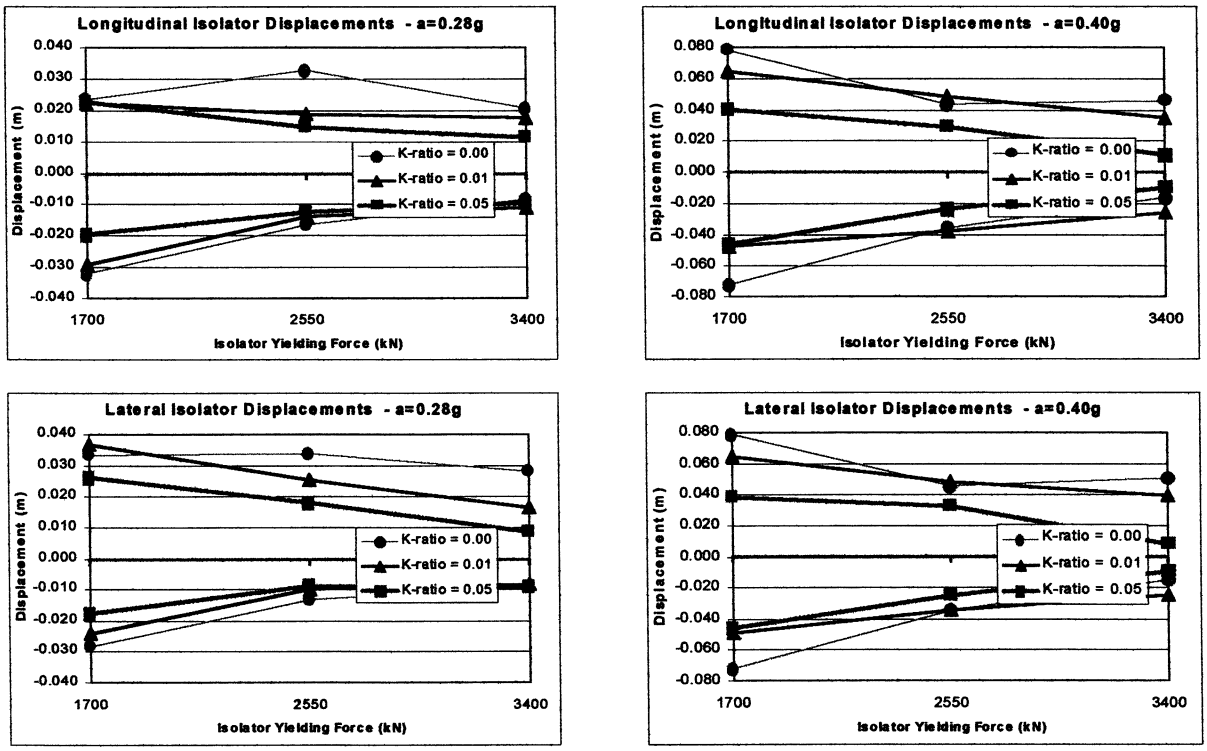


Figure 24. Displacements of the isolators in the isolated bridges.

In figs. 19-24 the response quantities of the bearings and the isolators are shown. In Figures 19 and 20 the envelope values and the time histories of the three displacement components of the bearings are reported. In fig. 21 there are shown the envelope values of the vertical reactions of the bearings. In fig. 22, the time histories relevant to case 14 and 20, for the horizontal reactions of the isolators (case 14) and of the bearings (case 20), and for the vertical reactions of the bearings (both cases) are given. The horizontal reaction of the isolators in the isolated bridge can be directly compared to the horizontal reactions of the corresponding fixed and unidirectional bearings of the conventional bridge. In figs. 23 and 24 there are shown the force-displacement cycles of some isolators of case 14, while the envelope values of the displacements of the isolators are shown in fig. 24.

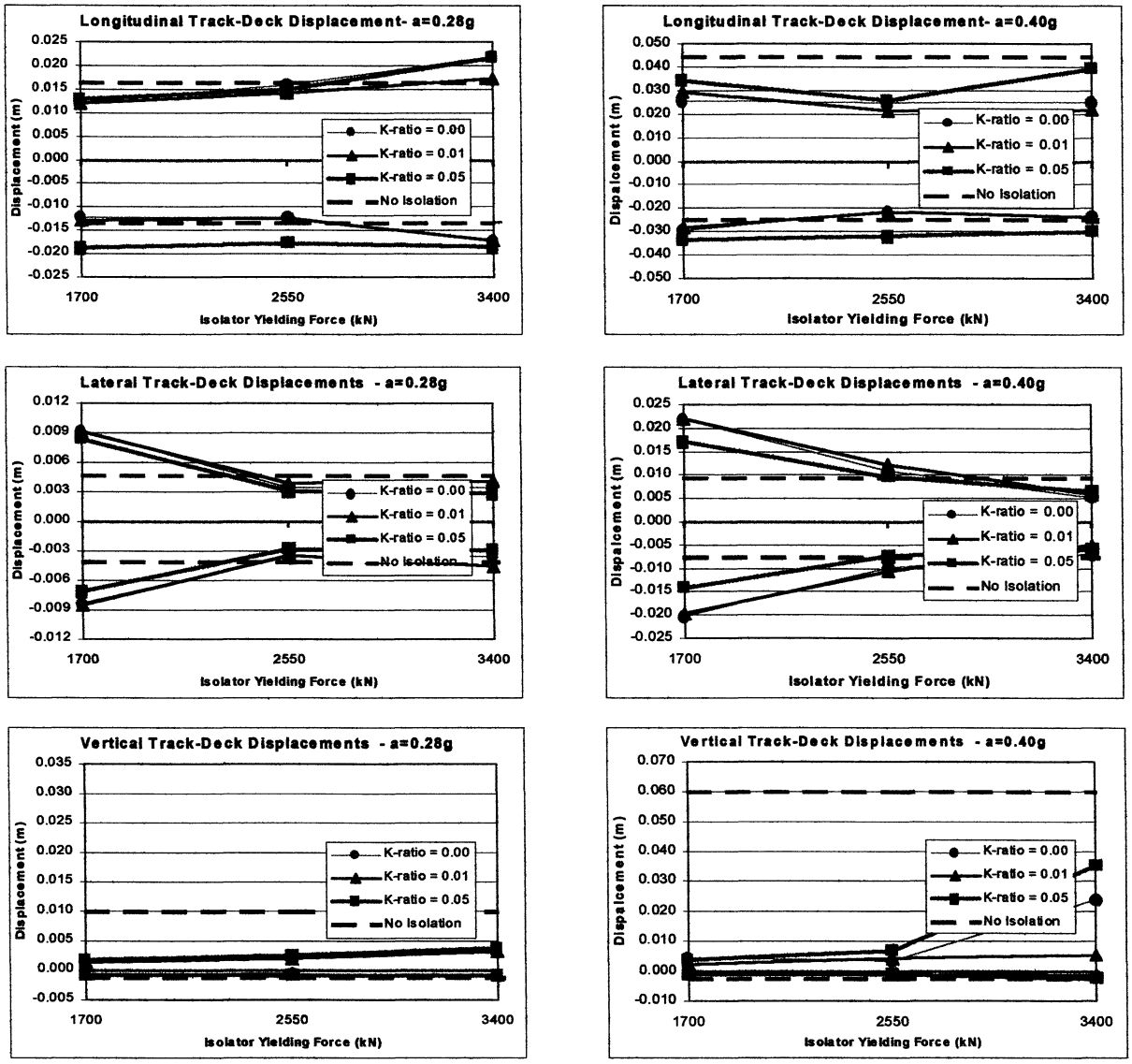


Figure 25. Envelope values of the relative track-deck displacements.

The effect of seismic isolation on the displacements of the bearings is different for the three directions and in the different points of the structural system. Looking at the envelope values (fig. 19), it is clear that the maximum longitudinal displacements are of the same order of magnitude for the isolated and the conventional bridge, though greater values are obtained for low yielding isolator forces and stiffness ratios. However the time histories of Figure 20, which are relevant to the middle bridge span, put in evidence a great difference, being the displacement in the isolated structure much greater than the displacement in the conventional structure. This occurs because, in the conventional bridge, large bearing displacements are recorded only in the external spans, while in the isolated bridges the bearing displacements are similar in all the spans.

Lateral displacements are, obviously, much greater in the isolated bridge, as the fixed condition is assumed in the transverse direction for the conventional bridge.

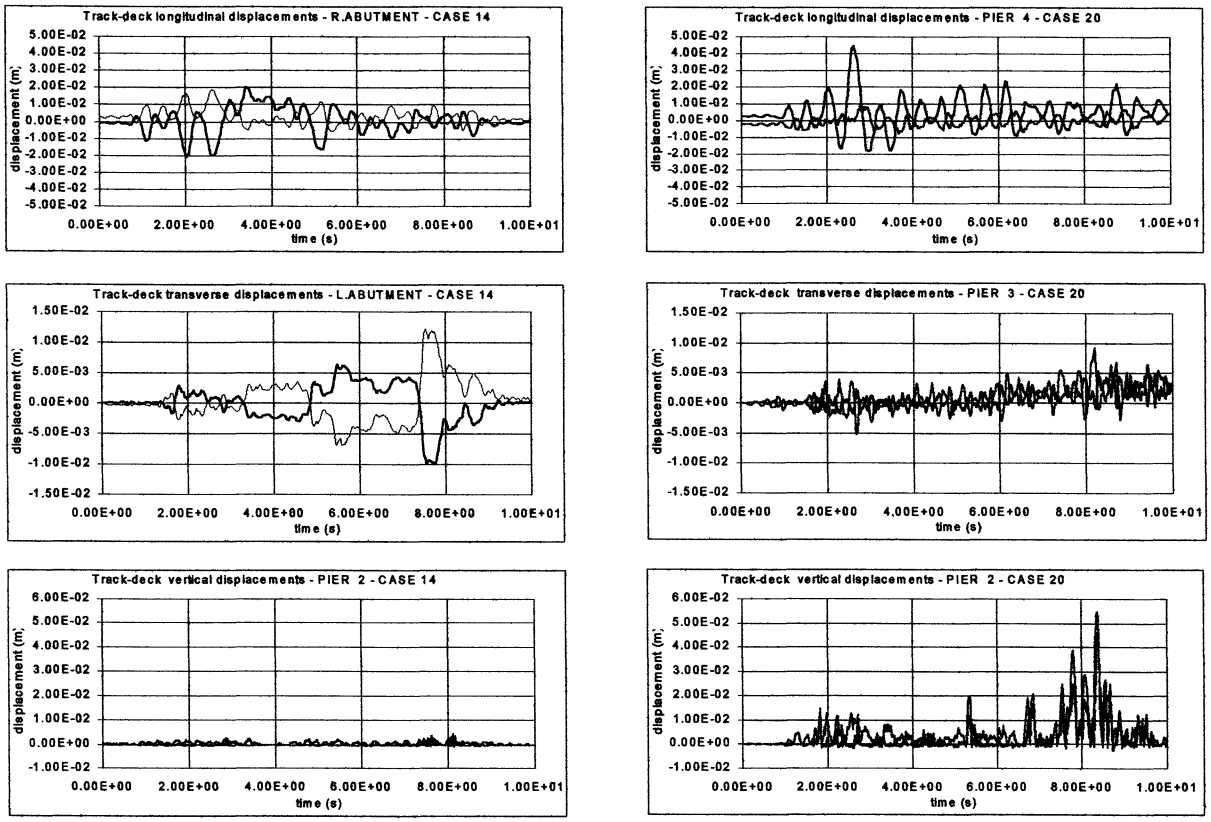


Figure 26. Time histories of the relative track-deck displacements for cases 14 and 20.

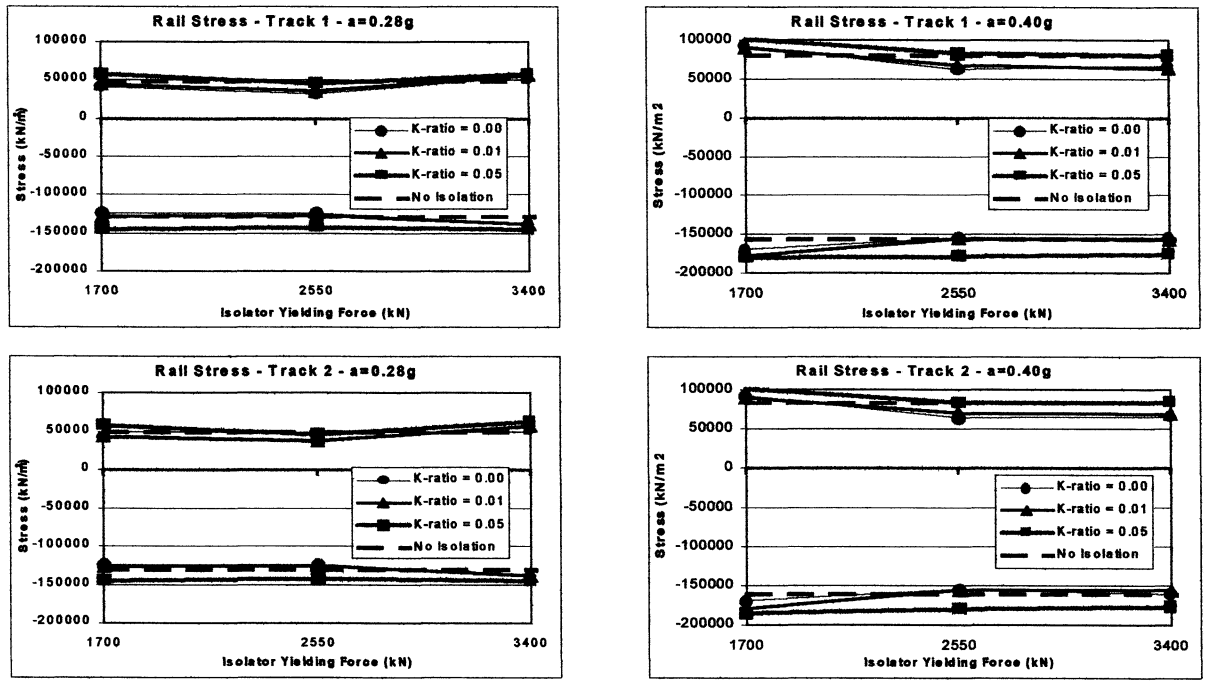


Figure 27. Envelope values of the rail stresses.

are not decreased. In fact seismic isolation reduces significantly the track uplift, thus improving the lateral resistance of the track.

Conclusion

Although the aim of this paper was just to explore the potential of passive control systems in the seismic design of railway bridges, and only a limited number of analyses have been carried out, some significant results have already been found. They emphasise the positive role that seismic isolation and energy dissipation can play for the seismic protection of railway bridges. Some of the results, particularly those relevant to the global structural behaviour, were already known from the numerous previous studies on highway bridges with seismic isolation. Some local effects, such as the beneficial influence of seismic isolation on bearing reactions and uplift, as well as on the vertical deck accelerations, were detected thanks to the very accurate modelling, and occur in railway bridges as well as in highway bridges. Moreover the specific aspects of track-bridge interaction and the possible beneficial effects of seismic isolation have been highlighted by the above shown results.

Summarising the main findings of the present investigation, seismic isolation:

- avoids collapse or even yielding of piers, also reducing considerably concrete cracking;
- avoids uplift of bearings;
- reduces considerably the vertical accelerations of decks;
- reduces considerably forces at the foundation;
- eliminates and reduces considerably vertical displacements (uplift) of rails

The main reason of the performance improvements provided by seismic isolation is due to the dramatic reduction of bending moments in piers. This results in two beneficial effects:

1) the reduction of the cyclic lengthening of the piers caused by concrete cracking;
2) the reduction of rotation of pier caps.

The first effect reduce vertical accelerations in the decks, while the second effect reduces the transverse rolling of the decks. Both result in the above listed positive effects. Moreover, although the presence of vehicles on the deck was not considered in the analysis, it can be supposed that seismic isolation, if suitably designed, could also reduce the risk of transverse tilting of vehicles.

Some savings in the structural costs could, probably, be obtained by seismic isolation, which partially or totally compensate the over-cost due to the devices. The decrease of shear and bending moment, in fact, permits to reduce the longitudinal and transverse steel reinforcements of piers as well as the size and reinforcement of the foundation structures.

The numerical results suggest that also the safety of track could be improved by a suitable design of the isolation system. Although normal stresses in the rails cannot be significantly decreased, track displacements, especially the vertical ones, can be considerably reduced, thus improving the safety to buckling.

To confirm the findings of this preliminary study, an extensive investigation shall be carried out to improve the understanding of the seismic behaviour of railway bridges with different seismic isolation systems. Like in the present investigation, both the safety of track and vehicles and the structural collapse shall be considered. Important additional parameters shall be taken into account, such as the

difference in pier height, the nonsynchronous motion of piers, the presence of train, the different types of isolation systems, the different structural arrangements. Such an investigation, besides confirming the benefits that railway bridge design and construction can gain from seismic isolation, could also give indications on the optimal type and arrangement of seismic isolation system to meet both the structural and the track requirements. Moreover some further studies are needed to assess the suitability of the different isolation system with respect to the normal service conditions of railway bridges, particularly related to the track-structure interactions.

References

1. CEN, "Eurocode 1: Basis of design and actions on structures – Part 3: Traffic loads on bridges", Brussels, 1994
2. FS - ASA Servizi di Ingegneria, "Actions for Railway Bridge Design - Guidelines for Design, Execution and Inspection (Sovraccarichi per il calcolo dei ponti ferroviari – Istruzioni per la progettazione, l'esecuzione e il collaudo)" Rome (in Italian), 1997.
3. M. Dolce, D. Liberatore, G. Traini, "Nonlinear Seismic Analysis of Railway Bridges", Italy-Japan Workshop on Seismic Design and Retrofit of Bridges", Rome, February 1997
4. FS - ASA Servizi di Ingegneria, "Guidelines FS 44b: Technical Guidelines for Railway Manufacts in Seismic Area (Istruzione FS 44b: Istruzioni tecniche per manufatti sotto binario da costruire in zona sismica)", Roma (in Italian), 1996
5. Pinto, A.V., Verzelletti, G., Pegon, P., Magonette, G., Negro, P., Guedes, J., "Pseudo-Dynamic Testing of Large-Scale R/C Bridges", Joint Research Centre - European Commission, Report EUR 16378 EN.
6. M. Dolce, "Passive Control of Structure", Proc. 10th European Conference on Earthquake Engineering, Wien, 1994.
7. M. Dolce, B. Filardi, R. Marnetto, D. Nigro, "Experimental Tests and Applications of a New Biaxial Elastoplastic Device for the Passive Control of Structures", Proc. 4th World congress on joint sealants and bearing systems for concrete structures, Sacramento, California, 1996.
8. CEN European Committee for Standardisation, "Eurocode 8, Design Provisions for Earthquake Resistance of Structures", Part 1.1. ENV1998.1.1. Brussels, 1994

APPLICATIONS OF ISOLATION BEARINGS TO BRIDGES

M. Karshenas Ph.D. P.E. and Iraj I. Kaspar P.E.
Illinois Department of Transportation
Springfileld, Illinois 62764

ABSTRACT

This article reviews applications using three specific types of passive isolation bearings for seismic retrofitting of existing and construction of new bridges in Illinois with emphasis on the selection process and cost of isolation bearings. Experiences on application of isolation bearings, and effective methods of cost reduction, such as competitive bidding for the selection of protective systems, are discussed. Finally, the costs of various protective systems from recent projects are presented for comparison.

INTRODUCTION

Vulnerability of bridge structures to seismic forces has caused a number of failures during recent earthquakes in the United States and other countries. Often, an efficient way to address this vulnerability, both in existing and new bridges, is the use of isolation bearings. In spite of the favorable performance of isolation bearings in reducing seismic force effects on bridge substructures, the use of these bearings is not very wide spread. One of the major reasons for the limited use of isolation bearings is their relatively high unit cost. The additional cost of isolation bearings over conventional bearings is often offset by savings in the substructure retrofitting or by savings in construction cost of bridges due to reduced seismic force level, as a result of using these bearings. In seismic areas, a large number of bridges exist and more are being built annually with the superstructures linked to the substructures by conventional bearing devices. These bearings may be easily replaced with isolation bearings to reduce seismic force effects and enhance the safety of bridges during earthquakes. The mechanism of seismic force reduction in a bridge with isolation bearings may originate from one or more of the following sources:

- Period shift caused by a reduction of lateral stiffness of the bridge
- Distribution of seismic forces to all supports.
- Increase in damping, through yielding of bearing components such as lead core or friction forces acting on sliding surfaces of the bearings.

Increasing the flexibility of a bridge in the lateral directions results in an increased horizontal displacement under lateral forces. Utilizing isolation bearings in bridges generally increases the lateral flexibility as well as the period of vibration during earthquakes at the expense of increased lateral displacements. These increased lateral displacements must be tolerable under service load conditions.

For a superstructure constructed on isolation bearings, all supports may contribute to resisting lateral forces in proportion to the transverse and longitudinal stiffness of the bridge. As will be shown later, altering the lateral load distribution between supports, is a powerful retrofit tool that

can be exploited by proper use of isolation bearings. Another important feature of isolation bearings in bridges is the capability to dissipate seismic energy through resisted displacements occurring within an internal mechanism. In an elastomeric bearing with lead core, energy dissipation is through plastic deformation of the lead core. In a friction type bearing energy is dissipated through the work of friction forces acting at the interface of the sliding surfaces.

PASSIVE ISOLATION BEARINGS USED ON ILLINOIS BRIDGES

Currently, all new and retrofitted bridges in Illinois are required be designed or upgraded for seismic forces in accordance with the AASHTO Standard Specifications for Highway Bridges (1). The utilization of isolation bearings is an alternative strategy in seismic upgrading of existing or design of new bridges that is allowed by the code. In recent years, three types of seismic isolation bearings have been used on Illinois bridges elastomeric type isolation bearings with lead core, friction type isolation bearings with sliding surface, and FIP bearings with attributes of the two previous bearing types. The design of these bearings is governed by the 1991 Guide Specifications for Seismic Isolation Design (2). To qualify the performance and capabilities of these bearings, production samples were subjected to various cyclic tests in addition to those specified by the guide specifications. Following is a brief description of the various types of isolation bearings that were available and found suitable for earthquake resistant bridges.

ELASTOMERIC ISOLATION BEARING

The elastomeric isolation bearing is a force-controlled bearing that has been developed and used as a tool to reduce seismic forces and to provide better distribution of lateral forces among bridge supports. Figure 1 shows the elements of an elastomeric isolation bearing manufactured by Dynamic Isolation Systems, DIS. This bearing provides a positive connection between the superstructure and substructure at each support and eliminates the danger of girders unseating that has often occurred in bridges with ordinary bearings during past earthquakes. The service load deformation of this bearing is a function of rubber properties, rubber dimensions, and lead core size. The force-displacement behavior of this isolation bearing remains elastic under service loads, however, the lead core deforms plastically during earthquakes. Generally, the flexibility of the bearing reduces the overall lateral stiffness of a bridge, increases lateral displacements of the superstructure and reduces inertial forces during an earthquake. While keeping the service load movements of the bridge to a tolerable limit, these isolation bearings allow a controlled movement of the superstructure relative to the substructure elements during an earthquake. The yielding and plastic deformation of the lead core increases the damping ratio of the structure. Also, the lateral forces will be distributed to all supports proportionally to the substructure stiffness that includes the softening effect of the isolation bearings.

FRICTION TYPE ISOLATION BEARING

In a friction type isolation bearing, displacements between the superstructure and substructure are accommodated through a PTFE sliding surface with controlled frictional resistance. Figure 2 shows a sketch of an Eradiquake EQS, sliding type isolation bearing, that was used for isolation bearings of a 6 span continuous bridge on Illinois Route 13. In the United

States, R.J. Watson Inc. is marketing EQS isolation bearings. The displacements between the superstructure and substructure and the frictional resistance at the sliding surface of the bearings, dissipate seismic forces during an earthquake. Hollow cylindrical elements of polyurethane, represented by springs in figure 2, control movements between the superstructure and substructure in both longitudinal and transverse directions during the service loading of the bridge. These elastic springs also provide a restoring force that is expected to bring the superstructure close to its original position after earthquakes. Rotation of these bearings is accommodated through a flexible disk under the steel bearing block. An advantage of these bearings is a sealed box that contains the sliding surface and provides some degree of protection against contamination of the sliding surface. However, a possible disadvantage of this bearing is the potential for variations of the sliding coefficients of friction with time due to wearing or deterioration of the sliding surfaces.

FIP ISOLATION BEARING

This type of bearing is manufactured by the FIP Structural Systems of Italy and has been used for seismic areas in Europe and the United States. Figure 3 shows a schematic view of type I and type II FIP bearings used on three fly-over ramps of the approaches to the Poplar Street Complex in East St. Louis, Illinois. The vertical load transfer element of the bearings could be a steel reinforced elastomer or a pot bearing, depending on the magnitude of the vertical loads. However, the lateral load transfer in each direction is controlled by a number of stainless steel pins that remain elastic under service loads, but are expected to yield and undergo plastic deformation during an earthquake. The frictional resistance at the sliding surface and plastic deformation of the steel pins dissipate seismic forces during earthquakes. In type I bearings, small thermal movements between the superstructure and substructure are permitted through the sliding surface and elastic deformation of the steel pins in each direction. The role of the shock transmitter and the second sliding surface in type II bearings is to accommodate large thermal movements over long periods of time. However, for sudden shocks such as earthquake movements, the shock transmitters lock up and engage the steel pins.

Two advantages of FIP bearings are prominence of steel pins that can be readily inspected after an earthquake and the possibility of different pin stiffnesses for the transverse and longitudinal directions of a bridge. The independent control of seismic behavior in each direction makes these bearings very versatile for design, as opposed to the lead core bearing that has identical nonlinear properties in all directions. The steel pins in these bearings, similar to the lead cores in DIS bearings, are subjected to frequent wind and braking forces during service loading of the bridge and fatigue considerations are warranted in the design of these elements. These bearings do not meet the restoring force requirements of the 1991 Guide Specifications. Therefore, a nonlinear analysis of the bearings must be performed to evaluate the accumulated displacements during a design earthquake. Other disadvantages include high initial cost, potential maintenance cost of the shock transmitters and a non-domestic source.

APPLICATIONS OF ISOLATION BEARINGS TO BRIDGES

The three types of isolation bearings discussed above have been used on a number of new as well as rehabilitated bridges that are located in areas of low to moderate seismicity. A brief description of a number of bridges in Illinois with seismic isolation bearings is given below.

Sexton Creek Bridge

This is a new bridge with three continuous spans of 120, 154, and 120 ft and 43 ft wide deck, built in Alexander County, Illinois, in 1989. The bed rock acceleration at the bridge site was assumed to be 0.2g, according to the AASHTO Standard Specifications, and the soil profile was type III. The superstructure consists of five continuous steel plate girders resting on pile supported 40 ft tall wall-piers and pile bent abutments. Two sizes of DIS isolation bearings were used on this bridge. At the abutments, 13" x 13" elastomeric bearings, 8.38" thick, with 4.25" diameter lead core were used. At both piers, 18" x 18" elastomeric bearings, 8.38" thick, without a lead core were used. This special selection and arrangement of isolation bearings was intended to reduce seismic forces and to direct both seismic and non-seismic forces to the abutments and away from the tall piers. This force distribution scheme takes advantage of the diaphragm action of the superstructure's concrete deck and was found to be an economical design alternative. No special design was employed for the deck slab since the reinforcement required for service loads was adequate to transfer lateral seismic forces to the abutments. This was the first bridge being seismically isolated in Illinois, and the first application to newly constructed bridge in the US, which may be a reason for the relatively low unit costs of $2000 and $3900 shown in table 1.

Cache River Bridge

This bridge, with three continuous spans of 86, 108 and 86 ft, carries Illinois Route 3 over the Cache River Diversion Channel and was scheduled for retrofit and seismic upgrading in 1991. The bed rock acceleration of the bridge site was assumed to be 0.2g per requirements of the AASHTO Standard Specification, and the soil profile was type III. The condition of the bridge and the requirement to keep one traffic lane open at all times during construction dictated rehabilitation of the bridge in lieu of full replacement. Consideration of alternative rehabilitation measures favored keeping the existing 45 ft tall solid wall-piers founded on pile supported footings, and replacing the abutments and the deteriorated superstructure in two construction stages. A technically feasible method to salvage the existing piers in spite of potentially high seismic forces was the use of isolation bearings. The piers were originally designed only for wind and service loads that were substantially smaller than seismic forces. The special arrangement of isolation bearings with no lead cores at the piers and isolation bearings with lead cores at the new abutments allowed transferring the majority of the seismically induced forces to the new abutments. The new abutments, coupled with the diaphragm action of the deck slab, were designed to take the lateral forces.

In this project all three features of the isolation bearings period shift, increased damping and special distribution of seismic forces were utilized to salvage the existing piers, playing a critical

role in allowing stage construction of bridge. The bearings that were considered in design and used on the bridge were DIS type with a furnishing and installing cost of $3000 and $3900 per bearing at abutments and piers respectively, as given in table 1.

Approaches to the Poplar Street Bridge

This six span continuous steel multi-girder superstructure with spans ranging from 108 to 161 ft was built in the late 1960s and rehabilitated in 1989 with no consideration for seismic forces. After the requirements for seismic design of bridges were established in the after-math of the Loma-Prieta earthquake, this bridge was upgraded for seismic forces. The bedrock acceleration of the site was 0.12g and the soil profile was type III. A retrofit alternative that replaced the original rocker bearings with isolation bearings was found adequate to reduce and redistribute seismic forces thus avoiding major substructure or foundation retrofits. The 128 original rocker and fixed bearings supporting the one year old deck slab were individually jacked and replaced by isolation bearings with no traffic disruptions. The bridge was designed and retrofitted using 128 DIS type bearings.

Mainlines of the Poplar Street Complex

The elevated structures of the Poplar Street Complex interchange, in East St. Louis, Illinois, were built in the late 1960s and consisted of two girder system superstructures with two or three-column substructures supported on a crash wall and pile footings. In 1993 and 1994 the mainlines of the interchange carrying I-55/70 were replaced with new bridge units 43 ft wide and span lengths ranging from 90 to 135 ft. The new superstructure consisted of 6 lines of 60" deep steel plate girders, and the substructures were two column piers rigidly framed into a cap beam and supported on a crash wall and pile footings. The acceleration coefficient of the bridge site was assumed to be 0.12g based on the AASHTO Standard Specifications, and soil profile was type III. The design alternative with isolation bearings was found suitable for the bridge units and 350 DIS elastomeric bearings with lead cores were used. The unit cost of the DIS bearings for this project ranged from $5000 to $6200, as given in table 1. The design was performed with reduction factor of one, assuring elastic behavior of the structural components during a design earthquake. Approximate savings from the use of isolation bearings, instead of strengthening these substructures, was estimated at 4% of the total construction cost.

Fly-Over Ramps of Approaches to the Poplar Street Bridge

The portions of three ramps that cross over the newly replaced mainlines in East St. Louis, were rehabilitated to protect mainlines in case of an earthquake. The substructure for these ramps consists of two circular columns on a crash wall with pile footings. The column heights varied from 40 to 60 ft with diameters ranging from 5 to 7 ft. The superstructure is two-girder system with steel plate girders and a concrete deck slab that was completed in the late 1960s with no seismic design considerations. The elastic capacity/demand ratios for various substructure components indicated insufficient splice length of the main column reinforcing bars, inadequate seat width at expansion bearings, and inadequate pile to pile-cap connections. Retrofitting with FIP isolation bearings was found an acceptable alternative that reduced seismic force demands

below the existing capacity and no seismic retrofitting of the structural components was theoretically required. External confinement bands were added to pier columns over bar splices due to concerns regarding the lap lengths provided and based on improvements demonstrated by field tests. A total of 30 FIP isolation bearings were used on three fly-over ramps with unit costs ranging from $8000 to $12000 for furnishing each type I and type II bearings.

Figure 4 shows the elastic capacity/demand (C/D) ratios for seismic moments at column bases in piers S7 to S18 of the fly-over ramp S (3). The C/D ratios were determined for two retrofit scenarios that replaced existing bearings in the structure with DIS and FIP bearings. A comparison of the reduced seismic moments at the base of the columns, with FIP isolation bearings, achieved C/D ratios larger than one that theoretically eliminated a substructure retrofit.

Illinois Route 13 Bridge

This is a new bridge with six continuous spans ranging from 131 to 198 ft over the Illinois Central Railroad. The superstructure consists of six continuous steel plate girders with a concrete deck 43-ft wide. The substructure consists of wall piers and abutment bents, all on pile supported footings. A study of various design alternatives showed more than 5% cost savings could be achieved by using isolation bearings on this bridge, for the site acceleration of 0.12g and soil profile type III. The bridge design plans were prepared considering DIS type isolation bearings with lead cores. However, the contract documents permitted the use of substitute bearings, provided they could reduce seismic forces to a level below the design capacity specified in the contract documents. As shown in table 1, 42 bearings were used on the abutments and piers with unit costs of $3700 and $4600, respectively for type I and type II bearings. This unit cost is substantially lower than previously incurred for bearings of similar sizes. The total isolation bearing cost amounted to 4.5% of the total construction cost of the bridge. Damping ratio of the bearings was about 55 percent of the critical, requiring a nonlinear analysis of the isolated bridge to satisfy the requirements of the 1991 Guide Specifications.

In the early 1990s, bridge designers had limited choices of protective systems, and substructure design was commonly performed based on a pre-selected type of isolation bearing. In recent years, however, due to the availability of various isolation devices, for cost savings through competition, designers have tried various contract procedures to provide better opportunities for any protective system manufacturer to participate in the selection process. The competitive bid process was used on a bridge that resulted in substantial bearing cost reduction as shown in the last two rows of table 1. For this bridge, the design documents were prepared with DIS bearing; however, substructure design forces were given in the contract documents. The design documents then allowed any alternative isolation bearing to substitute the DIS shown on the plans, if they could satisfy the design parameters. The bid price of the DIS isolation bearings with the equivalent diameters given in the last rows of table 1 was close to the price for the friction type bearings that were finally used on the bridge.

Experience in the use of isolation bearings has shown that the contract specifications should allow for various pre-approved bearing types, rather than calling for a specific type of bearing. Competition will not only result in lower prices, but will encourage new types of isolation

bearings to participate in the selection process. Drawbacks of this procedure include more research and inspection by the owner and the need for precise specification requirements. The service loads, including wind, braking force, temperature induced forces and displacements, and the energy dissipated in a cycle at maximum seismic displacement must be given. The substructure units are designed for the forces given and any isolation bearings that provide similar or better conditions with no need for redesign of the substructure should allowed be used on the bridge. Table 1 shows the size and cost of various types of isolation bearings that have been used on bridges in Illinois since 1990. The unit costs include furnishing and installation of bearings on new as well as retrofitted bridges. Part of the substantial cost reduction in bearings over the last 3 years can be attributed to competition among the various manufacturers.

Testing of Isolation Bearings

The requirements of the 1991 guide specifications for seismic design of isolation bearings specify a set of prototype tests to establish the design properties of protective systems and a set of quality control tests to verify the as-built system properties. These guidelines were used to satisfy design requirements prior to acceptance and installation of the isolation bearings used in Illinois. Some pre-qualification tests to established fundamental characteristics of the bearings were conducted previously by the manufacturers of these systems, and did not need to be repeated.

At the time, limited information was available on the effect of temperature, aging, freeze-thaw cycles and fatigue on most isolation bearing components, and the current 1991 guidelines remained silent on such issues. To verify the expected performance characteristics of isolation bearings, a series of quality control tests on randomly selected samples of isolation bearings were conducted. These quality control tests consisted of static and dynamic testing of the representative samples under service loading as well as cyclic loading to verify design parameters.

For the three types of isolation bearings used on Illinois bridges, a series of tests were conducted on bearing samples to verify both service and seismic loading properties of the completed bearings. For friction type isolation bearings, two test samples were subjected to a thousand-hour salt spray test (ASTM salt-fog) simulating conditions of isolation bearings in cold environments, where the bearings are likely exposed to cycles of salt spray in the winter. The fog-tested bearing samples were then subjected to axial and lateral cyclic forces and displacements in the lab to verify the properties of the bearings that were assumed for design. In addition, the stiffness sensitivity of the completed samples of isolation bearings was tested at 0° F, and at 90° F.

SUMMARY

The benefits of isolation bearings are well established as lateral- force-control devices that allow designers to reduce or redirect seismic forces to various supports. These benefits can be summarized as follows:

- Isolation bearings can be effectively utilized in retrofitting and the design of most new bridge structures in seismic regions.
- As a retrofit tool, isolation bearings can reduce construction costs and traffic disruptions by eliminating the need to strengthen substructure units.
- A generic design that allows competitive bidding for isolation bearings can reduce the initial cost of isolation bearings.
- Testing of isolation bearings should include the effects of temperature, aging, and other ambient conditions that could potentially affect their performance both in service and during earthquake events.

REFERENCES

1- AASHTO Standard Specifications for Highway Bridges, Published by the American Association of State Highway and Transportation Officials, Sixteenth Edition 1996.

2- Guide Specifications for Seismic Isolation Design, published by the American Association of State Highway and Transportation Officials, AASHTO, June 1991

3- Seismic Study Report, "Comparison of DIS and FIP Seismic Isolation Bearings, Retrofit of Ramp S", FAI-70, St. Illinois Department of Transportation, by Sverdrup Corporation, June 1992.

Table 1- Isolation bearings used on Illinois bridges since 1989

Type & Location	Construction Date	Size (In)	Number (Each)	Unit Cost $	Design
DIS- Abutment Sexton Creek	1989	13 x 13	10	2000	Specific
DIS, Pier Sexton Creek	„	18 x 18	10	3900	„
DIS, Abutment Cache River	1990	12 x12	10	3000	„
DIS, Pier - Cache River	„	14 x14	10	3900	„
FIP, Type I, Poplar St. Ramps	1993	16Φ **	12	8000	„
FIP, Type II, Poplar St. Ramps	1993	20Φ **	18	12000	„
DIS, Abut. Poplar Complex B	„	14 x 14	78	5300	„
DIS, Pier „	„	17 x 17	35	5900	„
DIS, Pier „	„	19 x 19	61	6200	„
DIS, Abut. Poplar Complex C	1994	13 x 13	70	5000	„
DIS, Pier „	„	17 x 17	105	5940	„
EQS, Friction Type-IL Rte. 13	1995	16Φ **	12	3700	Generic
EQS, Friction Type-IL Rte. 13	1995	20Φ **	30	4600	„

** Approximate diameter of equivalent elastomeric isolation bearing

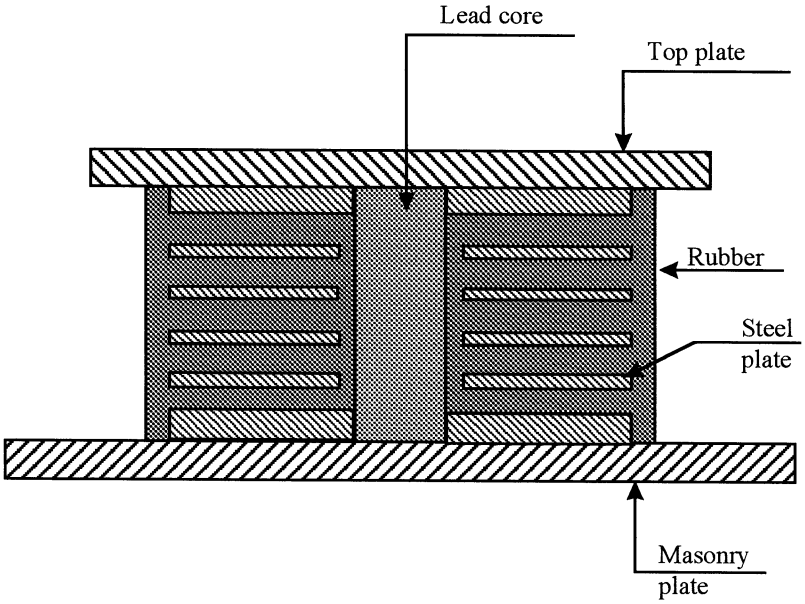


Figure 1- Elastomeric isolation bearing
with lead core

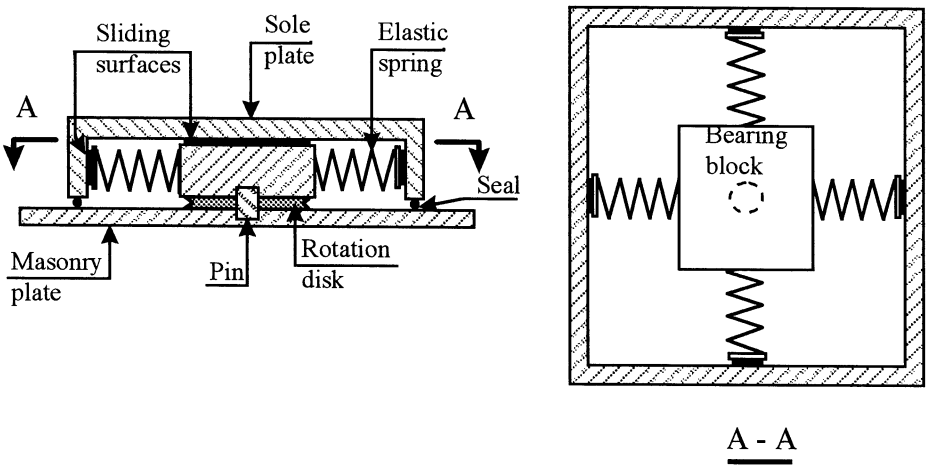


Figure 2 - Elements of an Eradiquake
isolation bearing

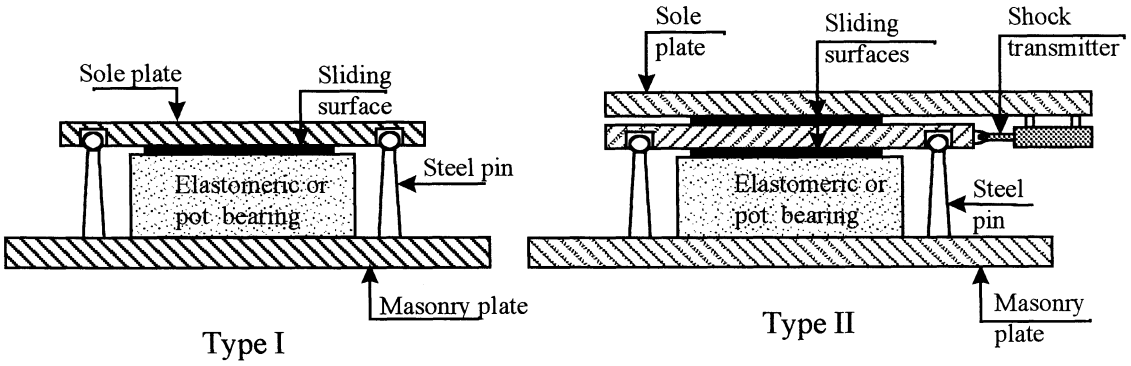


Figure 3 - FIP isolation bearings

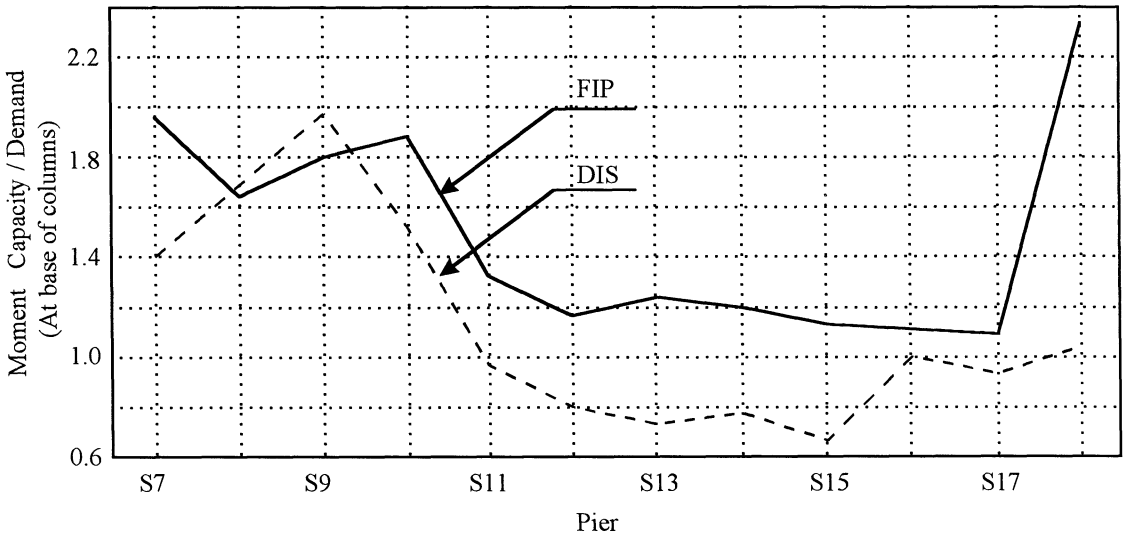


Figure 4 - Elastic C/D ratios for piers S7 to S18

SEISMIC BEARINGS FOR LARGE SPAN BRIDGES

Roy A. Imbsen, P.E., D.Engr.
Imbsen & Associates, Inc.
Sacramento, California

ABSTRACT

One of the most effective strategies in enhancing (or tuning) the seismic response of a bridge to seismic events is the effective use of isolation bearings. Implementing this strategy for long span bridges requires the use of large bearings (up to 3 m [10 ft] in diameter), designed to have properties specific to each application. Several types of bearings are currently available for this purpose which include 1) friction pendulum isolation bearing, 2) slider with elasto-plastic springs, 3) elastomeric isolation bearings (e.g., lead core - rubber bearing), 4) elastomeric with metallic dissipaters, etc. Use of these types of bearings on large bridges requires that they are designed to carry as much as 10,000 kips of vertical load and allow for displacements up to ±1.2 m (± 4 ft), i.e., 2.4 m (8 ft) total.

Imbsen & Associates, Inc. has incorporated isolation bearings in the seismic retrofit design of several major bridges, which include for example: The I-40 Mississippi River Crossing near Memphis, Tennessee, The Golden Gate Bridge in San Francisco, and the Benicia-Martinez Bridge in California. The elastomeric isolation bearing was used in the Golden Gate Bridge and the approaches on the Benicia-Martinez Bridge, and the friction pendulum bearing has been proposed for the I-40 and main span on the Benicia-Martinez Bridge.

Analysis methods for incorporating isolation in retrofit design is presented below, followed by a discussion of their specific applications to the three bridges mentioned above.

ANALYSIS AND DESIGN

The analytical procedures used for the design of bridges with isolation bearings must be able to model the nonlinear characteristics of the structure and the isolation bearings. A detailed nonlinear seismic analysis is usually required to obtain accurate results. However, simplified methods can be used for preliminary analysis to perform certain sensitivity studies and determine the best location and the most effective use of the isolation devices. Both methods are described below

Simplified Analysis

The system of a bridge with isolation bearings can be simplified to a two degree of freedom linear system as shown in Figure 1. The pier and foundation mass is lumped to the top of the pier as the primary mass m_1 and the tributary superstructure mass is lumped as the secondary mass m_2. The characteristics of isolation bearing is shown in Figure 2, in which k_i represents the initial elastic stiffness of the bearing with a yielding capacity of F_y, and k represents the post-yielding stiffness. If the maximum displacement of the bearing is u_{max}, then the equivalent bearing stiffness k_{eq} can be expressed as:

$$k_{eq} = \frac{F_{max}}{u_{max}} = \frac{F_y + k(u_{max} - u_i)}{u_{max}} = \frac{F_y\left(1 - 1/k_i\right)}{u_{max}} + k \qquad (1)$$

Either a frequency domain analysis or a time domain analysis can be used to evaluate the seismic performance of the simplified system [1].

For major bridges supported on massive piers, seismic isolation concept should be treated as part of the structural tuning for the overall lateral load path of the structural system including the foundation flexibility. By carefully selecting the locations and properties of the isolation devices, the force transferred to both superstructure and piers can be minimized. Different structures and site conditions may result in significantly different strategy in applying the seismic isolation concept. The simple two-DOF system and analysis methods can be used to evaluate the seismic responses of the bridges before proceeding to the detailed analysis and design.

Detailed Analysis

An integrated seismic analysis methodology for evaluation and retrofit design of major bridges has been developed using nonlinear global and local analytical models, and substructuring method. To carry out this analysis most efficiently, our philosophy has been to use rigorous but simplified analytical formulation. The motivation is that, with rigorous formulation, we can keep track of assumptions made; and with simplified method, we can obtain results quickly to establish an in-depth understanding of the engineering problem. Then, we can proceed to carefully scrutinize all assumptions made, establish sensitivity of the response with respect to assumptions and uncertainties, and ensure compliance with the structure seismic performance requirements [2].

For a large-span bridge seismic retrofit design, site specific seismic hazard is first established. The spatial variation of ground motion, along the bridge alignment, will be appropriately accounted for. The general substructure method is then applied for the global analysis formulation including soil-foundation-structure interaction effects. Foundation impedance and effective foundation input motion are developed at each foundation for use in global time history analysis. Assumptions made in the substructure formulation are verified through consistent development and analyses of local substructure models.

Global Model and Analyses

Having defined the effective foundation input motions and foundation impedance matrices, the global analytical model can be used in nonlinear time history analyses to establish seismic force and deformation demands in structural system and components. The global model contains nonlinear modeling of relevant components above the foundation, such as isolators, hinges, expansion joints and piers. The results of the global analyses are primarily used to:

1. Assess superstructure member responses (both existing and new members)
2. Assess nonlinear performance of isolator bearings (both displacements and forces)
3. Assess response of the superstructure at discontinuities (expansion joint and span hinge elements)
4. Establish foundation displacement demands (to be used in the pushover analyses of stand-alone foundation models)
5. Establish foundation force demands (to be used in feed-back verification analyses of substructure systems)

Local Models and Analyses

The key aspect of the detailed analytical procedure is the effective use of global and local analyses to establish response assessments, verification of assumptions, and/or to conduct sensitivity studies. The key local analyses can include:

1. Local Analyses of Isolation Systems
2. Foundation Feed-Back Analysis
3. Response Sensitivity to Caisson Yielding
4. Local Pushover Analysis of Stand-alone Substructure Models

TESTING

The isolation bearings have been used on several bridges in the past. However, what makes the applications that are discussed in this paper unique, is the size of the bridges, and the size of the bearings used to tune their responses. These bearings are more than 3 m (10 feet) in diameter, and carry loads of over 44,500 kN (10,000 kips). Bearings of similar size for seismic application have not been manufactured in the past, and new manufacturing techniques are required in some cases to produce them. As a result, extrapolation of the test results from smaller bearings may not be totally accurate. This has lead to a testing program by Caltrans to conduct performance characteristic and proof tests of full size bearings to better understand their behavior [3].

APPLICATION

In the San Francisco Bay region, there are seven major bay-crossing bridges. It is desirable but economically not possible to retrofit all seven bridges to meet the *serviceable performance goal* following an earthquake. Based on studies carried out for the region as a whole, only the Golden Gate Bridge and The Benicia-Martinez Bridge are classified as the "*lifeline*" structures.

For these lifeline structures, it is important that the immediate service will be available for the public following the earthquake. To satisfy the seismic performance requirements, the design procedures must be sufficiently refined to allow an adequate assessment in term of component deformation, not only the maximum value that can occur but also the cumulative inelastic deformation due to the cyclic nature of the earthquake responses.

For the two California bridges, the seismic performance of the bridge and the isolation devices is strongly influenced by the near-source velocity pulse in the ground motion input.

Due to the close proximity to active faults, this near-source feature in the ground motion input must be carefully accounted for.

Three specific applications of the isolation bearings will be discussed in the remainder of this paper. These include the two bridges mentioned above and the I-40 Mississippi River crossing. Each application is unique, as each bridge shows different characteristics. What is common among all applications is the fact that the use of isolation has lead to considerable savings in retrofit costs of superstructure, and has provided for higher levels of confidence in the predicted behavior.

APPLICATION TO THE NORTH APPROACH OF THE GOLDEN GATE BRIDGE

Bridge Description

The North Approach Viaduct of the Golden Gate Bridge extends from the north end of the North Anchorage Housing to the North Abutment. Figure 3 shows the location of the North Approach Viaduct in relationship to the suspension bridge. It consists of five truss spans of 53.3 m (175 feet) each on partially straight and horizontally curved alignment. These truss spans are supported on four intermediate steel braced frames, on Pylon N2 on the south end, and on the North Abutment. The braced frame tower heights are about 15.2 m (50 feet) at Tower 1, 39.6 m (130 feet) at Tower 2, and 45.7 m (150 feet) for Towers 3 and 4. The original construction of the viaduct consists of two parallel trusses spaced 15.2 m (50 feet) apart. Each braced frame tower has 4 vertical legs and plan dimensions of 15.2 by 15.2 m (50 by 50 feet). As part of a 1961 widening project, an additional line of trusses and two additional vertical legs at each tower were added. These new members are located 7.6 m (25 feet) west of the original structure. The towers are supported on concrete pedestals and spread footings at the original bridge and caissons at the widening. The peak ground acceleration at the site is estimated at 0.65 g from the San Andreas fault.

In 1982, the viaduct was retrofitted to the then-current Caltrans seismic retrofit guidelines. The following details were used: 1) threaded bar restrainers oriented in the longitudinal direction were installed at bearing supports to prevent excessive relative displacement; 2) transverse restrainers were installed to tie the truss spans to the supporting towers; 3) additional diagonal bracing members were added to the widening portion of the towers and at the lower portion of the original towers; and 4) foundations at the tower legs of the widening section were strengthened to provide stronger anchorage. During the mid 1980s, the original concrete deck was replaced with a lightweight orthotropic steel deck system.

Retrofit Strategy

A three-dimensional model of the complete viaduct was developed using the computer program Nonlinear Earthquake Analysis of Bridge Systems (NEABS), which is capable of performing multi-mode linear response spectrum analysis as well as linear and nonlinear time history analysis. Both the response spectrum analysis using 100 modes and direct-integration time history analysis were carried out for the as-built and retrofitted structure. Three component earthquake input (i.e., two horizontal and one vertical) were considered. Seismic deficiencies were identified in the superstructure, bearings, towers, foundations, and abutments. Some the deficiencies are listed below.

- Many truss members need to be reinforced or replaced
- Existing steel bearing anchor bolts fail in tension creating possible instability and unacceptable vertical displacements.
- Bearing support widths are inadequate to ensure that trusses will be supported after the earthquake.
- Most connections of diagonal braces and horizontal struts are inadequate.
- Column elements have a demand/capacity ratio higher than 1.
- Anchor bolts that connect the tower base to the concrete pedestals will fail in tension and shear.
- Concrete pedestals are underreinforced and overloaded and will fail.
- The footings provide insignificant resistance to uplift.
- The North Abutment is inadequate to absorb lateral forces and displacements.

The overall strategy used on the North Viaduct includes changing the simple spans of the steel truss superstructure to a system that is continuous in the longitudinal direction by making the bottom chord continuous. This ties the overall system together. Additionally, the overall system is tuned by replacing steel bearings with isolation bearings. A brief description of the retrofit is described in a paper by Mervin Giacomini and Roy A. Imbsen [4]. The isolation retrofit is described below.

Isolation Bearings

Isolation bearings will be installed at the top of the new towers. A typical isolator bearing is shown in Figure 4. The new isolation bearings at the top of the towers will serve to dissipate horizontal loads but there are also significant vertical uplift loads which must be transmitted from the superstructure to the tower. Vertical restrainers are incorporated into the design. Bearing performance will be confirmed by a comprehensive series of tests which will be performed over the life of the structure so that the effect of aging will be known. Provisions were made for bearing replacement should that be needed. The new jacking points were built into the bearing assembly as a part of the retrofit.

Advantages of Isolation

The North Viaduct of the Golden Gate Bridge is being retrofitted to be serviceable after a major event. A key aspect of this retrofit design is that the overall system is tuned by replacing steel bearings with isolation bearings.

APPLICATION TO THE BENICIA-MARTINEZ BRIDGE

Bridge Description

Benicia-Martinez Bridge (George Miller, Jr. Bridge) is a high-level, deck-type, welded truss bridge with welded girder approach spans. This 6,215-foot-long structure carries I-680 over the easterly end of Carquinez Strait between the cities of Benicia in Solano County and Martinez in Contra Costa County. The general plan and the typical sections of the bridge are shown in Figure 5. The structure was originally constructed in 1960, retrofitted by adding earthquake restrainers in 1980 and widened in 1989.

The eight approach girder spans (2 at the north side and 6 at the south side), vary from 27.4 m (90 feet) to nearly 61 m (200 feet) in length with all girders 3 m (10 feet) in depth. The main truss section of the bridge consists of seven 161 m (528-foot) spans, two 131 m (429-foot) spans and one 100 m (330-foot) span. All trusses are 10 m (33 feet) in depth. All bearings under the original construction were of steel. The truss bearings are of the rocker type, measuring 1.12 m (3'-8") from top of rocker to base of masonry plate. The truss spans are supported by reinforced concrete cellular pier shafts on cellular reinforced concrete footings resting on groups of 1.83 m (6-foot) diameter, concrete-filled steel caissons. The peak rock acceleration at the site is 1.0 g from the Green Valley fault resulting in 2.4 g horizontal and 1.7 g vertical peak ground acceleration.

Retrofit Strategy

In both approach structure and the main truss spans, one of the major deficiencies is the bearing support. Initially, one of the options considered was to let the bearing "fused," i.e., let bearings be damaged as long as there is enough support to prevent drop-span failure. However, disadvantages associated with this option are: (1) designers do not have much control of the expected behavior; (2) the friction, that may develop at the interface following the bearing fused, can still be high enough to cause significant overstress in the truss members. Based on these considerations, it was decided to replace all existing bearings by isolation bearings. The primary objective is a more predicable seismic performance during and following the earthquake. The truss members are protected from the earthquake by the limited force transfer through the isolation bearings. This results in significant saving in the retrofit of superstructure trusses.

As the bearings are placed on top of substructure pier with relatively large plan dimension of 4.57 m by 4.57 m (15 ft by 15 ft), there is sufficient room for relative bearing displacement to occur. Additionally, because of the high rigidity of the pier and foundation caisson groups, the rotation of the pier is very small in all cases, e.g. less than 0.1 degree. This aspect is quite different from steel braced frame towers where the joint rotations could be large and the performance of the bearings can be adversely affected. For those situations, the restoring force mechanism is required. For the Benicia-Martinez Bridge, because of the large support plan dimension and the negligible rotation, the relative displacement across the bearing can be reasonably large, e.g. 1.2 m (4 ft), without jeopardizing the performance of the bearings, other structural elements connected, and the post-earthquake services.

As shown in Figure 6, the response can be accurately predicted only if the system is idealized as a two-degree-of-freedom system. Recognizing this aspect, an alternative would be to treat bearings as a tuning device to optimize the overall response including both the superstructure and substructure.

This requires higher lateral load capacity in the superstructure. Then, the superstructure may act as the mass damper which, if tuned properly by adjusting the stiffness and damping in the bearing devices, can potentially reduce the substructure seismic demand. As the substructure retrofit is typically a significant portion of the total cost, it is of interest to further explore this concept in future retrofit projects.

Advantages of Isolation

The difficulty in strengthening conventional fixed bearings, and the serviceability performance goal require retrofit strategies which minimize load transfer from truss to the piers. Isolation systems were selected which displace at a set horizontal force level with restoring features to limit permanent relative movement between the superstructure and the piers.

Figure 7 shows placement of typical isolator bearings over the top of the columns. The existing truss connections required strengthening for the jacking points. The friction isolator devices are placed with the sliding elements connected to the truss joints. This will prohibit eccentricity of the service loads with respect to the truss connections, and therefore will not induce moments to the truss chords during seismic response.

APPLICATION TO THE I-40 MISSISSIPPI RIVER CROSSING

Bridge Description

The I-40 Mississippi River Bridge, built in the late 1960's as part of the interstate highway system, carries three lanes of traffic in each direction. The total length of bridge to be retrofitted is 5.3 km (3.3 miles), including main channel spans, approaches, and ramps. The bridge is comprised of 164 spans, 160 piers, and 10 abutments. The main channel spans consist of five steel box girder spans and two steel through tied arch truss spans. The west approach to the channel spans is primarily precast prestressed concrete I girder spans, except for twelve welded steel plate girder spans; while the east approach and connecting ramps are entirely welded steel plate girder spans.

The seismic activity in the area is governed by the New Madrid seismic zone. The ground acceleration for a 500 year return period (design level) is 0.2 g and for a 2500 year return period (contingency level) is 0.4 g. The Project Plan for the entire I-40 bridge is shown in Figure 8.

The focus of current retrofit design work has been the main channel spans, consisting of the five box girder and two tied arch spans. Other retrofit design work will include the remaining west approach, east approach, and ramp spans.

Box Girder Spans

The steel box girder portion of the bridge, which lies just west of the tied arch spans, is comprised of five continuous spans—two 100.6 m (330') spans and three 121.9 m (400') spans. This portion of the bridge extends from Pier W28 to Pier A at the tied arch spans. Two 4.9 m (16') deep continuous steel box girders are positioned 17.8 m (58'5") apart, and support welded steel built-up plate floorbeams. Each box girder is supported on piers consisting of lightly reinforced tapered concrete columns.

Tied Arch Truss Spans

The main channel crossing is a continuous steel through tied arch truss bridge with two 274.3 m (900') spans. These main spans are supported on Piers A, B, and C.

Piers A, B, and C each consist of two 38.4 m (126') tall tapered concrete columns with very light transverse reinforcing. The columns and webwalls are supported by lightly reinforced concrete

distribution blocks which sit on top of footings, that have only a light bottom mat reinforcing. The footings rest on deep massive rectangular concrete-filled steel caissons which are embedded into the soil below the river. There is no positive tie against uplift between the footing and the caisson.

Expansion Joints

The Pier W28, A, and C expansion joints are steel plate finger joints. They are capable of a maximum ±330 mm (±13") longitudinal movement; but have no transverse movement capability.

Bearings

Tall steel bearings at each pier support the box girders and tied arch truss. Bearings at Piers W29-W32 and Pier B are fixed against longitudinal movement, while the bearings at Pier W28, Pier A, and Pier C are expansion bearings. Bearings are as tall as 1.4 m (4'6") at Pier B, and 1.2 m (3'10") tall at Piers A and C.

Retrofit Strategy

A three-dimensional analytical model of the box-girder portion and the tied-arch portion of the bridge was developed using the IAI-NEABS program. Ground motion input consisted of spatially varying displacement time-histories at the multiple supports. The model also included soil-structure interaction effect and foundation rocking.

The bridges were originally analyzed using the existing structure configurations, then reanalyzed for various types of trial retrofit strategies, and finally reanalyzed for the preferred final retrofit strategy.

Seismic Performance Criteria

Seismic performance goals were established, in conjunction with the Departments of Transportation, that the bridge must remain "operational/serviceable" following the maximum probable "Contingency Level Earthquake" (2500 year return period). The bridge is a vital defense and commerce transportation link. Bridge closures are expected to last no longer than 2 to 3 days, the time needed for inspections. Any damage should be easily repaired under traffic.

Existing Deficiencies

- No adequate shear transfer system exists to transfer transverse deck shear down to the floorbeams.
- Excessive plastic hinges would form at the base of the columns and webwalls at those piers.
- Most pier footings are inadequate to withstand longitudinal seismic overturning.
- Many truss members and their connections would be considerably overstressed.
- Rocking of footings on top of caissons can occur due to longitudinal seismic motion.
- Finger type expansion joints are not adequate for expected seismic displacements.
- The expansion bearings at Piers W28, A, and C offer very little seismic resistance.
- The fixed bearings at Piers W29-W32 and B are extremely overstressed.

Initial Retrofit Strategy – Maintain Existing Bearing Strategy

Traditionally, the combination of "strength and ductility" have been the accepted approach to provide maximum seismic resistance. The strength approach provides retrofitting of inadequate bridge components to transfer loads through the entire system (i.e., superstructure, bearings, piers, and foundations, etc.).

The initial retrofit strategy maintained all existing steel rocker bearings. These bearings required extensive retrofit strengthening and would be locked in by shear blocks in the transverse and longitudinal directions.

The estimated cost of this Initial Retrofit Strategy escalated quickly, totaling more than $43,200,000. for the box girder and tied arch spans. At this point, a review of the retrofit strategy seemed appropriate based upon the extent of retrofit work that would be needed for the Maintaining Existing Bearing Strategy.

Final Retrofit Strategy and Design – Isolation Bearing Strategy

With recent advances in isolation bearing technology and understanding, isolation has become a viable retrofit strategy for many bridges. Isolation provides a means to limit structure forces; however larger displacements often occur. A retrofit strategy incorporating isolation bearings was investigated for the I-40 bridge. Figure 9 shows typical details of a friction pendulum bearing.

Box Girder Spans – Comparing to the "Existing Bearing Strategy", significant reductions of force and displacement in the superstructure result in major retrofit cost savings. Full-height concrete webwall extensions to tops of piers are not required. Foundation retrofits are also minimized, and even eliminated at Pier W32. Bearing replacement requires that jacks and temporary supports be employed to lift the superstructure. External temporary supports must be used because there is little room on top of the columns to do this work. An expensive modular swivel expansion joint is needed at Pier W28. The ends of the west approach plate girder portion of the bridge need to be cut back, re-framed and bearings relocated, to allow room for the expansion joint at Pier W28. Foundation, columns and caps at Pier W28 need major retrofit because of the expansion joint enlargement and west approach girder support relocation.

Tied Arch Truss Spans – Comparing to the "Existing Bearing Strategy," force levels are reduced significantly in both the superstructure and substructure. Displacements at the tops of the piers are reduced. Less retrofit work would be required for the superstructure (50% or greater reduction). No column jacketing is needed. No webwall extension is needed at Pier B. No webwall extension to the bottom of the floorbeams is needed at Piers A and C. Piers A and C now participate in resisting superstructure longitudinal seismic forces, instead of relying solely on Pier B. Selection of an isolation bearing strategy means less costly design and construction costs for this bridge.

More costly modular swivel expansion joints will be required at Piers A and C to accommodate the expected seismic movements from the tied arch spans and its neighboring spans. To provide room for the new expansion joint, the ends of the east approach plate girders need to be cut back and their bearings relocated to a new concrete cap beam and column. The ends of the box girders at Pier A will be cut back as part of the retrofit to provide room for longitudinal movement. Jacks and temporary supports would be required at each pier to lift the heavy tied arch superstructure and replace the existing bearings with isolator bearings.

Advantages of Isolation

The estimated cost of the Isolation Bearing Strategy for the box girder and tied arch spans resulted in approximately a 40% savings in construction cost from the initial Maintaining Existing Bearing Strategy.

As a result of the IAI strategy review process, the Isolation Bearing Strategy was presented to the Departments of Transportation as the preferred seismic retrofit strategy, and adopted. Final design and PS&E are being prepared for the isolation bearing retrofit strategy.

SUMMARY AND CONCLUSIONS

Isolation bearings can be used to tune the seismic response of large-span bridges, and result in considerable cost savings. This is especially true in the case of retrofitting existing bridges where the alternative is often costly substructure and superstructure retrofit. Three bridge seismic retrofits designed by Imbsen & Associates, Inc. has demonstrated that bearings of unusually large size and load carrying capacity can be used effectively, and the structure response can be tuned by carefully selecting the locations and properties of the isolation bearings. Simplified and detailed nonlinear seismic analysis procedures have been developed for engineer to perform sensitivity analyses and final detailed analyses as needed.

REFERENCES

1. Chang, G.S., Liu, W.D., Nobari, F.S., Kartoum, A., Chen, X. – "Design Issues of Seismic Isolation of Major Bridges," Second National Seismic Conference on Bridges and Highways, Sacramento, California, June, 1997.
2. Roy A. Imbsen, Wen David Liu, Farid S. Nobari, Robert A. Schamber, "Seismic Modeling and Analysis of the Benicia-Martinez Bridge," SEWC Structural Engineers World Congress, San Francisco, CA, July 1998.
3. Dorie Mellon, "Caltrans' proposed Testing of Seismic Response Modification Devices for the Toll Bridge Retrofit program," National Seismic Conference on Bridges and Highways, July 1997.
4. Mervin G. Giacomini and Roy A. Imbsen, "Seismic Retrofit of the North Approach Viaduct of the Golden Gate Bridge," SEWC Structural Engineers World Congress, San Francisco, CA, July 1998.

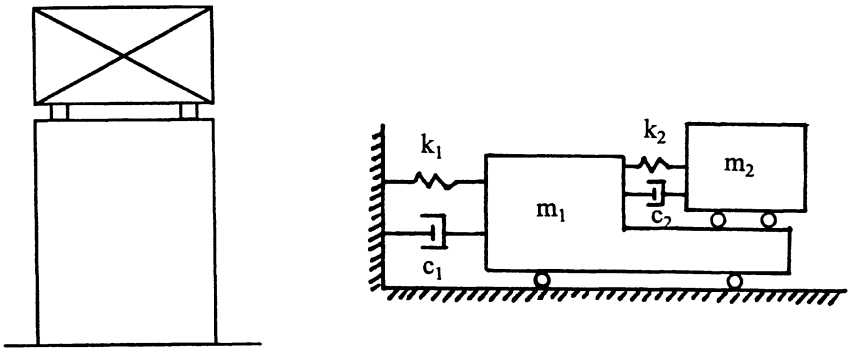


Figure 1 – Simplified 2-DOF model for bridges

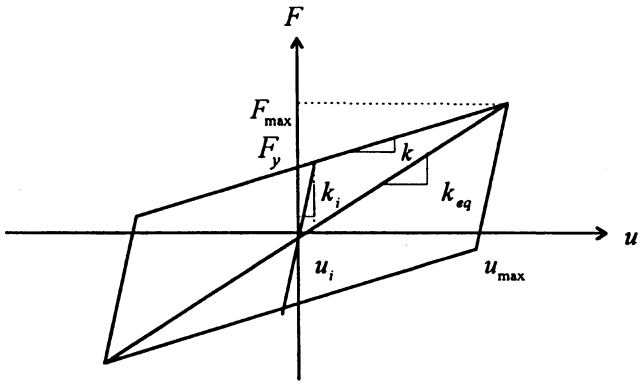


Figure 2 – Force-displacement relationship of isolation bearing

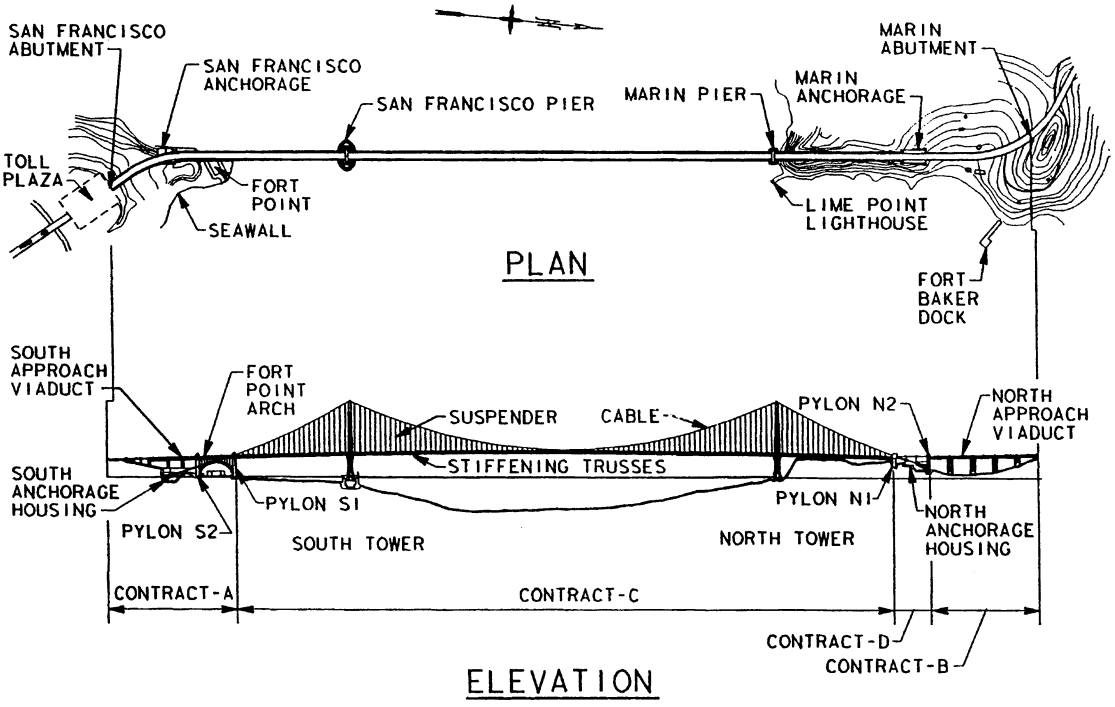


Figure 3 – Location of the north approach viaduct

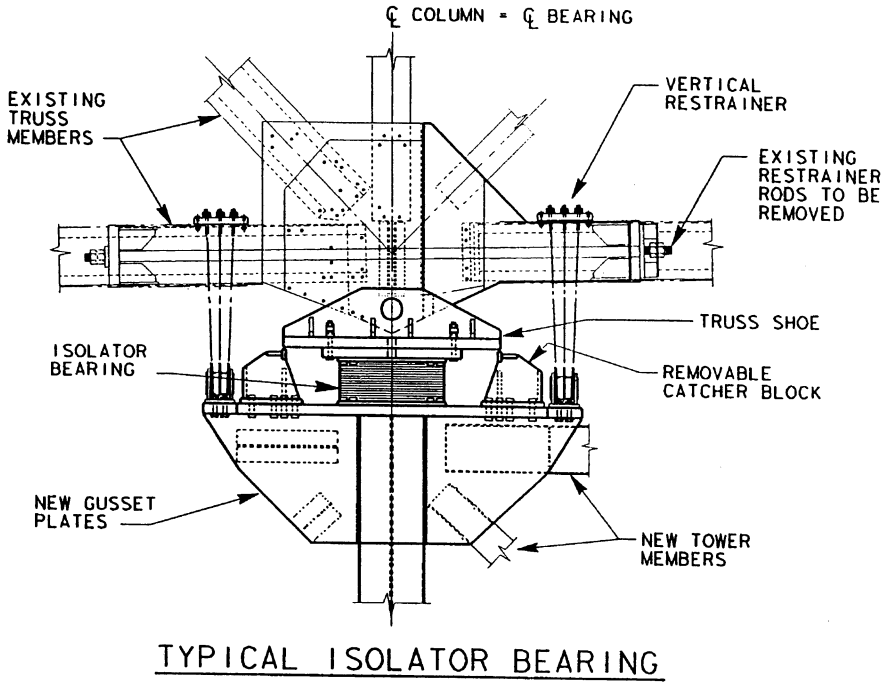


Figure 4 – Typical isolator bearing

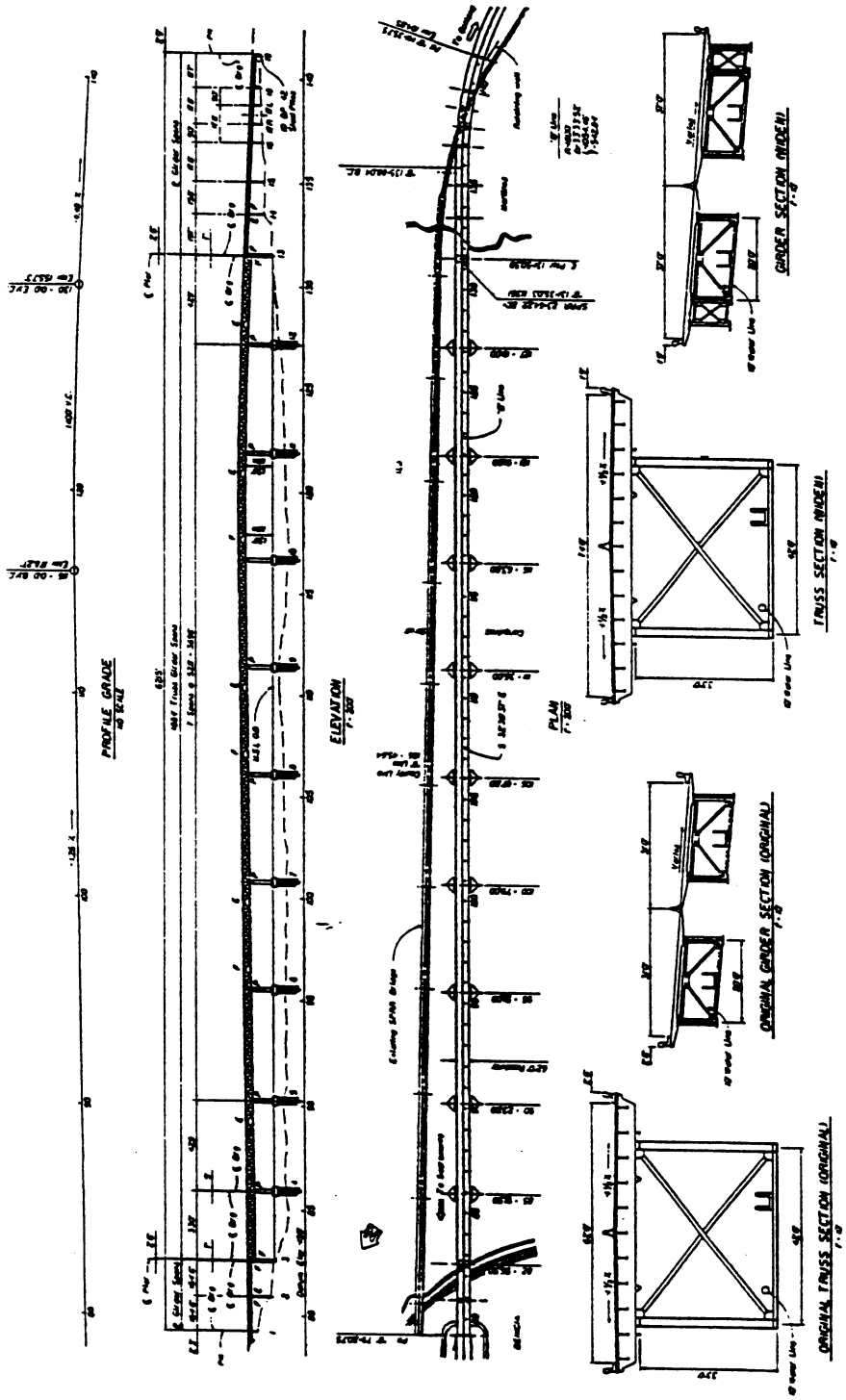


Figure 5 – Benicia-Martinez Bridge

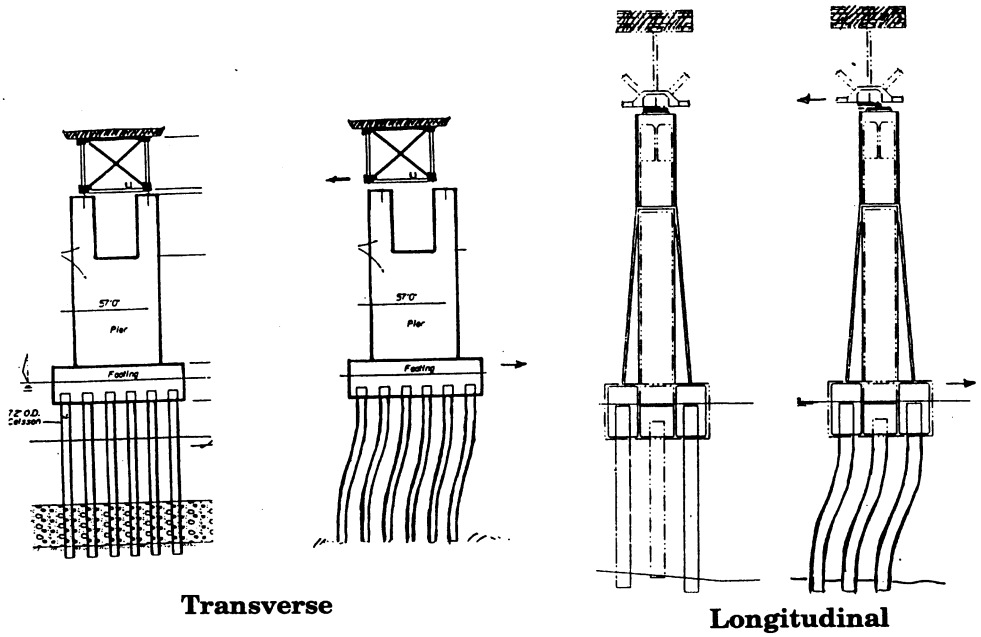


Figure 6 – Typical piers under earthquake loading, action of isolation bearings

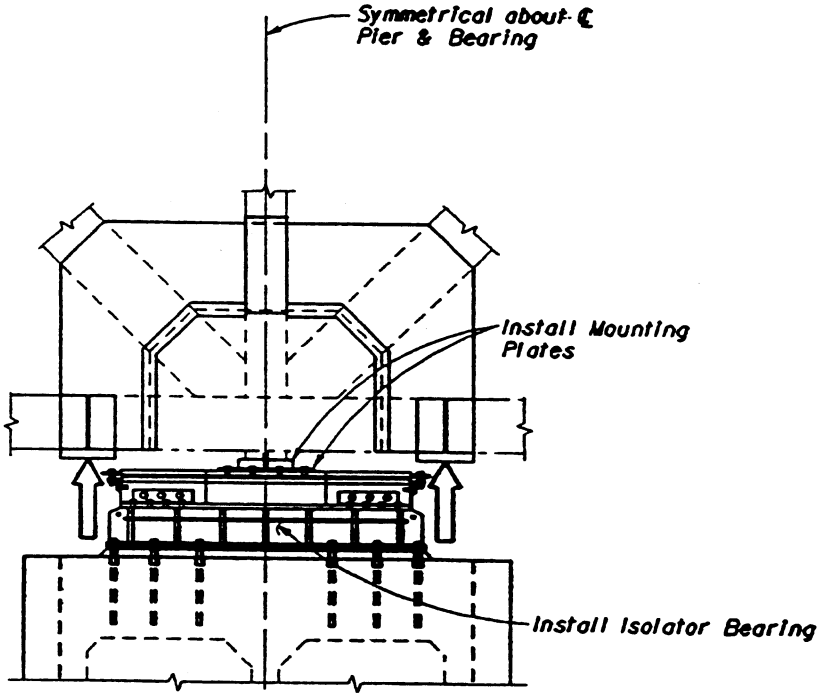


Figure 7 – Isolator bearing placement

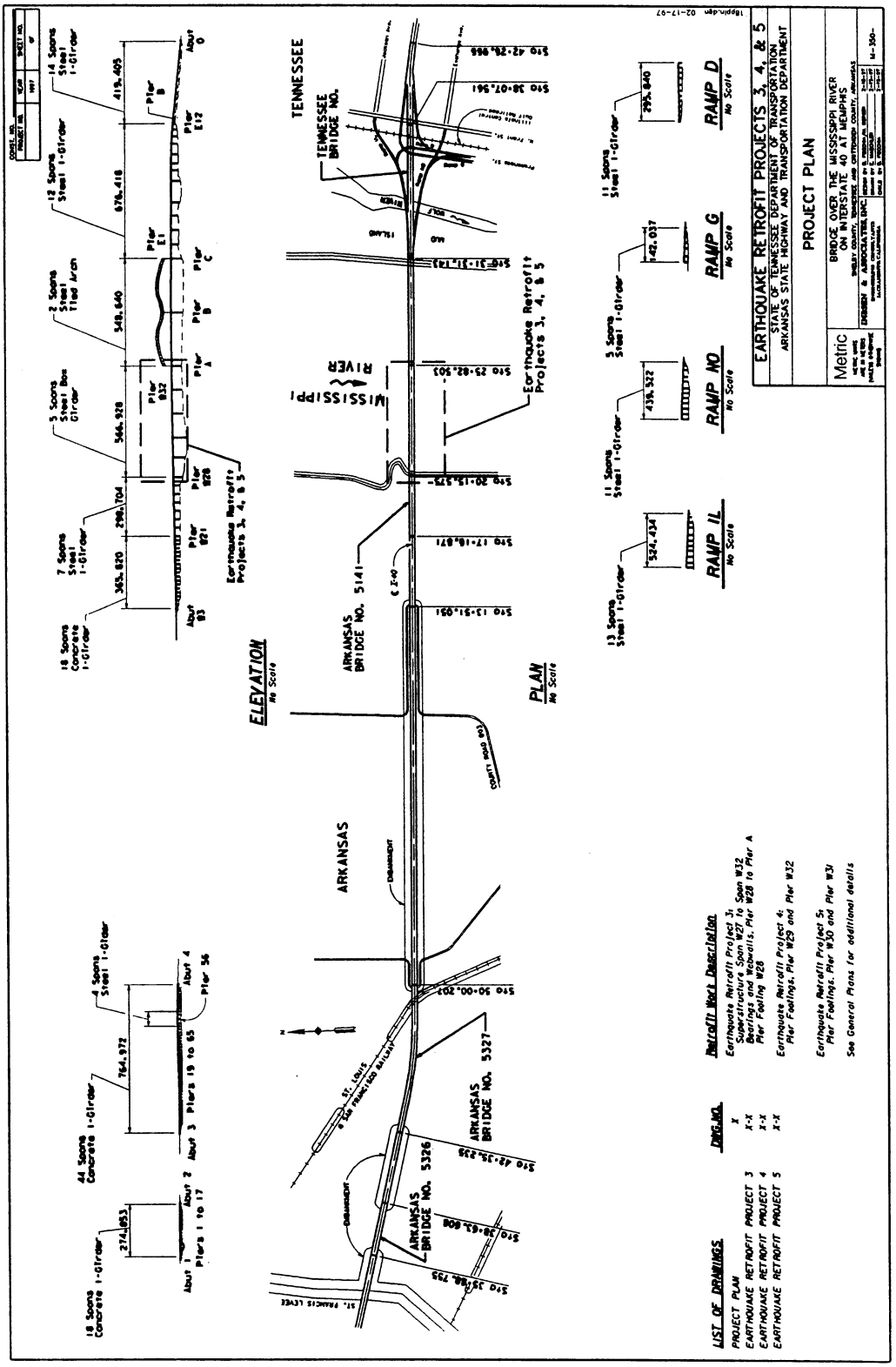


Figure 8 – I-40 Mississippi River bridge project plan

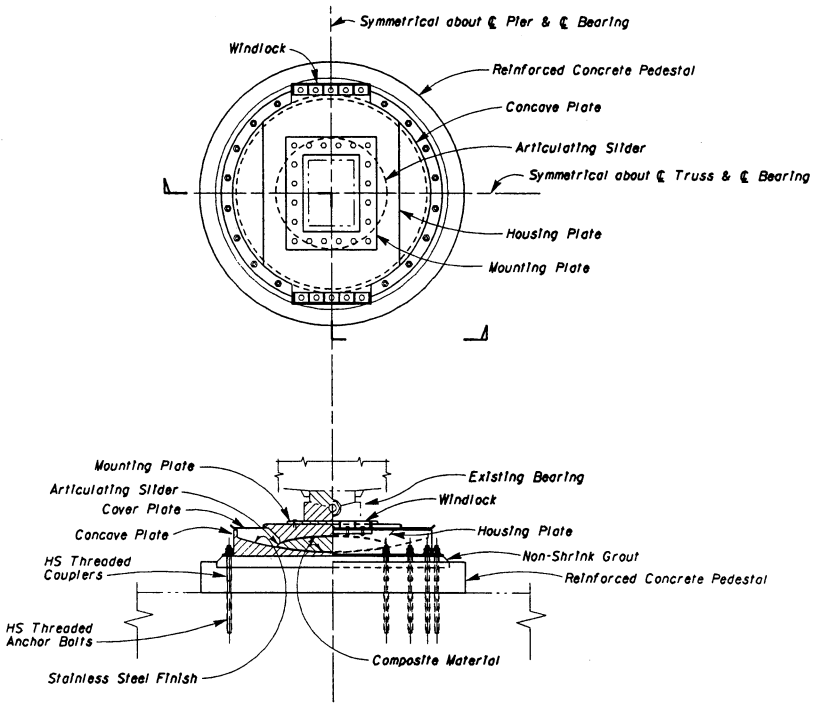


Figure 9 – I-40 typical friction pendulum bearing

DESIGN OF THE CALTRANS SEISMIC RESPONSE MODIFICATION DEVICE (SRMD) TEST FACILITY

Gianmario Benzoni – Frieder Seible
Division of Structural Engineering
University of California, San Diego
La Jolla, CA 92093-0085

ABSTRACT

In the Seismic retrofit design of California's Toll Bridges, seismic isolation is used in several bridges to limit the seismic force input into the superstructure and to avoid costly superstructure retrofit measures which would require partial lane closures and traffic interruptions. Isolation bearings and dampers of the size required for these large span bridges have not been built or tested to date. This paper describes the design and construction of a full scale testing facility which will allow the real-time 6-DOF dynamic characterization of the seismic response modification devices designed for California's Toll Bridges.

INTRODUCTION

Testing objectives and procedures

Technical requirements for the Caltrans Seismic Response Modification Device Test System (SRMD) were developed on the basis of current design projects for the California Toll bridge Retrofit Program, as well as the new AASHTO T-3 Guide Specification for Seismic Isolation Design /1/, /2/. Specifications have been adjusted during the design, to provide a very flexible test system, open to a wide spectrum of devices and testing possibilities.
The main technical capabilities of the 6-DOF system are summarized in table 1 together with the testing system acceptance requirements /3/.

Table 1- Technical specifications

		Accuracy of application	Accuracy of readout
Vertical force	53,400 kN (12,000 Kips)	±5%	0.5% full range
Vertical moment	8,136 kNm (72,000 Kip-in)		±1.35 kNm (12 Kip-in)
Long. force	8,900 kN (2,000 kips)		1.0% full range
Lateral force	4,450 kN (1,000 Kips)		1.0% full range
Vertical displ.	±0.127 m (5 in.)	±2%	1.0% full range
Longitudinal displ.	±1.22 m (48 in.)	±2%	1.0% full range
Lateral displ.	± 0.61 m (24 in.)	±2%	1.0% full range
Vertical velocity	±254 mm/s (10 in./s)	±10%	
Long. velocity	±1,778 mm/s (70 in./sec)	±10%	
Lateral velocity	±762 mm/s (30 in./sec)	±10%	
Height of Specimen	Up to 1.52 m (5 ft)		
Relative Platen rot.	±2°		

Together with the above specifications the different types of isolating devices and dampers to be tested and the testing objectives and procedures drove the overall design approach.
The isolating devices considered were Friction Pendulum (FPS) and elastomeric isolation bearings, proposed solutions for Benicia-Martinez and Coronado bridge, respectively, as well as viscous dampers, common to almost all the toll bridge retrofit projects. Testing objectives ranged from slow speed uni-directional testing for basic performance characterization to high speed, 3-D testing for energy based analysis. The investigation of the effect of wear and aging was also an important issue in the proposed test program, through re-characterization of the performance of the scale SRMDs already exposed to the actual bridge loads, deformations and environmental conditions.

Dedicated testing facility

Targeting the possibility of testing the SRMD devices that will be installed in the first of the Caltrans toll bridge retrofit projects (Benicia-Martinez bridge), the design and construction of the testing facility was put on a fast track 1 1/2 year schedule. This challenging time frame did not allow any time for construction of a new building space for the SRMD testing machine. For this reason the University of California, San Diego located and obtained a portion of the existing High Bay Physic Laboratory as permanent space for the testing machine. The building is located on the UCSD campus directly adjacent to the Powell Structural Research Laboratories, with the advantage of direct access to the support services of these Labs. The available space comprises about 300 square meters (3,200 ft^2) and is already serviced by a 20 ton (40 kips) overhead crane. The exceptional demand of hydraulic power for this test system requires about 19,000 liters (5,000 gal) of oil storage and a pressurization, through nitrogen gas, up to 34 Mpa (5,000 psi). For safety reasons the pumps and the 100 accumulators will be located in a separate building. Direct pumping, designed for long duration tests and for accumulator charge will provide 720 and 417 liters per minute (190 and 110 gpm) at 21 and 34 Mpa (3,000 and 5,000 psi), respectively.

DESIGN CONCEPT

Machine geometry and components

The design of the test facility was developed jointly by Caltrans, the University of California, San Diego and MTS Corporation of Eden Prairie, MN. Many preliminary configurations were re-visited and modified due to the complexity of the project, driven by the large demand of vertical forces and displacements, as indicated in table 1. The final design configuration of the testing machine is shown in figure 1.
The testing system, presently under construction, consists of prestressed concrete reaction frame (concrete box), and of a moving platen, connected by four horizontal actuators to the concrete box. The platen slides over four hydraulic hydrostatic low friction bearings attached to the floor of the concrete structure. The platen also extends with four steel outrigger arms that support four low friction sliding actuators at their tops.

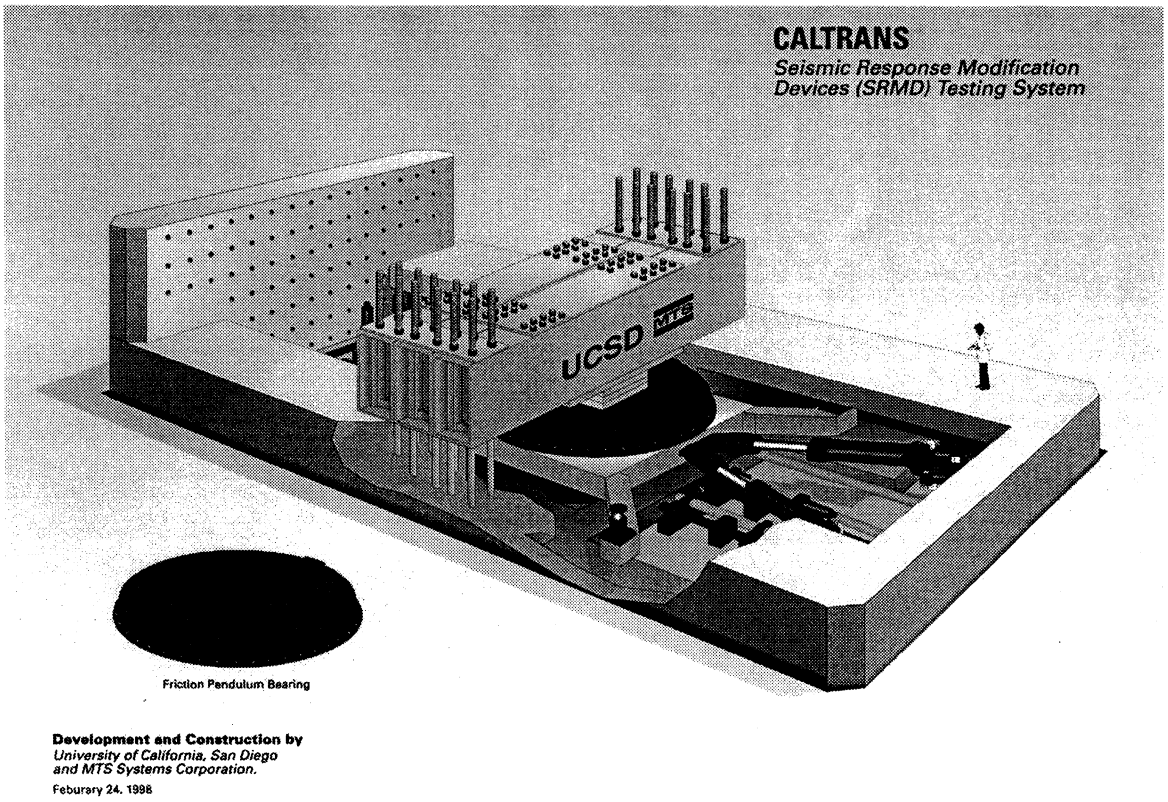
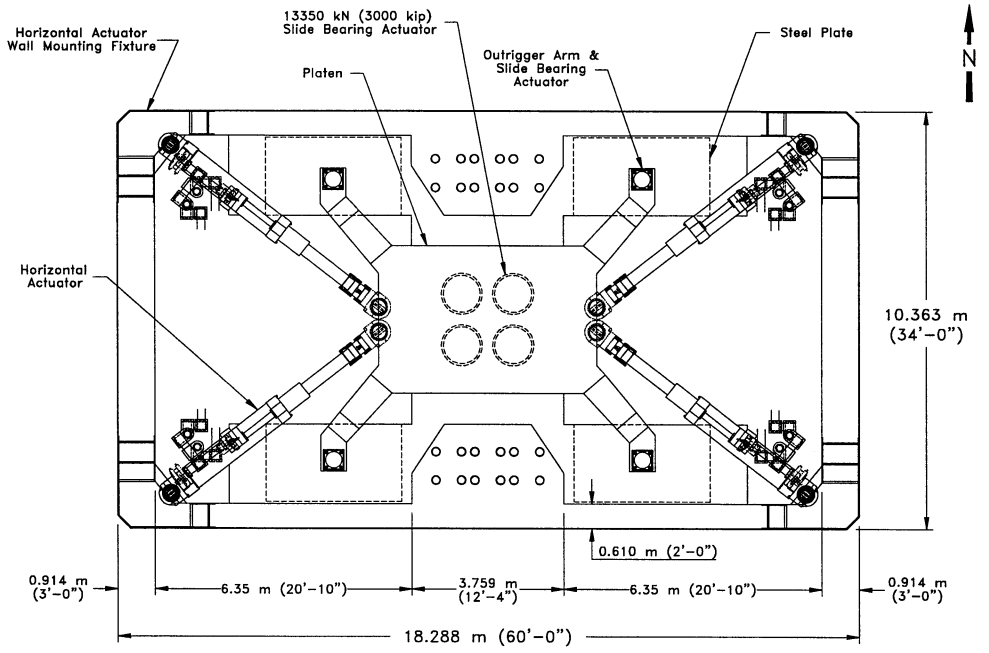


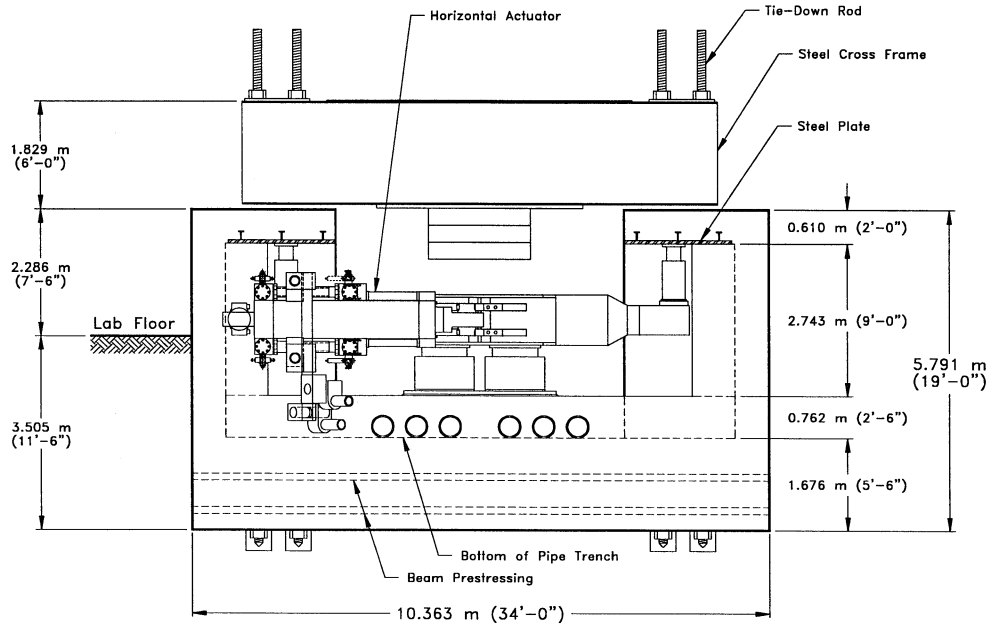
Figure 1 – SRMD testing system

The testing system is completed by two additional reaction structures: a steel cross beam, removable and linked to the concrete box through a tie-down rod system, and a heavily prestressed reaction wall on one end of the machine. Figure 2 shows a plan view and cross sections, with key dimensions.

Due to the large displacements of the test specimens in the longitudinal and transverse directions, the traditional solution of a platen with hinge connection to horizontal and vertical actuators was not practical. This configuration would have required very long stroke vertical actuators, with deep excavation inside the existing building. Space limitations, difficulties of access for tall excavating equipment and the need to maintain the rest of the existing laboratory in working condition during construction made this solution impractical. The technical option MTS provided was the use of 4 vertical hydraulic sliding bearings which support the moving platen, apply the vertical load, and allow horizontal motion and swivel capacity with very low friction (less than 0.2% of vertical force). Characteristics of all the actuators of the system are presented in table 2.



Plan View



Transverse cross section

Figure 2 – continue

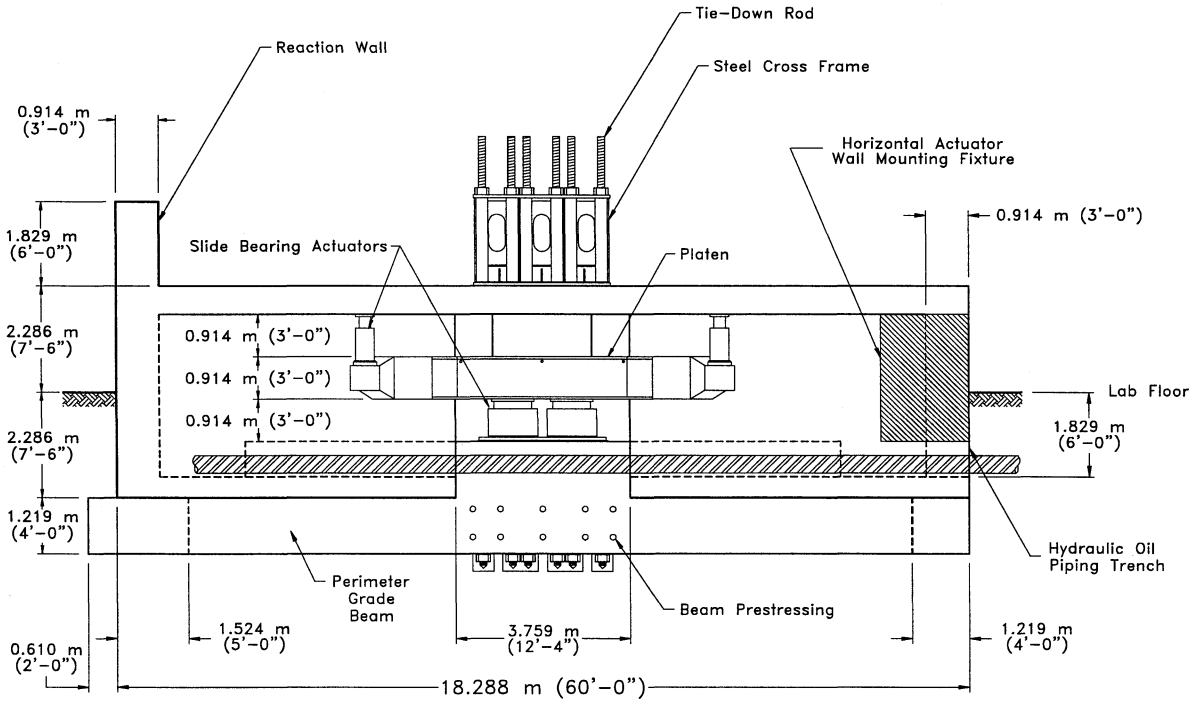


Figure 2 - SRMD system plan view and cross sections

Table 2- MTS actuators technical specifications

Function	Horizontal Actuator	Vertical Actuator- Bearing	Vertical (Outrigger) Actuator – Bearing
Quantity	4	4	4
Max Force (Tension)	4,500 kN (1,000 kips)	*NA*	*NA*
Max force (Compression)	7,000 kN (1,600 kips)	18,000 kN (4,000 kips)	534 kN (120 kips)
Stroke	2.5 m (100")	0.25 m (10")	0.5 m (20")
Rod diameter	0.3 m (12")	*NA*	*NA*
Bore	0.5 m (20")	0.81 m (32")	0.19 m (7.5")
Max velocity	1.8 m/s (70 in/s)	0.4 m/s (15 in/s)	0.5 m/s (18in/s)
Swivels	± 20° both ends	± 2°	± 2°
Servovalves	(19 m^3/min) (5,000 gpm)	(11 m^3/min) (3,000 gpm)	(0.7 m^3/min) (180 gpm)
Pressure	35 Mpa (5,000 psi)	35 Mpa (5,000 psi)	21 Mpa (3,000 psi)
Weight	13 ton (28 kips)	4.4 ton (9.7 kips)	0.4 ton (1 kip)

This solution strongly influenced the geometry of the facility, allowing a relatively shallow embedment of the moving platen into the support frame. The dimensions and strokes of the horizontal actuators determined the shape of the support structure. Its close box-like geometry, together with the property of self-reacting the horizontal forces, was desirable also for providing

containment of oil leakage and testing of specimens to failure. The large vertical loads which the testing machine can apply are transferred to the test specimen by the 4 vertical hydrostatic actuators through the platen and reacted against an assembled tubular cross-beam. A self-reacting frame in two directions is thus obtained, as sketched in figure 3.

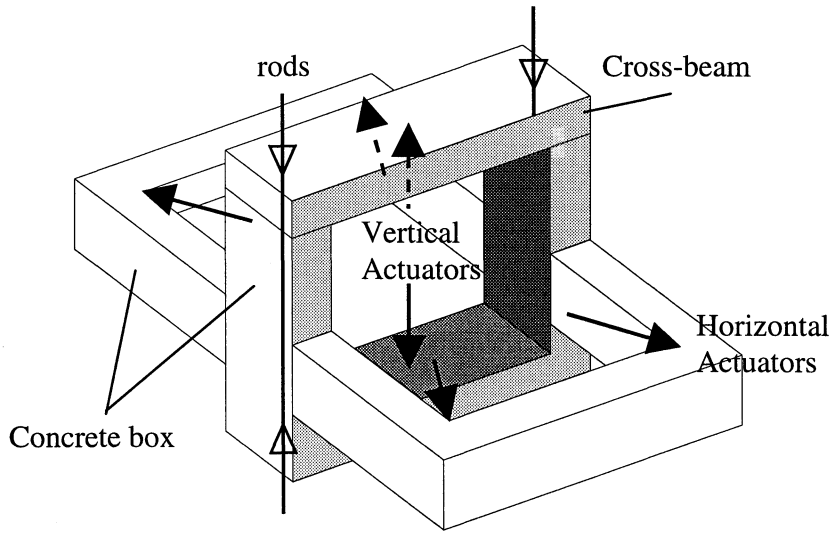


Figure 3 - The self-reacting frames

Platen Shape and Stability

The size of friction pendulum bearings under development, together with the overall dimensions of the concrete box, determined the geometry of the moving platen. As shown in figure 2 (and more in detail in figure 8) the actual dimensions are based on a rectangular shape of 3.65 by 4.88 m (12'x16'), extended in the longitudinal direction to accommodate the four outrigger arms at the corners and the mounting plates of the horizontal actuators. An initial analysis of the overall stability of the platen, at the most critical conditions of loads and displacements, showed the limits of the solution of a platen supported on four sliding bearings which provide vertical force only in compression. A large improvement in stability was achieved by adding eccentric points of vertical reaction through the four steel outrigger arms connected to the platen. On top of each of these extensions a sliding bearing provides extra vertical force needed to balance the overturning moment applied to the platen. One of the main issues was the location of the reaction structure for these actuators, given the large range of displacements they are allowed to cover. The solution of mounting these actuators to slide in pockets which are part of the surrounding concrete box was adopted. The pockets in the lateral walls are covered on the inside top face with steel plates, providing the finish conditions required for the optimum performance of the sliding actuators. The outriggers arms will be equipped, based on the actual design, with MTS 534 kN (120 kips) hydrostatic bearings, applied above the steel arms. They allow 0.5 m (20") of stroke. For design purpose their service capacity has been assumed at 490 kN (110 kips). The design of the system took into account also the possibility of more powerful actuators, up to 1,470 kN (330 kips), applied above and/or below the outrigger arms.

The mechanism of stability of the platen is shown in figure 4 for elastomeric and friction pendulum bearings. In the figure P represents the vertical load and H the applied shear force at mid height of the specimen, Δ the total platen displacement, O1 and O2 the vertical forces applied by the outrigger actuators, V1 and V2 the vertical forces applied by the sliding bearings mounted below the platen, and W the total weight of platen, specimen and outrigger actuators. For simplicity the model is here reduced to a 2-D system. However, the response of the platen has been analyzed with a 3-D finite element model which allowed the application of several critical combinations of loads and displacements /3/.

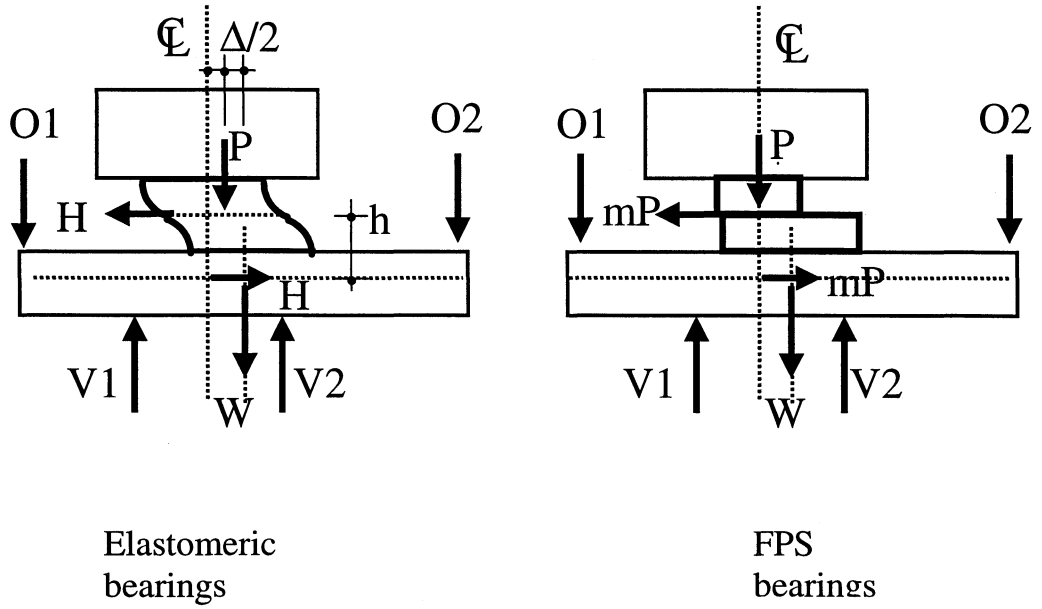
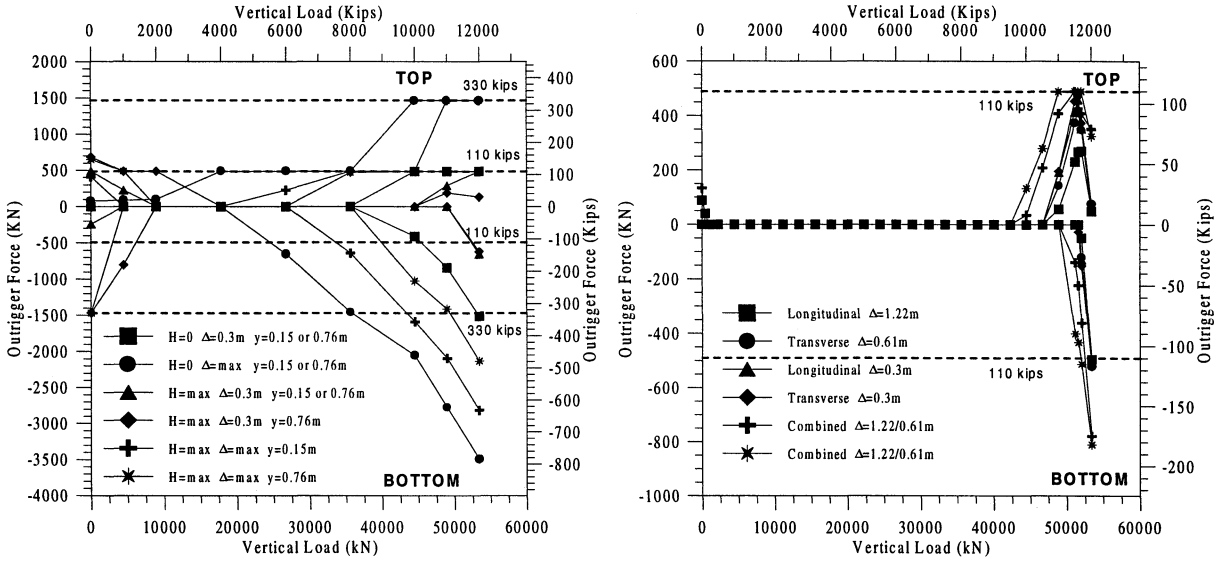


Figure 4 – Platen stability models

The two types of isolation devices present substantial differences in terms of forces transferred to the machine during a test. The elastomeric rubber bearings represent the most critical case for platen stability as well as for structural demand. In fact, due to their capacity to carry shear and end moments, they introduce a large overturning moment into the platen. This contribution is, as shown in figure 4, increasing with the size of the specimen. Additional moments are transferred to the platen when displacements occur. Due to P-Δ effect the applied vertical load P introduces a moment with the same direction of the one due to the horizontal forces. Opposing effects are exerted, in this case, by the platen self-weight and the vertical load eccentricity with respect to the center of sliding bearings (centerline of the machine). The remaining force components need to be balanced by the actions exerted by the installed vertical actuators (V,O). Several combinations of loads analyzed showed the difficulty of establishing a general rule for the governing force component in the stabilizing mechanism. Generally however the axial load P represents the main reason for instability at significant displacement whereas the horizontal shear governs for limited strokes. The balancing effect operated by the sliding actuators depends on the proportions between applied external forces and displacement. It must be noted that in several conditions only the actuators on one side of the platen are active (under "compression" force) while the other ones are instead following the displaced position of the platen without providing any force contribution.

Slightly different is the stability mechanism for friction pendulum bearings. The main reason is the low coefficient of friction between moving components, that results in reduced overturning moment to the platen. Also due to the articulated configuration of FPS devices, the applied vertical load always remains aligned with the resultant of the actions introduced by the vertical hydrostatic bearings. This condition eliminates the overturning moment due to P-Δ effect.
Figure 5 shows the stability response of the platen for combined transverse and longitudinal displacements, for elastomeric and FPS bearings.



(a) elastomeric bearing (b) FPS bearings

Figure 5 - Combined envelope of platen stability curves

The envelope curves show the outrigger forces necessary to stabilize the platen, assuming the vertical actuators below the platen are at their maximum level of reaction. In figure 5a the most critical conditions of horizontal loads (H), displacements (Δ), and half of the bearing height (y) are combined. The values of H and Δ are the same in both longitudinal and transverse direction. The maximum of y=0.76 m (2.5 ft) as indicated in the plot, corresponds to the highest specimen allowed with cross-beam installed, i.e 1.52 m (5 ft) clearance. It must be noted that also the condition of zero shear force was analyzed for elastomeric bearings. This limit state can be postulated to exist when an elastomeric bearing has failed in shear, while still being subjected to vertical load. Displacements and height of the specimens range from a moderate level to the peak values allowed by the system. The dashed horizontal lines correspond to the capacity of the outrigger actuators. The present configuration will include four actuators capable of 490 kN (110 kips) each, mounted on top of the outrigger arms. In order to complete the analysis of stability performance of the platen two other possible scenarios are reported in the same plot: the presence of 1,470 kN (330 kips) actuators on top of the outriggers and/or extra actuators installed below the platen extensions (negative values of outrigger force). For instance, the configuration of zero horizontal load and maximum displacement in both directions (black circle in figure 5a) does not present any stability problems up to a maximum vertical load of 17,800 kN (4,000 kips). At this level the capacity of the 490 kN (110 kips) top outrigger actuators is exceeded and

to reach stability at the vertical force of 26,700 kN (next data point) an extra force is needed from below the platen (about 650 kN, 146 kips). Above 35,600 kN (8,000 kips) of vertical load the capacity of the outrigger actuators is exceeded for any elastomeric bearing under maximum horizontal displacement or load conditions. In the graph unstable conditions in case of very low vertical load, maximum horizontal capacity and very tall specimens can be seen.

Figure. 5b shows the difference in behavior of FPS bearings with respect to the elastomeric devices. The stability of the system becomes an issue only at very low or very high vertical loads. For a large intermediate range of vertical forces the outrigger actuators are not required for stability purposes. The designed system configuration with 490 kN (110 kips) actuators above the platen arms allows stable tests at maximum displacement in both longitudinal and transverse directions with vertical load up to a maximum of about 50,000 kN (11,236 kips).

STRUCTURAL COMPONENTS DESIGN

Concrete Reaction Frame

As shown in figure 3 the two main self-reacting structures consist of two reacting frames placed in perpendicular planes. The specific nature of the applied loads was the basis for a "non standard" limit state definition. The system is in fact numerically controlled for the load and displacements application phase and the level of peak forces introduced into the system is of deterministic nature. Service loads assumed for the design of each structural element were:

Vertical Load = 53,400 kN (12,000 kips) (quasi static)
Vertical Load = 44,500 kN (10,000 kips) (dynamic)
Longitudinal Load =8,900 kN (2,000 kips)
Transverse Load = 4,450 kN (1,000 kips)

A service load factor of 1.2 was assumed for every possible combination of the above forces, with the structure behaving elastically in all its components. An ultimate load factor of 1.6 was introduced as design specification and applied to the combination of vertical and longitudinal load, vertical and transverse load and to longitudinal and transverse forces acting simultaneously. The ultimate load factor has been derived from the absolute maximum load the hydraulic actuators can express. This implies the failure of the control system in a situation of peak force applied. The degradation of the structural integrity of the system, in this case, has been carefully controlled and limited, introducing also, through some fabrication detail, preferential location for mechanisms of damage.

All structural concrete for the SRMD machine was specified with a nominal design strength of 48 Mpa (7,000 psi) and Grade 60 reinforcement. A maximum reinforcement spacing of 0.3 m (12") was specified for better crack control and preservation of structural stiffness integrity.

As shown in figure 2, the four vertical large actuators are connected to the vertical concrete frame at mid span of the 2.43m (8 ft) high horizontal beam that represents the main reaction block of the overall structure. The beam is 10.36 m (34 ft) long with a clear span of 5.18 m (17 ft) and is 3.75 m (12'-4") wide. It receives the vertical forces distributed, through a 2.74 x 2.74 m (9x9 ft) steel plate, from the hydrostatic sliding actuators. The point of application of the vertical reactions to these forces are instead the plates and nuts that restrain the tie-down steel rods at the

bottom of the beam itself. The structure was designed with post-tensioning strands, running horizontally at about 0.6 m (2 ft) from the bottom level. The post-tensioning force is about 5,800 kN (1,300 kips) for each tendon. A total of 10 tendons with 30, low relaxation, 7-wire, 15.24 mm (0.6") diameter strands are required. The limitation in space at the anchorage location on the south side of the machine necessitates the application of post-tensioning force only at one end of the prestressing system. Heavy transverse reinforcement, consisting in 25.4 mm (#8) 4 leg stirrups is used along the overall length of the concrete beam at 0.15m (6") spacing. This reinforcement was designed for the severe shear and torsional forces expected. As visible in the cross-section of figure 2, this main structural element will accommodate also 6 of the hydraulic lines, running, into steel tubes, all the way through the width of the concrete beam. The remaining structural components of the concrete box are the two longitudinal walls 0.61 m (2 ft) thick and the two end walls in the transverse direction. With exception of the reaction wall, the sides of the concrete box did not require particularly heavy reinforcement and prestressing. A post-tensioning system of 2 straight tendons, each one with an overall prestressing force of 5,385 kN (1,210 kips), is provided to react the horizontal actuator forces.

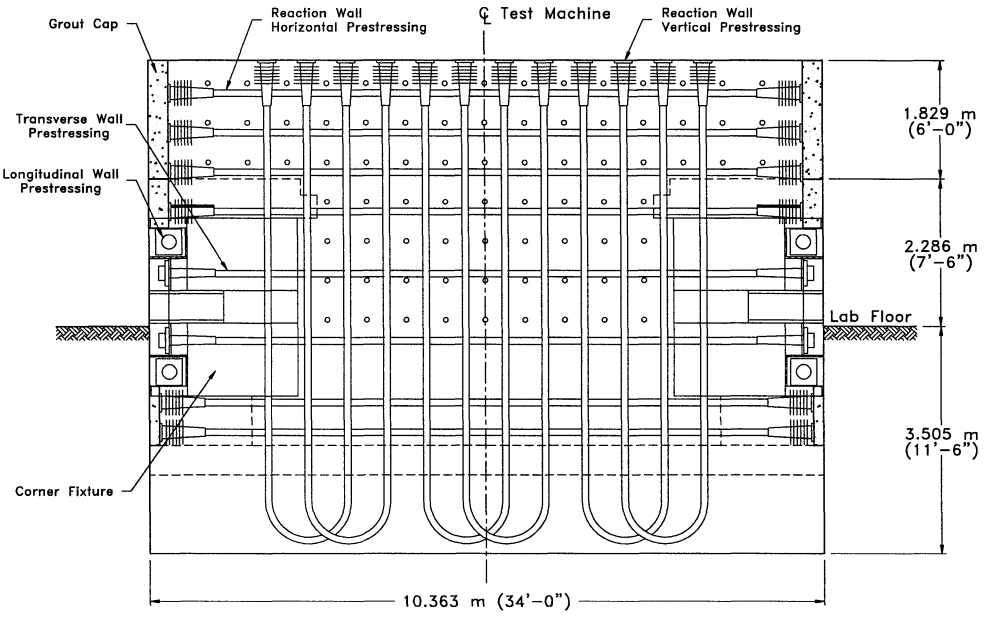


Figure 6 - Reaction Wall

The transverse cross-section of figure 2 shows the extent of the pockets realized along the longitudinal walls to provide a reaction surface to the outrigger actuators. The longitudinal wall, at its top, extends horizontally into the machine space producing an overhang about 1.8 m (6 ft) wide and 0.61m (2 ft) thick. Taking into account possible changes in terms of the capacity of the outrigger actuators, these structural components have been heavily reinforced with 35.8 mm (#11) longitudinal rebar at 0.15 m (6") spacing and 19.05 mm (#6) closed stirrups every 0.15 m (6"). The overhang beams will also support removable precast concrete panels which provide a cover to the machine space.

Particular attention has been paid to the design of the reaction wall of the SRMD concrete box. As mentioned above, the need to test devices like viscous dampers requires a reacting structural

element on one side of the specimen, while the other side is mounted to the moving platen. The reduced space around the test system does not allow the connection of the specimen to the lab floor. The required capacity of the wall was limited to the design horizontal load of 8,900 kN (2,000 kips), and was achieved with a system of horizontal and vertical post-tensioning. The basic tendon layout is shown in figure 6.
Fixed-end-loop-anchors were chosen for the vertical tendons, not requiring access to the bottom slab for the stressing operations. The 0.91 m (3 ft) thick wall is provided with 50 mm (2") diameter horizontal steel sleeves on a 0.61 m (2 ft) module for the attachment of specimens and external actuators. The hole pattern was intended to reproduce the existing ones in the Powell Structural Research Laboratories for compatibility with tools and mounting devices.

Steel Corner Fixtures

The horizontal actuators, shown in figure 2, are connected with spherical swivels on the rod end to the platen and with the swivel at the other end to the corner of the concrete box. Due to the high force capacity of these actuators and the required precision for their installation, the connection to the concrete structure was a delicate step in the design procedure. The co-existence of actuator connection and of the post-tensioning system for the concrete walls resulted in a quite articulated shape of the corner fixtures. The general geometry of these structural elements is shown in figure 7.

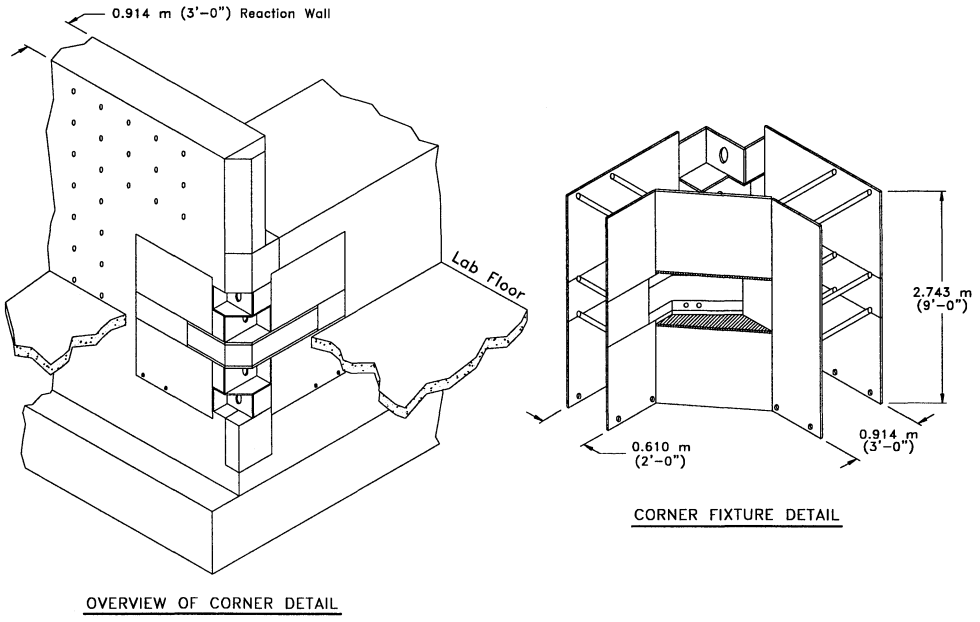


Figure 7 - Corner steel fixtures

The goal was to provide, through steel plates, an anchorage that transfers the loads applied from the actuators to both the external and internal faces of the concrete box. The elements are shaped to provide a chamfer to the structure portion above the laboratory floor. On the internal side of the fixtures, two 0.13 m (5") horizontal steel plates will accommodate the bolted connection with the actuators. The overall geometry of these corner details had to take into account also the

congested situation of valves and pressure hard lines located at the end of the actuators, with the complication of a system that is allowed to swivel horizontally and vertically to follow the platen displacements.

The Platen

In its configuration, the testing system does not differ significantly from a shake table configuration. The platen needs to exhibit very high stiffness without excessive weight. The advantage of actuators slightly oversized with respect to the design loads made the weight less critical in the design concept. The presence of stabilizing actuators, eccentric to the platen stressed the importance of a very stiff system. The proposed solution is schematically shown in figure 8.

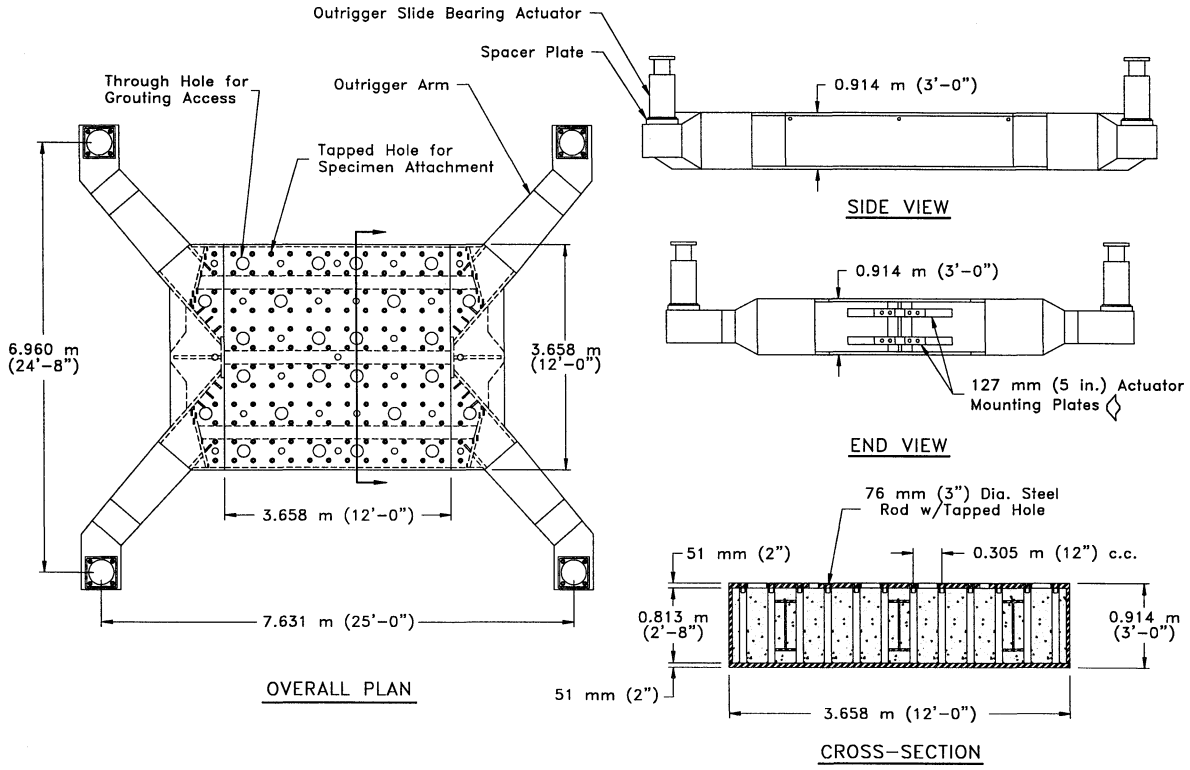


Figure 8 – Moving platen

Two 51 mm (2") thick steel plates spaced 0.91 m (3 ft) apart are connected through a pattern of welded steel rods 76 mm (3") in diameter. The rods, positioned in a grid of 0.3x0.3 m (12"x12") have tapped holes on the top for specimen attachment. The actuator mounting plates are connected, on the short sides of the platen, to a very stiff steel frame that transfers forces to the other side of platen through three longitudinally placed steel beams. This steel frame is welded to the top and bottom steel plate and to the lateral plates along the long sides, forming a closed box. The platen is grouted with concrete from holes in the top steel plate. The outriggers are designed as pre-assembled steel boxes that will be welded to the main body of the platen once in place in the machine space. The governing action in the platen design was the shear force transferred to

its top surface, in case of elastomeric bearings. The steel rods were calculated to resist these shear forces as well as axial stresses introduced by pure bearing and overturning moments.
One of the main difficulties, in the design of the platen, was the specification of a steel surface, at the bottom of the box assembly, with the flatness and finishing characteristics imposed by the four hydrostatic low friction actuators. Flatness was required to be at least 0.16 mm per meter (0.002" per foot) under full service conditions, resulting in a severe request of stiffness for the platen and a delicate fabrication process. The design process had to take into account the risk of the bottom plate warping during welding and fabrication. For this reason it was decided to design a complete steel box and, after all the welds are completed, to machine the bottom surface to the desired flatness and finish. The overall steel box weight of 272 kN (61 kips) without concrete and outriggers arms, complicated the search of a shop with appropriate hoisting and machining capabilities.

The Steel Cross Frame and Tie-Down System

As schematically indicated in figure 9, the vertical self-reacting frame of the system is completed by a cross-beam attached to the concrete box. It is evident that the flexibility of the testing facility is largely expanded in case of a removable cross beam, with the possibility of testing of specimens exceeding the clearance imposed by this transverse steel structure.

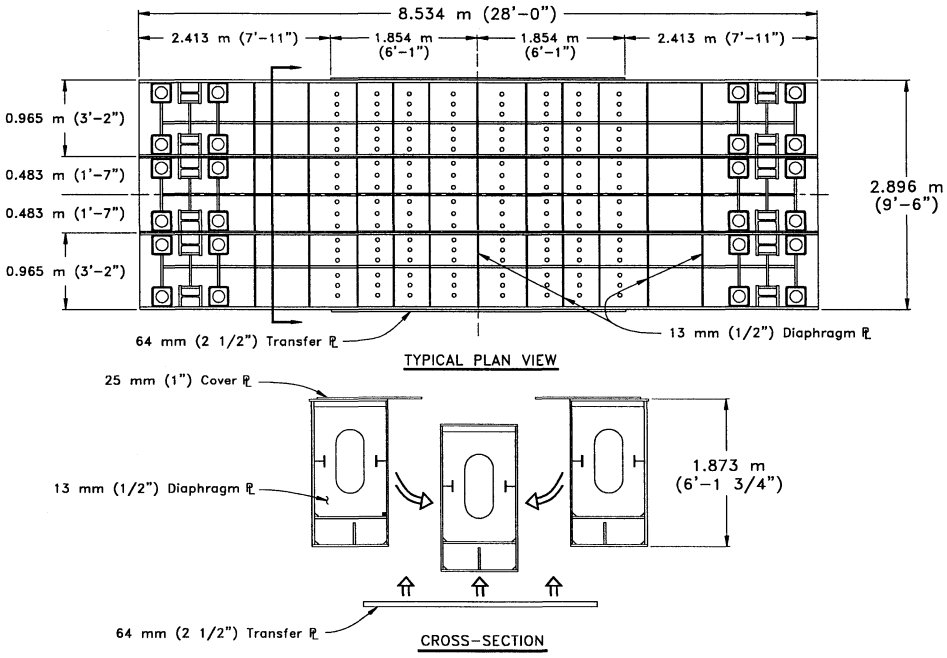


Figure 9 – Steel cross frame

The cross-beam, as shown in figure 9, is conceived as a modular box section, with each segment designed to remain below the weight limit of 20 tons, imposed by the crane capacity. Three steel beams, each one about 1 m wide and 1.8 m high (3'x6'), can be assembled, side by side, through bolted connections along the lateral plates and by cover plates overlapping the boxes at the top.

In order to allow the attachment of test specimens, a 64 mm (2 ½") thick, 3.7x2.95 m (12'x9.6') transfer plate is provided, with the additional purpose of connecting the three steel boxes at the bottom. To increase the stiffness, steel diaphragms are vertically placed inside the box section along the overall beam length. Figure 9 shows, at the two ends of the beams, the location of the 24 steel tie-down rods, with 152 mm (6") diameter each, used to connect the cross-frame to the concrete box. In this region of high stress concentration, square tubes are positioned, inside the steel boxes to directly transfer the tie-down forces and provide vertical stiffness to the system.
The design of the tie-down rods was driven by the need for a significant pre-loading tension force which will eliminate the risk of up-lift of the reaction steel frame and consequent loss of the friction forces at the steel-concrete interface. The goal was also to be able to remove the cross-frame from the concrete box without removing extra long rods and without having to access any space below the concrete frame. The design solution is based on lock off nuts, welded to plates permanently positioned at the bottom of the concrete frame. A lower segment of the rods, located inside a cast-in-place steel tube, will be screwed into the nut and connected to a steel coupler at the top edge. The steel coupler, while locked with pins into the concrete, will receive the top portion of the steel rods. The rods will be tensioned through hydraulic jacks and locked with nuts at the top of the steel cross-frame. The rods will be made from ASTM A193-B7 steel with 517 Mpa (75 ksi) yield stress. Figure 10 depicts the cross-head tie-down scheme.

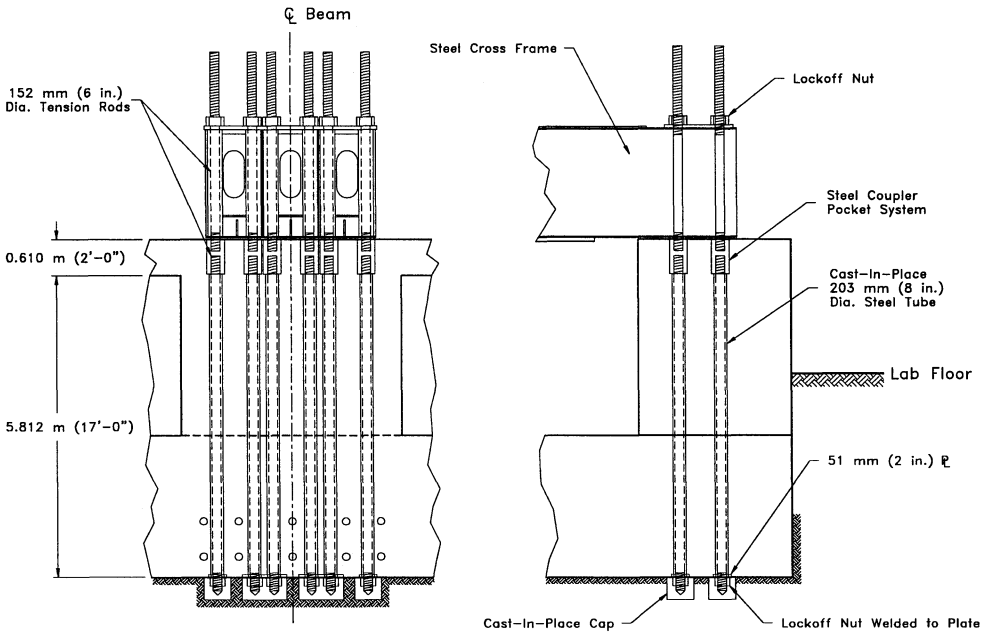


Figure 10 – Tie-down system

CONTROL SYSTEM and READOUT

The control and redout system has been developed by MTS and adapted specifically for the SRMD testing facility. It is based on a Direct Digital Control technology with a Host-Target architecture. The control computer interacts with the load cells applied in the horizontal actuators

rods and the pressure transducers of the vertical actuators. Closed loop control is performed in the rectangular coordinates. A coordinate transformation is used to convert errors in the rectangular positions to commands to the individual servovalves on the actuators. Control modes are: force in the vertical, and position control for the other degree of freedom. Additional force control loops minimize warping and compression of the platen due to mechanical overconstraint. Inevitably the system will introduce errors related to (1) friction of the vertical actuators, (2) friction of the horizontal actuators swivels, and (3) inertia effect of the platen and test specimen. Their extents are approximately quantified as 0.5%, 0.5% and 5% of the relative forces, respectively. The calibration of the system will include a measure of the friction values through a test bearing. Accelerometers, mounted on the platen surface, provide three component acceleration readings and will allow a compensation for the loading errors due to the inertial mass of the platen. All force, displacement and acceleration data will be collected in files. The position data files will provide location and direction of velocity data needed to determine the vector of the friction correction.

During the design phase, the review panel members, specifically addressed the need of a direct measure of the loads applied to the specimens. The goal is clearly the accurate readout of shear forces and axial load minimizing acceleration errors or actuator friction. The subject is presently under study at University of California, Irvine and San Diego.

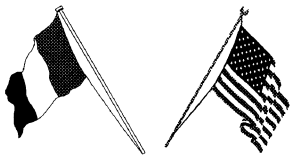
An accurate data acquisition and a camera monitoring system will provide the record of the specimen response. Particular attention will be dedicated to the measuring of surface temperature of FPS bearings and dampers.

POTENTIALITIES of the TESTING FACILITY

The geometry and configuration of the testing system, together with the dynamic characteristics of the hydraulic devices make a wide spectrum of tests possible with the SRMD system. With minor modifications the system is flexible to perform in different testing setups, with the characteristics of a unique shake table. The removable cross-frame and the configuration of the platen, allow the installation of tall specimens, possibly extended outside the existing size of the platen, without interfering with the reaction frame. Several different configurations of possible tests have been analyzed, including specimens in geotechnical sand boxes and devices tested under axial tensile load.

REFERENCES

1. Mellon, D.E, "Caltrans' Proposed Testing of the Seismic Response Modification Devices for the Toll Bridge Retrofit Program", National Seismic Conference on Bridges and Highways, July 1997, Sacramento, California, USA.
2. AASHTO T-3 Task Group, "Guide Specifications for Seismic Isolation Design", Draft 1997
3. Rich, T.R. "Platen Design for the Seismic Response Modification Device Testing System" Master Thesis, University of California San Diego, 1998.



Session IV

Design Criteria for Seismic Isolation Devices
Rosario Ceravolo, Alessandro De Stefano and Giuseppe Mancini

Sensitivity of Response of Isolated Bridges to Modeling and Design Parameters - A Case Study
Andrei M. Reinhorn, Vassil K. Simeonov, Grant DeRue and Michael C. Constantinou

Effects of Multi-support Excitation on Isolated Bridges
Giorgio Monti and Paolo E. Pinto

Development of Bridge Fragility Curves
Masanobu Shinozuka

Testing of Bridges with Isolation/Dissipation Devices at the ELSA Laboratory
Artur V. Pinto, Paolo Negro and Fabio Taucer

Design Criteria for Seismic Isolation Devices

Rosario Ceravolo, Alessandro De Stefano and Giuseppe Mancini

Dipartimento di Ingegneria Strutturale, Politecnico di Torino, Italy

Abstract

This paper examines the possible uses and the advantages of seismic isolation at the base of girder bridges. The attention is focused in particular on the feasibility of adopting a system based on the abatement of the horizontal stiffness of foundation piles, as is obtained by using piles partly non-confined by the surrounding soil.

A parameter sensitivity study was reported, first of all, conducted by means of simple idealisations and an analysis with response spectra. Then eight bridges with standard characteristics, representing a sufficiently wide class of girder bridges, were selected. On these eight structures, subjected to real seismic excitation, a more accurate parametric analysis was conducted with the aim of evaluating the optimal characteristics of the isolation and the applicability of the technique. Finally, the use of special jackets filled with a material with hysteretic non-linear behaviour was investigated in order to assess its potential advantages.

Introduction

Base isolation systems have proved very effective in the seismic isolation of buildings. In frame structures, in fact, the severity of seismic damage is correlated not only to maximum storey acceleration, but also to maximum inter-storey slip. The function of base isolation therefore has the twofold effect of serving as an effective filter for earthquake harmonics and at the same time of dislocating shear strains in the isolation devices.

When dealing with bridge structures, the latter requirement loses importance whilst, on the other hand, the success of isolation at the pier top for structures of this type (1,2) can be associated with the construction process and lower additional load-effects to which the isolation device is subjected (absence of the weight of the pier and second order effects). From a purely dynamic standpoint, the closer is the structural model to a single DOF system (with increasing span and decreasing pier height), the greater is the tendency of the two isolation systems to be equally effective.

Despite the foregoing considerations, base isolation may sometimes prove more effective even in bridge design. For instance, the use of foundation piles as an isolation system offers a number of advantages: conceptual simplicity, mature technology, considerable mechanical strength, the possibility of exploiting the hysteretic damping of the soil or filler materials, or even of adopting "ad hoc" damping systems by means of jackets filled with viscous fluids (mineral oils, silicone based oils, etc.).

The system examined in this investigation is schematised in Fig. 1. The upper part of the pile is released from the surrounding soil and is connected to the structure above it by means of a hinged restraint. The structure restrained to the set of piles therefore acquires a predominantly translational degree of freedom. This leads to an increment in the fundamental period of the structure, meeting the objective of providing a sufficient degree of isolation and at the same time filtering the excitation components of the higher modes.

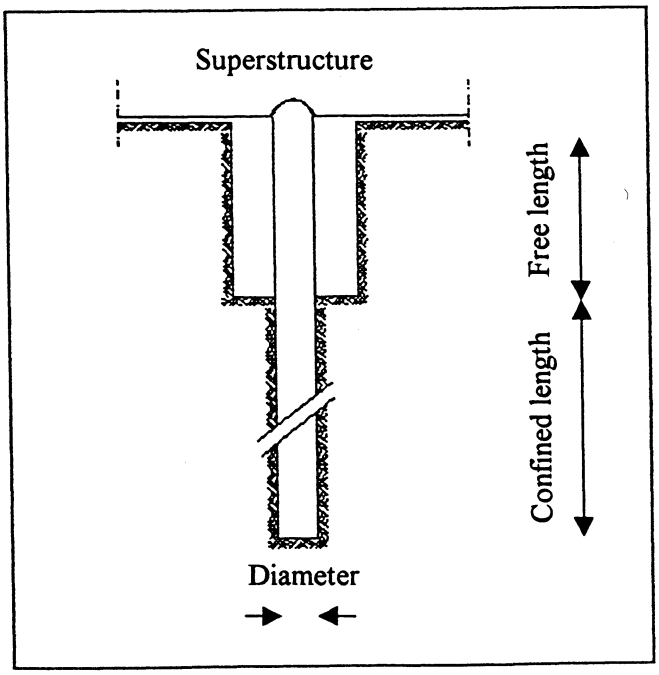


Figure 1. Scheme of the non-confined pile employed for isolation purposes.

In this paper, the effectiveness of this isolation system is studied in two stages: first of all the results of a study aimed at assessing the sensitivity of the different parameters involved, as determined through simple parametric analyses with response spectra, are presented. Then the response to seismic excitation of eight bridge structures, selected to embody standard bridge design characteristics, is analysed by means of 2-DOF models. This makes it possible to outline the realm of applicability of this technology.
Finally, numerical results are presented showing the improvements achieved in system design when the model adopted takes into account a hysteretic non-linear behaviour of the soil.

Stiffness matrix of laterally loaded piles

Let us now briefly go over a few of the formulations adopted in the literature to assess the stiffness of foundation piles (3). In general, two types of models are taken into account for the soil around the pile: Winkler's model, and, as an alternative, the continuous elastic medium model. Either approach requires appropriate numerical procedures and calibration processes.
A finite elements numerical analysis of a stiff body in a heterogeneous linear elastic semi-space, having a shear modulus which varies linearly as a function of depth, conducted by Randolph (4), leads to the following formulae for the determination of displacement and rotation values at the top of the pile:

$$\begin{aligned} u &= F_G \cdot \left[0.27 \cdot H \cdot (l_c/2)^{-1} + 0.3 \cdot M \cdot (l_c/2)^{-2}\right] \\ \vartheta &= F_G \cdot \left[0.30 \cdot H \cdot (l_c/2)^{-2} + 0.8 \cdot M \cdot \rho^{1/2} (l_c/2)^{-3}\right] \end{aligned} \tag{1}$$

where:

$$F_G = \frac{\left\{E_p / [G_c \cdot (1 + 0.75 \cdot \nu)]\right\}^{1/7}}{\rho \cdot G_c \cdot (1 + 0.75 \cdot \nu)} \tag{2}$$

$$l_c = D \cdot \left\{E_p / [G_c \cdot (1 + 0.75 \cdot \nu)]\right\}^{2/7}, \ \textit{critical depth} \tag{3}$$

$$G_c = G(l_c/2), \ \textit{shear modulus at a depth corresponding to half the critical value} \tag{4}$$

$$\rho = G(l_c/2)/G(l_c/4), \ \textit{degree of homogeneity} \tag{5}$$

where:
u, ϑ: displacement and rotation at the top of the pile (in the section of transition between the non confined and the confined portions of the pile);
H, M: shear and moment at the top of the pile;
D: pile diameter;
E_p: effective Young's modulus.

These formulae may be deemed to apply if the depth of the pile in the soil is at least equal to the critical length. If this condition is met, the pile can be regarded as a flexible element embedded in an elastic medium. The critical length can be taken to be the portion of pile effectively interacting with the soil. The degree of homogeneity expresses the variation in the elastic characteristics of the soil as a function of depth. It takes on a unit value in homogeneous soils.

The presence of a set of piles causes of loss of efficiency due to the interaction between the individual piles. The displacement at the top of a pile included in a set of n piles can be expressed through the following formula by Poulos (5):

$$\delta_i = \frac{1}{k}\sum_{j=1}^{n}\alpha_{ij} \cdot P_j \,, \tag{6}$$

where α_{ij} is the factor of interaction between piles i and j, and P_j is the generic load on the individual pile. The α_{ij} factors are markedly influenced by pile radius and, in particular, by pile spacing, and they can lead to an appreciable reduction in the efficiency of a group of piles. In several tests conducted by Williams (6) on sets of two and three piles in dense sand this reduction was seen to be as high as 40% of the efficiency coefficient. This can determine an increase of the isolation level, which in this study was not taken into account.

The seismic isolation system aims to reduce the translation stiffness of the piles by creating a length along which the pile is not confined in the soil. The connection with the structure above produces a hinged restraint, so as not to load the piles with a moment at the top. Fig. 2 shows the evolution of horizontal stiffness, in relation to the stiffness of a pile totally enclosed in the soil, as a function of free length, normalised with respect to the critical length. The results refer to a concrete pile, 400 mm in diameter, driven in clay soil (G_c=12 MPa and ν=0.15) with ρ=1 (homogenous soil) and ρ=0.5. In these conditions, the critical length comes to ca 4 m. It should be noted that, in homogeneous soil, releasing a pile over a length corresponding to one third of the critical value leads to a reduction in stiffness of about five times.

As for the load-effects on the pile, numerical tests on piles loaded with horizontal forces have shown that, with a good approximation, the maximum bending force on the pile corresponds to the moment in the section of transition between the confined and the non confined portions of a pile. Furthermore, the applicability of this principle increases with increasing free length-to-critical length ratio and with increasing soil homogeneity.

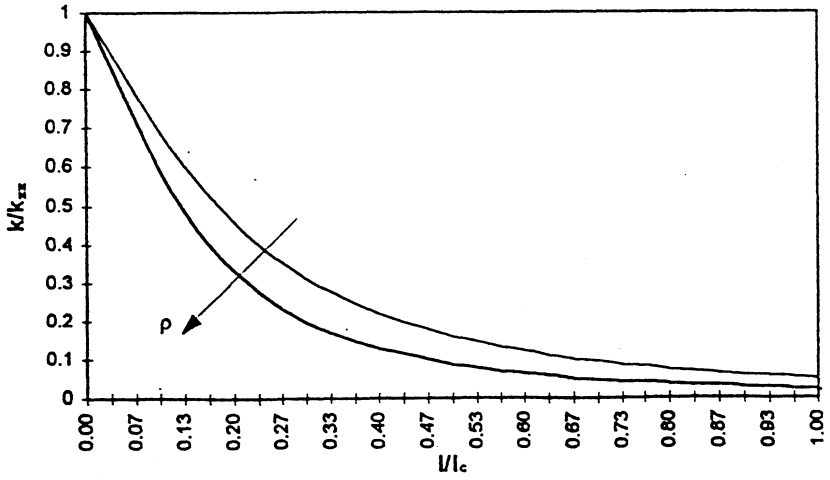


Figure 2. Horizontal stiffness relative to the stiffness of a fully driven pile (7).

Preliminary Sensitivity Analysis of the Parameters

The advisability of adopting the proposed system depends on a multiplicity of heterogeneous parameters which can be grouped into four classes: parameters of the structure on a fixed base, spectral characteristics of the excitation, parameters of the isolation system, soil parameters.

The sensitivity analysis was conducted with the aim of achieving results of a general scope, by focusing the attention on the isolation parameters. To this end, some of the results obtained in earlier research projects conducted at the Politecnico di Torino by Foti (7) are given below. In view of the relative simplicity and comprehensibility of the dynamic behaviour of a bridge, it was deemed sufficient, at the stage of preliminary analysis, to consider a 1-DOF model, consisting of a modal mass $\underline{m}$ and two springs arranged in series, associated with the stiffness of the isolation system, K_p , and the generic modal stiffness of the structure, K_s, respectively.

The spectral characteristics of excitation have been taken into account through the elastic response spectrum used in the analysis, which is the one supplied in Eurocode 8 (8), with peak ground acceleration of 0.35 g. Spectrum parameters relate to type C soil, characterised by higher periods which represent greater hazards for isolated systems. Furthermore, the isolation system being considered has been conceived to be applied whenever it is necessary to adopt pile foundations, i.e., in poor soil conditions in many cases.

Two parameters have been adopted to determine whether or not the isolation objectives are attained: one is the so-called "degree of isolation", α, i.e., the ratio between a structure assumed to be stiff on the isolation system and the period of the structure on a fixed base. In the following paragraphs reference shall also be made to the inverse of this parameter, called "degree of coupling", which is the ratio between the natural frequencies. The "degree of isolation" provides a quantitative measure of the shift towards lower isolation frequencies, of lesser significance in seismic spectra. Despite its qualitative nature, this parameter remains independent of the response spectrum employed. A number of standards and recommendations set minimum values for this degree of isolation, for instance by requiring that $\alpha \geq 2$. However, whilst values of α approaching 1 entail risks of coupling, exceedingly high values are often associated with an excessive global system flexibility, which is unsatisfactory. The other parameter adopted is the percentage response difference which, though it is strictly correlated with α, supplies more conclusive quantitative evidence.

The results given below refer to RC piles with a diameter of 600 mm and effective length collaborating with the soil of 20 m. The structure above the individual pile has a weight of 95,000 kg (ca 80% of admissible load) and a natural period of 0.7 s, corresponding to the zone of the spectrum most favourable to isolation efficiency. The soil is clayey, with $G = 2.5 \cdot z$ MPa and value of undrained cohesion of $c_u = 150$ kPa. In these conditions, it turns out that for free lengths of the order of 2 to 3 m, the degree of isolation obtained is 2.5, which is close to the degree achieved in traditional isolation system design, with acceleration abatement levels of around 50%.

Fig. 3 illustrates the percentage variation of the response as a function of the period of the oscillator for a pre-determined free length of 3 m. The shape of the diagram clearly reflects the response spectrum adopted. Thus, the best results are obtained for periods of fixed base structures of between 0.6 e 1.0 s, whilst the benefits for the oscillators situated beyond the maximum amplification zone are negligible.

Fig. 4 shows the non-dimensional moment as a function of free length for two different pile diameters. It can be seen that maximum moment values are recorded in the zone of greatest interest in terms of degree of isolation, which brings out the problem of strength control on the piles. Furthermore, an interesting observation we can make is that the maximum moment of the pile decreases appreciably with increasing pile diameter.

Finally, Figs. 5 and 6 show the modest influence of the soil modulus G. Relatively low sensitivity results are obtained for all soil deformability parameters. The degree of homogeneity has a slightly

more appreciable weight; however, assuming a degree of homogeneity lower than 1 reduces the response by 5 - 10% and leads to a reduced moment on the piles, which means that the assumption of a homogeneous soil is favourable in terms of safety.

Though it is not exhaustive, this analysis points out a number of aspects and parameters which may have a decisive effect on the applicability of the isolation system to girder bridges, the most important of which can be summarised as follows:

1) This technology, especially in view of the large pile diameters generally employed in bridge construction, will not supply a high degree of isolation. This entails the adoption of great free lengths, whose feasibility should be evaluated for the different types of structure.
2) The use of concrete piles might find a limitation in the strength of the material. It should be noted however that the problem is attenuated with increasing pile diameter (Fig. 4), this being an aspect of special interest in bridge isolation.
3) The influence of soil parameters is quite modest. The assumption of a homogenous soil is on the safe side.

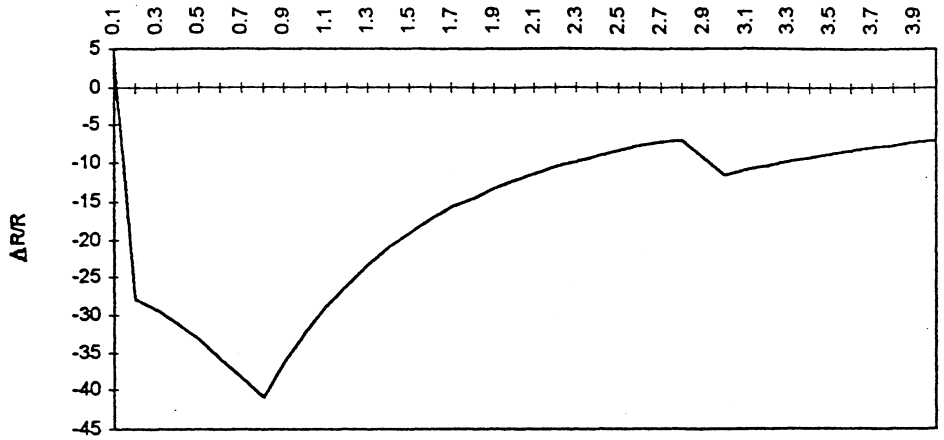


Figure 3. Percentage variation of the response as a function of oscillator period (free length of the piles = 3m).

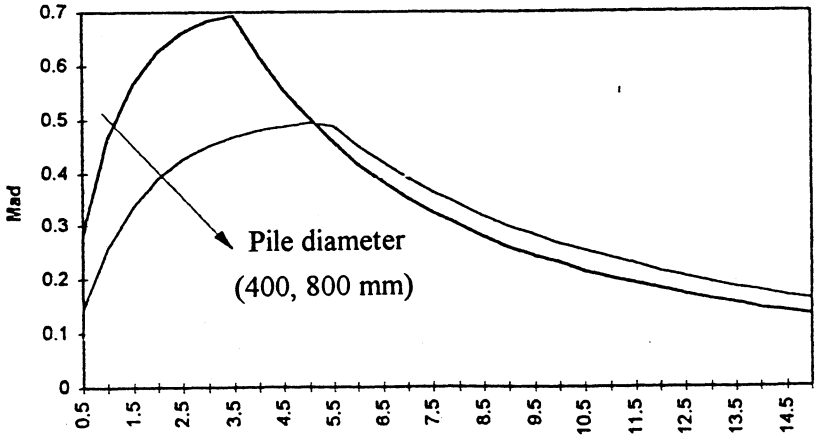


Figure 4. Non-dimensional moment as a function of free length for different pile diameters.

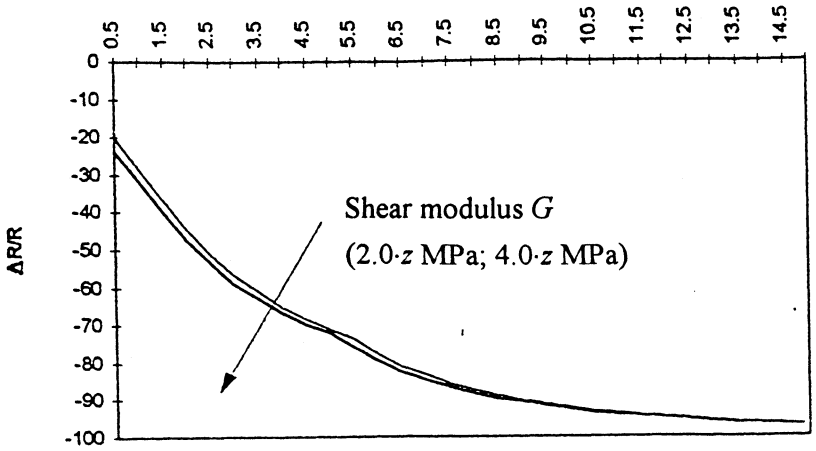


Figure 5. Percentage variation of the response as a function of the free length of the pile for different values of the soil's modulus G.

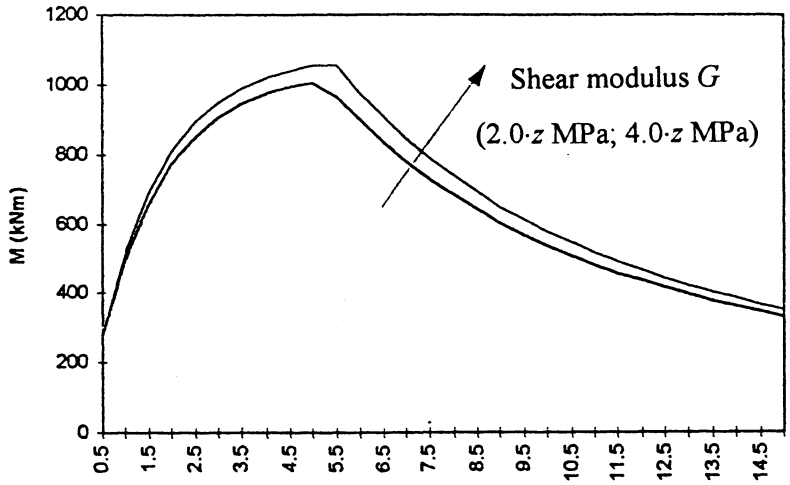


Figure 6. Moment as a function of free length for different values of the soil's modulus G.

2-DOF model of the isolated bridge

The numerical experiments described in the following paragraphs were conducted with reference to the discrete simplified model shown in Fig. 7. The dynamic equations associated with this model are:

$$\begin{aligned} &m_{tot}\ddot{x}_b + \mathbf{a}^{\mathrm{T}}\mathbf{M}\ddot{\mathbf{x}} + c_b\dot{x}_b + k_b x_b = -m_{tot}\ddot{x}_g; \\ &\mathbf{M}^{\mathrm{T}}\mathbf{a}\ddot{x}_b + \mathbf{M}\ddot{\mathbf{x}} + \mathbf{C}\dot{\mathbf{x}} + \mathbf{K}\mathbf{x} = -\mathbf{M}^{\mathrm{T}}\mathbf{a}\ddot{x}_g. \end{aligned} \tag{7}$$

where:
m_{tot} : total system mass;
c_b, k_b : damping and stiffness of the isolation;
M, **C**, **K**: mass, damping and stiffness matrices of the superstructure on a fixed base;

x_b : isolation displacement relative to the soil;
x : superstructure displacement vector relative to the fixed base;
a : entrainment vector;
$\ddot{x}_g$: soil acceleration.

Let us assume that the motion of the superstructure on a fixed base is closely approximated by its first vibration mode (9,10). This amounts to setting:

$$\mathbf{x} \cong {}_1\mathbf{w} x_n, \tag{8}$$

where x_n is the displacement at the top of the structure relative to the fixed base, and ${}_1\mathbf{w}$ is the first modal eigenvector, normalised so that ${}_1w_n=1$. By substituting exp. (8) into exp. (7) we get the following two equations:

$$\begin{aligned} &m_{tot}\ddot{x}_b + \Gamma_1 M_1 \ddot{x}_n + c_b\dot{x}_b + k_b x_b = -m_{tot}\ddot{x}_g; \\ &\Gamma_1 M_1 \ddot{x}_b + M_1\ddot{x}_n + 2\xi_1\omega_1\dot{x}_n + \omega_1^2 M_1 x_n = -\Gamma_1 M_1 \ddot{x}_g. \end{aligned} \tag{9}$$

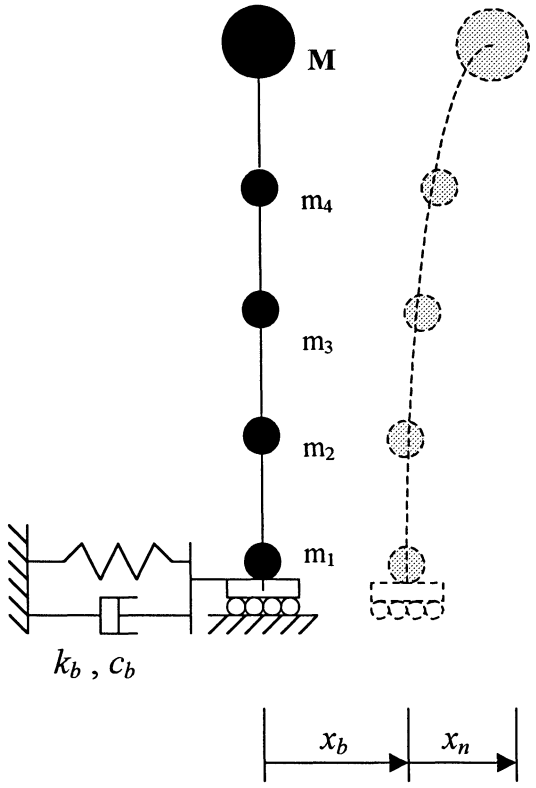


Fig. 7: Simplified 2-DOF model

Where ω_1 and ζ_1 are the frequency and the damping factor of the first mode of the structure on a fixed base. Furthermore M_1 and Γ_1 are the modal mass and the first mode participation factor, defined as:

$$M_1 = {}_1\mathbf{w}^T \mathbf{M}_1 \mathbf{w}$$
$$\Gamma_1 = \left({}_1\mathbf{w}^T \mathbf{M}\mathbf{a}\right)/M_1.$$

In this form, the problem of base isolation is governed not only by the stiffness and damping characteristics of the system adopted, but also by: the frequency and damping of the first mode of the superstructure, the modal mass, the total mass and the first modal participation factor (in bridges the latter is very close to 1).

Description of the numerical experiments

By referring to the 2-DOF model described above and, in particular, by integrating equation (9) step by step, it proved possible to study in an easy but sufficiently accurate manner the feasibility of the isolation system being considered.

The parametric study was conducted on a limited number of girder bridges (eight in all) suitably selected to be able to draw conclusions of a general nature. The main target of the parametric analysis was the stiffness of the piles and hence their free length. The study was performed for three types of reinforced concrete piles (diameters: 800, 1000, 1200).
The following variables were checked to evaluate the quality of the isolation, also on the basis of the considerations made in the previous paragraphs:

1) Percent reductions in the load-effects on the pier;
2) Pier top displacement;
3) Pile top displacement;
4) Load effects on the piles.

Table 1 gives the general data concerning the bridges examined, and Table 2 lists the number of piles to be fitted for three different pile diameters. Finally, Table 3 summarises the parameters characterising the dynamic model of the individual bridge.

Bridge	Type **1**	Type **2**	Type **3**	Type **4**	Type **5**	Type **6**	Type **7**	Type **8**
Pier height, H [m]	15	15	15	40	40	40	80	80
Deck length, L [m]	30	60	100	30	60	100	60	100
Deck mass [t/m]	20	26	30	20	26	30	26	30
Pier mass [t]	240	240	240	1500	1500	1500	4000	4000
Pulvino mass [t]	50	50	50	300	300	300	800	800
Pier section flex.stiffness (EJ) [Nm^2]e09	286	286	286	1228	1228	1228	1870	1870

Tab. 1. General data concerning the bridges examined.

Bridge	Type **1**	Type **2**	Type **3**	Type **4**	Type **5**	Type **6**	Type **7**	Type **8**
Pile Ø 800	6	12	-	14	20	-	-	-
Pile Ø 1000	4	8	14	10	14	20	-	-
Pile Ø 1200	3	6	10	8	10	14	18	22

Tab. 2. Number of piles adopted for the different bridge types.

Bridge	Type **1**	Type **2**	Type **3**	Type **4**	Type **5**	Type **6**	Type **7**	Type **8**
ω_1 [rad/s]	19.08	12.38	9.06	6.92	5.16	3.99	1.86	1.54
ζ_1 [%]	5	5	5	5	5	5	5	5
m_{tot} [t]	840	1800	3240	2100	3060	4500	5560	7000
M_1 [t]	698	1658	3098	1205	2163	3603	3173	4610
Γ_1	1.0358	1.0151	1.0081	1.1316	1.0731	1.0438	1.1332	1.0916

Tab. 3. Parameters of the dynamic model of each bridge.

The excitation values used are taken from accelerometric records relating to the earthquake of Loma Prieta (1989, Natural Science Building at UC Santa Cruz, E/W direction, PGA=0.4248 g). The elastic response spectrum, shown in Fig. 8, reveals a rather typical frequency content, with a main peak at the low periods and a secondary peak on periods slightly higher than 1 s. In the following applications the acceleration values were normalised so as to have a PGA of 0.35g.

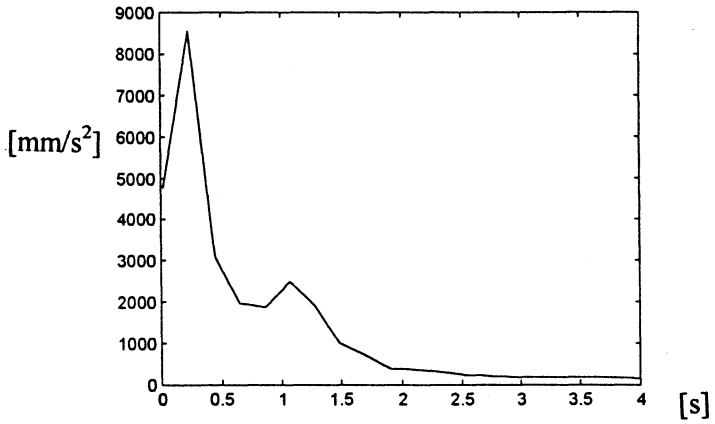


Figure 8. Loma Prieta response spectrum (1989, Natural Science Building at UC Santa Cruz, E/W direction, PGA=0.4248 g, ζ=5%).

Qualitative considerations on the performances of the isolation device

With the bridge data calculated through modal analysis (as given in Table 3), it proves possible to obtain preliminary qualitative estimates as to the effectiveness of isolation systems. Figs. 9 and 10 show the diagrams of the degree of isolation, α, plotted as a function of the free length of the pile, for each of the three pile diameters considered. The diagrams are grouped for bridges of the same height. In view of the relatively modest influence of the elastic properties of the soil - as demonstrated by the preliminary sensitivity analysis - from now on we shall always refer to concrete piles driven in clayey soil (G_c=12 MPa and ν=0.15) under the assumption (to be on the safe side with respect to the degree of isolation) that ρ=1 (homogeneous soil).
Apart from the obvious observation that, pile stiffness being the same, α increases markedly with natural frequency and, to a lesser extent, the frequency being the same, with total mass, the diagrams provide the following indications on the practical feasibility of the isolation system:

a) The high period of bridges with very tall piers may be viewed as the parameter playing a decisive role in making this type of isolation unfit for practical design purposes (Fig.10); lower pile diameter does not make an appreciable contribution to the degree of isolation.
b) Conversely, in the design of bridges with relatively high natural frequencies, the system can be rated as satisfactory: in other words, system performance improves with decreasing pier height and span length. In this case too, the effects of fitting stiffer piles do not seem appreciable and therefore it might be advisable to adopt larger diameters to cope with strength problems.

It should be pointed out, however, that the degree of isolation is a qualitative parameter and the results may vary a great deal for different seismic spectra. Furthermore, so far we have failed to take into account the elasto-plastic behaviour of the soil, or the possibility of employing high-damping

systems. A quantitative study, in terms of effective response, is discussed in the following paragraphs.

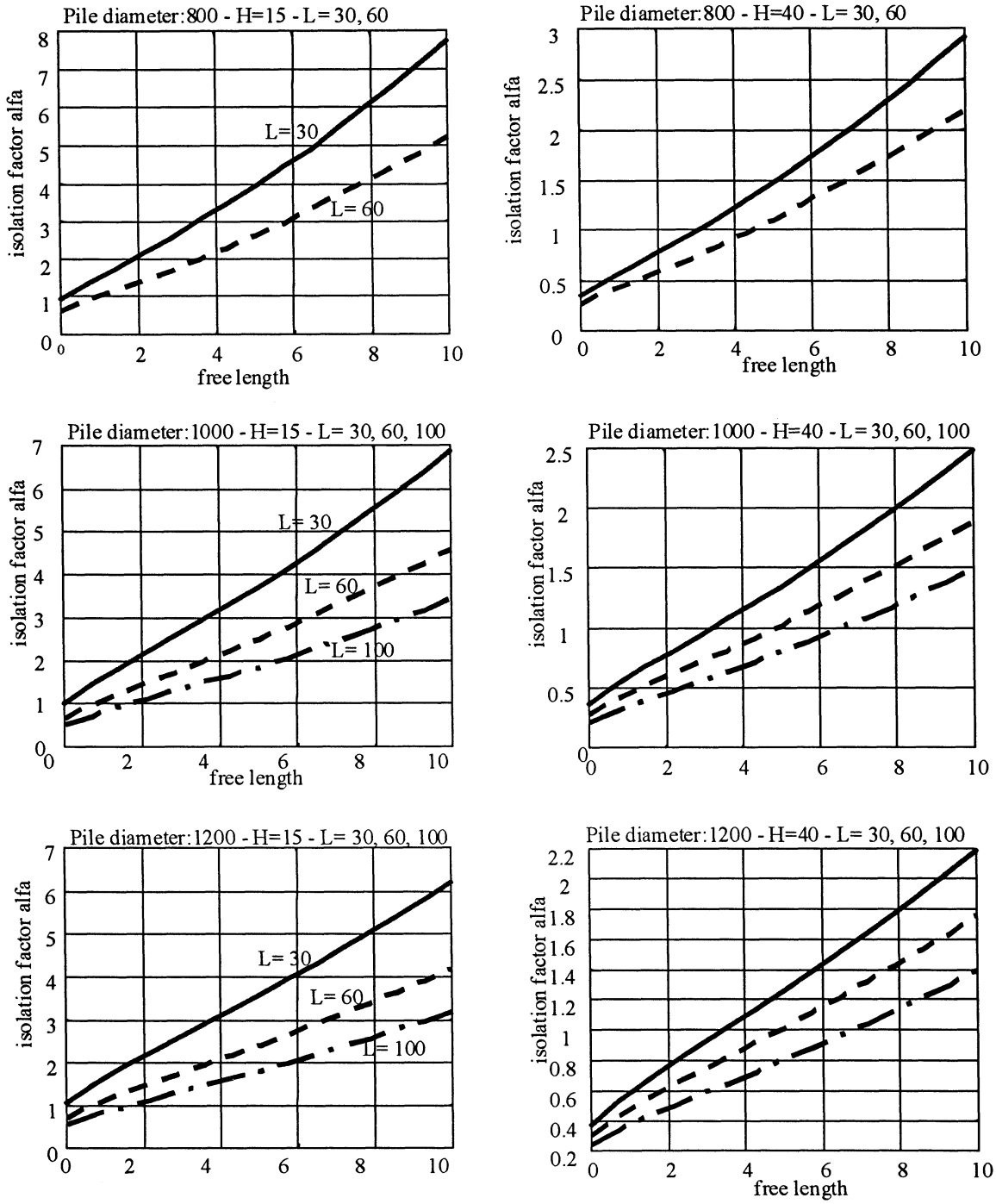


Figure 9. Degree of isolation α as a function of free length for the different types of bridge (types 1-6).

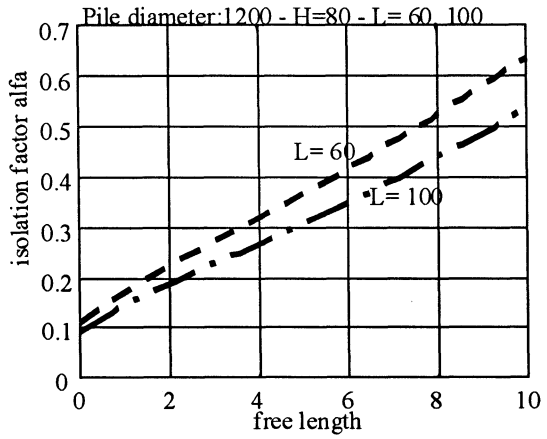


Figure 10. Degree of isolation α as a function of free length for tall bridges (types 7-8).

Response of the isolated system under a severe earthquake

Fig. 11, on the Loma Prieta earthquake, illustrates the response of the different types of bridge to increasing isolator stiffness levels, which is more conveniently expressed in terms of "degree of coupling", Ω. In this connection it should be kept in mind that the following relationships apply:

$$\Omega^2 = \frac{1}{\alpha^2} = \frac{k_b}{\omega_1^{\,2} \cdot m_{tot}} \tag{10}$$

It can be seen, first of all, that the diagrams are clearly comparable, confirming that Ω, or α, are highly significant parameters. Ω being the same, the displacements required of the isolation device to achieve a certain level of reduction of the response increase from type 1 to type 8 bridges, this increase being acceptable, however, with respect to the height of the pier. At the same time, deck displacements increase by one order of magnitude but, within the range of isolation degrees of interest, they remain at sufficiently low levels.

It may be of some interest to note, in type 1 bridges, for $\Omega \cong 0.3$, the amplification effect produced on the piles by the secondary peak which the spectrum has on periods slightly higher than 1 s. In this range of periods, the system is governed by pile deformability, and this, in the presence of high period harmonics, might pose severe problems of displacements and load-effects on the piles.

In the portion of the diagram of greatest significance for design purposes (values of Ω lower than 0.5) we observe a similar law in the attenuation of the response, but clearly, in tall bridges, with huge total mass, a certain degree of isolation can only be attained at the price of much higher deformability levels, whose feasibility is discussed later on.

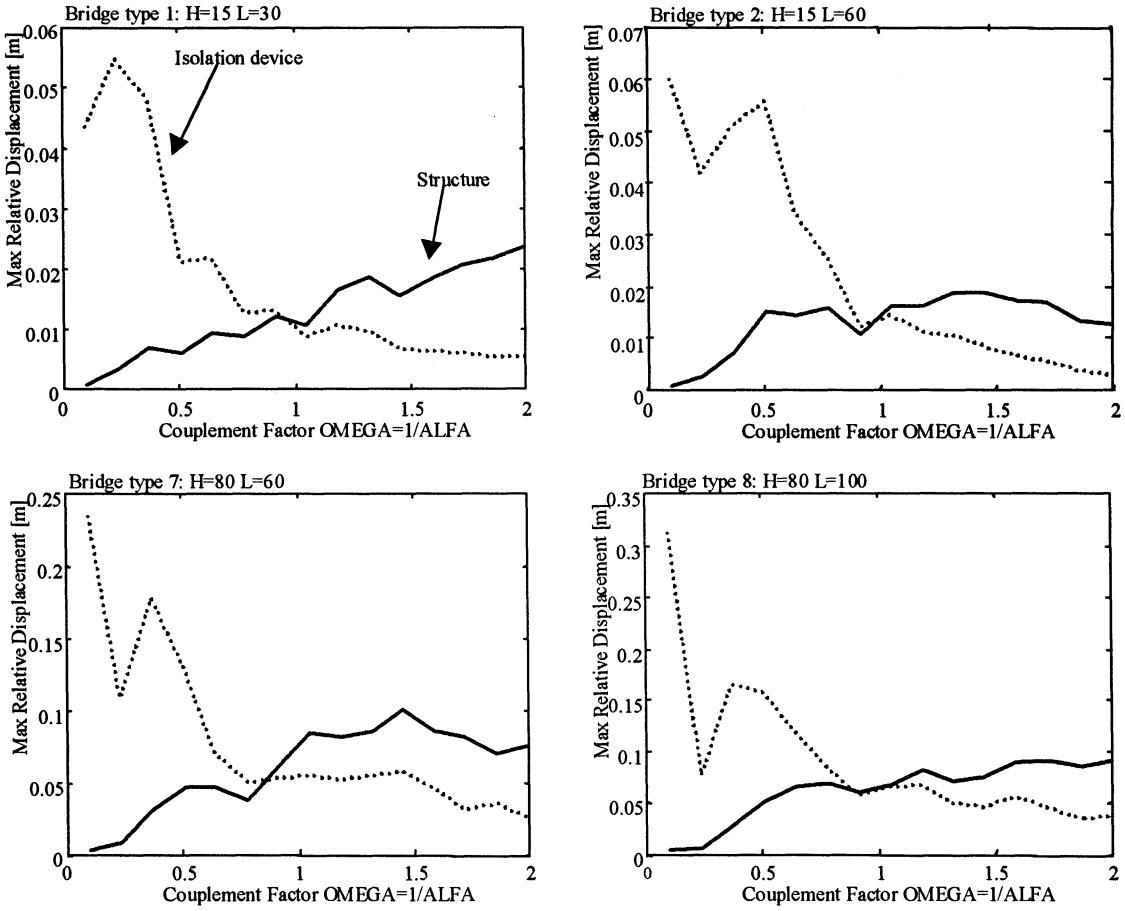


Figure 11. Relative displacements of the isolation system and the pier as a function of the degree of coupling Ω for bridge types 1,2,7,8.

Results of the numerical experiments

The tests being considered were extended to the eight bridges described in Table 1, each of which was associated, compatibly with individual bridge design, with three different pile diameters, as listed in Table 2. For each of the corresponding dynamic models the integration of the equations of motion led to three types of charts:

1) Pile top displacement and relative displacement of the bridge top relative to the fixed base, as a function of the free length of the piles.
2) Percentage response of the bridge vs. the response of the non isolated one, as a function of the free length of the piles.
3) Maximum non-dimensional moment on the foundation piles, as a function of the free length of the piles.

The diagrams of the first type provide a general understanding of dynamic behaviour and make it possible to check for incompatible displacements. Admissible deck displacement relative to the ground has been assumed to be, indicatively, 1/300 the height of the pier (H/300). The diagrams of

the second type express the efficiency of the isolation system. Finally, the moment diagrams illustrate the actual feasibility of the system, in terms of strength.
The results concerning the Loma Prieta earthquake already give an exhaustive picture of the situation, by displaying the effects of the two peaks of the spectrum, on high and low periods, respectively, in a separate form.
Fig. 12 shows the relative displacements of the piles and structure as a function of the free length of the piles. These charts refer to type 1 - 6 bridges, with 1200 mm piles. Furthermore, we can discern two marked displacement peaks, caused by the passage at the second peak of the spectrum (after ca 1.05 s). These peaks move towards the origin with increasing initial period, i.e. with decreasing degree of isolation required.

Type 1-3 bridges (H=15m)
In the three bridges of lesser height, at the peaks, pile displacements can be as high as H/100. Hence, in such bridges, free lengths of over 4 m give rise to excessive displacements, whilst in order to achieve a good degree of isolation (α=2.5 for average characteristic spectra), pile free length must be comprised between 2.5 and 8 m (see Fig. 9).
This last consideration is confirmed by the diagrams given in Figs. 13, which illustrate the percentage response, with reference to that of a non isolated system, for pile diameter of 1200 mm. In type 1 bridge, hinged restraint alone makes it possible to obtain considerable response reductions, so that free lengths lower than 4 m provide a satisfactory degree of isolation without posing excessive displacement problems. In type 2 - 4 bridges, instead, free length values must be higher than 6 m, to reduce the response sufficiently and at the same time cross the displacement peaks. In type 3, and especially type 4, bridges, the negative results are compounded by the fact that their natural period falls in a trough of the spectrum, where the isolation device causes a raise in the response.
Figs. 14 and 15 show the non-dimensional maximum peaks on the individual pile $\mu = M/\left(\pi \cdot R^2 \cdot f_{cd}\right)$, where M is the moment on the pile, R is the radius, and $f_{cd} = 18.75\ \mathrm{N/mm^2}$ is the design strength of concrete, with $R_{ck} = 37\ \mathrm{N/mm^2}$. The results seem encouraging, if one considers that, by designing the piles so as to confer sufficient ductility to the section, we obtain resisting moments of $\mu = 0.4 \div 0.5$. It should be noted that the risk of pile failure is limited to particular free length values and to the bridges with the lowest period. Thus, the problem of excessive pile displacement, due to the low frequency energy contents, go hand in hand with excessive load-effect problems. It should be noted, however, that the use of larger diameter piles has a beneficial effect, both in terms of displacements and in terms of moments, without giving rise to an appreciable increase in response in the range of free length of interest.
Apart from the result relating to the bridge of type 1, which is markedly influenced by the shape of the spectrum, it can be seen that pile displacement and load-effect peaks correspond to the optimal isolation levels. This suggests that, in bridges of this type, free lengths lower than 6 m should be used with great caution, after a careful study of displacements and load-effects in the foundation piles. In this range of initial periods, the degree of isolation, α, is well correlated with the attenuation of the response.
Fig. 15, instead, gives the results obtained on 1000 mm piles (only bridge type 1 and 4), and it can be seen that the increase in diameter gives rise to a very modest shift of the response to greater free length. Instead it is of some interest to note the increase in the maximum moment on the piles.

Type 4-6 bridges (H=40m)
Where H=40m bridges are concerned (types 4-6), the displacements are seen to be modest with respect to the height of the bridge (ca H/400). The presence of a peak in the spectrum on high periods (ca 1.05 s) means that in bridges with periods just beyond the peak (bridges 4 and 5), the response is reduced with free lengths of only 4 to 6 m, which, surprisingly, correspond to low

degrees of isolation (of about 1.5). In these bridges, in the presence of highly deformable soils, which widen the earthquake spectrum, no matter how the degree of isolation, even relatively small period increments might be decisive for the survival of the structure. Type 4-8 bridges display moment values on the safe side, decreasing with the initial period, on account of their being situated in low amplification zones of the spectrum (Fig. 8).

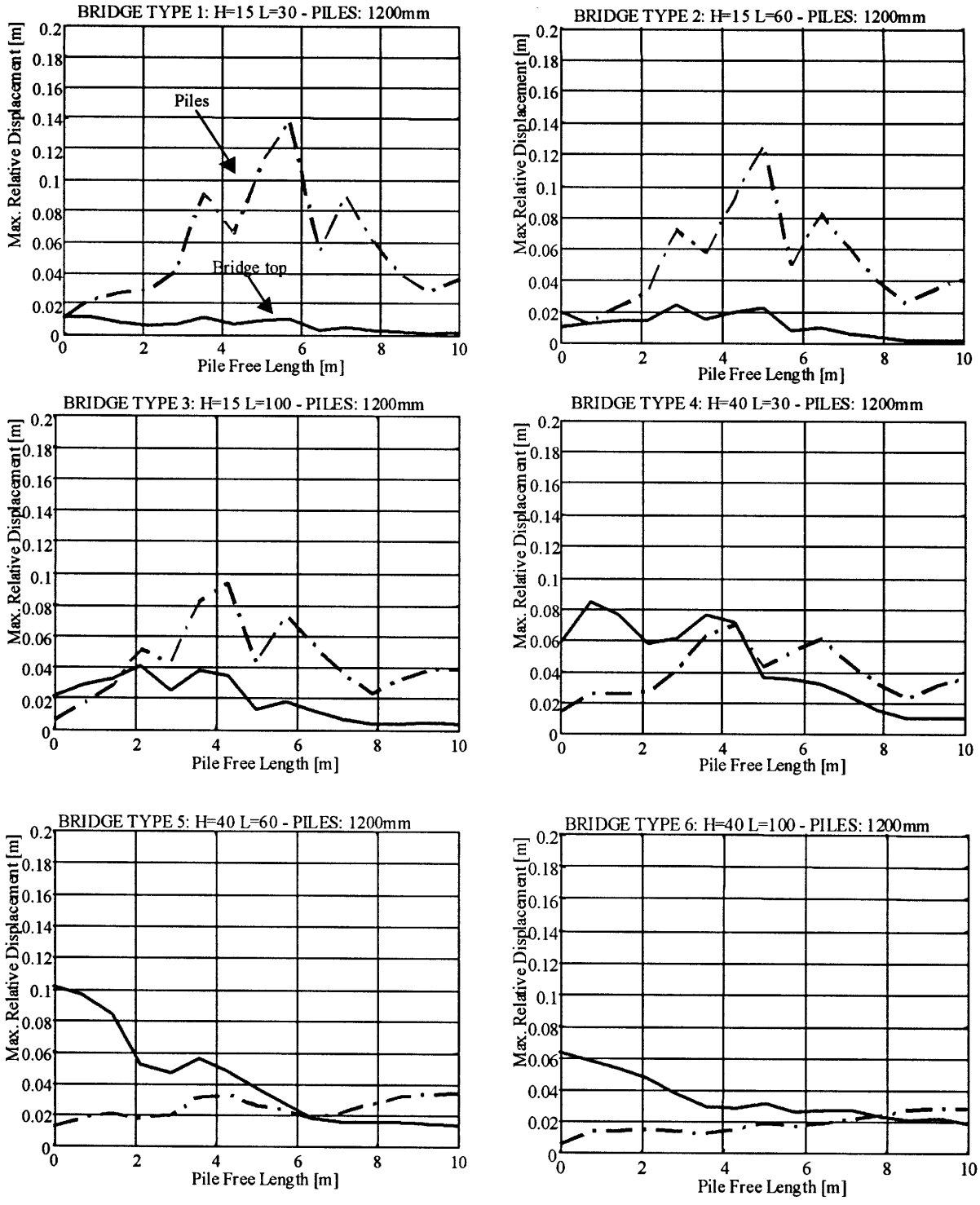


Figure 12. Relative displacements of the isolation system and the pier as a function of the free length of the (1200 mm) piles for type 1 - 6 bridges.

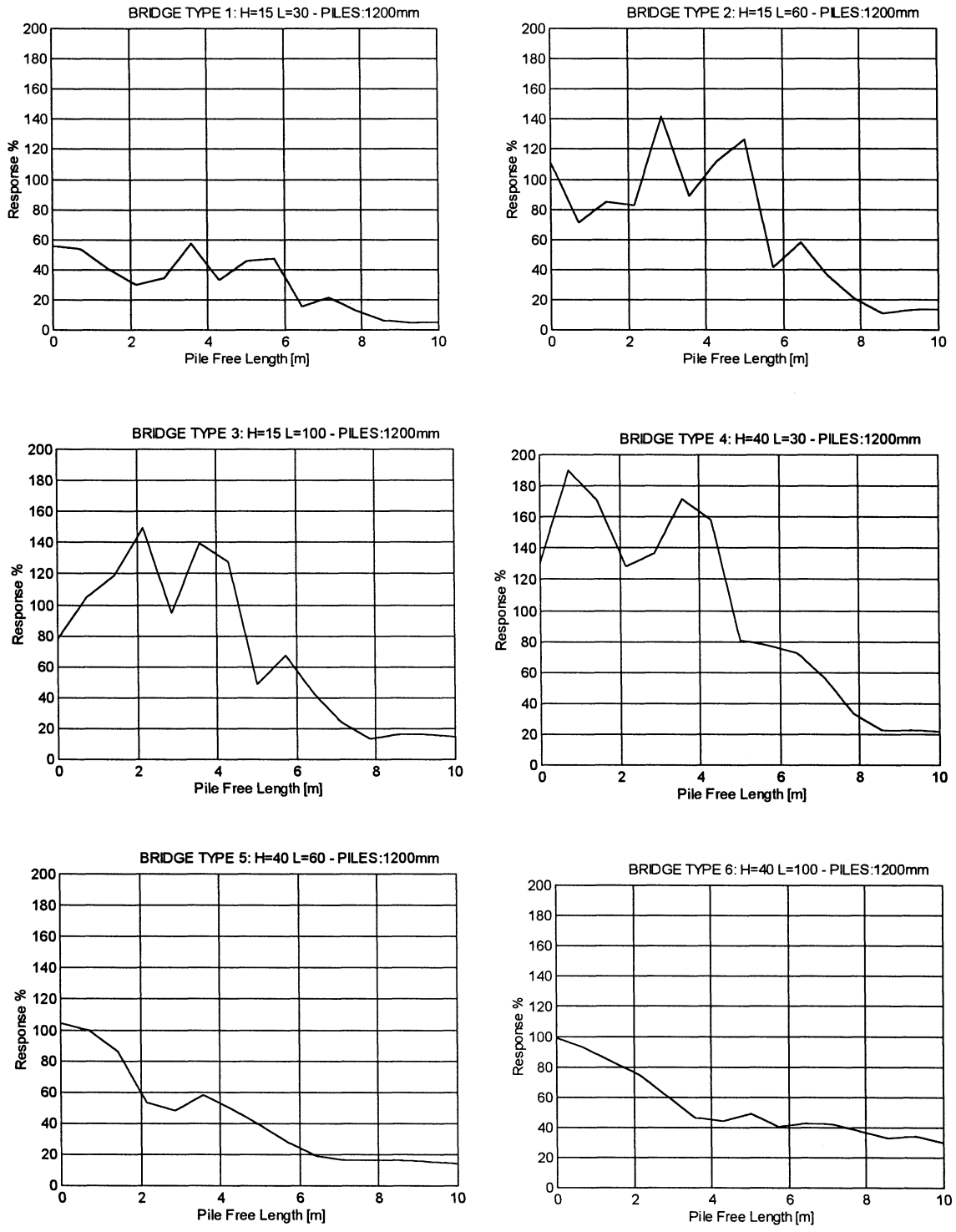


Figure 13. Percent response of the pier (vs. the response with no isolation system) as a function of the free length of the (1200 mm) piles for type 1 - 6 bridges.

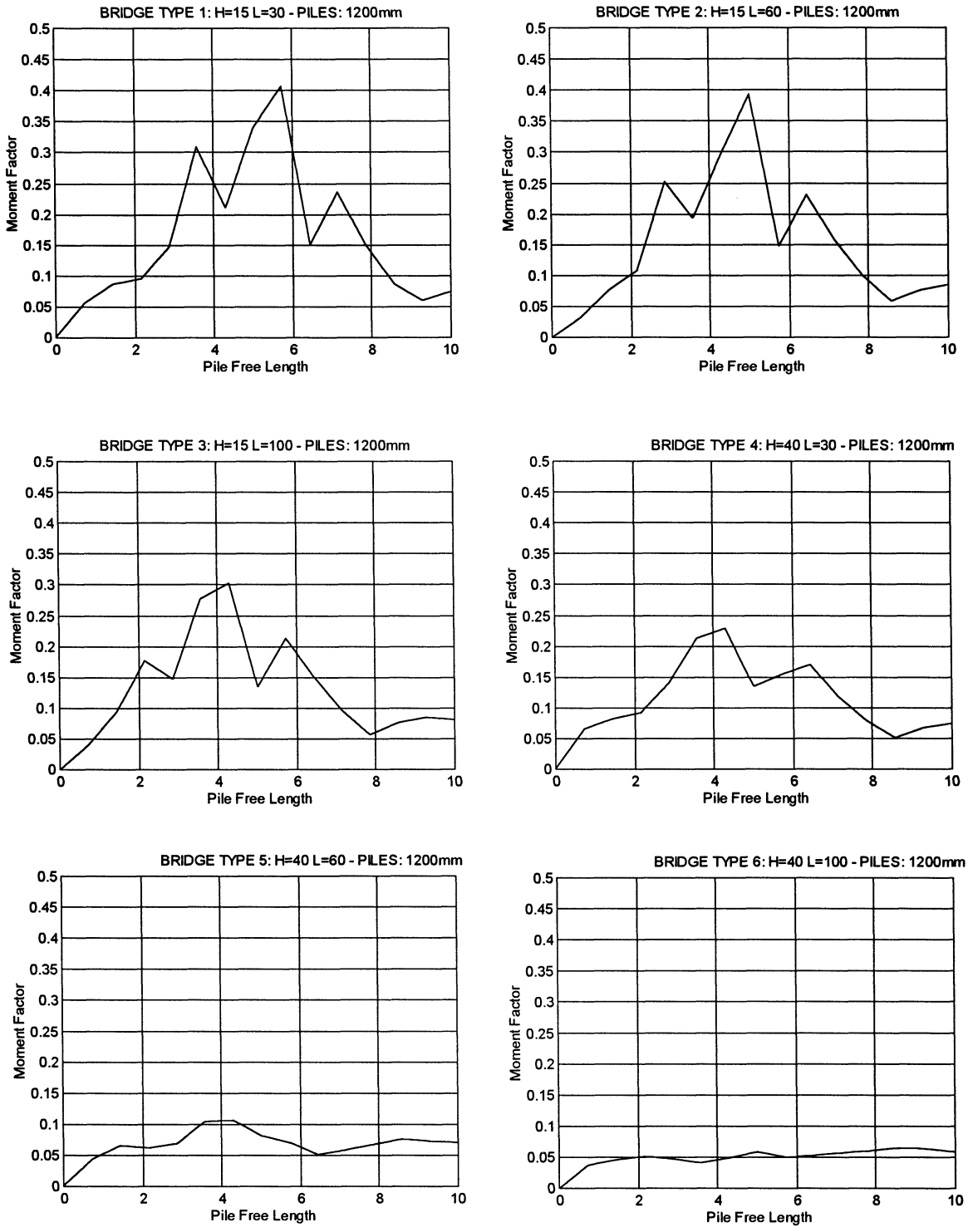


Figure 14. Maximum non-dimensional moment on the piles (1200 mm) for type 1 - 6 bridges.

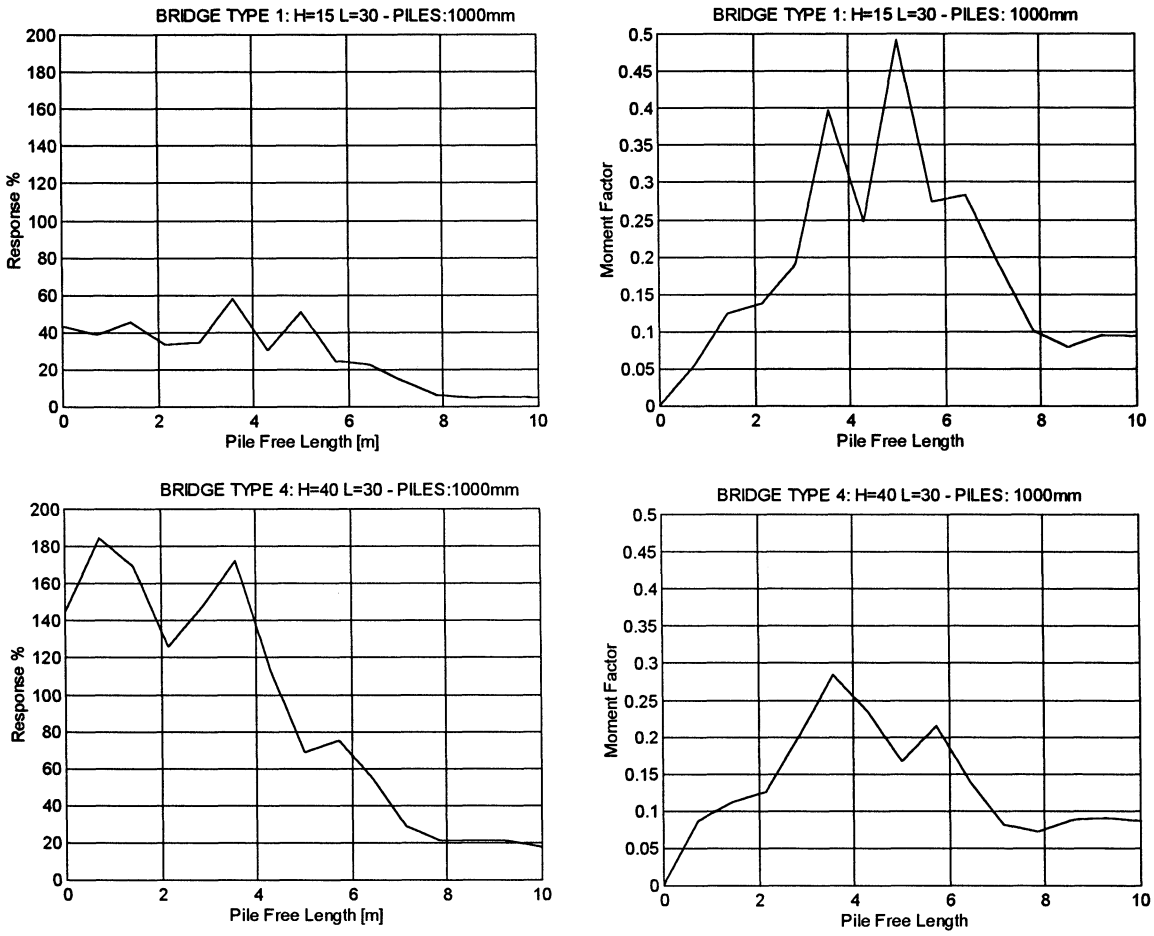


Figure 15. Percent response of the pier and maximum non-dimensional moment piles (1000 mm) for type 1 and 4 bridges.

Effect of non-linearity and hysteresis

So far, this analysis has disregarded the non-linear and hysteretic behaviour of the isolation system. The latter may be activated for small pile displacement levels, on account of the elasto-plastic and hysteretic behaviour that takes place at the pile-soil interface, causing considerable energy dissipation. The determination of the type of force-displacement law governing the isolation system is a complex problem which cannot be dealt with in this context and which is affected by a multiplicity of factors. From an operational standpoint, we may refer to the experimental results given in the literature.

For the time being, we shall be content with the qualitative results obtained from a simple numerical simulation process by adopting a quadratic softening force-deformation law with a hysteretic Masing type law (Fig. 16). Figs. 17-18 show the relative displacements caused by the Loma Prieta earthquake on type 1 and type 4 bridges, respectively, assuming that an 0.01 m displacements leads to a 50% reduction of isolation system secant stiffness. In reality, this reduction is a function of the length of the pile non confined by the ground. In the same figures, to the side, the percentage response of the linear system is compared to that of the hysteretic non-linear system.

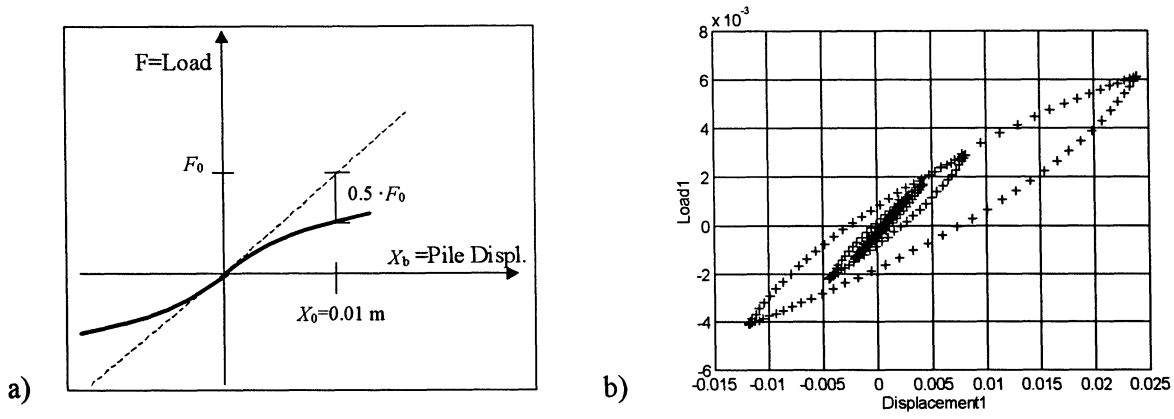


Figure 16. a) Quadratic hardening constitutive law adopted for the isolation device. b) Example of Masing hysteresis law adopted (impulsive load).

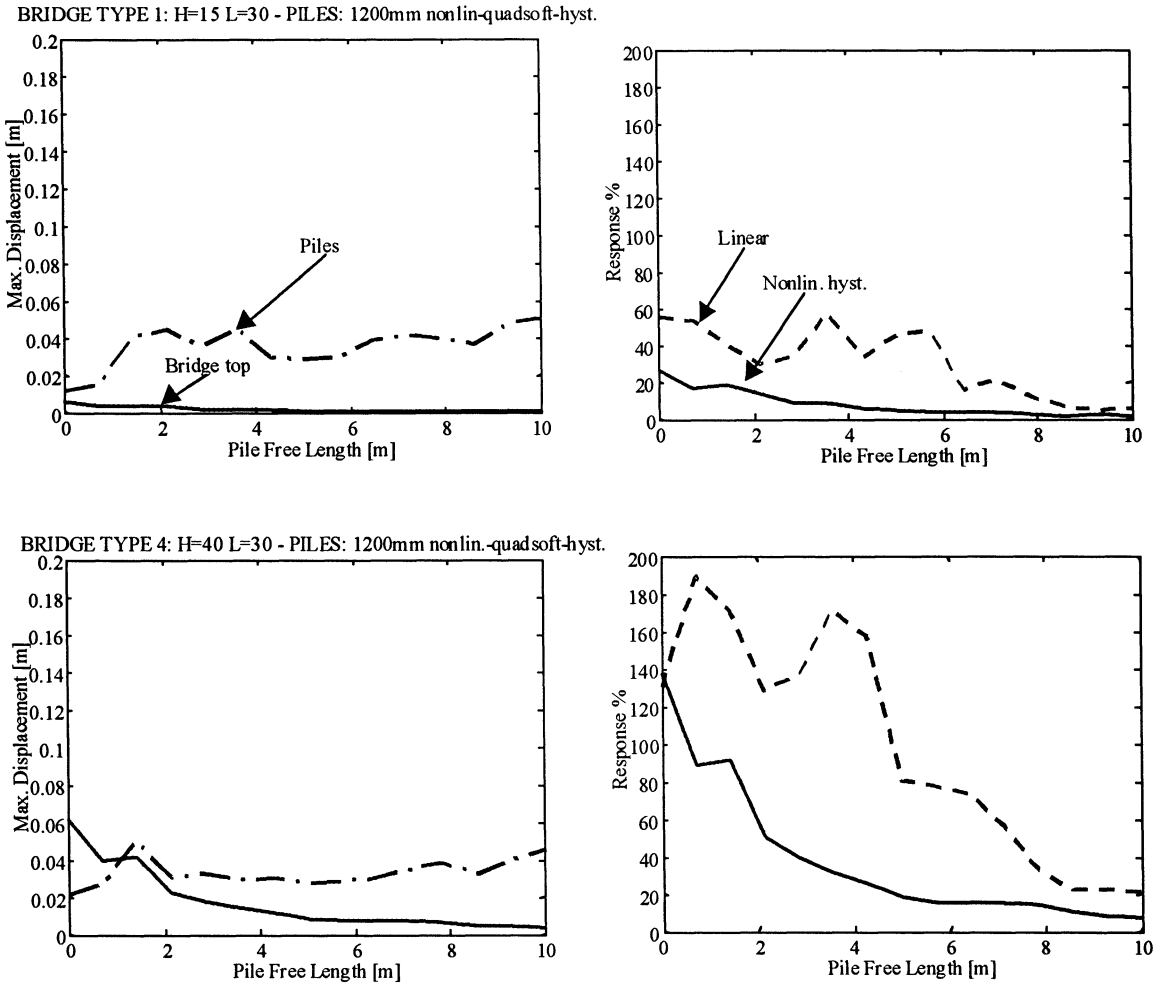


Figure 17. Relative displacements of the isolation system and the pier as a function of the free length of the (1200 mm) piles for type 1 and 4 bridges in the assumption of a hysteretic non linear isolation system.

Figure 18. Percent response of the pier (vs. the response with no isolation system) as a function of the free length of the (1200 mm) piles for type 1 and 4 bridges: comparison between linear and hysteretic isolation systems.

In general, we found a clear-cut and progressive improvement in isolation system performance. The non-linear behaviour can also be obtained artificially and it offers the advantage of mobilising system flexibility only in seismic loading conditions.

Conclusions

In this paper we have explored the possibility of applying seismic isolation to the base of girder bridges. The isolation device examined, which is obtained through the partial release of foundation piles from the surrounding soil, offers a number of intrinsic advantages: simplicity, the fact that bridges lend themselves well to the use of this type of isolation, the possibility of adjusting the degree of stiffness on the basis of design considerations, durability. Conversely, the main problem is the limited degree of isolation that can be achieved, first of all because the free lengths that can be realised are modest and secondly on account of pile displacement and load-effects.

On these types of structure, characterised by highly variable and often high periods, the degree of isolation parameter (α) is not sufficient to predict the effectiveness of the isolation system. In such conditions, in fact, a decisive role is taken on by the shape of the seismic spectrum. A parametric study of the seismic response of eight types of isolated bridges has led to the following observations:

1) When the seismic spectrum is concentrated on the low periods, the degree of isolation required is low enough to be able to apply the proposed isolation system to bridges characterised by low natural periods. In 15 m tall bridges (types 1-3), the optimal degree of isolation is achieved with free lengths of 4 to 8 m, not far, that is, from the values for which displacements and load-effects reach critical levels. This problem, however, can be partially overcome by fitting larger diameter piles. In the field of interest, in fact, this intervention has minor effects on the response and it proves advantageous in terms of displacements and load-effects. It should be noted, among other things, that excessive pile displacement values (0.05-0.08 m) are found to occur precisely for those values of free length which are most detrimental to pile strength (μ=0.45-0.5). We conclude that in bridges with short piers (~15 m), the advisability of pile isolation should be evaluated case by case and its use should be rated as particularly critical in the presence of seismic components with high periods and in highly deformable soils. Furthermore, the isolation system is especially vulnerable to irregular spectra, with peaks at the periods higher than 1 s.
2) 40 m tall bridges (types 4-6), with periods of ca 1 s, fall in a zone of the spectrum where, particularly in deformable soil, even a limited degree of isolation achieves a substantial attenuation of the response. In this case, displacement values are generally acceptable with respect to the height of the pier and moments are reduced, since we are working in lower amplification period zones. On such bridges, the efficiency of the isolation depends greatly on the seismic spectra adopted and the use of the proposed system may prove advantageous. Taller bridges (types 7-8) are in zones of the spectrum where the isolation becomes ineffective.
3) Of greater interest is the possibility of taking into account the elasto-plastic and hysteretic behaviour of the soil, as this may improve system efficiency and lead to a drastic reduction in displacements. The workings of the isolation system can be optimised through the use of special filler materials.

The investigation will be carried on to examine more closely the non-linear behaviour of this type of isolation and to explore the possibility of obtaining "ad hoc" damping effects by means of jackets filled with viscous fluids (mineral or silicone oils, etc.).

References

1. *Passive and Active Structural Vibration Control in Civil Engineering*, T.T. Soong and M.C. Costantinou eds., Springer-Verlag, 1994.
2. G.M. Calvi, A. Pavese, "Conceptual Design of Isolation Systems for Bridge Structures", *Proc. 2nd Italy-Japan Workshop on Seismic Design and Retrofit of Bridges*, pp. 351-374, Rome, February 27-28, 1997.
3. R. Lancellotta, "Geotecnica", Zanichelli, Bologna, 1993 (in Italian).
4. M.F. Randolph,"The Response of Flexible Piles to Lateral Loading", *Geotechnique*, vol. 31, n. 2, pp. 247-259, 1981.
5. H.G. Poulos, "Behaviour of Laterally Loaded Piles: I – Single Piles, and II – Pile Groups", JSMFD, ASCE, SM5, pp. 711-751, 1971.
6. D.J. Williams, "The Behaviour of Model Piles in Dense Sand", PhD thesis, University of Cambridge, 1979.
7. S. Foti, "Aspetti di Isolamento Sismico Connessi alla Tipologia delle Fondazioni", MSc. Thesis, Dipartimento di Ingegneria Strutturale, Politecnico di Torino, Italy, 1996 (in Italian).
8. Eurocode 8 "Design Provisions for Earthquake Resistance of Structures", ENV 1998-1, CEN, Brussels, 1994.
9. J.M. Kelly,"Base Isolation: Linear Theory and Design", *Earthquake Spectra,* Vol.6, pp. 223-244, 1990.
10. B. De Nicolo, M. Mezzina, Z. Odoni, "Analisi delle Prestazioni dei Dispositivi Viscoelastici di Isolamento alla Base", *Ingegneria Sismica,* Anno XIV- N. 1 – gennaio-aprile 1997 (in Italian).

SENSITIVITY OF RESPONSE OF ISOLATED BRIDGES TO MODELING AND DESIGN PARAMETERS - A CASE STUDY

by

Andrei M. Reinhorn[1], Vassil K. Simeonov[2], Grant DeRue[2], Michael C. Constantinou[1]

ABSTRACT

The concept of base isolations in bridges implies that structural components should experience limited inelastic behavior associated only with minor damage. Most isolation systems are designed to eliminate altogether inelastic behavior. The estimation uncertainties during the design process of the future ground motions, associated with the uncertainties involved in the constructed practice, leave the possibility that the entire system will experience inelastic behavior with permanent deformations and damage.

The fundamental objective of providing pertinent protection against undesired failure modes of base isolated bridges relies on estimates of the piers properties, such as flexure or shear capacities, or estimates of foundation deformation limits. It relies also on good knowledge of isolation properties. Design choices based on nominal material properties may miss the physical features of the structure, rendering the isolation system inefficient in preventing large ductility demands on the substructure. One of the objectives of this paper is to examine the effect of variation of the ratio of isolator and pier yield characteristics on the response of isolated bridges. It has been recognized that, due to low redundancy and domination of the deck mode of vibration, isolated bridges are extremely sensitive to the characteristics of the ground motion (Calvi and Pinto, 1996). After yielding, the stiffness properties and the periods of the deck-bridge system may be entirely dominated by the secondary stiffness of the isolators because of the larger mismatch with the support stiffness. This study investigates the sensitivity of bridge' response to small variations of the post-yield stiffness of the isolation system. Since most of the mass of the bridge is contributed by the deck, analytical models for design tend to diminish the attention to the masses of the piers and to the vibration modes they induce. However, in deck isolated bridges the local modes of tall massive columns may contribute substantially to the drift demand of the respective isolator-pier systems. This paper also studies the response implications of neglecting the column mass in modeling of bridges.

[1] Professor, Department of Civil Structural and Environmental Engineering, University at Buffalo, USA
[2] Graduate Research Assistant, Department of Civil Structural and Environmental Engineering, University at Buffalo, USA

INTRODUCTION

The concept of base isolations in bridges implies that structural components should experience limited inelastic behavior associated only with minor damage. Most isolation systems are designed to eliminate altogether inelastic behavior. The uncertainties in estimating during the design process the ground motions in future earthquakes, associated with uncertainties involved in the constructed practice, leave the possibility that the entire system will experience inelastic behavior with permanent deformations and damage. Moreover, the design of the isolation system of an existing bridge is a more challenging task. This is because the structural properties of the bridge piers, decks and abutments cannot be precisely determined due to lack of materials' information as influenced by past loading history. Nonlinear seismic analysis of base isolated bridges becomes a necessity. The development of new analytical tools, such as IDARC-BRIDGE (Simeonov at al, 1998), allows for more accurate evaluation of the expected response while the estimate of parameters is uncertain and the structure is expected to undergo damage.

The fundamental objectives of an isolation system can be summarized as to:
(i) localize the damage in the isolators to protect the underlying piers/abutments and their foundations and, consequently, permit reparability after a seismic event,
(ii) reduce the shear forces transmitted into the supporting elements to avoid undesired failure modes,
(iii) regulate the global response so that the deck-translation mode induces similar forces in each isolator-pier-foundation-soil system and, therefore, remove possible concentrations of ductility demand in stiff supports,
(iv) increase the energy dissipation capacity by use of high damping isolation systems.
These goals may be pursued individually or concurrently.

The fundamental assumption is that all isolator-pier-foundation-soil systems resist the maximum accepted (rigid) displacement of the deck with identical forces. Furthermore, capacity design principles usually require that no (or little due to the spread yield most RC columns exhibit) ductility is demanded from the substructures during the design earthquake. It is recommended that the actual strength of an isolation-damping bearing (I/D) device at the maximum displacement does not exceed certain percentage of the strength of the corresponding column (Priestley et al, 1996). While this approach can be easily integrated in the design procedure for new bridges, in case of retrofit of existing bridges, where the pier strengths and stiffness are predetermined, it may be difficult to achieve the desired. The reason is that the non-isolated bridge design, a *status quo*, has already attributed larger strengths to the shorter columns and vice versa – a mirror image of the expected outcome of the design of an isolated bridge. A possible solution of this problem is to provide identical I/D devices at all supports (except possibly the abutments) tailored to the strength of the weakest pier. The design of the isolation system of the bridge model, studied herein, uses such reasoning.

This study explores the influence of several parameters of the structure-isolation system, which may influence crucially the overall response. The main issues in the paper are:
(1) Sensitivity of Response of Isolated Bridges to the Relative Magnitude of the Yield Strengths of the I/D Devices and the Bridge Piers. The objective of capacity design is to avoid undesired failure modes or protect certain components (such as the piers) by concentrating damage in preferred locations – in isolated bridges invariably in the isolators. However, depending on the

analysis procedure employed, predictions of the actual yield level of the piers (in flexure or shear) may fluctuate widely from method to method especially for columns with multiple reinforcement layers and unknown loading history. The relative magnitude of the yield strengths of the elements of the pier-isolator system and, especially, the post-yield stiffness of the I/D devices control the response of the bridge. The isolator drift and pier ductility demands imposed by an actual strong motion are used to assess the sensitivity of response to variation of these parameters.

(2) Sensitivity of Response of Isolated Bridges to Common Modeling Assumptions. Inserting the isolation system below the deck at the top of the piers changes the global structural scheme. The piers respond as structures restrained by the foundation at base level and by the isolators at the top. The common assumption of neglecting in analysis the own mass of the columns may result in distorted simulation of behavior of irregular bridges. The dynamics of the deck and the piers may lead to out of phase response with large deformations.

To illustrate the sensitivity issues a case study was selected and parametric studies were performed using a newly developed computer platform for nonlinear analysis of bridges using extremely large ground motion, yet realistic, which produced substantial inelastic response.

NONLINEAR ANALYSIS PLATFORM FOR BRIDGE EVALUATION

A computational platform for *three-dimensional nonlinear* analysis and damage assessment of bridges IDARC-BRIDGE (Simeonov et al, 1998) was developed and used to conduct this study. The program models bridge structures using macromodels of structural components, i.e. piers, decks, abutments, bearings, etc, which may experience inelastic hysteretic behavior. The platform employs a number of advanced programming and numerical techniques, which rarely coexist in research or, even, commercial packages. The internal data handling combines the advantages of sparse matrix storage format with dynamic memory allocation. The set of algebraic equations, resulting from the numerical integration of the system of linearized differential equations of dynamic equilibrium, is solved iteratively by the method of gradients in combination with the conjugate directions convergence technique and Jacobi preconditioning algorithm. The program offers several analysis types, applicable to both performance evaluation and design situations:

(i) time-history analysis with ground acceleration input,
(ii) time-history analysis for uniform or spatially variable ground displacements,
(iii) time-history analysis for nodal force excitation,
(iv) quasi-static analysis using incremental displacements as input,
(v) quasi-static analysis for incremental forces,
(vi) monotonic pushover (collapse mode) analysis with lateral load pattern governed by the distribution of mass,
(vii) monotonic adaptive pushover analysis in which the distribution of lateral forces acting on the structure is adjusted with the instantaneous mode shapes,
(viii) dynamic pushover analysis for a linearly increasing ("ramped") acceleration input, and
(ix) eigenvalue analysis.

Nonlinear inelastic or linear elastic analysis is performed depending on the properties of the elements used for constructing the structural model. The damage of all components exhibiting hysteretic behavior is monitored through cumulative indexing.

The program offers an exhaustive element library for modeling the stiffness and damping properties of commonly encountered constituents of bridge structures. Five of the eight elements, currently available have the capability to represent nonlinear behavior: "inelastic 3d beam", "isolator hysteretic", "isolator slider", "bilinear gap", "pile group". As suggested by an element name, its force-displacement rule reflects the distinctive features of the respective component of a typical bridge assembly: deck, piers, isolation system, expansion joints and foundations. All elements are macro-model based and, with the exception of the "bilinear gap", utilize smooth hysteretic laws. However inexact, due to the assumption of existence of unique envelope of a given load-deformation relationship, these models are computationally efficient in terms of resource demands. The utility of this approach is supplemented by the versatility of the smooth hysteretic rule in simulating a wide range of possible behaviors occurring by virtue of strength deterioration, stiffness degradation, hardening and pinching phenomena. Furthermore, a limited number of user-supplied parameters are required to fully define the underlying capacity curve. The list of remaining elements includes the basic tools of three-dimensional linear structural analysis: beam-columns, springs and dampers.

CASE STUDY

The bridge selected in this study is representative of multi-span highway bridges with continuous superstructure – a prestressed concrete hollow-box girder with four 50-meter spans supported on three hollow-core piers and two abutments (see Fig. 1). Seven 1:2.5-scaled models of this prototype have been tested with PSD techniques at the ELSA-JRC laboratory in Ispra, Italy. Details of reinforcement design, material properties and test results can be found elsewhere (Pinto, 1996). The model used in this study has isolators over the abutments and all piers, as one of the isolation solutions for the irregular bridge tested in the ELSA study (Pinto, 1996). The deck is assumed free to move longitudinally and transversely at all supports, restrained only by the isolators. Free rotations are allowed at the deck-support interface in the horizontal, longitudinal vertical and transverse vertical planes. At the abutments, the rotations in the intersecting plane are fixed to neutralize the effect of assuming single, rather than multiple, point of contact of the superstructure and the isolation system. All bridge columns are fixed at ground level; i.e. the foundation flexibility is ignored.

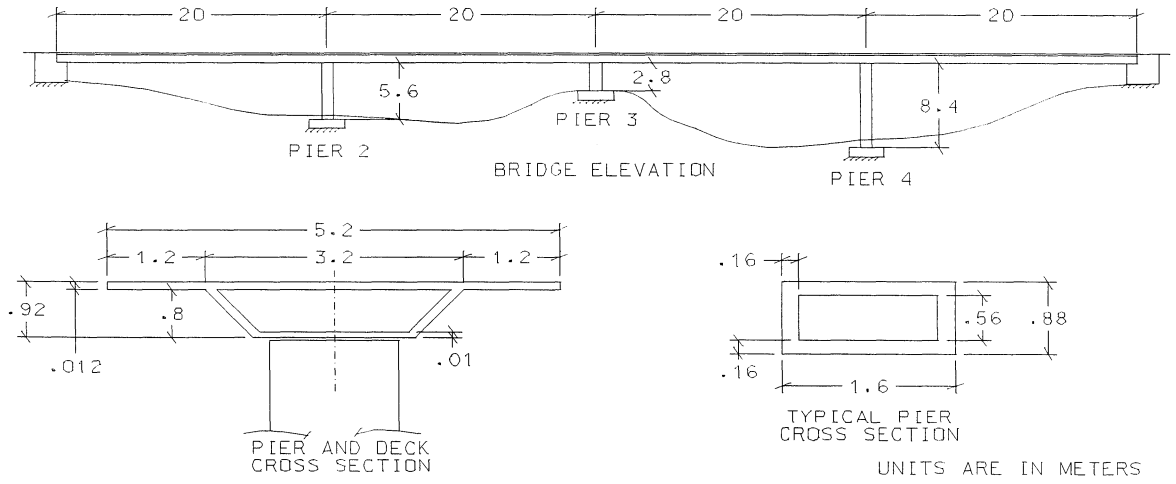


Figure 1 - Bridge Model Geometry, Deck and Pier Cross Sections

Component Modeling in Case Study:

Bridge Piers and Deck: Each column (pier) is modeled with a single 3D inelastic beam-column element (see Fig. 3). A spread-plasticity model is used to infer the distribution of flexibility along the element from the moment-curvature of the two end sections, as defined by a smooth hysteretic rule (Simeonov et al, 1998). The backbone curve of piers inelastic properties is generated by monotonic curvature-controlled loading of a fiber model of the cross section under constant axial load (Collins and Mitchell, 1991) – see Fig. 2 and Table 1.

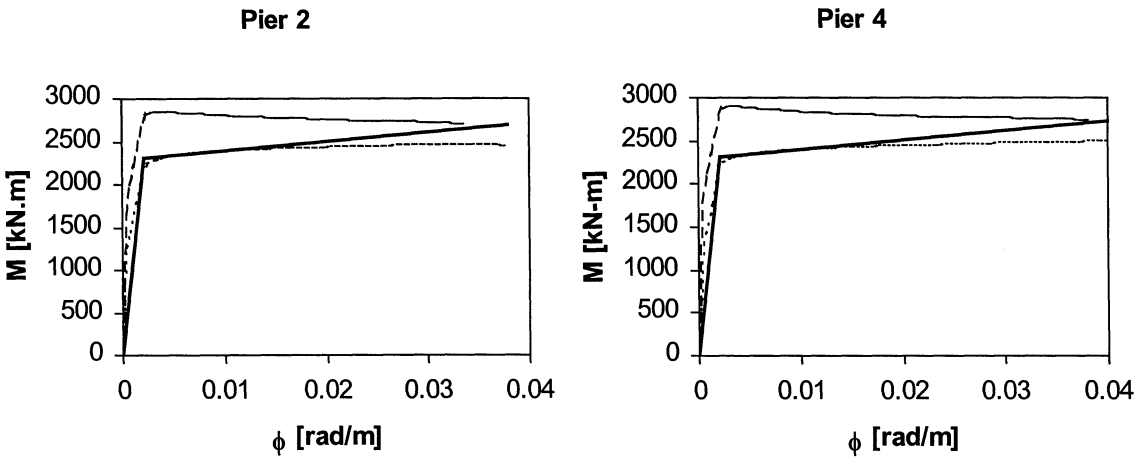


Figure 2 - Moment-Curvature Relations at the Bases of Piers 2 and 4 (notation in Fig.1)

The elastic stiffness of the element is derived from the secant slope through the point of first yield of a reinforcing layer. The bridge deck is divided into 32 segments of equal length and modeled by linear elastic beam-column elements, the stiffness properties of which are based on the uncracked cross section – see Fig. 3 and Table 2. The contribution of shear to element flexibility is included through the appropriate shear area. The mass of the deck and piers is lumped in the nodes of the *finite-element mesh. In some analysis cases, the pier masses are omitted to quantify the effect.*

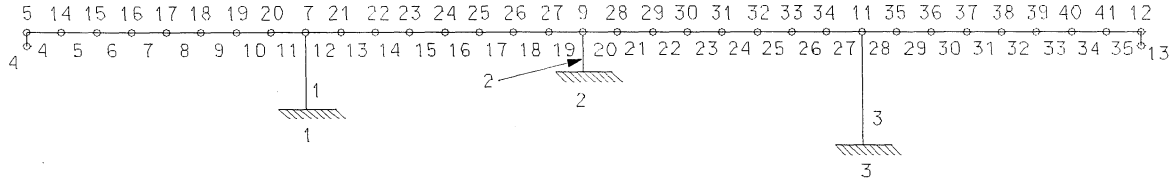


Figure 3 - Computer Model: Nodes and Elements

Seismic Isolators: The isolators at all bridge supports are identical I/D devices composed of distinct parts for carrying vertical load (sliding bearings with negligible friction) and complementary energy dissipation (a metal rod system operating in flexural bending). A bilinear hardening force-displacement curve is assumed to provide sufficiently accurate representation of the behavior of the I/D system devices. The yield strength and post-yield stiffness of the isolation system are varied to simulate the uncertain properties estimation, whereas, the initial stiffness is kept invariant.

Table 1 - Pier Strength (Yield) and Stiffness Properties

Pier	M_y	ϕ_y	$K_{o,col}$	$K_{o,iso}$	$K_{o,col}/K_{o,iso}$
	[kN.m]	[rad/m]	[kN/m]	[kN/m]	-
P2	2307	0.0021	18064	30500	0.59
P3	3506	0.0025	169641	30500	5.56
P4	2312	0.0021	5512	30500	0.18

Table 2 - Uncracked Properties of Bridge Components

Component	A	I_{xx}	I_{yy}	I_{zz}	w
	[m^2]	[m^4]	[m^4]	[m^4]	[kN/m]
Pier	0.666	-	0.189	0.017	40.760
Deck	1.101	0.325	2.333	0.135	67.470

Ground Motion

The ground motion, used to represent the extreme earthquake in numerical simulations reported herein, was recorded during the 1994 Northridge event. The accelerogram belongs to the suite of near-fault recordings scaled to match the target spectra for Los Angeles in the FEMA/SAC Project (Somerville et al, 1997). The probability of occurrence of the modified motion is 2% in 50 years.

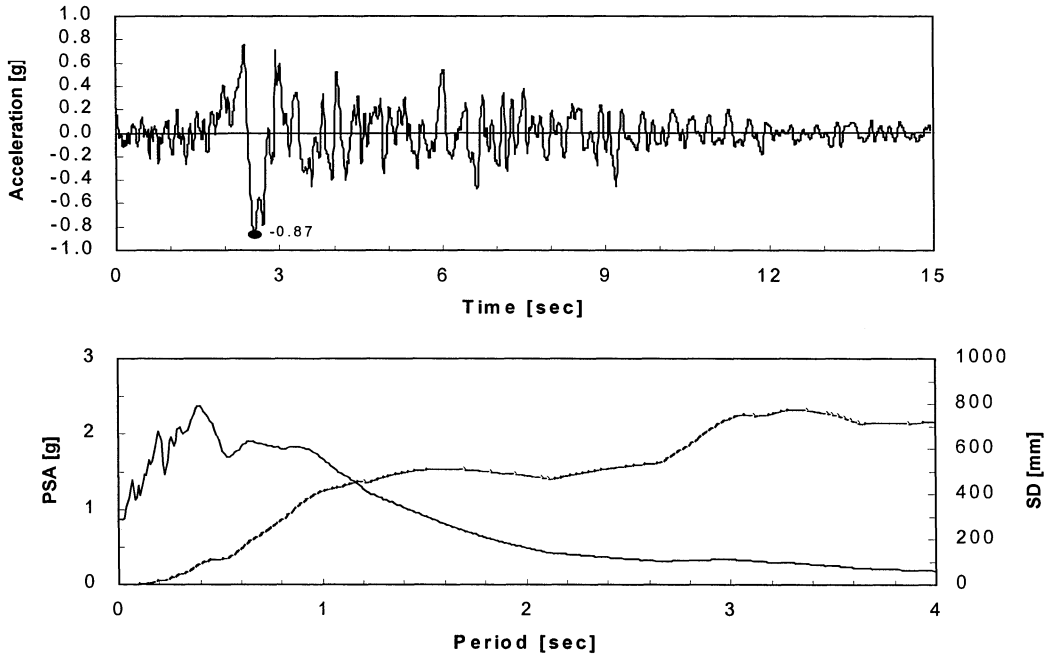


Figure 4 - Ground Motion Time History and Elastic Spectra

RESULTS OF CASE STUDY

Response Sensitivity to Yield Characteristics of I/D Devices and Bridge Columns

The study investigates the sensitivity of the relative magnitude of the yield strengths of the I/D devices and the piers, which affect the damage pattern in case of expected severe excitation of 2% probability of occurrence in 50 years. The estimates of the yield characteristics of existing columns are less precise than for the isolators. For the most part, the uncertainties in such estimates are related to prior deterioration of properties. Strength deterioration has been shown to occur in R/C columns subjected to cyclic loading even at moderate ductility demands. Furthermore, tension stiffening, which may account for as much as 20% of the flexural yield capacity, by virtue of increasing the strength of the reinforcing steel in the tension zone of the cross section, reflects the condition of material bond - a consequence of cyclic, as well as, environmental effects itself. It is realistic, therefore, to anticipate some deviation from the isolator-pier strength ratio, which is intended to serve as a protection factor against damage of columns. Moreover, strain hardening in the isolation system must be taken into account when calculating the forces transferred through the I/D devices and into the underlying supports at expected displacements. In view of the objective to concentrate most of the energy dissipation in the isolation system, the secondary stiffness of the isolators is probably their most-important property, since it controls entirely the fundamental period of the deck-bridge system after yield. This is especially true in design of seismic retrofit, where placing identical devices at all supports might be the only option to control the uniform response of the bridge.

First, the analysis of the bridge with rigid connections of the deck and the piers indicates a large demand for ductility in shortest pier, P3, which will induce the failure of the bridge. The displacement demands in the piers (P2, P3, P4) for the tested motion is 73mm, 94mm, 93mm, which represent ductility demands of 3.2, 12.6 (!), and 1.9.

The bridge with the isolators was then analyzed. The yield level of the isolators was set to a fraction of the yield shear force F_y of the weakest pier, P4. Four different values of isolator post-yield stiffness were used: 0.5%, 1.0%, 2.0% and 5.0% of the initial stiffness. The isolator-pier strength ratio causing first yielding in the bridge piers (pier P4, the weakest) was established by gradually increasing the strength of the isolators, while keeping the original yield levels of columns constant. The strength ratio, at which second yielding occur (at the other exterior column, P2), was then obtained in a similar manner.

Based on the numerical analyses the ductility demands in the piers were plotted in Fig. 5 and the displacement demands in the isolators shown in Fig. 6. Several remarks can be pointed out:

(1) The first and second yields in the bridge occur predictably in the taller piers, P4 and P2, respectively. Both have similar cross section strength and flexural rigidity, but different heights.

(2) The higher the strength of the isolators (i.e. their yield level) the larger the ductility demand in the yielding piers. The increase is not proportional and occurs more severely immediately after the initial yield. However, the maximum ductility demands are dramatically smaller than in the unisolated bridge.

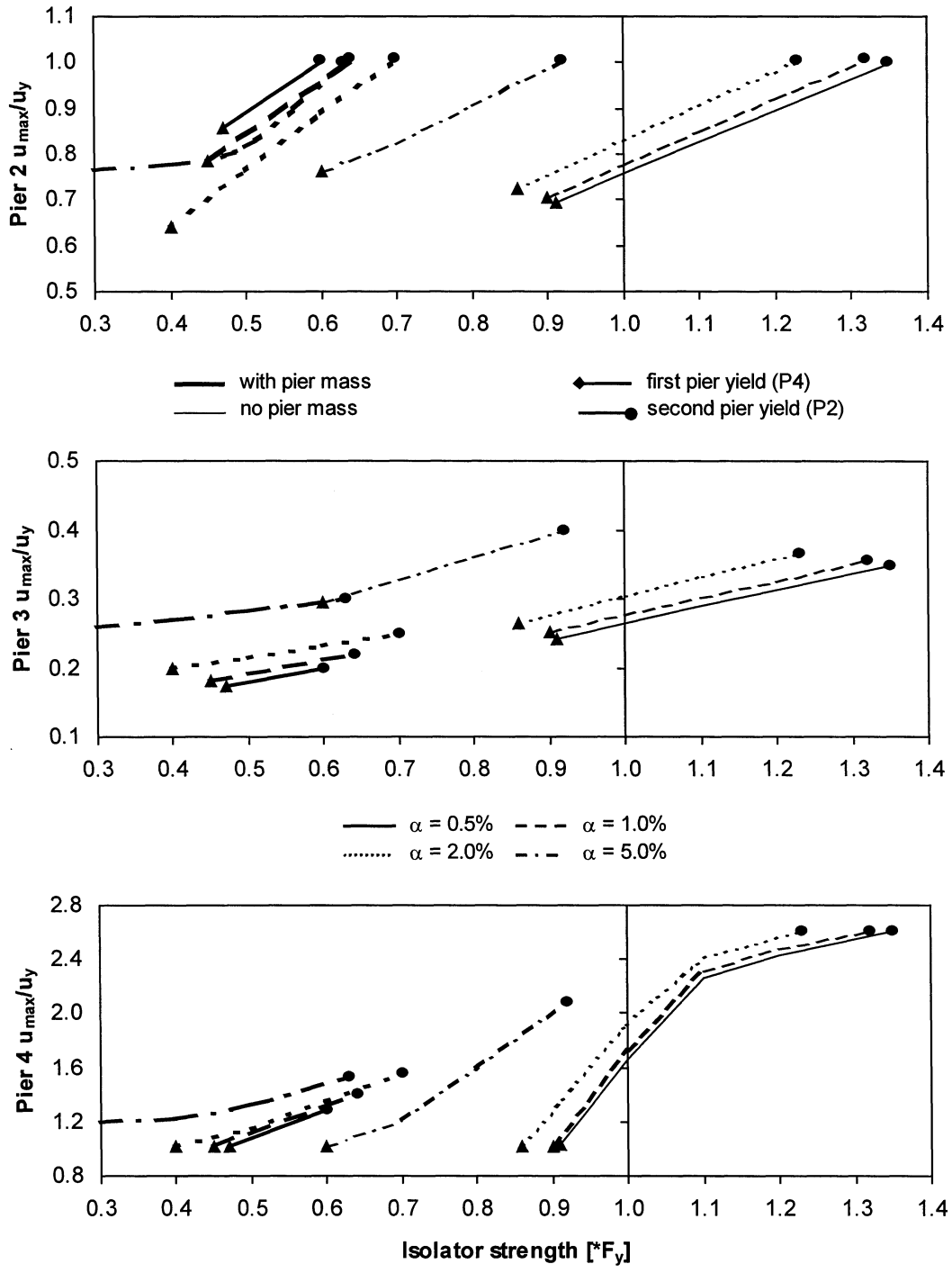


Figure 5 – Sensitivity of Pier Drift to the Properties of Isolators vs. Properties of Piers

(3) At lower yield strength of the isolators system, yielding of columns may be entirely prevented. However, in some cases extremely low yield level is required to achieve such protection (see Fig. 5). This requires large displacements in the isolators, 80 to 200 mm. Some of the isolators may not have such capability.
(4) For large isolators strength, more piers yield, while the ductility demands increase in the yielded piers beyond the amount in the unisolated bridge (2.4-2.5 vs. 1.9 in P4).
(5) In presence of post-yield hardening in the isolation system, the yielding of the columns may occur for weak isolators also. A variation from 1% to 5% hardening may lead to yielding of multiple piers (P4, P2) and large ductility demands for isolators were the response would have been only elastic otherwise.

Response Sensitivity to Modeling Pier Mass

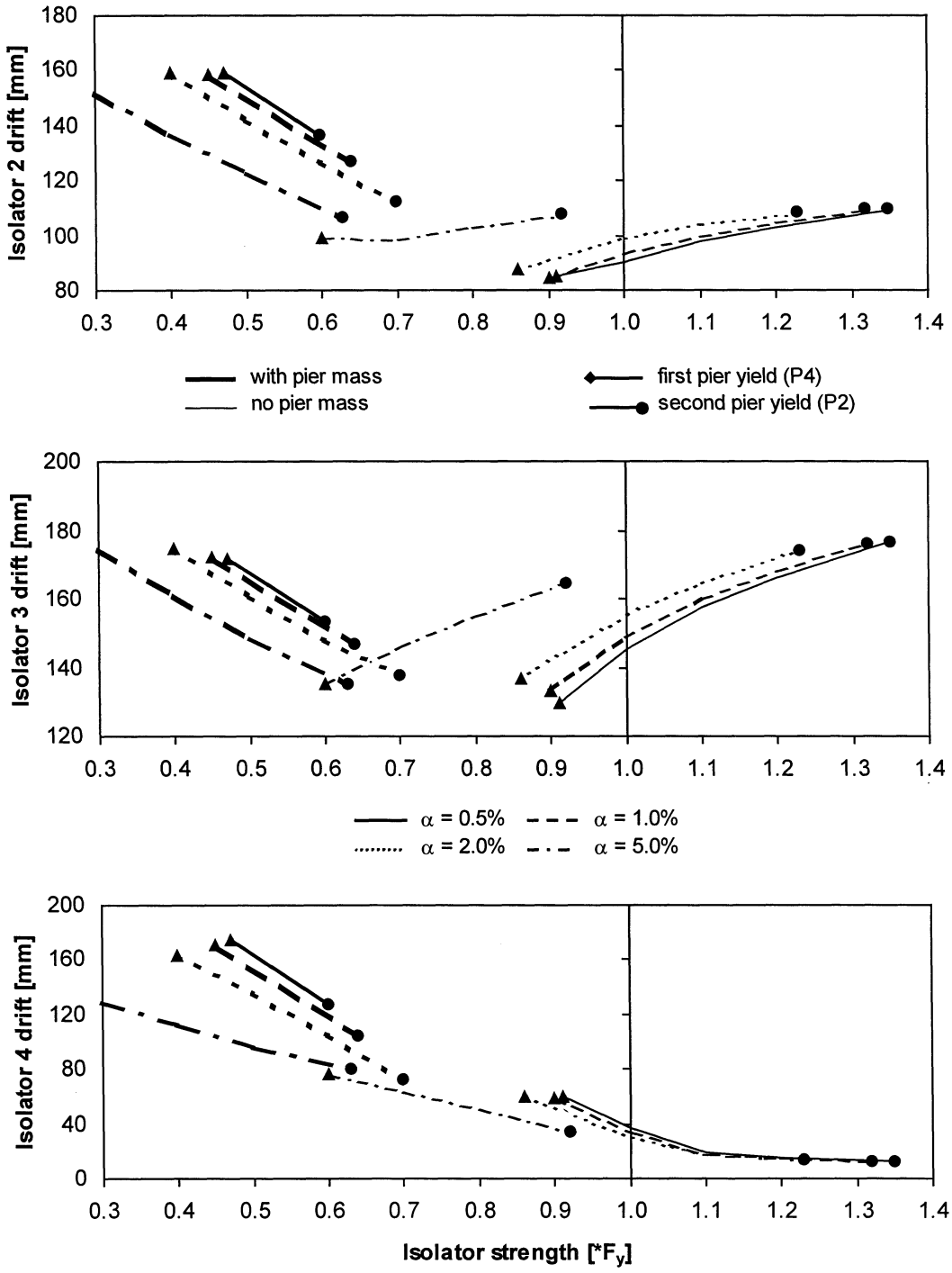
One of the consequences of placing the isolation at deck level is the independent response of each pier-isolator system with little or no coupling effect of the deck. Under these circumstances, local dynamics may have an important contribution to the response of the substructure, especially in cases where the isolation system has low stiffness. The task of quantifying the effect of the local modes of vibration is accomplished by comparing response of models with the pier masses considered and neglected. The isolator-pier strength ratio causing yielding of the tallest column was used as a basis for comparison – a premise similar to that of the previously conducted study. If the pier masses are taken into account, then the first yield of pier P4 occurs at much lower isolator-pier strength ratios - 47%, 45%, 40% and 15%, compared the pier-mass-excluded analyses - 91%, 90%, 86% and 60%, respectively, for the four different post-yield stiffness coefficients. The maximum drift demand on the isolators at the flexible piers is almost twice higher in the case when the mass is considered. It can be speculated that the inertia forces in the piers may produce out of phase motion with the deck, which results in larger demands in the isolators. The results were unexpected in view of the common practice of lumping the masses in the bridge deck.

CONCLUSIONS

The case study demonstrates the utility of nonlinear dynamic analysis in investigating aspects of structural behavior, which are difficult to capture by static or linear procedures. The fundamental results of isolation - increased energy dissipation and change of support stiffness, may still be modeled by simplified methods in the preliminary design phase. However, the consequences of isolator (and possibly pier) yield in conjunction with the harmonic content of the ground motion and the hysteretic damping can be quantified only through inelastic time-history analysis. Several observations can be summarized:

(1) Yielding of piers, in a bridge with multiple elements having various strength, may occur even when the isolators have yielding strength lower than the weakest pier.
(2) Severity of (a) yielding of piers and (b) the post-yielding behavior of the entire bridge is dependent on the post yielding characteristics of isolator system.
(3) Although low yield isolators provide a better protection for the piers, the displacement demand for the isolators may be prohibitive.

Fig


Isolator 2 drift [mm]
180
160
140
120
100
80
0.3 0.4 0.5 0.6 0.7 0.8 0.9 1.0 1.1 1.2 1.3 1.4
with pier mass
no pier mass
first pier yield (P4)
second pier yield (P2)
Isolator 3 drift [mm]
200
180
160
140
120
α = 0.5%
α = 1.0%
α = 2.0%
α = 5.0%
Isolator 4 drift [mm]
200
160
120
80
40
0
Isolator strength [*Fy]

(4) A bridge with multiple piers but identical properties and with identical isolators behaves like a single pier bridge. However, bridges with multiple piers with different properties, have a behavior, which is difficult to predict by simplified models.
(5) A small variation of the post-yielding stiffness of the isolation system produces a substantial change in the yielding pattern and expected failure modes of the bridge.
(6) The contribution of the local modes of vibration of massive flexible piers to the drift demand of the respective columns may be quite substantial in bridges with isolation inserted at deck level, effect particularly pronounced in cases of low stiffness of the I/D devices. Due to phase mismatch of deformations at the top and bottom of isolator, the drift demand may become excessive. The results of preliminary design techniques, using the tributary mass of the superstructure but excluding the column mass must be verified by time history analysis.

AKNOWLEDGEMENTS

This study was made possible by a project of National Center for Earthquake Engineering Research (NCEER) sponsored by the Federal Highway Administration (FHWA). Task Number 106-E.7.2.3. the support is greatly acknowledged.

REFERENCES

1. Calvi, M. G. and Pinto, P. E., editors, (1996), "Experimental and Numerical Investigations on the Seismic Response of Bridges and Recommendations for Code Provisions", LNEC-Laboratorio Nacional de Engenharia Civil, Lisbon, Portugal.
2. Collins, M. P. and Mitchell, D., (1991), "Prestressed Concrete Structures", Prentice Hall, Englewood Cliffs, NY, pp. 707-746.
3. Pinto, P. E., editor, (1996), "Pseudodynamic and Shaking Table Tests on R.C. Bridges", LNEC-Laboratorio Nacional de Engenharia Civil, Lisbon, Portugal.
4. Priestley, M. J. N., Seible, F., and Calvi, G. M., (1996), "Seismic Design and Retrofit of Bridges", 1996, John Wiley & Sons, Inc, pp. 457-533.
5. Simeonov, V. K., Reichman, Y., Mylonakis, G., and Reinhorn, A. M. (1998), "IDARC-Bridge - A Computational Platform for Seismic Damage Assessment of Bridge Structures", Report No. NCEER-98-XXXX, National Center for Earthquake Engineering Research, State University of New York at Buffalo (in print).
6. Somerville, P., Smith, N., Punyamurthula, S., and Sun, J., (1997), "Development of Ground Motion Time Histories for Phase 2 of the FEMA/SAC Steel Project", Report No. SAC/BD-97/04, SAC Joint Venture.

Effects of Multi-Support Excitation on Isolated Bridges

Giorgio Monti and Paolo E. Pinto

Dipartimento di Ingegneria Strutturale e Geotecnica,
Università La Sapienza di Roma, Italy

Abstract

Multi-support seismic excitation can affect the response of isolated bridges, and particularly the performance of the isolating devices, which are generally designed for synchronous action. Three phenomena are of major interest for bridge structures, denoted as: a) incoherence, b) wave-passage, c) site-response, of which the former two, grouped under the term 'nonsynchronism', have been object of an extensive parametric study in the past. Here, the third phenomenon is addressed, which is due to spatially varying local soil profiles, and its effects on the bridge response are evaluated. The technique adopted is that of a random vibration analysis of linear systems, equivalent to the examined bridges equipped with hysteretic-type isolating devices, whose response is represented through linear elements of equivalent stiffness and damping.

Introduction

Recently recorded soil time histories obtained from strong motion arrays installed in seismic areas have clearly demonstrated that the motion of relatively close points on the soil surface is not synchronous, that is, even relatively close points can experience significant relative displacements. This phenomenon is due both to reflection and refraction of seismic waves

through underlying soil layers with different mechanical characteristics and to the presence of soils of different nature under different support points.

From the point of view of structural analysis, the most important implication of this observed behavior is that the conventionally adopted assumption of equal seismic input under all the supports of a structure is a pure abstraction, acceptable only when dealing with conventional buildings of moderate dimensions, and it is even farther from reality if extended-in-plan structures are to be studied. In some cases, such as long-span isolated bridges like those examined in this paper, due consideration should be given to the non-synchronism of the seismic action, since different input motions experienced at adjacent supports can significantly modify the overall structural response thus jeopardizing the design concept.

This manifest lack of knowledge on the subject is reflected in modern seismic codes for bridge design, where the non-synchronous nature of seismic input is accounted for only by means of semi-empirical provisions for extra seating lengths, adequate gaps in the joints, minimum imposed relative displacements between adjacent foundations, etc.

Studies on the response of extended-in-plan structures subjected to different motions at the supports have started some thirty years ago (Bodganoff et al. 1965) and continue until today. Many of these studies focus on the algorithm to obtain the response (for ex., Perotti 1990), while others (for ex., Der Kiureghian and Neuenhofer 1992, Heredia-Zavoni and Vanmarcke 1994) are more design-oriented. Few studies (Moerland et al. 1993, Monti et al. 1995, 1996) deal with the inelastic behavior.

This is surprising, because if it is true that present design practice is based on a linear analysis, where the protection offered by the non-linear behavior of the isolators is globally accounted for by means of a simple factor, there is no evidence that this approach may extend its validity to non-synchronous situations, or at least not with the same protection factors.

The purpose of the present study is to make a further step into this question: the relevance of non-rigid input motion on the inelastic response of isolated bridge structures, and the extent of validity of the "protection factor" approach.

It consists in a parametric analysis of a bridge with 6 spans, of 50 m length each and piers 10 m tall, whose isolators are designed according to common design practice. The bridge is subsequently analyzed under different multi-support excitation conditions. The method employed is that of a stationary random vibration analysis where the non-linear isolators are linearized with Kelvin elements, having effective stiffness and equivalent damping determined through an equivalence equation. To this purpose, the accuracy of three different equations is evaluated.

The soil motion is represented through a second moment random field fully characterized by (equal or different) power spectral densities at each station and by a coherence spectrum, assumed to depend on three different sources of incoherence. All the parameters controlling the loss of coherence have been made to vary between their respective extremes.

Fully incoherent ground motion

From a physical point of view, the spatial variation of seismic ground motion may be schematically thought of as the result of the combination of three different phenomena: a) the *incoherence* effect, resulting from reflections and refractions of waves through the soil during their propagation (this effect is also referred to as *geometric incoherence*), b) the so-called *wave-passage* effect, that is the difference in the arrival times of seismic waves at different stations, and c) the *site response* effect, due to differences in local soil conditions under the various stations.

Within the stochastic model assumed here, spatial variability is described by means of the cross-PSD matrix of the ground acceleration as follows

$$\mathbf{S}_{\ddot{U}\ddot{U}}(d,\omega) = \Gamma(d,\omega) \times \mathbf{S}_{AA}(\omega) \tag{1}$$

where the symbol $\times$ denotes the Hadamard product by which each element of $\Gamma(d,\omega)$ is multiplied by the corresponding element of $\mathbf{S}_{AA}(\omega)$, ω = circular frequency, and $\mathbf{S}_{AA}(\omega)$ is the (full) matrix of the ground acceleration cross-PSD functions at the N locations, given as

$$\mathbf{S}_{AA}(\omega) = S_{A_j A_l}(\omega) = \sqrt{S_{A_j A_j}(\omega) S_{A_l A_l}(\omega)} \qquad j,l = 1 \ldots N \tag{2}$$

and $\Gamma(d,\omega)$ is the (full) matrix of the complex coherency functions accounting for the three effects of incoherence, wave passage (Luco and Wong 1986) and site response (Der Kiureghian and Neuenhofer 1996)

$$\begin{aligned} \Gamma(d,\omega) = \gamma_{jl}(d,\omega) &= \gamma_{jl}(d,\omega)^{\text{incoherence}} \cdot \gamma_{jl}\left(d^L,\omega\right)^{\text{wave passage}} \cdot \gamma_{jl}(\omega)^{\text{site response}} \\ &= \exp\left[-\left(\frac{\alpha\,\omega\,d_{jl}}{v_s}\right)^2\right] \cdot \exp\left[-i\frac{\omega\,d_{jl}^L}{v_{app}}\right] \cdot \exp\left\{i\theta_{jl}(\omega)\right\} \qquad j,l = 1 \ldots N \end{aligned} \tag{3}$$

The *incoherence* term decays exponentially with the circular frequency ω, with the horizontal separation distance d_{jl} between two stations j and l and, through the shear waves

velocity v_s, with the inverse of the mechanical characteristics of the soil. The second term depends on the projected horizontal distance d_{jl}^{L} along the wave propagation direction and on the wave circular frequency ω, and is a measure of the *wave-passage* delay due to the surface apparent velocity of waves v_{app}. The *site response* term is represented through a phase shift independent of the distance

$$\theta_{jl}(\omega) = \tan^{-1} \frac{\mathrm{Im}\left[H_j(\omega) H_l(-\omega)\right]}{\mathrm{Re}\left[H_j(\omega) H_l(-\omega)\right]} \tag{4}$$

and dependent on the frequency-response functions of the soil columns at the different stations

$$H_j(\omega) = \frac{\omega_j^2 + 2i\zeta_j \omega_j \omega}{\omega_j^2 - \omega^2 + 2i\zeta_j \omega_j \omega} \qquad j = 1 \ldots N \tag{5}$$

which represent the amplitude of a harmonic motion at the surface of the ground caused by a harmonic motion of the form $\exp(i\omega t)$ at the bedrock level. It is important to note that the phase shift is completely defined in terms of the two frequency-response functions, which only depend on the properties of the two soil columns. In particular, it does not depend on the distance between the two stations, or the power spectral densities of the bedrock motion. It should be emphasized that the site-response component of the coherency function does not account for the effect of incoherence resulting from scattering of waves within the two soil columns. This contribution is rather included in the incoherence term.

Apart from the site response effect, which depends on the locally selected PSD functions, in this study the coherency function is considered basically as a two-parameter function, having lumped the mechanical characteristic of the soil and the factor α into a single parameter expressed as the ratio v_s/α, and the second one being v_{app}. When $v_s/\alpha \to \infty$, the first term tends to 1 and the incoherence effect results from wave travelling and site effect only; if $v_{app} \to \infty$, the second term tends to 1 and the incoherence is due to the incoherence and the site effect only. Note that in this formulation the geometric incoherence effect is given a higher weight (square power) with respect to the wave-passage effect.

In the soil frequency-response functions $H_j(\omega)$ in (5) the parameters depend on the soil type (F=firm, M=medium, S=soft) as follows (Der Kiureghian and Neuenhofer 1996):

$$\begin{aligned} &\omega_j(\mathrm{F}) = 6\pi \text{ rad/sec}, \zeta_j(\mathrm{F}) = 0.6 \\ &\omega_j(\mathrm{M}) = 3\pi \text{ rad/sec}, \zeta_j(\mathrm{M}) = 0.4 \\ &\omega_j(\mathrm{S}) = \pi \text{ rad/sec}, \zeta_j(\mathrm{S}) = 0.2 \end{aligned} \tag{6}$$

The PSD function adopted in this work is the well-known modified Kanai-Tajimi spectrum of ground accelerations (Clough and Penzien 1975), expressed as

$$S_{A_jA_j}(\omega) = S_{0_j}\, S_{CP_j}(\omega) = S_{0_j} \frac{\omega_{f_j}^4 + 4\zeta_{f_j}^2\, \omega_{f_j}^2\, \omega^2}{\left(\omega_{f_j}^2 - \omega^2\right)^2 + 4\zeta_{f_j}^2\, \omega_{f_j}^2\, \omega^2} \frac{\omega^4}{\left(\omega_{g_j}^2 - \omega^2\right)^2 + 4\zeta_{g_j}^2\, \omega_{g_j}^2\, \omega^2} \tag{7}$$

where S_{0_j} = scale factor, $S_{CP_j}(\omega)$ = normalized (two-sided) Clough-Penzien spectrum, ω_f and ζ_f may be thought of as characteristic ground frequency and damping, and ω_g and ζ_g are the parameters of an additional filter, introduced to assure finite power for the PSD. All these parameters depend on the location j.

Note that the PSD of the ground displacement process is:

$$S_{D_jD_j}(\omega) = S_{0_j}\, \omega^{-4}\, S_{CP_j}(\omega) = S_{0_j} \frac{\omega_{f_j}^4 + 4\zeta_{f_j}^2\, \omega_{f_j}^2\, \omega^2}{\left(\omega_{f_j}^2 - \omega^2\right)^2 + 4\zeta_{f_j}^2\, \omega_{f_j}^2\, \omega^2} \frac{1}{\left(\omega_{g_j}^2 - \omega^2\right)^2 + 4\zeta_{g_j}^2\, \omega_{g_j}^2\, \omega^2} \tag{8}$$

The scale factors S_{0_j} at all location can be found based on either the peak ground acceleration or the peak ground displacement (PGA and PGD, respectively, selected in this work as equal for all locations) according to the following relation:

$$S_{0j} = \frac{\mathrm{PGA}^2}{p_{A_j,0.5}^2 \cdot \mathrm{Var}_{A_j}^*} = \frac{\mathrm{PGD}^2}{p_{D_j,0.5}^2 \cdot \mathrm{Var}_{D_j}^*} \tag{9}$$

where $p_{A_j,0.5}$, $p_{D_j,0.5}$ = peak factors corresponding to a 50% probability of exceedance of the peak level (either PGA for the ground acceleration process or PGD for the ground displacement process) at location j.

For a generic process Y, the peak factor can be calculated according to (Vanmarcke 1977):

$$p_{Y,0.5} = \sqrt{2 \cdot \ln \frac{2.8 \cdot \Omega_Y \cdot t_s}{2\pi}} \tag{10}$$

where t_s = duration of the (stationary part of the) process and

$$\Omega_Y = \sqrt{\frac{\mathrm{E}\left[\dot{Y}^2\right]}{\mathrm{Var}[Y]}} \tag{11}$$

where $\mathrm{E}\left[\dot{Y}^2\right]$ = mean square of the derivative of the process and $\mathrm{Var}[Y]$ = variance (total power) of the process having PSD $S_{YY}(\omega)$:

$$\mathrm{E}\left[\dot{Y}^2\right] = \int_{-\infty}^{\infty} \omega^2 S_{YY}(\omega) d\omega \tag{12}$$

$$\mathrm{Var}[Y] = \int_{-\infty}^{\infty} S_{YY}(\omega) d\omega \tag{13}$$

Note that Ω_Y only depends on the shape of the PSD and not on the scale factor; thus, it can be written for the ground acceleration and the ground displacement processes, respectively, as:

$$\Omega_{A_j} = \sqrt{\frac{\mathrm{E}^*\left[\dot{A}_j^2\right]}{\mathrm{Var}^*\left[A_j\right]}} \qquad \text{and} \qquad \Omega_{D_j} = \sqrt{\frac{\mathrm{E}^*\left[\dot{D}_j^2\right]}{\mathrm{Var}^*\left[D_j\right]}} \tag{14}$$

where

$$\mathrm{E}^*\left[\dot{A}_j^2\right] = \int_{-\infty}^{\infty} \omega^2 S_{CP_j}(\omega) d\omega \qquad \text{and} \qquad \mathrm{E}^*\left[\dot{D}_j^2\right] = \int_{-\infty}^{\infty} \omega^{-2} S_{CP_j}(\omega) d\omega \tag{15}$$

$$\mathrm{Var}^*\left[A_j\right] = \int_{-\infty}^{\infty} S_{CP_j}(\omega) d\omega \qquad \text{and} \qquad \mathrm{Var}^*\left[D_j\right] = \int_{-\infty}^{\infty} \omega^{-4} S_{CP_j}(\omega) d\omega \tag{16}$$

The characteristic ground frequency ω_f of the Clough-Penzien spectrum depends on the soil type (F=firm, M=medium, S=soft) as follows (Der Kiureghian and Neuenhofer 1992):

$$\begin{aligned} \omega_f(\mathrm{F}) &= 15 \text{ rad/sec} \\ \omega_f(\mathrm{M}) &= 10 \text{ rad/sec} \\ \omega_f(\mathrm{S}) &= 5 \text{ rad/sec} \end{aligned} \tag{17}$$

while the other parameters can be determined as follows:

$$\zeta_f = \frac{\omega_f}{25} \qquad \omega_g = \frac{\omega_f}{10} \qquad \zeta_g = 0.6 \tag{18}$$

The PSD functions of the three soil types are presented in Figure 1 along with the acceleration and displacement response spectrum.

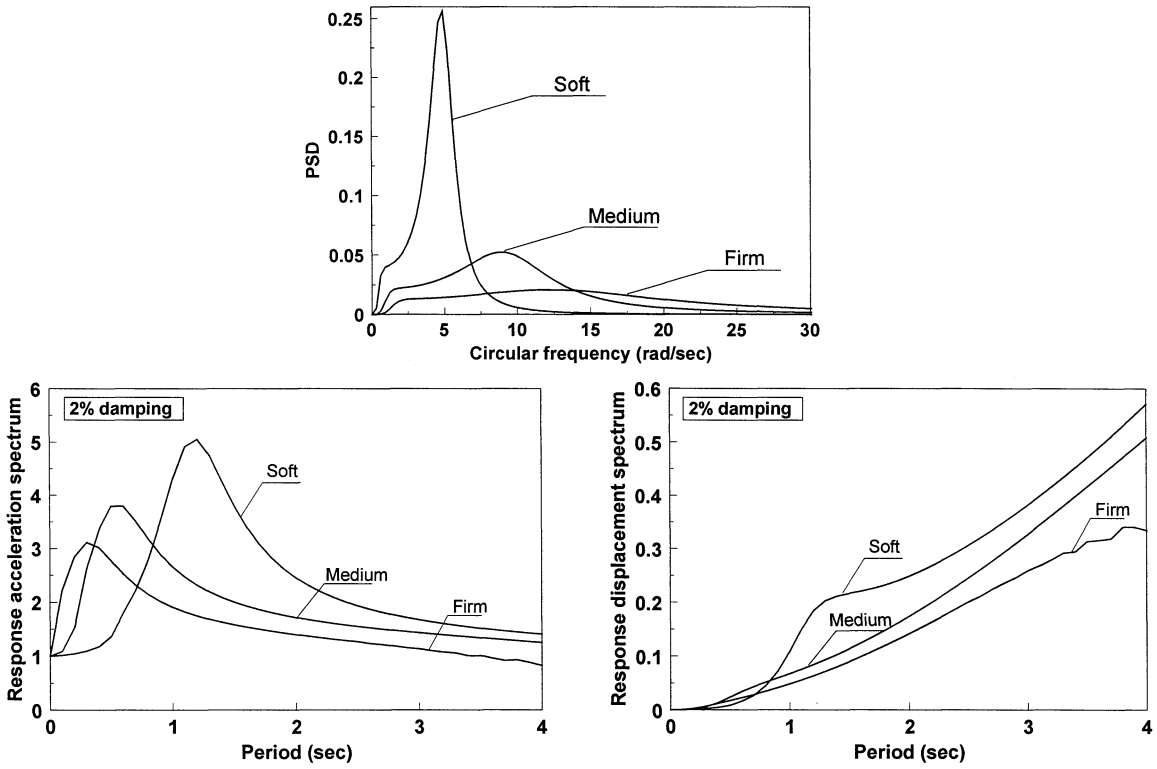


Figure 1. PSD and response spectra for soil types F, M and S.

The values of Var^* and Ω for the three soil types are:

$$\mathrm{Var}^*_{A_j}(\mathrm{F}) = 92.055 \qquad \mathrm{Var}^*_{A_j}(\mathrm{M}) = 62.764 \qquad \mathrm{Var}^*_{A_j}(\mathrm{S}) = 45.082 \tag{19}$$

$$\Omega_{A_j}(\mathrm{F}) = 46.276\,\mathrm{rad/sec} \qquad \Omega_{A_j}(\mathrm{M}) = 21.963\,\mathrm{rad/sec} \qquad \Omega_{A_j}(\mathrm{S}) = 6.4977\,\mathrm{rad/sec} \tag{20}$$

$$\mathrm{Var}^*_{D_j}(\mathrm{F}) = 0.78974 \qquad \mathrm{Var}^*_{D_j}(\mathrm{M}) = 2.6690 \qquad \mathrm{Var}^*_{D_j}(\mathrm{S}) = 21.403 \tag{21}$$

$$\Omega_{D_j}(\mathrm{F}) = 1.5521\ \mathrm{rad/sec} \qquad \Omega_{D_j}(\mathrm{M}) = 1.0578\,\mathrm{rad/sec} \qquad \Omega_{D_j}(\mathrm{S}) = 0.5622\ \mathrm{rad/sec} \tag{22}$$

Thus, the peak factor of the three soil types can be directly expressed as follows:

$$\begin{aligned} p_{A_j,0.5}(\mathrm{F}) &= \sqrt{2\ln t_s + 6.053} & & p_{D_j,0.5}(\mathrm{F}) = \sqrt{2\ln t_s - 0.737} \\ p_{A_j,0.5}(\mathrm{M}) &= \sqrt{2\ln t_s + 4.562} & \text{and} \quad & p_{D_j,0.5}(\mathrm{M}) = \sqrt{2\ln t_s - 1.504} \\ p_{A_j,0.5}(\mathrm{S}) &= \sqrt{2\ln t_s + 2.126} & & p_{D_j,0.5}(\mathrm{S}) = \sqrt{2\ln t_s - 2.768} \end{aligned} \tag{23}$$

Note that from (9) it is observed that:

$$\psi_{soil}(t_s) = \frac{\text{PGD}}{\text{PGA}} = \frac{p_{D_j,0.5}}{p_{A_j,0.5}} \frac{\sigma^*_{D_j}}{\sigma^*_{A_j}} \tag{24}$$

where $\sigma^*_Y = \sqrt{\text{Var}^*_Y}$ and ψ_{soil} is a function of the soil type and of t_s through the peak factors. For example, for a stationary duration $t_s = 20$ sec, it is:

$$\psi_F(20) = 0.0612 \text{ sec}^2 \qquad \psi_M(20) = 0.1345 \text{ sec}^2 \qquad \psi_S(20) = 0.4342 \text{ sec}^2 \tag{25}$$

Bridge model

The bridge is modeled as an elastic system, where both the piers and the isolators are considered as elastic. As regards the piers, this assumption is valid if the adopted procedure for the design of the isolators is such to maintain them in the elastic range, whereas the isolators, which of course enter well into the inelastic range, are represented through equivalent linear elements whose hysteretic damping is condensed into a viscous damping ratio. Both these quantities can be expressed as function of the required ductility.

Equivalent stiffness and damping ratio of the isolator

The equivalent stiffness $k_{eq,j}$ and the damping ratio $\xi_{eq,j}$ of the $j = 1 \ldots N$ isolators, equivalent to their hysteretic dissipation can be evaluated according to different criteria. Three are selected in this work, based on k_E = isolator elastic stiffness and α = isolator hardening ratio:

a) the first one is that adopted in AASHTO (Guide specification 1991)

$$k_{eq,j} = k_E \frac{1+\alpha(\mu_j - 1)}{\mu_j} \qquad \xi_{eq,j} = \frac{2}{\pi} \frac{(1-\alpha)(\mu_j - 1)}{\mu_j \left[1+\alpha(\mu_j - 1)\right]} \tag{26}$$

b) the second one is that presented in (Hwang et al. 1995)

$$k_{eq,j} = k_E \frac{1+\alpha(\mu_j - 1)}{\mu_j} \cdot \left(1 - 0.737 \frac{\mu_j - 1}{\mu_j^2}\right)^{-2} \qquad \xi_{eq,j} = \frac{2}{\pi} \frac{(1-\alpha)(\mu_j - 1)}{\mu_j \left[1+\alpha(\mu_j - 1)\right]} \frac{\mu_j^{0.58}}{6-10\alpha} \tag{27}$$

c) the third one is that presented in (Hwang et al. 1994)

$$k_{eq,j} = k_E \left\{1 + \ln\left[1 + 0.13(\mu_j - 1)^{1.137}\right]\right\}^{-2} \qquad \xi_{eq,j} = 0.0587(\mu_j - 1)^{0.371} \tag{28}$$

On passing, it should be observed that the first of the above equations is obtained through simple geometrical considerations, while the other two have been calibrated on the response of sdof oscillators: in particular, the second one is just a correction of the first one in order to maximize the accuracy in predicting the inelastic maximum response of bi-linear elastic bearings, while the third one is based on the optimal prediction of the period shift of a base-isolated regular bridge.

Note that the purpose of the equivalence is to substitute the hysteretic isolators with equivalent Kelvin elements. A Kelvin element, a linear spring in parallel with a pure viscous damper, satisfies the following equation:

$$f_j = k_{eq,j}\, y + c_{0j}\, \dot{y} \tag{29}$$

which can be transformed in the frequency domain as follows:

$$f_j(i\omega) = \left(k_{eq,j} + i\, c_{0j}\, \omega\right) y(i\omega) \tag{30}$$

Its transfer function from deformation y to force f is therefore:

$$H_j(i\omega) = k_{eq,j} + i\, c_{0j}\, \omega = k_{eq,j} + i 2 \xi_{eq,j}\, k_{eq,j} \tag{31}$$

where the real and the imaginary parts are the non-negative real-valued storage and loss moduli, respectively. This representation will be used in the following developments.

Equations of motion of the bridge

The equation of motions for the deck (subscript D) masses and the pier (subscript P) masses with the interposed isolators (subscript I) are, respectively:

$$\begin{aligned} &\mathbf{M}_D\left(\ddot{\mathbf{X}}_P + \ddot{\mathbf{X}}_I + \ddot{\mathbf{U}}\right) + \mathbf{C}_D\left(\dot{\mathbf{X}}_P + \dot{\mathbf{X}}_I + \dot{\mathbf{U}}\right) + \mathbf{K}_D\left(\mathbf{X}_P + \mathbf{X}_I + \mathbf{U}\right) + \mathbf{C}_I\left(\dot{\mathbf{X}}_I\right) + \mathbf{K}_I\left(\mathbf{X}_I\right) = \mathbf{0} \\ &\mathbf{M}_P\left(\ddot{\mathbf{X}}_P + \ddot{\mathbf{U}}\right) + \mathbf{C}_P\left(\dot{\mathbf{X}}_P\right) + \mathbf{K}_P\left(\mathbf{X}_P\right) - \mathbf{C}_I\left(\dot{\mathbf{X}}_I\right) - \mathbf{K}_I\left(\mathbf{X}_I\right) = \mathbf{0} \end{aligned} \tag{32}$$

where $\mathbf{K}_I = diag_j\left(k_{eq,j}\right)$. Eq. (32) can be written in matrix form as:

$$\begin{aligned} &\begin{bmatrix} \mathbf{M}_D & \mathbf{M}_D \\ \mathbf{0} & \mathbf{M}_P \end{bmatrix} \cdot \begin{Bmatrix} \ddot{\mathbf{X}}_I \\ \ddot{\mathbf{X}}_P \end{Bmatrix} + \begin{bmatrix} \mathbf{C}_D + \mathbf{C}_I & \mathbf{C}_D \\ -\mathbf{C}_I & \mathbf{C}_P \end{bmatrix} \cdot \begin{Bmatrix} \dot{\mathbf{X}}_I \\ \dot{\mathbf{X}}_P \end{Bmatrix} + \begin{bmatrix} \mathbf{K}_D + \mathbf{K}_I & \mathbf{K}_D \\ -\mathbf{K}_I & \mathbf{K}_P \end{bmatrix} \cdot \begin{Bmatrix} \mathbf{X}_I \\ \mathbf{X}_P \end{Bmatrix} = \\ &\begin{bmatrix} \mathbf{M}_D & \mathbf{C}_D & \mathbf{K}_D \\ \mathbf{M}_P & \mathbf{0} & \mathbf{0} \end{bmatrix} \cdot \begin{Bmatrix} \ddot{\mathbf{U}} \\ \dot{\mathbf{U}} \\ \mathbf{U} \end{Bmatrix} \end{aligned} \tag{33}$$

If it is assumed that: a) the contribution to the overall damping given by $\mathbf{C}_D \cdot \dot{\mathbf{X}}_I$, $\mathbf{C}_D \cdot \dot{\mathbf{X}}_P$ and $\mathbf{C}_P \cdot \dot{\mathbf{X}}_P$ is negligible with respect to that of the isolators $\mathbf{C}_I \cdot \dot{\mathbf{X}}_I$; b) $\mathbf{C}_D \cdot \dot{\mathbf{U}}$ can be neglected with respect to the other quantities on the left-hand side of the equation. Thus, the resulting equations are:

$$\begin{aligned}&\begin{bmatrix}\mathbf{M}_D & \mathbf{M}_D \\ \mathbf{0} & \mathbf{M}_P\end{bmatrix}\cdot\begin{Bmatrix}\ddot{\mathbf{X}}_I \\ \ddot{\mathbf{X}}_P\end{Bmatrix}+\begin{bmatrix}\mathbf{C}_I & \mathbf{0} \\ -\mathbf{C}_I & \mathbf{0}\end{bmatrix}\cdot\begin{Bmatrix}\dot{\mathbf{X}}_I \\ \dot{\mathbf{X}}_P\end{Bmatrix}+\begin{bmatrix}\mathbf{K}_D+\mathbf{K}_I & \mathbf{K}_D \\ -\mathbf{K}_I & \mathbf{K}_P\end{bmatrix}\cdot\begin{Bmatrix}\mathbf{X}_I \\ \mathbf{X}_P\end{Bmatrix}= \\ &=\begin{bmatrix}\mathbf{M}_D & \mathbf{K}_D \\ \mathbf{M}_P & \mathbf{0}\end{bmatrix}\cdot\begin{Bmatrix}\ddot{\mathbf{U}} \\ \mathbf{U}\end{Bmatrix}=\begin{bmatrix}\mu & \kappa\end{bmatrix}\cdot\begin{Bmatrix}\ddot{\mathbf{U}} \\ \mathbf{U}\end{Bmatrix}\end{aligned} \tag{34}$$

The advantage of casting the equation in this form, rather than the more classical version in (Clough and Penzien 1975) where a dynamic and a pseudo-static part are separately solved and subsequently added up, stems from the fact that this is computationally of great convenience, since it allows to directly obtain the expression of the PSD matrix of the isolators response, instead of deriving it as PSD of a sum process, where also the cross PSDs between the dynamic and the pseudo-static process must be evaluated.

The whole problem can then be stated as:

$$\mathbf{M}\ddot{\mathbf{X}}+\mathbf{C}\dot{\mathbf{X}}+\mathbf{K}\mathbf{X}=\mu\ddot{\mathbf{U}}+\kappa\mathbf{U}=\mathbf{F} \tag{35}$$

Response of the isolators

Using elementary notions of stationary random vibration theory, the matrix of the response PSD is obtained by filtering the cross-PSD matrix $\mathbf{S}_{FF}(\omega)$ of the action $\mathbf{F}$ with the frequency response matrix $\mathbf{H}_X(i\omega)$ of the system

$$\mathbf{S}_{XX}(\omega)=\mathbf{H}_X(i\omega)\,\mathbf{S}_{FF}(\omega)\,\mathbf{H}_X^T(-i\omega) \tag{36}$$

where the first N values on the diagonal are the auto-PSD of the isolators.

The cross-PSD matrix $\mathbf{S}_{FF}(\omega)$ in (36) is obtained from the cross-correlation matrix of the action $\mathbf{F}$:

$$\mathbf{R}_{FF}(\tau)=\mu\,\mathbf{R}_{\ddot{U}\ddot{U}}\,\mu^T+\kappa\,\mathbf{R}_{UU}\,\kappa^T+\mu\,\mathbf{R}_{\ddot{U}U}\,\kappa^T+\kappa\,\mathbf{R}_{U\ddot{U}}\,\mu^T \tag{37}$$

which is then Fourier-transformed into the cross-PSD matrix

$$\begin{aligned}\mathbf{S}_{FF}(\omega)&=\mu\,\mathbf{S}_{\ddot{U}\ddot{U}}\,\mu^T+\kappa\,\mathbf{S}_{UU}\,\kappa^T+\mu\,\mathbf{S}_{\ddot{U}U}\,\kappa^T+\kappa\,\mathbf{S}_{U\ddot{U}}\,\mu^T \\ &=\mu\,\mathbf{S}_{\ddot{U}\ddot{U}}\,\mu^T+\frac{1}{\omega^4}\kappa\,\mathbf{S}_{\ddot{U}\ddot{U}}\,\kappa^T+\frac{1}{\omega^2}\left(\mu\,\mathbf{S}_{\ddot{U}\ddot{U}}\,\kappa^T+\kappa\,\mathbf{S}_{\ddot{U}\ddot{U}}\,\mu^T\right)\end{aligned} \tag{38}$$

(where in the above equation the relation $S_{U_\circ} = S_{\ddot{U}_\circ}/\omega^2$ has been used).

The frequency response matrix $\mathbf{H}_X(i\omega)$ in (36) can be obtained from the modal frequency response (diagonal) matrix

$$\mathbf{H}_Z(i\omega) = diag_k\left[\left(\hat{\omega}_k^2 - \omega^2 + 2i\xi_k\hat{\omega}_k\omega\right)^{-1}\right] \tag{39}$$

where $\hat{\omega}_k$ is the circular frequency of the *k*-th mode and ξ_k the associated modal damping. The frequency response matrix $\mathbf{H}_Z(i\omega)$ is transformed into the frequency response matrix $\mathbf{H}_X(i\omega)$ through the eigenmatrices of the system (35), which implies that an eigenproblem has to be solved.

Before solving the eigenproblem, it should be noticed that the matrices **M** and **K** in (35) are non-symmetrical. In this case, it is convenient to cast the equation in the following form:

$$\ddot{\mathbf{X}} + \mathbf{M}^{-1}\mathbf{C}\dot{\mathbf{X}} + \mathbf{M}^{-1}\mathbf{K}\mathbf{X} = \mathbf{M}^{-1}\mathbf{F} \tag{40}$$

Thus, modal decomposition can be performed of the (assumed classically damped) eigenproblem

$$\mathbf{M}^{-1}\mathbf{K}\Phi = \Phi\Lambda \tag{41}$$

whose solution is the eigenvalues matrix $\Lambda = diag_k\left(\hat{\omega}_k^2\right)$ and the couple of eigenmatrices: the right-hand eigenmatrix Φ, and the left-hand eigenmatrix Φ_L, for which the following relation holds: $\Phi_L^T = \Phi^{-1}$.

Treatment of damping

The equations of motion can be uncoupled by writing $\mathbf{X} = \Phi\mathbf{Z}$

$$\ddot{\mathbf{Z}} + \Phi^{-1}\mathbf{M}^{-1}\mathbf{C}\Phi\dot{\mathbf{Z}} + \Phi^{-1}\mathbf{M}^{-1}\mathbf{K}\Phi\mathbf{Z} = \Phi^{-1}\mathbf{M}^{-1}\left(\mu\ddot{\mathbf{U}} + \kappa\mathbf{U}\right) = \mathbf{Y} \tag{42}$$

where it is noted that the modal damping matrix $\hat{\mathbf{C}} = \Phi^{-1}\mathbf{M}^{-1}\mathbf{C}\Phi = \overline{\Phi}_L^T\mathbf{C}\Phi$ (where $\overline{\Phi}_L^T = \Phi^{-1}\mathbf{M}^{-1} = \Phi_L^T\mathbf{M}^{-1}$ is the mass-normalized left-hand eigenmatrix) is not diagonal, therefore the equations are not completely uncoupled. An analysis of the error resulting from neglecting the off-diagonal terms can be found in (Veletsos and Ventura 1986) where it is shown that for modal damping ratios lower than 30% the error is acceptable, if not negligible.

Under this consideration, the modal damping ratios are obtained as

$$\xi_k = \frac{1}{2\hat{\omega}_k} diag_k\left(\Phi^{-1}\mathbf{M}^{-1}\mathbf{C}(\hat{\omega}_k)\Phi\right) = \frac{1}{2\hat{\omega}_k} diag_k\left(\overline{\Phi}_L^T\mathbf{C}(\hat{\omega}_k)\Phi\right) \tag{43}$$

where the damping matrix $\mathbf{C}(\hat{\omega}_k)$ is built for each eigenvalue as follows (Zambrano *et al.* 1996):

$$\mathbf{C}(\hat{\omega}_k) = diag_j\left(\frac{\mathrm{Im}\{H_j\}}{\hat{\omega}_k}\right) = diag_j\left(\frac{2\,\xi_{eq,j}\,k_{eq,j}}{\hat{\omega}_k}\right) \tag{44}$$

where the numerator is the imaginary part of the transfer function (31) of the j-th isolator.

With the values of the modal damping ratios in (43) the modal frequency response matrix $\mathbf{H}_Z(i\omega)$ in (39) can be built and then transformed into the frequency response matrix $\mathbf{H}_X(i\omega)$

$$\mathbf{H}_X(i\omega) = \Phi\ \mathbf{H}_Z(i\omega)\ \overline{\Phi}_L^T \tag{45}$$

This expression, along with that of the cross-PSD of the action in (38), can be inserted into (36) to get the PSD matrix of the response.

Iterative procedure

The response of the bridge depend on the isolator stiffness and damping. Since this is evaluated with either (26) or (27) or (28) as function of the ductility required to the isolators, which in turn depends on the isolators characteristics, an iterative procedure must be followed. This can be summarized as follows:

1) Guess value for the required ductility μ_j in all $j = 1 \ldots N$ isolators along the bridge (usually, $\mu_j = 1$)
2) Calculate the vector of the variances of the response of each isolator through (36) (that is, only the first N values on the diagonal need to be evaluated, since they are the auto-PSD of the isolators)

$$\sigma^2_{iso,k} = \mathrm{Var}\left[X_{iso,k}\right] = \int_{-\infty}^{\infty} S_{X_k X_k}(\omega)\, d\omega \qquad k = 1 \ldots N \tag{46}$$

3) Update the vector of the required ductility in each isolator

$$\mu_k = \frac{p \cdot \sigma_{iso,k}}{X_{y,k}} \qquad k = 1 \ldots N \tag{47}$$

where p is a peak factor taken as 2.5.

4) Compare the ductilities with the current value: if convergence is attained then exit, else repeat procedure with the new estimate of ductilities.

Design of the isolated bridge

The bridge under consideration is represented in Figure 2, purposely selected equal to that extensively studied in (Monti et al. 1996). It is a 6-span continuous deck with 5 piers of the same height H= 10 m and of 2.5 m diameter. The span length is 50.0 m. The deck, transversely supported by isolators to the piers and the abutments, has a dead load of 200 kN/m. The piers (acting as cantilevers) are considered as fixed on the soil. All the analyses of the bridge have been performed in the transverse direction.

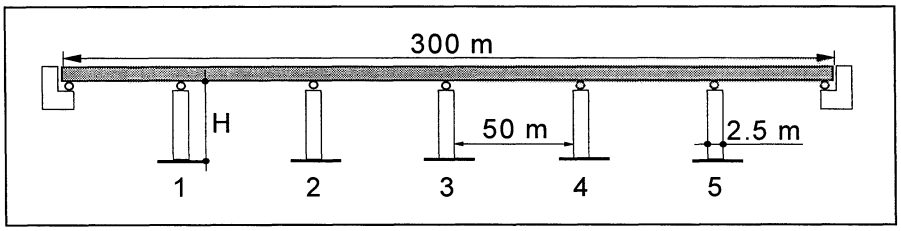


Figure 2. Schematic view of the bridge.

The isolated bridge has been designed elastically for the transverse direction only, under synchronous ground motion ($v_s/\alpha = \infty$ and $v_{app} = \infty$) which corresponds to the usual design assumption adopted in engineering practice.

In the elastic analyses performed to design the bridges, the cracked stiffness of the piers has been used, obtained from the uncracked stiffness (gross section) divided by a factor 2.5. The following material strengths have been used: for concrete $f_c = 35{,}000$ kPa, for steel $f_y = 440{,}000$ kPa, with ultimate strains equal to $\varepsilon_{cu} = 0.008$ and $\varepsilon_{su} = 0.10$, respectively. Material design factors were: 1.5 for concrete and 1.15 for steel.

The design has been made for the average of the maximum values of the response (force at the pier top) obtained using ten sets of accelerograms scaled to a PGA of 0.42 g. A protection level equal to μ = 4.2, which correspond to the design PGA= 0.10 g, was considered. For the design phase, the deck was considered as rigid, hinged on the piers and supported by rollers on the abutments.

The design criterion aimed at equally sharing the total shear force among all the elements (piers and abutments), which basically imply that the same isolators are used on all the piers and abutments and that all the piers have the same strength.

The design of the isolators is performed according to:

$$F_{Y,iso} = \frac{F_{D,\max}}{\mu} \tag{48}$$

where $F_{Y,iso}$ is the isolator yield strength, $F_{D,\max}$ is the maximum force (average on 10 analyses) transmitted from the deck to the pier below, and μ is the reduction factor of this force. The isolator stiffness is obtained as: $K_I = 150 \cdot F_Y$, which basically assures that the isolator yield displacement is always equal to 6 mm. The isolator hardening ratio b was selected as $b = \bar{b}$ such that the hardening ratio of the pier-isolator system be equal to $b_{\text{tot}} = 0.10$. The value of $\bar{b}$ is easily obtained from

$$\bar{b} = b_{\text{tot}} \cdot \left(\frac{1}{K_P} + \frac{1}{K_I} \right)^{-1} \cdot \frac{1}{K_I} \tag{49}$$

where K_P is the stiffness of the pier considered as a cantilever. In the bridge examined, the isolators hardening ratio turned out to be: $\bar{b} \approx 0.03$.

The piers, of height H, are designed to satisfy the following inequality

$$M_u \geq H \cdot \left(F_{Y,iso} + F_{P,\max} + c \cdot N_D + N_T \cdot \Delta_{\max} \right) \cdot \gamma_o \tag{50}$$

where M_u is the resisting moment of the section at the pier base, $F_{P,\max}$ is the base shear due to the mass of the pier itself and of the pier top (which are under the isolator), c is a friction coefficient, taken equal to 0.03 (teflon bearings assumed), N_D is the load applied on the isolator by the supported deck, N_T is the total load (deck+pier) considered lumped at the pier top, $\Delta_{\max}$ is the maximum displacement (average on 10 analyses) at the pier top and $\gamma_o = 1.2$ is an overstrength factor recovering the uncertainties in the evaluation of $F_{Y,iso}$, c and $\Delta_{\max}$. The reinforcement ratio in all piers resulted equal to 2.07%. Such conservative design procedure ensures that all the piers remain in the elastic range.

Results of the Analyses

The bridge in Figure 2, whose isolators were designed with the above described procedure, was analyzed through stationary random vibration analysis to assess the effect of fully incoherent ground motion on the isolators response. In the linear bridge model, all isolators are substituted with equivalent Kelvin elements, with stiffness and damping proportional to the required ductility.

It is known, (see for ex., Clough and Penzien 1975), that the response of an elastic structure subjected to non-synchronous input can be obtained from the superposition of two contributions: a *dynamic* component induced by the inertia forces and a so-called *pseudo-static* component, due to the differences in the support displacements. These latter can induce significant distortions in the structure thus modifying the internal forces with respect to the case of synchronous input. The two components can be represented at each time step by means of two values: the mean ground displacement under the supports, which corresponds to a rigid body motion of the structure and can be partly identified with the dynamic component, and the ground displacements standard deviation, which can be considered as representative of the pseudo-static distortion imposed to the structure. The ground displacements for the three types of soils can be evaluated through (24) and considering that all the analyses are performed under a PGA=0.42g: this corresponds to a PGD of 0.20 m, 0.50 m and 1.70 m for the soil types F, M and S, respectively. Since the latter value appears unrealistically high, it has been decided not to include the soil type S in the analyses.

It should be kept in mind while observing the following figures that *geometric incoherence* (*i.e.* that ruled by the first term in Eq. 3) decreases as v_s/α increases from 300 m/s to ∞ m/s. In each diagram the *wave-passage* delay (*i.e.* that ruled by the second term in Eq. 3) decreases as the apparent velocity v_{app} increases from 300 to ∞ m/s.

As reported in (Monti et al. 1996), for soil F an evident phenomenon is the significant reduction of the mean displacement for increasing geometric incoherence, therefore we expect a reduction of the dynamic component as v_s/α decreases from ∞ m/s to 300 m/s. For soil M this is less evident and we rather expect an increase of the dynamic component when v_{app}= 300 m/s. For both soils a remarkable increase of standard deviation is observed as v_s/α decreases but this phenomenon is less evident as v_{app} decreases from ∞ to 300 m/s. Therefore, high pseudo-static distortions are expected either for low values of v_s/α or, if $v_s/\alpha = \infty$, for low values of v_{app}. Note that in all cases the variation of v_{app} has a notable effect only for $v_s/\alpha = \infty$, while in the presence of a certain degree of geometric incoherence its effect is sensibly reduced.

A first task pursued was to assess the relevance on the simulated response of the selected equivalence equation, either (26) or (27) or (28), referred to as: AASHTO, Hwang and CALTRANS, respectively. In Figure 3 the adopted equations are compared for two different hardening ratios: 0% and 3% (the CALTRANS equation is insensitive to the hardening ratio). It can be observed that major differences exist in the estimation of the equivalent damping ratio, with relative differences of the order of 300%, whereas for the effective stiffness ratio the

differences are less evident with the only exception of the CALTRANS equations, which yields a lower stiffness reduction with increasing ductility.

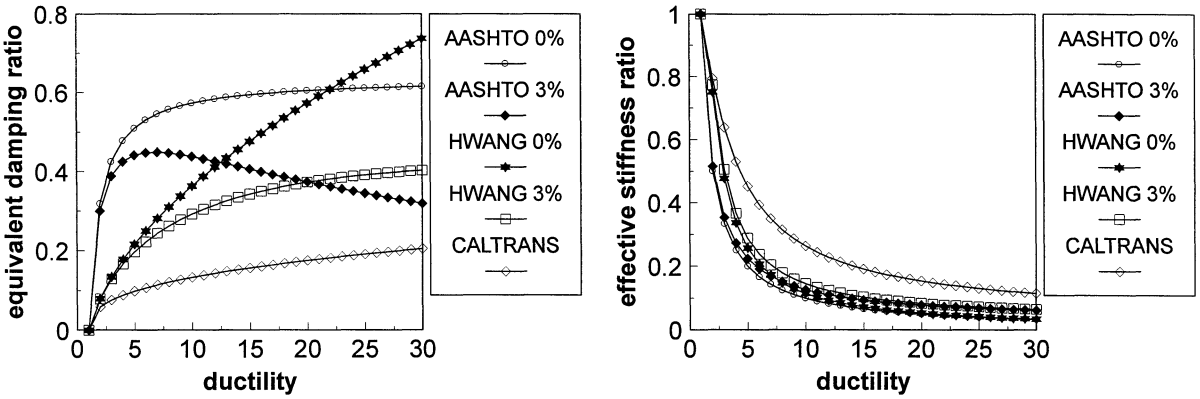


Figure 3. Isolator equivalent damping and stiffness ratios as function of the required ductility according to Eqs. 26 (AASHTO), 27 (Hwang) and 28 (CALTRANS), with hardening ratio 0% and 3%.

In Figure 4, the response of the isolators, in terms of peak displacement (where the peak factor is exactly computed), is represented for each of the above equivalence equations, compared with Montecarlo simulations on 300 nonlinear analyses. The benchmark cases considered are those on Firm and Medium soil, with either fully coherent or low coherence ground motion, corresponding to v_s/α and v_{app} equal to infinity and 300 m/s, respectively. All the comparisons above are conducted without accounting for the site response effect on the incoherence of the ground motion, but it is deemed that the conclusions reached above can be extended to the case of site response effect.

It is seen that in all cases the best approximation to the Montecarlo response is obtained with the CALTRANS equations but it is recognized that the accuracy decreases with increasing incoherence. The weakness of the AASHTO equivalence equations can be attributed to the fact that those are obtained through simple geometrical considerations, whereas the other two equations are derived by minimizing the RMS error of the inelastic maximum responses of sdof bi-linear hysteretic isolators. The two equations have a satisfactory performance when the bridge deforms according to the first modal shape, whereas they have a lower accuracy for high incoherence. In the following analyses the equations (28) are adopted to linearize the isolators.

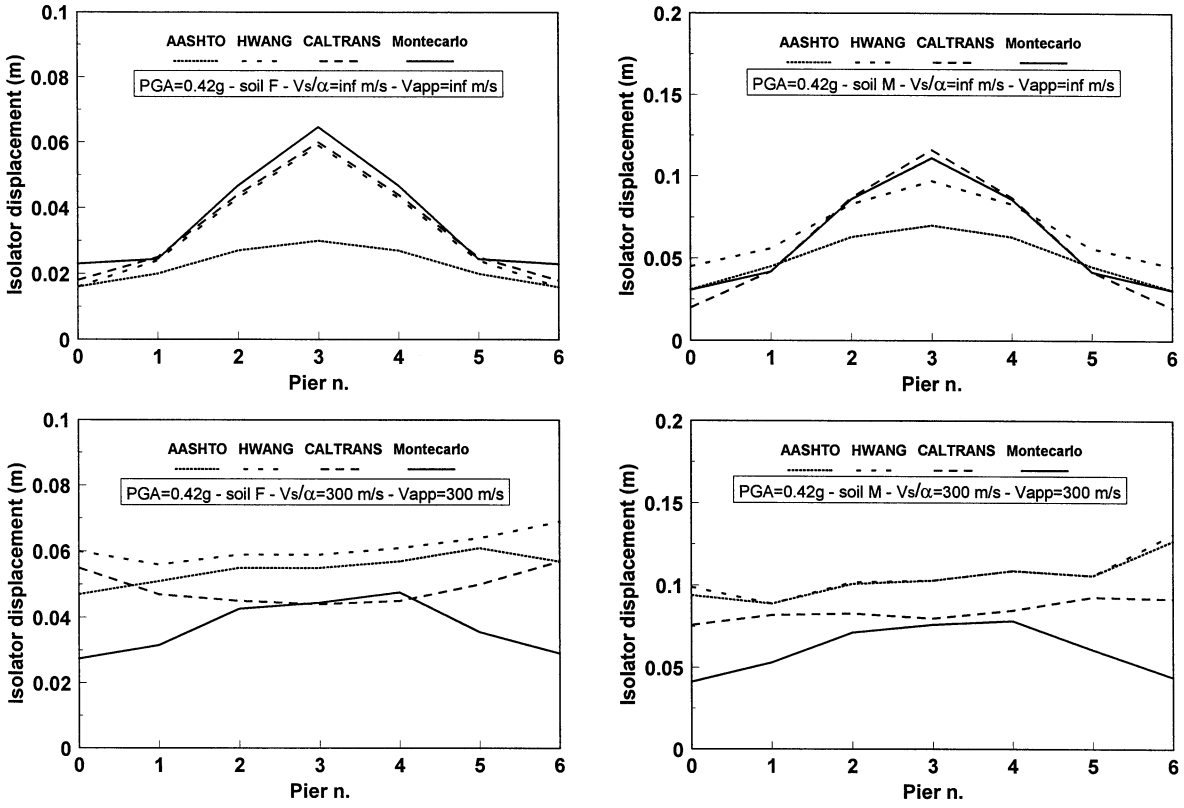


Figure 4. Validation of equivalence equations 26 (AASHTO), 27 (Hwang) and 28 (CALTRANS) for Firm (left) and Medium (right) soil and with high (top) and low (bottom) coherence.

For the cases examined above, in Table 1 the equivalent damping ratios and effective stiffnesses of the isolators are reported along with the modal damping ratio ξ_k, computed with (43), of the first four modal shapes, for the bridges in full synchronism on soil types F and M (reference is therefore made to Figure 4, top). It is noted that the AASHTO and Hwang equations yield approximately the same fundamental period, as expected because of the slight differences in the estimation of the effective stiffness, whereas the periods computed with the CALTRANS equation are sistematically lower. On the other hand, it is noted that both the damping ratios of the single isolators and the modal one are significantly higher in the two former equations, while the latter gives rise to low damping ratios. Thus, it can be said that the two former equations rely on the dissipation to predict the peak response of the isolators, whereas the latter, with lower damping ratios, relies on the stiffness.

Table 1. Equivalent and modal damping ratios with three different equivalence equations (A=AASHTO, H=Hwang, C=CALTRANS) for full synchronism.

		Equivalent damping (%) and effective stiffness			Modal damping (%) and period (sec)			
Eq.	Soil	1	2	3	ξ_1 (T_1)	ξ_2 (T_2)	ξ_3 (T_3)	ξ_4 (T_4)
A	F	36.4 (.40)	41.2 (.30)	42.4 (.28)	41.6 (0.75)	32.0 (0.63)	24.1 (0.47)	26.6 (0.38)
H	F	13.4 (.48)	21.5 (.25)	25.7 (.18)	22.3 (0.81)	14.6 (0.62)	9.0 (0.45)	7.9 (0.33)
C	F	7.8 (.62)	10.4 (.41)	11.9 (.32)	12.2 (0.68)	9.2 (0.57)	6.7 (0.43)	6.7 (0.33)
A	M	44.8 (.19)	44.4 (.14)	44.0 (.13)	44.4 (1.01)	35.1 (0.79)	35.4 (0.59)	34.9 (0.48)
H	M	25.1 (.19)	30.8 (.13)	32.8 (.11)	30.8 (1.05)	21.9 (0.80)	20.6 (0.61)	18.9 (0.50)
C	M	10.2 (.43)	14.1 (.24)	15.8 (.19)	15.3 (0.82)	10.8 (0.64)	7.2 (0.46)	7.0 (0.34)

After having chosen the model to linearize the isolators, it is now possible to consider the isolators response under different incoherence conditions. For the sake of clarity, we recall that the overall phenomenon of multi-support excitation can be split into two parts: one is the so-called non-synchronism effect, which are the two effects of *geometric incoherence* and *wave passage*, the other is the *site response* effect. In Figure 5 the isolators response with no site response effect is represented, therefore only the case FFFFF and MMMMM are considered, that is, soil type F and M under all supports: on the left, the response under perfectly synchronous conditions is graphed, while on the right the effect of non-synchronism is represented.

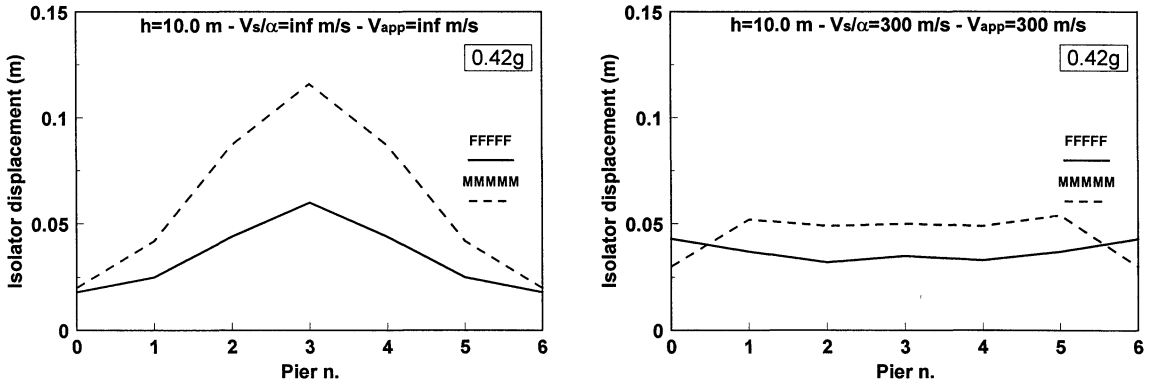


Figure 5. Isolators response without site response effect: synchronous (left) and non-synchronous (right).

The non-synchronous action has a twofold effect: one is to reduce the peak response (which is more than halved for the case of soil F), the other is to break the modal response, which in the first case is driven by the first modal shape, while in the second becomes practically flat. It is therefore confirmed that non-synchronism has a favorable effect on the response of isolated bridges, as already reported in (Monti et al. 1995, 1996).

The consequences of the site response effect are depicted in Figure 6 where the effect of one-step and three-step variations are considered, for the case of synchronism and non-synchronism. Four different combinations between soil type F (Firm) and M (Medium) are considered, denoted with the sequence of soil types under the five piers of the bridge under consideration. One-step and three-step combinations are considered, defined as a change in the soil type in the mid pier and the three mid piers, respectively. It should be noted that for each combination, the reciprocal is considered as well, that is, both FFMFF and MMFMM are studied.

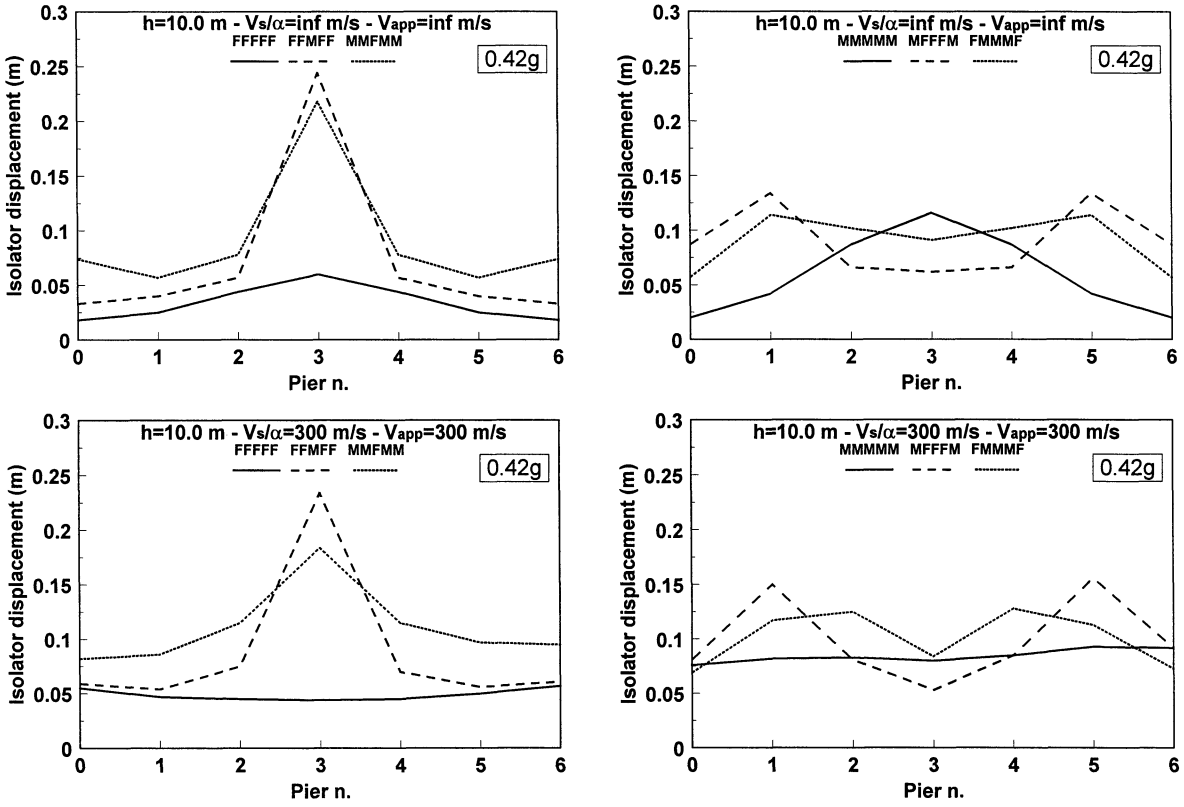


Figure 6. Isolators responses with varying site response effect:
one-step combinations (left) and three-step combinations (right) of Firm and Medium soil, synchronous (top) and non-synchronous (bottom).

From the diagrams, the following observations can be made:

- when site effect is present, the response is only slightly affected by non-synchronism; this essentially confirms the deterministic nature of the site response effect which implies the application of differential displacements at the supports, as opposed to the non-synchronous part of the action, which implies instead both a dynamic and a pseudo-static part,
- the effect on the response of the one-step combinations is more significant than that of the three-step combinations,
- reciprocal combinations produce similar response shapes.

Site effect can be interpreted as a problem of differential displacements imposed at the pier supports. It has been noticed above that soil type F and M have a PGD of 0.20 m and 0.50 m, respectively, which can be appreciated in the case depicted in Figure 6 (top, left) where a differential displacement of about 0.20 m affects the isolators 2, 3 and 4.

From the above, it can be concluded that, in case one wants to consider the presence of varying soil profiles under different support, the effect of non-synchronism can be disregarded.

Since we have now reduced the case of multiple-support excitation to a case where only the site effect is considered, one could wonder what is the difference in the global response if one models the site response effect considering only different soils in the diagonal terms of the PSD functions matrix (2), as opposed to the above described model where, in addition to this, all the off-diagonal terms in the coherency functions matrix (3) are calculated as function of distance-independent phase shifts in (4) and representing the cross-coherence among the different ground motions. In order to assess such difference, analyses have been carried out where the results obtained with the complete model of the ground motion are compared with results obtained by taking the site response coherence functions in (3) equal to 1. These comparisons are shown in Figure 7 for the same different soil combinations as above, but only for the case of full synchronism.

By observing the results it can be concluded that a model that does not account for the cross-coherence terms, yields quite different results, even though it should be recognized that the differences are in most cases acceptable. This amounts to saying, for instance, that time history analyses could be performed by applying, at different supports, accelerograms generated from different power density spectra, without introducing any significant error on the estimation of the peak response of the isolators.

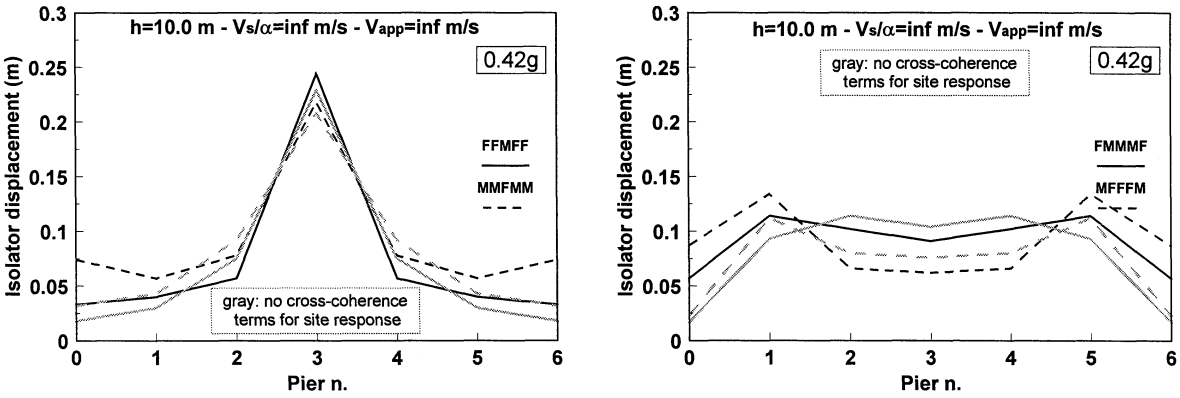


Figure 7. Isolators response considering the complete ground motion model (black lines) and the simplified model with no cross-coherence terms for the site response (gray lines), for one-step combinations (left) and three-step combinations (right) of Firm and Medium soil.

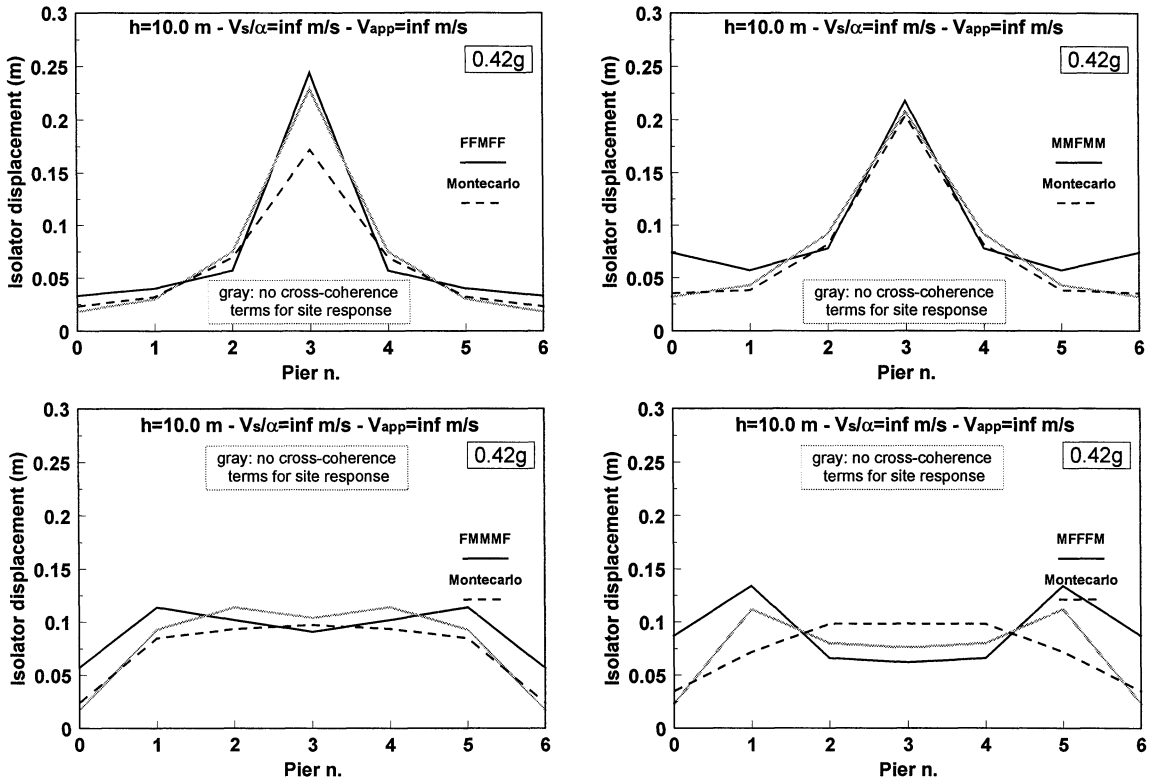


Figure 8. Isolators displacements obtained with Montecarlo analyses (dashed lines), compared with random vibration analyses with the complete ground motion model (black lines) and the simplified model with no cross-coherence terms for the site response (gray lines): one-step (top) and three-step (bottom) combinations.

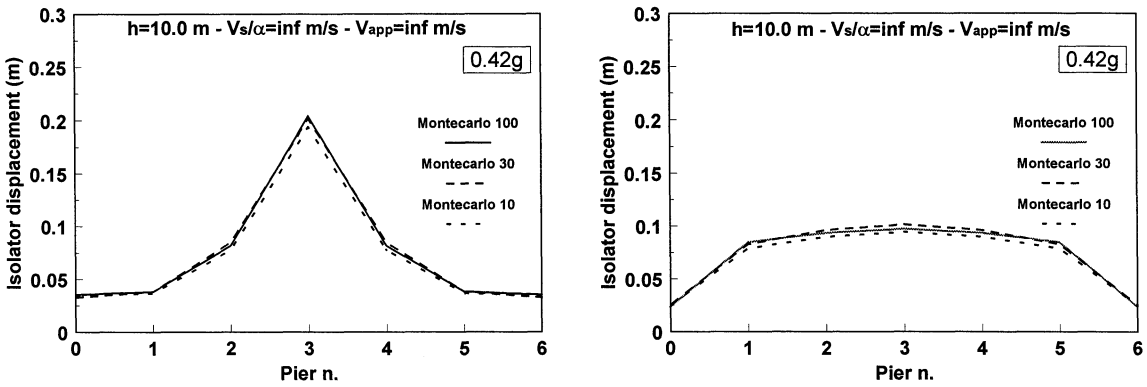


Figure 9. Isolators response with different number of Montecarlo analyses: case MMFMM (left) and FMMMF (right).

This is exactly what has been done in Figure 8 where the results of the random vibration analyses are compared with results obtained from Montecarlo analyses (dashed lines) on 100 samples, with accelerograms applied as mentioned above. It can be seen that for those cases with prevailing M soil (top-right and bottom-left) there are minor differences with respect to the case of the random vibration analysis with the complete model (black line), while for the cases with prevailing F soil (top-left and bottom-right) the differences are more significant but still acceptable.

Thus, a conclusion is reached, of course relative to the cases at hand but of sufficient generality, that in case the site response effect is to be included into the analysis of an isolated bridge, an acceptable estimate of the isolators peak displacement can be obtained through Montecarlo nonlinear analysis. An optimal number of 10 analyses (Figure 9) can be selected to approximate with sufficient accuracy the exact result, thus confirming the deterministic nature of the site response effect.

References

1. AASHTO (1991). 'Guide Specifications for Seismic Isolation Design'. American Association of State Highway and Transportation Officials, Washington, D.C.
2. Bodganoff, J.L., Goldberg, J.E. and Schiff, A.J. (1965). Bull. of Seismological Society of America, 55, 627-640.

3. Clough, R.W. and Penzien, J. (1975). Dynamics of Structures. McGraw-Hill, New York, N.Y.

4. Der Kiureghian, A. (1996). 'A coherency model for spatially varying ground motions'. Int. J. of Earthquake Engineering and Structural Dynamics, Vol. 25, 99-111.

5. Der Kiureghian, A. and Neuenhofer, A. (1992). 'Response spectrum method for multiple support seismic excitations'. Int. J. of Earthquake Engineering and Structural Dynamics, Vol. 21, 713-740.

6. Hwang, J.S., Change, L.H. and Gates, J.H. (1994). 'Practical analysis of base-isolated bridges with bi-linear hysteresis characteristics', Earthquake Spectra, Vol. 10, No. 4, 705-727.

7. Hwang, J.S., Chiou, L.H. and Change, L.H. (1995). 'Establishment of an equivalent linear model of seismically isolated bridges using a system identification method', Proc. 4th U.S. Conference on Lifeline Earthquake Engineering, ACE, San Francisco, 416-423.

8. Luco, J.E. and Wong, H.L. (1986). 'Response of rigid foundation to a spatially random ground motion'. Int. J. of Earthquake Engineering and Structural Dynamics, Vol. 14, 891-908.

9. Monti, G., Nuti C. and Pinto P.E. (1995). 'Response of conventional and isolated bridges under non-synchronous seismic motion'. Proc. SECED Conference European Seismic Design Practice, Chester, UK.

10. Monti, G., Nuti C. and Pinto P.E. (1996). 'Nonlinear response of bridges under multi-support excitation'. Journal of Structural Engineering ASCE, Vol. 122, n. 10.

11. Perotti, F. (1990). 'Structural response to non-stationary multiple-support random excitation'. Int. J. of Earthquake Engineering and Structural Dynamics, Vol. 19, 513-527.

12. Vanmarcke, E.H. (1977). 'Structural response to earthquakes'. Seismic Risk and Engineering Decision. Lomnitz Ed., McGraw-Hill, New York, N.Y., 287-337.

13. Veletsos, A.S. and Ventura, C.E. (1986). 'Modal analysis of non-classically damped linear systems'. Earthquake Engineering and Structural Dynamics, Vol. 14, 217-243.

14. Zambrano A., Inaudi, J.A. and Kelly, J.M. (1996). 'Modal coupling and accuracy of modal strain energy method'. Journal *of Engineering Mechanics*, ASCE, Vol. 122, No. 7, July, 603-612.

DEVELOPMENT OF BRIDGE FRAGILITY CURVES

Masanobu Shinozuka

Department of Civil Engineering
University of Southern California
University Park, CA 90089-2531

ABSTRACT

This paper presents preliminary results of an on-going research on bridge fragility curve development focusing on (1) development of empirical fragility curves utilizing bridge damage data obtained from the past earthquakes, particularly the 1994 Northridge earthquake, (2) development of analytical fragility curves, on the basis of dynamic analysis, (3) the issues of hypothesis testing and confidence intervals of these fragility curves, and (4) demonstration, on the basis of dynamic analysis, of effective use of a protective system for fragility enhancement using a representative bridge in the Memphis area.

INTRODUCTION

While performing a seismic risk analysis of a highway system, it is imperative to be able to identify seismic vulnerability associated with various damage states of bridges, since bridges are among the most seismically vulnerable structures in the system. The development of vulnerability information in the form of fragility curves, however, represents a major challenge. This paper outlines methods of fragility curve development for bridges by empirical as well as analytical means.

In principle, the development of bridge fragility curves will require synergistic use of the following methods; (1) Professional judgment, (2) quasi-static and design code consistent analysis, (3) utilization of damage data associated with past earthquakes and (4) numerical simulation of bridge seismic response based on structural dynamics. To amplify this observation, the following comments are in order.

1. Extent of damage should be evaluated and quantified in terms of physical quantities (such as interstory drift and ductility factors), but not necessarily in terms of repair

cost relative to replacement cost. Input from and consensus judgment by an invited group of professional engineers should be utilized here.

2. Fragility curves for various levels of damage should then be derived, taking into consideration a set of uncertain factors arising from structural characteristics, site conditions, damage states, ground motion attenuation laws, liquefaction and permanent ground motion potential.

3. More rigorous detailed response information based on time-history analysis accounting for complex damage states (e.g., multiple damage modes) should be generated by Monte Carlo simulation for a relatively small but statistically appropriate number of cases.

4. Quasi-static nonlinear analysis, a simplified and approximate method derived from the more rigorous method mentioned in 3 above, should be developed to establish fragility curves at a large number of earthquake intensity levels. This method should be validated by comparison of results from a number of representative cases obtained from both methods. In addition to the usual measure of earthquake intensity in terms of MMI and PGA, ARS should be employed as much as possible (where ARS is the acceleration response spectrum averaged over the frequency range of each structural category).

5. Experimental calibration of fragility curves for selected structures and structural components should be carried out.

This paper, however, summarizes preliminary results of the on-going research on bridge fragility curve development being carried out by this author focusing on (1) development of empirical fragility curves utilizing bridge damage data obtained from the past earthquakes, particularly the 1994 Northridge earthquake, (2) development of analytical fragility curves, on the basis of dynamic analysis (3) the issues of hypothesis testing and confidence intervals of these fragility curves, and (4) demonstration, on the basis of dynamic analysis , of effective use of a protective system for fragility enhancement using a representative bridge in the Memphis area.

EMPIRICAL FRAGILITY CURVE DEVELOPMENT

First, empirical fragility curves for the Caltrans' bridges are developed on the basis of the record of the damage resulting from the 1994 Northridge Earthquake under the assumption that the curves can be expressed in the form of two parameter log-normal distribution functions and with the aid of the maximum likelihood method for estimation of the two parameters (median c and log-standard deviation ζ of the log-normal distribution).

The likelihood function L is expressed as

$$L = \prod_{i=1}^{N} [P(a_i)]^{q_i} [1 - P(a_i)]^{1-q_i} \quad (1)$$

where $P(\cdot)$ represents the fragility curve for a specific state of damage, a_i the PGA value to which bridge i is subjected, q_i = 1 or 0 depending on whether or not the bridge sustains the state of damage under PGA = a_i, and N is the total number of bridges within the region affected by the earthquake of interest. Under the current log-normal assumption, the function $P(a)$ takes the following form

$$P(a) = \Phi\left[\frac{\ln(a/c)}{\zeta}\right] \quad (2)$$

in which "a" represents PGA and $\Phi[\cdot]$ is the standardized normal distribution function.

The two parameters c and ς in equation 2 are estimated as c_0 and ς_0 satisfying the following equations and maximizing L;

$$\frac{\partial \ln L}{\partial c} = \frac{\partial \ln L}{\partial \zeta} = 0 \quad (3)$$

This estimation is performed numerically by implementing a straightforward optimization algorithm.

Four fragility curves for Caltran's bridges associated with the four states of damage are plotted in figure 1 (with their respective median and log-standard deviation values indicated) for Caltrans' bridges. These fragility curves are constructed on the PGA vs damage state database developed by overlaying the Caltrans' bridge map (figure 2) on the Northridge earthquake PGA contour map by USGS (figure 3) and by utilizing the corresponding bridge damage report by Caltrans for the classification of damage state. The fragility curve identified by "minor" in figure 1 is associated with the state of at least minor damage. Similar significance applies to other three fragility curves identified by "moderate", "major" and "collapse".

It is cautioned that, in this analysis involving Caltrans' bridge, no attempt was made to develop fragility curves for each of the different sets of bridges classified in terms of such attributes as age, design code used, structural type and materials. The decision not to pursue elaborate bridge classifications at this time is made primarily because doing so requires significant effort and a detailed database, and partly because some of potentially many classes of bridges thus created will consist of statistically too small a number of

bridges to permit a meaningful statistical analysis. Hence, the usage of current fragility analysis is limited to a population of Caltrans' bridges which are assumed to have a statistical homogeneity, although its application in the ensuing transportation systems and socio-economic analyses still produce quite revealing and useful results.

HYPOTHESIS TESTING AND CONFIDENCE INTERVALS

The issues of hypothesis testing and confidence intervals as they relate to fragility curve development have not been addressed so far primarily because the earthquake engineering community has never had the opportunity to collect damage database of a sufficiently large size that can be used to develop fragility curves on the basis of legitimate statistical analysis. However the 1994 Northridge and 1995 Kobe earthquake, inflicting devastating damage upon many buildings, bridges, port facilities, other engineered structures and natural environment, made it possible to apply statistical methods to analyze the probabilistic characteristics of damage in a more judicious fashion rather than relying on an ad hoc curve fitting exercise.

Test of a Goodness of Fit

The fundamental probabilistic interpretation of a fragility curve P(a) as a function of "a" suggests that a structure (or a bridge in the present study) will sustain a designated state of damage with probability P(a) and will not sustain the damage state with probability $1 - P$(a) under the earthquake intensity represented by PGA equal to "a". This means that, under each PGA value, the probabilistic phenomena one deals with can be described by random variable X_i following the Bernoulli distribution such that $X_i = 1$ when the state of damage is reached under PGA = a_i and $X_i = 0$ otherwise. Then,

$$\chi_i^2 = (X_i - p_i)^2 \tag{4}$$

has mean and variance equal to

$$\mu_{\chi_i^2} = p_i(1 - p_i) \tag{5}$$

and

$$\sigma^2{}_{\chi_i^2} = Var(\chi_i^2) = p_i(1 - p_i)(1 - 2p_i)^2 \tag{6}$$

,respectively, where $p_i = P(a_i)$. This should not be confused with the well known χ^2 statistic.

The sum of χ_i^2 shown below

$$\chi^2 = \sum_{i=1}^{N}(X_i - p_i)^2 \tag{7}$$

approaches asymptotically Gaussian as N becomes large where N is the sample size (the total number of the bridges considered) and in this analysis it is indeed a large value (>>1).

Recalling X_i is independent of X_j ($i \neq j$) and governed by the Bernoulli distribution, a straightforward analysis shows that the expected value $\mu_{\chi^2} = \mathrm{E}(\chi^2)$ and the variance $\sigma^2_{\chi^2} = \mathrm{var}(\chi^2)$ can be written as

$$\mu_{\chi^2} = \mathrm{E}(\chi^2) = \sum_{i=1}^{N} p_i(1-p_i) \tag{8}$$

and

$$\sigma^2_{\chi^2} = \mathrm{var}(\chi^2) = \sum_{i=1}^{N} p_i(1-p_i)(1-2p_i)^2 \tag{9}$$

On the other hand, if x_i represents the realization (observation) of X_i , then

$$x^2 = \sum_{i=1}^{N} (X_i - p_i)^2 \tag{10}$$

is the realization of χ^2.

Since p_i depends on the values of c_0 and ζ_0, the standard procedure of hypothesis testing suggests that if α is a significance level and

$$P_{\chi^2} = \Phi\left(\frac{x^2 - \mu_{\chi^2}}{\sigma_{\chi^2}}\right) \geq 1-\alpha \tag{11}$$

then, the hypothesis that c_0 and ζ_0 are indeed the true values of c and ζ will not be accepted with the significance level α usually set equal to 0.05 or 0.10. For the four fragility curves shown in figure 1, the values of P_{χ^2} are

$P_{\chi^2} = 0.638$	for minor (and severer) damage
$= 0.668$	for moderate (and severer) damage
$= 0.548$	for major (and severer) damage
$= 0.497$	for collapse

with all cases passing the test of goodness of fit at the significance level of 10%.

Confidence Intervals

The estimators $\hat{c}$ and $\hat{\zeta}$ of c and ζ cannot be explicitly given in terms of analytical forms as they represents optimal solutions obtained numerically by solving equation 3. Since the confidence intervals pertain directly to the uncertainty associated with c_0 and ζ_0, it is most desirable to demonstrate the extent of the statistical variations of these estimators. To this end, Monte Carlo simulation techniques are used to generate realizations of $\hat{c}$ and $\hat{\zeta}$. This calls for the simulation of X_i at each a_i using p_i based on c_0 and ζ_0. Upon simulating X_i for all a_i and obtaining their realizations ξ_i (i = 1, 2,...,N), equation 3 is solved for estimations c_0' and ζ_0' of c and ζ utilizing the values of ξ_i (rather than x_i).

Repeating this process a large number k of times (say, k = 1,000), one obtains the k sets of realizations of c_0' and ζ_0' as plotted in figure 4 with k = 1,000. Leaving the detailed analysis to a later study, it appears prudent to choose, by observation, c =0.8g and ζ = 0.80 for constructing a pessimistic fragility curve for the state of minor damage, and c = 1.2g and ζ = 1.10 for an optimistic fragility curve. The difference between these two curves indicates a confidence band (of the fragility curve constructed based on c_0 and ζ_0) in an engineering sense. A later analysis will define the confidence band associated with a more rigorously defined level of confidence utilizing two-dimensional distribution of $\hat{c}$ and $\hat{\zeta}$.

Only for the purpose of gaining insight to this issue of statistical confidence, the pessimistic and optimistic fragility curves corresponding to the one associated with the minor state of damage are plotted in figure 5 together with the (solid) curve replotted from figure 1. The confidence analysis described here will have a significant impact on the way in which the results of the ensuing socio-economic analysis are interpreted.

DEMONSTRATION OF EFFECTIVENESS OF PROTECTIVE SYSTEMS

A representative bridge with a precast presstressed continuous deck in the Memphis area studied by Jernigan and Hwang [1] is shown in figure 6 where the plan, elevation and column cross-section are depicted. Other pertinent structural and material data are given in table 1. It is noted that the strength f_c' of 3000 psi concrete used for the bridge is assumed to be best described by a normal distribution with a mean average strength of 4500 psi and a standard deviation of 900 psi, and that the yield strength f_y of grade 40 reinforcing bars used in design is best described by a log normal distribution having a mean strength of 48.8 ksi with a standard deviation of 5.22 ksi. Then, a sample of ten nominally identical but statistically different bridges are created by generating ten sample values each of and f_c' according to respective probability distribution functions assumed.

For the seismic ground motion, the time histories generated by Hwang and Huo [2] at the Center for Earthquake Research and Information at the University of Memphis are used. These time histories are generated by making use of the Fourier acceleration amplitude on the base rock derived under the assumption of a far-field point source by Boore [3]. In fact, the study area is located 40 km to 100 km from Marked Tree, Arkansas, the epicenter for all the scenario earthquakes considered in this study. Upon using seismologically consistent values for the parameters in the Boore and other related models and converting the Fourier amplitude to the power spectrum, corresponding histories are generated on the base rock by means of the spectral representation method by Shinozuka and Deodatis [4]. The seismic wave represented by these time histories is propagated through the surface layer to the ground surface by means of the SHAKE 91 computer code (Idriss and Sun [5]) and used, upon modulating in the time domain, for the response analysis. A sample of 10 time histories each representing the following six (6) combinations of M (magnitude) and R (epicentral distance); M = 6.5 with R = 80 km and 100 km, M = 7.0 with R = 60 km and 80 km, M = 7.5 with R = 40 km and 60 km, and M = 8.0 with R = 40 km and 60 km.

Typical ground motion time histories for two combinations M = 7.5 and R = 40 km and M = 6.5 and R = 100 km are shown in figure 7. A sample of ten time histories generated from each M and R combination is matched with a sample of ten bridges in the Latin Hypercube format. The spectral accelerations averaged over 50 acceleration time histories generated by Hwang and Huo [2] from each of the combinations M=7.5 for R=40, 60, 80 and 100 km are shown in figure 8.

The state of damage considered are major (three sets of columns all subjected to the ductility demand ≥1 and minor (the set in the middle subjected to the ductility demand ≥1, but not the two sets on the side) to the longitudinal applications of ground motion. The analysis performed under the ground motion in the transverse direction produced lesser degrees of damage state and hence not reported in this paper. The fragility curve for the state of major damage is plotted in figure 9. Two types of base isolators are considered for analysis with their dynamic/mechanical properties listed in table 2. Two fragility curves corresponding to these isolator types (cases 1 & 2) are plotted in figure 9 which clearly demonstrate the effectiveness of the base isolators. The extent of deformation the base isolators are allowed to undergo is an integral part of design consideration, and due attention should be paid to this issue also from safety point of view. Therefore, it is necessary for the type of analysis performed here to take this into consideration for the fragility curve development. This issue will be addressed in a later study.

CONCLUSIONS

This study empirically developed four fragility curves associated with four different states of damage for Caltrans' bridges utilizing the damage data complied by Caltrans for

the 1995 Northridge earthquake event. Two parameter log-normal distribution functions were used to represent the fragility curves with the two parameters estimated by the maximum likelihood method treating each bridge damage event as a realization from a Bernoulli distribution. The goodness of fit of each of the four fragility curves was tested favorably at a significance level of 10% by computing an appropriate sample statistic. An engineering confidence band was also established for the two parameters. Then, the effectiveness of base isolators to protect bridges from earthquake damage was demonstrated in terms of fragility curve enhancement by performing dynamic analysis of bridges in a Monte Carlo simulation. While the numerical result presented here needs to be extended further for generalization, the conceptual and theoretical treatment dealt in this study is believed to provide analytical tools of lasting usefulness for fragility curve development.

REFERENCES

1. J. B. Jernigan and H. M. Hwang, "Inventory and Fragility Analysis of Memphis Bridges", Center for Earthquake Research and Information, The University of Memphis, Technical Report, September 15, 1997.

2. H. Howard, M. Hwang and Jun-Rong Huo, "Simulation of Earthquake Acceleration Time Histories," Center for Earthquake Research and Information, The University of Memphis, Technical Report, July 25, 1996.

3. D. M. Boore, "Stochastic Simulation of High-frequency Ground Motions Based on Seismological Models of the Radiation Spectra," Bulletin of the Seismological Society of America, 73, 1865-1894, 1983.

4. M. Shinozuka and G. Deodatis, "Simulation of Stochastic processes by Spectral Representation," Applied Mechanics Reviews, Vol. 44, No. 4, April 1991, pp. 191-204.

5. I. M. Idriss, and J. I. Sun, "SHAKE91, a Computer Program for Conducting Equivalent Linear Seismic Response Analyses of Horizontally Layered Soil Deposits, User's manual," Center for Geotechnical Modeling, Department of Civil and Environmental Engineering, University of California, Davis, CA, 1992.

ACKNOWLEDGMENT

This study was supported by the Multidisciplinary Center for Earthquake Engineering Research under the auspices of the Federal Highway Administration under FHWA Contract No. DTFH61-92-C-00106 and also by the National Science Foundation under Grant No. NSF-CMS-9633386.

Testing of Bridges with Isolation/Dissipation Devices at the ELSA Laboratory

Artur V. Pinto, Paolo Negro and Fabio Taucer

ELSA-Structural Mechanics Unit, ISIS,
Joint Research Centre, European Commission, TP 480, 21020 Ispra (VA), Italy

Abstract

Large-scale pseudo-dynamic (PsD) tests on seismically isolated bridges were recently carried out at the ELSA Laboratory. Two alternative solutions were adopted, one solution with isolation/dissipation (I/D) devices over the abutments and over all piers, and another solution with I/D devices over the central short pier only, where the demands concentrated for the conventionally designed structure. The main aim of the test campaign was to assess the seismic performance of two isolation schemes for irregular bridges against the behavior of geometrically similar ones designed following the classical strength reduction factor approach.

As expected, the dissipation of energy was totally concentrated in the I/D devices and the bridge piers were completely protected. It is however important to underline that the fully isolated bridge requires significant clearances at the abutments in order to accommodate the dynamic displacements in those zones. In addition to the fact that the partial isolation is more economical (one isolator against five for the full isolation solution), the partial isolation exploits in a more effective way the deformation capacity of the lateral piers.

The present paper describes the tests on isolated structures performed at ELSA and collects the most important findings concerning the feasibility of the PsD tests, and the characteristics and effectiveness of the isolation systems.

INTRODUCTION

The ELSA Laboratory is involved in several projects aiming at the mitigation of the seismic risk of existing and new constructions. In particular, ELSA is performing large/full-scale tests on structures (buildings, bridges) [1] [2] in order to contribute to the calibration of Eurocode 8, the European design code for structures in earthquake prone regions.

Concerning structures with isolation/dissipation (I/D) devices, recent tests were carried out and devoted to the use of seismic devices in irregular bridges [3].

Two alternative solutions were adopted for the bridges: the first solution included I/D devices over the abutments and over all piers -labeled Full-Isolation (FI)- and the second solution included I/D devices over the central short pier only -labeled Partial-Isolation (PI)-, where seismic demands for the conventionally designed structure were concentrated. The main aim of the test campaign of the bridges with isolators was, therefore, to assess the seismic performance of two isolation schemes for irregular bridges against the behavior of geometrically similar ones designed following the classical strength reduction factor approach.

The experimental part of the research program on bridges included shaking table tests performed at ISMES, Bergamo, Italy and pseudo-dynamic (PsD) tests of six bridge models carried out at Ispra (JRC-ELSA). In particular, a series of tests devoted to the regularity issue for bridges [4] were carried out, which are the object of this paper. Detailed results on the testing campaign at ELSA and corresponding analysis can be found in [8], [9] and [10].

THE LARGE-SCALE TESTING PROGRAM

The testing program at ELSA included a preliminary cyclic test of one squat pier, and PsD tests on six complete structures, representative of typical multi-span continuous-deck motorway bridges. The deck was made up of a hollow-core pre-stressed concrete girder, with a full-scale width of 14 m. The deck ended at the abutments with shear-keys, to allow end rotations. The bridges had four identical spans of 50 m, for a total length of 200 m.. The piers had a constant

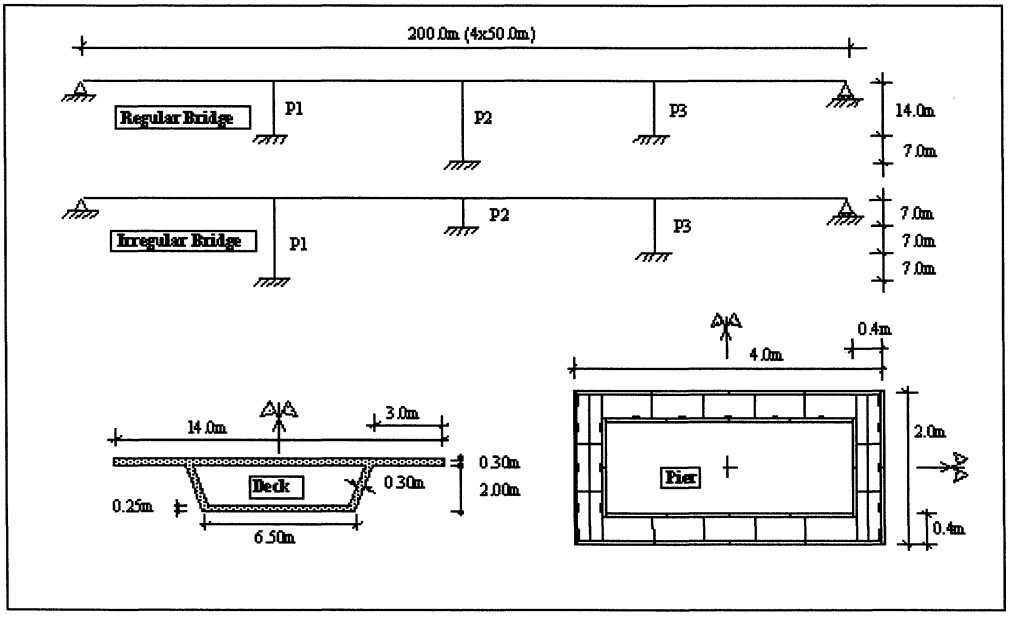


Figure 1: Full-scale schemes of the bridges tested pseudodynamically.

rectangular reinforced concrete (RC) hollow-core cross-section of 400 mm thickness, with heights ranging from 7 to 21 meters. The schemes of the full-scale bridges are shown in Figure 1. The geometric and reinforcement characteristics of the piers are shown on Table 1.

Table 1: Bridges tested pseudodynamically

Bridge Identification Label	Pier 1		Pier 2		Pier 3	
	Full-size height [m]	Steel percentage	Full-size height [m]	Steel percentage	Full-size height [m]	Steel percentage
B232	*14.0*	*1.15*	*21.0*	*0.62*	*14.0*	*1.15*
B213A	*14.0*	*0.50*	*7.0*	*0.92*	*21.0*	*0.50*
B213B	*14.0*	*0.50*	*7.0*	*1.69*	*21.0*	*0.50*
B213C	*14.0*	*1.15*	*7.0*	*0.50*	*21.0*	*1.15*
B213A I/D	*14.0*	*0.50*	*7.0*	*0.92*	*21.0*	*0.50*

Two different schemes were adopted, having in mind to test the structures in the direction orthogonal to the bridge axis. The first scheme represented a regular configuration and corresponds to a bridge for which the fundamental deflected shape of the deck alone is similar to that of the complete structure (i.e. a symmetric bridge having the tallest pier in the center). The second scheme represented an irregular configuration and corresponds to a bridge for which the first mode of the structure is very different from the first-mode deflected shape of the deck alone. The bridge was non symmetric with the shortest pier in the middle, resulting in much higher forces in the central, stiffer pier.

As shown on Table 1, six bridge specimens were tested. The numbers appearing in the test identification labels represent the height modules in each of the three piers. The height module was 7 meters for the full-scale bridges, thus bridge B232, corresponding to the regular bridge, had piers of 14, 21 and 14 meters high respectively. The other bridges -with 213 in the label- were irregular, with piers of 14, 7 and 21 meters high respectively. A scale factor of 1:2.5 was selected for the testing of the bridge prototypes in the laboratory.

The letters A, B and C in the label refer to the different design approaches. The label B213A stands for standard design according to EC8, Part 2. The bridge B213B corresponded to the most straightforward design solution to the high ductility demands expected for the central pier, i.e. the central pier has been made stronger. In bridge B213C the taller piers have been made stronger instead, in an attempt to relieve the central pier from relatively high forces.

The other bridge specimen (B213A I/D) was identical to specimen B213A, but was tested with seismic isolation devices.

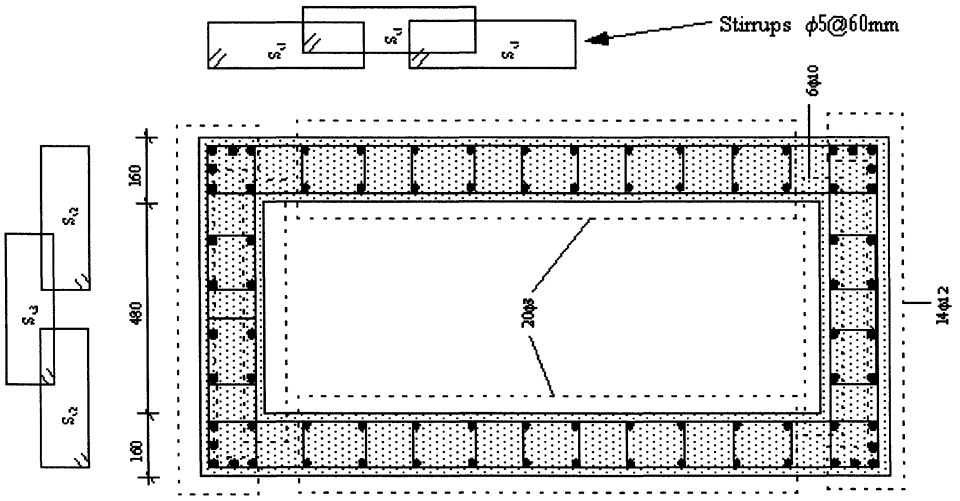


Figure 2: Typical reinforcement lay-out, 1:2.5 scale (central pier of B213A).

The design of the piers was first carried out according to the current version of EC8, Part 2, Bridges [2]. As for the irregular structure, two different design approaches, non Eurocode 8-conforming, were adopted, based on the findings of the preliminary non-linear analyses. These may represent the two possible conceptual solutions to the irregularity issue. In one case (B213B), the reinforcement percentage of the shortest pier was significantly increased (from 0.92% to 1.69%), with the aim to reduce the high ductility demand which was anticipated in the analysis. For the remaining case (B213C), the strength of the taller piers was increased (from 0.50% to 1.15%), so that the forces attracted by the shortest pier can, in principle, be reduced. A typical cross section layout of the tested models is shown in Figure 2.

The bridge B213A, corresponding to the standard application of the design code, was also tested with the view of including non-synchronous base-motions and seismic isolation devices. No special provisions were, however, included in the design.

IMPLEMENTATION OF THE PSEUDODYNAMIC TEST METHOD

Pseudo-dynamic Testing

A PsD test is one, which, although carried out quasi-statically, uses on-line computer calculation and control together with experimental measurement of the actual properties of the structure to provide a realistic simulation of the dynamic response. The equations of motion for a discrete parameter model of the test structure are solved on-line using a step-by-step numerical time integration method. Inertial and viscous damping forces are modeled analytically - a relatively straightforward matter compared to the non-linear structural restoring forces, which are measured experimentally because of the practical impossibility of modeling them accurately. The process automatically accounts for the hysteretic damping due to inelastic deformation and damage of the structural materials, which is the major source of energy dissipation.

To simulate the earthquake response of a structure, a record of an actual or artificially generated earthquake ground acceleration history is given as input data to the computer running the PsD algorithm. The horizontal displacements of the controlled degrees of freedom (where the mass of the structure can be considered to be concentrated) are calculated for a small time step using a suitable time integration algorithm. These displacements are then applied to the test structure by servo-controlled hydraulic actuators fixed to the reaction wall. Load cells on the actuators measure the forces necessary to achieve the required displacements and these structural restoring forces are returned to the computer for use in the next time-step calculation. Details of the capabilities of the ELSA Laboratory and of the PsD implementation are given elsewhere [6].

Substructuring Technique

The PsD test method is a hybrid technique, which combines the numerical integration of equations of motion of complex structures condensed on a reduced number of degrees-of-freedom (d.o.f.), with the experimental measurement of the reaction forces resulting from this motion. Despite the potential of the PsD technique, direct testing of very large civil engineering structures like bridges would require a number of controlled d.o.f. that could exceed the experimental capabilities. It is, however, possible to extend the field of application of the method, at least when the behavior of a part of the structure is well known, by introducing a substructuring technique [5]. This technique takes advantage of the hybrid character of the PsD test method by combining the numerical simulation of the known part of the structure, the substructure, with the physical testing of the remaining structural part, the tested structure. The method is well suited for bridges since their largest part, the deck, can be assumed to be linear elastic and therefore modeled by any finite-element software: only the piers, whose dimensions remain reasonably small, and where damage is expected, are tested in the laboratory.

A further advantage, which is again well suited for bridges, is the possibility of dealing with situations where the seismic excitation is asynchronous or presents different amplitudes along the foundation.

The use of substructuring techniques in PsD testing implies, for the substructure, a model and the time integration of its spatially discrete equations of motion. This model may present a number of d.o.f. greater, by some orders of magnitude, than the number of nodes actually controlled by the PsD algorithm. Thus, if the substructure were handled by a Personal Computer (PC) program driving the PsD algorithm, the current capabilities of this controller program could easily be exceeded. To overcome this difficulty, the adopted strategy was to have two processes running in parallel: the one responsible for the PsD algorithm running in the PC (controller) and the other, responsible for the substructure, running in a remote workstation and communicating between them using standard network capabilities such as Berkeley sockets.

Consider the following system of semi-discrete differential equations:

$$Ma + Cv + r(d) = f \tag{1}$$

which describes the motion of a structure with m degrees-of freedom, where a, v and d represent the acceleration, the velocity and the displacement vectors, r and f the structural internal force and external force vectors, M and C are the mass and damping matrices.

To solve the system of Equation 1, a numerical step-by-step integration method is adopted. The displacement and velocity vectors at step *(n+1)* can be written in terms of the acceleration vector and the previous step values which, when introduced in Equation 1, lead to a discrete system of linear equations at time *(n+1)*:

$$\hat{M} a_{n+1} = \hat{f}_{n+1} \tag{2}$$

where

$\hat{M}$ is a pseudo mass matrix and $\hat{f}_{n+1}$ a pseudo force vector.

Distinguishing between the quantities coming from the substructure *(S)* and the tested structure *(T)*, the system of Equation 2 may be rewritten as

$$\begin{bmatrix} {}^{S}\hat{M}_{ij} & {}^{S}\hat{M}_{i\beta} & 0 \\ {}^{S}\hat{M}_{\alpha j} & {}^{S}\hat{M}_{\alpha\beta} + {}^{T}\hat{M}_{\alpha\beta} & {}^{T}\hat{M}_{\alpha J} \\ 0 & {}^{T}\hat{M}_{I\beta} & {}^{T}\hat{M}_{IJ} \end{bmatrix} \bullet \begin{bmatrix} a^{j}_{n+1} \\ a^{\beta}_{n+1} \\ a^{J}_{n+1} \end{bmatrix} = \begin{bmatrix} {}^{S}\hat{f}^{j}_{n+1} \\ {}^{S}\hat{f}^{\beta}_{n+1} + {}^{T}\hat{f}^{\beta}_{n+1} \\ {}^{T}\hat{f}^{J}_{n+1} \end{bmatrix} \tag{3}$$

where i, j, refer to the internal d.o.f of the substructure, α, β to the common connection d.o.f. and I, J to the internal d.o.f. of the tested structure.

Condensing the unknowns a_j the controlling equation becomes

$$\begin{bmatrix} {}^{T}\hat{M}_{\alpha\beta} + ({}^{S}\hat{M}_{\alpha\beta} - {}^{S}\hat{M}_{\alpha j}\, {}^{S}\hat{M}^{-1}_{ji}\, {}^{S}\hat{M}_{i\beta}) & {}^{T}\hat{M}_{\alpha J} \\ {}^{T}\hat{M}_{I\beta} & {}^{T}\hat{M}_{IJ} \end{bmatrix} \bullet \begin{bmatrix} a^{\beta}_{n+1} \\ a^{J}_{n+1} \end{bmatrix} = \begin{bmatrix} ({}^{S}\hat{f}^{\alpha}_{n+1} - {}^{S}\hat{M}_{\alpha j}\, {}^{S}\hat{M}^{-1}_{ji}\, {}^{S}\hat{f}^{i}_{n+1}) + {}^{T}\hat{f}^{\alpha}_{n+1} \\ {}^{T}\hat{f}^{I}_{n+1} \end{bmatrix} \tag{4}$$

and the substructure is governed by

$${}^{S}\hat{M}_{ij}\, a^{j}{}_{n+1} = {}^{S}\hat{f}^{i}_{n+1} - {}^{S}\hat{M}_{i\beta} a^{\beta}_{n+1} \tag{5}$$

Equation 4 points out the differences between the conventional PsD test case and the one with substructuring. In the substructuring case, the pseudo mass matrix is modified by adding the term within parentheses supplied by the substructure process. In addition, at each time step, the pseudo force vector includes the terms from the substructure. The equation governing the substructure (Equation 5) requires the acceleration at the connection nodes.

Details of the ELSA implementation of PsD testing with substructuring are given in [6].

Test set-up

The piers were aligned in front of the reaction wall, with the shorter one in the middle, as shown in Figure 3. The plinths of the piers were rigidly attached to the strong floor by means of steel

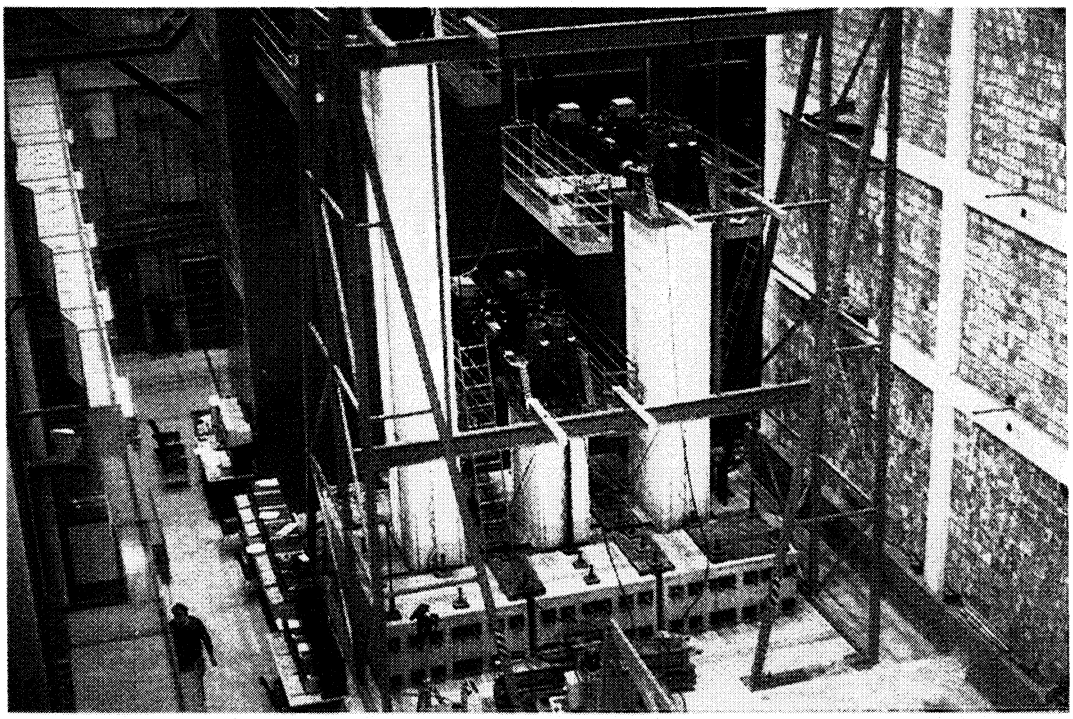


Figure 3: Test set-up for the PsD tests of the irregular bridge prototypes.

bars passing through the floor itself. A stiff steel cap was connected with bolts and epoxy resin to the top of the piers. The cap was used to apply the vertical load corresponding to the weight of the deck, as well as to apply the horizontal loads required to impose the computed displacements.

The pier axial force (1700 kN) was applied by means of vertical actuators connected to the cap, placed inside the hollow core pier with instrumented steel bars embedded in the pier plinth. The vertical force was imposed at the beginning of the test and remained practically constant by means of the hydraulic accumulators that compensated the effects of the horizontal displacement.

Two double-acting servo-hydraulic actuators (three for the central pier in the test B213B), each one capable of applying a load of 1.0 MN, were used to impose the horizontal displacements. They were connected by spherical joints to the steel cap at one side, and to a steel plate attached to the reaction wall at the opposite side. The imposed displacements were measured with respect to two independent steel frames using digital optical transducers.

Instrumentation

The instrumentation of the piers included both active measurements -those which are related to the PsD control algorithm-, and passive instruments. Passive instruments can be grouped in four sets. *Rotations*: pairs of displacement transducers were placed at different levels on the two external opposite faces of the specimens to measure local rotations. Additional pairs of transducers were placed to monitor unexpected orthogonal rotations. Another set of transducers was used to measure both the total rotation of the pier and its elongation. *Diagonal deformations:* the two diagonals were instrumented to measure shear deformations. *Horizontal displacements*: another set of transducers were placed at different levels between the side of the pier and a steel bar connected with swivel joints to the base and to the cap. This allowed to monitor the deflected shape. *Section warping: a* set of transducers were placed on the same horizontal basis to follow the in-plane deformation of the cross-section, enabling to measure the section warping due to shear.

PSEUDO-DYNAMIC TESTS ON THE CONVENTIONAL RC BRIDGES

Input Motion and Testing Procedure

The tests used one of the artificial accelerograms used in the analysis, with a nominal peak acceleration of 0.35 g. The accelerogram is depicted in Figure 4, together with the corresponding elastic response spectrum. The accelerogram was intended to fit the response spectrum specified in EC8 for peak ground acceleration 0.35 g and medium soil conditions.

The mass matrix used in the substructured part was scaled by λ^3, λ=2.5 being the geometrical scale factor, consequently the ordinates of the accelerogram were multiplied by λ, and the time scale was accordingly reduced. The original accelerogram of ten seconds became 4 seconds long. The axial load applied by the vertical actuators was independent from the mass values. A constant value of 1700 kN was applied, to keep the normalized axial load the same as in the real structure (ν=0.1).

No specific testing procedure (type of loading and corresponding intensity) is presently available for dynamic tests of earthquake resistant structures. In principle, the testing procedure is tailored to the general objectives of the tests that must be well clarified in advance.

Concerning the PsD testing of the bridges the main objectives are recalled: evaluation of the seismic performance of bridges designed in accordance with the present version of EC8; comparison of three design solutions for irregular bridges; evaluation of safety margins for each design solution.

Thus, it was decided to test the bridges using first the 'design earthquake' as input motion and then an intensity of the input motion as close as possible to the one causing failure (high level earthquake). Additionally, for the set of irregular bridges the intensity of the high level earthquake was tailored to the weak design solution (bridge B213C).

Accordingly and based on the numerical predictions [11], [12], the scaling factors adopted for the high level earthquake were 1.2 and 2.0 for the irregular and the regular bridges respectively. A smaller scaling factor would not have caused major damage to the regular bridge.

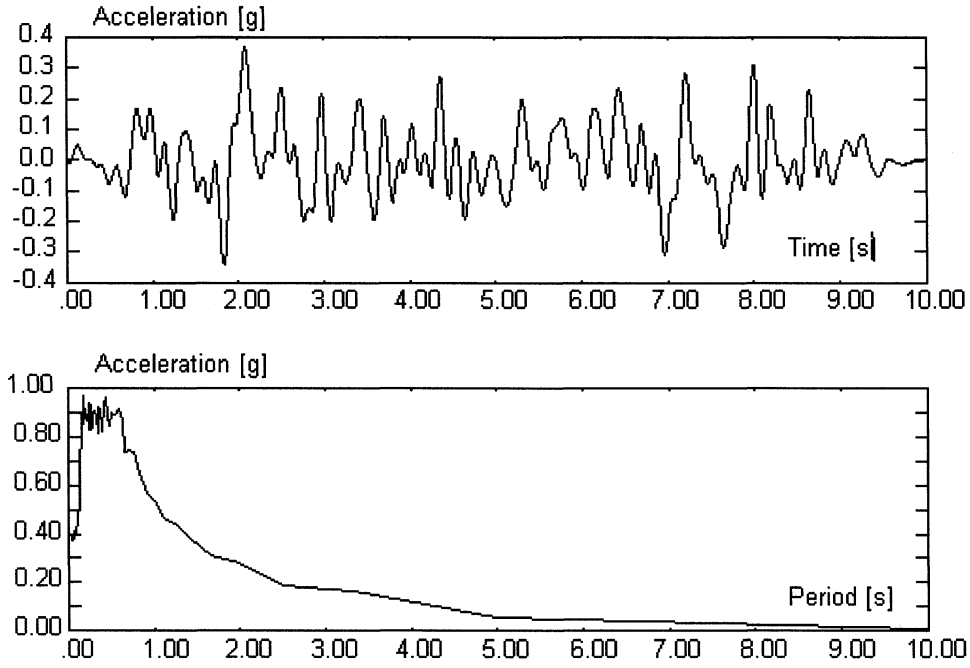


Figure 4: Artificial accelerogram and corresponding response spectrum (5% damping)

As expected, the external piers in bridge B213A did not suffer significant damage during the test with the reference accelerogram at the nominal intensity. Hence, they were used again in bridge B213B, and were also used in the tests with seismic isolation. The tests with the accelerogram multiplied by 1.2 were physically performed on the short pier only, by providing a numerical model for the other piers (bridges B213A and B213B). This was done by using the substructuring capabilities of the PsD implementation. A nonlinear elastic model, calibrated with the results of the 1.0 test was used.

Test Results for the Conventional Bridges

The extreme values of displacement, ductility and damage are given in Table 2; the damage index was computed from the Park and Ang model [7]. The displacement profiles of the three irregular bridges are shown on Figure 5 for the two earthquake levels. Representative results of the tests are given in Figures 6-7, in terms of global hysteresis loops

The results of the test on bridge B232 comply with the regularity issue, as mentioned in EC8, Part 2. The behavior of the bridge was considered ductile, with energy dissipation taking place at all piers. The energy dissipation mechanism was stable and efficient, with demands roughly proportional to capacities, and an input signal 2 times larger than the design signal was applied without loss of capacity.

In the case of test B213A the dissipation of energy was limited to the short pier. This corresponds to the situation for which a warning is issued in EC8, part 2: "*Behavior factors > 1.2 should not be used without special consideration, if the development of plastic hinges in the piers* [i.e. the lateral piers] *is not probable, because the piers do not reach yielding under the design seismic action*". The ductility demand on the short pier was, however, reasonably small.

In the test B213B the short pier, which was stronger than in the previous bridge, attracted much larger forces, but experienced considerably lower ductility demands. Again, energy dissipation took place in the short pier only. The crack pattern was found to be much more spread than in the previous test.

In test B213C, the goal to obtain a more regular force distribution was achieved. The distribution of the maximum bending moment among the piers was, in fact, fairly constant. Ductility demands in the short pier were, however, much larger than in test B213A. The advantages of the corresponding design approach are, therefore, debatable.

It should be underlined that the maximum values of ductility demand and damage index for the Design Earthquake are quite similar for all bridges (except for the ductility demand of Bridge B213C). However, the irregular bridges, tested with an input motion slightly higher than the design earthquake (1.2 times) and much lower than the intensity used for the regular bridge (2.0 times), were heavily damaged. The safety against collapse of the irregular bridges was quite low, compared to the safety level possessed by the regular bridge.

Table 2: Seismic response of the bridges (1:2.5 scale) for the two earthquake levels

Bridge Label	Pier	Design Earthquake			High Level Earthquake[1]		
		Top Disp. [m]	Ductility	Damage Index	Top Disp. [m]	Ductility	Damage Index
B232	*1*	*.044*	*1.4*	*.22*	*.089*	*2.8*	*.47*
	2	*.062*	*1.9*	*.34*	*.132*	*4.1*	*.79*
B213A	*1*	*.022*	*<1*	---	*(.029)*[2]	---	---
	2	*.024*	*2.0*	*.30*	*.052*	*4.0*	*.70*
	3	*.028*	*<1*	---	*(.050)*	---	---
B213B	*1*	*.025*	*<1*	---	*(.028)*	---	---
	2	*.023*	*1.5*	*.25*	*.043*	*2.5*	*.50*
	3	*.028*	*<1*	---	*(.048)*	---	---
B213C	*1*	*.017*	*<1*	*.09*	*.041*	*1.3*	*.22*
	2	*.020*	*4.2*	*.35*	*.057*	*11.9*	*1.03*
	3	*.026*	*<1*	*.09*	*.049*	*<1*	*.16*

1. 1.2 and 2.0 times the design earthquake respectively for bridge B232 and for the irregular bridges (B213A, B213B and B213C.

2. (.) Values obtained from the numerical model (pier substructured)

The test results confirm that the strategy adopted for the design of the bridge B213B, which corresponds to the use of a lower local behavior factor, is the 'less worse' and could lead to a suitable design approach for irregular bridges. An alternative solution for these highly irregular bridges lays on the use of Isolation/Dissipation devices, which was the object of the second part of the testing campaign in ELSA.

Finally it should be underlined that, after the PsD tests, the bridge piers were tested cyclically until collapse exhibiting a ductile behavior. This confirms the adequacy of detailing provisions included in Eurocode 8 for this kind of structures.

Detailed analysis of the PsD test results are reported elsewhere [9].

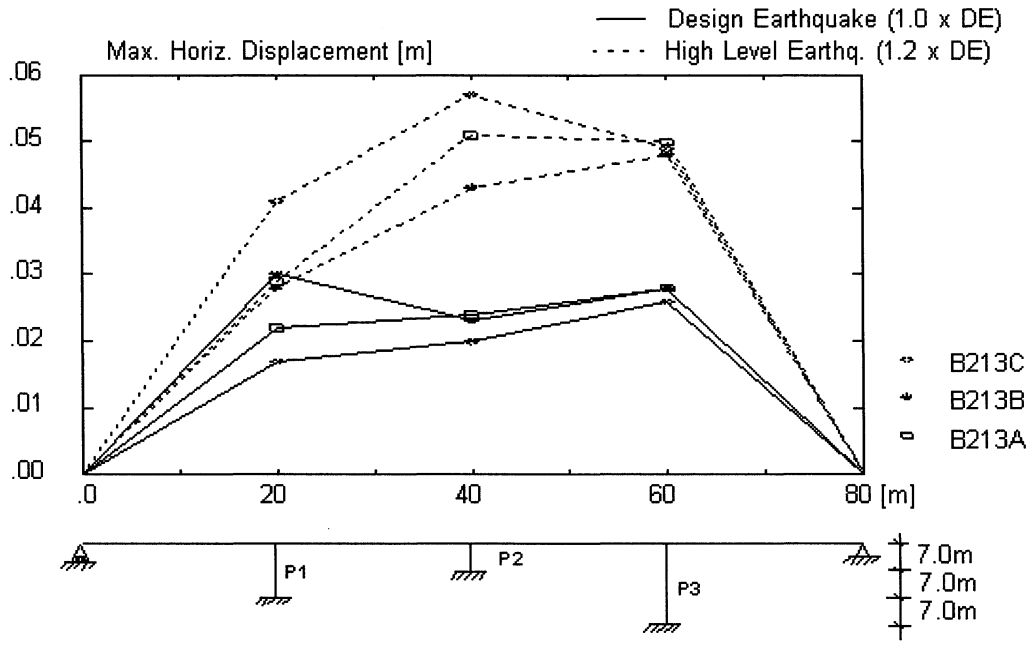


Figure 5: Displacement profiles of the 1:2.5 scale irregular bridges for the two earthquake intensities.

BRIDGES WITH ISOLATION/DISSIPATION DEVICES

The tests on the *conventionally* designed bridges concentrated on alternative design methods for irregular bridges, based on the use of non-uniform (local) behavior factors, while the second part of the test campaign, devoted to the irregularity issue, was concerned with the use of I/D devices.

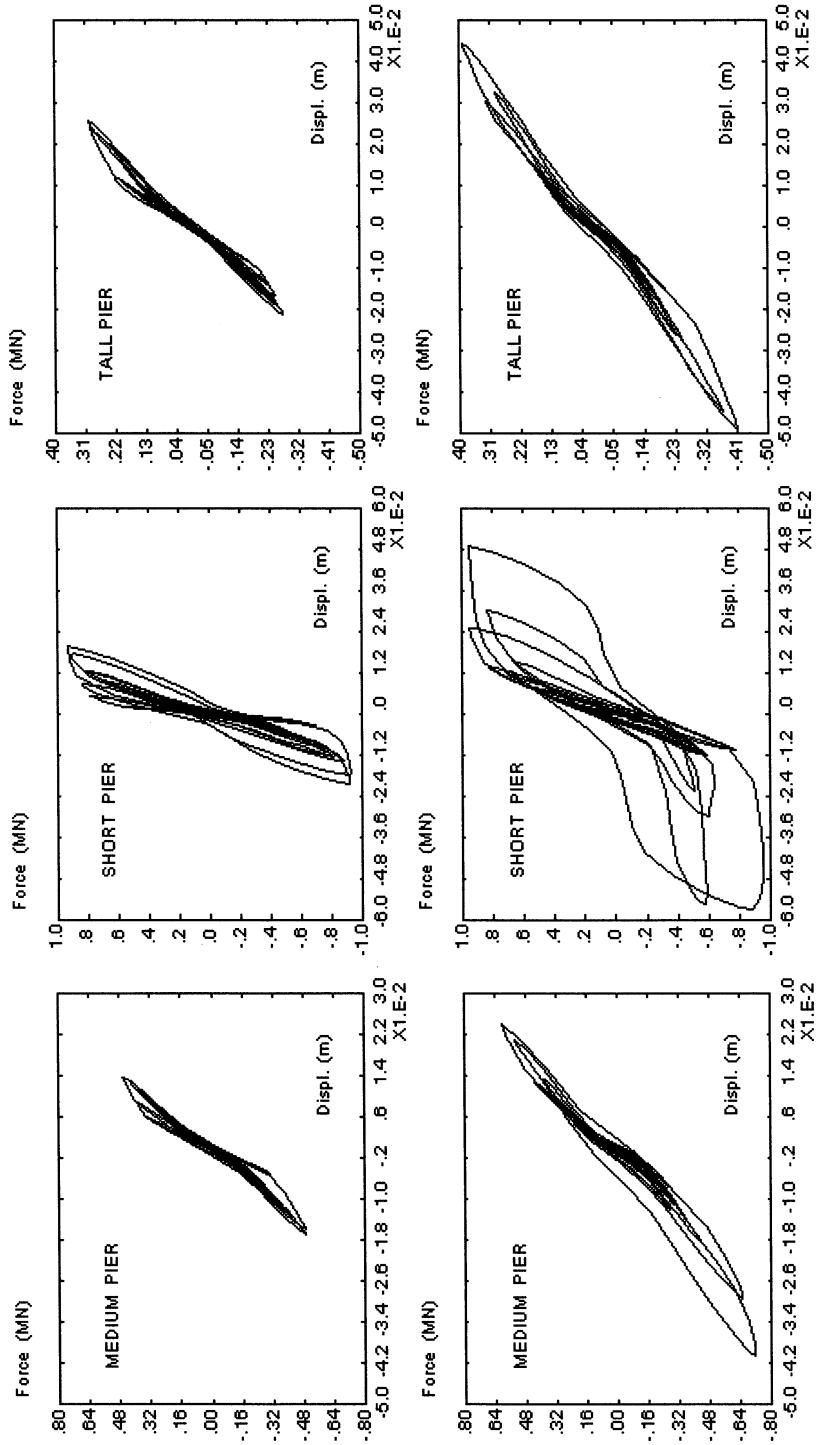


Figure 6: Force-displacement diagrams for piers of bridge B213C for the design earthquake (1.0xDE) and the high level earthquake (1.2xDE).

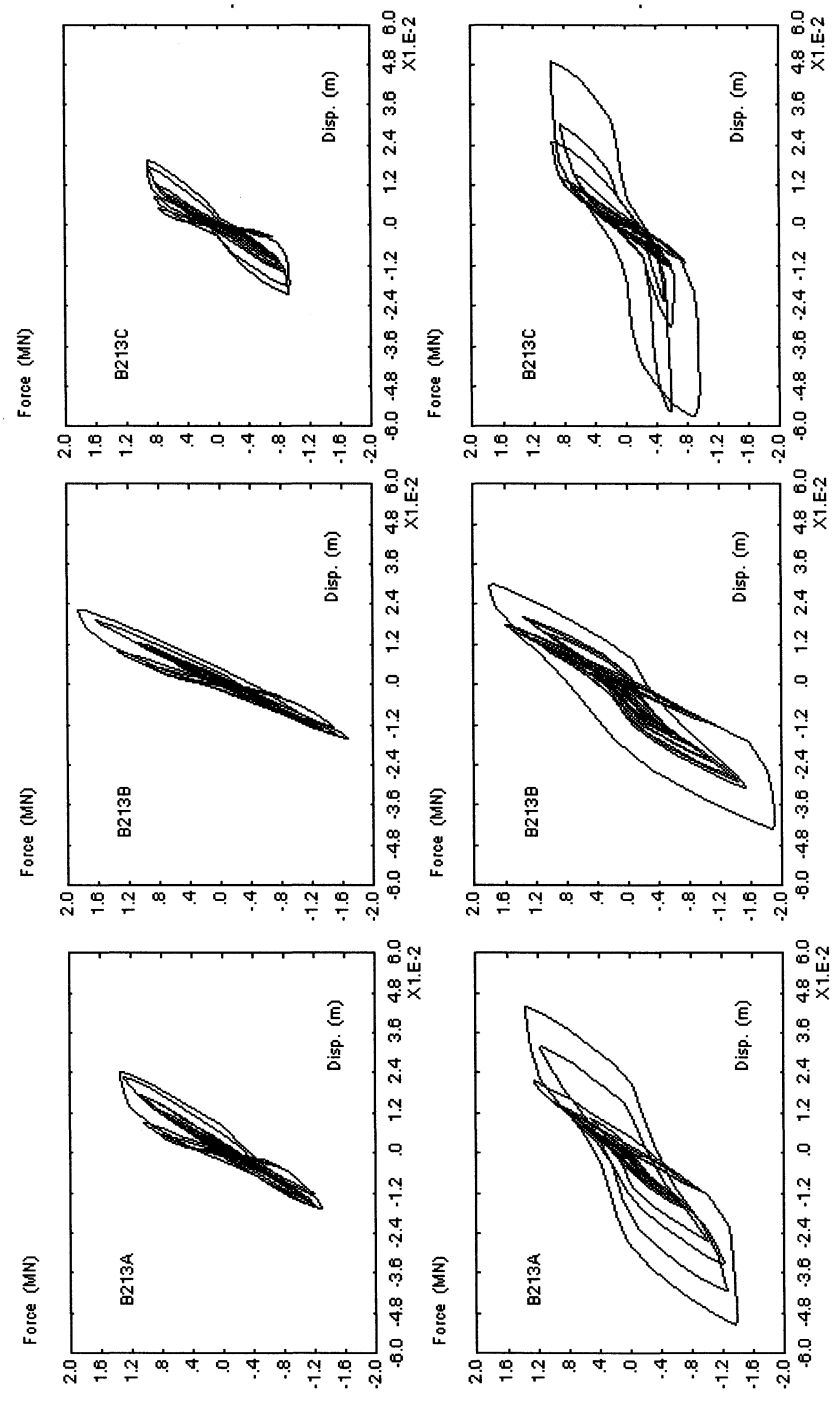


Figure 7: Force-displacement diagrams of the short piers of the irregular bridges for the two earthquake levels.

The scope of isolation systems is in general to reduce the force response and increase the global damping, while maintaining the stiffness of the whole system within acceptable values for service loading. The isolation system designed for the bridges tested at ELSA was essentially regarded as an alternative structural solution for highly irregular bridges. In fact, the previous tests on bridges without isolation confirmed that it is quite difficult to find suitable design solutions for very irregular bridges. In spite of the improved earthquake performance of the bridge designed with non-uniform strength reduction factors (Bridge B213B), the earthquake demands, for input accelerations higher than the design ones, were quite high compared to the ones of the regular structures. Therefore, the isolation appeared to be a potential and economical solution that to satisfies the requirements for an adequate seismic performance of such an irregular structure.

The Isolation System

Two isolation solutions, shown schematically in Figure 8, were adopted for the irregular bridge. One solution with I/D devices over the abutments and over all piers -labeled Full-Isolation (FI)- and another solution with I/D devices over the central short pier only, where demands concentrated in the conventionally designed structure. This solution was labeled Partial-Isolation (PI). Details on the design of the isolation systems can be found elsewhere [10].

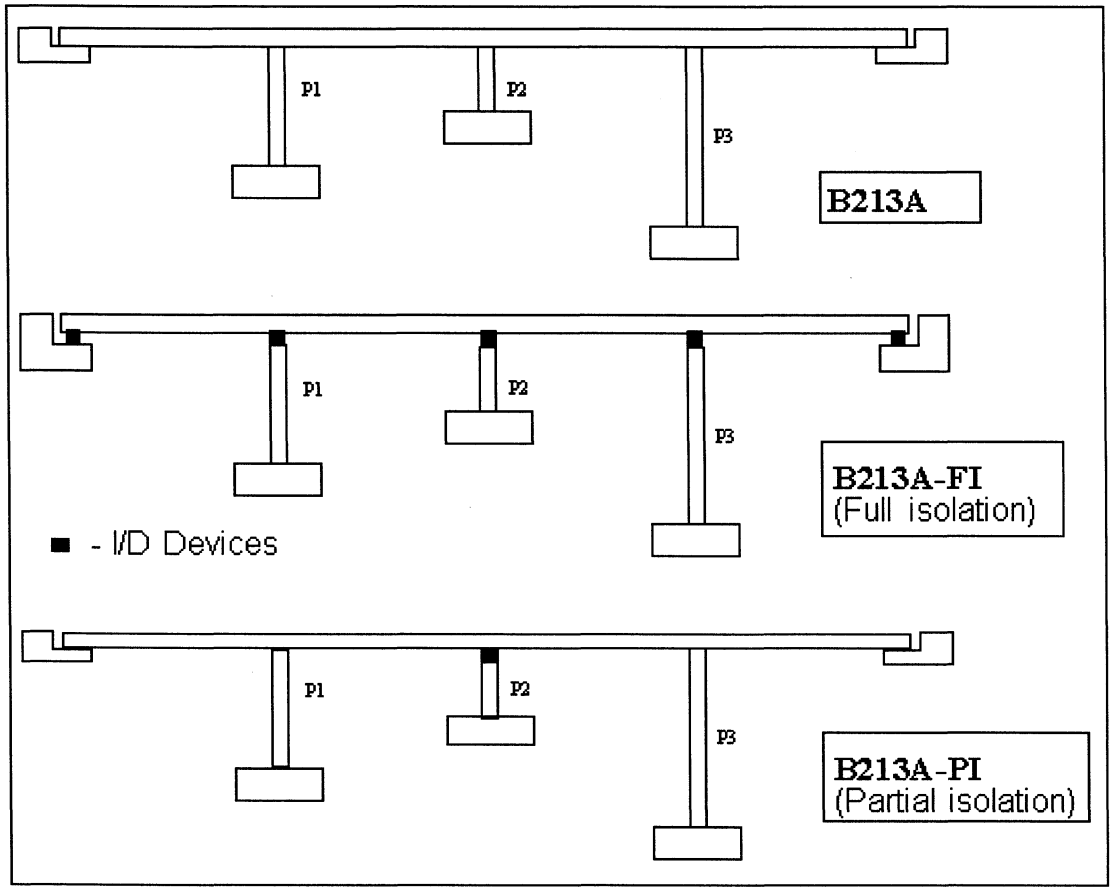


Figure 8: Schematic representation of the three test conditions: Conventionally designed bridge, fully isolated bridge and partially isolated bridges

The aim of the test campaign of the bridges with isolators was to assess the seismic performance of two isolation schemes for irregular bridges against the performance of geometrically similar bridges designed following the classical behavior factor approach.

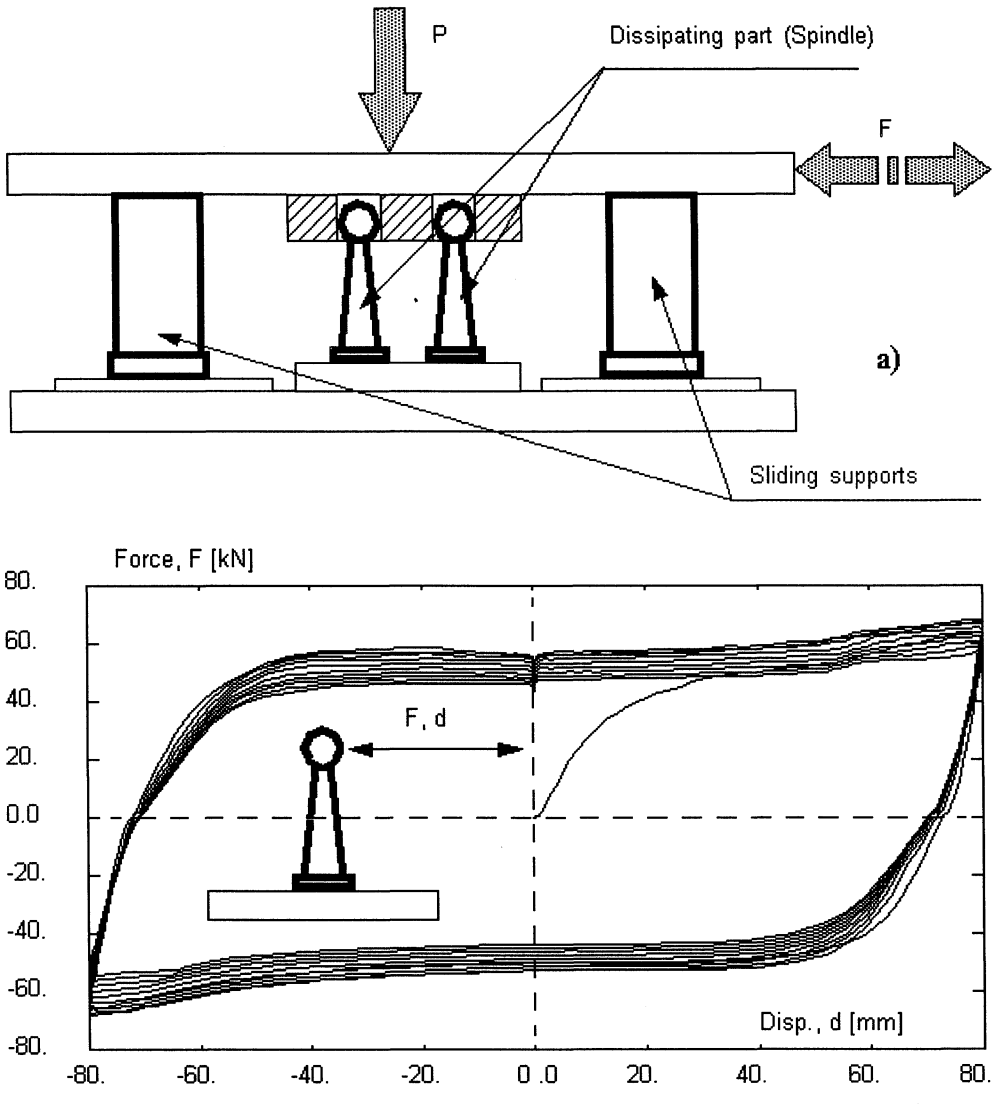


Figure 9: Isolation/Dissipation devices: a) Schematic representation and functioning b) Cyclic force displacement diagram for one dissipating element (spindle).

The adopted isolation/dissipation devices are represented schematically in Figure 9a. They are composed of two distinct mechanical parts. The first part is composed by sliding supports over teflon bearing pads designed to bear the vertical loading due to self weight of the superstructure and to service loads. The second part is composed by a dissipating component (spindle), intended as the device part where the energy dissipation, through significant plastic deformations, takes place. Furthermore, this part contributes to the lateral stiffness of the isolator.

The dissipating part is essentially composed of vertical ductile steel spindles (cantilever vertical beams) of non-uniform cross section. This geometric configuration induces spread plasticity, exploiting thus all the available dissipating potential of the spindle.

Each isolating device is composed by several dissipating elements. However, the behavior of the device, in terms of strength and ductility, can be characterized from the testing of one element only. A typical curve for one of these elements is presented in Figure 9. Very high ductility can be expected from these devices with a large number of quite stable dissipative loops.

It should be underlined that the use of these devices appears to be very promising for civil engineering applications. They are quite simple, with well-separated parts for load carrying and energy dissipation, and are fabricated using well-known conventional materials.

Test Set-up and Test Results

The test set-up for the bridges with I/D devices was similar to the one for the conventional bridges. However, the devices were positioned between the top of the piers and the steel cap, which moved up the load application point. Therefore, the effective height of the isolated piers was increased by about 340 mm. Furthermore, the test set-up for the fully isolated bridge (isolators over all deck supports) included two additional controlling actuators, one for each abutment, to impose to the isolators at the abutments the corresponding dynamic displacements.

The physical realization of the test set-up corresponding to the abutments was performed by fixing the base of the isolator to the reaction floor and connecting the upper part of the device to the servo-hydraulic actuator. As the vertical force, corresponding to the weight of the deck on the abutments, was not required (however, the same did not apply to the piers, because the axial force may play an important role in their non-linear behavior), the isolation devices for the abutments only comprised the dissipating part indicated in Figure 9; the sliding supports that carry the vertical loading were not included.

As mentioned above, the isolation of the bridges were essentially considered as a means of designing an irregular bridge for adequate earthquake performance. Therefore, the test sequence and the earthquake intensities considered in the tests on the previous non-isolated irregular bridges were assumed in the tests on the isolated ones. Thus, comparison of the seismic performance of the different design solutions becomes certainly easier.

Preliminary stiffness tests were performed on the bridge piers with and without earthquake isolators. From the results of these tests a decrease of the 'pier' stiffness with the isolators in place was apparent. The earthquake tests on the isolated bridges followed the stiffness tests mentioned above. The earthquake input signal with 10 seconds duration (prototype time-scale) used in the previous tests was also used for the tests with isolation. Furthermore, the two level earthquake intensity (design earthquake (DE) and 1.2 times the design earthquake) testing strategy was also maintained.

Table 3 gives the maximum displacements measured at the top of the piers for the three bridges for the two earthquake tests. For the isolated internal deck supports the displacements were split into pier and relative device displacements. The total displacement (deck displacement) can be obtained summing the two partial displacements.

Table 3: Maximum displacements for the isolated and non-isolated bridges for the two earthquake tests

Test	Bridge	Location	Displacement [cm]				
			Left Abutment	Medium Pier	Short Pier	Tall Pier	Right Abutment
1.0 x DE	***B213A***	*Pier*	-	*2.16*	*2.42*	*2.79*	-
	B213A/FI	*Device*[1]	*4.00*	*4.23*	*5.22*	*3.71*	*5.39*
		Pier	-	*0.64*	*0.21*	*1.90*	-
	B213A/PI	*Device*	-	-	*3.79*	-	-
		Pier	-	*2.50*	*0.28*	*3.68*	-
1.2 x DE	***B213A***	*Pier*	-	*2.95*	*5.15*	*4.99*	-
	B213A/FI	*Device*	*4.43*	*4.68*	*6.06*	*4.24*	*6.20*
		Pier	-	*0.90*	*0.26*	*2.27*	-
	B213A/PI	*Device*	-	-	*4.55*	-	-
		Pier	-	*2.99*	*0.29*	*4.23*	-

1 Relative displacement for the isolation/dissipation device

Figures 10-11 give more informative results concerning the overall earthquake behavior of the bridges. In fact, as expected, the dissipation of energy is totally concentrated in the I/D devices and the bridge piers have been completely protected. It is however important to underline that the fully isolated bridge requires quite important clearance at the abutments in order to accommodate the dynamic displacements in those zones.

A clear picture of the global behavior of the irregular bridges with and without isolators is given in the plots included in Figure 12. The envelop displacement profiles for the deck and for the top of the piers were plotted together, allowing for an easy comparison between the three design cases, namely: the conventionally design bridge (B213A), the bridge with isolators over the short central pier (B213A-PI) and the fully isolated one (B213A-FI). Looking at the deck displacements, it is apparent that the tendency for all cases is to approach the regular deformation of the deck similar to the deformation of the first mode of vibration, which is effectively controlled by the dynamic characteristics of this structural part. Concerning the top-pier displacements of the short central pier, extremely severe in the case of bridge B213A, there is clearly a significant reduction in the pier displacement demands for both isolated structures. In fact, the earthquake displacements of such a pier are insignificant. As shown in Figures 10-11,

the piers did not yield and the dissipation of energy concentrated in the isolation device, which was one of the basic assumptions in the design of the isolation system.

From the analysis of the test results of the isolated bridges it is possible to conclude that: a) Seismic isolation is an effective way to protect bridge structures against the damaging effects of earthquakes; b) Isolation can be considered as a very good alternative solution for irregular bridges. In fact, both isolation solutions regularize the earthquake behavior of the bridge; c) Furthermore, partial isolation (isolation of the critical piers) presents some advantages relatively to the full isolation. As confirmed by the test results, full isolation leads to considerably large displacements at the abutments, which may require large clearances to accommodate those displacements. In addition to the fact that partial isolation is more economical (one isolator against five for the full isolation solution), partial isolation exploits in a more effective way the deformation capacity of the lateral piers.

Finally, it should be underlined that the test set-up for this test campaign with isolators was particularly designed for horizontal loading only. Practical application of these I/D devices will require more detailed analysis considering for example, the effects of the vertical components of the seismic action, in order to avoid premature malfunctioning of the mechanical devices. An up-lifting of the upper plate of the devices would lead to a loss of horizontal stiffness of the bearing and would inhibit the required dissipation of energy.

CONCLUSIONS

A testing program was carried out as a part of the activities of the Bridge Group of the Network for Pre-normative Research in support of EC8. The main scope of the tests was to study the implications of irregularity when using the q-factor design approach.

Four RC bridges have been tested pseudodynamically, namely: one regular and three highly irregular bridges designed according to different design philosophies. The test results confirmed that safety against collapse of the irregular bridges is quite low compared with the safety of the regular bridge designed with the same procedure. Furthermore, the comparison between the test results obtained for the three irregular bridges confirms that the strategy adopted for the design of the bridge B213B, which corresponds to the use of a lower local behavior factor, is the 'less worse' and may lead to a suitable design approach for these bridges.

The tests on the isolated bridges confirmed that isolation is an effective approach for earthquake protection of bridges. In particular, isolation can be considered as a 'rational' alternative design solution for highly irregular bridges. Both isolation schemes have shown very good seismic performance, reducing the seismic response of the bridges to levels at which the piers were kept in the elastic range for the two earthquake tests. Moreover, partial isolation (isolation of critical piers) showed some advantages with respect to the full isolation scheme. In addition to the fact that partial isolation is more economical, this solution exploits more efficiently the deformation capacity of the lateral piers and does not require large clearances at the abutments.

Finally, the potential of the PsD test method with substructuring used in this test campaign was highlighted. The on-line analytical simulation of the bridge deck and of some piers have shown the practical advantages of the method as implemented at ELSA for the seismic testing of large scale bridges.

Acknowledgements

This work has been developed under the Human Capital Mobility program of the European Commission and was part of the research program of the Bridge Group of the PREC8 Research Network.

The participation to the ELSA testing campaign of the members of the Bridge Group, in particular, the contributions of Professor G. M. Calvi, coordinator of PREC8 and of the Bridge Group and Professor P. E. Pinto, chairman of the technical committee for EC8 is gratefully acknowledged.

It should be mentioned that the testing program is a joint effort of the staff of the Structural Mechanics Unit, JRC. The experimental program was directed by G. Verzeletti, Head of the Experimental Mechanics Sector. The implementation of the substructuring technique is due to P. Buchet, G. Magonette, P. Pegon and P. Tognoli. E. Gutierrez designed the instrumentation scheme, D. Tirelli was in charge of the reduction of experimental data and J. Guedes provided both the numerical simulations and the preliminary interpretation of results. The enthusiasm of the laboratory staff has made possible the preparation and execution of the tests.

Finally, the support to the research project on seismic isolation of FIP Industriale is gratefully acknowledged.

References

[1] Eurocode No 8, Structures in Seismic Regions - Design - Part 1 - General and Buildings - May 1988 edition, Report EUR 12266 EN, Commission of the European Communities, 1988.

[2] Eurocode No 8, Structures in Seismic Regions - Design - Part 2 - Bridges - Draft April 1993 - CEN, DOC. TC250/SC8/N76, 1993.

[3] Donea J., G. Magonette, P. Negro, P. Pegon, Pinto A. and G. Verzeletti. Pseudo-dynamic testing of large-scale models of civil engineering structures at the ELSA reaction wall. *Proc. of the 10th European Conference on Earthquake Engineering*, Vienna, 1994.

[4] Calvi G.M. and Pinto P.E. Seismic design of bridges: Experimental and analytical research. *Proc. of the 10th European Conference on Earthquake Engineering* Vol.4, Vienna, 1994.

[5] Dermitzakis, S.N. and S.A. Mahin. Development of substructuring techniques for on-line computer controlled seismic performance testing. *Report No. UCB/EERC-85/04*. Berkeley, California, 1985.

[6] Buchet, P. and P. Pegon. PsD testing with substructuring - Implementation and use. *Special Publication* AMU, STI, EC, JRC, Ispra, Italy, 1994.

[7] Park, Y.J. & A.H-S. Ang. Mechanistic Seismic Damage Model for Reinforced Concrete, *Journal of Structural Engineering,* ASCE, Vol. 111, N. 4., 1985.

[8] Pinto A.V., G. Verzeletti, P. Negro and J. Guedes. Cyclic testing of a squat bridge-pier. *EUR Report N.16247EN* - AMU, STI, EC, JRC, Ispra, Italy, 1995.

[9] Pinto A.V.; G. Verzeletti; P. Pegon; G. Magonette; P. Negro. Pseudo-Dynamic Testing of Large-Scale R/C Bridges. *Report EUR 16378 EN,* EC, JRC, Ispra, Italy, 1996.

[10] Pinto, A.V. (Editor). Pseudo-Dynamic and Shaking Table Tests on RC Bridges. *ECOEST/ PREC8 Report.* LNEC, Lisbon, 1996.

[11] Guedes, J., P. Pegon & A.V. Pinto. A Fibre/Timoshenko Beam Element in CASTEM 2000. *Special Publication* N. I.94.31, STI, JRC, EC, Ispra, Italy, 1994.

[12] Guedes, J. & A.V. Pinto. Numerical Predictions for the PsD testing of R/C Bridges. *Report EUR No. 16358 EN*, EC, JRC, Ispra, Italy, 1996.

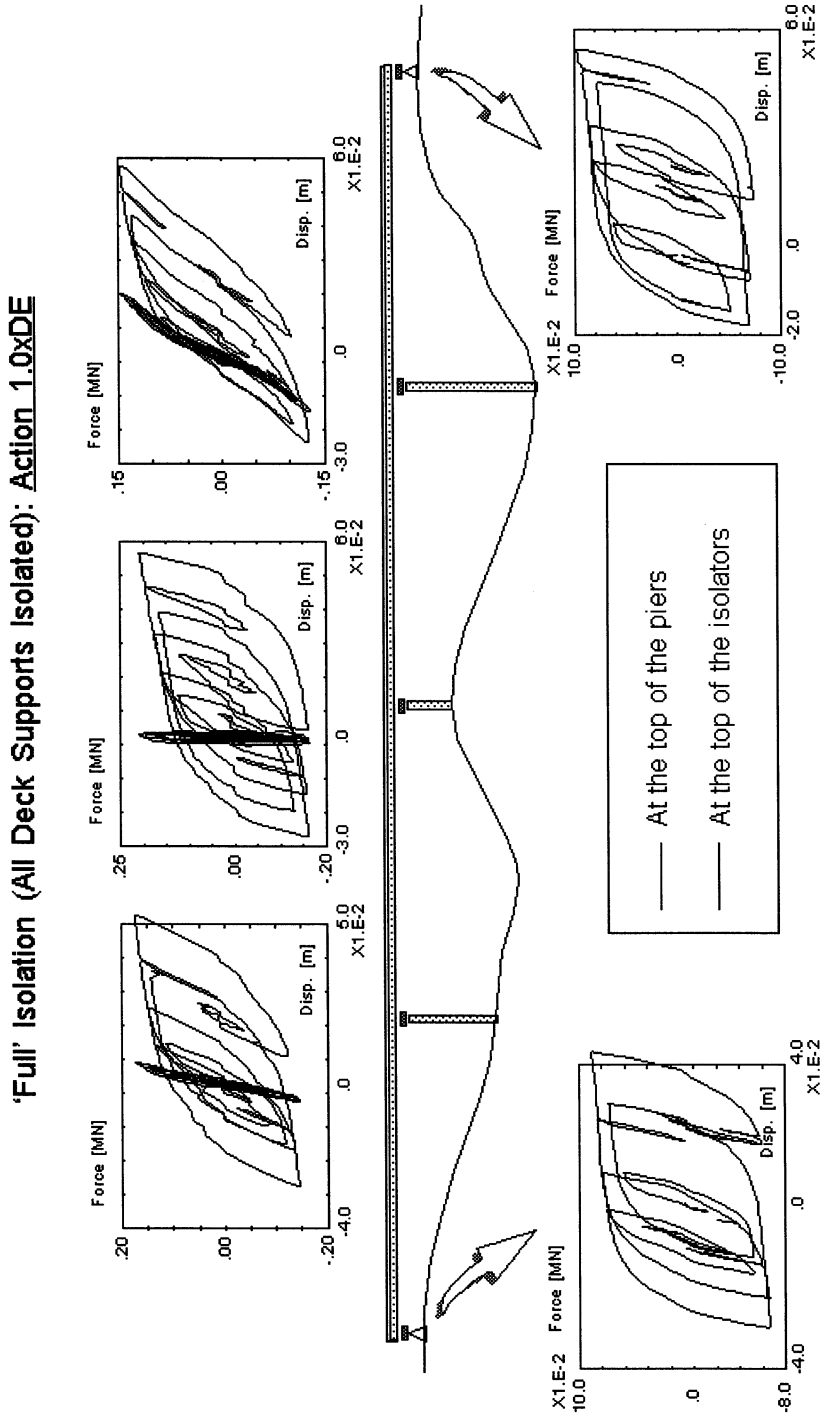


Figure 10: Bridge B213A-FI: Force-displacement diagrams for the isolator and for the bridge piers for the (1.0xDE) test.

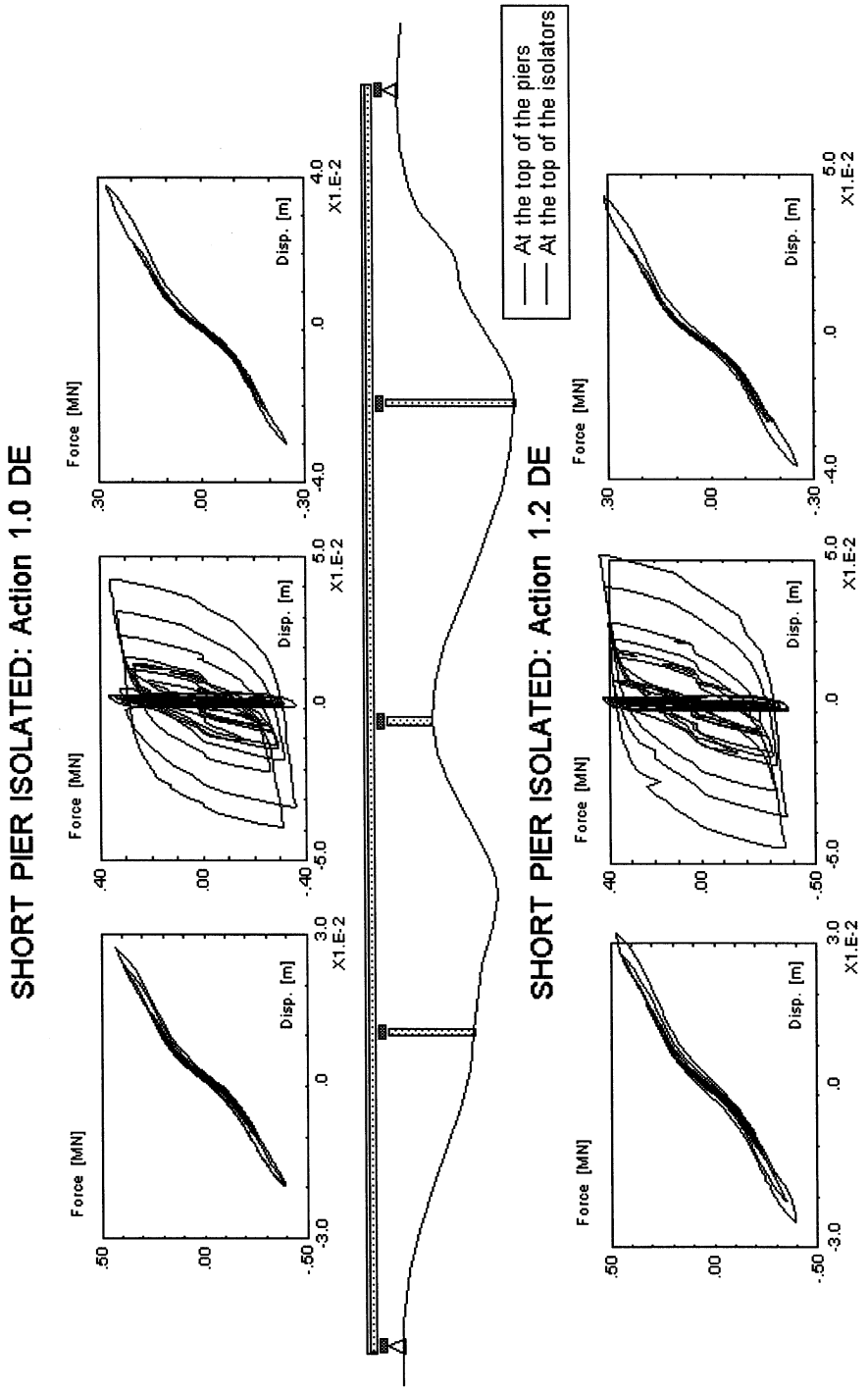


Figure 11: Bridge B213A-PI: Force-displacement diagrams for the isolators and for the bridge piers for the (1.0xDE) and the (1.2xDE) test.

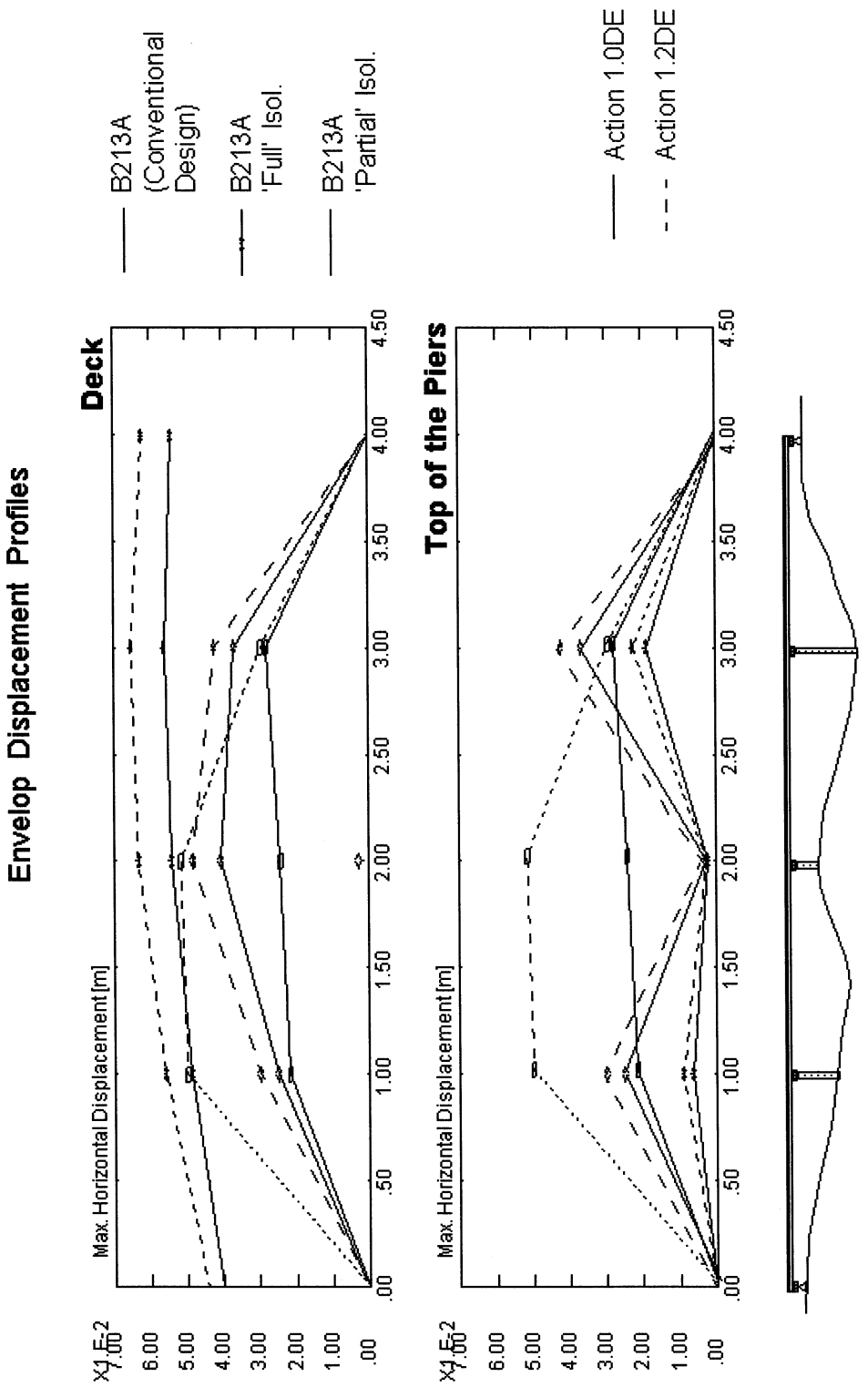
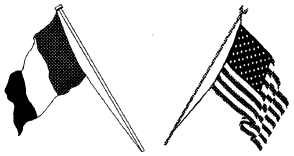


Figure 12: Envelope displacement profiles for the deck and for the top of the piers of the irregular bridges for the two earthquake tests.



Session V

The Use of Advanced Composites in Seismic Retrofitting
Frieder Seible

Stress Reduction System of Medium Span Bridges Using Semiactive Controls
William Neff Patten, Jinghui Sun and Guangjun Li

SMA Devices for Seismic Isolation of Bridges: Design and Experimental Behaviour
Mauro Dolce and Roberto Marnetto

Rocking Columns: An Effective Means of Seismically Isolating a Bridge
John B. Mander, R. Contreras and R. Garcia

THE USE OF ADVANCED COMPOSITES IN SEISMIC RETROFITTING

Frieder Seible, Ph.D., P.E.
Division of Structural Engineering
University of California, San Diego
La Jolla, CA 92093-0085

ABSTRACT

Advanced composites known as polymer matrix composites (PMCs) or fiber reinforced polymers (FRPs) have been shown to be structurally very efficient in the seismic retrofit of constructed facilities. Light weight and ease of application also result in cost effective retrofit measures despite higher material costs compared to conventional retrofit systems.

Design and application issues with advanced composite retrofits are discussed together with structural performance validations from large and full scale laboratory experiments. Examples for seismic response and retrofit design will include laboratory tests and field applications on seismic retrofits of structural concrete wall buildings and reinforced concrete bridge columns. Detailed design guidelines for seismic retrofits using FRPs are presented together with critical detailing and application issues.

INTRODUCTION

Advanced composite materials, predominantly developed for use in the aerospace industry, have shown a great potential for strengthening, retrofitting and repair of existing buildings and bridge structures to extend their service life well into the 21st century. With the broader availability of glass, aramid and carbon fibers, as well as automation in the manufacturing process, PMCs can be affordable and competitive with conventional structural rehabilitation materials and processes.

While the low density and the high mechanical characteristics of advanced composite materials were long recognized, applications in the civil engineering sector were limited to date due to (1) high materials and manufacturing costs, and (2) the component by component replacement of existing structural members rather than a comprehensive design approach with these new materials. This paper provides an overview of the use of advanced composites for the seismic retrofit of existing civil structures.

The structural effectiveness of PMCs in retrofitting existing structural systems has repeatedly been demonstrated with full or large-scale structural tests at the University of California, San Diego. Carbon fabric overlays have been used to retrofit reinforced and unreinforced masonry walls for seismic loads and to restore and more than double the displacement capacity in the repair of a full-scale 5-story reinforced masonry building tested under simulated seismic loads to failure. Bridge columns were seismically retrofitted and repaired with fiberglass, carbon and hybrid composite jackets and these FRP retrofits were shown to be just as effective as conventional steel jacket column retrofit technology.

The success of structural rehabilitation measures with advanced composite materials has led to the development of new lightweight structural concepts utilizing FRP shells and tubes to form new structural systems. FRP tube systems are introduced in the following, combining construction simplifications and outstanding short and long-term structural characteristics for use in new lightweight framing systems for seismic zones.

ADVANCED COMPOSITES FOR CIVIL ENGINEERING APPLICATIONS

The most common advanced composites fibers used in PMC structural applications are carbon, aramid and glass, and the most commonly used matrices are epoxies and esters. While a detailed discussion of materials, and manufacturing processes of these PMCs can be found elsewhere [1], only their key characteristics, including cost, will be summarized here with direct reference to civil engineering applications. High performance fibers developed and used in the aerospace industry are cost prohibitive in the civil sector, limiting the choice to advanced composite materials referred to under the low to medium performance category.

The range of realistic properties can be summarized as follows:
strength: For quasi-isotropic material considerations or design assumptions strength values comparable to high strength structural steels can be achieved. However, due to the non-ductile failure characteristics only a limited range of these capacities can be utilized. Uni-directional fiber geometry can result in strength characteristics similar to high strength prestressing wires and strands.
strain: Failure strains are low and typically limited to the 1 to 3% range with carbon fibers at the lower and glass and aramids at the upper end of the range.
modulus: Moduli for quasi-isotropic assumptions range from 10% to 30% of steel and for uni-directional fiber applications from 1/3 to 2/3 of the structural steel modulus.
cost: Cost is dominated by the price of the fiber material, ranging currently per pound from $1-3 for glass to $10-25 for carbon (T300, AS4). Typical resins are $1-2 per pound.

With a 40 to 60% typical fiber volume fraction and automated manufacturing techniques, PMC structural component costs in place can range from $3-15 per pound, with glass at the lower and carbon at the upper end of the range.

It should be noted that both strength and modulus decrease rapidly with deviation of the fiber orientation from the loading direction which is largely a function of a very low shear modulus of the matrix or resin system, typically 1% or less of Young's Modulus for steel. For retrofitting of existing concrete structures, the reduced weight of these advanced composite materials in the form of thin overlays is a major benefit, as will be discussed in the following.

While the chemical resistance of these PMCs to acid or corrosive environments is very good in general, durability aspects such as ultra violet degradation of the matrix, alkaline reactions between glass and concrete, water absorption by the resin system as well as fire and vandalism protection typically require a form of external coating. Furthermore, only limited information on the creep and relaxation characteristics of affordable PMCs in the civil engineering environment exist to date and require comprehensive evaluations. Also, significant differences in thermal

characteristics between the existing concrete substrate and the PMC overlays need to be addressed.

SEISMIC RETROFIT OF CONSTRUCTED FACILITIES

Structural wall overlays

Seismic repair and retrofitting of structural walls can be accomplished very economically with thin advanced composite wall overlays. Tests have focused to date on (1) reduction of shear deformations in structural walls, (2) retrofitting of shear walls to achieve ductile in-plane behavior, (3) repair of damaged walls to increase in-plane ductility, as well as (4) retrofitting of out-of-plane unreinforced structural walls.

A series of seven single-story structural wall panel tests were performed on fully grouted hollow core concrete masonry walls at full-scale. Subsequent to sandblasting and filling of voids and mortar joints with epoxy or polymer concrete, advanced composite overlays were applied to the wall surface either single or double-sided in the form of mats or woven fabrics saturated with resin in an impregnator.

a) Shear retrofit:
Especially for in-plane wall response or shear, very thin overlays (only one or two layers t_i = *0.5 to 1.0 mm*) can show significant seismic improvements. Composite fibers are oriented horizontally to cross diagonal or shear cracks, while allowing horizontal or flexural cracks to open. Forces to be transferred in the composite overlays are limited by the laminar shear or principal tensile strength of the existing structural wall material since the polymer resin typically features significantly higher tensile capacities than the concrete or masonry substrate.

To improve shear capacities of structural walls of length d with advanced composite overlays of thickness t_o and a conservative diagonal tension crack angle assumption of 45•, the resulting shear capacity increase can be determined based on an allowable overlay stress level derived for a maximum horizontal wall strain of 0.004 above which aggregated interlock is assumed to be lost. For typical structural wall aspect ratios, i.e. height and length of approximately the same dimensions, the above strain criteria inherently assumes large shear deformations, namely 0.4% drift due to shear alone. Thus, additional limitations on the total allowable shear deformations can be imposed by reducing the allowable overlay stress level. Alternatively, stiffness criteria can be employed in the wall overlay design, limiting shear deformations to deformation levels which can be expected in concrete walls with conventional horizontal reinforcement A_{sh}^{req} (determined based on conventional design requirements), by scaling the amount of horizontal overlay fabric A_{oh} from the equivalent required horizontal steel reinforcement and the ratio of steel to overlay stiffness.

Since the bond between the composite overlays or the resin matrix and the concrete substrate is at least as good as the bond capacity between individual reinforcing bars and unconfined concrete, upper limits to the total improvement of shear capacity can also be taken as those encountered in conventional concrete design codes.

The seismic deformation limitations of many structural walls are controlled by compression toe crushing or lateral stability of the compression toe region. A nominal level of compression toe confinement can be provided by wrapping additional layers of composite overlay material around the toe region if access is available.

Three full scale 2 x 2 m (6 x 6 ft) structural wall panels constructed with 152 mm (6 in.) fully grouted and reinforced concrete block masonry, see Fig. 1b, were tested in (1) the as-built condition, (2) repaired condition following diagonal shear failure, and (3) retrofitted condition.

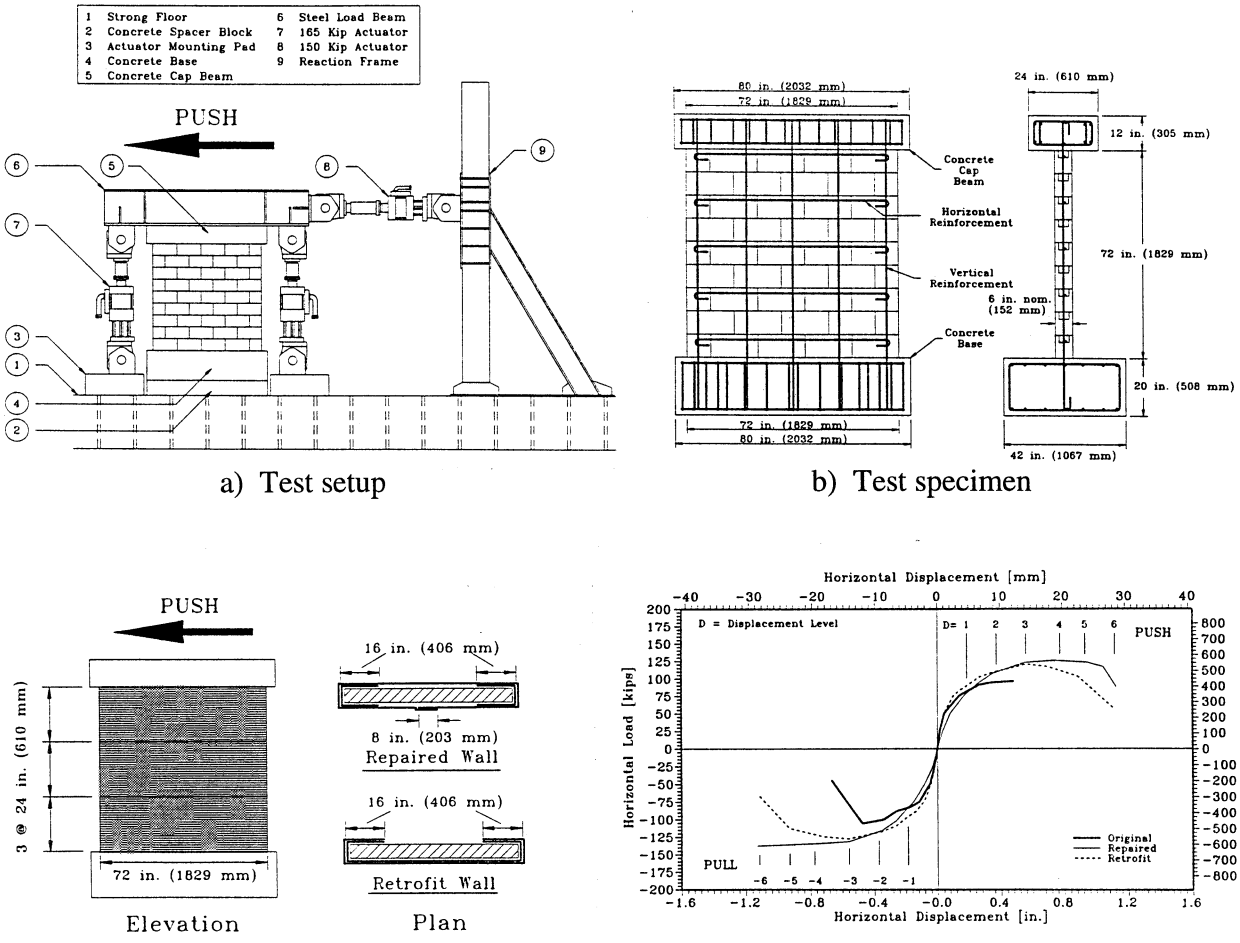


Figure 1 – In-plane retrofit of structural walls

The repair of the original failed wall panel consisted of epoxy injection of the diagonal corner-to-corner shear failure crack, reconstruction of the crushed compression toe with polymer concrete and double sided horizontal carbon wall overlays 490 g/m^2 (25 oz/y^2 unidirectional fabric). The retrofit specimen was a new as-built wall with two layers of single sided horizontal carbon wall overlays. Thus, the amount of horizontal carbon fabric was the same in both cases, see Fig. 1c. The mild reinforcement consisted of Grade 60 #6 bars for vertical and #3 bars for horizontal reinforcement, see Fig. 1b. For the horizontal cyclic load test, the wall panels were first loaded

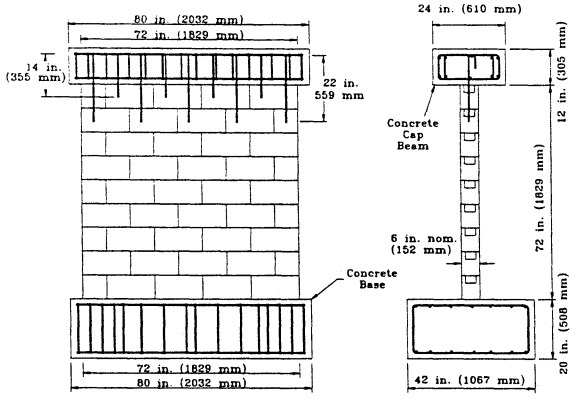
with 1.80 MPa (270 psi) axial or vertical load and subsequently restrained against rotation at the wall top.

Envelopes for the load-deflection hysteresis curves are depicted in Fig. 1d and show that both, double sided repair and single sided retrofit with horizontal carbon overlays result in twice the deformation capacity observed in the as-built wall specimen. The seemingly better performance of the repaired wall specimen can be attributed to the polymer concrete rebuilt wall toe.

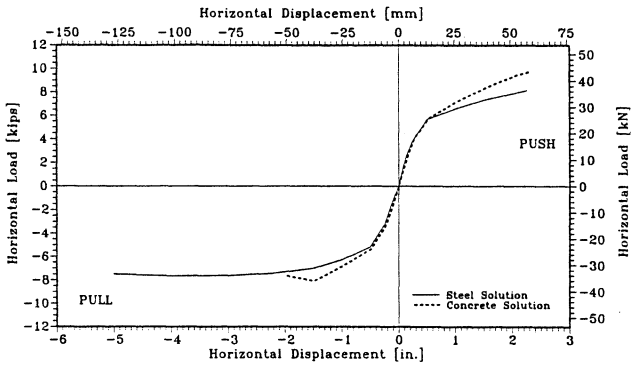
b) Flexural retrofit:

For out-of-plane wall retrofitting the key design aspects are (1) the development of the overlay material in regions of high moment gradients, and (2) the potential for buckling and delamination of the thin and stiff overlays on the compression side of the flexural member.

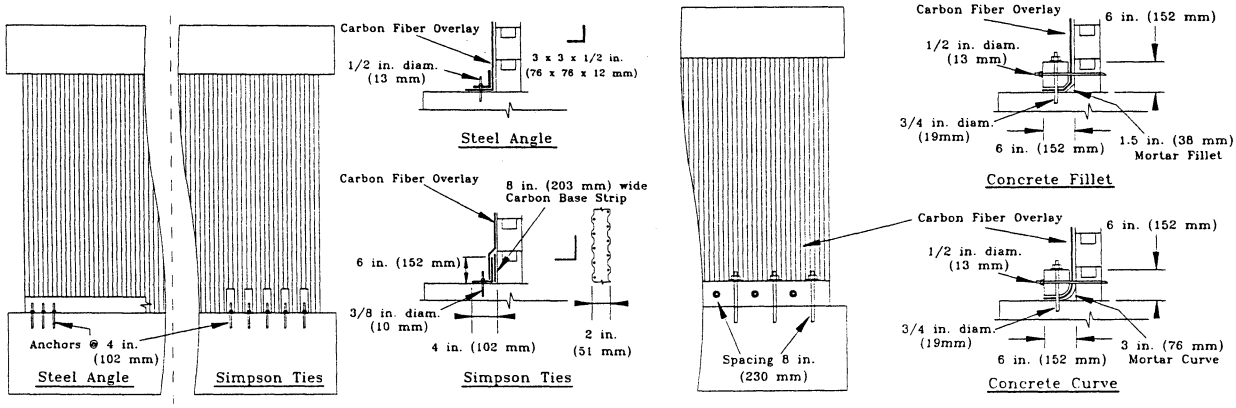
Two out-of-plane flexural wall tests were performed on 2 x 2 m (6 x 6 ft) unreinforced fully grouted masonry wall panels, see Fig. 2a, with the same geometry and axial load condition as the



a) Test specimen



b) Load-displacement response envelopes



c) Steel base anchorage d) Concrete base anchorage

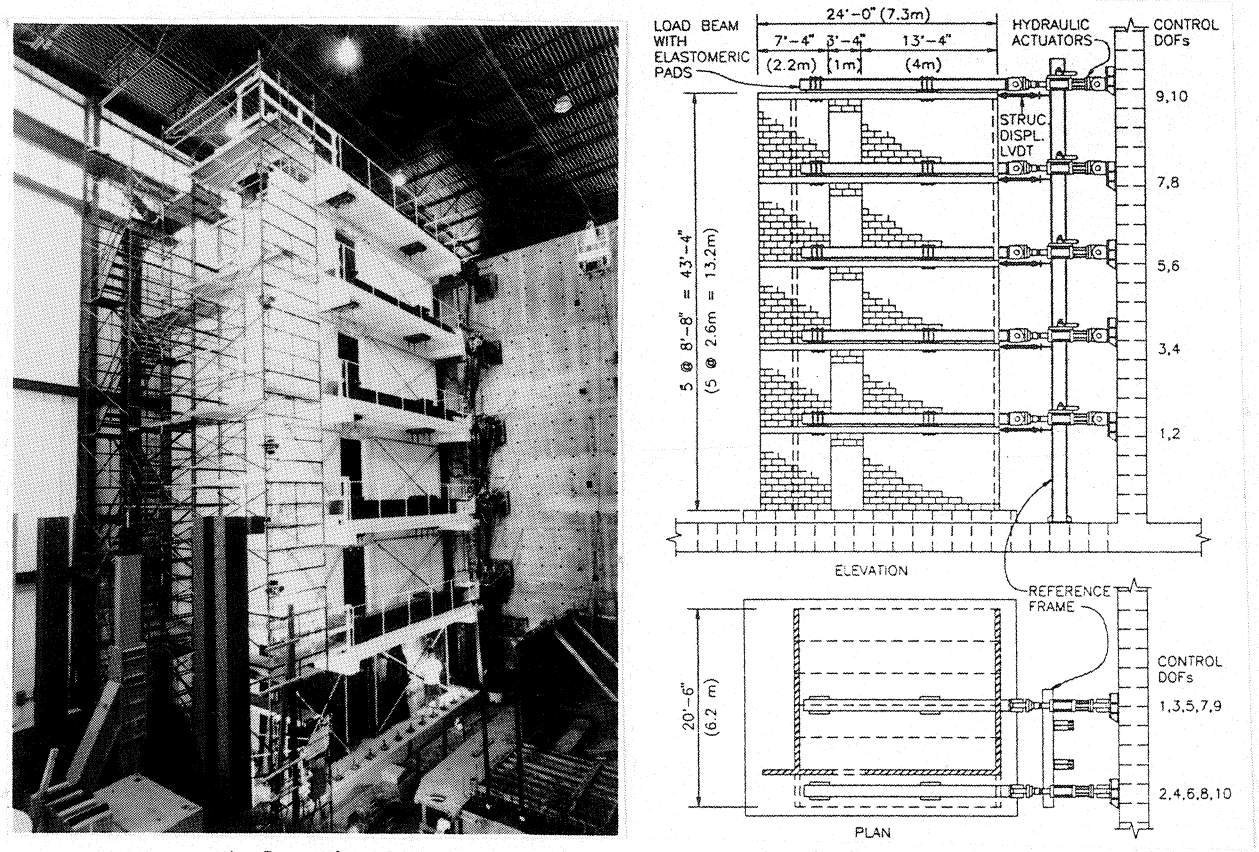
Figure 2 – Out-of-plane retrofit of unreinforced walls

shear walls in Fig. 1. The vertical single layer carbon fabric needed to be developed at the base of the cantilever wall to provide flexural capacity to the wall. End anchorage or fabric development was achieved with four different anchorage types, namely two steel anchorage solutions with a bolted steel angle or individual steel straps, and two concrete anchorage solutions with bolted base beams and different wrap-around curvature for the carbon fabric, see Figs. 2c and d, respectively.

The cantilever load-deflection envelopes are depicted in Fig. 2b for the four different connection details. By far the largest deformation capacity was obtained with individual steel straps on the tension side, since the right-angle-bent steel straps straighten out with increasing cantilever loads. Lateral load capacities do not depend on the anchorage type as long as the full carbon fabric capacity can be developed.

c) Full scale building test:

The effectiveness of the application of advanced composite wall overlays for seismic repair and retrofitting of structural wall systems can best be demonstrated by the example of a full-scale five-story reinforced masonry building, see Fig. 3, which was tested under pseudo-dynamic simulated seismic loads to failure [3]. Subsequent to the original testing, the building was repaired by means of structural carbon overlays to the first two stories of the structural walls, (see Fig. 3b), subsequent to reconstruction of the crushed wall toes with polymer concrete.



a) Overview b) Carbon overlay areas

Figure 3 – Five-story full scale building test

The load-deflection envelopes for the original and the repaired five-story building, (see Fig. 4), show that a single layer of carbon fabric overlay [t = 1.25 mm, predominately horizontal woven carbon fabric, (12 k toe AS4), with epoxy resin matrix], applied on each side of the structural walls with two layers in the toe regions, contributed significantly to doubling the inelastic deformation capacity in the critical push direction. Measured shear deformations in the overlayed wall panels were reduced to half the shear deformations in the original five-story building test. Detailed information of the repair and retrofit installation and seismic response data can be found in [3].

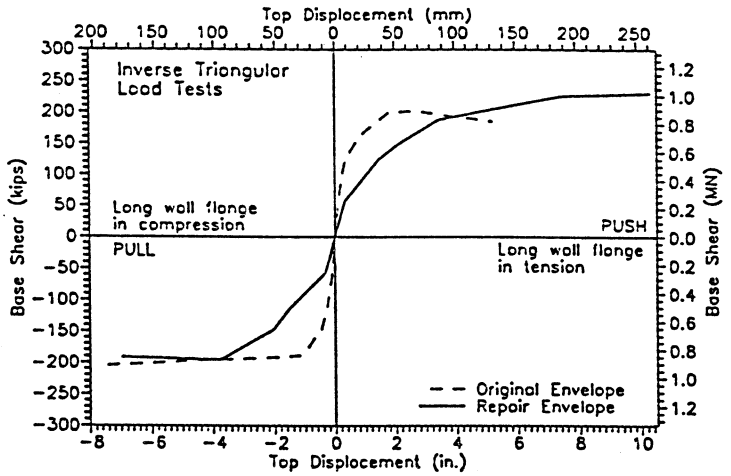


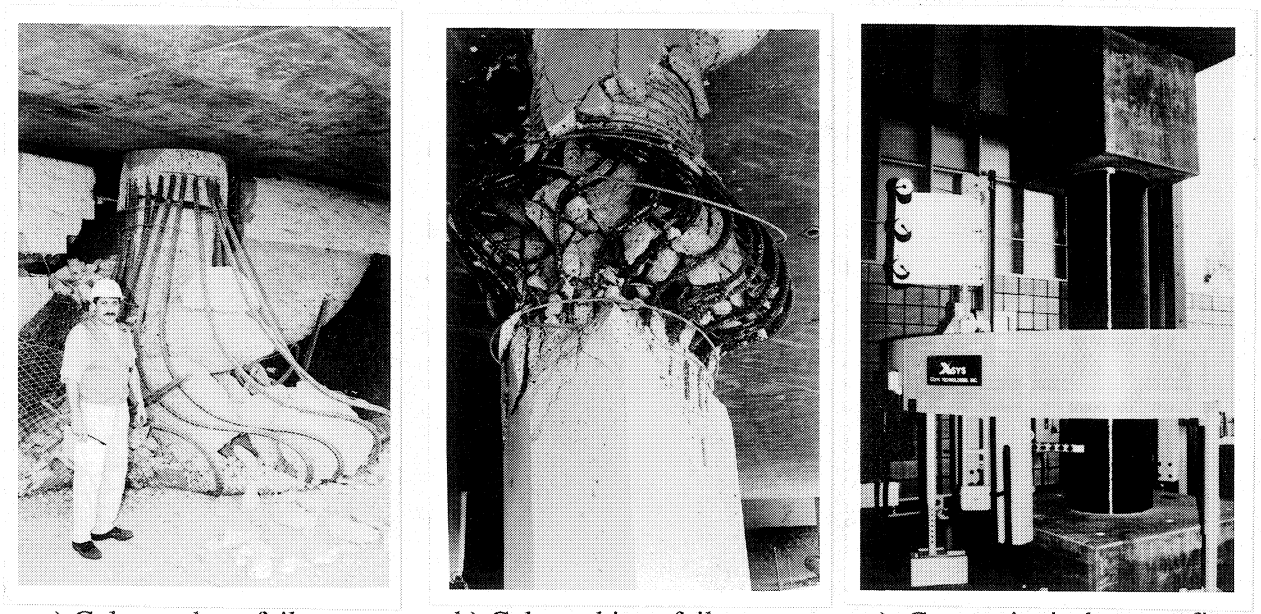
Figure 4 – Load-displacement envelope comparison for carbon overlay repair test

SEISMIC RETROFITTING OF BRIDGE COLUMNS

The seismic response of concrete columns is to a large extent controlled by the amount and detailing of the horizontal or transverse reinforcement. Since the transverse reinforcement for many existing columns was not designed based on current design knowledge and criteria but only nominally provided to support the longitudinal column reinforcement during construction, the retrofit solution is to provide the missing horizontal reinforcement externally. External jackets need to be designed to prevent three critical column failure modes, namely (a) shear, (b) flexural hinge confinement/bar buckling, see Fig. 5, and (c) lap splice clamping. Advanced composite jacket design issues for these three predominant failure modes are discussed in the following.

a) Shear:

The column shear failure is primarily a strength and a dilation problem. Shear strength can be added to concrete columns by hoop or horizontal reinforcement in the form of 90• (from the column axis) oriented composite fibers, where the opening of inclined cracks, and with it the loss of aggregate interlock in these cracks which is one of the key shear force transfer mechanisms, can be controlled by limiting the column dilation in the loading direction to experimentally



a) Column shear failure b) Column hinge failure c) Composite jacket retrofit

Figure 5 – Critical column failure modes

determined dilation strains of $\varepsilon_d < 0.004$ or 0.4%, [1,3]. The jacket thickness for shear retrofit can be determined based on Eqn. (1) for circular and rectangular columns as

$$\text{circular} \quad t_j = \frac{\frac{V_o}{\phi_v} - (V_c + V_s + V_p)}{\frac{\pi}{2} \times 0.004 E_j \cdot D}$$

$$\text{rectangular} \quad t_j = \frac{\frac{V_o}{\phi_v} - (V_c + V_s + V_p)}{2 \times 0.004 E_j \cdot D} \qquad (1)$$

where V_0 is the column shear demand based on full flexural overstrength in the potential plastic hinges, ϕ_v a shear capacity reduction factor (typically taken as 0.85), V_c, V_s and V_p the three shear capacity contributions from the concrete, horizontal steel reinforcement and axial load based on the UCSD three component shear model [4] with reductions for the concrete component V_c in the flexural plastic hinge region based on the ductility demand, and E_j and D the composite jacket modulus and the column dimension in the loading direction, respectively.

From Fig. 6 it is obvious that the high strengths in the composite materials can typically not be utilized due to the limitation on the dilation strains to ensure aggregate interlock. Thus, the proportional relationship for composite jacket thickness for shear retrofit can be expressed as

$$t_j^v \sim \frac{1}{E_j D} \times C_v \qquad (2)$$

where C_v denotes the remaining coefficient derived from Eqn. (1). Equation (2) shows that for most advanced composite jacket retrofits the jacket thickness is inversely proportional to the jacket modulus and the column dimension in the loading direction.

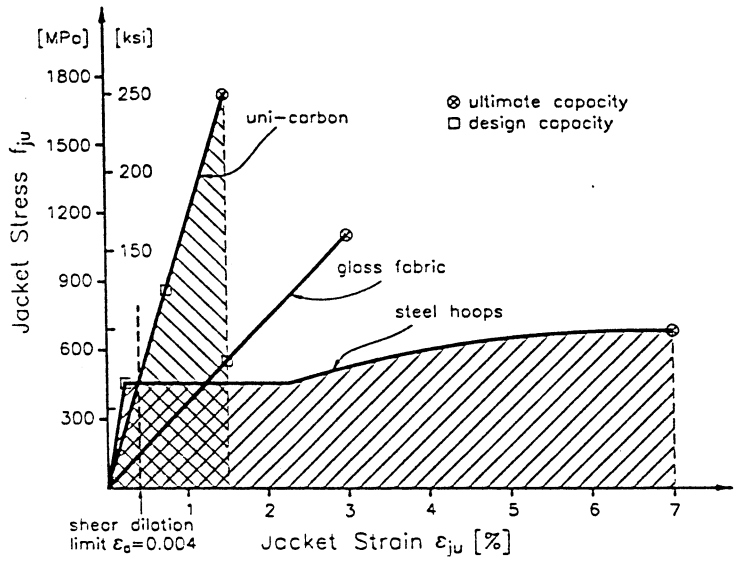


Figure 6 – Typical mechanical characteristics of column jackets in the hoop direction

b) Flexural hinge confinement:

Inelastic deformation capacity of flexural plastic hinge regions can be increased by stabalizing the longitudinal bars against buckling and by confinement of the column concrete with hoop reinforcement from an advanced composite fiber jacket system. For circular columns the required jacket thickness can be expressed as

$$t_j = 0.09 \frac{D(\varepsilon_{cu} - 0.004) f'_{cc}}{\phi_f \cdot f_{ju} \cdot \varepsilon_{ju}} \tag{3}$$

where f'_{cc} is the confined concrete compression strength which depends on the effective lateral continuing stress and the nominal concrete strength and can be conservatively taken as 1.5 f'_c, for most retrofit designs [4] f_{ju} and ε_{ju} are the strength and deformation capacity of the composite jacket in the hoop direction, ϕ_f is a flexural capacity reduction factor (typically taken as 0.9), ε_{cu} is the ultimate concrete strain which depends on the level of confinement provided by the composite jacket and can be determined as

$$\varepsilon_{cu} = 0.004 + \frac{2.8 \rho_j f_{ju} \varepsilon_{ju}}{f'_{cc}} \tag{4}$$

with ρ_j representing the volumetric jacket reinforcement ratio. In turn, ε_{cu} can be obtained from

$$\varepsilon_{cu} = \Phi_u \cdot c_u \tag{5}$$

based on the ultimate section curvature Φ_u and the corresponding neutral axis depth c_u which both can be determined from a sectional moment-curvature analysis and directly related to a structural member ductility factor

$$\mu_\Delta = 1 + 3\left(\frac{\Phi_u}{\Phi_y} - 1\right)\frac{L_p}{L}\left(1 - 0.5\frac{L_p}{L}\right) \tag{6}$$

where L_p represents a semi empirical plastic hinge length [3], L represents the shear span to the plastic hinge, and Φ_y is the section yield curvature [3].

Expressing the flexural jacket thickness Eqn. (3) for hinge confinement in proportional terms similar to the shear Eqn. (2) the required jacket thickness

$$t_j^c \sim \frac{D}{f_{ju}\varepsilon_{ju}} \times C_c \tag{7}$$

is proportional to the column dimension D in the loading direction and inversely proportional to the product of ultimate jacket stress and strain in the hoop direction.

To ensure that column bar buckling in the plastic hinge does not control the flexural failure mode, additional checks on the transverse reinforcement ratio ρ_j need to be performed [4] particularly for slender columns where $M/(V \cdot D) > 4$ (with M and V the maximum column moment and shear). The expression for the required thickness

$$t_j^b \sim \frac{D}{E_j} \times C_b \tag{8}$$

The confinement effects provided by circular jackets originate directly from the radial pressure forces generated by the jacket curvature and the tensile hoop strains in the jacket generated by the dilation of the plastic hinge. For rectangular columns an oval jacket should be provided by means of added precast concrete segments with changing radii of curvature in the different loading directions. An equivalent circular column diameter D_e can be derived from the average of the oval jacket principal radii of curvature, and the jacket thickness calculations can follow those outlined for circular columns using the equivalent column diameter D_e. It should be noted that mid side or unsupported column bars in rectangular columns cannot be stabilized against buckling with thin FRP overlays.

c) Lap splice clamping:

Finally, lap splice clamping requires sufficient lateral pressure f_ℓ onto the splice region to prevent starter bars and the column reinforcement to slip relative to each other. With this simplified failure model, basic shear friction type considerations for a monolithically cast interface can be employed. Furthermore, experimental test results showed that onset of lap splice debonding or relative slippage starts when measured hoop or dilation strain levels are between 1,000 to 2,000

με. At strain levels of 2,000 με debonding of the lap splice was in progress as indicated by a loss in lateral load carrying capacity of the test columns [4].

Limiting dilation strain levels to 1,000 με, the composite jacket thickness to ensure lap splice clamping can be derived as

$$t_j = 500\frac{D(f_\ell - f_h)}{E_j} \tag{9}$$

where f_h represents the horizontal stress level provided by the existing hoop reinforcement in a circular column at a strain of 0.1% and f. the lateral clamping pressure over the lap splice L_s can be determined as

$$f_\ell = \frac{A_s \cdot f_{sy}}{\left[\frac{p}{2n} + 2(d_b + cc)\right]L_s} \tag{10}$$

where p is the perimeter line in the column cross-section along the lap spliced bar locations, n is the number of spliced bars along p, A_s is the area of one main column reinforcing bar, and cc the concrete cover to the main column reinforcement with diameter d_b [4].

Expressing the splice clamping problem again in terms of a proportionality relationship in the form of

$$t_j^s \sim \frac{D}{E_j} \times C_s \tag{11}$$

indicates that the required composite jacket thickness is inversely proportional to the jacket modulus E_j in the hoop direction and directly proportional to the column diameter.

For rectangular columns with lap splices, the curvature from circular or oval jackets is required to provide the necessary lateral clamping pressure. An equivalent circular column diameter D_e as outlined for the plastic hinge confinement, can be used to determine jacket thicknesses. For three different advanced composite jacket systems with hypothetical mechanical properties, relative jacket thicknesses for the four column failure modes based on the proportional relationships from Eqns. (2), (7), (8), and (11) are listed in Table 1.

System A is representative of a towpreg based graphite/epoxy composite similar to that used in automated winding of jackets, system B is representative of a Kevlar/epoxy composite, and system C is representative of an E-glass/Vinylester composite similar to that used in prefabricated adhesively bonded shells. All values in Table 1 are normalized to the thickness values derived for system A which represents a unidirectional carbon tow winding system with an epoxy matrix. Table 1 shows that jacket thicknesses for shear and lap splice clamping are driven by the modulus of the jacket in the hoop direction which favors higher modulus materials,

whereas the flexural plastic hinge confinement can also efficiently be achieved with a lower modulus and higher strain capacity material.

Table 1 - Comparison of hypothetical jacket thicknesses

System	Mechanical Characteristics	Normalized Jacket Thickness			
		Shear Strength	Plastic Hinge Confinement	Bar Buckling	Lap Splice Clamping
System A	E_j = 124 GPa f_{ju} = 1,300 MPa ε_{ju} = 1%	1	1	1	1
System B	E_j = 41 GPa f_{ju} = 690 MPa ε_{ju} = 1.5%	3.0	1.3	3.0	3.0
System C	E_j = 21 GPa f_{ju} = 552 MPa ε_{ju} = 3%	6.0	0.8	6.0	6.0
	Design Relationships	$t_j^v \sim \frac{1}{E_j D} \times C_v$	$t_j^c \sim \frac{D}{f_{ju}\varepsilon_{ju}} \times C_c$	$t_j^b \sim \frac{D}{E_j} \times C_b$	$t_j^s \sim \frac{D}{E_j} \times C_s$

1 MPa = 0.145 ksi, 1 GPa = 145 ksi

The above advanced composite jacket design guidelines clearly show, that (1) in most cases the full jacket strength cannot be utilized due to strain limitations in the substrate to limit crack width and loss of aggregate interlock in concrete and that therefore (2) the design of the advanced composite system is modulus driven, which is beneficial from a long term behavior point-of-view since variations in moduli seem smaller than strength degradations under various civil engineering environments. Finally, (3) for rehabilitation (retrofit) measures, the advanced composite retrofit can and should be designed such that brittle failures in the FRPs do not control the response, a design objective which can be achieved with simple capacity design principles.

DESIGN DETAILING

Because composites can be easily applied to existing concrete structures either through in-situ overlay installation on the structure itself or through the adhesion of prefabricated panels or strips, there is a tendency to follow with the FRP the contours of the element to be rehabilitated without sufficient thought given to the consequences of such designs. Common examples of the misuse of ease of conformance are shown in Figs. 7 and 8 wherein composites are used for the shear strengthening of T and I-beams respectively, through FRP overlays on the beam faces. As can be seen in the right hand side of the Fig. 7, in new conventional concrete T-beam, shear stirrups are never curtailed in the beam region, but are carried over into the slab section to be anchored in the compression zone and to provide the sought after truss mechanism. When FRPs are curtailed in the vertical section below the slab, there is a distinct possibility that the composite will debond or delaminate at the bottom corner and along the vertical edge below the slab, significantly reducing safety and reliability margins. For good detailing, the composite should be continued or anchored into the slab and wrapped around the beam bottom. Also, re-entrant corners, see Fig. 8, should be avoided.

Composite plates are routinely bonded with adhesives to the bottom of beams in order to strengthen beams as shown in Fig. 9. This however disregards the fact that the presence of the beam causes very high shear stresses at the end of the composite plate resulting in peel stresses and ultimate failure due to premature debonding of the plate/strip from the concrete.

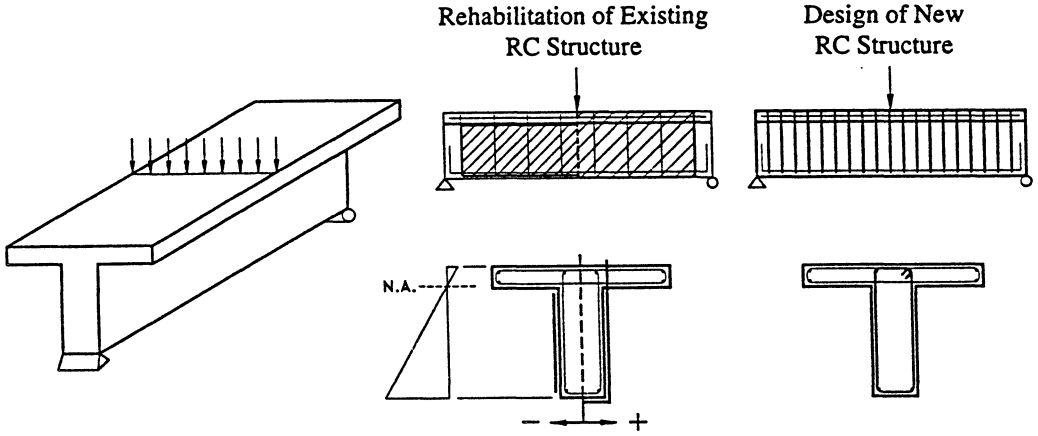


Figure 7 – Design detailing for shear strengthening of T-beams

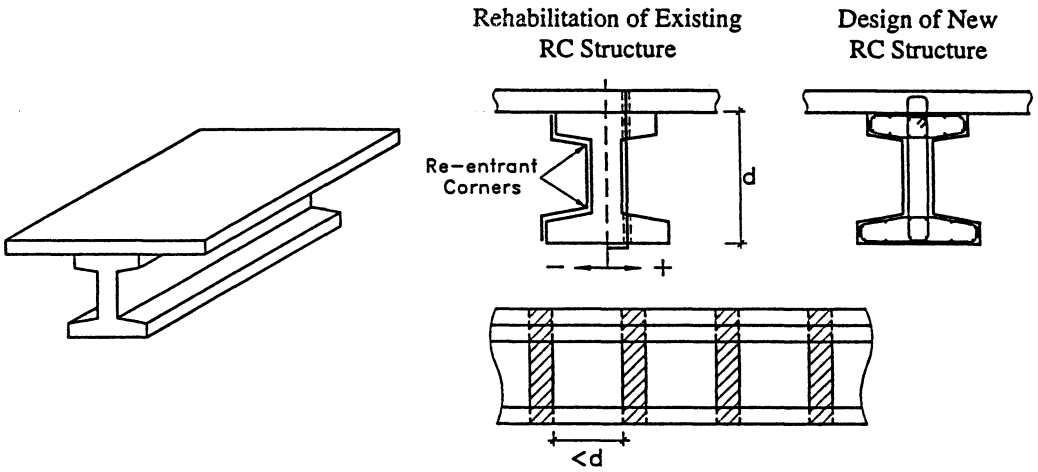


Figure 8 – Design detailing for shear strengthening of I-beams

Appropriate detailing should follow the procedure prescribed for internal rebar which would be carried through to the support. FRP strengthening can be developed through partial embedment of the composite in the concrete so as to provide anchorage and stress buildup over its length and in case termination short of the support region is required strict limits on the maximum allowable strength/capacity enhancement should be applied.

The successful application of composites to the bottom surface of beams has resulted in some use of strips on the soffit of slabs with strips being adhesively bonded to the soffit at wide spacings. Again this is poor detailing practice due to shear lag between tension and compression mechanisms and since it allows for punching shear failure in the large unreinforced gaps between

the external composite strips as shown in Fig. 10. Correct procedure would be to place the strips closer together similar to the placement of internal steel rebar or to use continuous fabric over the entire soffit.

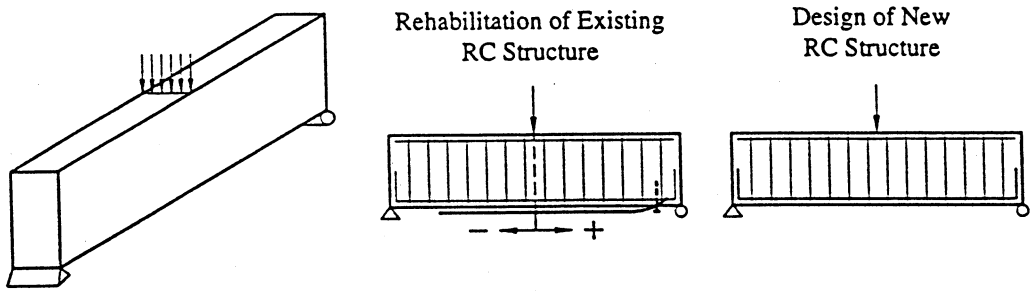


Figure 9 – Design detailing for the flexural strengthening of beams

Composite sheets can be easily applied to large aspect ratio rectangular columns or pier walls. However due to the long length between corners, the composite does not confine the internal concrete structure if just applied to the surface. In order to achieve confinement, the composite wraps need to be constrained on both sides along the length through the use of dowels or bolts that anchor the composite to the pre-existing structure, thereby creating shorter distances which are confined between bolts. This is actually similar to the technique used in conventional construction (Fig. 11) wherein the transverse reinforcement on the two side faces I tied together through the use of J-hooks.

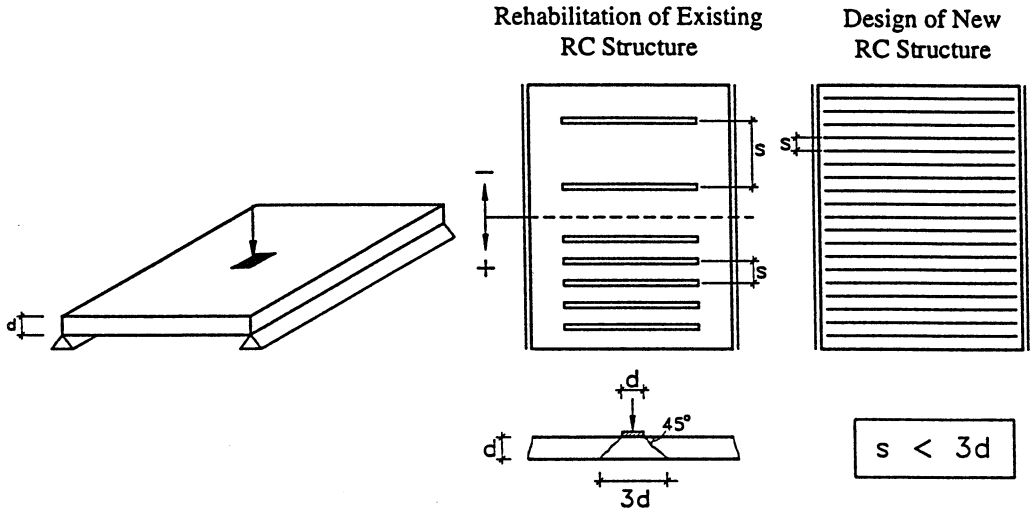


Figure 10 – Design detailing for the flexural strengthening of slabs

As a general rule, external FRP retrofit rehabilitation measures on concrete structures should emulate conventional internal reinforcement detailing as much as possible. In cases where this is not practical, strict limitations on the allowable capacity enhancement for the rehabilitation measure should be applied.

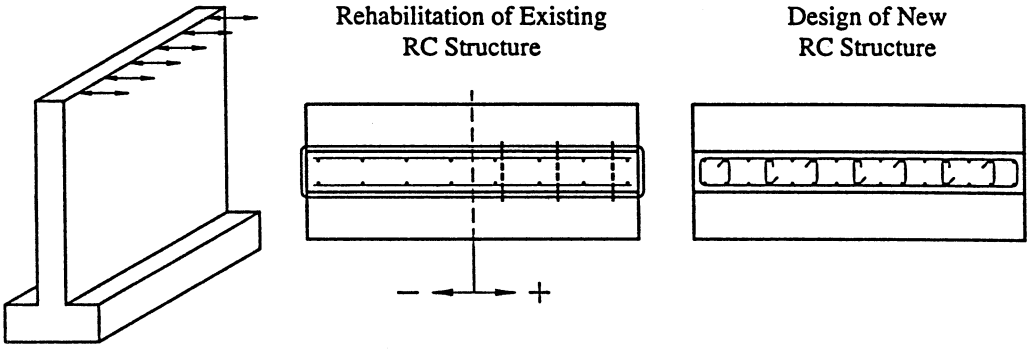


Figure 11 – Design detailing for the seismic retrofit of rectangular columns/pier walls

SUMMARY AND CONCLUSIONS

The use of fiber reinforced composites for the seismic retrofitting of concrete structures requires that appropriate design philosophies, guidelines and detailing be established and that the design be conducted using a methodology that ensures appropriate use of the material. With the appropriate design criteria for FRPs in structural seismic retrofit significant advantages can be derived form the light weight properties of these new materials and their ease of handling and installation. The structural effectiveness of FRPs in retrofitting of in-plane structural walls, out-of-plane unreinforced walls and concrete columns with shear, flexure and lap-splice problems has been demonstrated with large or splice problems has been demonstrated with large or full scale laboratory tests.

REFERENCES

[1] Seible, F., and Karbhari, V., "Seismic Retrofit of Bridge Columns using Advanced Composite Materials," Proceedings, National Seminar on Advanced Composite Materials, May 1997, 29 pp.

[2] Laursen, P.T., Seible, F., and Hegemier, G.A., "Seismic Retrofit and Repair of Masonry Walls with Carbon Overlays" University of California, San Diego, Structural Systems Research Project Report No. SSRP-95/01, January 1995, 192 pp.

[3] Weeks, J., Seible, F., Hegemier, G., and Priestley, M.J.N., "The U.S.-TCCMAR Full-Scale Five-Story Masonry Research Building Test: Part V - Repair and Retest," University of California, San Diego, Structural Systems Research Project Report No. SSRP-94/05, January 1994, 115 pp.

[4] Priestley, M.J.N., Seible, F., and Calvi, G.M., "Seismic Design and Retrofit of Bridges," John Wiley & Sons, Inc., 1996, 686 pp.

STRESS REDUCTION SYSTEM OF MEDIUM SPAN BRIDGES USING SEMIACTIVE CONTROLS

W. N. Patten, Ph.D., P.E.
Principal, SOTec Inc.
and
Director,
Center for Structural Control (CSC)
The University of Oklahoma
Norman, Oklahoma 73019
Ph: (405) 325-4242; Fax: (405) 325-1088
CSC@ou.edu; wpatten@ou.edu

Co-Authors: Jinghui Sun & Guangjun Li

ABSTRACT

Vehicle-induced vibrations of bridges tend to accelerate deck wear and to produce high cycle fatigue effects. Many U.S. interstate bridges constructed of continuous girders with composite concrete decks are now considered to have reached the limit of their useful life due to truck impact loads. The Center for Structural Control at The University of Oklahoma has spearheaded the development of an intelligent stiffener for bridges (ISB). The ISB consists of a computer-controlled hydraulic system that is easily retrofitted to an existing bridge superstructure. Field tests of the system indicate that the ISB reduces maximum stress range in the NCHRP 299 suggests that the ISB system extends the safe working life of a bridge by at least five decades. The ISB system will make it possible to avoid the reconstruction of many highway bridges at about 10% of the cost of replacement.

INTRODUCTION

Research conducted at the CSC has produced a structural vibration control system that can be retrofitted to a bridge in order to add many additional years of service life to the structure. The system is, in effect, a muscle-like structure that flexes when heavy trucks pass over a bridge and otherwise remains relaxed. The attachment of the controllable muscle to the structure produces an Intelligent Highway Bridge (IHB). The IHB utilizes Intelligent Stiffener for Bridges (ISB) as a controllable element. ISB is distinct from active control systems in that they require very little power to operate (the system relies on a 12 volt automobile battery). The technology is now being field-tested on an in-service interstate bridge and the results from that testing are expected to be published soon. Preliminary results from the testing effort are described herein.

REVIEW OF LITERATURE

The typical highway bridge is constructed with girders and composite decks. The active control of bending vibrations of a girder was considered by Abdel-Rohman *et al* (1980). They suggested a

bridge attachment of a moment-producing actuator assembly to reduce maximum deflections. They simulated the response of the girder to a moving load and determined that the suggested mechanism could provide a significant reduction of the vibration amplitude. The authors there noted that the moving load creates a nonautonomous control problem. They proposed a feedback control, where the feedback gain is obtained at each time step by solving a time-varying Riccatti Equation. While the approach is elegant, there is little possibility of accomplishing the computational effort required in real time. A more recent paper by Lin and Tretheway (1993) re-examines the girder vibration problem essentially using the same active control assembly used in the preceding reference. They also utilized an optimal tracking control (where they assume a knowledge of the magnitude and velocity of the moving load). Their control requires the solution of a time-varying Riccatti Equation. Shelley *et al* (1993) reported recent results of an experimental effort to demonstrate the effectiveness of active control when applied to a decommissioned 250' steel through-truss highway bridge in Ohio. They employed a electro-hydraulic reaction mass to dampen the in plane vibrations of the structure. The device was capable of 32" of stroke and used a 150 lb reaction mass, making it possible to develop a force output of 1000 lb. The authors employed an adaptive modal filter approach to synthesize a modal controller. The experiment produced an order of magnitude reduction of the fundamental mode of the bridge. The application of semiactive control to structures remains an uncharted area of research.

SYSTEM MODELING

The control of a simple pin-pin bridge girder with a quarter vehicle representation of a truck is examined first (Figure 1).

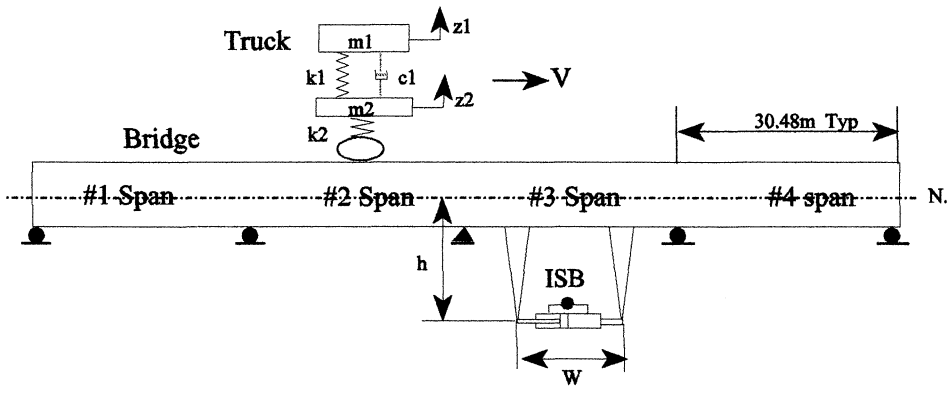


Figure 1: Four Span Bridge with Moving Vehicle

The analysis assumes that each moment arm is attached to the girder at a point. A finite element model (FEM) of the span is first established. Typical beam elements were used (Zienkiewicz (1977)). The domain is discretized and a vector of generalized coordinates is defined as $\hat{y} = [z^T, z'^T]$. $\mathbf{z}$ is the vector of global nodal displacements, and z' is a vector of the slopes at each nodal point (the prime over indicates differentiation with respect to the length of the beam). The FEM takes the form

$$M_b \hat{\ddot{y}} + C_b \hat{\dot{y}} + K_b \hat{y} = \Gamma v + \hat{d}(t) \; ; \quad \hat{y} \in R^m \tag{1}$$

The matrices, M_b, C_b, and K_b, represent the consistent mass, the proportional damping and the stiffness of the discretized girder respectively. The first term, on the right-hand side of Eqn. (1), represents the input moments to the girder produced by the ISB assembly. The matrix Γ_{mxn} is a Boolean matrix that affords a mapping between the global nodal unknowns and the inputs. The input equation assumes that the left and right control moments are equal in magnitude and of opposite sign. The input vector, $\hat{d}(t)$, represents the tire force imposed by the moving vehicle. While it is well known that the response of the system is dependent on the speed of the vehicle, vehicles traveling on roadway bridges typically move at or near the posted speed. The work here assumes that the vertical tire force is distributed to the nodes of the elements, with the relative force at each node is determined by proportioning the total load in a linear fashion. The layout of the ISB actuator is shown in Figure 2. The coordinate S represents the stroke of the piston rod, which corresponds to the relative displacement between the two moment arms.

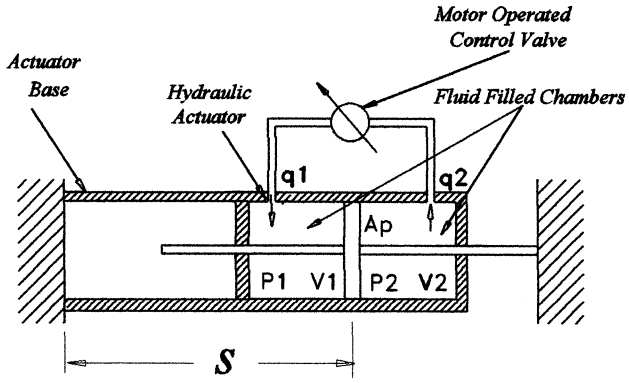


Figure 2: Semiactive Actuator

The hydraulic analysis presented here is an abbreviation of a recent article on the subject (Patten *et al* (1995)). The analysis here assumes that the compressibility of the hydraulic fluid plays an important role in the dynamics of the actuator. With that assumption, then the ISB dynamics can be expressed as

$$\Delta \dot{P} = -\alpha \beta \{A_p \dot{S} + C_d A_v g(\Delta P)\} \tag{2}$$

The valve orifice area, A_V, is bounded $0 \le A_V \le A_{VMAX}$. The nonlinear expression, $g(\Delta P)$, has the following form (Patten *et al* (1995))

$$g(\Delta P) \triangleq sign(\Delta P)\left(\frac{2}{\rho}|\Delta P|\right)^q \tag{3}$$

where the exponent **q** is **0.5** for turbulent flow through the valve. When the flow through the valve is laminar, the exponent **q** is approximately **1**. The transition from laminar to turbulent flow through a valve is usually indicated when the Reynolds number is approximately 270 (Dulay *et al* (1988)). The parameter, α, represents the change in the volumetric ratio $\alpha = (4 V_1 V_2) / (V_1 + V_2)$; where V_1 and V_2 are the instantaneous volumes of each of the actuator chambers, and β is the bulk modules of the fluid-air mix in the actuator. If β is extremely large, then the fluid-air mix is essentially incompressible. In the case of a nearly incompressible fluid, the division of both sides of Eqn. (2) by β indicates that the right-hand side of the expression is zero, leading to the simpler Bernoulli energy balance. A more rigorous analysis that includes the variation of density ($\dot{\rho}$) with respect to time is sometimes necessary when very large pressures are treated. The work here assumes the mechanical model given in Eqn. (2), adequately portrays the hydrodynamics of the ISB actuator. The relative velocity across the actuator is

$$\dot{S} = h(\dot{\theta}_A - \dot{\theta}_B) \triangleq h(\hat{R}, \hat{y}) \tag{4}$$

where $\hat{R}$ is an appropriately defined Boolean vector. Substitution of Eqn. (4) in Eqn. (2) yields

$$\Delta \dot{P} = -\alpha \beta \{A_p h(\hat{R}, \hat{y}) + g(\Delta P) C_d A_v\} \tag{5}$$

Equation (5) makes it clear that the actuator dynamics couple with the dynamics of the girder. The two terms in the bracket on the right-hand side of Eqn. (5) represent a combination of stiffening and

damping. If the valve is closed ($A_V = 0$), then stiffness dominates. On the other hand, if the valve is open $(0 < A_V < A_{VMAX})$, then the change in pressure is due impart to the elastic deformation of the fluid and to the pressure drop across the valve. Eqns. (1) and (5) are combined here in a more compact form. Defining $\hat{x} = \{\hat{y}^T, \hat{\dot{y}}^T, \Delta P\}$, and noting that the applied moment in Eqn. (1) produced by the actuator is defined as $v = h A_p \Delta P$. Then the following state space model is adopted.

$$\dot{\hat{x}} = A\hat{x} + B g(\Delta P) A_v + D \tag{6}$$

where,

$$A = \begin{bmatrix} [0]_{mxm} & [k]_{mxm} & [0]_{mx1} \\ [-M_b^{-1}K_b]_{mxm} & [-M_b^{-1}C_b]_{mxm} & [h C_d A_p M_b^{-1}\Gamma]_{mxk} \\ [0]_{kxm} & [-\alpha A_p \hat{R}]_{kxm} & [0]_{1x1} \end{bmatrix}_{rxr} \tag{7}$$

$$B = \begin{bmatrix} [0]_{mxk} \\ [0]_{mxk} \\ -[hA_p]_{1xk} \end{bmatrix}_{2m+1xk}, \qquad D = \begin{bmatrix} [0]_{mxk} \\ [d(t)]_{mxk} \\ [0]_{1xk} \end{bmatrix}_{2m+1xk}$$

k is the number of actuators, **m** is the order of the beam model, and **r=2m+1**.

Controller Synthesis

The work presented here relies on a classic Lyapunov formulation that produces a direct control decision, and seeks to achieve a sequence of control decisions that maximize the rate of dissipation of the system. It is noted, that every valve controller will produce a stabilizing solution. A Lyapunov approach that has been posed many times in the past for the regulation of nonlinear plants with saturation limits on the control variable, is adopted (Mohler (1991)). A quadratic Lyapunov function, **V**, is first posed;

$$V = \frac{1}{2}(\hat{x}^T, Q\hat{x}) \; ; \quad Q > 0 \tag{8}$$

Differentiating **V**, then

$$\dot{V} = \hat{x}^T(A^T Q + QA)\hat{x} + \hat{x}^T Q B g(X) C_d A_v + \hat{x}^T Q D \tag{9}$$

If $\dot{V}$ is negative, then we can conclude that the system is dissipative(stable). It is assumed that a **Q** exists and that $A^T Q + QA$ can be selected negative semi-definite. The last expression on the right-hand side of Eqn. (9) is disregarded, because there is nothing that can be done to effect the dissipativeness of that term. Writing **Q** as a matrix of column vectors;

$$Q = [\hat{q}_1, \hat{q}_2, \ldots\ldots \hat{q}_r] \tag{10}$$

and noting that the only nonzero entry in **B** is the last element ($b_n = hA_p$), then maximum dissipation is assured if A_V (the valve orifice) is selected using the following bi-state control law.

$$x^T q_r \, sign(\Delta P) \begin{cases} \geq 0, & A_v = A_{vmin} \\ < 0, & A_v = A_{vmax} \end{cases} \tag{11}$$

The vector $\hat{q}_r$ provides a means of weighing the different states to emphasize a particular control objective; here the reduction of the nodal displacement amplitude at the center of the bridge is the objective of the control action.

System Design

A design study was undertaken to determine the best possible combination of specific design parameters. Noting a computer simulation program was used to determine a most feasible design con figuration. The study examined the effectiveness and cost implications of the following design variables:

a) number of actuator assemblies and location on girders
b) distance between moment arms
c) high of moment arms (from natural axle of girders)
d) size of the actuator (diameter and stroke)
e) stiffness and weight of ISB assembly
f) number and location of sensors
e) bandwidth of control electronics
f) size of the control valve
g) fatigue life of the bridge and ISB components

The trade-off between cost and effectiveness was used to make a final decision. The final kinematic design of the system is shown in Figure 3. Three ISB assembly were installed on the girder #1, #3,

#5 in the third span (see Figure 3). The dimensions of the actuator cylinders and details of the moment arm assemblies are shown in Figure 4.

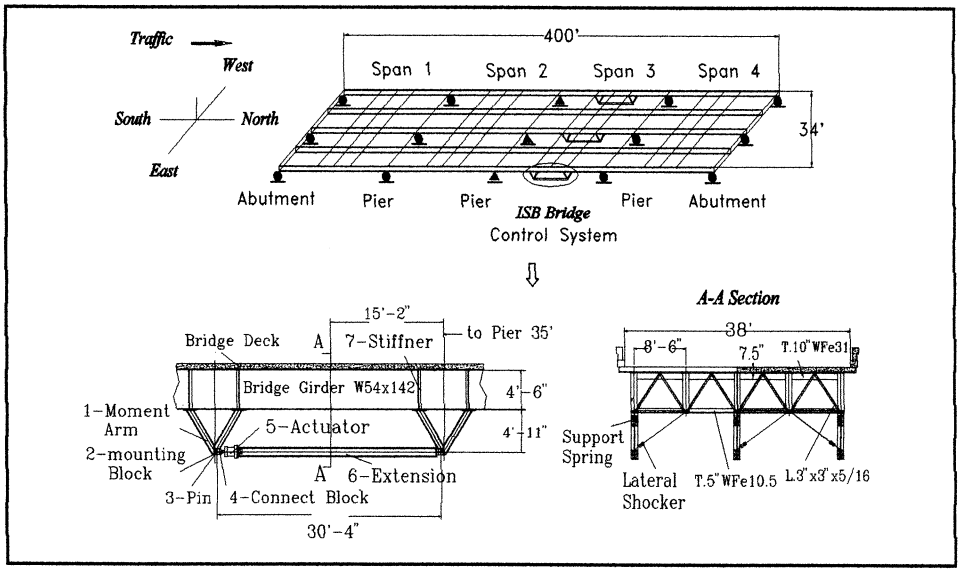


Figure 3 The final ISB system setup in the I-35 Walnut Creek Bridge

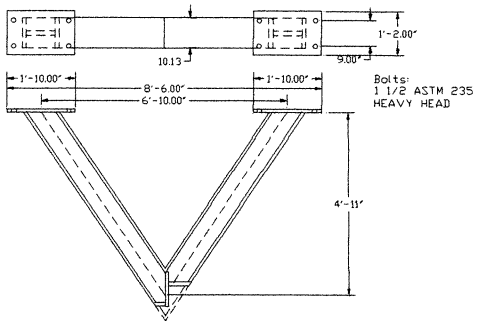


Figure 4 Design draw of moment arm

The installation on the bridge superstructure was accomplished by using monorails and block & tackle systems. First, holes were drilled in the girder to install web stiffeners. Then, holes were carefully drilled in the flange of one girder at a time. The effectiveness of the design relies in part on the ability of the ISB system to transmit forces at a specified moment in time. The installation required considerable care in the location and size of the holes drilled in the flanges. Tapered bolts and reamed holes were also used, to guarantee a no-slip condition between the moment arm

assembly and the girder that the moment arms were attached to. Next, the moment arms for the ISB assembly were hoisted into position, and bolted. Following installation of the moment arms, the actuator/extension assembly was tucked to the site. The assembly was then hooked to the monorail system, transported to its proper location, and hoisted into place. The process was repeated for each ISB assembly. Traffic was never impeded during the construction effort.

Once the mechanical hardware was installed, then the CSC team installed the computer systems and electronic components that were used to produce a intelligent semiactive control system. The ISB assembly consists of a special hydraulic actuator that is outfitted with a motor controlled valve. As Figure 5 shows, the control valve position is regulated by a DC motor which was controlled by a intel microcontroller 196 which was mounted near the actuator.

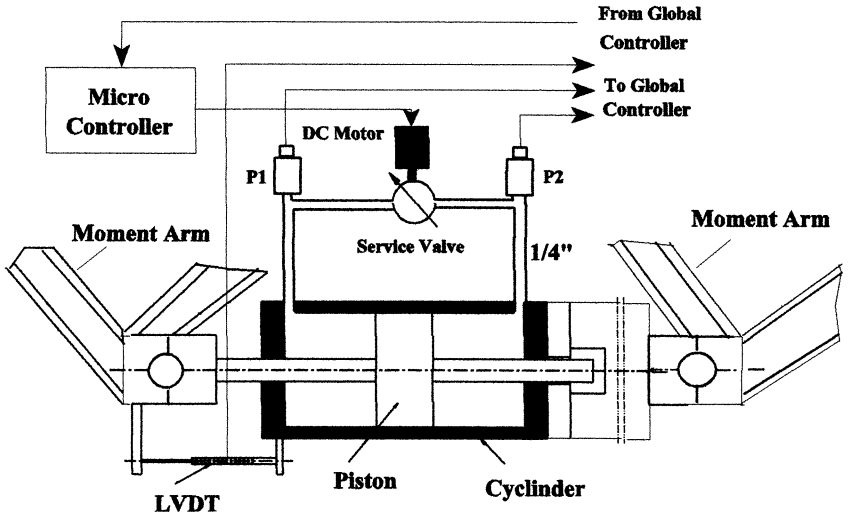


Figure 5 Kinematic assembly of an ISB actuator

A PC was used to collect all the control sensor outputs. The valve orifice area (A_V) needed to accomplish the control objective was computed at each update of the control. Figure 6 depicts the general frame work of the semiactive feedback control system which was set up on the Walnut Creek Bridge.

The closed loop operation of the ISB relies on the physical states of the bridge and of the hydraulic pressure in each of the actuators. Each actuator was outfitted with two absolute pressure sensors and an LVDT to measure the stroke of the actuator piston. The stroke of hydraulic piston for 80 klb truck load on is typically +3 mm.

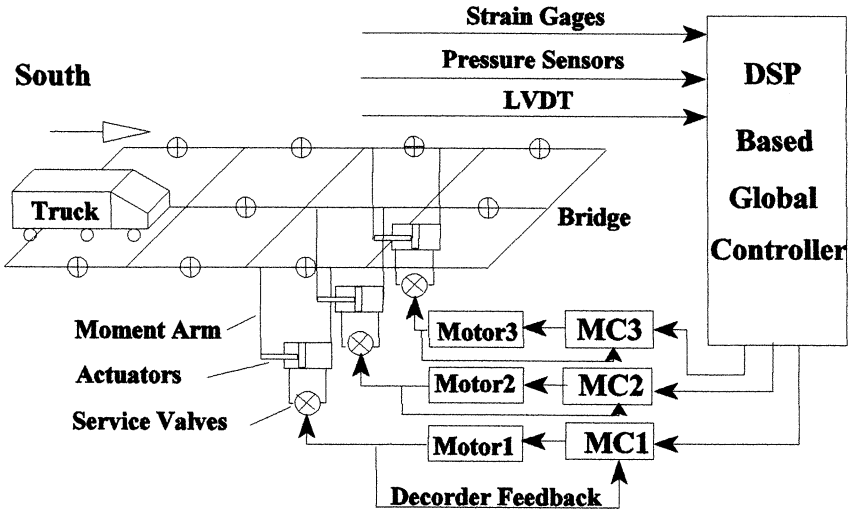


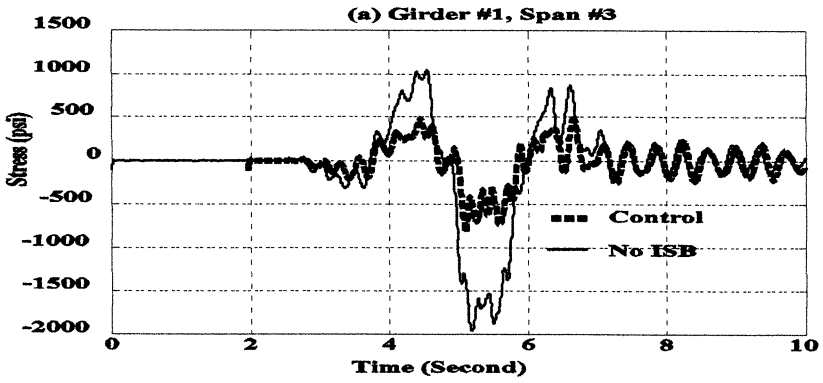
Figure 6 The control system layout; MC = micro controller

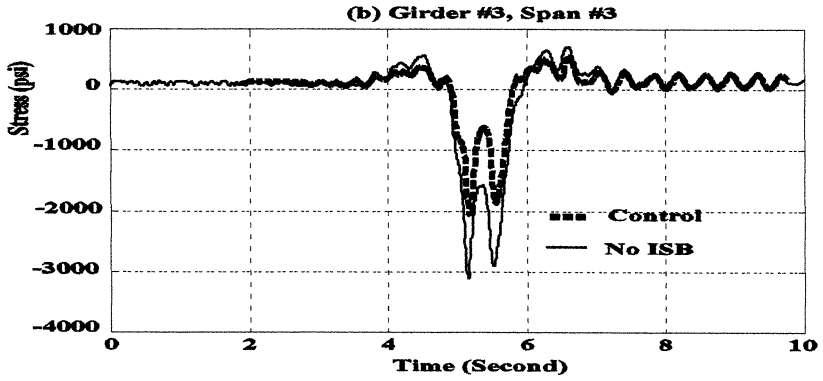
Field Test

The tests presented here rely on a Lyapunov bistate control logic. The closed loop control relies on eleven measurements: the differential pressure at each actuator (3), the relative displacement of each actuator (measured with the LVDT) (3), and the 5 strain at the bottom of the flange at the center of each of the three girders that the ISB system is attached to. Each of those measurements was weighted with a specific gain which is obtained from simulations. The weighted readings were then used to determine whether each valve should be opened or closed at each point in time.

Controlled Response

Several field tests have been conducted at the bridge to examine the performance of the control system.. The results of a test conducted in April, 1997 are reproduced here to demonstrate the closed loop performance of the ISB system.. The test included four types of test trucks. Figure 7 depicts the bridge stress response to the passage of the Heavy Truck with and without control. The test truck passed over the bridge in the right lane and at a speed of 105 km/h. The effectiveness of the ISB system is easily recognized. The ISB reduced maximum stress range by approximately 50%.





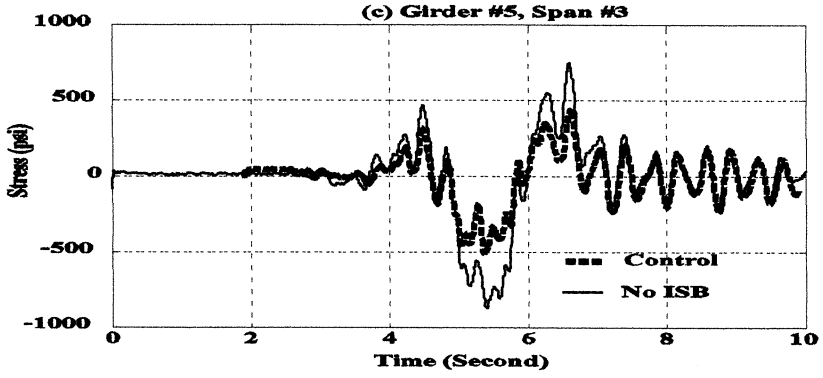


Figure 7: Close loop versus open loop control performance, HT traveling in the right lane at 105 km/h; girder #1, b: girder #3, c: girder #5.

Safe Life Predictions

The primary purpose of the ISB design was to afford a means of extending the remaining useful service life of the test bridge. The ISB accomplishes that goal by reducing the maximum deflection and maximum stress range that accompanies with the passage of heavy trucks. The assessment of the effect that the ISB had on the remaining service life of the bridge was conducted by using a specific rule prescribed for that purpose by NCHRP 299. Data obtained from the field measurements was used to make the determination of added fatigue life. Figure 8 depicts the maximum stress measured at center of the girders when the RT crosses the bridge. The tests were conducted several times for various trucks traveling in each lane. The stress reduction that accompanies the use of the ISB is significant at the posted speed limit. The calculated differences of remaining safe life when a test vehicle crossed the bridge is shown in Table 1. The differences are listed for the east girder (#1), the central girder (#3) and the west girder (#5). The minimum addition of safe life produced was 49.6 years. The equation used to conduct the calculation is given in Table 1. The table indicates that prior to the installation of the ISB system, the code indicated negative safe life. A calculation of mean life with and without the ISB system also indicates a dramatic increase in useful life. That computation always produces much more optimistic projection of remaining life than does the estimate of safe life.

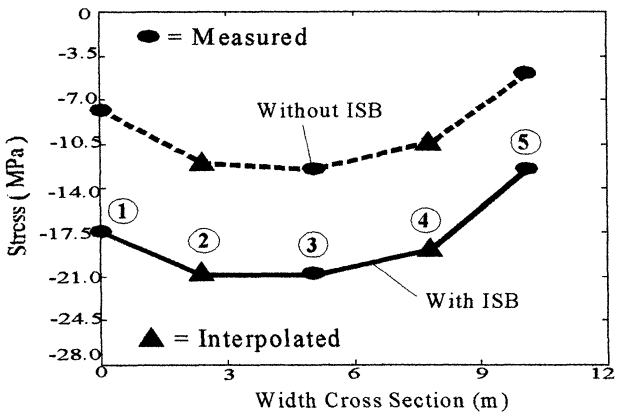


Figure 11 Maximum stress measured at span #3 mid-section, Rock Truck traveling in the right lane; girder numbered in circle

Table 1 Remain Safe Life (Ys) of Walnut Creek Bridge Using Field Measured Test Data

Span with ISB	East Girder	Center Girder	West Girder
No ISB	-12.4	-13.7	0.4
ISB Controlled	167.7	35.8	110.5
Life Extension	180.1	**49.5**	110.9

Truck = 80,000 lb., 32 ft. wheel base, 5-axle tandem tractor/trailer

Note:

Safe Life (see NCHRP 299) : $$Y_f = \frac{f \times K \times 10^6}{T_a \times C \times (R_s \times S_{re})^3} - a;$$

f=1, K=12, Rs=1.35,C=1(Rainfull count),

Ta=3000=Estimated Life Time Average Daily Truck Volume,

a=25 (present Age of the Bridge),

Sre=Maximum Stress Range: (1) With ISB=1.54 x 10^7 N/m;

(2)Without ISB=3.41 x 10^7 N/m.

CONCLUSIONS AND RECOMMENDATIONS

This paper presented a tutorial on the methods used to design a semiactive vibration absorber (ISB) for application to bridges. The control synthesis was accomplished assuming the vehicle loads to be exogenous. A Lyapunov analysis was utilized to discover a feedback control rule. Field tests were conducted with several multi-axle trucks with collaborated loads. Open loop testing (without control) indicated that almost all the heavily-laden trucks produce impact levels in excess of 1.8 times the static load. The large impacts result from the fact that truck chassis vibrations couple strongly with bridge modal vibrations. Close loop testing confirmed the effectiveness of the ISB design. The semiactive system can typically reduce maximum stresses of the most heavily loaded girders by over 40%, producing a significant increase in the expected safe life of a bridge.

REFERENCES

Abdel-Roman, M., Quintana, V.H., and Leipholtz, H.H., (1980), "Optimal Control of Civil Engineering Structures," *Journal of Engineering Mechanics Division*, Proceedings of ASCE, **106**(EM1), 57-73.

"Fundamentals of Hydraulic Power Transmission," (1988), Dulay, I.K. (ed.), with Fureze, F., Harkey, G., and Lukacs, J., In *Studies in Mechanical Engineering*, **7**, New York, NY: Elsevier .

Lin, Y.H., and Trethewey, M.W., (1993), "Active Vibration Suppression of Beam Structures Subjected to moving Loads: A Feasibility Study Using Finite Elements," *Journal of Sound and Vibration*, **166**(3), 383-395.

Mohler, R.R., *Nonlinear Systems*, (1991) Englewood Cliffs, New Jersey: Prentice-Hall, Inc.

Patten, W.N., He, Q., and Sack, R L., (1995), "New Life for Highway Bridge via Semiactive Vibration Absorbers (SAVA)," Submitted to *Journal of Bridge Engineering*, ASCE, Nov.

Patten, W N., He, Q., He, J., and Hu, J., (1994), "A New Algorithm of Semiactive Control for Suspension with Nonlinear Leaf Spring," *ASME Winter Annual Meeting*, Chicago, IL, 147-156.

Patten, W., He, Q., Kou, C.C., Liu, L., and Sack, R.L., (1994), "Suppression of Vehicle Induced Bridge Vibration Damper (SAVA)," *First World Conference on Structural Control*, Los Angles, CA, Aug. 3-5, **FA2** 83-89.

Patten, W.N., Sack, R.L., and He, Q., (1996), "A Controlled Semiactive Hydraulic Vibration Absorber for Bridges," *Journal of Structural Engineering*, ASCE, **122**(2), 187-193.

Shelley, S.J., Aktan, A.E., and Frederick, N., (1993), "Active Vibration Control of a 250 Foot Span Steel Truss Highway Bridge," *Second IEEE Conference on Control Applications*, Vancouver, B.C., Sept.

Zienkiewicz, O.C., (1977), "The Finite Element Method (third Edition)." Maidenhead Berkshire, England: McGraw-Hill Book Company (UK).

NOMENCLATURE

A The plant matrix

A_p Effective piston area of actuator; M^2

A_v Hydraulic valves orifice area; M^2

A_{vmax} Maximum hydraulic orifice area; M^2

A_{vmin} Minimum hydraulic orifice area; M^2

B Control input matrix

c_1 Damping coefficient of truck suspension; N*S/M

C_b Bridge damping matrix

C_d Service valve fraction coefficient

d(t) Truck disturbance; N

D Truck disturbance input matrix; N

E Young's module; N/M^2

$g(\Delta P)$ Nonlinear damping function

h Height of moment arms; m

I Inertia of the bridge girder; M^4

k_1 Stiffness of suspension; N/M

k_2 Stiffness of tire; N/M

K_b Bridge stiffness matrix

K_t Truck stiffness matrix

K_{tire} Stiffness of tire N/M

L Span length of the bridge; m

m_1 Mass of tire; kg

m_2 Mass of truck body; kg

M_b Bridge mass matrix

M_t Truck mass matrix

Q Weighing matrix of control

q_r Last column weighing matrix of control

$\hat{R}$ Boolean matrix

v Truck traveling speed; m/s

V Lyapunov function

V_1 Volume of actuator chamber

V_2 Volume of actuator chamber

w Static weight of truck; kg

W Width of moment arms; m

$\hat{x}$ State vector of bridge; m

$\hat{y}$ Generalized coordinate of bridge

$\hat{z}$ Displacement vector of bridge

$\dot{z}_0$ Initial velocity of truck suspension; m/s

α Coefficient of hydraulic damper; N/M^2

β Coefficient of hydraulic damper; N/M^2

Δ Beam element length; m

ΔP Differential pressure of hydraulic damper; N/M^2

Γ Boolean matrix

ν Semiactive control force vector

ρ Density of hydraulic damper; N/M^3

θ_A Angle of A moment arm

θ_B Angle of A moment arm

SMA Devices for Seismic Isolation of Bridges: Design and Experimental Behaviour

Mauro Dolce[(1)] and Roberto Marnetto[(2)]

[(1)]USB-DiSGG (Dipartimento di Strutture, Geotecnica, Geologia applicata all'ingegneria, Università della Basilicata), Italy

[(2)]T.I.S. (Tecniche Idraulico-Stradali) S.p.A., Rome, Italy

Abstract

Shape Memory Alloys, for their peculiar properties, have a great potential in the field of passive seismic protection of structures. The MANSIDE (Memory Alloys for New Seismic Isolation DEvices) project is aimed at exploiting this potential, through comprehensive experimental and theoretical studies. MANSIDE is funded by the European Commission, within the BRITE-EURAM program. It has started on December 1995 and will end on March 1999. It has lead to the conceptual design, the implementation and the experimental testing of a family of devices for seismic isolation and passive energy dissipation of buildings and bridges.

In the proposed paper the main experimental results on the mechanical behavior of some selected shape memory elements are shown. The conceptual design of a family of energy dissipating devices having full re-centering and high energy dissipation capabilities, as well high resistance to large strain cycle fatigue and great durability, are described. The experimental behavior of the devices is shown by the results of the cyclic tests on the devices and of shaking table tests on scaled frame models. Finally the applicability to bridges is demonstrated by an example.

Introduction

Passive protection of bridges against seismic vibrations with the use of special devices is widely accepted as a very effective antiseismic technique, both for new constructions and for the retrofitting of existing ones. Several types of devices have been implemented and used, however the increasingly demanding performance requirements push towards the development of new devices, exploiting the peculiar characteristics of new advanced materials. Indeed the present technologies present some limitations such as problems related to ageing and durability (e.g. for rubber components), to maintenance (e.g. for those based on fluid viscosity), to installation complexity or

replacement and geometry restoration after strong events (e.g. those based on steel yielding or lead extrusion), to variable performances depending on temperature (e.g. polymer based devices).

The present achievements in quantity production of smart materials, and specifically shape memory alloys (SMA), to date applied mainly in medical sciences, electrical and mechanical engineering, can open a new application field within civil engineering, specifically in the protection of constructions against seismic vibrations. SMA's show the potential to eliminate some limitations involved in present technologies, allowing a broader application. This is achievable thanks to a combination of behaviour, installation and maintenance advantages, connected to a more reliable and constant behaviour over time.

Some experimental and theoretical studies have already been performed with the aim of exploring the potential of SMA in seismic vibration control. Some of them (1, 2) were related to assess the experimental behaviour of SMA elements stressed under different conditions, or to compare behaviour of frames with energy dissipating braces based on SMA and other materials, some others were mainly aimed at the conceptual design of devices (3, 4, 5). A comprehensive study, with experimental results both on the material and on frame models embodying SMA devices in energy dissipating braces is presented in (6). However a more comprehensive research was needed in order to fully explore the possibilities of applying SMA in both seismic isolation and energy dissipation systems.

Within this framing, the MANSIDE (Memory Alloys for New Seismic Isolation and energy dissipation DEvices) project, whose total value is about 4000 KECU, was proposed to the European Commission and funded with 2385 KECU within the BRITE-EURAM framework. The total duration of the research project is 40 months, starting from December 1995.

Aim of MANSIDE is the conceptual development, design, construction and testing of seismic devices based on SMA. The specific application field considered shall be the protection of buildings and infrastructures against seismic events. Major products of the project will be:

- Isolation-dissipation components based on SMA
- Completed and tested prototypes of passive protection devices
- Engineering processes for design, manufacturing and installation
- Guidelines for design and use, including system reliability requirements.

N.	Organisation	Function	
1	DSTN-SSN	Developer	• coordination / guidelines
2	AMT	Supplier	• material and components for devices
3	TIS	Developer/end-user	• design of devices
4	AIAS	End-user	• construction and tests of structural models
5	USB-DiSGG	Developer	• lab tests of devices / numerical modelling
6	KULeuven R&D	Developer	• material characterisation
7	COMET	Manufacturer	• device manufacturing
8	SMM	Developer	• material and component for devices
9	EDIN	End-user	• structural design/technical-economical validation

Table 1. Partners in the MANSIDE project.

The research program is conceptually divided into the 4 tasks, as described in fig. 1. The first three tasks (T1, T2, T3) are relevant respectively to:

- the design, production and testing of SMA materials and components,
- the design, manufacturing and testing of SMA devices,
- the design, construction and testing of structural models equipped with SMA devices and, for comparison, with steel or rubber devices or without devices.

In the fourth task all the design, production and test data are collected and examined, to validate the new devices with respect to technical and economical aspects and to develop technical guide-lines for an optimal use of SMA devices in structural vibration control.

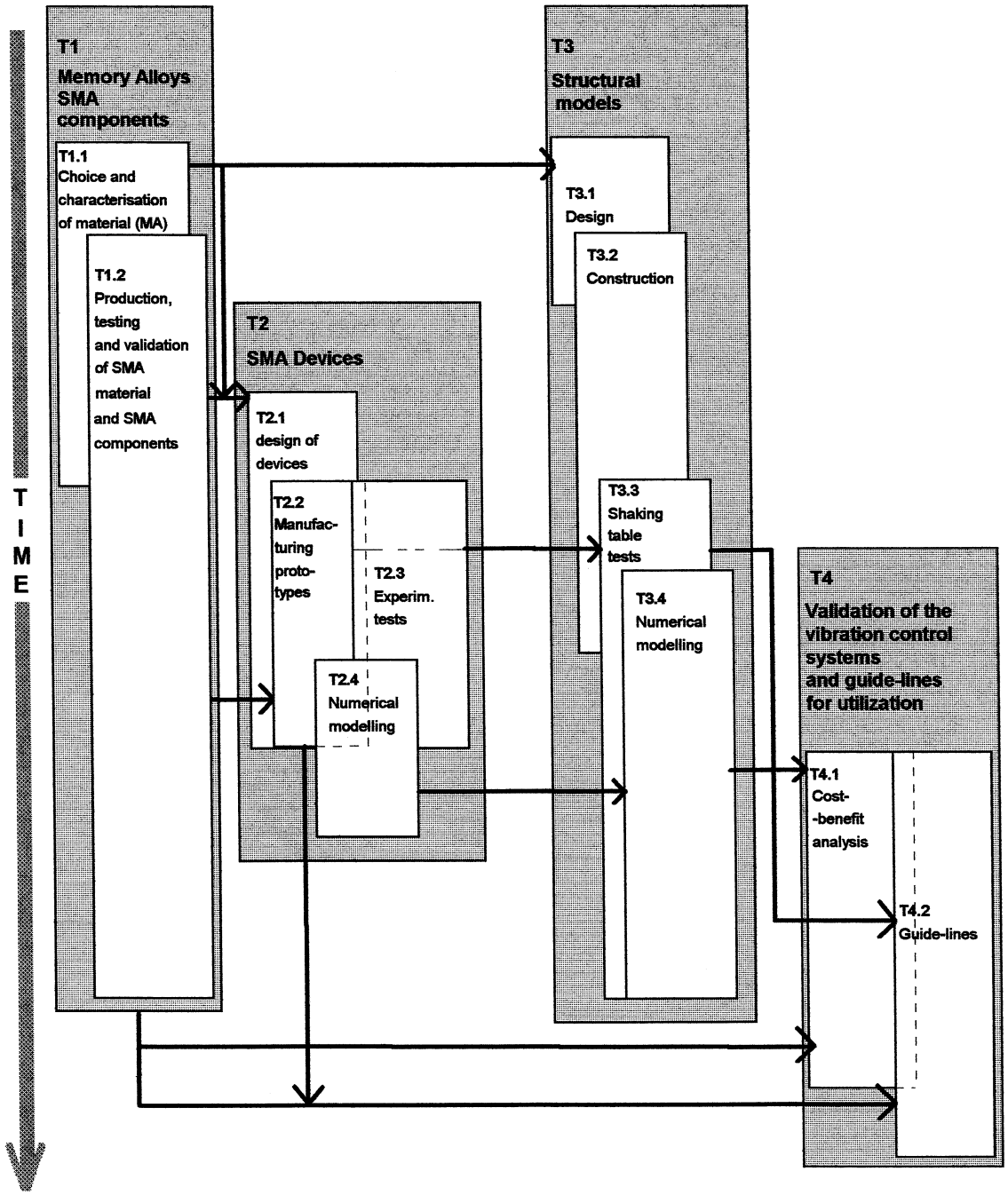


Fig. 1 - Flow-Chart of the research programme.

An overview of the participants and their role in the project is given in tab. 1. The team comprises nine organisations from four European countries, with the industrial partners encompassing all the classes in the relevant product chain, from material production (SMM, Sw), to material manufacturing (AMT, Be), device production-installation (TIS, It,) and civil engineering construction (AIAS, Gr). The co-ordination is provided by an Authority (SSN, It), with unique expertise and statutory role in the field of seismic problems, while two Academic Institutions provide scientific support and advanced methodological capabilities on SMA's (KULeuven, Be) and seismic isolation (USB, It). Finally, a civil engineering consultant company (EDIN, It) supplies engineering design expertise and point of view. Two main subcontractors have been enrolled to co-operate in the shaking table testing (Technical University of Athens) on 1/3.3 scaled structures and in the development of theoretical models to simulate the behaviour of SMA and SMA-based devices (University of Rome 3).

A comprehensive description of the MANSIDE project as well as the first achievements during the first year and half is provided in (7). In this paper the aspects related to the conception, design, testing of the devices are specifically addressed, with particular attention focused on the possible applications in bridge design.

Shape Memory Alloys

Memory Effect and Superelasticity are the functional properties that mostly distinguish Shape Memory Alloys from other metallic alloys. Both effects depend on the transformation temperatures between different phases, namely M_s, M_f, A_s, A_f, and on the current temperature of the material T. The transformation temperatures are properties of a specific material and can be varied according to their treatments.

If $T<M_f$ and the material is slowly strained up to 6-8%, it shows a "stress plateau" and a residual strain at the end of the action. This is only apparently similar to what happens in steel. In fact if the specimen is heated up to a temperature T>Af, the residual strain is completely recovered (*Memory Effect*).

If $T>A_f$ and the material is slowly strained up to 6-8%, then it shows again a "stress plateau", but the deformation is completely recovered when unloading (*Superelasticity*).

The first type of behaviour occurs for the material being in the martensitic phase, while the second behaviour is typical of the material initially being in the austenitic phase. If the loading process is cyclic, a considerable energy dissipation is obtained for martensite, while lower energy dissipation is obtained for austenite, with a very large fatigue resistance for both, even under repeated strains up to 6-8%.

These peculiar performances are made possible by the reversible solid-solid transformations (i.e. transformations of the crystalline structure) involving the martensite and austenite phases. Such transformations can be stress-induced or thermally induced. These two aspects are dual and not independent: the application of a constant stress varies the transformation temperature, while different ambient temperature determine different stress levels at which the phase transformation is activated and completed.

In order to explain memory effect and superelasticity in terms of phase transformation the following considerations hold.

If $T<M_f$, the material is initially in its martensitic state. Its crystalline structure is characterised by a series of variants, which are coupled among them. The application of a load produces the un-coupling of the variants, their re-orientation and the growth of the variants aligned along the loading direction. This phenomenon corresponds to the stress plateau in a force-displacement cycle. When unloading, only the elastic part is recovered and a large residual strain remain. When heating beyond A_f, martensite is completely transformed into austenite, which is characterised by a unique (cubic) crystalline structure. Therefore the specimen recover its initial shape, which is maintained even after cooling down to the starting temperature $T<M_f$, thus re-transforming into martensite.

If $T>A_f$, the material is initially in the austenitic state. The application of a load induces the transformation of austenite into uncoupled martensite. This transformation correspond to the stress plateau. When unloading, the inverse martensite-austenite transformation occurs and the initial shape is recovered, as unstressed martensite is unstable if $T>A_f$.

The mechanical behaviour of SMA also depends on the strain rate, i.e. on the frequency of the loading, as energy dissipation decreases and hardening increases when increasing load frequency. However it is clear that SMA, in both the martensite and the austenite states, could be favourably used in vibration control systems. In particular, the superelasticity of austenite and the energy dissipation capability of martensite at high strain levels, as well as the unique fatigue resistance of both, appear as the most appealing features for such kind of applications.

Several metallic components can be used to make SMA. The most popular and suitable for vibration control are those based on Nickel and Titanium and on Copper, Zinc and Alluminium. In the present work, all the activities were concentrated on the alloys based on Nickel and Titanium, as they were judged to be the most suitable for passive control applications.

The main drawback of these materials are related to their high costs, which is of the order of 100-200$ per kilogram. However, it can be counterbalanced by the superior performances of SMA. In any case the high cost calls for a very careful design of the passive control system, aimed at maximising the exploitation of the material.

Tests on SMA Elements at DiSGG

A large number of static and dynamic tests were carried out on SMA elements at the Laboratory of DiSGG, University of Basilicata – Italy. The tests were aimed at characterising the behaviour of different SMA elements (wires and bars), under different stress conditions, as well as finding the best solutions to exploit SMA properties in seismic devices for energy dissipating braces and seismic isolation. Both martensite and austenite elements were tested by applying cyclic sinusoidal deformation to the specimens.

The following groups of tests were carried out at ambient temperature (approximately 20° C):

1. Tensile tests on austenite and martensite wires
2. torsional tests on 8 mm diameter austenite bars
3. torsional tests on 6.7 mm diameter martensite bars
4. torsional tests on 30 mm diameter hexagonal austenite and martensite bars
5. flexural tests on 6.7 mm diameter martensite bars in double bending
6. flexural tests on 6.7 mm diameter martensite bars in roller bending (U elements)
7. flexural tests on 13 mm diameter martensite bars in roller bending (U elements)
8. axial tension-compression tests on 6.7 mm diameter bars.

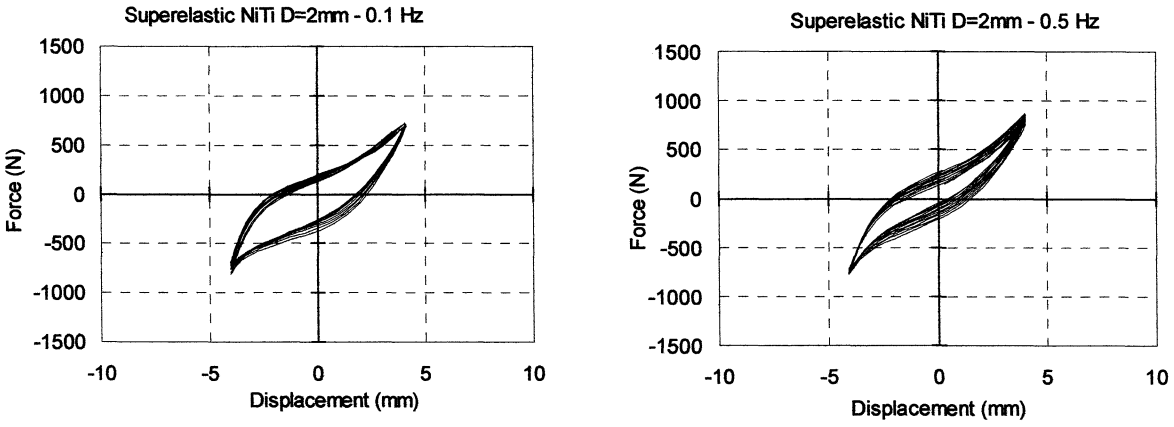


Fig. 2. Tension cyclic tests on ϕ2 mm austenitic NiTi wire at 0.1 and 0.5 Hz frequency, 4% strain.

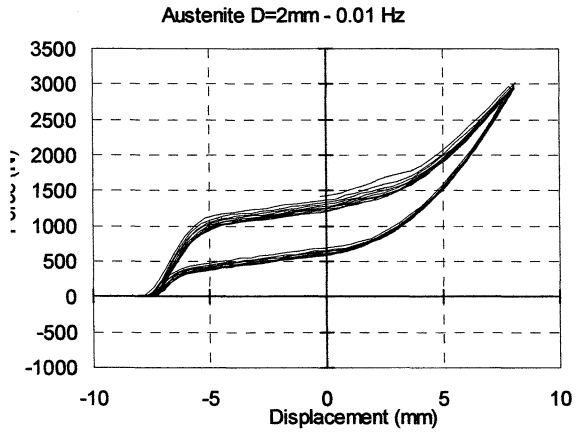


Fig. 3. Tension cyclic tests on ϕ2 mm austenitic wire at 0.01 Hz frequency, 8% strain.

Axial tensile loading-unloading tests were made on several wire samples of superelastic binary and ternary NiTi alloy, and on a couple of NiTi martensitic samples. The tests were carried out for two values of the maximum strain, 4% and 8%, at different frequencies, from 0.01 Hz to 4 Hz (strain rate 0.0008-0.32 sec^{-1}). In figs 2 and 3 some typical experimental force-displacements diagrams for NiTi alloy, for different frequency and strain values are reported, while tab. 2 summarises the results of several tests at different strain amplitude and rates. The influence of frequency is apparent. The tests on martensitic wire specimens were only monotonic, and were aimed at evaluating their general behaviour up to failure.

Gauge L (mm)	Test N.	Test Freq. (Hz)	Start displ. (mm)	Cyclic displ. (mm)	Strain (%)	Strain rate (s^{-1})	N. of cycles	K (N/m)	Wd (N*m)	Wd (J/g)	ξeq. (%)
200	1	0.01	5	4	4%	0.0008	3	202671	4.855	1.199	23.67%
	2	0.1	5	4	4%	0.008	10	215945	2.814	0.695	13.16%
	3	0.5	5	4	4%	0.04	10	225228	2.126	0.525	9.48%
	4	1	5	4	4%	0.08	10	227332	1.826	0.451	8.08%
	5	2	5	4	4%	0.16	10	223924	1.399	0.345	6.22%
	6	4	5	4	4%	0.32	10	200305	1.329	0.328	6.62%
	7	Slow-Beyond yelding		20	10%		1				
	8	0.1	12	8	8%	0.016	10	145507	5.991	1.479	9.90%

Tab. 2. Summary of experimental results for NiTi superelastic wires.

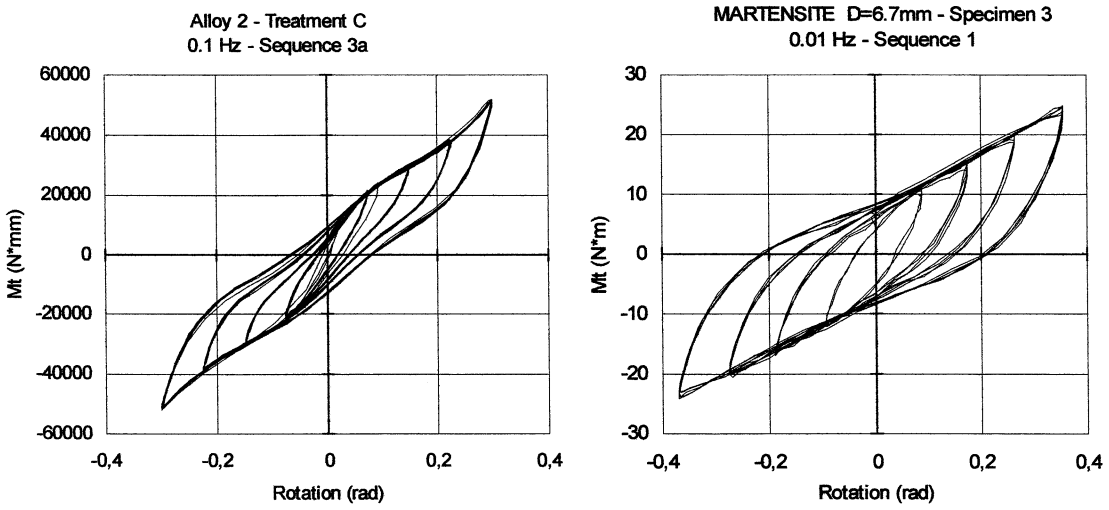


Fig. 4. Moment-rotation cycles in torsional tests on SMA \austenite ϕ8mm bars (left) and martensite ϕ6.7mm bars (right).

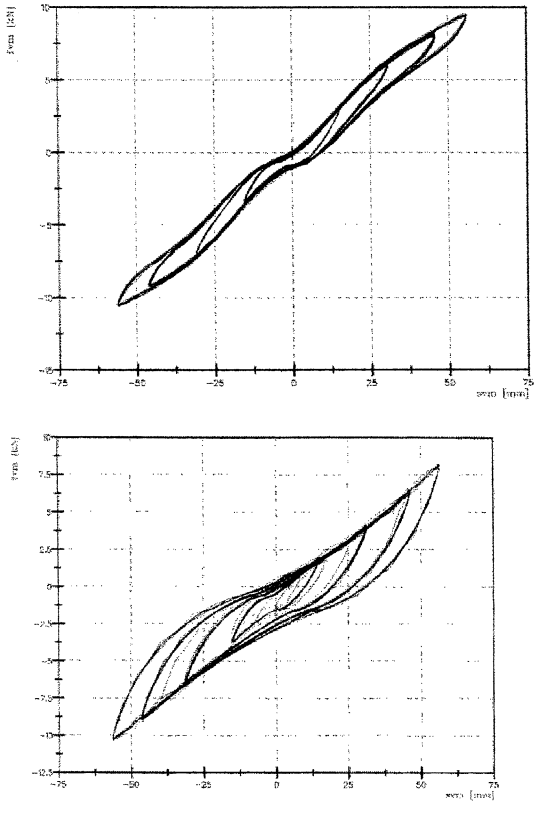


Fig. 5. Torsion test on austenite (top) and martensite (bottom) ϕ30mm bar.

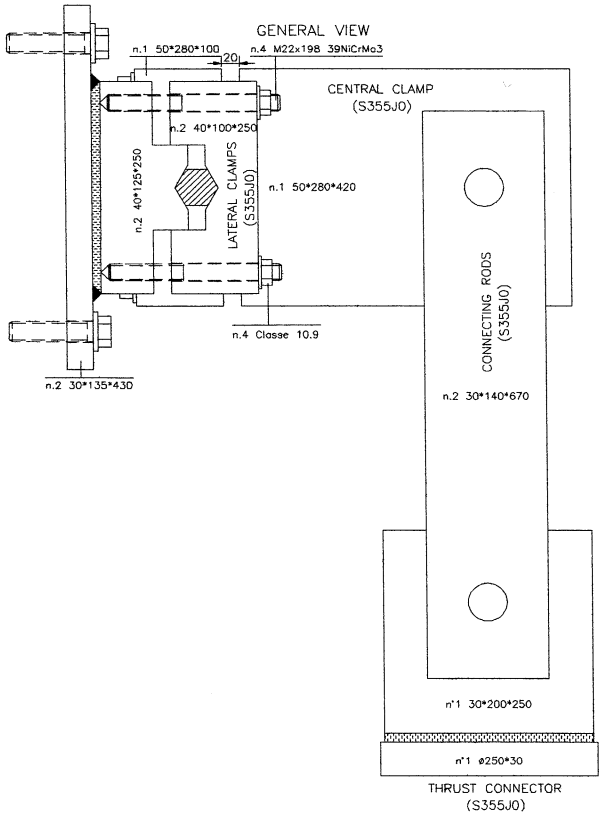


Fig. 6. Mechanical equipment for torsional tests on big size bars.

The first torsional tests were carried out on five cylindrical ϕ8 mm austenitic specimens, made of 3 alloys and 3 types of treatment (2nd group of tests), as well as on some ϕ6.7 mm martensite specimens (3rd group of tests). Torsion was applied through a rigid arm, as it can occur in the arrangement of seismic devices. The length of the arm could be varied from test to test. Therefore, specimens were subjected to shear and bending, besides torsion. The torsional tests were made for different values of the surface maximum nominal strain γ, namely 3%, 6%, 9%, 12%, 15%, 18% and at various strain rates and frequency. For all specimens, failure was reached after some hundreds (austenite) or thousands (martensite) of large strain cycles (up to18%). Typical moment-rotation diagrams are provided in fig. 4.

The 4th group includes torsional cyclic tests on big size (30, 40, 50 mm diameter) hexagonal austenitic and martensitic bars. At this purpose, a special mechanical equipment was manufactured (see fig. 6), whose working principle is the same as the one used for the small size bar testing. Only three 30 mm diameter bars have been tested up to now. One martensite and two different austenite specimens were tested. The typical cyclic behaviours obtained for the martensite bars appear quite similar to the results obtained for the small size bars. For the austenite bars a lower energy

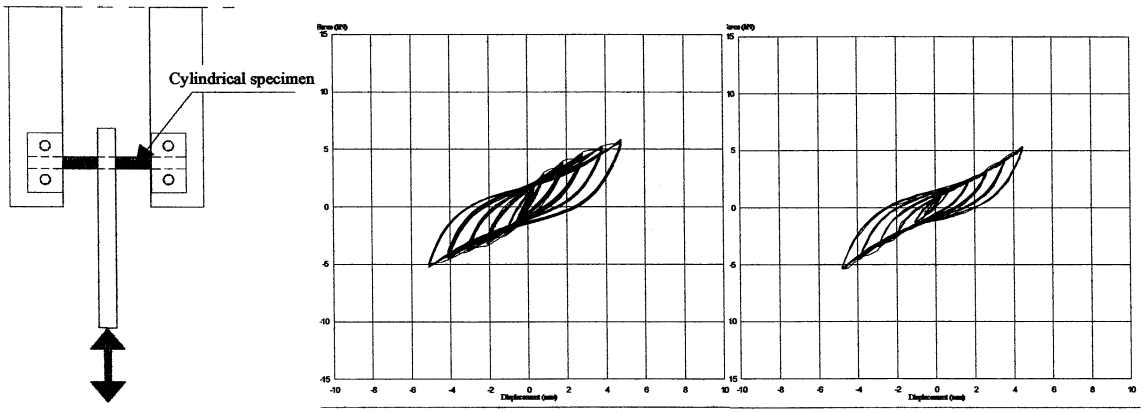


Fig. 7. Test setup tests of bars in double bending and force-displacement cycles of SMA martensite ϕ6.7mm bars at 0.2 Hz (left) and 1 Hz (right) frequency.

dissipation capability was found. Two typical diagrams are shown in fig. 5.

The 5th test group was aimed at evaluating the behaviour of cylindrical martensite bar specimens, arranged in a very simple way to be subjected to double bending (see fig.7). Although the induced stress state is not optimal for what concerns the exploitation of the material, the easy mechanical arrangement justifies the interest for this test. Three series of tests were carried out. They differ for the value of the deformable length L, taken equal to 30, 20 and 10 mm. Many sequences of cyclic displacements from 0.5 mm up to 10 mm, at different frequencies (from 0.2 up to 4 Hz), were made. Typical force-displacement diagrams are shown in fig. 7.

The test groups 6 and 7 were aimed at evaluating the behaviour of martensite U-shaped bar specimens subjected to roller bending (see fig. 8). Although the induced stress state is not optimal for what concerns the exploitation of the material, the easy arrangement and compactness of the energy dissipating SMA component, with respect to the large displacement allowed, justifies the

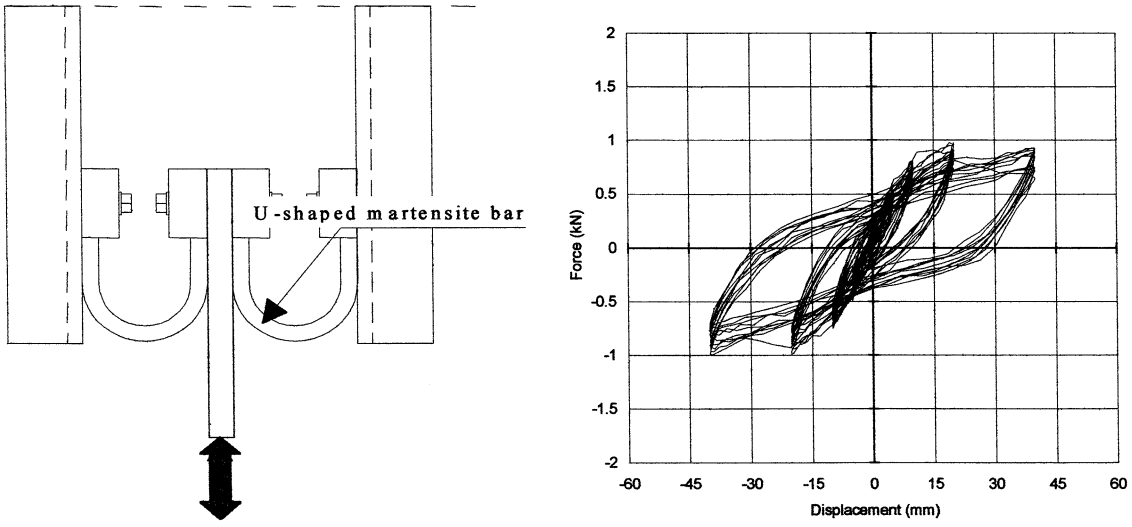


Fig. 8. Test set up for bars in roller bending and force-displacement cycles of SMA martensite ϕ6.7mm bars at 0.2 Hz frequency

interest for this test. The tests were carried out by applying many sequences of cyclic displacements from 1 mm up to 40 mm, at different frequencies (from 0.2 up to 1 Hz), to bar specimens, bent with 45 and 25 mm internal curvature radius, corresponding to about 7% and 12% maximum surface initial strain.

Finally a few tests were carried out on some short 6.7 mm diameter bars, under cycling tension-compression, in order to check the possibility of exploiting this kind of stress condition for energy dissipating braces. The tests confirmed the strong difference in the behaviour under compression and tension stresses, already emphasised by the tests carried out at KULeuven.

Selection of SMA Elements for Devices

In view of their use in seismic devices, the mechanical performances of martensite and austenite are to be examined separately.

As far as martensite materials and components are concerned, the failure tensile tests and the cyclic tests in tension-compression, torsion, and bending emphasised a mechanical behaviour generally favourable to applications in passive control devices. Such behaviour, which depends on the annealing temperature of the production process, is characterised by a great capacity of deformation, eventually recoverable by the memory effect, and of energy dissipation.

The torsion and the flexure tests, carried out on the same alloy, provided qualitatively similar results. They showed good dissipation capability and some hardening. However energy dissipation tends to reduce and hardening tends to increase when increasing frequency,.

In deciding the shape and the stress mode of martensite elements to be included in seismic devices, wires can be definitely excluded for their instability in compression and their permanent deformation in tension. Martensite elements can then be used only as round or hexagonal bars of different diameters.

Taking into account the cost of the material, the most efficient stress mode in terms of energy dissipation is tension-compression, followed by torsion and then bending. Such consideration, however, is purely theoretical, and must be related to the practical difficulties in realising a seismic device. A particular attention shall be devoted to:

a) the mechanism to transmit or transform the movement of the device into the deformation of the SMA energy dissipating elements;
b) the clamping length needed to connect the SMA elements to the moving parts of the device with respect to the active length.

It can occur that the most efficient stress modes imply such complications in the device construction and functioning, that the material savings in the energy dissipating part of the SMA element is largely overcome by the greater cost of the device and the additional clamping lengths. Generally speaking, it may be observed that, while tension-compression and flexure-shear modes can be easily obtained by directly connecting the end portions of the element to the mutually moving parts of a devices, the torsion mode needs a suitable mechanism to transform displacements into rotations. Moreover, torsional bars, especially round bars, require large clamping lengths. On the other hand, for tension-compression mode, lateral constraints shall be provided to the bar to avoid buckling in compression. The double bending mode (shear and flexure) is undoubtedly the easiest to realise with respect to the two aforementioned problems.

As far as austenite materials and components, the cyclic tensile tests on wires, as well as torsion tests and tension-compression tests on bars, permit to make important considerations.

The superelastic features appear perfectly attained in wires subjected to loading-unloading cycles in tension, while residual deformations occur in bars subjected to tension-compression and to torsion Therefore these latter cannot be effectively used to get re-centering devices.

The energy dissipation capabilities of the austenitic alloys strongly depend on the frequency. It has turned out to be rather low, if not insufficient, in the usual field of application of seismic devices (0.4 - 4 Hz), being the equivalent viscous damping equal to or less than 10%.

Finally the variability of the mechanical properties of austenite as a function of the temperature must be considered and related to the actual temperature variation in the field of application of devices in civil structures. In this respect, a careful design of the alloy is required.

Requirements of the Seismic Isolation Devices

The main scope of the MANSIDE project is the design of two families of engineered devices based on SMA:

- energy dissipating braces for framed structures
- seismic isolation devices for buildings and bridges.

In order to optimise the overall response of the structural system embodying them, a preliminary evaluation was carried out by a series of numerical simulation analyses at different levels of detail. The same numerical models were also used to check the effectiveness of the SMA passive control systems, with respect to other conventional systems, and to verify the improvement of performance with respect to the same structures without passive control.

The re-centering and the energy dissipation capabilities, were chosen as the main objectives of the design. Functional simplicity, no maintenance, i.e. durability and fatigue resistance, limited encumbrance and economy were selected as additional objectives.

After some theoretical studies, aimed at exploiting martensitic and austenitic bars in torsion within seismic devices, and taking into account the experimental results on SMA components, the conceptual design was especially focused on the possibility of achieving the two aforementioned main objectives (re-centering and energy dissipation capacities) by means of two separate groups of SMA elements.

The re-centering capability can be obtained by using austenite wires. The energy dissipation capability can be provided either by martensite bars subjected in bending or torsion, or by austenite superelastic pretensioned wires, acting as a double counteracting system of springs. A hybrid solution, which appear suitable from many points of view, relies upon the energy dissipation capabilities of compact and low-cost steel elements (e.g. see (8)). From the technical point of view, the advantages of this solution come from the high energy dissipation capability of steel (see fig. 9), its very low hardening, the independence from temperature, with the only drawback of the eventual need of substituting the elements after very strong earthquakes. However the self-centering capability of the system is preserved, as will be seen later. From the economical point of view the costs of the dissipating group is dramatically reduced.

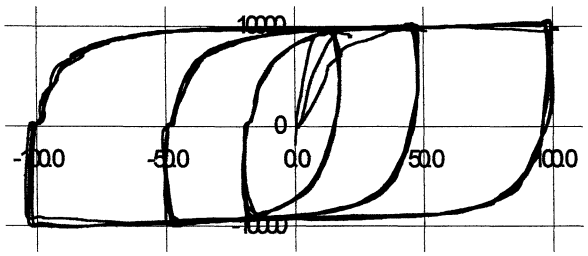


Fig. 9. Typical experimental force-displacement cycles on a steel-base energy dissipation device (8).

In order to explain the conceptual design and the actual behaviour of such devices, it is necessary to examine separately the theoretical behaviour of the two complementary functional groups.

If one refers to a simplified scheme, in which the self-centering SMA group has a nonlinear elastic behaviour, while the energy dissipating group has a perfectly plastic behaviour, the force-displacement cycles separately shown in fig. 10 are obtained.

In order to improve the re-centering capability of the first group, some pre-strain shall be applied, so that an initial infinite stiffness is obtained. If these two behaviours are combined together, just summing up the forces of the two components relevant to the same displacement, the cycles of fig. 10 are obtained. The energy dissipation can be varied according to the number of elements in the energy dissipating group. However in order to keep the re-centering feature, the maximum force corresponding to the zero displacement value must be not greater than the prestress force of the recentering group. The desired behaviour is then obtained by calibrating the number and the charactestics of the elements of both groups, as well as the level of prestress. According to the supplemental recovering force or the residual displacements of the force-displacement cycles, the family of devices that can be obtained by applying the above explained concepts can be subdivided into the following main categories (see fig. 11):

- Supplemental Re-Centering Devices: a supplemental recovering force is available to re-center the structural system, even in presence of parasite forces (e.g. friction in devices, plastic forces in structural elements, etc.), external to the device;
- Self-Centering Devices: the device recover the initial position at the end of the action, but no supplemental force is available;

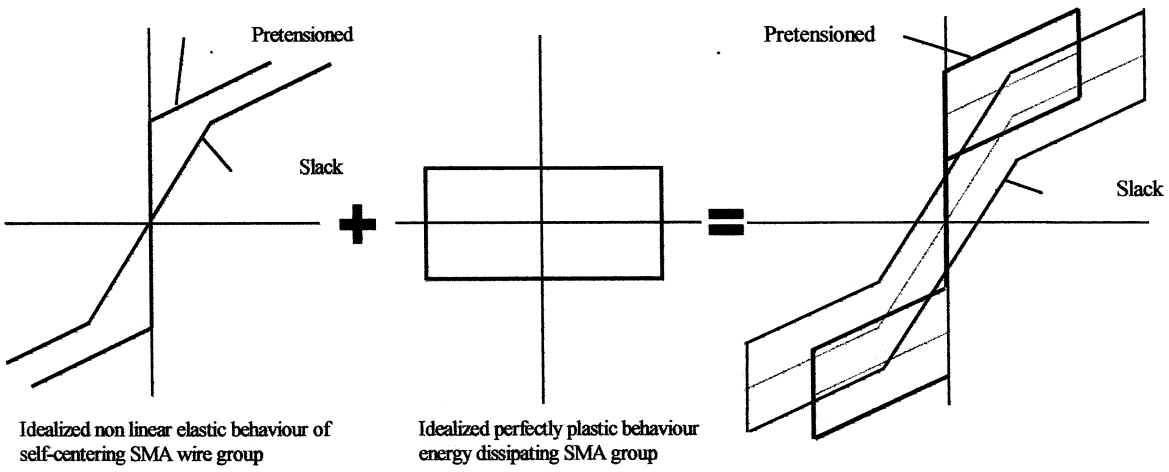


Fig. 10. Idealised separated and joint behaviour of the two SMA groups of a self-centering / energy dissipating device.

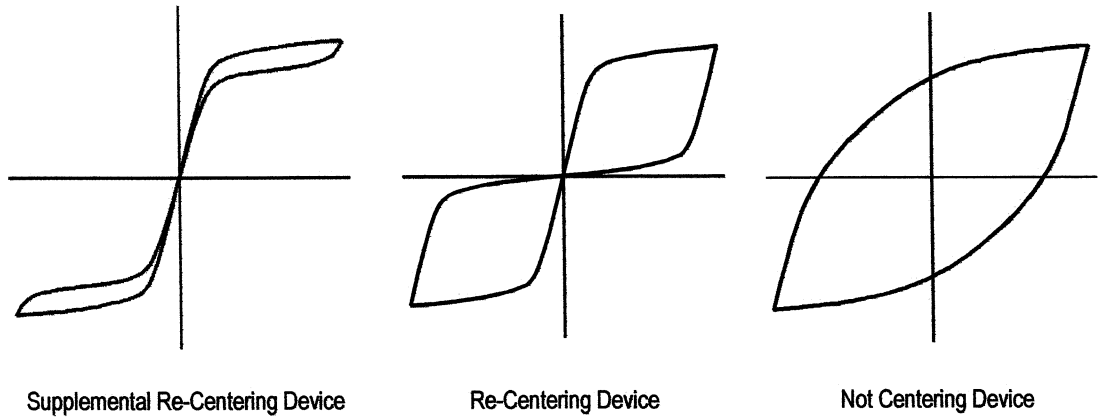


Fig. 11. Categories of the types of devices based on SMA.

- Not-Centering Devices; high energy dissipation is provided but large residual displacements occur at the end of the action.

As above seen, the actual behaviour of the SMA austenite and martensite elements, in the practical frequency range, are somewhat different from the idealised ones. The superelastic wires give some energy dissipation, the martensite elements are initially elastic (not rigid) and show some strain hardening. However the main behavioural features are maintained and the above explained working principles, with some approximation, are still valid.

According to these design principles, and to the results of the experimental tests, the bracing dampers and the isolators can be obtained as shown in tab. 3. For some applications one of the two requirements can be relaxed, so that devices having only either re-centering or energy dissipating capability can be needed. In such cases only one group of SMA elements must be implemented in the seismic device.

	Bracing damper	Isolator
RE-CENTERING GROUP	• PRETENSIONED SUPERELASTIC AUSTENITE WIRES ARRANGED TO BE ALWAYS STRESSED IN TENSION	• PRETENSIONED SUPERELASTIC AUSTENITE WIRES ARRANGED TO BE ALWAYS STRESSED IN TENSION
ENERGY DISSIPATING GROUP	• MARTENSITE BARS IN DOUBLE BENDING • PRETENSIONED SUPERELASTIC AUSTENITE WIRES • STEEL BARS IN DOUBLE BENDING	• MARTENSITE BARS IN ROLLER BENDING • PRETENSIONED SUPERELASTIC AUSTENITE WIRES • STEEL BARS IN ROLLER BENDING

Tab. 3. Combination of re-centering and energy dissipating SMA groups to realise bracing devices and isolators.

The design efforts were mainly focused on the arrangement of the re-centering SMA group, for both

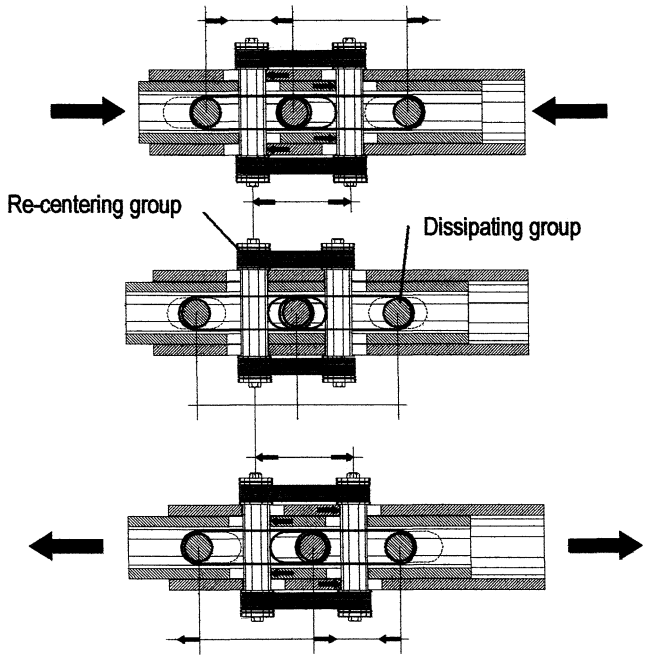


Fig. 12. functional scheme of a complete device, including two functional groups based on SMA wires.

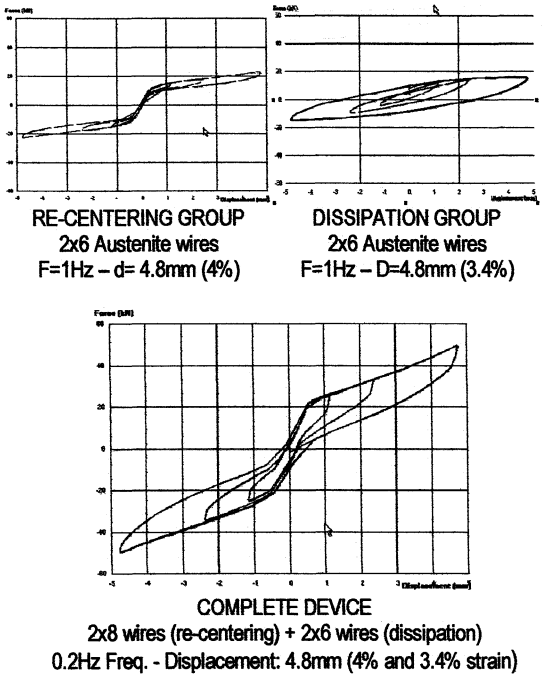


Fig. 13. Experimental behaviour of the single SMA wire groups and of the complete SMA wire system.

the braces and the seismic isolation system. Then the arrangement of an energy dissipating SMA group based on pre-tensioned wires in the same device including the SMA re-centering group was studied. The resulting complete device works according to the scheme shown in fig. 12. The same concept was used for both the brace and the isolation devices. They are made of two concentrical pipes that moves mutually when inserted in a structure subjected to seismic actions. The pipe ends

are connected to mutually moving parts of the structural systems, e.g. two consecutive stories in a frame, the pier and the deck in a bridge, the base and the superstructure in a building.

To realise the SMA wire re-centering group, two studs are inserted transversely in the two tubes, into oval-shaped holes. An adequate number of superelastic wire are winded around the studs, which also have a mechanism to apply and calibrate pretension (not shown in fig. 12). The special arrangements of studs and holes is such that, for any positive or negative mutual movements of the tubes, the wires of the re-centering group are always subject to elongation, thus increasing the tensile strains.

Similarly three studs, two of which move with the internal tube and the other with the external tube (or vice versa), as well as the wire looped around the studs and the mechanism to calibrate pretension, constitute the energy dissipation group. When the two tubes move reciprocally, one loop elongates and the other shortens, thus acting as a double counteracting system of springs and exploiting the austenite wires to dissipate energy in an optimal way.

All the three categories of devices can be obtained by simply varying the number and diameters of wires of the two functional groups, as well as by calibrating the pre-tensioning of the SMA re-centering group, as shown by the experimental results on the brace, in fig. 13.

A full-scale prototype of energy dissipating brace was designed, realised and tested. It acts as a uni-directional device, developing forces that depend on the number of the wire loops and displacements that depend on their base-length. The prototype brace was designed to carry up to 200 KN and reach displacements up to 10 mm in normal working conditions and more than 20 mm at failure, depending also on the applied pre-strain level. The brace also include an alternative dissipating group based on SMA martensite or even steel bars acted in double bending. Three 1/3.3 scale prototypes of braces, with similar features, were realised and tested both separately at the DiSGG Laboratory and within the frame model, in the shaking table tests.

The devices for the 1/3.3 scale seismic isolation system, to be used for the shaking table tests were

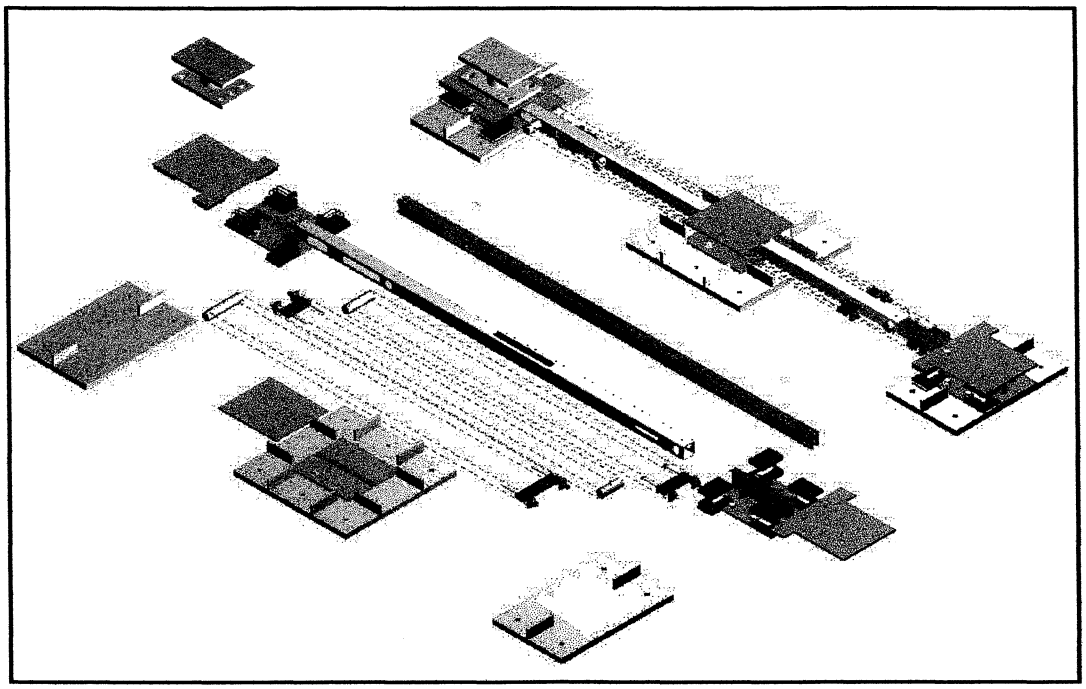


Fig. 14. Arrangement of the isolation systems for the scaled frame model.

designed and realised as shown in fig. 14. Like the SMA-based brace, this system is especially conceived to test several configurations. It is made of a SMA wire re-centering and/or dissipating device, based on the same scheme as the brace, but allowing up to ±100 mm displacement, and three sliding steel-teflon bearings. These latter can incorporate U-shaped SMA bars or steel plates, as energy dissipation groups, alternative to the SMA wire dissipating group. This arrangement made it possible to make tests on different configuration of the isolation systems, with very simple and fast operations.

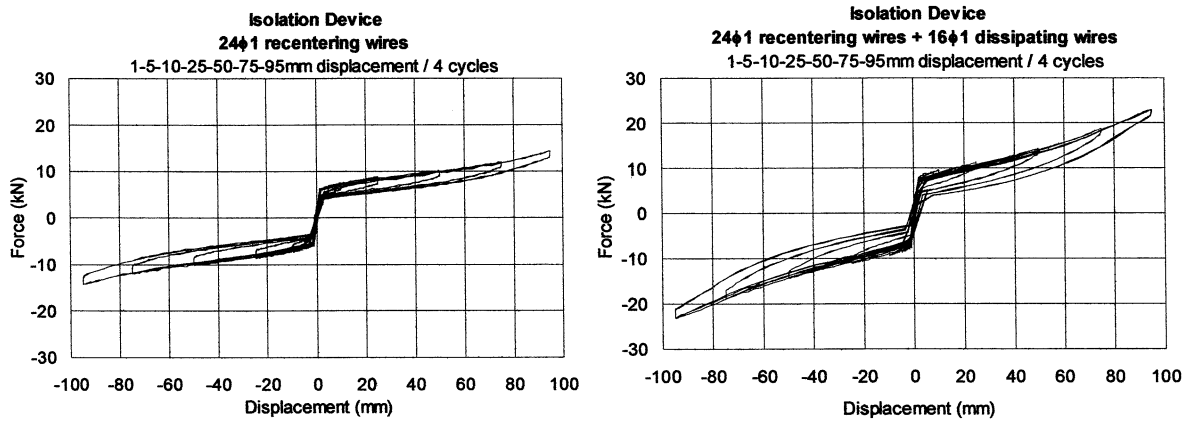


Fig. 15 Force-displacement cycles of the recentering only device (left) and of the complete device (right).

Preliminary tests on all the 1/3.3 devices were carried out at the Laboratory of DiSGG, to verify their correct behaviour. Fig. 15 shows the force-displacement diagrams of the main device having the SMA-wire re-centering group alone and with dissipating group, in the same configuration (and with the same wires) subsequently used for the shaking table tests. As can be seen, even the complete device had a supplemental re-centering force of about 3 kN. This was purposely done to counteract the 3% friction of the bearings, experimentally evaluated. The weight of the frame being about 100 kN, the friction force resulted to be just 3 kN. The calibration of the re-centering and of the dissipating groups for the shaking table tests was carried out by a series of accurate numerical simulation analyses of the frame model.

Shaking table tests on 1/3.3 scale frames

In order to verify the effectiveness of the devices for both the bracing and isolation systems, an extensive experimental program has been carried out at the Laboratory of Earthquake Engineering of the Technical University of Athens. The frame, models (see fig. 16) were built by AIAS, the greek partner of MANSIDE. 8 frame models, without and with infilled panels, were constructed and equipped with steel-based and SMA-based energy dissipation braces, as well as with rubber-based, steel-based, SMA-based, Hybrid SMA-steel-based isolation systems, according to the program reported in tab. 4.

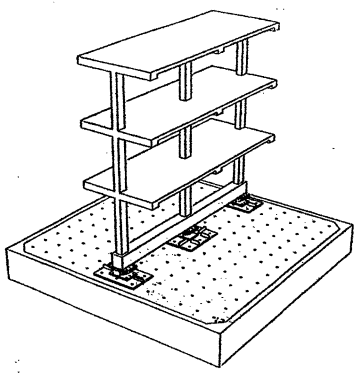


Fig. 16. Frame model for shaking table tests

The program was aimed at comparing the seismic behaviour of structures without any passive control systems, to similar structures

equipped with conventional and with SMA-based control systems. The tests were completed in March 1998, and some preliminary, but significant, results will be presented in the following paragraph. The tests on model No. 8, i.e. on the base-isolated infilled frame, have been selected, as they are thought to be the most significant ones, in view of the possible application of the SMA technologies on seismic isolation of bridges.

Model Nr.	Vibration control	Devices	Infill	Height (m)	Plan Sizes (m)
1	conventional	NO device	bare frame	3.15	3.3 by 1.3
2	conventional	NO device	brick masonry	3.15	3.3 by 1.3
3	base isolation	rubber bearings	bare frame	3.15	3.3 by 1.3
4	base isolation	rubber bearings	brick masonry	3.15	3.3 by 1.3
5	energy dissipation	steel energy diss. braces	bare frame	3.15	3.3 by 1.3
6	energy dissipation	SMA energy diss. braces	bare frame	3.15	3.3 by 1.3
7	base isolation	SMA-kernel isolators	bare frame	3.15	3.3 by 1.3
8	base isolation	SMA-kernel isolators	brick masonry	3.15	3.3 by 1.3

Tab. 4 - Characteristics of the 1/3.3-scale frame model.

Results of the tests on the base-isolated infilled frame

In table 5 there is reported the complete program of the tests on model No. 8, as it was actually carried out.

Test No.	Device name	Isolation system characteristics	Table (%g) acceleration
8-1	SMA1a: Complete SMA device	24ϕ1 recentering wires + 16ϕ1 dissipating wires	8
8-2	SMA1a: Complete SMA device	24ϕ1 recentering wires + 16ϕ1 dissipating wires	16
8-3	SMA1a: Complete SMA device	24ϕ1 recentering wires + 16ϕ1 dissipating wires	24
8-4	SMA1a: Complete SMA device	24ϕ1 recentering wires + 16ϕ1 dissipating wires	36
8-5	SMA2a: Hybrid SMA/steel device	recentering wires + 2U-shaped steel elements	36
8-6	SMA2b: Hybrid SMA/steel device	recentering wires + 1U-shaped steel element	36
8-7	SMA2c: Recentering SMA device	24ϕ1 recentering wires	36
8-8	SMA3: SMA Dissipating device	16ϕ1 dissipating wires	36
8-9	SMA3: SMA Dissipating device	16ϕ1 dissipating wires	48
8-10	SMA1b: Complete SMA device	8ϕ2 recentering wires + 24ϕ1 dissipating wires	36
8-11	SMA1b: Complete SMA device	8ϕ2 recentering wires + 24ϕ1 dissipating wires	48
8-12	SMA1b: Complete SMA device	8ϕ2 recentering wires + 24ϕ1 dissipating wires	54
8-13	SMA1b: Complete SMA device	8ϕ2 recentering wires + 24ϕ1 dissipating wires	60
8-14	SMA1b: Complete SMA device	8ϕ2 recentering wires + 24ϕ1 dissipating wires	72
8-15	SMA1b: Complete SMA device	8ϕ2 recentering wires + 24ϕ1 dissipating wires	78

Tab. 5. Detailed program of the tests carried out on model No. 8 at L.E.E of TUA.

Several configurations of the isolation system (namely 6) could be tested under high intensity earthquakes (0.36g nominal table acceleration), thanks to the effectiveness of the isolation systems in preserving the structure from any damage. The seismic action was given by an artificial EC8 type B (fig.17) compatible accelerogram (9) with about 10 secs. scaled duration (fig. 18).

The main results are shown in figs. 19 and 20. The time histories of the displacements of the isolation device and of the accelerations of the 2nd floor compared to the accelerations of the shaking table are reported for the 7 cases shadowed in table 5.

Looking at the diagrams of figs. 19 and 20, it is possible to compare the behaviour of 4 different configurations of the isolation system, as well as the respons of the structural system with the complete re-centering/dissipating device for acceleration from 0.36g up to 0.78g.

0.78 g is the maximum acceleration reached during tests, as it produced the maximum design displacement of the device (100 mm). Under such acceleration, no apparent damage to the frame and to the infilled panels was observed, except for the failure of the anchorage of the base beam of the frame to the connecting plate, due to the knocking at the end stroke of the device.

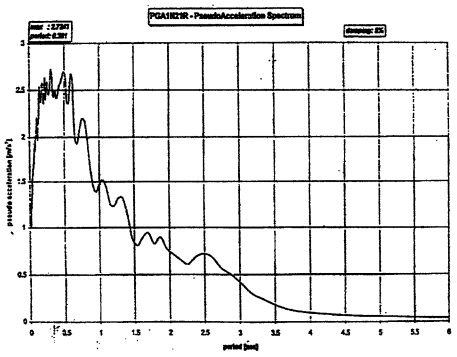


Fig. 17. Response spectrum of the earthquake for shaking table tests.

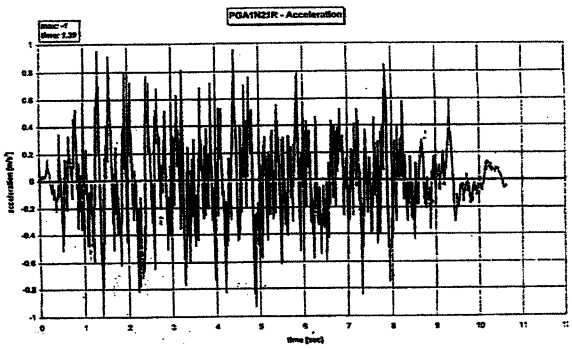


Fig. 18. Artificial accelerogram of the earthquake for shaking table tests.

Comparing the response of the different devices and of the structure equipped with them, in fig. 19, the excellent behaviour of all of them is evident. The acceleration of the second floor resulted to be always reduced with respect to the base.

The hybrid isolation system turned out to be the most effective one in limiting the isolation system displacements, even with respect to the complete system named SMA1b. On the other hand, the de-amplification of accelerations in the structure improves as long as the maximum force of the isolation system reduces. That is why the most effective system in terms of de-amplification is the system equipped with dissipating wires only. However it can be also observed that this system has the maximum displacements, for the same acceleration (0.36g) and it shows a residual displacement at the end of the action. On the contrary, none of the other isolation systems, all of them being supplemental re-centering systems, show any residual displacement at the end of the action, even for accelerations up to 0.72g. The residual displacement at 0.78g can be ascribed to the failure of the plate-frame connection.

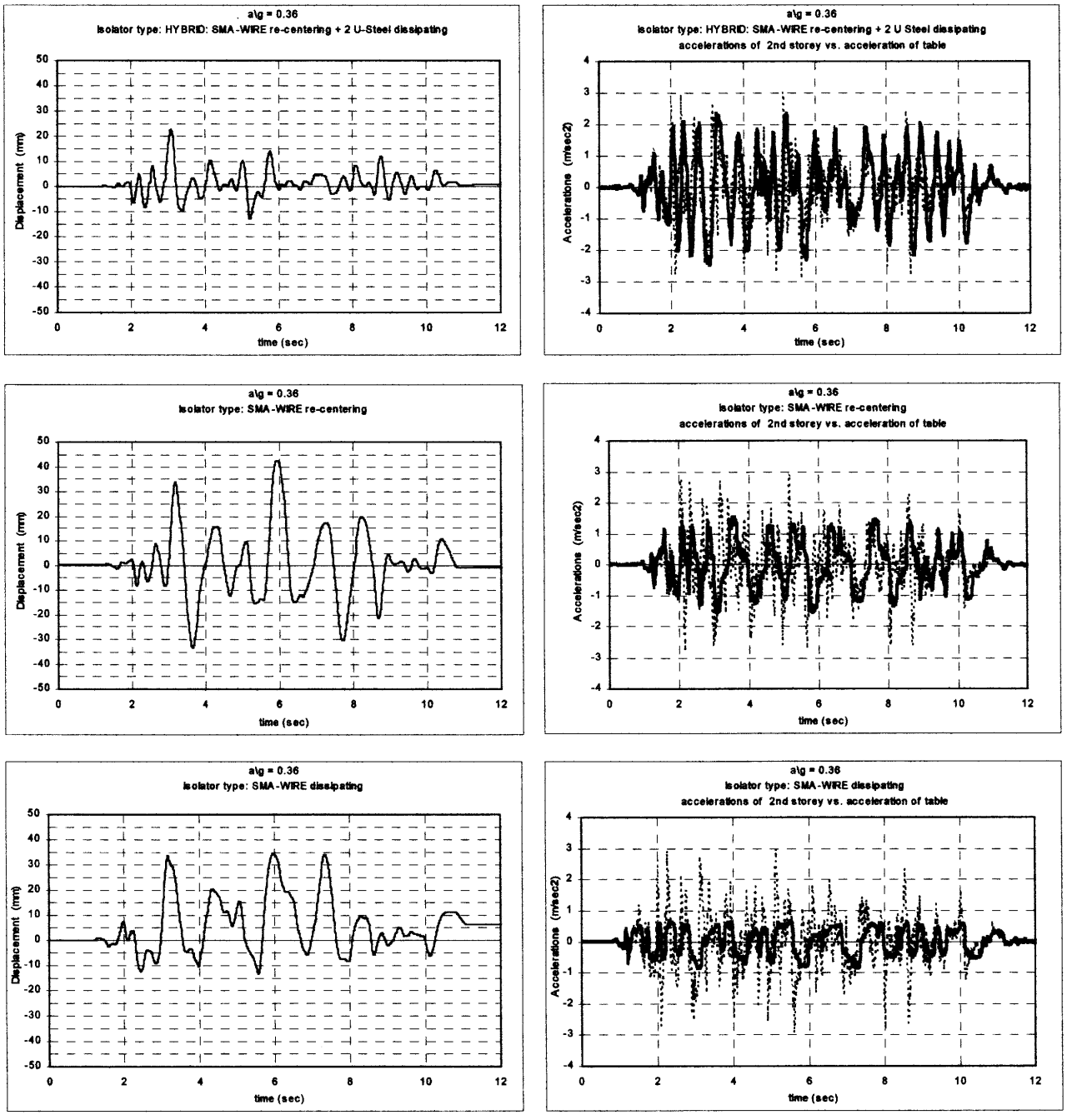
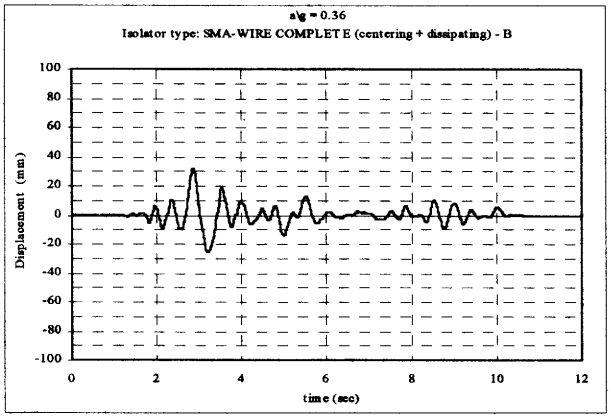
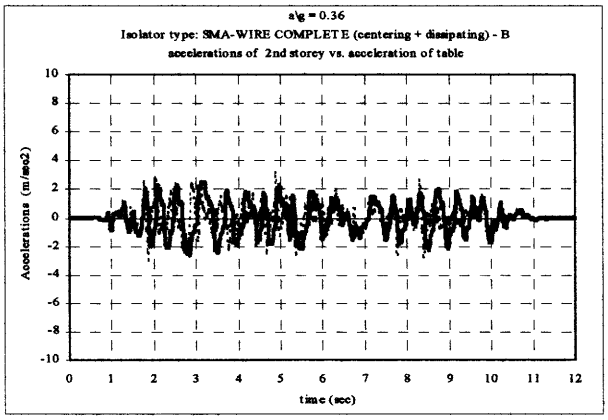
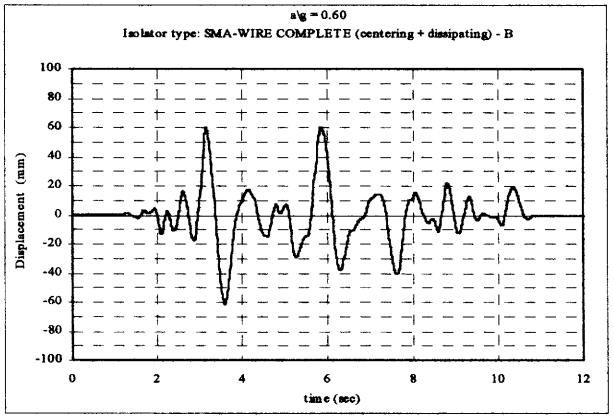


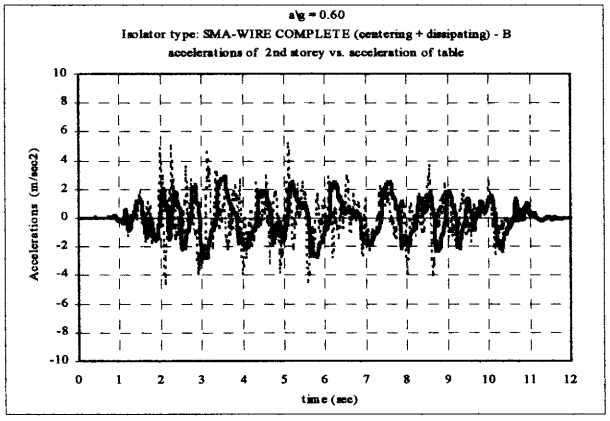
Fig. 19. Displacements of the isolation system (left column) and comparison between acceleration of the table and of the 2nd story for tests 8-5, 7, 8.

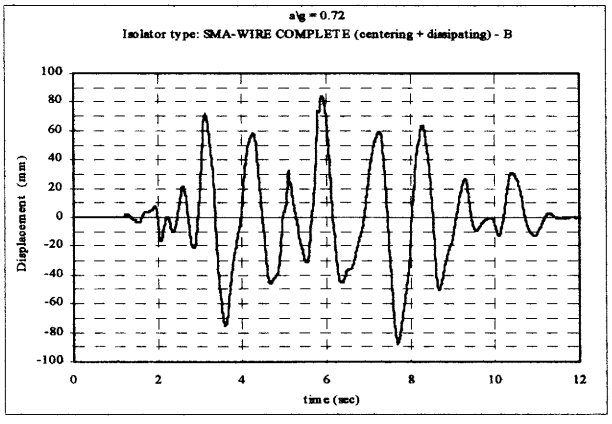
A general outcome of the shaking table tests is the excellent behaviour of the entire family of the tested isolation systems. All of them protected the model from structural and even non-structural damage, with significant de-amplification of the acceleration and showing a full re-centering capability, even considering that the steel-teflon bearings had 3% friction.

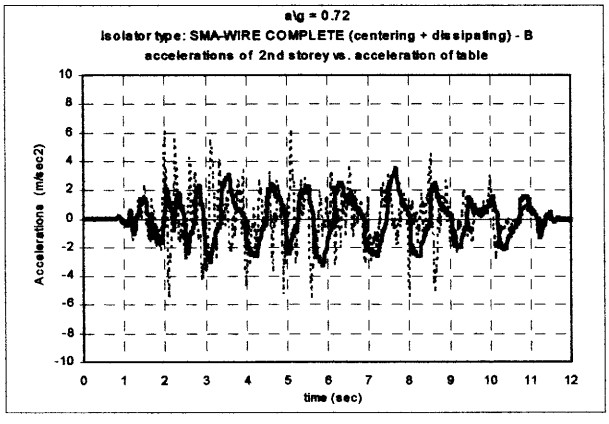


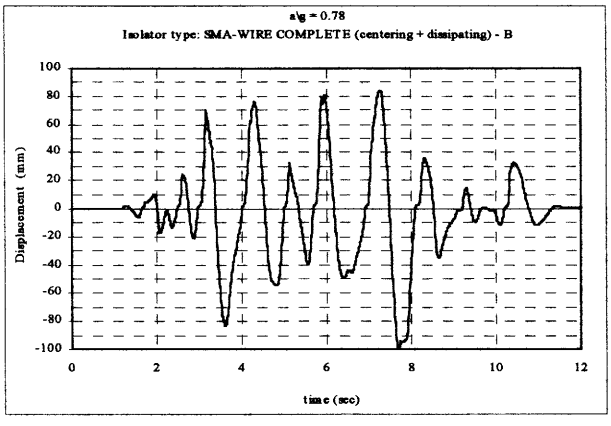












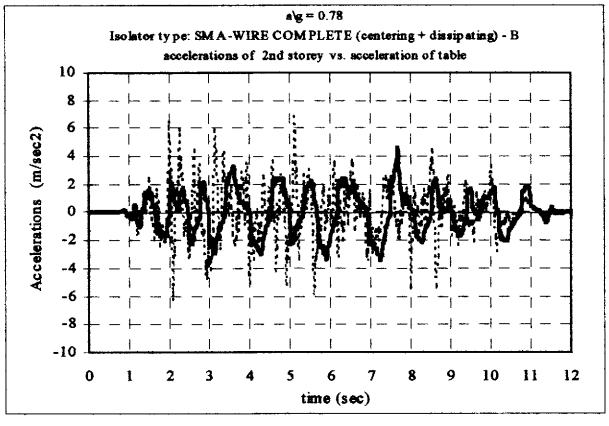


Fig. 20. Displacements of the isolation system (left column) and comparison between acceleration of the table and of the 2nd floor, for tests 8-10, 13, 14, 15.

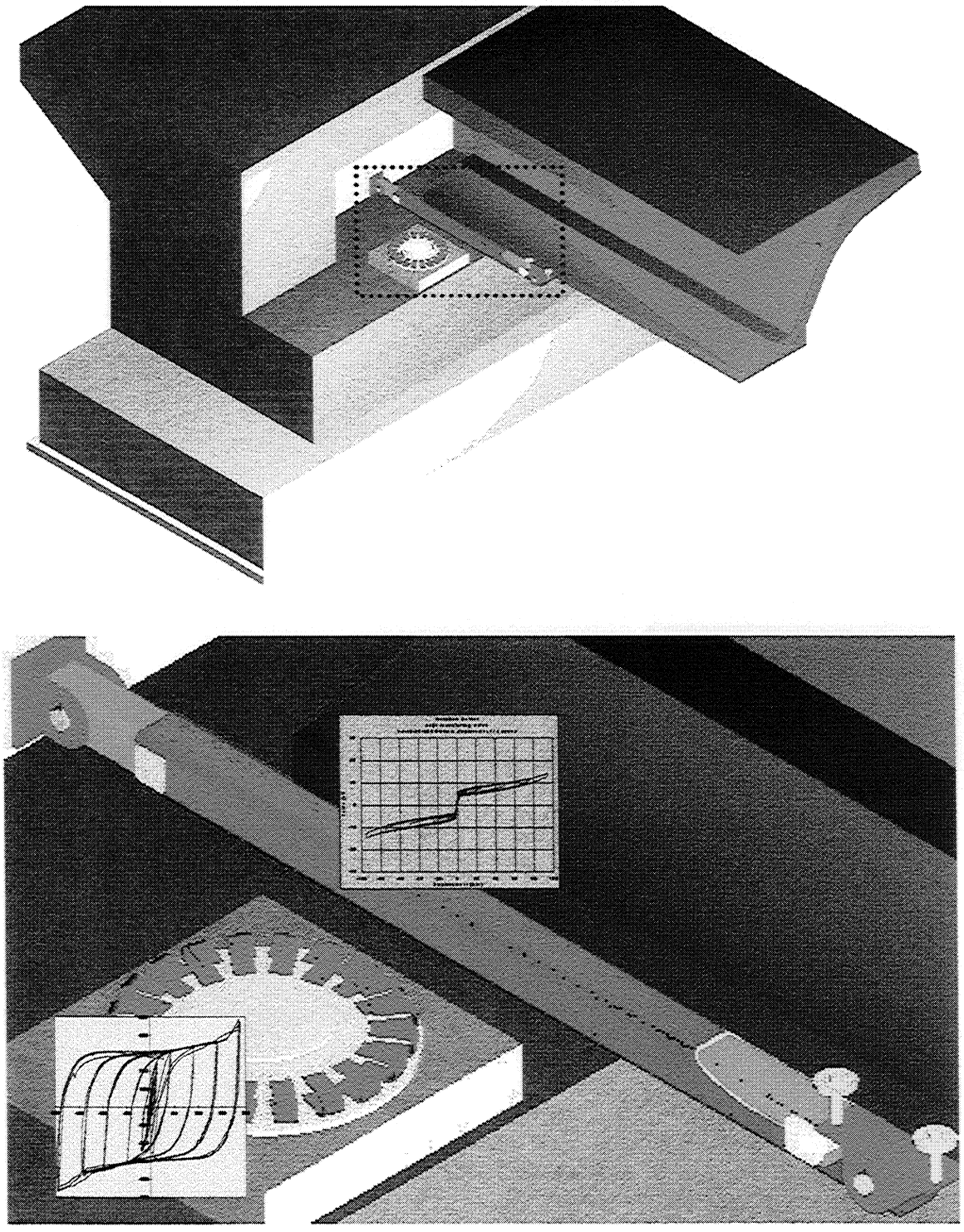


Fig. 21. Possible arrangement of a hybrid isolation system in a bridge.

Potential applications to bridges

The possibility of using the isolation devices set up within the MANSIDE project in bridges was verified by designing a real scale device system for a 600 m long continuous bridge. Several solutions can be adopted, however the hybrid SMA-steel isolation system shown in fig. 21 was selected, to exemplify the adaptability of the SMA based devices. The two functions, re-centering and energy dissipation, are clearly separated and carried out by two different devices:

- SMA wire re-centering device
- bearings embodying U-shaped steel elements (8).

The re-centering device was designed to have ±280 mm maximum displacement, 1000 kN maximum force. Its sizes are 5.00 m length by 0.27 x 0.27 m. Its encumbrance is therefore very limited and one or more of them can be easily arranged in the usual structural configurations of bridges.

Acknowledgments

Funding for the MANSIDE research was provided by the European Commission, EC, DGXII, within the BRITE-EURAM Program, Project BE95-2168

References

1. E.J. Graesser, F.A.Cozzarelli, "Shape-Memory Alloys as New Material for Aseismic Isolation", ASCE Journal of Engineering Mechanics, Vol. 117, No. 11, 1991.
2. P.R. Witting, F.A. Cozzarelli, "Shape Memory Structural Dampers: Material Properties, Design and Seismic Testing", Technical Report NCEER-92-0013, State University of New York, Buffalo (USA). 1992
3. I.D. Aiken, D.K. Nims, A.S. Whittaker, J.M. Kelly, "Testing of Passive Energy Dissipation Systems", Earthquake Spectra, Vol. 9, No. 3, 1993.
4. Inaudi, "Active Isolation and Innovative Tuned Mass Dampers for Vibration Reduction", PhD Dissertation, EERC Library, UCB, 1993.
5. Hodgson, R.C.Krumme, "Damping in Structural Applications", Proc. of the 1st International Conference on Shape Memory and Superelastic Technologies, Pacific Grove, California (USA), 1994.
6. A.S. Whittaker, R.C. Krumme, J.R. Hayes, "Structural Control of Building Response using Shape Memory Alloys", Headquarters U.S. Army Corps of Engineers, Washington D.C. 1995
7. M. Nicoletti, F. Braga, F. Brancaleoni, J. J. Cederström, M. Dolce, R. Marnetto, E. Papacharalabous, C. Valente, J. Van Humbeeck, W. Van Moorleghem "Memory Alloys for New Seismic Isolation and Energy Dissipation Devices: first achievements of the MANSIDE project (EC Project BE95-2168)", Proceedings of the International Post SMiRT Conference Seminar on Seismic Isolation, Passive Energy Dissipation and Active Control of Vibrations of Structures, Agosto 1997, Taormina.
8. M. Dolce, B. Filardi, R. Marnetto, D. Nigro, "Experimental Tests and Applications of a New Biaxial Elastoplastic Device for the Passive Control of Structures", Proc. 4th World congress on joint sealants and bearing systems for concrete structures, Sacramento, California 29.9-3.10.96.
9. CEN European Committee for Standardisation, "Eurocode 8, Design Provisions for Earthquake Resistance of Structures", Part 1.1. ENV1998.1.1.. Brussels, 1994.

ROCKING COLUMNS: AN EFFECTIVE MEANS OF SEISMICALLY ISOLATING A BRIDGE

by

J.B. Mander, R. Contreras and R. Garcia
Department of Civil, Structural and Environmental Engineering
University at Buffalo, SUNY

INTRODUCTION

Recent earthquakes such as Loma Prieta (1989), Northridge (1994) and Kobe (1995) have all demonstrated the need for a new bridge design philosophy that avoids damage in order to maintain post-earthquake serviceability. Conventional seismic resistance construction is based on the *ductile design* philosophy which aims at preventing loss to life and limb. Seismic energy is dissipated in plastic hinge zones that occur at the ends of bridge columns. This form of energy dissipation induces damage to those hinge zones and may result in permanent lateral displacements that may be so severe that it is necessary to either rebuild or replace that part of the bridge structure. Therefore, irreparable damage to structures designed in accordance with the *ductile design* philosophy is both inevitable but undesirable. Perhaps a more attractive form of seismic resistant design is to use *seismic isolation*. This increasingly popular approach that has been developed over the past two decades relies on energy being dissipated by mechanical means through various devices such as: lead cores within lead-rubber bearings, friction in sliding bearings, viscous dampers, or metallic yielding devices. The major disincentive for using this design philosophy is that large horizontal displacements need to be accommodated in the bearing system. It is conceivable that under a maximum credible earthquake, particularly with near-field (fling) effects, the provided design displacement can be exceeded. The bearings can thus fail, resulting in unseating of the deck. Therefore, even seismically isolated structures may be damaged in a strong earthquake.

It follows that there is a need for new design philosophies that have the attributes of the present *ductile design* (that is limited displacement plus energy dissipation) and *seismic isolation* design (that is the absence of damage under service-like excitation). In other words, new types of bridge pier designs and forms of construction are needed that can avoid damage entirely. The purpose of this paper is to describe a form of isolation that relies on rocking columns. This approach permits large displacement while avoiding seismically induced damage.

The concept of rocking structures is not really new. Two state-of-the-practice examples of rocking structures may be found in New Zealand: the South Rangitikei Railway Bridge, and an industrial chimney at the Christchurch Airport (Skinner et al., 1993). The South Rangitikei Rail Bridge is the largest concrete bridge in the southern hemisphere. The bridge is a tall (72 m) structure with twin hollow column piers supporting a single cell box girder. The box girder, which consists of 58 m continuous deck spans, is designed to carry a single narrow-gauge railway track for Coopers E-40 loading. Hollow columns are used as a weight saving measure; an important consideration in seismic design. Torsional beam mechanical energy dissipating devices are installed at the foot of each column as the bridge piers step from one column leg to the other (Cormack, 1988). Subsequent research by Priestley et al. (1978) showed that such devices may not be needed as the rocking piers dissipate considerable energy when each leg slams onto the foundation. Nevertheless, the mechanical energy dissipators are intended to restrain uplift as well as attenuate the number of rocking cycles.

This paper first describes the seismic resistance of a rocking bridge pier both with and without the effects of prestress. Although the subject of rocking structures is not new, dating back to the early work of Housner (1963), much of the work that followed was aimed at investigating the seismic response of *rigid* rocking block systems. Although Meek (1978) introduced aspects of structural flexibility coupled with rocking structures, and Aslam et al. (1980) considered the influence of prestress that provided some resistance in anchoring a rigid structure to the ground to increase its rocking resistance, neither investigator specifically addressed issues pertaining to bridge structures. Only recently did Priestley et al. (1996) describe in their monograph the behavior and design of rocking bridge piers. However, Priestley et al. did not integrate the inter-related aspects of rocking, structural flexibility and prestressing in their design recommendations. This paper attempts to address these issues and to present unified analysis and design procedures.

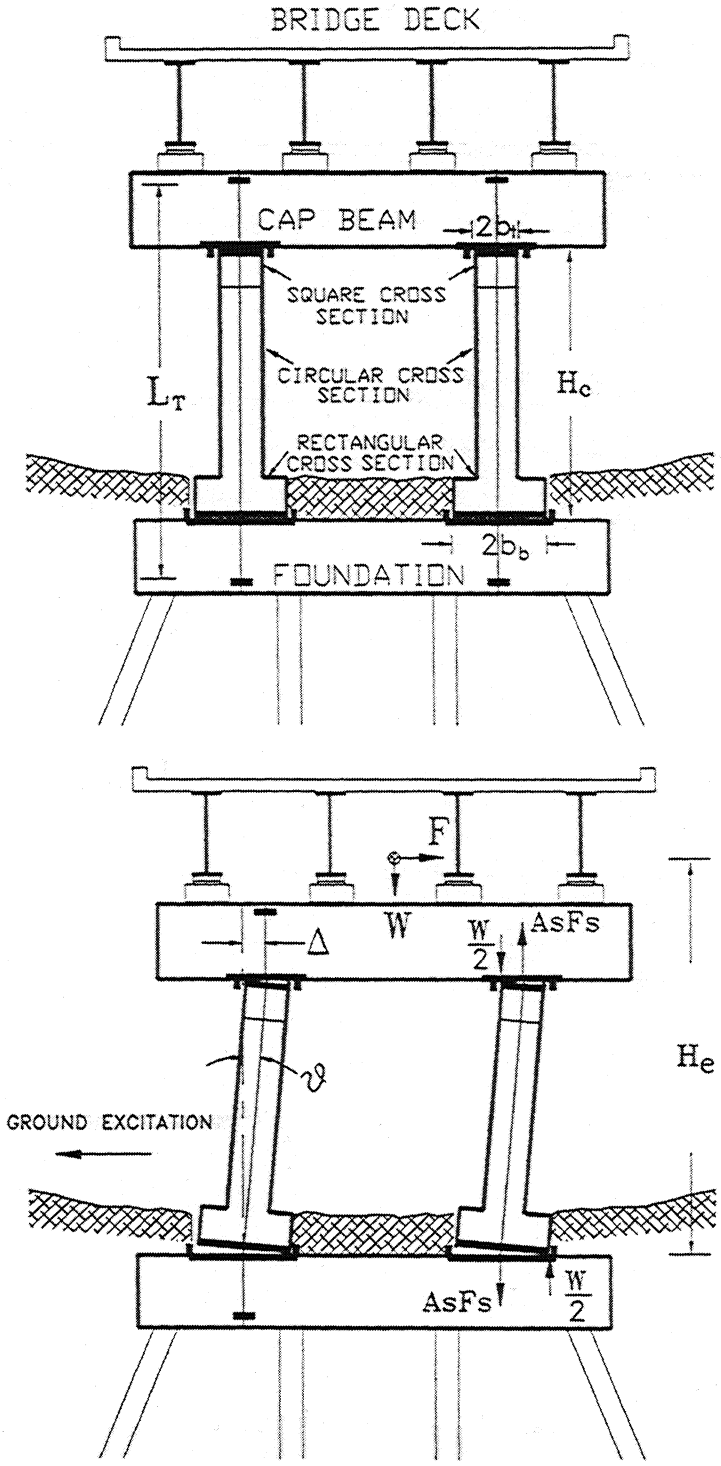


Fig. 1 Bridge Pier with Rocking Columns

One of the most fascinating aspects of the dynamics of rocking structures is the way in which energy is dissipated. This is explored in the present paper based on an energy balance approach which is in contrast to the dynamics approach developed previously by Housner (1963). The design philosophy of rocking bridge piers is validated experimentally in two ways. First, an experimental study is conducted on the resistance of a near full-sized rocking bridge column with and without the presence of prestressing action. Next, a shaking table study is described for a one-quarter scale model bridge pier.

SEISMIC RESISTANCE OF ROCKING PIERS

Prior to uplift, rocking structures behave like any regular fixed-based elastic structural system. However, when the lateral load exceeds certain limits, the columns uplift forming a rocking mechanism. Consider the rocking bridge pier shown in Fig. 1. In order to determine the magnitude of the lateral load necessary to induce uplift, a virtual work method of analysis will be adopted. The external work done following uplift is given by

$$EWD = F\Delta = FH_c\theta + W(b_b + b_t)\theta \tag{1}$$

The internal work done resisting this uplifting action is

$$IWD = \Sigma M_r\theta \tag{2}$$

where M_r = resisting moment at the rocking toe of each column end given by

$$M_r = (P_g + P_p)e \tag{3}$$

respectively in which e = eccentricity of the axial load respectively taken as b_b and b_t (the semi-base width) at bottom and top of the column, P_g = gravity load in the column where for the two column bent shown in Fig. 1, $P_g = 0.5W$, and P_p = axial prestress force in each column, ΣP_p being the total axial prestress forces for the bridge.

Equating $EWD = IWD$, substituting equation (3) into (2) and normalizing with respect to the structural weight (W), gives the base shear capacity:

$$C_C = \frac{F}{W} = \left(1 + \frac{\Sigma P_p}{W}\right)\left(\frac{b_b + b_t}{H_c} - \theta\right) \tag{4}$$

If $b_b = b_t = 0.5D$ where D = column diameter or overall width, then

$$C_c = \left(1 + \frac{2P_p}{W}\right)\left(\frac{D}{H_c} - \theta\right) \tag{5}$$

If there is no internal prestress applied to the columns, then it is evident that the uplift resistance is a function of the structural geometry alone (D and H_c).

ANALYSIS OF DAMPING

An energy approach is adopted herein to assess the effective viscous damping factor of a rocking pier system. Using this energy approach, damping can be found from the energy absorbed and dissipated on each half-cycle. Considering <u>one</u> impact per half-cycle, the equivalent viscous damping factor (ξ_{eq}) of the pier system is given by

$$\xi_{eq} = \frac{\delta E}{\pi F\Delta} = \frac{\delta E}{\pi WC_c\Delta} \tag{6}$$

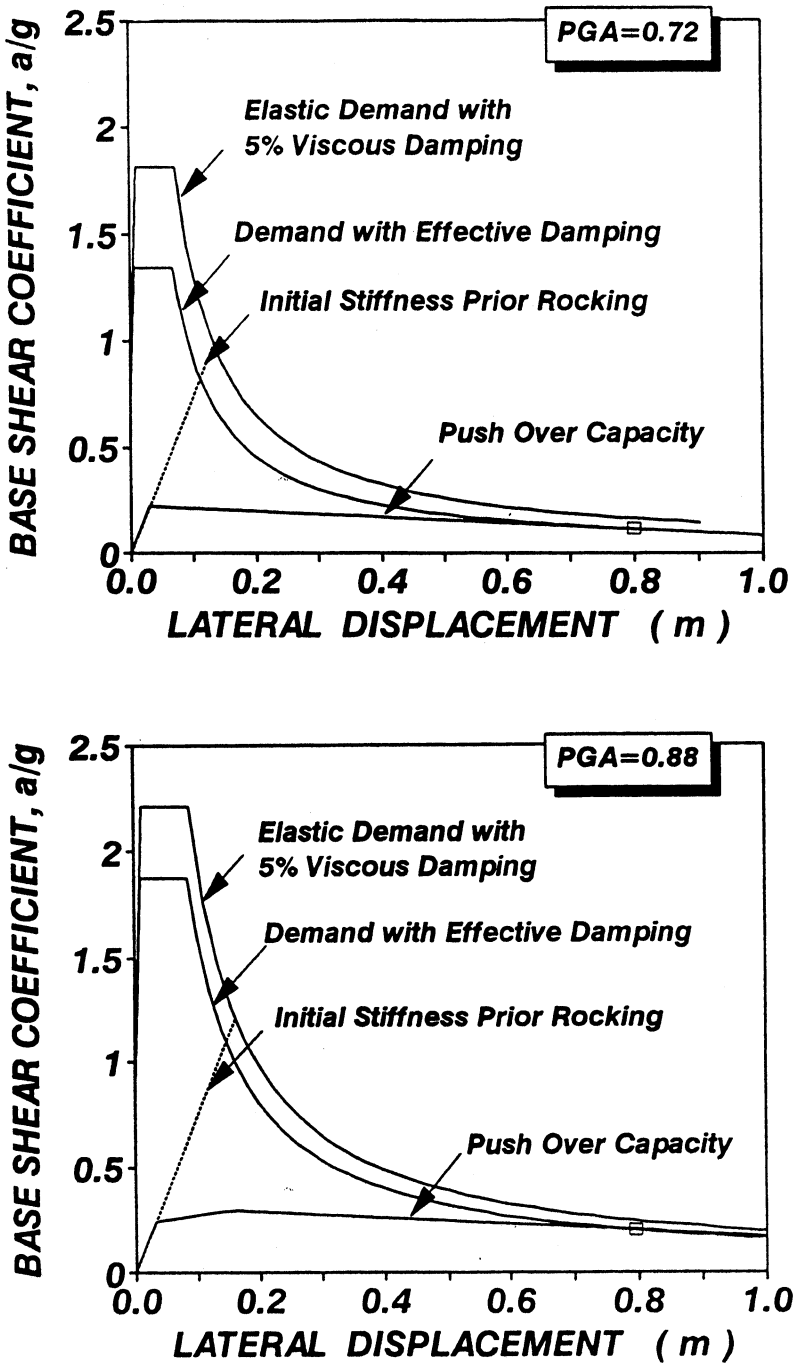


Fig. 2 Linearized Capacity-Demand Response Spectrum Analysis. Upper graph shows a rocking pier without prestress. Lower graph shows a pier with post-tensioned tendons.

where F = uplift force, Δ = displacement amplitude, and δE = dissipated/radiated energy. The energy lost is given by

$$\delta E = (1 - r)E_p = (1 - r)\, W \frac{D}{H} \Delta \tag{7}$$

Thus

$$\xi_{eq} = \frac{1 - r}{\pi} \frac{\left(\frac{D}{H}\right)}{C_c}$$

where r = ratio of the kinetic energy before and after impact defined by (Mander and Cheng, 1997) as

$$r = \frac{\frac{1}{2} I_{deck}\, \dot{\theta}_2^2}{\frac{1}{2} I_{deck}\, \dot{\theta}_1^2} = \left(\frac{\dot{\theta}_c}{\dot{\theta}_1}\right)^2 = \left(1 - \frac{m_{deck} D^2}{m_{deck}(D^2 + H_c^2)}\right)^2 = \left(\frac{1}{1 + \left(\frac{D}{H_c}\right)^2}\right)^2 \tag{9}$$

for small $\left(\frac{D}{H}\right)$ values, $1 - r$ can be simplified using a binomial expansion as $2\left(\frac{D}{H_c}\right)^2$

$$\xi_{eq} = \frac{2}{\pi} \frac{\left(\frac{D}{H}\right)^3}{C_c} = \frac{2}{\pi} \frac{\left(\frac{D}{H}\right)^3}{\left(1 + \frac{\Sigma P_p}{W}\right)\left(\frac{D}{H} - \theta\right)} \tag{10}$$

For bridges without prestress and with small lateral drifts, the above equation is further simplified to give

$$\xi_{eq} = \frac{2}{\pi}\left(\frac{D}{H}\right)^2 \tag{11}$$

Capacity-Demand Spectrum Response Analysis

For a given rocking structural geometry, it is essential that the designer assess the maximum expected response displacement imposed on the structure by the design ground motion. This is referred to herein as seismic displacement demand. A modified AASHTO code-type of elastic spectra, as shown in Fig. 2, can be adopted for design purposes as to find the base shear demand in the presence of non-standard ($\neq 5\%$) damping follows:

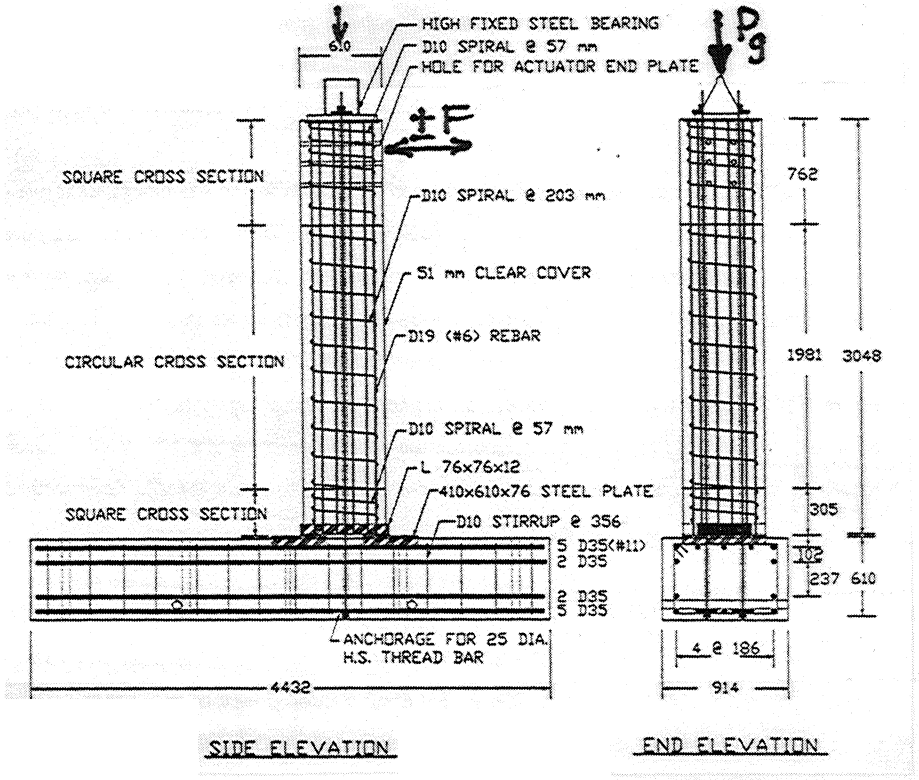
"Short" period structures:

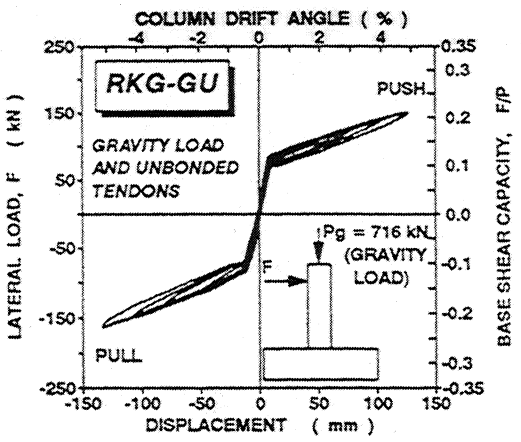
$$C_d = 2.5 \frac{K_s}{B_s} A \tag{12}$$

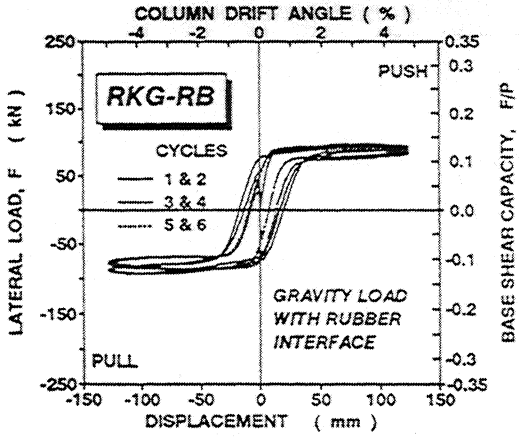
"Long" period structures:

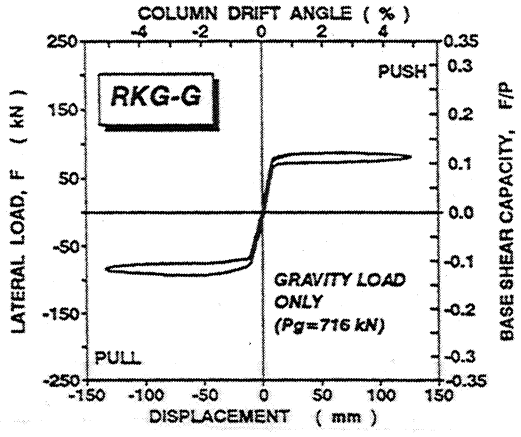
$$C_d = \frac{K_L}{B_L} \frac{SA}{T} \tag{13}$$

in which subscripts S and L, respectively, stand for the short and long period portions of the response spectra, A = peak ground accelerations ratio, S = code recommended soil-type factor, T = natural period of vibration,









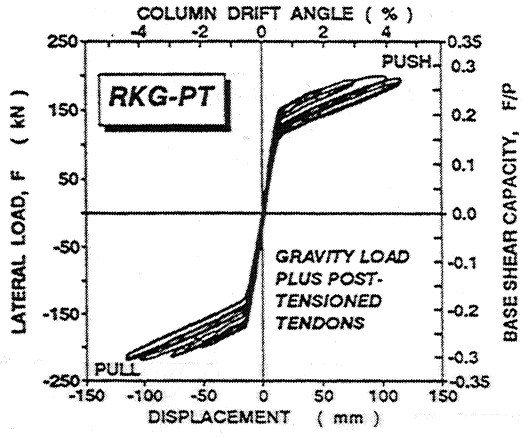


Fig. 3 Near Full Size Rocking Colu340 Specimen and the Force-Deformation Behavior

K = a factor that can be used to adjust the shape of the standard AASHTO spectra either for site effects, or for accounting for randomness and uncertainty and B = reduction factor that accounts for damping which is defined for short and long period ranges as follows:

$$B_S = \left(\frac{\xi}{0.05}\right)^{0.5} \tag{14}$$

and

$$B_L = \left(\frac{\xi}{0.05}\right)^{0.3} \tag{15}$$

The first of the design equations governs for short period fixed-based structures. However, for rocking structures, it is inevitable that equation (13) govern in a displacement-based design. The effective (secant) period of a rocking structure can be found as follows:

$$T = 2\pi\sqrt{\frac{W/g}{K}} = 2\pi\sqrt{\frac{W}{g}\frac{\Delta}{C_c W}} = 2\pi\sqrt{\frac{\Delta}{C_c g}} \tag{16}$$

Substituting into equation (13), setting demand equal to capacity ($C_d = C_c$), and solving for the structural displacement gives

$$\Delta = \left(\frac{SA}{2\pi}\frac{K_L}{B_L}\right)^2 \frac{g}{C_c} \tag{17}$$

It is of interest to note that the displacement demand is inversely proportional to the rocking-uplift capacity (C_c). Moreover, displacement response variability due to randomness in the ground motion is proportional to the square of K_L. Thus if there is a 50% variation in ground motion response, there will be a variation in response uncertainty that may range from 45 to 225% of the expected value.

It follows that due to this wide variation in expected response, a conservative design displacement should be adopted to avoid toppling. It is therefore suggested that the design displacement be limited to 50% of the maximum displacement limit — that is $0.5D$.

EXPERIMENTAL PERFORMANCE OF ROCKING BRIDGE PIERS

One of the keys to the success of this design approach is to ensure that while rocking damage does not occur to the column due to the higher stresses generated on uplift and impact. To this end a special steel-steel rocking connection is proposed. Steel is an ideal material as it is able to withstand the very high point stresses at the rocking toe of the column. Fig. 3 shows the near full-sized rocking column specimen that was tested quasi-statically under combining axial load (to represent gravity) and reversed cyclic loading (to represent an earthquake). A 75 mm thick steel plate was placed at the bottom of the column to which the longitudinal bars were mechanically attached. The steel plate was seated on thick steel masonry plates that were imbedded into the foundation beams and anchored to the longitudinal reinforcement of that beam. Two high-strength 25 mm diameter threadbars were passed through the column and anchored in the foundation beam. These bars were either left: (a) slack, (b) snug, or (c) prestressed to various levels. Fig. 3 also shows the test results for the rocking column specimen. Each test was performed under displacement control where the command signal was a sine wave. Lateral load was applied to a series of variability amplitude cycle which consisted of two cycles of loading at drift amplitude of $\pm 0.25\%$, $\pm 1\%$, $\pm 2\%$, $\pm 3\%$, $\pm 4\%$ and $\pm 5\%$ at a cycling period of 30 seconds.

The test RKG-G was conducted with the tendons slack under gravity load alone, and from the results it was evident that a bi-linear response was obtained (note the hysteresis seen in the test results is due to the inability of the vertical actuator to accurately apply a consistent gravity load). The test RKG-GU is similar, but the tendons

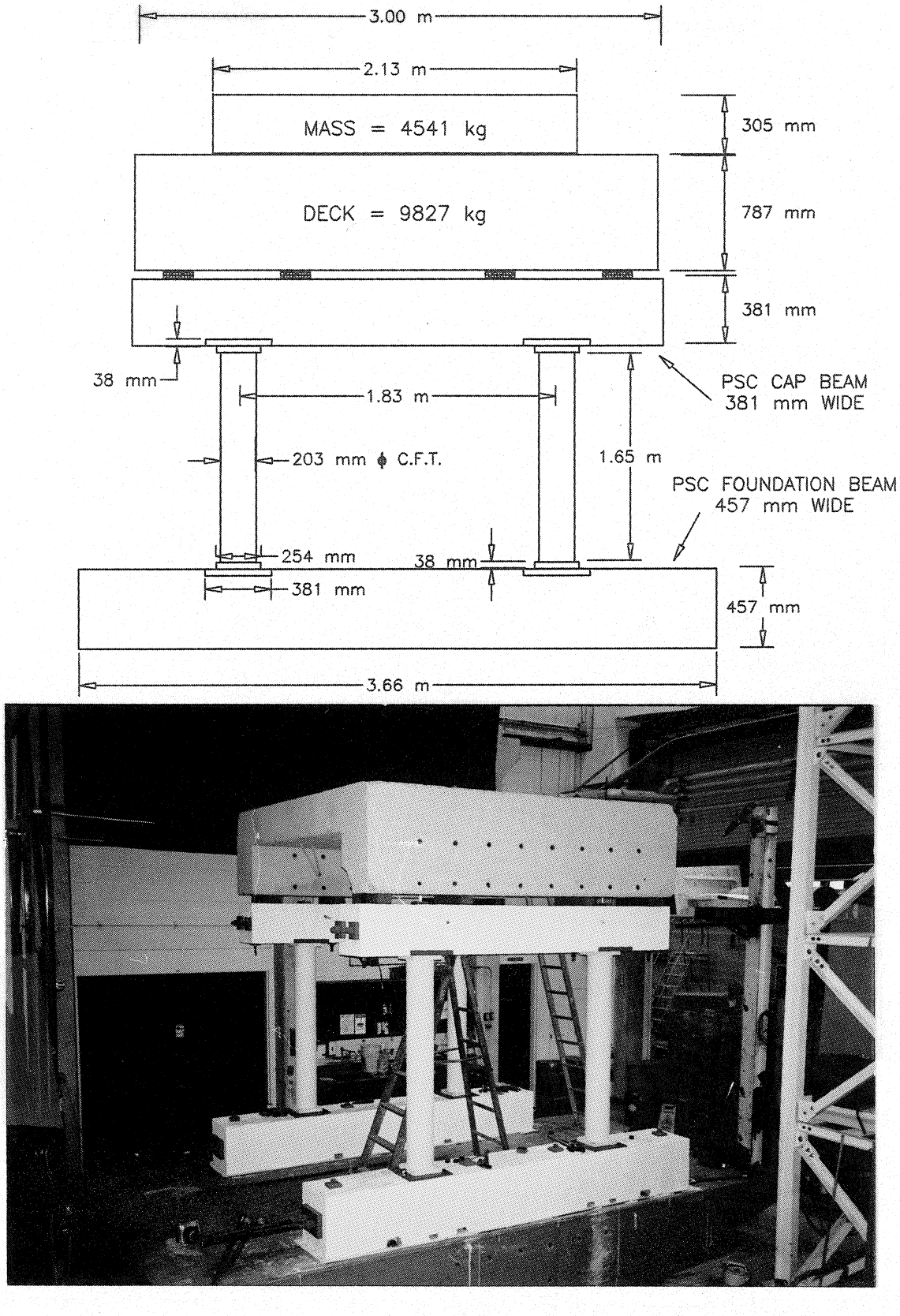


Fig. 4 Experimental One-Quarter Scale Bridge Model

were snug tight at the commencement of the test. This RKG-PT is where some post-tensioning of the tendons was provided. This increases the base shear capacity from 0.1 to 0.2 on uplift giving a total base shear capacity at first yield of the tendons of 0.3.

From these experiments, it is clearly evident that the performance of the rocking columns is very satisfactory. Good strength and deformation capacity may be attained — without damage. Finally, it should be emphasized that there was no residual drift observed at the end of each cycle of loading and hence re-centering is always ensured.

SHAKING TABLE EXPERIMENTAL STUDY

The Bridge Model

Based on the foregoing design theory, together with the proof of concept column experiments, further experimentation was conducted on entire bridge piers. As the dynamics of rocking structures are difficult to predict from a theoretical perspective, it was determined necessary to conduct several shaking table experiments to validate the entire rocking bridge pier concept. Therefore, a one-quarter scale model bridge was designed, constructed, and tested on the University at Buffalo shaking table. The deck of the model bridge was supported by two twin-column piers. The piers consisted of prestressed concrete foundation and cap beams, while the columns were built from concrete-filled steel tubes. Fig. 4 presents details of the model bridge structure.

The model bridge structure was intended to represent a prototype possessing 18 m spans having a width of 10 m. The superstructure was assumed to have a deck weight of 7 kPa, inclusive of girders, deck and guardrails. The experimental model was scaled based on constant acceleration similitude principles. Therefore, ground motion acceleration amplitudes were unscaled while the time scale was multiplied by 0.5. Constant acceleration similitude requires supplementary mass to be added to the model structure. Therefore, the concrete deck was represented by two large concrete blocks weighing 96 and 45 kN. Some additional lead bricks were also seated on the deck to provide required weight.

The ends of the concrete-filled steel tube rocking columns were capped with 254 mm square by 38 mm thick steel plates. These plates were seated on steel masonry plates that were cast into the foundation and cap beams. In this way, a steel-steel rocking interface was provided. Each column had a 40 mm plastic tube located along the axis of the member. Through these tubes ungrouted high-strength, high-alloy, prestressing threadbars were passed and anchored in both the foundation beam, as well as the cap beam.

The key dimensions of the model used later in the analysis of the experimental results are: $D = 254\,mm$ and $H_c = 1726\,mm$.

The rocking behavior of the structure was studied through the analysis of the response of the bridge model to impulses and earthquake motions such as Taft, El Centro, Northridge and Kobe. These earthquake records were scaled to different peak ground accelerations with and without vertical acceleration.

EXPERIMENTAL DAMPING — RESULTS OF PULSE TESTS

In order to initiate a free rocking vibration motion for the purpose of determining damping effects, pulse tests were performed. The bridge model was subjected to different single pulse excitations with a frequency of 2.0 Hz which was very close to 2.6 Hz, the average predominant frequency of the structure obtained from White Noise tests. The amplitudes of the pulses were 0.20 g, 0.22 g and 0.30 g. These characteristics of the pulses lead to a high excitation of the structure and a free rocking response. From time domain response results, the equivalent viscous damping characteristic of the structure during the rocking stage, as well as the rocking frequencies and periods, were determined. The response to the 0.22 g pulse is shown in Fig. 5. The test was performed on the structure without prestress (the tendons were completely loose). The maximum relative deck displacement response was 132 mm, corresponding to a drift of $\theta = 0.076$.

The free rocking vibration decay curve permits the evaluation of damping of a single-degree-of-freedom system. Accordingly, by evaluating the decay of the free-vibration time history response of the structure, the

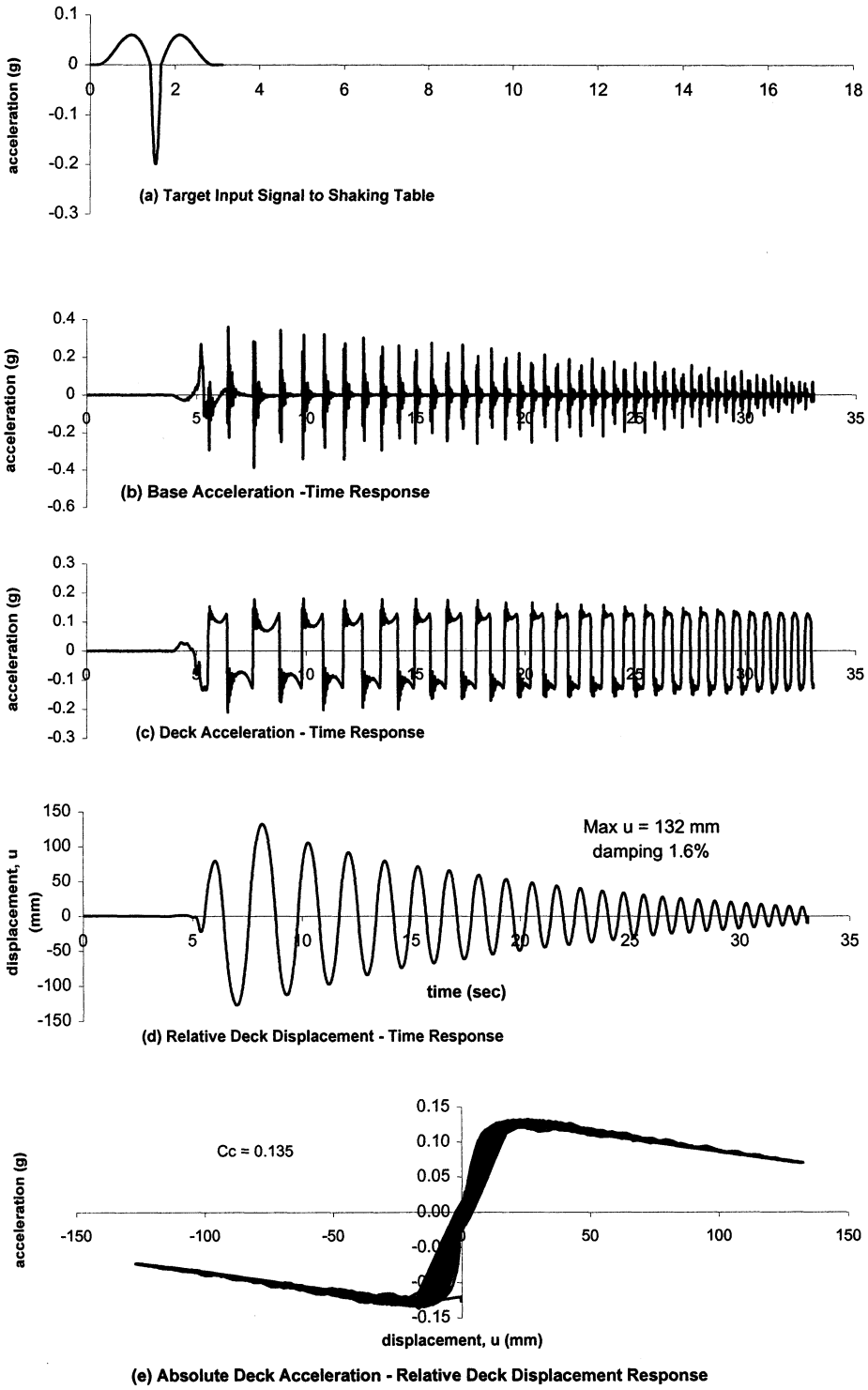


Fig. 5 Response to 2.0 Hz, 0.22 g Pulse Test without Prestress

viscous damping factor was determined by applying the well-known logarithmic decrement method.

The equivalent damping ratios of the bridge model were obtained from the displacement response time history of the structure when subjected to different single pulse excitations. The average damping ratios obtained were 1.4% for 0.20 g, 1.6% for 0.22 g, and 2.0% for 0.30 g pulse. The reason the damping increased with the PGA is due to the danger drift (θ) amplitude. Consider the results shown in Fig. 5. The average drift midway through the experiment is 0.02. According to equation (10), the theoretical damping is $\xi_{eq} = 1.7\%$. This agrees very well with the experimental observation.

RESULTS FOR EARTHQUAKE EXCITATIONS

With No Prestress

The bridge model without prestressing was subjected to the Taft ground motion, with amplitude of 0.16 g. The response of the structure to this test is shown in Fig. 6. For this particular test, no clear rocking was observed as indicated in the seismic capacity curve shown in Fig. 6.

The maximum relative deck displacement response obtained for Taft 0.16 g was 12 mm. This corresponds to a drift ratio of 0.7%. The time history of relative deck displacement is shown in Fig. 6. It should be noted that for this test only a limited amount of uplift was obtained. This is evident from the acceleration-displacement plot for the Taft earthquake in Fig. 6.

With Prestressing Tendons Snug

The earthquake records selected for the experiments with snug prestressing tendons were Taft 0.16 g, 0.25 g and 0.25 g with vertical acceleration, El Centro 0.17 g, 0.25 g, 0.34 g, 0.40 g, and Northridge 0.66 g. The response of the structure to El Centro 0.34 g and Northridge 0.66 g motions are shown in Fig. 6(b) and (c), respectively.

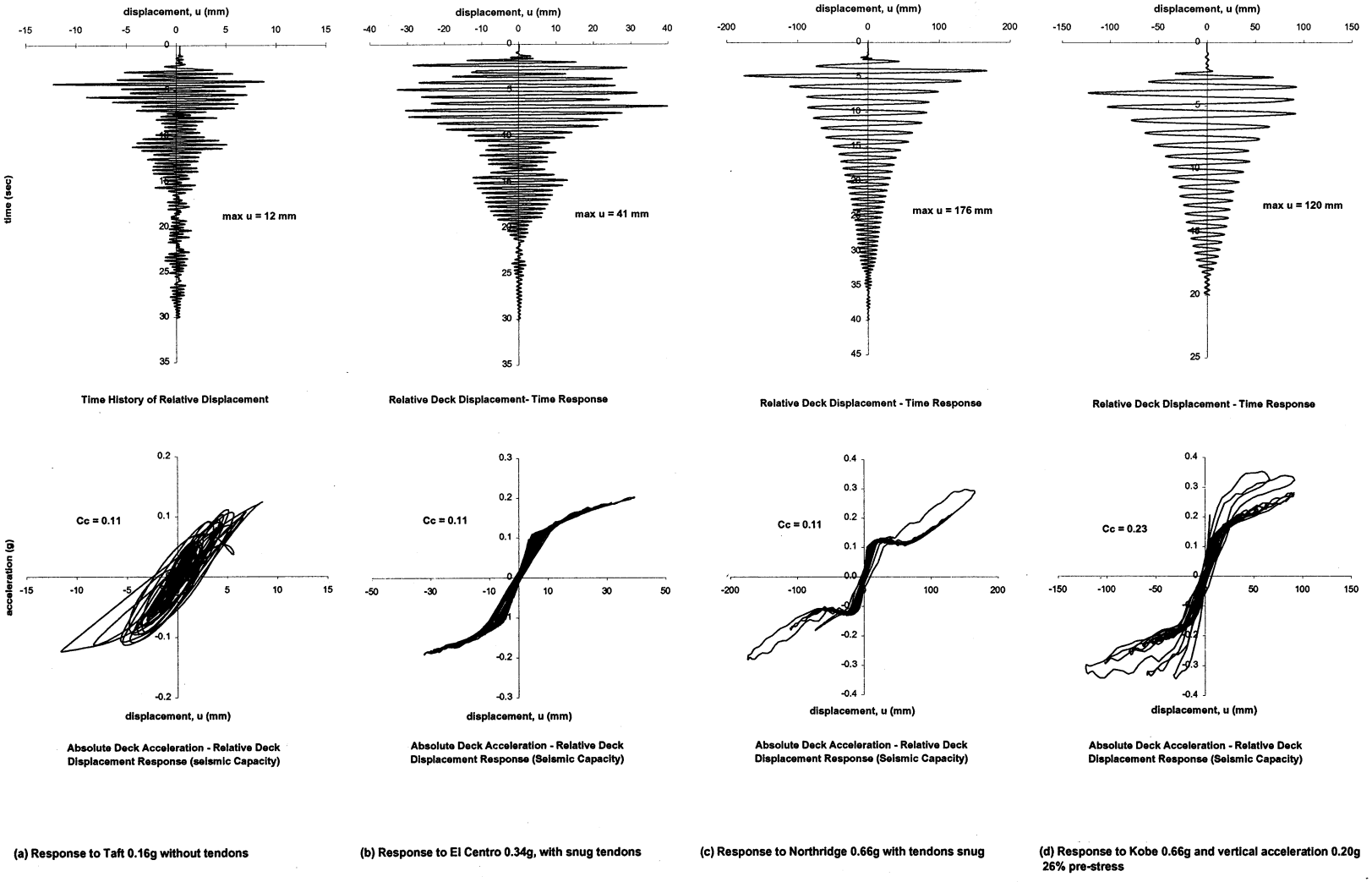
The expected behavior of the rocking column bridge under seismic excitation is bi-linear elastic. The first elastic range, which is the pre-rocking stage, is determined by the structural flexibility of the rocking columns. The second elastic range, on the other hand, is determined by rigid body kinematics of the rocking mechanism including the effects of the prestressing tendons. When the structure is provided with snug tendons, the first elastic range stays the same since there is no prestressing force to alter the lateral flexibility (stiffness) of the structure. When the structure starts to rock, the second elastic part is enhanced by the presence of the tendons which provide additional restraint that also reduces the lateral displacements. Similarly, the seismic capacity is also increased. The beneficial effect of the presence of the tendons is evident when one examines the deck acceleration (force)-displacement plots in Fig. 6.

The maximum relative deck displacement obtained for El Centro 0.34 g was 41 mm, that is $\theta = 0.024\ rad$. Similarly, for Northridge 0.66 g the maximum relative deck displacement obtained was 176 mm with $\theta = 0.102\ rad$. The time history of relative deck displacement for both earthquakes is shown in Fig. 6.

With Post-Tensioned Tendons

When the tendons within bridge columns are post-tensioned, the lateral resistance is provided by the gravity load and the supplementary prestressing. The base-shear capacity is limited by tendon yielding, which in the case of the present tests, $C_c = 0.36$. The effect of post-tensioning is to not only increase the lateral resistance, but also limit post-uplift displacement response. The earthquake records selected to test the bridge model with the tendon post-tensioned were El Centro 0.34 g, 0.40 g and 0.50 g, Northridge 0.2 g, 0.4 g, 0.6 g and 0.66 g, and Kobe 0.66 g and 0.66 g with vertical acceleration. The response of the structure to Kobe 0.66 g with vertical acceleration is shown in Fig. 6(d).

When comparing the results among same input motions with same PGA but different conditions of the tendons, it was observed that the restraint of central tendons in the columns effectively reduced the lateral



(a) Response to Taft 0.16g without tendons

(b) Response to El Centro 0.34g, with snug tendons

(c) Response to Northridge 0.66g with tendons snug

(d) Response to Kobe 0.66g and vertical acceleration 0.20g 26% pre-stress

Fig. 6 Response to Earthquake Excitations

displacement of the rocking piers. The maximum relative deck displacement response of the structure when subjected to Kobe 0.66 g with vertical acceleration was 120 mm. This represents a drift angle of $\theta = 0.07\ rad$.

In agreement with the results obtained from the theoretical analysis, the capacity coefficients of the bridge model increased with higher levels of prestress. One of the most interesting tests performed was the one chosen for this paper — Kobe 0.66 g with vertical acceleration. The initial uplift capacity coefficient obtained from the response to this ground motion was 0.23. This is in contrast to the non-prestressed or snug tendon case where at uplift $C_c = 0.13$. Note that this enhancement of uplift capacity was obtained with only limited axial prestress of $0.26f_{pu}$.

Although yielding of the prestressing tendons may occur during a large seismic evaluation, plastic strains in the tendons are expected to be very small. Therefore, after a strong earthquake, the tendons do not need to be replaced, but the prestress (if any) should be checked and re-tensioned, if necessary.

COMPARISON OF EXPERIMENTAL RESPONSE WITH THEORETICAL PREDICTIONS

Fig. 7 presents the theoretical response of the model bridge structure obtained by the linearized capacity-demand spectrum method. The theoretical push-over capacity curve (C_c) is shown along with two demand curves. The inner (left-hand side) of the two curves is for 2% damping, whereas the outer curve is for 0% damping. Also shown on each graph is a large bullet which is the experimentally obtained performance point. Strictly this should lie on the capacity curve about midway between the two demand curves.

The experimental results compare favorably with the theoretical prediction for the El Centro and Northridge ground motions. However, the Kobe prediction is unconservative. This is presumably due to the fact that the vertical ground motion component was not accounted for in the analysis. Clearly this should be accounted for in design if high near-fault vertical motions are expected.

CONCLUSIONS

In summary, rocking bridge piers have certain distinct advantages: no earthquake induced structural damage, re-centering of the structure, and therefore immediate post-earthquake serviceability. Thus the advantages of a seismic isolation philosophy consistent with the ductile design approach can be realized when one adopts a rocking column design.

Further advantages can be realized in terms of economy of construction. As rocking bridge piers lend themselves to an assemblage of precast elements, considerable time savings can be made in the construction schedule. This is an especially important consideration for construction sites where the harsh winter climate necessitates cessation of all work activity for several months. This winter period can be utilized manufacturing and curing the precast elements under cover in controlled factory-like conditions.

REFERENCES

Aslam, M. Goddon, W.G. and Scalise, D.T. (1980) "Earthquake Rocking Response of Rigid Blocks," *Journal of Structural Engineering, ASCE*, Vol. 106, No. 2, February 1980, pp. 377-392.

Cormack, L.G. (1988). "The Design and Construction of the Major Bridges on the Mangaweka Rail Division," Transactions, Institution of Professional Engineers, New Zealand, 15, I/CE, pp. 16-23.

Housner, G.W. (1963). "The Behavior of Inverted Pendulum Structures During Earthquake," *Bulletin of the Seismological Society of America*, Vol. 53, No.2, pp. 403-417.

Mander, J.B. and Cheng, C-T. (1997), "Seismic Resistance of Bridge Piers Based on Damage Avoidance Design", National Center for Earthquake Engineering Research, Technical Report NCEER-97-0014, December 10, 1997.

Priestley, M.J.N. and Tao, J. (1993). "Seismic Response of Precast Prestressed Concrete Frames with Partially Debonded Tendons," *PCI Journal*, Vol. 38, No. 1, January-February 1993, pp. 58-69.

Priestley, M.J.N., Seible, F. and Calvi, G.M. (1996). *Seismic Design and Retrofit of Bridges*, John Wiley & Sons, New York.

Skinner, R.I., Robinson, W.H. and McVerry G.H. (1993). *An Introduction to Seismic Isolation*, John Wiley & Sons Ltd., England, p. 10.

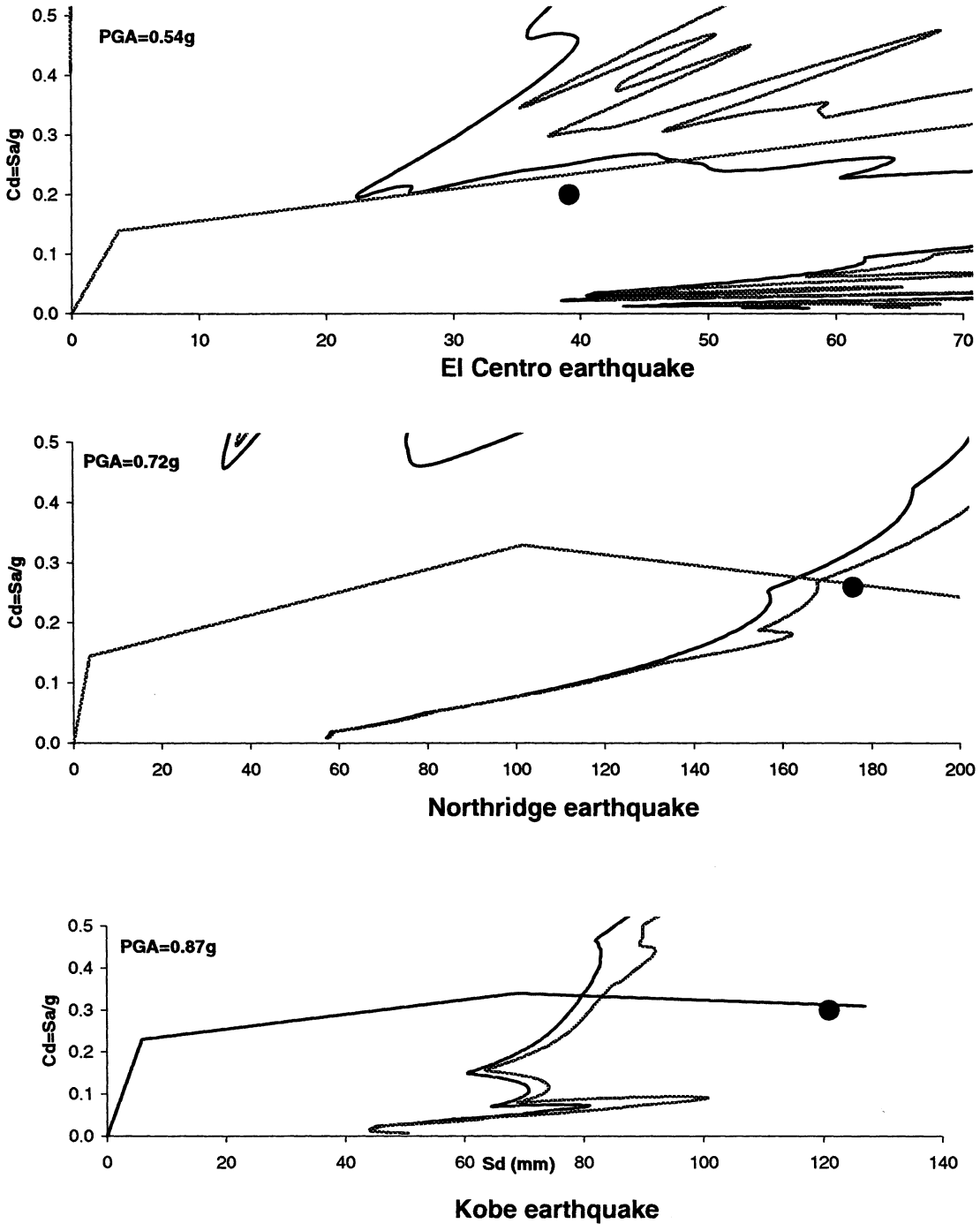
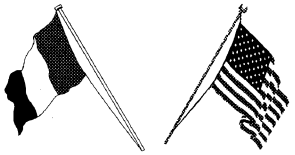


Fig. 7 Linear Elastic Capacity-Demand Spectra



Session VI

Modeling of Elastomeric Devices in the Dynamic Linear and Nonlinear Range
Antonello De Luca and Giuseppe Faella

Modeling and Characterization of Seismic Isolation Bearings
Gregory L. Fenves, Wei-Hsi Huang, Andrew S. Whittaker, Peter W. Clark and Stephen A. Mahin

High Damping Elastomeric Bearings (HDEB): Experimental Tests and Preliminary Results
Franco Braga

Optimal Design of Isolated Bridges and Isolation Systems for Existing Bridges
Gian Michele Calvi and Alberto Pavese

Modeling of Elastomeric Devices in the Dynamic Linear and Nonlinear Range

by
Antonello De Luca[1] and Giuseppe Faella[1]

[1] Dipartimento di Analisi e Progettazione Strutturale, Università di Napoli Federico II, Italy

Abstract

A hysteretic model able to simulate the behaviour of elastomeric devices for seismic base isolation is presented. The model is an extension of the Wen's model which has been modified in order to introduce a dependency of some coefficients on the achieved shear deformation, so that the shape of the hysteretic cycles of the high damping rubber devices is reproduced with suitable precision at all amplitude of deformation. A comparison with experimental data from shaking table tests and with other typical modelings (equivalent viscous model and Bouc-Wen's model) has been carried out to prove the adequacy and advantages of the proposed model. The comparison has shown a satisfactory agreement between the numerical simulation provided by the proposed model and the experimental response both for low and for high deformations, thus overcoming the drawbacks typical of the hysteretic models existing to date.

Introduction

Isolation devices are usually made of rubber bearings or high damping rubber bearings which exhibit highly non-linear response, especially when subjected to large deformations from dynamic excitations deriving from an earthquake-type motion. This earthquake motion produces, during the time history, different cycles yielding to unequal values of deformations, each one corresponding to a different response in terms of stiffness and damping because of the high non-linearity of the material.

In the dynamic analysis of base isolated structures, refined modeling of the devices, as the finite element method, is usually not convenient because of the large number of degree of freedom necessary for an appropriate discretization and of the lack of mathematical procedures able to reproduce the behaviour, and in particular the energy dissipation, of the hyperelastic materials. Therefore, macroscopic simplified models, which are able to simulate both the damping and the stiffness characteristics of the bearings, are usually adopted.

Several models (Nagarajaiah et al., 1989, Serino et al., 1993) were developed so far to specifically simulate the behaviour of base isolation devices. Among these models it is possible to distinguish two limit approaches. The first one, commonly referred to as equivalent linear viscous model, makes a linearization of the problem by assuming an equivalent viscous damping, derived from the equivalence of the dissipated energy, and an effective secant stiffness. The simplicity of the model, due to the hypothesis of linearization, is counterbalanced by the fact that the actual secant stiffness depends on the deformation and therefore it is not possible to adequately match the response when the external signal is highly variable as in the case of the earthquake input motion. The second approach, commonly referred to as hysteretic model, ignores the dependency on velocity since it assumes that the restoring force is the result of an elastic and a hysteretic contribution both proportional to the extent of deformations. Within this philosophy it is possible to define a secant stiffness able to follow any type of seismic history. The problem arises in the simulation of the equivalent viscous damping at very small deformations since the dissipated energy, represented by the area embodied in the hysteretic loop, is not able to represent the actual damping properties.

Based upon the need of overcoming the limitations of the two above cited methods, a new model is presented in this paper. Feature of the model is the capability to reproduce the stiffness and the damping properties at any value of deformation. The model is an extension of the Wen's model which has been modified in order to introduce a dependency of some coefficients on the current value of the shear deformation. The parameters which need for using the model can be evaluated on the basis of standard static tests and/or sinusoidal dynamic tests performed on the isolation devices.

The adequacy both of the equivalent viscous damping model and the Wen's model and of the proposed model to simulate the response of isolation devices subjected to several dynamic loads is verified by comparing the analytical response with some shaking table time histories.

Existing models

Though many mathematical models were developed in the past years to study the behaviour of elastomeric devices for vibration isolation, most of such models cannot be used to analyse the response of devices for seismic isolation of structures. In fact, the base isolation requires to work in a rather bounded range of frequencies where the expected very large deformations do not allow to neglect the non-linear characteristics of the elastomeric materials; furthermore, the response of the base isolated structures is dependent both on the imposed deformations and on the frequencies of the excitation. Therefore, the models for simulating the behaviour of base isolation devices, usually made of rubber bearings or high damping rubber bearings, have to account for the strongly non-linear properties of the elastomers and for the characteristics of the dynamic loading. However, as it has been previously evidenced, when elastomeric devices are employed for seismic base isolation, it is possible to operate under simplified hyphoteses and, hence, to assume a linearized behaviour for the estimated range of variation of frequencies and deformations. For this reason,

simplified models characterised by viscous or hysteretic damping are usually employed and in the next sections the main characteristics of the equivalent viscous damping model and of the hysteretic models are summarised.

Equivalent viscous damping model

The dynamic response of single degree-of-freedom systems with viscous damping is governed by the following equation of motion:

$$m\ddot{u}(t)+c\dot{u}(t)+ku(t)=p(t) \tag{1}$$

In most cases, the mass m and the stiffness k can be determined rather easily using physical considerations or generalised expressions, while the evaluation of the damping coefficient c is usually not simple because the basic energy-loss mechanisms are seldom fully understood.

Damping of the linear viscous form is commonly used because it leads to a convenient form of equation of motion and it generally is possible to compute an appropriate equivalent viscous-damping coefficient from experimental data. In fact, if the system is subjected to a harmonically varying load $p(t) = p_o \sin \bar{\omega} t$, under steady-state harmonic condition at frequency $\bar{\omega}$, the average rate of energy dissipation is given by (Clough and Penzien 1993):

$$P_{avg} = \frac{c\,\bar{\omega}}{2\pi} \cdot \int_0^{2\pi/\bar{\omega}} \dot{u}(t)^2\, dt = \xi\, m\, \omega\, \bar{\omega}^2\, u_{max}^2 \tag{2}$$

where ω is the undamped natural circular frequency, ξ is the ratio of the given damping to its critical value and u_{max} is the displacement response amplitude. Therefore, the energy loss per cycle is equal to:

$$E_d = \frac{2\pi}{\bar{\omega}} \cdot P_{avg} = 2\pi \xi\, m\, \omega\, \bar{\omega}\, u_{max}^2 \tag{3}$$

Equation (3) shows that at a fixed amplitude u_{max}, the energy E_d is dependent upon the excitation frequency $\bar{\omega}$ while tests evidenced that the energy loss per cycle is essentially independent on frequency.

If the system truly posses linear viscous damping, the shape of the applied-force/displacement diagram is an ellipse. If damping is of a non-linear viscous form, the shape of such diagram will not be elliptical and the response will be a distorted harmonic, even though the applied loading is a pure harmonic. Nevertheless, the energy input per cycle can be computed as the area under the applied-force/displacement diagram and, therefore, an equivalent viscous damping ratio for the corresponding displacement amplitude, which dissipate the same amount of energy per cycle as in the real experimental case, can be evaluated. The equivalent damping ratio is associated with an elliptical applied-force/displacement diagram having the same area E_d as the measured non-elliptical diagram; at resonance ($\omega=\bar{\omega}$), the energy equivalence requires to write Equation (3) by assuming $\xi=\xi_{eq}$ and leads to:

$$\xi_{eq} = \frac{E_d}{2\pi m \omega^2 u_{max}^2} = \frac{E_d}{2\pi k u_{max}^2} = \frac{E_d}{4\pi E_s} \tag{4}$$

being $E_s = k u_{max}^2 / 2$ the elastic dissipated energy.

Since the spring force f_s and the damping force f_d are 90° out of phase with each other, the amplitude of the maximum base reaction force is given by:

$$f_{max}(t) = \sqrt{f_{s,max}(t)^2 + f_{d,max}(t)^2} = k u_{max} \sqrt{1 + (2\xi\beta)^2} \tag{5}$$

Then, the effective stiffness k_{eff} is equal to:

$$k_{eff} = \frac{f_{max}}{u_{max}} = k\sqrt{1 + (2\xi\beta)^2} \tag{6}$$

and, at resonance, Equation (6) provides:

$$k_{eff} = k\sqrt{1 + 4\xi^2} \tag{7}$$

Therefore, the restoring force is assumed proportional to the displacement and the model maintains linear characteristics.

In conclusion, the equivalent viscous damping assumption allows to obtain a convenient expression of the equation of motion, because of the simplifications connected with the hypothesis of linearity; moreover, in many applications it provides a response which is reasonably approximated and, for this reasons, it is widely used in the analyses of the base isolated structures. However, the experimental results generally do not show this form of damping since the elastomeric materials are not purely viscous but present a hysteretic energy dissipation which does not depend on the frequency.

Hysteretic models

The main deficiency of the equivalent viscous damping models is the dependency of the energy loss per cycle on the frequency of the applied loading which is at variance with a great deal of test evidence.

In order to remove this dependency, the damping force can be modelled by using the so-called hysteretic form of damping in place of the viscous damping. Mathematical models which satisfy the above condition are the hysteretic models where a damping force, whose gradient is in phase with the velocity and is proportional to the variation in displacements, is defined. In such case, the dissipated energy is given by the area of the hysteretic loop and, obviously, is independent on the velocity by which the loop is covered. Moreover, it has to be noted that, in the range of application of the isolation devices, this assumption is quite close to the actual behaviour.

In order to simulate the hysteretic phenomenon in systems subjected to dynamic actions, many mathematical models have been developed, but the hysteretic model more utilised is the one originally proposed by Bouc (1971) and subsequently extended by Wen

(1976). The advantages of such model, which is described by differential equations, are the capability to simulate a wide range of behaviours and the high computational efficiency.

In the model, the restoring force F is assumed equal to the sum of a linear elastic component and of a hysteretic component as follows:

$$F = \alpha \frac{F_y}{\gamma_y} \gamma + (1-\alpha) F_y Z \tag{8}$$

where γ is the shear deformation and α is the post yielding to elastic stiffness ratio ($\alpha = k_2/k$); F_y is the yield value of the restoring force and γ_y is the yield deformation, while Z is a nondimensional hysteretic parameter provided by the following differential expression:

$$\frac{dZ}{d\gamma}\gamma_y = \left\{ A - |Z|^{\eta} \left[\beta + sign\left(Z \frac{d\gamma}{dt} \right) \zeta \right] \right\} \tag{9}$$

where the sign of ζ is opposite to the sign of Z in the unloading branches and is concordant in the loading and reloading branches.

In Equation (9), A, β, ζ, and η are nondimensional coefficients which control the shape of the hysteresis loop. In particular, the coefficient A controls the initial slope of the first loading branch which is equal to $A \cdot k$ while the initial slope of the unloading and reloading branches, in addition to A, is controlled by β and ζ (Figure 1): if the ratio ζ/β is lower than 1 the slope is smaller than k while if it results $\zeta/\beta > 1$ the slope is greater than k.

Parameter η governs the joining curve between the elastic and the post-elastic branches: if η is very large the loading branch tends to the one of the elastic-plastic model. Furthermore, η influences also the area of the hysteresis loop since at large deformations the area shrinks as η decreases, while at low deformations the behaviour is opposite and the influence of η on the loop area is more sensible.

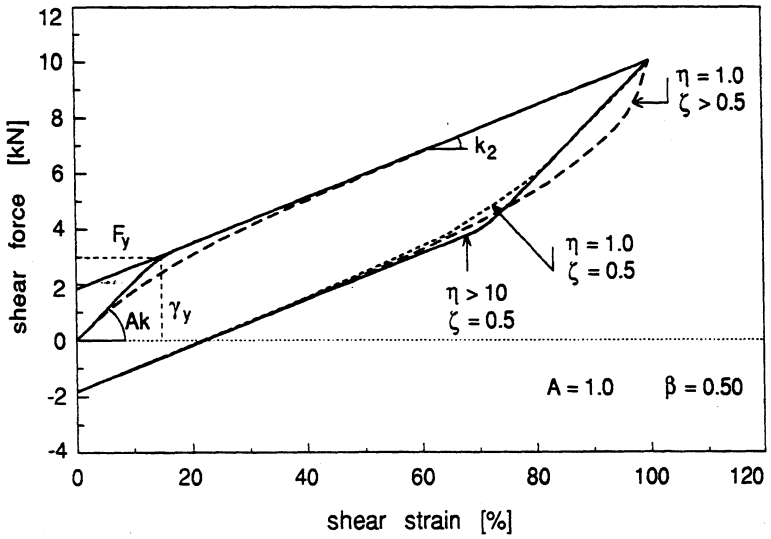


Figure 1. Parameters of the Wen's model

Finally, by setting Equation (9) equal to zero, the maximum value of Z is obtained:

$$Z_{max} = \left(\frac{A}{\beta + \zeta} \right)^{1/\eta} \tag{10}$$

and, hence, if the ratio $A/(\beta+\zeta)$ is kept constant, it is possible to vary the shape of the hysteresis loop without changing the values of the other coefficients.

The coefficients A, β, ζ, and η can be evaluated on the basis of a given experimental loop but it is immediate to evince that matching of the response for one cycle will not lead to matching at other different cycles.

The proposed model

From the above section, it emerges that the equivalent viscous damping model can match all values of the damping as the shear deformation varies but it is not able to reproduce the trend of the actual secant stiffness. The hysteretic models, instead, do not allow to approximate the experimental curve of the damping though they well simulate the value of the secant stiffness. This derives from the fact that both models are settled for a given value of the shear deformation and, then, they do not allow to obtain the same degree of approximation as the shear deformation varies.

The model which is presented in this section is finalised to simulate the response of elastomeric devices characterised by loops highly variable with the extent of deformation and it has been developed for seismic applications where the moderate dependency of external loads on frequency has been demonstrated by experimental tests (Aiken et al., 1992).

The model is of the hysteretic type and can be considered as an extension of the Wen's model which has been modified in order to introduce the dependency of some coefficients on the current values of deformation, so that the limitations of the original model are overcome. In fact, in the Wen's model the equivalent damping ξ_{eq} and the secant stiffness k_s, in a generic cycle, in addition to the maximum deformation, depend on the values of the coefficients α, F_y, k_2, A, β, ζ, and η, which are initially settled on the basis of the experimental data. The proposed model, instead, updates the damping coefficient and the stiffness as a function of the maximum shear deformation γ_c achieved in each cycle, which depends on the frequency of the applied loading.

Referring to the differential relation between the hysteretic parameter Z and the shear deformation γ, Equation (9) of the Wen's model has been rearranged in the following form:

$$\frac{dZ}{d\gamma}\gamma_y = \left\{ A - \beta |Z|^{\eta_1} - \zeta \, sign\left(Z \frac{d\gamma}{dt} \right) |Z|^{\eta_2} \right\} \tag{11}$$

If the following positions are made:

$$A=1.0 \qquad \eta_1=0 \tag{12}$$

Equation (11) leads to:

$$\frac{dZ}{d\gamma}\gamma_y = \left\{1-\beta-\zeta\, sign\left(Z\frac{d\gamma}{dt}\right)|Z|^{\eta_2}\right\} \tag{13}$$

In this case, the maximum value of the parameter Z in the loading branch is equal to:

$$|Z|_{max} = \left(\frac{1-\beta}{\zeta}\right)^{1/\eta_2} \tag{14}$$

which, by imposing Z_{max}=1, provides:

$$\zeta = 1-\beta \tag{15}$$

and, therefore, Equation (13) can be rewritten as follows:

$$\frac{dZ}{d\gamma}\gamma_y = \zeta\left\{1-sign\left(Z\frac{d\gamma}{dt}\right)|Z|^{\eta_2}\right\} \tag{16}$$

As it has been said above, coefficients ζ and η_2 of Equation (16) are assumed to be function, within each cycle, of the maximum current value γ_c of deformation achieved in that specific cycle. Therefore, it is possible to integrate Equation (16) for each γ_c and the evaluation of α, F_y and k_2 on the basis of experimental tests performed on isolation devices at a settled value of deformation γ_c allows to adopt Equation (8) to compute the effective secant stiffness k_s and the equivalent damping ξ_{eq}. In functional form this means to formulate the following relations:

$$\begin{aligned} \xi_{eq}(\gamma_c) &= f_1(\gamma_c,\zeta,\eta_2) \\ k_s(\gamma_c) &= f_2(\gamma_c,\zeta,\eta_2) \end{aligned} \tag{17}$$

which represent a system of non-linear non-algebraic equations in the unknowns ζ and η_2.

The value of the ratio α can be evaluated by imposing that the curve $\xi_{eq}(\gamma_c)$ is tangent to the correspondent experimental curve.

The yielding force F_y can be instead computed from the expression:

$$F_y = \frac{F_o}{1-\alpha} \tag{18}$$

where F_o is the value of the shear force at a shear deformation equal to zero. The value of F_o is obtained by equating the area E_d of the experimental hysteresis loop relevant to the maximum shear deformation γ_{max} (see Equation(4)) with the area E_d^p of the parallelogram which envelops such experimental loop ($E_d^p = 4\,F_o\,\gamma_{max}\,t_r/C_s$), thus obtaining:

$$F_o = \frac{\pi C_s\,\xi_{eq}\,k_s\,\gamma_{max}\,t_r}{2} \tag{19}$$

where t_r is the total rubber height of the devices and C_s is a coefficient which accounts for the difference in the shape of the parallelogram and the experimental loop.

Finally, the post-yielding stiffness k_2 is computed by imposing that the experimental restoring force F_{exp} at the maximum shear strain is equal to the one F_{par} which characterises the enveloping parallelogram. Being $F_{exp} = k_s \gamma_{max} t_r$ and $F_{par} = F_o + k_2 \gamma_{max} t_r$, the above equivalence leads to:

$$k_2 = k_s - \frac{F_o}{\gamma_{max} t_r} \tag{20}$$

Therefore, the procedure stems from the knowledge of the experimental values of k_s and ξ_{eq} for some settled values of deformation γ_c and the steps to be followed are hereafter summarised. A value of the deformation γ_c is selected. A trial value is assigned to ζ and η_2 in order to integrate Equation (16) and to derive the values of k_s and ξ_{eq} through Equation (8). These computed k_s and ξ_{eq} are then compared with the experimental values corresponding to the settled deformation γ_c in order to establish if iteration on the procedure has to be carried out in order to find out the correct ζ and η_2 values. The procedure is then reiterated for the entire range of γ_c values so to define two curves for the coefficients ζ and η_2 as functions of the shear deformation.

In conclusion, the model is completely defined by Equations (8) and (16) combined with the $\zeta(\gamma_c)$ and $\eta_2(\gamma_c)$ functions. In particular, in the evaluation of the dynamic response of the bearings, ζ and η_2 are updated at each change of velocity on the basis of the current value of the shear deformation. This procedure has been also implemented in the 3D-BASIS computer program (Nagarajaiah et al., 1991) in order to verify its efficiency in accomplishing, besides the requirement of a refined simulation at any deformation and for any type of elastomeric device, the requirement of simplicity, that is the possibility to be introduced in the complete modeling of the structure.

Experimental results used in the verification procedure of the mathematical models

The adequacy of the equivalent viscous damping model and of the Wen's model, as well as of the proposed model, to simulate the response of isolation devices subjected to several dynamic loads has been verified by comparing the analytical response with some experimental data. Tests on high damping rubber bearings have been used since they exhibit higher non linearities with respect to the common rubber bearings and, therefore, the comparison between the experimental response and the numerical simulation is even more critical. In particular, results both from shake table tests of a 1/2.5 scale base isolated r.c. building performed by Aiken, Clark and Kelly at Berkeley (Aiken et Al. 1993) and from mock-up tests performed by ENEA in the ISMES laboratory (Serino et Al. 1992) have been used.

The geometric properties of the scaled base isolated building tested at Berkeley are shown in Figure 2 while column and girder cross-section dimensions are reported in Table 1 along with the story weights. High damping steel-laminated rubber bearings and lead-rubber bearings characterised by different sizes were used for the tests; in this paper reference to the

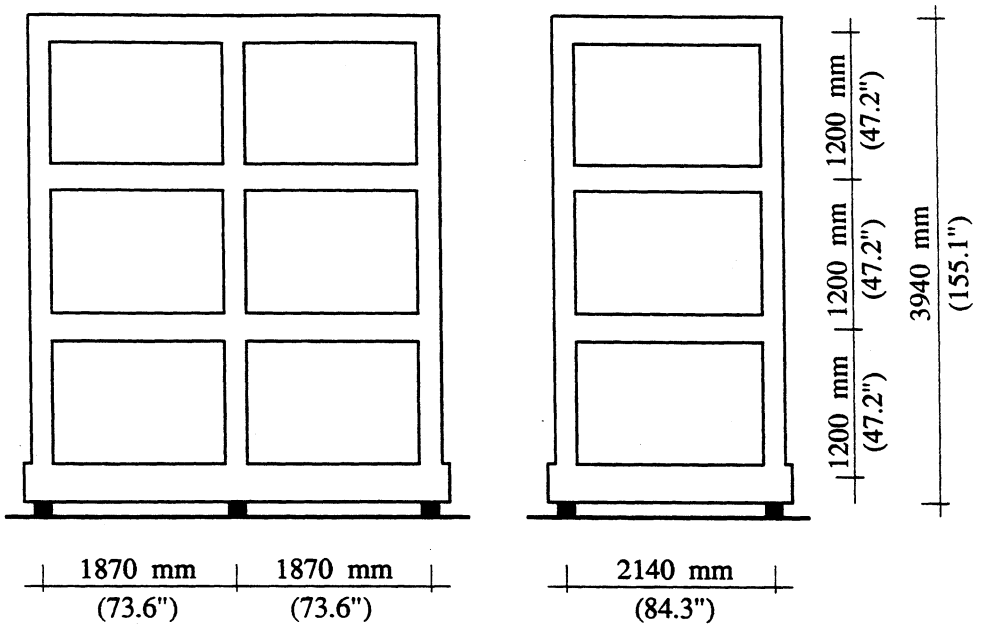


Figure 2. Transverse and longitudinal sections of the shake table scale model

base isolation system constituted by six high-damping devices having a circular cross section with a diameter equal to 176 mm and a total rubber height of 44 mm is made. The dynamic properties of the devices were previously determined by carrying out a large experimental program (Kelly, 1991, Aiken et al., 1992): in particular, characterisation sinusoidal tests on the bearings were performed in order to compute the values of the effective stiffness and of the equivalent damping. In the shake table tests three earthquake motions were applied to the model with varying effective peak ground acceleration. The earthquakes used were the 1940 El Centro (NS), 1968 Hachinohe (NS) and 1978 Miyagi (NS) records. In this paper, the comparison between experimental response and numerical simulation is carried out by using El Centro records. During the tests accelerations and displacements were measured at each floor level, including the bearing level. Significant yielding was observed throughout the structure since the records were amplified up to produce damage in the frame members. More details can be found in the relevant reports.

Table 1. Scale model data.

Story	Girder cross sections		Column cross sections		Story weights	
	[mm]	([in])	[mm]	[in]	[kN]	[in]
3	120x240	(4.7x9.4)	200x200	(7.9x7.9)	94.87	(21.32)
2	120x240	(4.7x9.4)	200x200	(7.9x7.9)	97.58	(21.93)
1	120x240	(4.7x9.4)	200x200	(7.9x7.9)	97.58	(21.93)
B	240x340	(9.45x13.4)	-	-	110.49	(24.83)

A further comparison has been carried out by using data relevant to a 394 kN isolated mock-up tested on the shaking table by ENEA in the ISMES laboratory: the mock-up was formed by three r/c blocks tightly connected to a very rigid steel frame and supported by four 1:4 scale isolation high damping steel-laminated rubber bearings. Each device had a circular cross section with a diameter equal to 125 mm and a total rubber height of 36 mm. Shake table tests were conducted both under harmonic loads and under seismic excitations. In the first case, the tests were repeated in order to achieve four values of the maximum shear strain, that is 10%, 25%, 50% and 100%: results from these tests have been used to compute the secant stiffness and the equivalent viscous damping which need to calibrate the parameters of the proposed model. In the second case, three complete sets of acceleration records, characterised by different predominant period, were used: namely, the San Rocco and Tolmezzo records of the 1976 Friuli earthquake and the Calitri record of the 1980 Campano-Lucano earthquake. Each test was repeated more times scaling the applied records at different levels (from -20 dB up to 15 dB) in order to analyse the non-linear characteristics of the response. In this paper, only the records from the Friuli earthquake are used for comparing experimental response and numerical simulation.

Comparison between experimental and analytical results

Application of the equivalent viscous damping model and of the Wen's model

In order to check the capability of the equivalent viscous damping model and of the Wen's model to simulate the actual behaviour of the bearings, in a first step, the capacity of such models to fit the actual curves of stiffness and damping as the shear deformation varies is examined; subsequently, the shaking table time histories are compared to the analytical response in terms of displacements and accelerations.

The experimental values of the effective stiffness and of the equivalent damping ratio obtained from the sinusoidal tests performed on the bearings of the scaled r/c building are plotted in Figures 3a and 3b respectively. In the figures, the correspondent interpolation curves and the values of the secant stiffness and of the equivalent damping computed by the linear viscous model and by the Wen's model are also provided.

Figure 3 evidences that both such models are not able to match, at the same time, the actual values of secant stiffness and equivalent damping for all values of the shear deformation. In fact, both the models have to be calibrated on a single value of the shear deformation, which usually corresponds to the largest strain. This limitation results in an incapacity of the linear viscous model in fitting the effective stiffness and in an incapacity of the Wen's model in fitting the actual equivalent damping. In particular, Figure 3a shows that the linear viscous model is able to fit only a value of the stiffness, that is the value on which the model is calibrated (in the examined case the deformation is equal to 200%). Figure 3b, instead, evidences how in the Wen's model the dissipated energy, which is conventionally measured by the equivalent viscous damping, is strongly dependent on the deformation: such behaviour is very different from the experimental one, evidencing moreover a significant hysteresis also at rather low deformations.

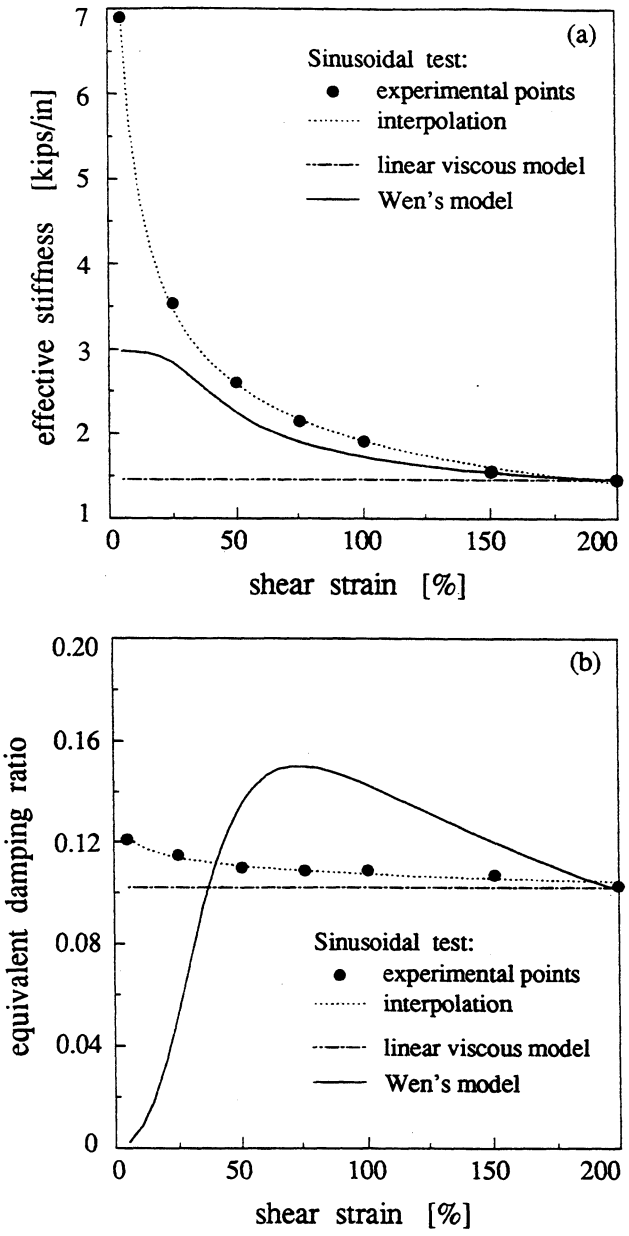


Figure 3. Comparison between experimental data and existing models in terms of effective stiffness (a) and equivalent damping ratio (b)

In Figures 4 through 9 the equivalent linear viscous model and the hysteretic Wen's model, in the version originally implemented in the 3D-BASIS computer program (Nagarajaiah et al. 1991), are adopted to simulate the experimental response both of the shake table tests on the scaled building under the El Centro record and of the shake table excitation on the mock-up test under the Tolmezzo input ground motion. In particular, the analytical response computed by using the above models is compared with the experimental one in terms of displacement and accelerations at the bearing level.

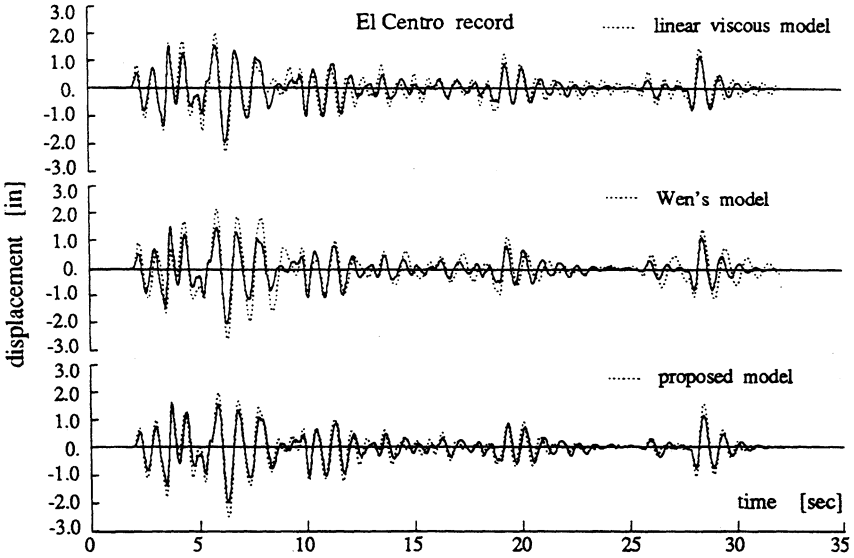


Figure 4. Comparison of the shake table response (experimental curve ——) with the simulation provided by the mathematical models - El Centro record.

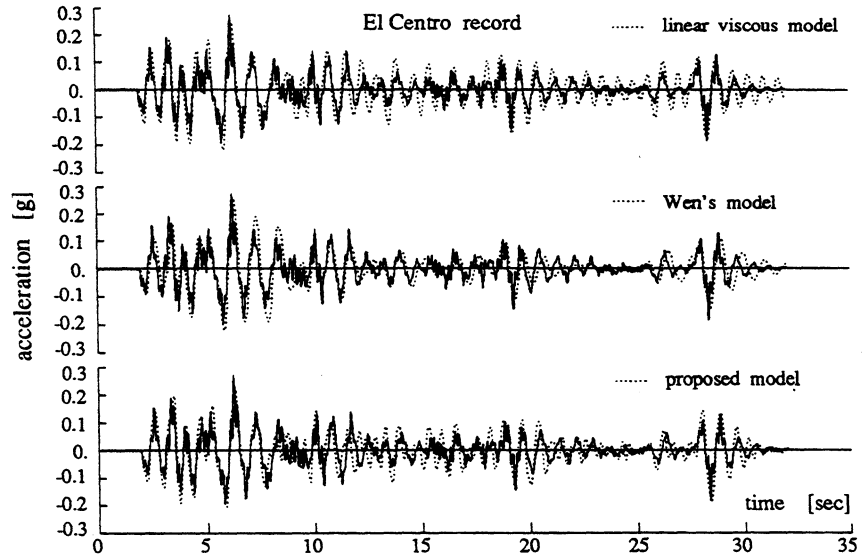


Figure 5. Comparison of the shake table response (experimental curve ——) with the simulation provided by the mathematical models - El Centro record.

In the first case (Figures 4 and 5), a maximum shear deformation equal to 200% was attained during the test and, in the application of the viscous model, an equivalent viscous damping equal to ξ_{eq}=10.2%, computed by Equation (4), and an equivalent stiffness k_{eff}=1.46 kips/in, computed by Equation (7), were used. In the application of the Wen's model, the coefficients which characterise the model were fixed as reported in (Nagarajaiah et Al., 1991) and then $A = 1$, $\zeta = 0.9$, $\beta = 0.1$ and $\eta = 2.0$ were used while values of $\alpha = 0.428$, F_y = 0.7675 kips, $\gamma_y = 61.17\%$ and $k_2 = 0.31$ kips/in were computed on the basis of the maximum deformation γ_{max} measured during the test.

In the comparison with the mock-up response, the Tolmezzo record was also scaled at a value of -20dB (Figures 6 and 7) and at a value of +8dB (Figures 8 and 9), which correspond to a reduction equal to 10 and to an amplification equal to 2.51 of the real record respectively; the corresponding maximum shear deformations γ_{max} achieved during the test were equal to 4.7% and 99.7%. Therefore, in the application of the viscous model, an equivalent viscous damping equal to ξ_{eq}=10.2% and a stiffness k_{eff}=288 kN/m were used since γ_{max} was equal to 99.7%. The Wen's model was applied with values of A, ζ, β and η equal to the ones of the above analyses while values of $\alpha = 0.39$, $F_y = 3.0$ kN, $\gamma_y = 14.2\%$ and $k_2 = 229$ kN/m were computed on the basis of the maximum experimental deformation.

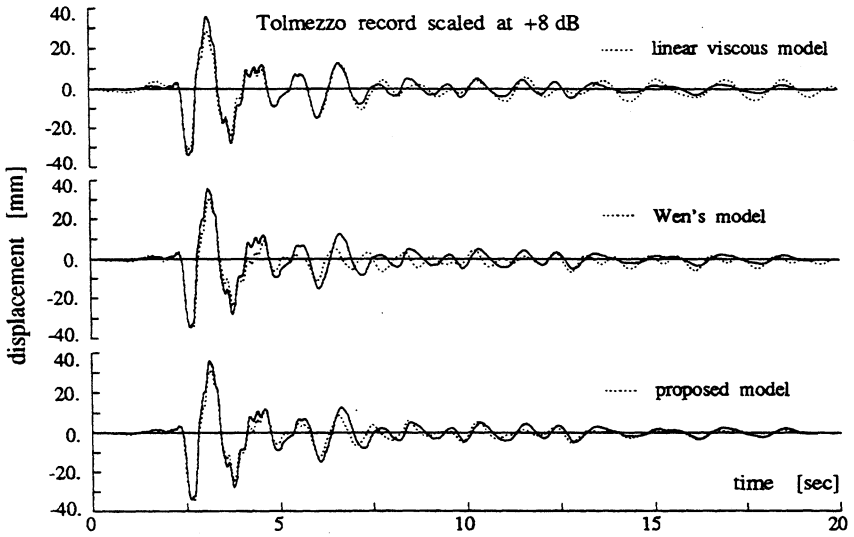


Figure 6. Comparison of the shake table response (experimental curve ——) with the simulation provided by the mathematical models - Tolmezzo record scaled at +8 dB.

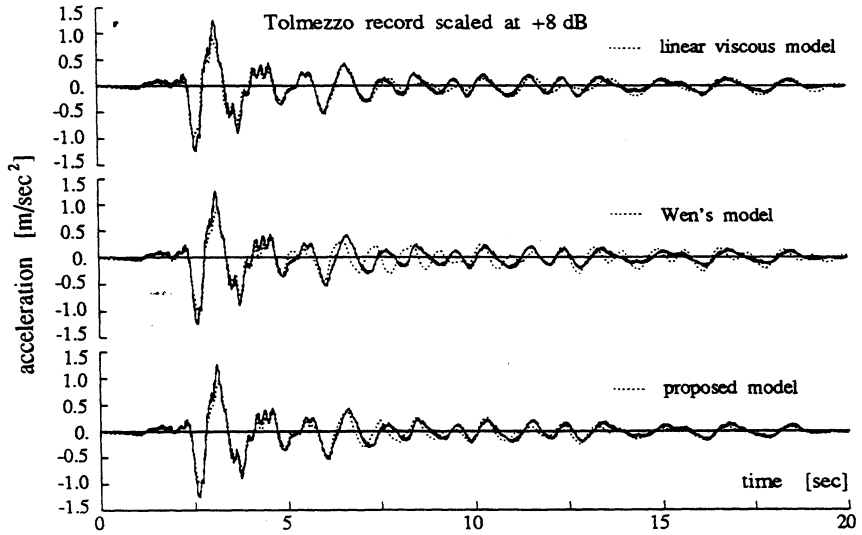


Figure 7. Comparison of the shake table response (experimental curve ——) with the simulation provided by the mathematical models - Tolmezzo record scaled at +8 dB.

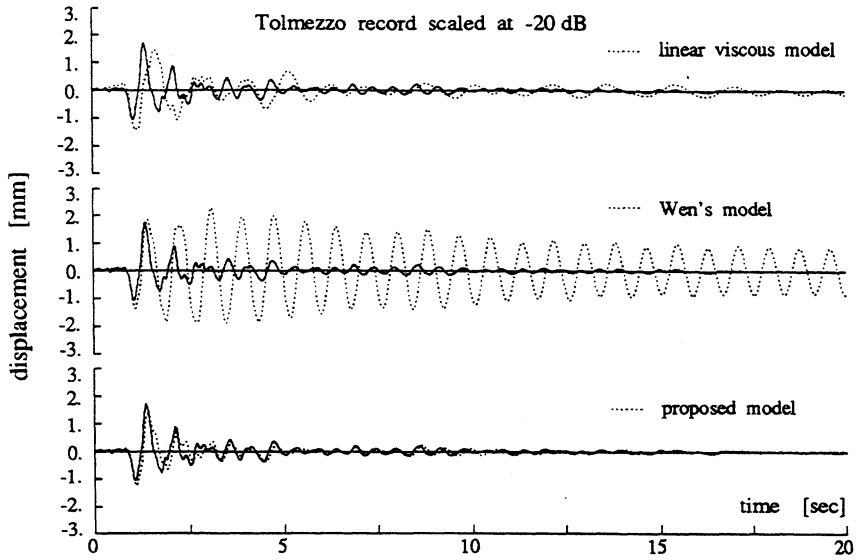


Figure 8. Comparison of the shake table response (experimental curve ——) with the simulation provided by the mathematical models - Tolmezzo record scaled at -20 dB.

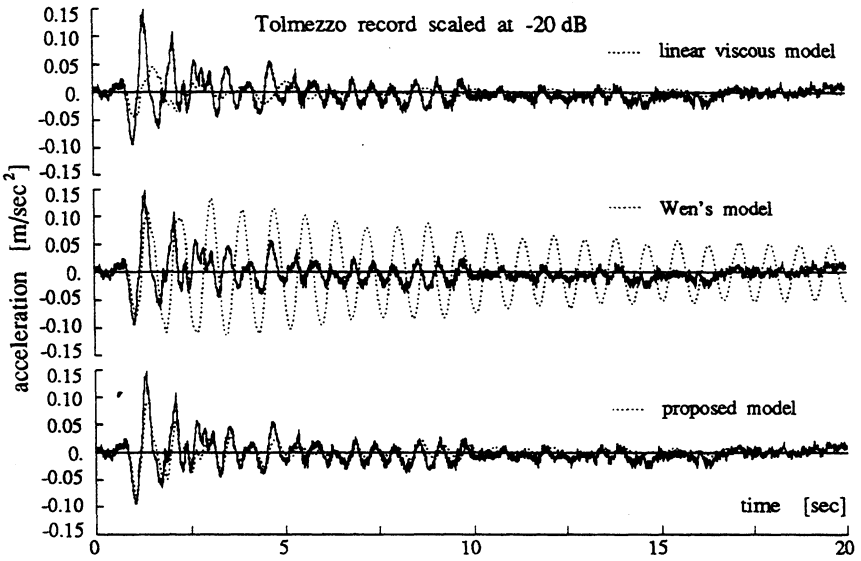


Figure 9. Comparison of the shake table response (experimental curve ——) with the simulation provided by the mathematical models - Tolmezzo record scaled at -20 dB.

All comparisons evidence that the experimental maximum values of displacements and accelerations are suitably fitted by the linear viscous model while the lesser displacements are lightly overestimated; furthermore, this model is not able to well fit the period in correspondence of the low displacements. These results can be easily explained since the equivalent viscous damping model, as shown in Figure 3, underestimates the stiffnesses at low shear deformations.

Also the Wen's model is able to well fit the experimental response only at large values of the shear deformation while the responses are strongly different as the maximum

deformation γ decreases. Therefore, it can be observed that this model, though the higher computational effort, does not seem to provide results significantly better than the ones obtained by the equivalent viscous damping model.

In conclusion, the comparison immediately evidences the limitations of the equivalent viscous damping model and, mainly, of the Wen's model. In fact, both models are able to simulate the response of first cycles but they loose this capacity after few cycles both in terms of displacement and acceleration. Furthermore, in any case, both models, being calibrated on the maximum values of the shear deformation, are not able at all to accomplish the response in the range of small deformations.

Application of the proposed model

The capability of the proposed model to reproduce the dynamic response of the high damping rubber bearings for a wide range of shear deformations has been verified by comparing the analytical response with the same experimental time histories previously used for analysing the adequacy of the equivalent viscous damping model and of the Wen's model.

As underlined before, the proposed procedure stems from the experimental values of the secant stiffness k_s and the equivalent damping ξ_{eq} at different shear deformations γ_c. These values are commonly provided by characterisation tests carried out on isolation devices. It is evident that data from shake table tests are not usually available to the designers since they require costly experimental procedures; the experimental values from sinusoidal tests, instead, are always available since codes require a preliminary characterisation of the devices. For this reason, the application of the proposed model to simulate the response of the shaking table response of the scaled r/c buildings, for which data both from sinusoidal tests and from shaking table on the bearings were available, were carried out by using only the results from the sinusoidal tests, that is the values plotted in Figure 3.

The application of the procedure requires the interpolation curves of the experimental values of k_s and of ξ_{eq}, as the ones plotted in Figures 3a and 3b, to compute the ζ and η_2 coefficients; in fact, the introduction of the values of such parameters into the Equation (16) and, then, into the Equation (8) allows to compute the response of the devices. Values of parameters ζ and η_2, relative to the numerical simulations which are shown in this paper, are reported in (De Luca et Al. 1993, 1994).

The comparison of the shaking table responses with the ones obtained by the proposed model is once again shown in the Figures 4 through 9, both in terms of displacement and acceleration. Verification of the model has been carried out by means of a modified version of 3D-BASIS computer program in which the proposed procedure has been implemented. Therefore, in the verification of the model against the shake table tests on the scaled r/c building it would be possible to analyse both the response of the devices and of the superstructure: however, only the comparison at the bearing level was performed since the comparison among the displacements of the upper stories was not satisfactory because the scale model registered significant yielding. These inelastic deformations in the elevation members are not accounted for in the 3D-BASIS modified computer program since it

presently assumes a linear elastic behaviour for the superstructure, as in the original version of the computer code.

Figures 4 through 9 evidence a satisfactory agreement between simulation and experimental data: stiffness and damping properties are matched since the response is rather in phase and the magnitude of the signals provided by the proposed model is consistent with the experimental values for all amplitudes of deformations. However, slight improvement of the model can still be envisaged in order to accomplish some discrepancies existing in the maximum values of the response under the Tolmezzo record scaled at -20db. In fact, in this case the error reaches about 20%, as it is shown in Figure 10 where the scatter S_{max}:

$$S_{max} = \frac{d^s_{max} - d^e_{max}}{d^e_{max}} \tag{21}$$

between the maximum experimental and numerical displacements, d^e_{max} and d^s_{max} respectively, is reported. However, it is worthy to note that this result is relevant to a very low values of the shear deformations (equal to about 5%) while at larger deformations values of S_{max} are rather low and, in any case, lower than the ones computed for the response obtained by the other models.

Adequacy of numerical simulation in fitting the experimental results was also measured by computing the relative standard errors S_E between experimental and numerical values:

$$S_E = \frac{Q}{M} \tag{22}$$

where the standard error Q is given by:

$$Q = \left[\frac{\sum_{i=1}^{n} (e_i - s_i)^2}{n} \right]^{1/2} \tag{23}$$

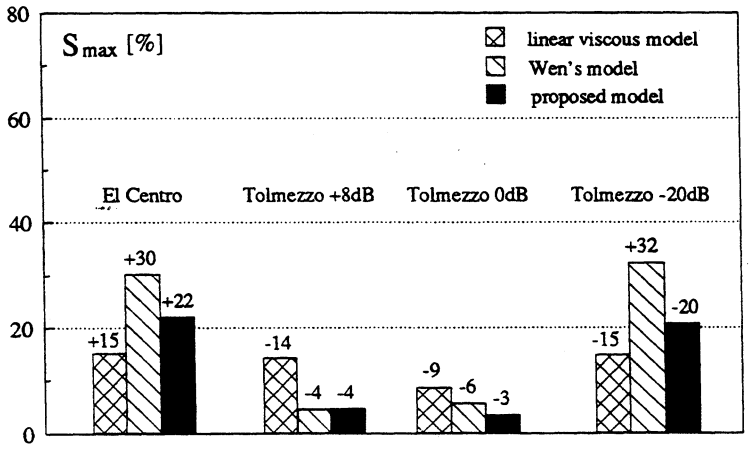


Figure 10. Scatter S_{max} between the maximum experimental and numerical displacements

and the average value M is equal to:

$$M = \frac{\sum_{i=1}^{n} |e_i|}{n} \tag{24}$$

In Equations (23) and (24), e_i and s_i are the experimental and the numerical value of the displacements or of the accelerations, while n is the total number of points.

Values of errors S_E are plotted in Figure 11 which confirms that the equivalent viscous damping model and the Wen's model are not able to properly reproduce a signal different from what expected, since they are calibrated on a settled value of deformation; the proposed model, being calibrated for all values of γ, can instead provide a suitable response even at very small shear deformation.

Therefore, examination of the numerical responses evidences that, by adopting the proposed model, also the results achieved using data from simple characterisation tests allow to obtain very satisfactory responses at any shear deformation and for all the dynamic excitations. Then, though by means of a hysteretic model, and then in lack of purely viscous forces, it seems to be possible to well simulate the response of the bearings also at very low values of the deformations where usually most of the existing models show a drawback. In fact, the comparison among the responses obtained from the models used in this paper has shown a evident amelioration in the response computed by the proposed procedure, even at deformations which are different from the ones used to calibrate the existing models.

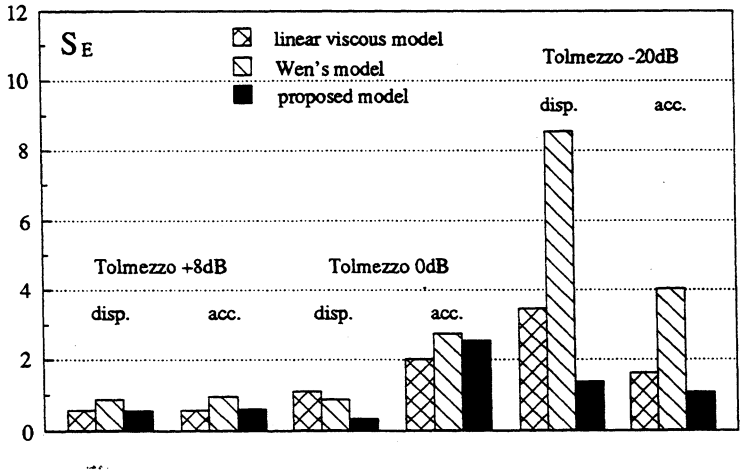


Figure 11. Relative standard error S_E between experimental and numerical values

In conclusion, it has to be noted that the computational effort which needs to adopt the proposed procedure is not larger than the one needed to use other hysteretic models: in fact, it requires only to have and to analyse some experimental data at several shear deformations from tests which, nevertheless, are usually performed. However, the tests have to be conducted for a range of shear deformations which includes the expected ones.

Conclusions

In this paper the capacity of the equivalent viscous damping model and of the hysteretic model proposed by Bouc and modified by Wen in simulating the seismic response of high damping rubber bearings has been initially analysed. The study has been carried out by comparing the analytical response provided by the two models with some experimental data from shake table tests of a scaled base isolated r.c. building and from some mock-up tests.

Being both the equivalent viscous and the Wen's model calibrated on a single value of the shear deformation, which usually corresponds to the largest strain, it has been confirmed that this limitation results in an incapacity of the linear viscous model in fitting the effective stiffness and in an incapacity of the Wen's model in fitting the actual equivalent damping at all amplitude of shear deformation.

Based on the results of the comparison between the experimental data and the numerical simulation provided by the above two models, the capacity of the equivalent viscous model in matching the experimental data better than the hysteretic model has been shown. However, such capacity is satisfactory mainly when the maximum shear deformation attained during the time history is close to the one adopted to calibrate the model.

Therefore, the need of developing models able to simulate the response of elastomeric devices characterised by loops highly variable with the extent of shear deformation deriving from earthquake-type motion has been clearly evidenced. Based on this remark, a new hysteretic model, which is an extension of the Wen's model, has been presented. The adequacy of simulation provided by the new model has been again analysed by performing a comparison with the experimental data and the comparison has evidenced the capacity of the model in overcoming the limitations present in the models existing to date. Furthermore, the implementation of this model within the 3D-BASIS computer program has allowed to show its efficiency in accomplishing the requirement of simplicity which is needed when a complete modeling of structures is required.

Acknowledgements

This research has been partially supported by Ministry of Education and Scientific Research (MURST) and by Italian National Council of Research (C.N.R.).

The authors would like to thank Prof. J.M.Kelly (University of California at Berkeley) for having provided the experimental results on devices and the shake table tests data.

The contribution of ing. A.Martelli (ENEA), who has provided the mock-up test data, and Prof. A.M. Reinhorn (University of New York at Buffalo), who has provided the original version of 3D-BASIS computer program, modified in this paper, is acknowledged.

References

Aiken I.D., Kelly J.M., Clark P.W., Tamura K., Kikuchi M and Itoh T., (1992), *Experimental Studies of the Mechanical Characteristics of Three Types of Seismic Isolation*

Bearings, Tenth World Conference on Earthquake Engineering, Madrid, pp. 2281-2286.

Aiken I.D., Clark P.W. and Kelly J.M., (1993), *Design - and Ultimate - Level Earthquake Tests of a 1/2.5-scale Base-Isolated Reinforced-Concrete Building*, Seminar on Seismic Isolation, Passive Energy Dissipation, and Active Control, ATC 17-1, 1, San Francisco, California, pp. 281-292.

Bouc R., (1971), Modele Mathematique d'Hysteresis, Acustica, 24 (1), pp. 16-25.

Clough R.W. and Penzien J. - Dynamics of structures, Secon edition, McGraw-Hill Inc., 1993

De Luca A., Faella G., Pellegrino C., Ramasco R. and Siano F., (1993), *Un Modello per la Simulazione di Dispositivi Elastomerici di Isolamento Sismico*, 6° Convegno Nazionale "L'Ingegneria Sismica in Italia", Perugia, pp. 13-15, (in italian).

De Luca A., Faella G., Pellegrino C., Ramasco R. and Siano F.,(1994), *A refined model for simulating the behaviour of base isolation devices*, Fifth U.S. National Conference on Earthquake Engineering, Chicago.

Kelly J.M., (1991), *Dynamic and Failure Characteristics of Bridgestone Bearings*, Report No. UCB/EERC-91/04, Earthquake Engineering Research Center, University of California, Berkeley.

Nagarajaiah S., Reinhorn A.M. and Constantinou M.C., (1989), *Nonlinear Dynamic Analysis of Three-dimensional Base Isolated Structures (3D-BASIS)*, Technical Report NCEER-89-0019, National Center for Earthquake Engineering Research, State University of New York at Buffalo.

Nagarajaiah S., Reinhorn A.M. and Constantinou M.C., (1991), *3D-BASIS - Nonlinear Dynamic Analysis of Three-dimensional Base Isolated Structures: part II*, Technical Report NCEER-91-0005, National Center for Earthquake Engineering Research, State University of New York at Buffalo.

Serino G., Martelli A. and Bonacina G., (1993), *Analysis of Free and Forced Excitation Tests of a 394 kN Isolated Structure Mock-up*, 1993 ASME Pressure Vessel and Piping Conference, Denver, Colorado, pp. 25-29.

Serino G., Bonacina G. and Spadoni B., (1992), *Implications of shaking table tests in the analysis and design of base isolated structures*, 10th WCEE, Madrid, pp. 2405-2410.

Wen Y.K., (1976), *Method For Random Vibration of Hysteretic System*, J. of the Engineering Mechanics Division, New York, 102 (EM2), pp. 249-263.

MODELING AND CHARACTERIZATION OF SEISMIC ISOLATION BEARINGS

Gregory L. Fenves, Wei–Hsi Huang, Andrew S. Whittaker, Peter W. Clark, Stephen A. Mahin

Pacific Earthquake Engineering Research Center
University of California, Berkeley
Richmond, California 94804

ABSTRACT

A coordinated experimental and analytical research program sponsored by the California Department of Transportation is underway to improve knowledge about seismic isolation and supplemental damping for highway bridges. The first phase of the study is to characterize the bi–directional response of elastomeric and sliding isolation bearings for static and dynamic excitation in a thorough static and dynamic testing program. Analytical models based on classical plasticity and smoothed plasticity (Bouc–Wen) are used for representing bearing behavior. Static bi–directional load histories and earthquake response studies show the effect of bi–directional coupling in these models compared with independent uni–directional models.

INTRODUCTION

Isolation bearings and supplemental damping devices can be effective techniques for controlling the forces and deformations transferred from a bridge superstructure to the substructure and footings. Hysteretic energy dissipation in the isolation bearings and dampers, with careful design, can limit bearing deformations and overall displacements to acceptable levels. The use of protective systems in new bridge construction, however, has been hampered by questions about system behavior, long–term durability, and clear definition of performance. Concerning system behavior, there is a lack of information about the following questions:

- Can isolation bearing and supplemental dampers be used close to faults which can generate ground motions with large velocity pulses?
- How can isolation devices be used effectively for bridges with flexible piers?
- Can limited yielding of piers be tolerated?
- What are the trade–offs between hysteretic energy dissipation in isolation bearings versus viscous or hysteretic energy dissipation in supplemental dampers?
- What is the bi–directional behavior of bearings and how does it affect bridge response?

To address these issues, the California Department of Transportation (Caltrans) is sponsoring a research project at the University of California, Berkeley, on seismic protective systems for bridges. The project consists of coordinated experimental and analytical studies that address the fundamental issues of how isolation bearings and supplemental damping devices can be used to achieve specified bridge performance. The current project follows previous experimental and analytical studies of protective systems for bridges by Kelly et al. (1986), Constantinou et al. (1991, 1994), and Tsopelas et al. (1996). Extending these important studies, the current project examines bi–directional behavior of isolated bridges, a range of isolation and damping devices, the response to near–fault ground motion, and the effect of pier yielding.

The first phase of the project is to characterize the bi–directional behavior of elastomeric and sliding bearings. Limited experimental studies have been performed in Japan, such as reported by Nagarajaiah et al. (1989) for high damping rubber bearings. To address this lack of information, the testing of isolation bearings under bi–directional static and dynamic excitation is now underway. This paper focuses on the models for bi–directional behavior, the experimental test program, and selected pre–test analyses.

BI–DIRECTIONAL MODELS OF ISOLATION BEARINGS

Elastomeric bearings have highly nonlinear behavior that is a function of the shear strain, vertical stress, number and order of deformation cycles, and temperature. An accurate and detailed understanding of all these effects under multi–directional loading is an ultimate goal. At this point simpler models with properties selected to account for the vertical stress and shear strain levels are addressed in this study. The approach focuses on macro–models of bearing behavior, as compared to constitutive models at the micro– or meso–scale or phenomenological models. Experimentally verified macro–models are readily incorporated into standard dynamic analysis procedures and can be effectively utilized in design. Although much progress has been made in understanding the constitutive behavior of elastomers, such models are difficult to use for design applications. Phenomenological models, such as by Kikuchi and Aiken (1997), are accurate for uni–directional behavior, but they have many parameters and are difficult to generalize for bi–directional behavior.

Two approaches for modeling the bi–directional behavior of bearings are investigated in this paper. The first approach utilizes classical, rate–independent plasticity. The second approach utilizes a smoothed idealization of plasticity, commonly referred to as the Bouc–Wen model. The concept of "yield" in an elastomeric or sliding bearing is, of course, a simplifying idealization. Both approaches are based on assumption of isotropic behavior and neglect torsion of the bearing. The restoring force in a bearing is assumed to depend only on the translational (shear) deformation of the bearing. The restoring force, $\mathbf{F} = \left[F_1 \; F_2\right]^T$, for the bearing is a function of deformation $\mathbf{U} = \left[U_1 \; U_2\right]^T$, in which F_i, U_i are the restoring force and deformation in orthogonal horizontal direction, i=1,2. Two methods for determining the bi–directional relationship between **F** and **U** are summarized below.

Rate–independent Plasticity

The first approach for representing behavior of bearings is to utilize rate–independent plasticity (Lubliner, 1990). The restoring force has an elastic–hardening component and a hysteretic component as follows:

$$\mathbf{F} = \alpha K_0 \mathbf{U} + \mathbf{F}_p \tag{1}$$

In equation 1 $\mathbf{F}_p$ is the hysteretic force, the initial stiffness of the bearing is K_0, and the post–yield hardening stiffness is αK_0. A circular yield function is postulated,

$$F(\mathbf{F}_p) = \|\mathbf{F}_p\| - (1-\alpha)F_y \tag{2}$$

where F_y is the uni–directional yield force. The plastic potential is selected to be the yield function, which is an associated flow rule for the plastic displacement rate:

$$\dot{\mathbf{U}}_p = \dot{\gamma} \cdot \frac{\partial F}{\partial \mathbf{F}_p} \tag{3}$$

in which γ is the plastic multiplier. During plastic flow, $F = 0$, the plastic displacement rate is given by equation 3, and the consistency condition must hold. Using standard procedures, the plastic displacement, plastic force $\mathbf{F}_p$, and tangent matrices are computed in incremental form.

Bouc–Wen Model

The Bouc–Wen model an endochronic model (Valanis, 1971), which utilizes an internal time. This class of models are used in stochastic analysis because evolution of the model is governed by a differential equation and it is not necessary to keep track of the yield state. The model represents a smooth transition between elastic and yield states. Wen (1980) applied to the model to uni–directional hysteretic behavior and Park et al. (1986) generalized it to bi–directional behavior. The bi–directional model is widely used, such as in 3D–BASIS (Nagarajaiah et al. 1991). The bi–directional form of the model considered here was generalized by Casciati (1989). Plasticity using a yield function (such as equation 2) is replaced by smoothed functions for the transition between no–yield and yield states. With this approach, the plastic force in equation 1 is defined as $\mathbf{F}_p = (1-\alpha)K_0(\mathbf{Z}U_y)$, where $\mathbf{Z} = \begin{bmatrix} Z_1 & Z_2 \end{bmatrix}^T$ is a dimensionless variable that governs the plastic behavior and $U_y = F_y/K_0$. The evolution equation is then written as (Casciati, 1989):

$$\dot{\mathbf{Z}}U_y = A\dot{\mathbf{U}} - (\gamma + \beta \operatorname{sgn}(\mathbf{Z}^T\dot{\mathbf{U}}))\|\mathbf{Z}\|^{\eta-2}(\mathbf{Z}\mathbf{Z}^T)\dot{\mathbf{U}} \tag{4}$$

The parameters, γ, β, and η govern the evolution of the plastic variable, $\mathbf{Z}$. For $A > 0$ and $\beta + \gamma > 0$, it can be shown that,

$$\max\|\mathbf{Z}\| = \left(\frac{A}{\beta+\gamma}\right)^{\frac{1}{\eta}} \tag{5}$$

For A=1 and $\beta + \gamma = 1$, the model represents a circular yield surface. The parameter η governs the transition to yield. In the limit as $\eta \to \infty$, the transition between elastic and plastic states is instantaneous, as for the rate–independent, plasticity model. Integration of equation 4 provides the plastic state, and the tangent matrix in incremental form can be derived. It should be noted that equation 4 is similar to the bi–directional equations given in Park et al. (1986) and Nagarajaiah et al. (1991). However, equation 4 includes complete information in the term $\operatorname{sgn}(\mathbf{Z}^T\dot{\mathbf{U}})$ which represents the direction of loading. Although Bouc–Wen model is widely used for representing hysteretic behavior, some studies have show that the model violates plasticity conditions and exhibits

drift under unsymmetrical displacement or load cycles (Thyagarajan and Iwan, 1990). An additional discussion on this point is found in Appendix B of Spacone et al. (1992).

BI–DIRECTIONAL DISPLACEMENT CONTROLLED TESTING

Most testing of isolation bearings is uni–directional because of the complexity of loading in two directions. Earthquake response of an isolated bridget is two–dimensional, so there is an urgent need to perform bi–directional testing of bearings in order to understand the behavior and evaluate the efficacy of the models described in the previous section. The recent upgrade of UC Berkeley's earthquake simulator allows bi–directional testing of small– to moderate–scale isolation bearings. Testing of the bearings is planned for April and May 1998.

The testing program involves an isolation system subjected to specified displacement histories in two horizontal directions. Figure 1 shows the plan and elevation of the a rigid frame supported by four bearings with five–component load cells on the earthquake simulator. The rigid frame supports concrete and lead weights totalling 65 kip provide the vertical stress on the bearings. Four struts brace the frame against reaction buttresses located around the simulator platform. Figure 2 shows the testing frame supported on four bearings before placing the added weights. With the struts fixing the frame against the buttresses, the platform is moved under displacement control according to specified bi–directional horizontal displacement histories. With the struts removed the isolated frame can be tested with earthquake ground motion histories.

The choice of the displacement histories for bi–directional testing is based on a variety of factors. The displacement histories should be simple enough to illustrate bi–directional interaction effects without the random nature of an actual earthquake. The displacement–controlled orbits are shown in figure 3. Varying levels of maximum strain in the two directions ranging from 25% to 250% are used to evaluate the path–dependent behavior of the bearings. The box and hourglass orbits will be run at a very slow rate. The uni–directional and figure–8 orbits will be run over a range of velocities to assess rate effects.

SELECTION OF BEARINGS

The program involves testing and analysis of bridge systems with three generic types of bearings: high damping rubber, lead–rubber, and spherical sliding bearings (Friction Pendulum System). The high damping rubber bearings have been investigated in an extensive study of uni–directional behavior (Aiken et al., 1992). The KL301 Bridgestone bearings are 6.93 in. in diameter, 2.48 in. in height, with a total rubber thickness of 1.73 in. rubber thickness (shape factor=20). The lead–rubber bearings and FPS bearings will be used with the target specifications in table 1.

The pre–test prediction of the bi–directional behavior has been examined for the bi–directional displacement controlled tests. Previous uni–directional tests (Aiken et al., 1992) of the high damping rubber bearings were used to estimate the parameters for the mathematical model. The downhill simplex method (Nelder and Mead, 1965) is an estimation procedure that only requires function evaluations and no gradient information. Given a displacement history, the procedure minimizes the square of the difference in force between the model and the test over one or more cycles. For the 100% shear strain level, the estimated properties are F_y=1.52 kip (C_y=0.093),

U_y=0.115 in., α=0.065, which gives a second slope of 0.86 kip/in. The period of the frame based on the second slope is 1.39 sec, and the secant period is 1.17 sec at a displacement of 4 in. For the Bouc–Wen model the parameters are: A=1, γ=β=0.5, and η=2.

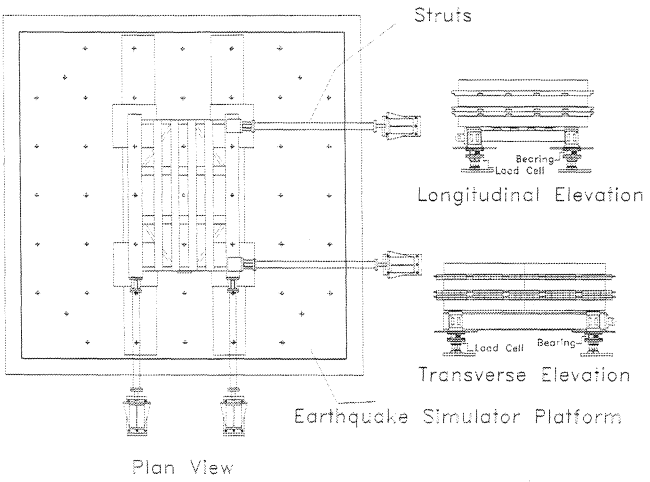


Figure 1 – Bi–directional bearing test apparatus on earthquake simulator

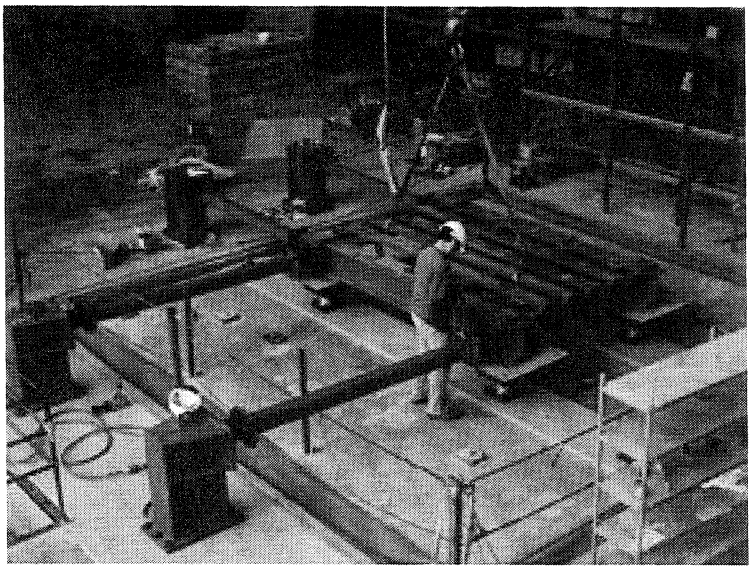


Figure 2 – Bi–directional testing apparatus on shaking table without added weight

The model response for the box orbit at 100% shear strain is shown in figure 4 and for the figure–8 at 100% strain in figure 5. Each figures shows the total force and plastic force trace and the hysteretic loops in the two directions (X and Y) computed with the plasticity and Bouc–Wen models.

The solid line gives the computed response for the bi–directional formulation. For comparison, the dotted lines shows the response from independent uni-directional models in X and Y. In figure 4 the independent uni–directional models overpredict the maximum force in the bearing by 25% because of the square yield surface. In comparison, loading in one direction while on the bi–directional circular yield surface requires unloading in the other direction. The plasticity and Bouc–Wen models give nearly identical results for the bi–directional models.

Figure 5 shows the model response for the figure–8 orbit at 100% shear strain. The bi–directional interaction effects are important in the Y direction because it is changing more rapidly than the X direction. Similar results are shown in Nagarajaiah et al. (1991). As can be seen in the force plots, the uni–directional model overestimates the maximum force in the bearing. The uni–directional model also overestimates the hysteretic energy dissipation, particularly in the Y direction. The plasticity and Bouc–Wen models are very similar when considering bi–directional effects, and both are superior for this load pattern compared with the uncoupled models.

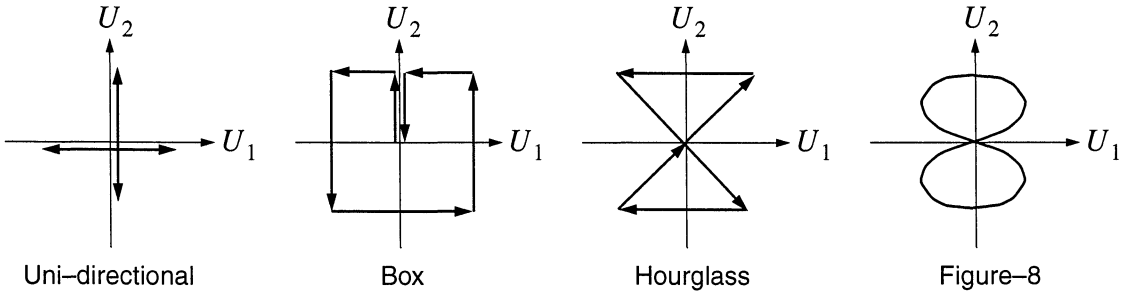


Figure 3 – Displacement controlled orbits for bi–directional testing

Table 1 – Target specifications for isolation bearings

	High Damping Rubber Bearings	Lead–Rubber Bearing	FPS Bearing
Design Vertical Load (kip)	16.25	16.25	16.25
Isolated Secant Period (sec)	0.9	0.9	1.5
Equivalent Damping Ratio	0.13	0.15	0.15
Equivalent Yield Coefficient	—	0.05	0.06
Uni–directional Displacement Capacity (in.)	5+	5+	6

EARTHQUAKE TESTING

The isolation bearing testing frame in figure 1 can be used for dynamic earthquake testing by removing the struts. The objective of the earthquake testing is to examine the bi–directional earthquake response of the isolated frame, evaluate the effects of different types of ground motions, including near–fault ground motions, and calibrate the bearing models. With an appropriate length scale factor, the testing frame represents a bridge with rigid superstructure and rigid substructure.

The challenge in selecting earthquake time histories lies in balancing the need to include motions representing different source types, soil types, intensities, and durations with the desire to limit the number of tests. The displacement and velocity limitations of the earthquake simulator necessitate the adjustment and scaling of the structural models and ground motions to represent the prototype bridges and ground motion accurately.

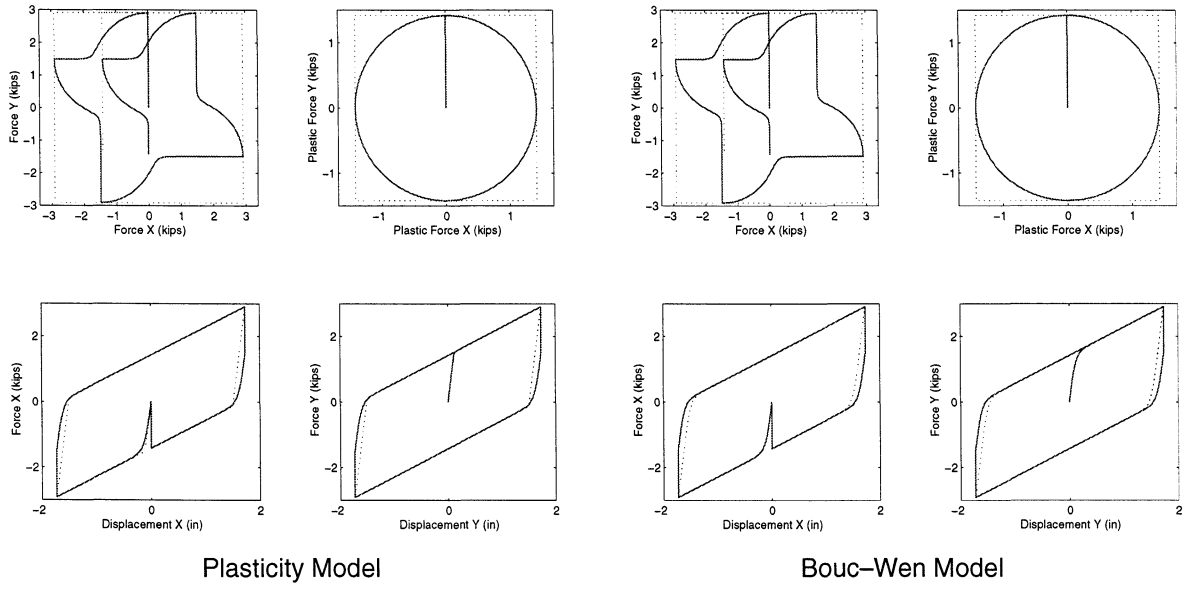


Figure 4 – Box displacement controlled history (γ=100%); solid line is bi–directional model, dotted line is uncoupled uni–directional model

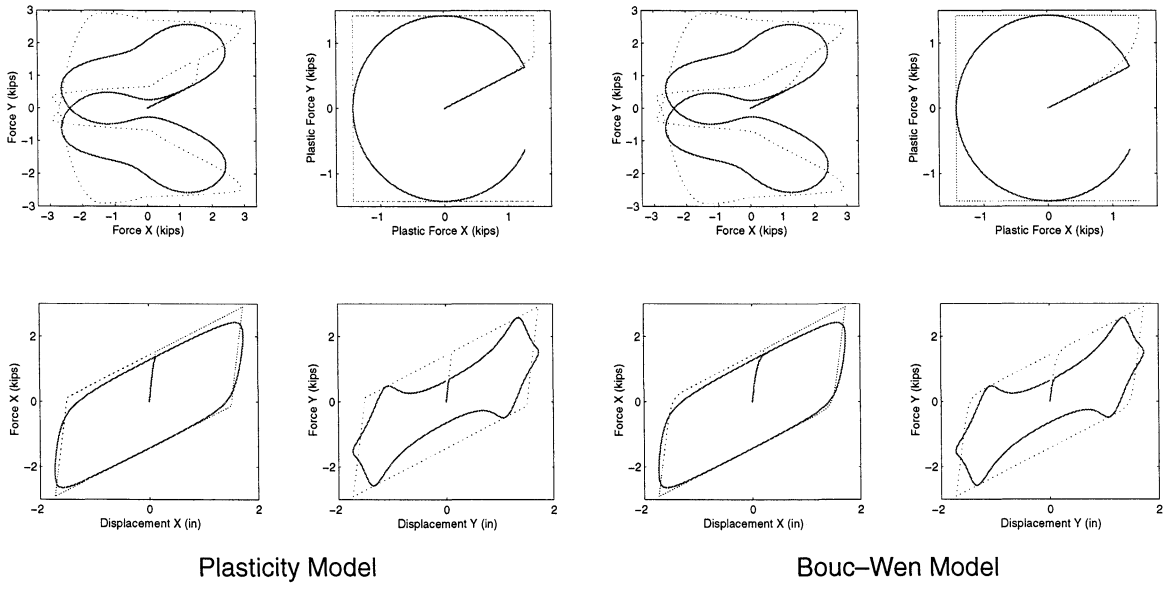


Figure 5 – Figure–8 displacement controlled history (γ=100%); solid line is bi–directional model, dotted line is uncoupled uni–directional model

Earthquake Ground Motions

In support of Phase 2 of the FEMA/SAC project to develop guidelines for the seismic design of steel structures, a comprehensive set of earthquake ground motion time histories has been developed by Woodward–Clyde Federal Services of Pasadena, California (SAC, 1997). The records are compatible with the national seismic hazard maps released in 1997 by the United States Geological Survey (USGS). The mean spectra of all of the records in each subset are matched to the USGS target spectra at periods of 0.3, 1, 2, and 4 seconds. Only the ground motions developed for the Los Angeles region have been evaluated for use in the current testing program. There are six sets of records:

- Los Angeles — 10% probability of exceedence in 50 years (LA01 to LA20, 10 pairs of time histories)
- Los Angeles — 2% probability of exceedence in 50 years (LA21 to LA40, 10 pairs of time histories)
- Los Angeles — 50% probability of exceedence in 50 years (LA41 to LA60, 10 pairs of time histories)
- Recorded near–fault records (NF01 to NF20, 10 pairs of time histories)
- Simulated near–fault records (NF21 to NF40, 10 pairs of time histories)
- Soft soil records (LS01A to LS20I, 90 pairs of time histories)

Records LA01 to LA60 have been amplitude and frequency scaled such that the mean 5% damped elastic spectrum for each set matches the USGS target spectrum corresponding to the associated probability of exceedence. They are intended to be representative of stiff soil sites (NEHRP site type D). The near–fault records have not been matched to any specific spectrum in terms of amplitude or in the frequency domain. The resulting scatter in the suite of records is therefore representative of the scatter anticipated in ground motions near the source of major earthquakes. Records NF01 to NF20 are from actual recorded time histories. Records NF21 to NF40 are computed from seismological source modeling. The near–fault records are oriented along the principal directions of the fault rupture. The soft soil records have been derived from the stiff soil, 10% in 50–year records by propagating them through various soil profiles. Soft soil sites 1 and 2 correspond to NEHRP site types E and F, respectively.

Selection and Processing of Ground Motions

The limitations of the earthquake simulator and the considerations for scaling the model are:

- The peak displacement of the simulator platform is 5 in. in each direction.
- The peak attainable velocity of the simulator platform is 23 in/sec in each direction.
- The longest–period isolation system considered is 3.2 seconds.
- The maximum length scale factor considered is 6.

For each record in each suite of time histories, the peak acceleration, velocity, and displacement were calculated for scale factors ranging from 1 to 6. Spectral responses were also calculated at periods of 1, 2, 3, 4, and 5 seconds. These calculations were then repeated assuming that the records were filtered with bandpass filters (0 to 5) that have a high corner and cut of 12 Hz and 15

Hz, respectively, and low cut frequencies between 0 and 0.25 Hz. A record is acceptable if the scaled velocity and displacement are within the limits of the earthquake simulator and the spectral values of the filtered record are not reduced substantially below the unfiltered version.

Based on the above criteria, and assuring that an ensemble of records reflecting a variety of source parameters, soil conditions, intensities, and durations, the records in table 2 have been selected as the ground motions for the experimental and analytical studies.

Table 2 – Earthquake records selected for testing

SAC ID	Record	M	R (km)	Amplitude Scale	Length Scale	Filter No.
LA01/LA02	Imperial Valley, 1940 El Centro	6.9	10	2.01	2–6	0
LA09/LA10	Yermo, 1992 Landers	7.3	25	2.17	2–6	3
LA13/LA14	Newhall, 1994 Northridge	6.7	6.7	1.03	3–6	0
NF09/NF10	1992 Erzincan	6.7	2	1	4–6	4
NF15/NF16	Olive View, 1994 Northridge	6.7	6.4	1	4–6	5
NF17/NF18	1995 Kobe	6.9	3.4	1	5	3
NF01/NF02	1978 Tabas	7.4	1.2	1	5	3
LA21/LA22	1995 Kobe	6.9	3.4	1.15	6–6	0
LS01C/LS02C	1940 El Centro – soft soil 1	6.9	10	2.01	4–6	0
LS01E/LS02E	1940 El Centro – soft soil 2	6.9	10	2.01	3–6	0
LS17C/LS18C	1940 El Centro – soft soil 1	6.7	6.4	0.99	6	0
LS17E/LS18E	1940 El Centro – soft soil 2	6.7	6.4	0.99	6	4

Figure 6 shows the 5% damped response spectra for the Kobe record near–fault record (NF17/NF18), Olive View record (NF15/NF16), and the record from the 1978 Tabas earthquake (NF01/NF02). The spectra in figure 6 are plotted in fault normal (FN) and fault parallel (FP) components with a length scale of 5 and a corresponding time scale of $\sqrt{5}$.

Response Predicted by Analytical Model

The response of the rigid frame using the properties of the HDR bearing for the Olive View (1994 Northridge) record is shown in figures 7 and 8. The displacement histories have a strong bias in the fault normal direction with a maximum displacement of 4 in. (γ=230%), which corresponds to a prototype bearing displacement of 20 in. The force space for the coupled model shows the circular yield surface, whereas the uncoupled model shows a square surface. The maximum force in the bearing is 4.8 kip, which corresponds to a seismic coefficient of 0.30. The coupled model shows considerable interaction effects in hysteresis loops, particularly in the FP direction. The uncoupled FP hysteresis loop is a poor representation of the bi–directional loading history. The response of the Bouc–Wen model in figure 8 is very similar to the plasticity model in figure 7. Figures 9 and 10 show the response for the Kobe and Tabas earthquakes, respectively, using the plasticity model. The response for the same cases using the Bouc–Wen model is very similar to

the plasticity model and is not shown here. The Kobe record produces strong FN bias in the response with two large displacement excursions in the FN direction. The FP force history is strongly affected by the yielding in the FN direction.

The response for the Tabas record in figure 10 has more equal FN and FP components than the other near–fault records. The displacement orbits for the uncoupled model is different in the details of the large FN excursion and FP excursion compared to the uncoupled model. The effect of bi–directional interaction is clearly seen in the FP hysteresis loop which shows a "turning around" in the FP direction near a displacement of 2 in. as the large negative FN displacement takes place. This bi–directional interaction is not represented with the uncoupled model.

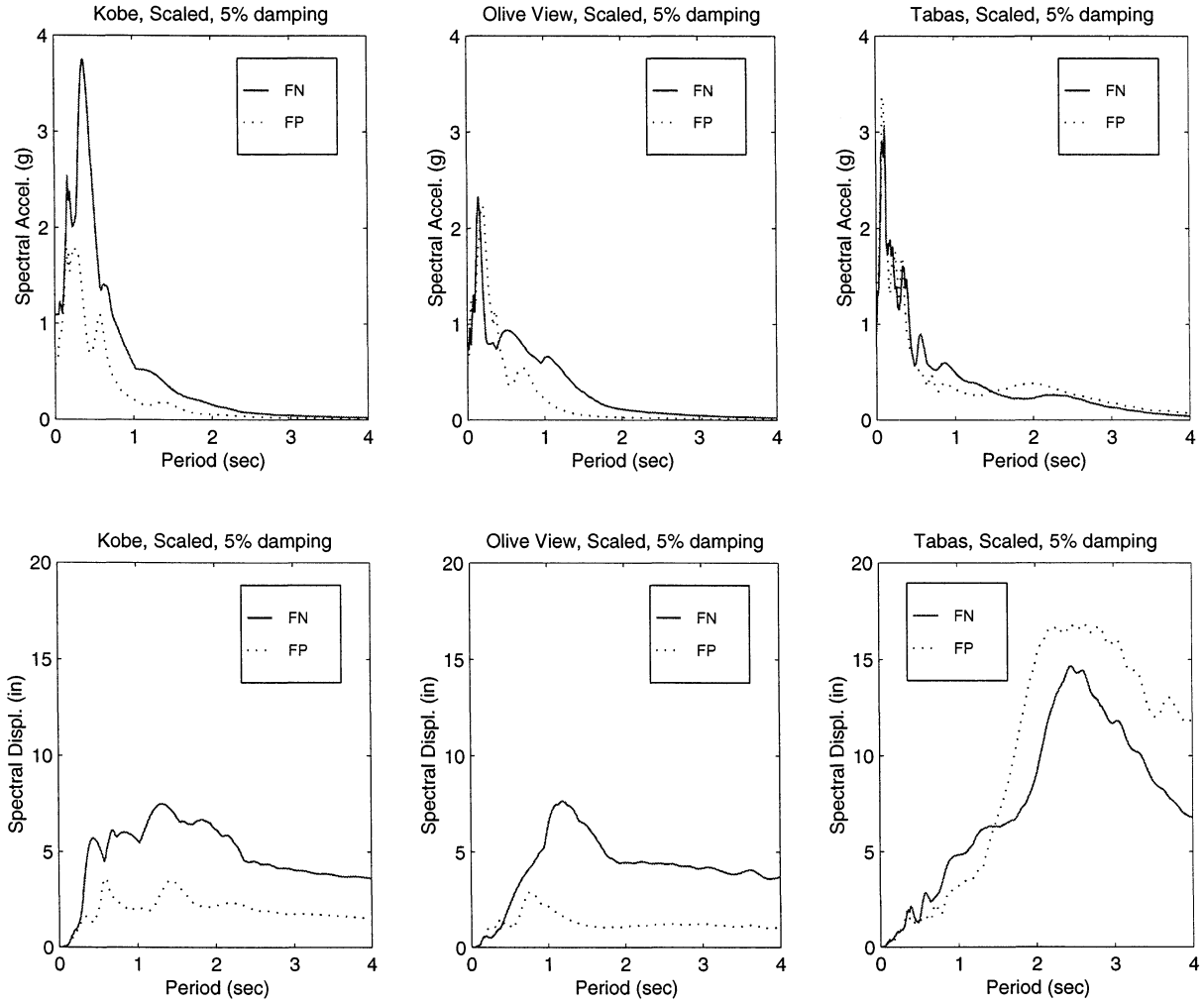


Figure 6 – Earthquake response spectra (5% damping) for three near–fault records with length scale factor of 5 (time scale=$\sqrt{5}$), in fault normal (FN) and fault parallel (FP) components.

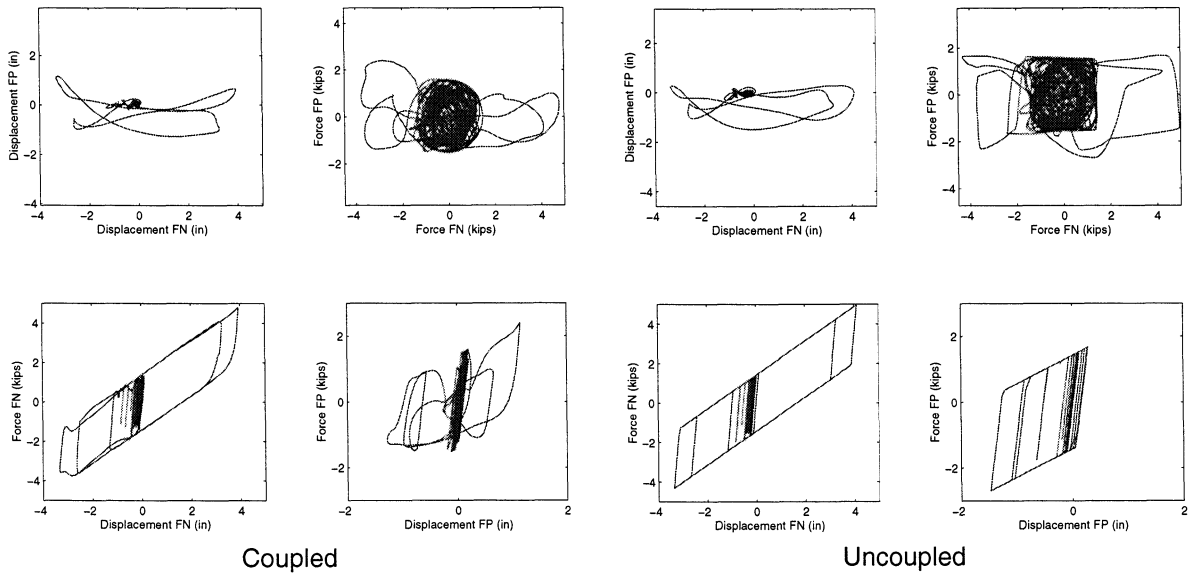


Figure 7 – HDR bearing response for Olive View record (1994 Northridge), length scale 5, plasticity model

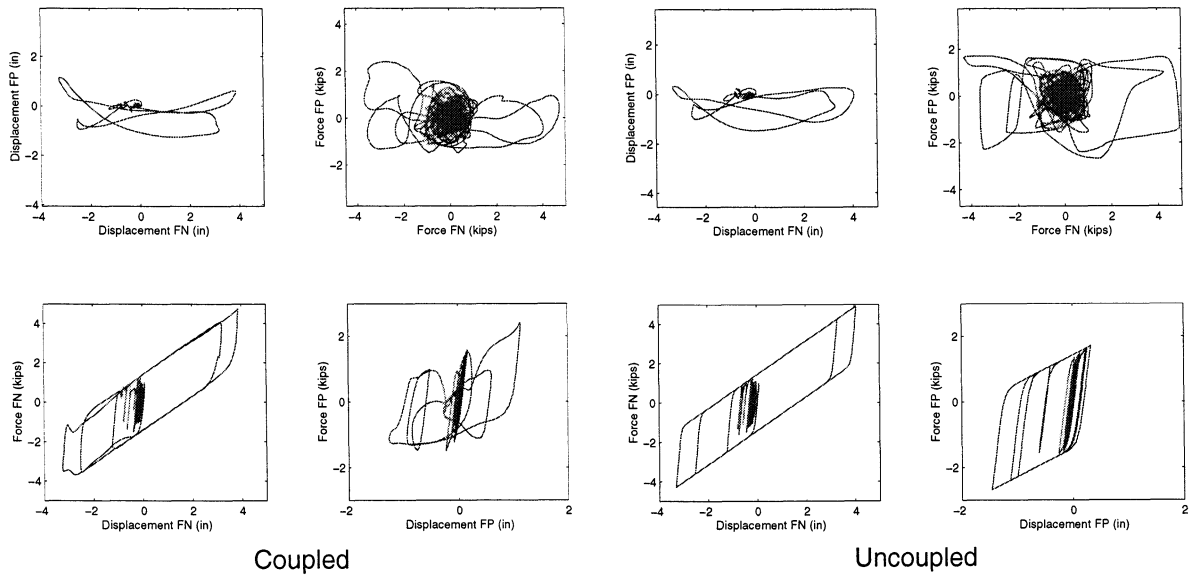


Figure 8 – HDR bearing response for Olive View record (1994 Northridge), length scale 5, Bouc–Wen model

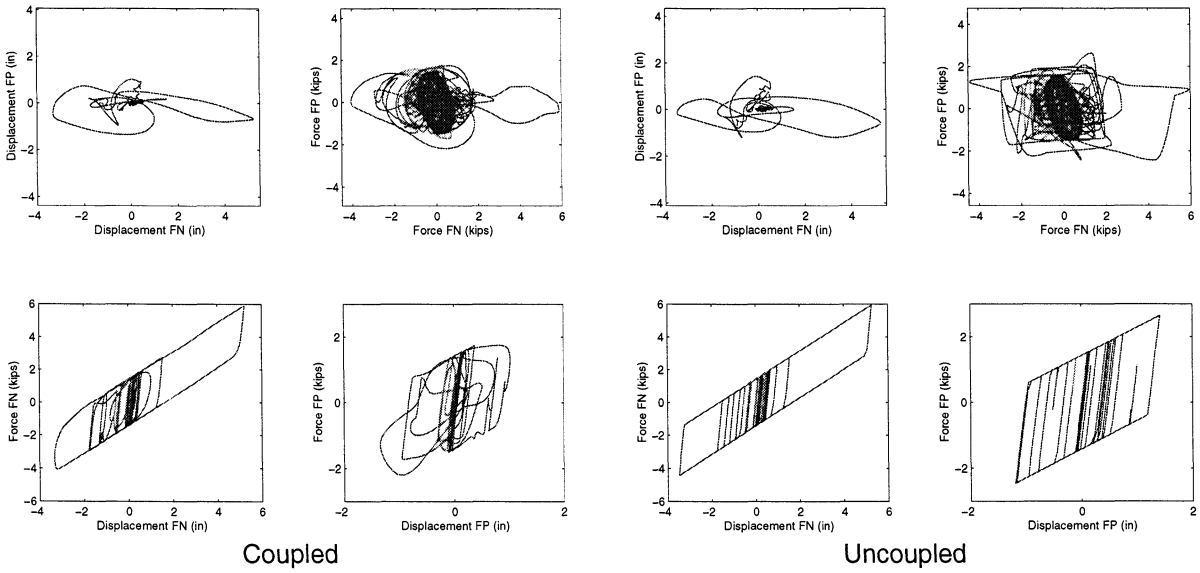


Figure 9 – HDR bearing response for 1995 Kobe near–fault record, length scale 5, plasticity model

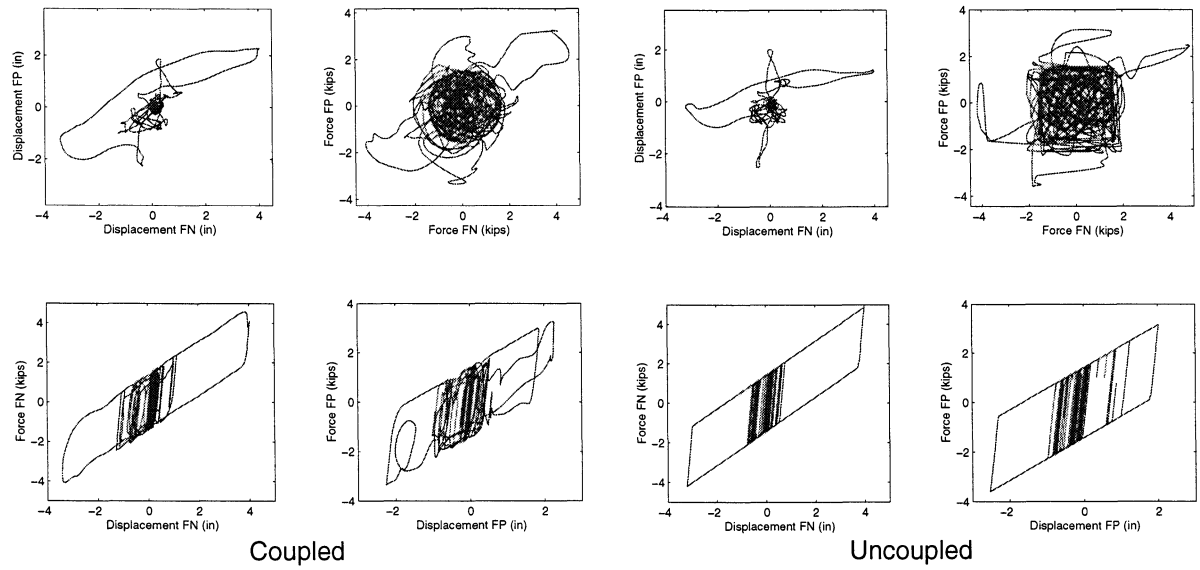


Figure 10 – HDR bearing response for 1978 Tabas near–fault record, length scale 5, plasticity model

SYSTEM RESPONSE

Another phase of the experimental program involves bi–directional testing of an isolated superstructure on flexible piers. The earthquake response of a rigid superstructure with four bearings,

each on a linear elastic pier, is examined in this section. The effective stiffness, K_{eff}, of a single pier is defined from the sum of the linearized bearing and pier flexibilities:

$$\frac{1}{K_{eff}} = \frac{1}{K_i} + \frac{1}{K_s} \tag{6}$$

where $K_i = \alpha K_0$ is the second slope stiffness of the bearing and K_s is the stiffness of the substructure. For a given K_{eff} and bearing–to–pier stiffness ratio K_i/K_s, the bearing stiffness is:

$$K_i = K_{eff}\left(1 + \frac{K_i}{K_s}\right) \tag{7}$$

The previously considered cases with the test frame and no substructure had $K_s = \infty$, $K_i = K_{eff}$ =0.86 kip/in. with a period of 1.39 sec (prototype period=3.1 sec) based on the second slope for the bearing.

Figure 11 shows the maximum response of the frame with four HDR bearings on flexible piers, subjected to the Olive View (1994 Northridge) record for length scale factor of 5. The bearings have the non–dimensional parameters considered previously (C_y=0.093, α=0.065). The figure shows the superstructure displacement in each direction, the bearing deformation in each direction, and the displacement and deformation (in any direction) for a range of periods based on the effective stiffness (equation 6) and for bearing–to–pier stiffness ratios from zero to unity. The FN response has a peak at about 1.2 sec (prototype period=2.68 sec). The maximum displacement is not just a function of period, but depends on the relative bearing and substructure stiffness. As the substructure becomes more flexible, the bearing deformation decreases and the maximum displacement increases because of reduced hysteretic energy dissipation in the bearing. For periods greater than 1.8 sec (prototype period=4.0 sec), the constant displacement portion of the spectrum (figure 6) gives a maximum displacement fairly independent of the bearing–to-pier stiffness ratio. As a result, the bearing deformation decreases as the pier becomes more flexible.

Nonlinear spectra, such as in figure 11 are being used in the design of the shaking simulator models with flexible piers. They also provide a convenient mechanism for design of isolated bridges which do not require an equivalent linearization procedure.

SUMMARY AND FUTURE WORK

The static and dynamic tests will provide valuable information about bi–directional behavior of seismic isolation bearings. Considering the models, bi–directional effects should be included in any analysis. Designs based on uncoupled inelastic springs may not accurately represent the forces transferred to the substructure and hysteretic energy dissipation. The plasticity and Bouc–Wen models produce very similar results, particularly with the complete terms for loading direction in the latter model. Extensions of the models to account for softening under cyclic load and stiffnening of the elastomeric bearings are under investigation. Development of models for sliding isolation bearings is being pursued.

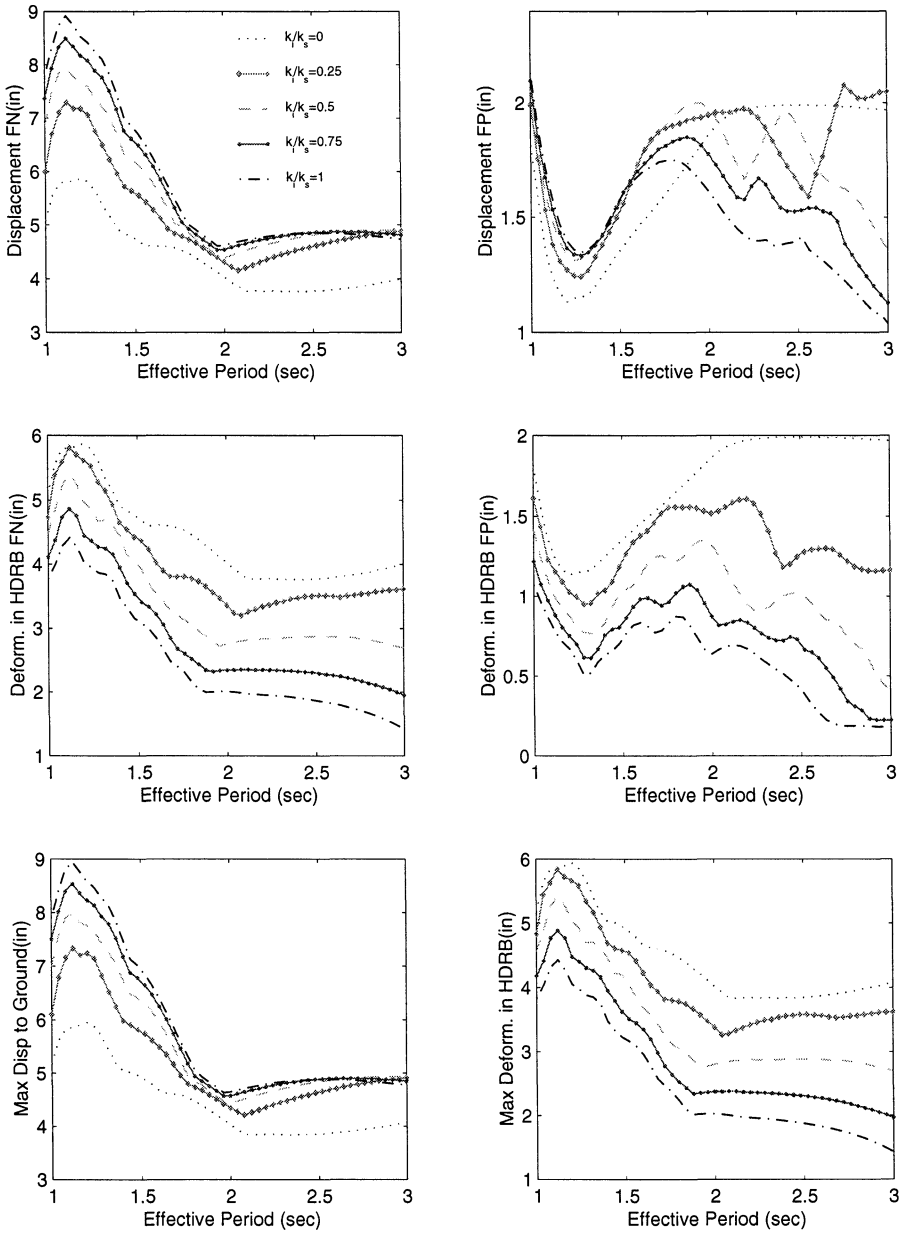


Figure 11 – Maximum responses of isolated bridge on flexible piers, Olive View record (1994 Northridge), length scale 5 (time scale=$\sqrt{5}$), plasticity model

ACKNOWLEDGEMENTS

The protective systems project is supported by the California Department of Transportation under Contract 59A169. Caltrans staff Tim Leahy, Dorie Mellon, Mohsen Sultan, Roberto Lacalle, and Li–Hong Sheng have worked closely with the project team. Dr. Amir Gilani assisted in the design and fabrication of the testing frame.

REFERENCES

Aiken, I.D., Kelly, J.M, Clark, P.W., Tamura, K., Kikuchi, M., and Itoh, T. (1992). "Experimental studies of the mechanical characteristics of three types of seismic isolation bearings," *Proceedings*, Tenth World Conference on Earthquake Engineering, Vol. 4, Madrid, pp. 2281-2286.

Casciati, F. (1989). "Stochastic dynamics of hysteretic media," *Structural Safety*, Vol. 6, pp. 259-269.

Constantinou, M.C., Kartoum, A., Reinhorn, A.M., and Bradford, P. (1991). "Experimental and theoretical study of a sliding isolation system for bridges," *Report No. NCEER-91-0027*, National Center for Earthquake Engineering Research, State University of New York at Buffalo.

Constantinou, M.C., Tsopelas, P., and Okamoto, S. (1994). "Experimental study of a class of bridge seismic isolation systems," *Proceedings*, Fifth U.S. National Conference on Earthquake Engineering, EERI, Vol. I, Chicago, pp. 901-910.

Kelly, J.M., Buckle, I.G., and Tsai, H.-C. (1986). "Earthquake simulator testing of a base-isolated bridge deck," *Report No. UCB/EERC-85/09*, Earthquake Engineering Research Center, University of California, Berkeley.

Kikuchi, M. and Aiken, I.D. (1997). "An analytical hysteresis model for elastomeric seismic isolation bearings," *Earthquake Engineering and Structural Dynamics*, Vol. 26, pp. 215-231.

Lubliner, J. (1990). *Plasticity*, Macmillan, New York.

Nagarajaiah, S., Reinhorn, A.M., Constantinou, M.C. (1989). "Nonlinear dynamic analysis of 3–D base isolated structures (3D-BASIS)," *Report No. NCEER-89-0019*, National Center for Earthquake Engineering Research, State University of New York at Buffalo.

Nagarajaiah, S., Reinhorn, A.M., Constantinou, M.C. (1991). "Nonlinear dynamic analysis of 3–D base isolated structures," *Journal of Structural Engineering*, ASCE, Vol. 117, pp. 2035–2054.

Nelder, J.A., and Mead, R. (1965). "Downhill simplex method on multi-dimensional minimization," *Computer Journal*, Vol. 7, p. 308.

Park, Y.J., Wen, Y.K., and Ang, A.H.–S. (1986). "Random vibration of hysteretic systems under bi-directional ground motions," *Earthquake Engineering and Structural Dynamics*, Vol. 14, pp. 543-557.

SAC (1997). "Suites of earthquake ground motion for analysis of steel moment frame structures," Report No. SAC/BD-97/03, Woodward–Clyde Federal Services, SAC Steel Project.

Spacone, E., Ciampi, V., and Filippou, F.C. (1992). "A beam element for seismic damage analysis," *Report No. UCB/EERC-92/07*, Earthquake Engineering Research Center, University of California, Berkeley.

Thyagarajan, R.S., and Iwan, W.D. (1990). "Performance characteristics of a widely used hysteretic model in structural dynamics," *Proceedings*, Fourth U.S. National Conference on Earthquake Engineering, EERI, Vol. 2, Palm Springs, pp. 177-186.

Tsopelas, P. et al. (1996). "Experimental study of FPS system in bridge seismic isolation," *Earthquake Engineering and Structural Dynamics*, Vol. 25, pp. 65-78.

Valanis, K.C. (1971). "A theory of viscoplasticity without a yield surface, Part I: General theory," *Archives of Mechanics*, Vol. 23, pp. 517-533.

Wen, Y.-K. (1976). "Method for random vibration of hysteretic systems," *Journal of the Engineering Mechanics Division*, ASCE, Vol. 102, pp. 249-263.

High Damping Elastomeric Bearings (HDEB) : Experimental Tests and Preliminary Results

Franco Braga

Dip.to di Strutture, Geotecnica, Geologia applicata all'Ingegneria (DiSGG),
Ateneo della Basilicata, Potenza, Italy

Abstract

In this paper an outline of a huge test program carried out at the Laboratory of Testing Materials and Structures of the DiSGG of the University of Basilicata, at Potenza, is given. About 500 high damping elastomeric bearings (**HDEB**) for seismic isolation were tested, and the mechanical and hysteretical characteristics of both new and artificially aged bearings were evaluated.

Three different groups (A, B, C) of devices were tested, each group being relevant to a different compound based on a different elastomer (olefinic, dienic and nitrilic base). For each group of devices, 24 different specimen types were tested, whose differences are relevant to dimensions, shape (circular or square), primary and secondary shape factor.

These characteristics do not change from one group to another, so that immediate comparisons among the different compounds can be made. In this paper the peculiar characteristics of the three compounds studied are briefly described, comparing them with the corresponding characteristics of the natural rubber.

Then, the geometric characteristics of all the bearings are illustrated (dimensions, shape, thickness and number of elastomeric layers, thickness of steel shims, primary and secondary shape factor).

Finally, the types of test performed on the specimens as well as the test equipment and set up are described. Particular attention is devoted to the accelerated aging procedures, used to evaluate the durability of compounds and devices.

The preliminary results obtained during the aging tests are briefly exposed and discussed.

Characteristics of the Devices

The experimental program herein described was designed and carried out for the **COSMES** Consortium, under the scientific supervision of professors Giangreco and De Luca (University of Naples "Federico II"). It is part of the wider research program named "Products and technologies for the reduction of seismic effects on constructions", which was financed by the Italian **M**inistry of the **U**niversity and of the **S**cientific and **T**echnological **R**esearch (**MURST**). Its main objective is the setting up and validation of new base isolation devices for the seismic protection of bridges and buildings.

The mechanical and hysteretic characteristics of new and artificially aged devices under shear and compression actions, both statically and dynamically applied, were evaluated in the tests. All the tests were carried out at the Laboratory of Testing Materials and Structures of the Department of Structures, Geotechnics and Geology (DiSGG) of the University of Basilicata, at Potenza.

HDEB devices, i.e. devices realized with artificial elastomer (synthetic rubber), have been examined, instead of the more usual HDRB, i.e. devices made of natural rubber. Using artificial elastomers is particularly interesting. While natural rubber has a set of mechanical characteristics pre-defined and substantially not modifiable, once the Shore hardness has been fixed, in the artificial elastomers some characteristics, e.g. the ones which are more significant for the particular use, can be upgraded, thus obtaining the required performances. Obviously other characteristics, which are less important in the specific application, result to be in some extent degraded.

The resistance to environmental actions, the durability and the energy dissipation properties were considered the most significant characteristics in the present program. In fact, the three produced elastomers (respectively with oleifinic, dienic, and nitrilic base) achieved better performances, as regards the above reported characteristics, than natural rubber, even if other characteristics, as tensile and tear strengths, were degraded.

In particular:

- the elastomer of oleifinic base (Terpolymer Ethylene Propylene Diene **EPDM**) is characterized by a greater resistance to the aggressive environmental actions and to the aging;
- the elastomer of dienic base (**Polybutadiene**) is characterized by a very low vitreous transition temperature, so that it is well suited in particularly severe environmental conditions;
- the elastomer of nitrilic base (**Nitrilic Rubber**) is characterized by greater dissipative capacities while having a low mechanical resistance.

Adopting the three different elastomers as the basic components of three different compounds, the following three groups (A, B, C) of seismic isolation devices, meant for three different uses, have been realized:

- **Group A**, suitable for aggressive environment and having high durability;
- **Group B**, suitable for low temperature environments;
- **Group C**, suitable for soft soil foundations, having high energy dissipating capacity.

Characteristics of the basic components

The peculiar characteristics of the materials used and the relevant standards are reported in Tab.1. To enable some comparisons, the characteristics of a typical natural rubber compound, used for the production of **HDRB**, is also reported (indicated by **Rubber**).

Moreover, the characteristics of the steels used for the end plates and for the internal shims (with the exception of the B Group specimens n° 3bis and 12bis, whose internal shims are made of composite material) are reported. The above data have been provided by the Elastomers Division of EniChem, that designed and produced the elastomers and the compounds, and by the Antivibration Systems Division of Pirelli, that realized all the devices.

Examining closely the characteristics of the different compounds is beyond the purpose of the present paper. However a summary examination of the data in Tab. 1 highlights some indubitable advantages in using a compound based on artificial elastomer, and then the interest of this research.

For instance, if a reduction of the tensile and tear strengths can be accepted, as they are beyond the usual demands to seismic devices, then a significant increase in durability and a significant decrease of the shear modulus, while increasing shear strain, can be obtained (see Group A for shear strain = 200%).

Characteristics	Group A EPDM	Group B Polybut.	Group C Nitrilic	Rubber	Adopted Standards
Vitreous transition temperature	-54 °C	-100°C	-10°C	-70°C	DSC scanning 10°C/m
Shore Hardness A	63	62	47	65	ASTM D 2240
Tensile strength	16.6 MPa	16.2 MPa	13.6 MPa	21.1 MPa	ASTM D 412
Elongation at break (EB)	620%	580%	760%	550%	ASTM D 412 DIE C
Elastic yield	33%	32%	12%	——	DIN 53512 A
Compression set	18.2%	28%	38%	28.6%	ASTM D 575 A
Tear resistance	23.7 N/mm	21.2 N/mm	14.6 N/mm	37.4 N/mm	DIN 53507
Curing time	32 min.	9 min.	15 min.	——	ASTM D 2084 T90(160°C)
Thermo-oxidative ageing resistance	Hardness var.: +4	Hardness var.: +2	Hardness var.: +6	Hardness var.: +2	ASTM D 573
Aging resistance	1440 hours	1344 hours	1000 hours	500 hours	ASTM D 518 20% All, 40°C, 25pphm O_3
Thermal life at 30°C (residual EB = 100%)	51 years	35 years	63 years	39 years	ISO/TC 45 N 5846 (Arrhenius Plot)
Elastomer-Steel bond Elast.-Composite bond	21.2 N/mm ...	18.0 N/mm 14.9 N/mm	14.5 N/mm	18.0 N/mm	ASTM D 429B
Shear modulus 100% shear Strain 200% shear Strain	0.90 MPa 0.35 MPa	0.80 MPa ——	< 0.48 MPa ——	0.90 MPa 0.62 MPa	CNR 10018/85
Damping coefficient 0.5Hz, 100% shear strain static 100% shear strain	13% 11.9%	12.1% 10.1%	16.5% 14.8%	12% 10.2%	SEAONC 90
STEEL (internal shims)	FeP01	FeP01	FeP01	FeP01	UNI 5866
STEEL (end plates)	Fe510B	Fe510B	Fe510B	Fe510B	UNI 7070

Tab. 1. Chemical, physical and mechanical characteristics of the basic components.

Geometric characteristics of the devices

The geometric characteristics of all the tested devices are reported in Tab. 2.

N.	Group	Shape	D_{max} [mm]	D'_{max} [mm]	n	s [mm]	h_e [mm]	s' [mm]	s'' [mm]	h_{tot} [mm]	Type	S_1	S_2
1	A, B, C	O	75	72	6	2.4	14.4	0.5	25	66.9	e	7.50	5
2	A, B, C	O	75	72	3	4.8	14.4	0.5	25	65.4		3.75	5
3	A, B, C	O	75	72	10	2.4	24	0.5	25	78.5	c	7.50	3
3bis	B	O	75	72	10	2.4	24	0.5	25	78.5	c	7.50	3
4	A, B, C	O	75	72	5	4.8	24	0.5	25	76	d	3.75	3
5	A, B, C	□	150	144	12	2.4	28.8	1.0	25	89.8		15	5
6	A, B, C	□	150	144	6	4.8	28.8	1.0	25	83.8		7.50	5
7	A, B, C	□	150	144	20	2.4	48	1.0	25	117		15	3
8	A, B, C	□	150	144	10	4.8	48	1.0	25	107		7.50	3
9	A, B, C	O	150	144	12	2.4	28.8	1.0	25	89.8		15	5
10	A, B, C	O	150	144	6	4.8	28.8	1.0	25	83.8	e	7.50	5
11	A, B, C	O	150	144	20	2.4	48	1.0	25	117	b	15	3
12	A, B, C	O	150	144	10	4.8	48	1.0	25	107	c	7.50	3
12bis	B	O	150	144	10	4.8	48	1.0	25	107	c	7.50	3
13	A, B, C	O	150	144	40	2.4	96	1.0	25	185		15	1.5
14	A, B, C	O	300	288	12	2.4	28.8	2.0	25	100.8		30	10
15	A, B, C	O	300	288	6	4.8	28.8	2.0	25	88.8		15	10
16	A, B, C	O	300	288	40	2.4	96	2.0	25	224	a	30	3
17	A, B, C	O	300	288	20	4.8	96	2.0	25	184	b	15	3
18	A, B, C	O	400	384	40	3.2	128	3.0	25	295	a	30	3
19	A, B, C	O	400	384	20	6.4	128	3.0	25	235	b	15	3
20	A, B, C	O	400	384	10	12.8	128	3.0	25	205	c	7.50	3
21	A, B, C	O	400	384	5	25.6	128	3.0	25	190	d	3.75	3
22	A, B, C	O	400	384	20	3.2	64	3.0	25	171		30	6

Tab. 2. Geometric characteristics of all the specimens.

The symbols used in the table have the followings meanings:

N. = identification number (from 1 to 22 + 3bis and 12bis) of the 24 different bearings;
Group = group which the device belongs (**A**, **B**, **C**);
Shape = shape of the device (O circular, □ square);

$\mathbf{D_{max}}$ = max dimension of the device (**Diameter** for circular devices, **Side** for square devices);
$\mathbf{D'_{max}}$ = max dimension of the internal steel shims and of the end plates;
n = number of elastomeric layers;
s = thickness of elastomeric layers;
$\mathbf{h_e}$ = total elastomeric height ($\mathbf{h_e = n \times s}$);
s' = thickness of steel shims;
s'' = thickness of end plates;
$\mathbf{h_{tot}}$ = total bearing height ($\mathbf{h_{tot} = h_e + (n-1) \times s' + 2 \times s''}$);

Type = type of bearing (**a**, **b**, **c**, **d**, **e**, **f**);
S_1 = primary shape factor ($S_1 = D'_{max}/4s$);
S_2 = secondary shape factor ($S_2 = D'_{max}/ h_e$).

Some preliminary considerations have to be made in order to understand the criteria adopted in defining the dimensions of the specimens reported in Tab. 2. As already said, a reliable evaluation of the mechanical characteristics of single isolators ask for tests on the basic materials as well as on devices as a whole. However, real devices, besides being very expensive, often have so large sizes that it is difficult to find Laboratories which are able to test them and obtain a reliable evaluation of the main mechanical characteristics. It is then necessary to perform tests on reduced scale specimens identical to the real ones (on the basis of materials, dimensional ratios, shape factors, execution process), knowing the extent of the differences, if any, to be expected in the experimental response between the reduced and the full scale specimens.

At this purpose, in selecting the dimensional ratios of the specimens, the starting point was the design of the bearings with the maximum values of D_{max} , to be considered as full scale devices; the dimensions of the reduced scale devices have been defined in such a way that they are models of the real ones in a suitably reduced scale. Circular bearings with diameter D_{max} = 400 mm and total elastomer height h_e = 128 mm, have been chosen as full scale devices. To the purpose of examining the influence of the primary shape factor S_1 on the mechanical characteristics, four different specimens have been defined. These specimens have the same h_e = 128 mm, but different primary shape factor. Once a basic value of S_1 = 3.75 was selected, the other values ensued: 3.75 (N.= 21), 7.5= 3.75 x 2 (N.= 20), 15= 3.75 x 4 (N.= 19), 30= 3.75 x 8 (N.= 18).

The change of S_1 , while keeping he constant, was obtained by varying the thickness s of the individual layers of elastomer and then the number of elastomeric layers n; four values of n (each one multiple of a basic value equal to 5) were selected, respectively equal to 5, 10, 20 and 40. The only exception to this plan is the bearing N. 22, having total elastomeric height h_e = 64 mm, i.e. half the height of the other ones, and S_1 = 30. A bearing with such an unusual dimensions has been considered to understand the role of the total elastomeric height, when S_1 is kept constant.

Once the dimensions of the full scale devices were defined, other 17 different reduced scale devices were designed. They are divided into 4 categories, which are characterized by 3 different loading areas and 1 shape variation. The 3 categories with circular shape have D_{max} respectively equal to 75 mm, 150 mm and 300 mm, while the category with square shape has D_{max} = 150 mm. By examining the data in Tab. 2, relevant to the circular bearings, it appears clear that most of the bearings of the three small scale categories (D_{max} = 75 mm, 150 mm, 300 mm) represents reduced-scale models of a full scale bearing, having the same S_1 and S_2 and smaller D_{max}.

This is true as long as the behavior of the bearings is substantially not affected by the thickness of the steel parts, as it is for the currently used thickness values. In particular, the last but two columns (Type) of table 2 highlights the direct correspondences, thus identifying 5 types, each one marked by a lowercase letter (a, b, c, d, e). It has to be noted that all the bearings belonging to the same type are similar but differently scaled.

It was not possible to establish the above described correspondence for all the bearings, particularly, for bearings N. 2, 9, 13, 14, 15, 22. They are however useful to evaluate the influence of the primary and secondary shape factors, whose values are differently combined. Finally the square-shaped specimens N. 5, 6, 7, 8 have shape factors identical to the circular-shaped specimens N. 9, 10, 11, 12 respectively, thus permitting a direct comparison to study the influence of the shape.

Description of the Mechanical Tests Performed

Four different types of mechanical tests were performed:

- static compression tests (**B1**);
- static shear failure tests with constant axial load (**B2**);
- cyclic static shear tests with constant axial load (**B3**);
- cyclic dynamic shear tests with constant axial load (**B4**).

All the tests, with the exception of the B1 tests, have been carried out on a couple of two equal bearings.

This test modality, fairly common and sometimes used also for testing in simple compression, was chosen to avoid complicated test facilities, otherwise needed when testing devices one by one, to eliminate any relative rotations between the external plates of a bearing.

It comes out that in all the **B2**, **B3** and **B4** tests, a mean value of the mechanical characteristics relevant to a couple of bearing was evaluated.

N.	Group A					Group B					Group C				
	New			Aged		New			Aged		New			Aged	
	B1	B3	B4	B1	B3	B1	B3	B4	B1	B3	B1	B3	B4	B1	B3
1	2	2	2	–	–	2	2	2	–	–	2	2	2	–	–
2	2	2	–	–	–	2	2	–	–	–	2	2	–	–	–
3	2	2	2	–	–	2	2	2	–	–	2	2	2	–	–
3 bis	–	–	–	–	–	2	2	2	–	–	–	–	–	–	–
4	2	2	2	–	–	2	2	2	–	–	2	2	2	–	–
5	2	2	–	–	–	2	2	–	–	–	2	2	–	–	–
6	2	2	–	–	–	2	2	–	–	–	2	2	–	–	–
7	2	2	–	–	–	2	2	–	–	–	2	2	–	–	–
8	2	2	–	–	–	2	2	–	–	–	2	2	–	–	–
9	2	2	–	–	–	2	2	–	–	–	2	2		–	–
10	2	2	2	–	–	2	2	2	–	–	2	2	2	–	–
11	2	2	2	–	–	2	2	2	–	–	2	2	2	–	–
12	2	2	2	–	–	2	2	2	–	–	2	2	2	–	–
12 bis	–	–	–	–	–	2	2	2	–	–	–	–	–	–	–
13	2	2	–	–	–	2	2	–	–	–	2	2	–	–	–
14	2	2	–	–	–	2	2	–	–	–	2	2	–	–	–
15	2	2	–	16	24	2	2	–	16	24	2	2	–	16	24
16	2	2	2	–	–	2	2	2	–	–	2	2	2	–	–
17	2	2	2	–	–	2	2	2	–	–	2	2	2	–	–
TOT	34	34	16	16	24	38	38	20	16	24	34	34	16	16	24

Tab. 3. Number of reduced-scale specimens new and artificially aged, and relevant tests.

To avoid that the experimental results of one test were depending on the sequence of the previous tests, each couple of specimens was subjected only to one test among **B1**, **B2**, **B3**, **B4**. A summary of all the tests performed and the total number of the relevant specimens subjected to those tests is reported in Tabs. 3 (reduced-scale bearings) and 4 (full scale bearings). On the whole, 162 specimens of Group A, 174 specimens of Group B and 162 specimens of Group C were tested. Finally, the total number of tests carried out, equal to 837, is given in Tab. 5.

N.	Group A				Group B				Group C			
	B1	B2	B3	B4	B1	B2	B3	B4	B1	B2	B3	B4
18	2	2	2	2	2	2	2	2	2	2	2	2
19	2	2	2	2	2	2	2	2	2	2	2	2
20	2	2	2	2	2	2	2	2	2	2	2	2
21	2	2	2	2	2	2	2	2	2	2	2	2
22	2	2	2	–	2	2	2	–	2	2	2	–
TOT	**10**	**10**	**10**	**8**	**10**	**10**	**10**	**8**	**10**	**10**	**10**	**8**

Tab.4 Number of new and artificially aged full scale specimens, and relevant tests.

	GROUP A		GROUP B		GROUP C	
	Reduced-scale	Full scale	Reduced-scale	Full scale	Reduced-scale	Full scale
B1	34 + 2x16 = 66	2 x 10 = 20	38 + 2x16 = 70	2 x 10 = 20	34 + 2x16 = 66	2 x 10 = 20
B2	–	5	–	5	–	5
B3	3x17 + 2x2x12 = 99	3 x 5 = 15	3x19 + 2x2x12 = 105	3 x 5 = 15	3x17 + 2x2x12 = 99	3 x 5 = 15
B4	2x2 x 8 = 32	3x3 x 4 = 36	2x2 x 10 = 40	3x3 x 4 = 36	2x2 x 8 = 32	3x3 x 4 = 36
TOT	**197**	**76**	**215**	**76**	**197**	**76**

Tab. 5 Total number of tests performed.

As shown in Tables 3 and 4, the tests were performed both on new and artificially aged bearings. The specimens to be aged were tested before and after the artificial ageing. Low levels of load, which were taken equal to the design ones, were applied, so that no degradation could occur during testing and the effects of the aging could be correctly evaluated.

All the tests have been performed by controlling displacements, with a mean sampling frequency of about 100 points (applied displacements and relevant loads) per cycle, to have a detailed description of the behavior of the devices, and evaluate suitably their mechanical and hysteretic characteristics.

Static compression tests (B1 tests)

Both reduced-scale bearings (N. 1÷17 with $\mathbf{D_{max}}$ = **75** mm, **150** mm, **300** mm) and full scale bearings (N. 18÷22 with $\mathbf{D_{max}}$ = **400** mm) were subjected to **B1** tests. The tests were conducted in a static way, by applying a monotonically increasing compression load and measuring the relevant displacements.

A maximum compression stress equal to 21 MPa was applied on all the specimens, corresponding to three times the design stress (7 MPa). However, for the above stated reasons, the specimens to be subjected to accelerated aging were loaded with a maximum compression stress equal to 7 MPa.

Creep tests were also carried out on all the full scale specimens, by applying the design load for 24 hours and measuring the displacement increases.

For the static compression tests (Tests B1) a press with the maximum capacity of 3000 kN was used (Figs.1 and 2). The loads applied by this press were measured by precalibrated load cells, whose capacities vary between 100 kN and 4000 kN, according to the maximum load applied during test.

The displacements were measured by inductive linear transducers linked to the anchorage plates of the isolators. The transducers were arranged to evaluate also possible rotations of the top plate of the isolator (Fig. 3).

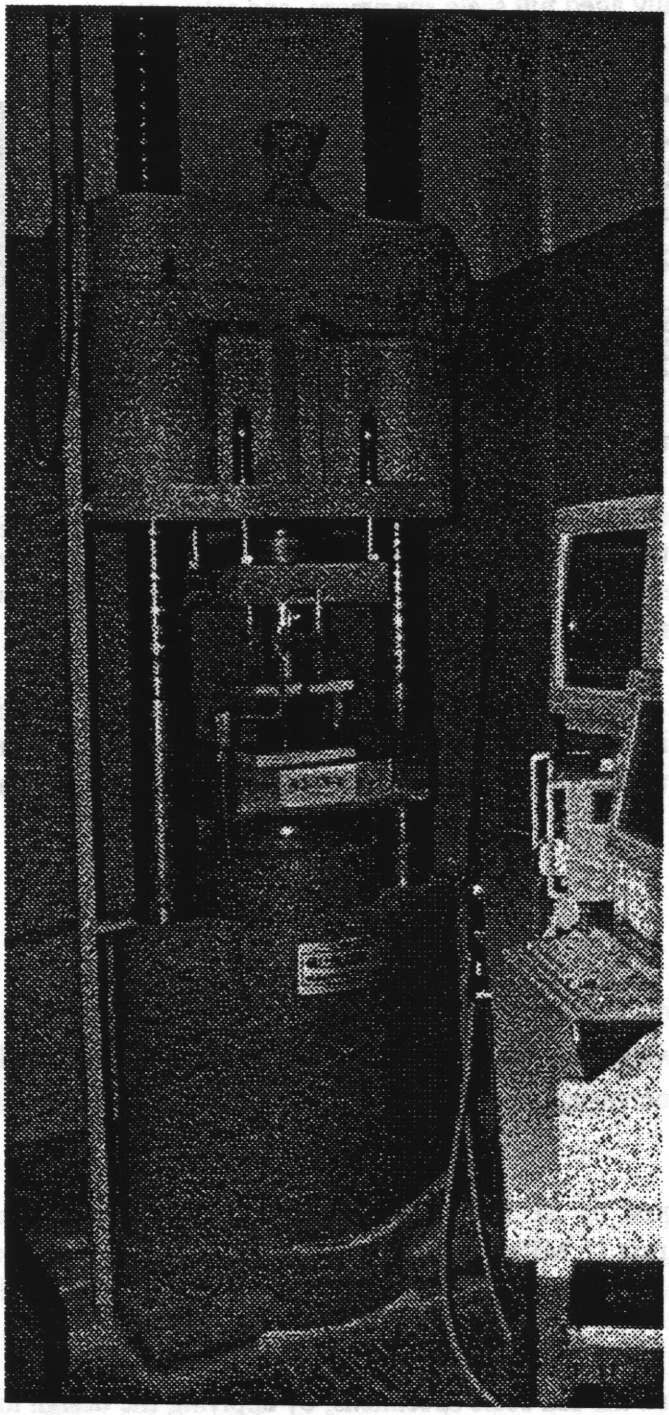


Fig. 1 Static compression test rig.

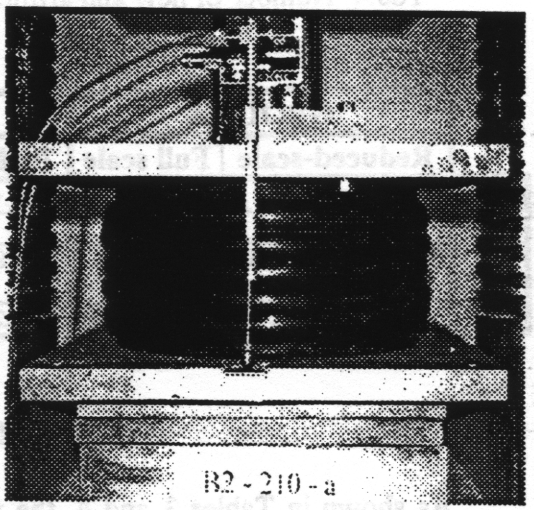


Fig. 2 A compression test.

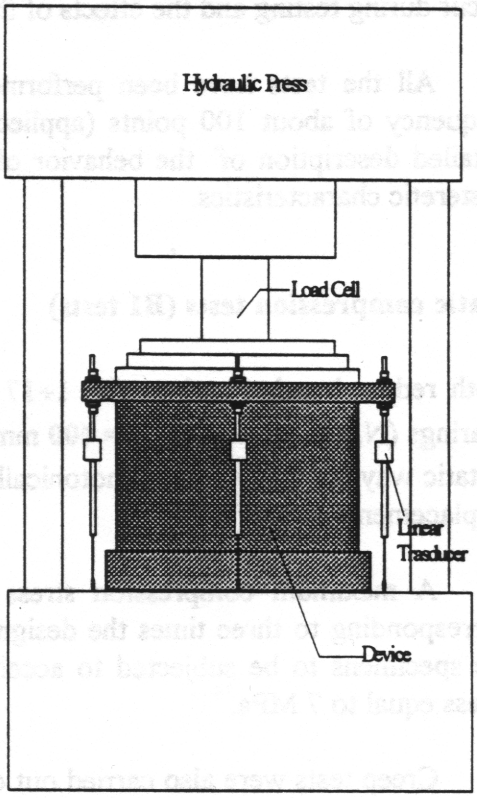


Fig.3 Compression test instruments.

Static and dynamic shear tests with constant axial load (B2, B3, B4 tests)

The shear tests were performed in three different static and dynamic modes. The axial load was always constant and applied statically, whereas the shear deformations were applied both statically (frequency < 0.05 Hz) and dynamically (frequency > 0.05 Hz). In the latter case the frequencies have been selected in the working field of the base isolation devices (0.2-0.6 Hz).

The tests were performed always by controlling displacements, as described below.

- Static shear failure tests with constant axial load (**B2** tests)
  These tests were performed only on real scale specimens not subjected to accelerated aging, by applying a constant axial load giving the design stress (7 MPa) together with a monotonically increasing shear strain up to failure or at least 300% (maximum applied displacement > 384mm for the bearings N. 18-21).

- Cyclic static shear tests with constant axial load (**B3** tests)
  These tests were performed both on reduced-scale and on full-scale specimens, by applying a constant axial load giving 50%, 100% and 150% the design stress (7 MPa) together with a sinusoidal shear strain varying according to the following sequence of maximum strain: ±10%, ±30%, ±50%, ±75%, ±100%, ±150%. The sequence included 10 and 5 consecutive cycles at each strain level, on the full and the reduced scale bearings respectively. The full scale bearings were subjected to a larger number of cycles, in order to detect any possible degradation effect. As regards the specimens subjected to artificial aging, a constant axial load giving 50%, and 100% the design stress (7 MPa) together with a sinusoidal shear strain varying according the following sequence of maximum strain: ±10%, ±30%, ±50%, ±75%, ±100% were applied. The sequence included 5 consecutive cycles at each strain level.

- Cyclic dynamic shear tests with constant axial load (**B4** tests)
  These tests were performed both on reduced-scale and on full-scale specimens, by applying a constant axial load resulting in 50%, 100% and 150% the design stress (7 MPa) on the full scale specimens, while on the reduced-scale specimens only two levels of axial load were applied (100% and 150%). Together with the axial load, a sinusoidal shear strain was applied according to the following sequence of maximum strain: ±10%, ±30%, ±50%, ±75%, ±100%. The sequence included 10 and 5 consecutive cycles at each strain level, on the full and the reduced scale bearings respectively. The shear strains were applied dynamically at the following frequencies: 0.2 Hz, 0.4 Hz and 0.6 Hz on the full-scale bearings, 0.4 Hz and 0.6 Hz on the reduced-scale bearings.

All tests **B2** were carried out with the test rig shown in Figs. 4 and 5, where two or four identical bearings can be simultaneously tested under static or cyclic shear forces together with a constant axial load. The test rig is made up of a steel reaction structure, whose main elements are a "I" shaped base beam, a horizontal stiff beam and two frames that react the axial loads. The structure, thanks to its rigidity, guarantees the complanarity of the end plates of the specimens during test. It also follows passively the axial displacements of the devices caused by the axial load and by the second order effects due to the shear load, thanks to the horizontal stiff beam put between the specimens and the vertical jacks. The shear load is applied by two synchronised ENERPAC double effect jacks, horizontally mounted and linked, through two loading plates, to the adjacent faces of the specimens. The compression load, which is kept constant, is applied by two ENERPAC double effect jacks, vertically mounted.

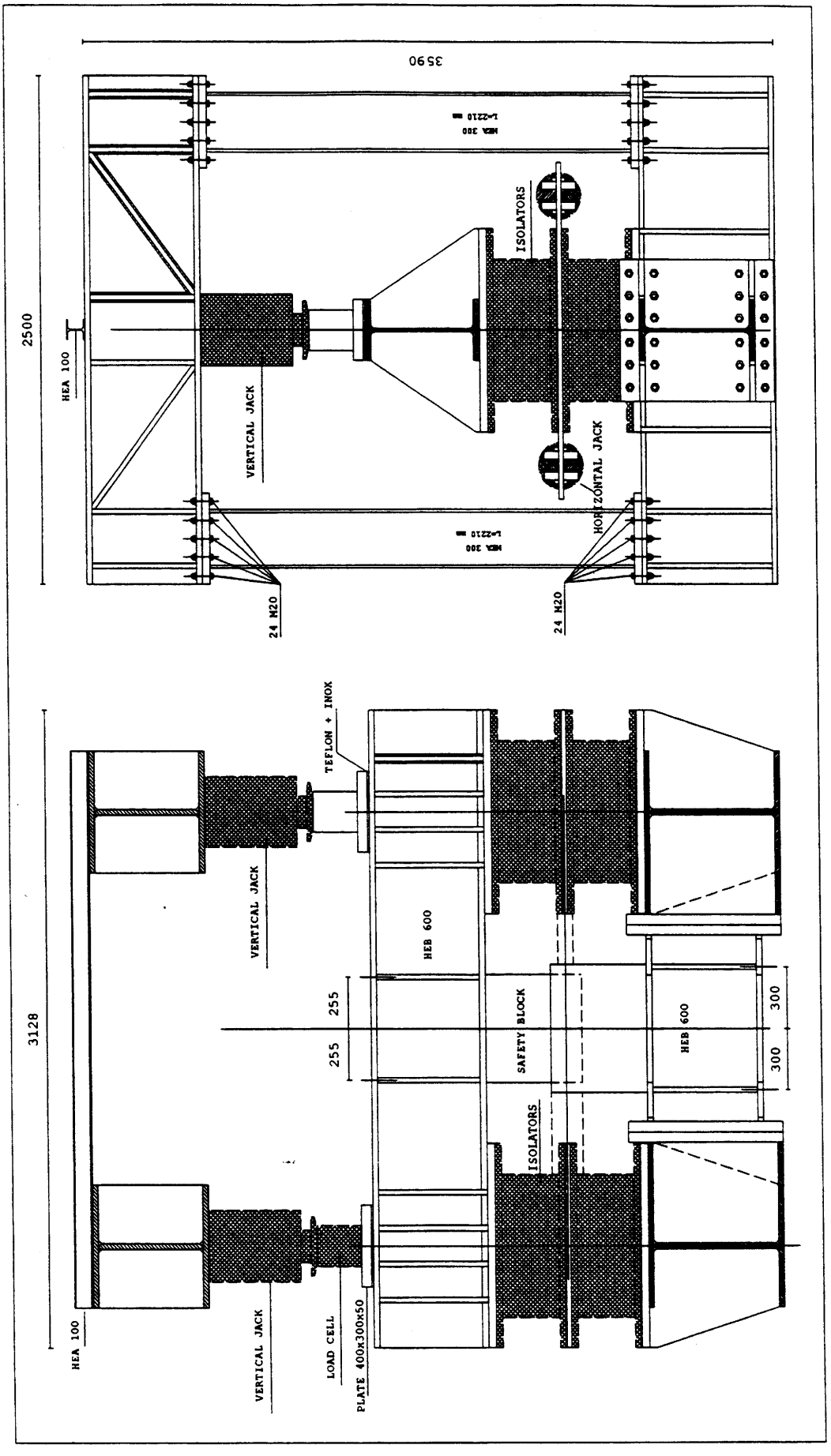


Fig. 4 Layout of the four-bearings test machine.

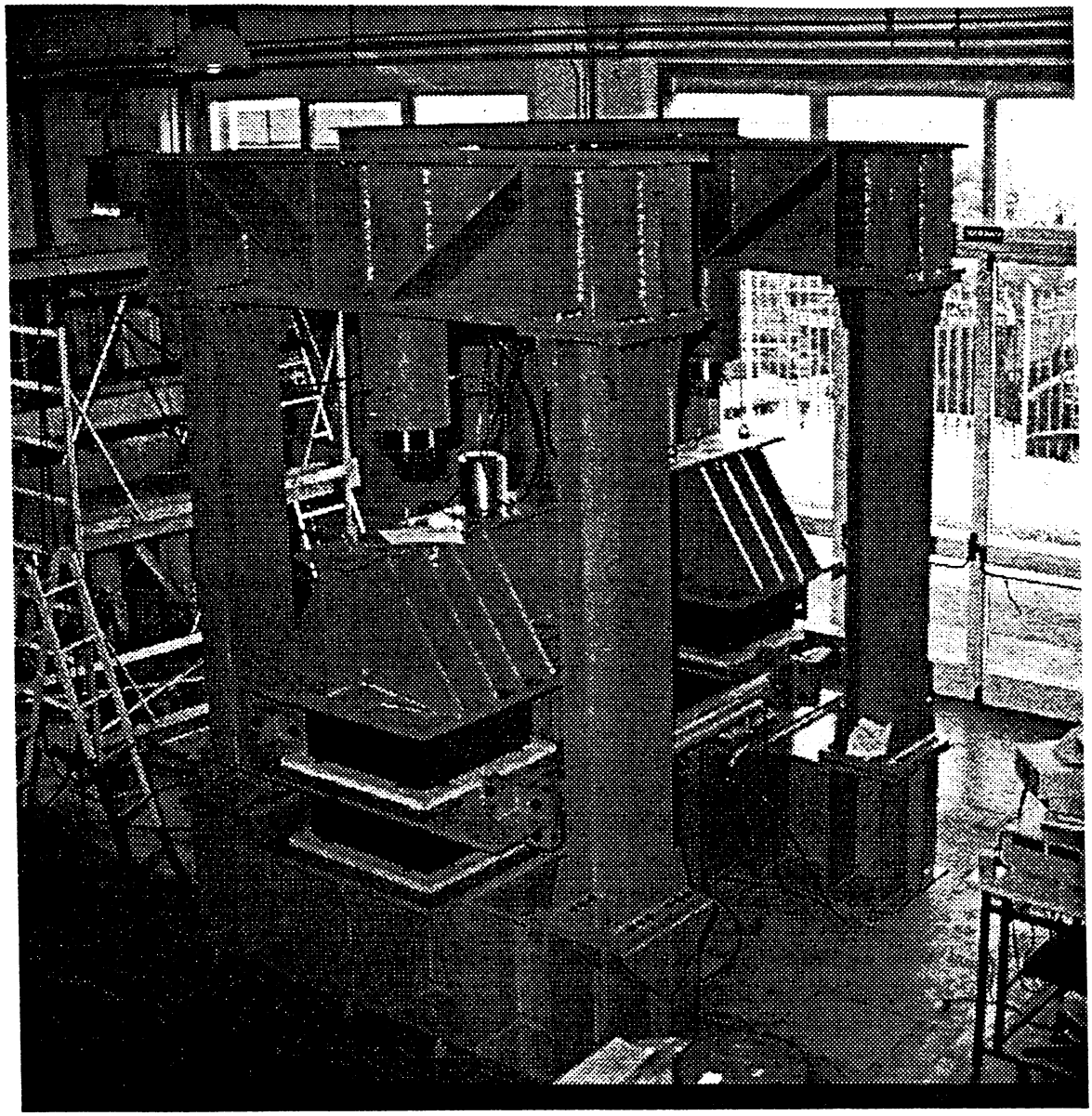


Fig. 5 Four-bearings test machine.

The maximum vertical capacity of the equipment is 4000 kN. 750 kN maximum horizontal load in compression and 350 kN in tension are the capacity of the two ENERPAC horizontal jacks, for a maximum 900 mm stroke.

When testing four specimens the maximum shear displacements was then ±450 mm for each couple. All the loads were measured by pre-calibrated load cells.

The presence of suitable slide-ways do not allow displacements of the specimens in direction other than the shear force direction, so that the horizontal displacements of each couple of specimens could be measured by only one inductive transducer.

The axial displacement was measured by a couple of inductive transducer for each couple of isolators.

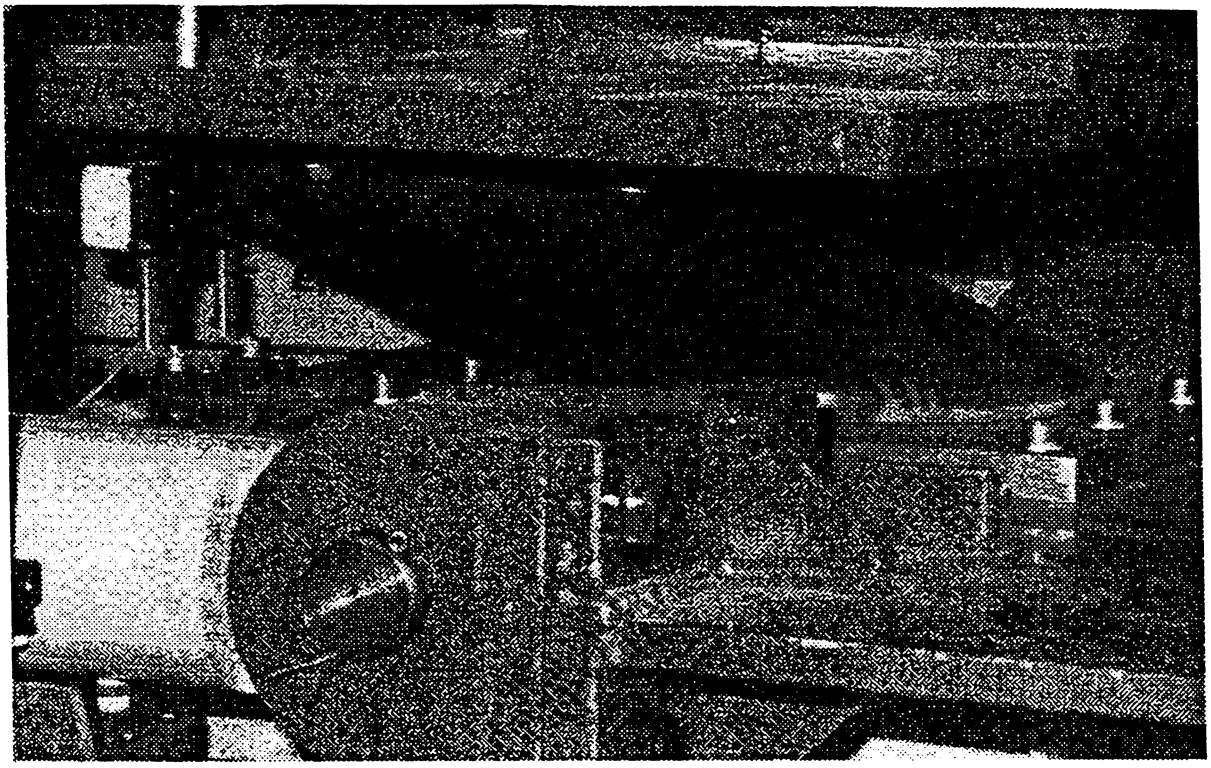


Fig. 6 Particular of a shear failure test.

For the cyclic static (Tests **B3**) and dynamic (Tests **B4**) shear tests, both performed by keeping the axial load constant, the test apparatus was able to apply simultaneously compression (in the horizontal direction) and shear (in the vertical direction) to a couple of identical bearings.

Figs. 7 and 8 show, respectively, a detailed layout and an overall view of the test apparatus, while Fig. 9 shows a detail during a shear dynamic test.

The test machine is made up by a steel reaction frame, whose main elements are a base beam and three stiff columns. Two of them are linked to the base by a double pendulum constraint and one by a hinge.

This structure guarantee the complanarity of the bases of the specimens and allows to follow passively, thanks to a system of cylindrical hinges, the axial displacements of the devices caused by the axial load and by the second order effects caused by the shear deformation.

The shear load is applied by a SCHENK hydraulic actuator, which is vertically mounted and linked to the adjacent faces of the two specimens through a loading plate. The compression load is applied and kept constant during test by a ENERPAC double effect jack, which is horizontally mounted between the hinged and the adjacent columns.

In order to make it possible the positioning of all the types of isolators to be tested, having different total heights, a series of special rigid connecting pieces were manufactured, to be placed between the columns and the end plates of the isolators.

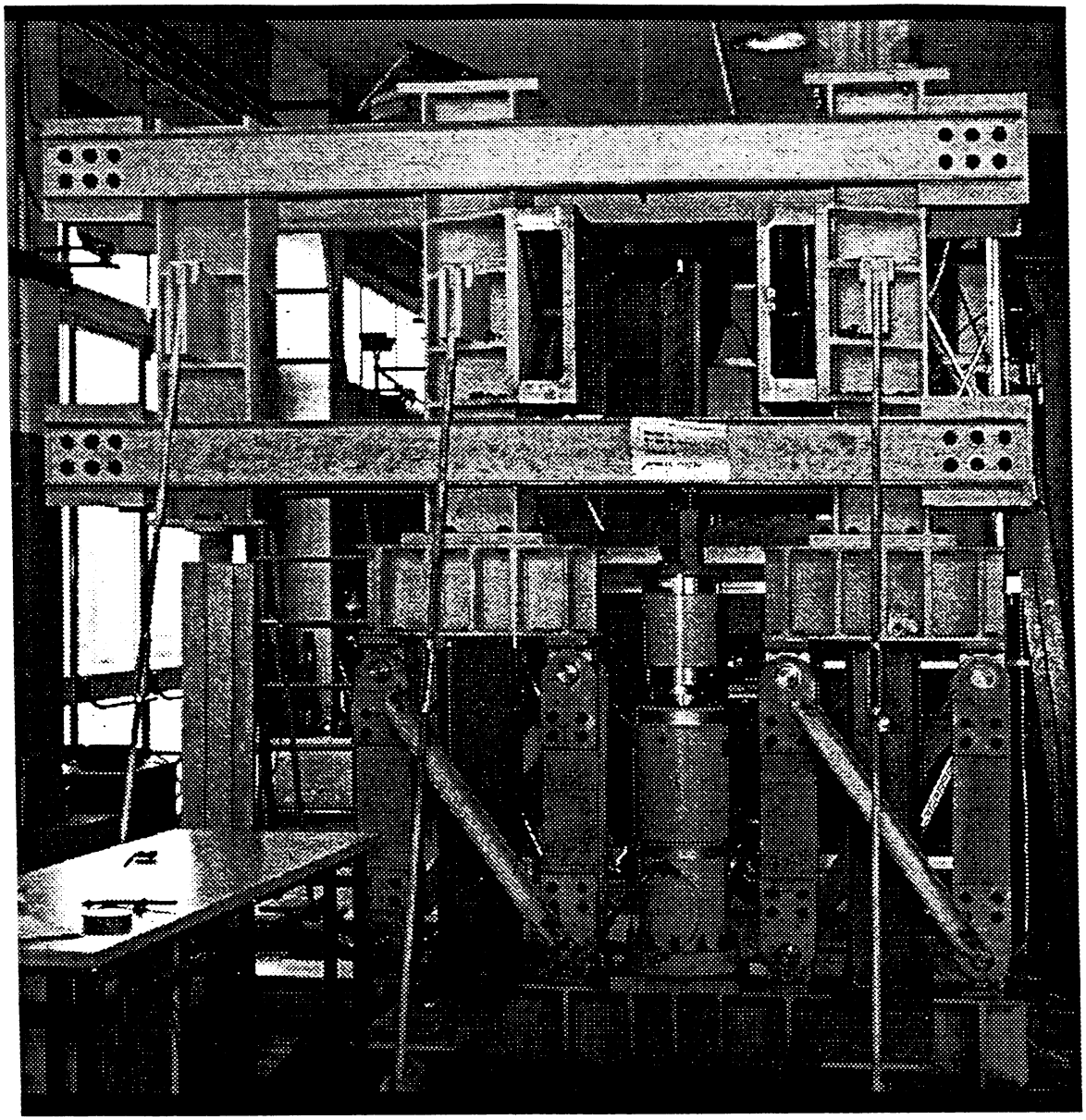


Fig. 8 Double bearing dynamic test machine.

The SCHENK actuator can develop 200 kN maximum dynamic force and ±125mm maximum displacement. The maximum static force is equal to 250 kN. The force of the actuator was measured by a pre-calibrated load cell of 250 kN, mounted between the head of the cylinder and the shear loading plate. The actuator is fed by a hydraulic power pack, made up of two pumps, each one having a maximum delivery of 80 litres/min, and by two 63 litres/min servo-valves. Control of the hydraulic system is performed by an electronic controller.

The displacements of the actuator are measured and controlled by an internal transducer, while the shear displacements of the specimens were measured by linear transducers connected to the shear loading plate. The axial displacements of the specimens were measured by two linear transducers, positioned between the end plates of the two specimens, in such a way that also rotations out of the shear loading plane could be evaluated. Fig. 10 shows an overall layout with the arrangement of the measuring devices.

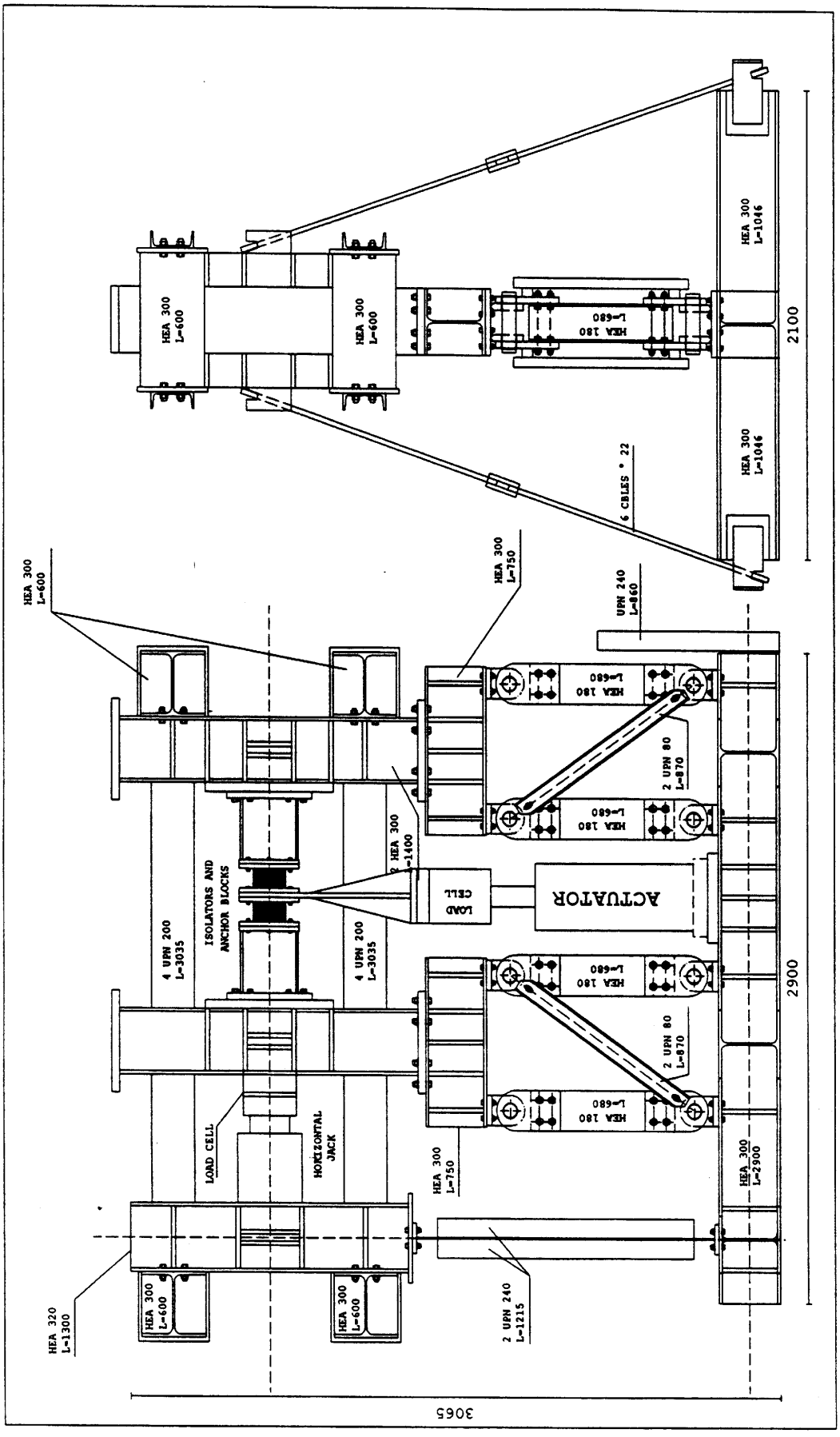


Fig. 7 Layout of double bearing dynamic test machine.



Fig. 9 Two bearings during a shear dynamic test.

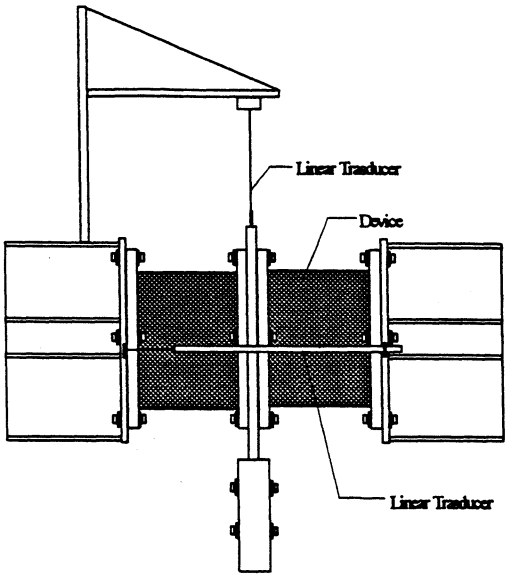


Fig. 10 Instrumentation of the double bearing dynamic test machine.

A series of ENERPAC double effect jacks, able to develop with sufficient accuracy loads ranging from 30 kN to 3000 kN according to the size of the specimen, were used to apply axial forces.

Pre-calibrated load cells of different capacity were mounted between the horizontal jack and the central column of the reaction frame, through a ball joint that guarantees a perfect load centering.

The hydraulic power pack feeding the axial load jack, managed by an electronic controller, is composed by a pump, whose maximum delivery is 5 litres/min, and by a system of electrovalves suitably designed.

The hydraulic system used to feed the axial load jacks in the double-bearing test machine, during the B3 and B4 tests was also used to feed all the jacks during the B2 tests.

Data Acquisition and Analysis System

The data acquisition and analysis system was managed by computer, through a managerial software which is able to process and display the experimental results coming from a HBM DMC 9012A signal filter, in real time.

The acquired results were filtered and amplified by the HBM filter and converted from analog signals to 16 bit digital signals, with a maximum sampling frequency per channel equal to 9600 Hz.

During the dynamic tests the acquisition frequency per channel ranges from (20 to 60 Hz), according to the type of test and the load frequency.

The system is able to simultaneously manage up to 72 canals. However, during the tests, at most 8 channels were used to directly acquire the signals and a few other channels were used to simultaneously process data.

Accelerated Aging

Reference to specimens, particularly bearing N. 15, to be subjected to accelerated aging was frequently made in the previous section. At this regard, some preliminary considerations have to be stated to clarify what is meant by accelerated aging and the reasons of its execution.

It is common knowledge that the characteristics of polymers (synthetic and natural rubbers) are time-dependent; thus, it is necessary to evaluate the relevant changes in the behavior of elastomeric bearings. This evaluation presents the same difficulty already illustrated when dealing with the evaluation of the mechanical properties, i.e. the difficulty to extrapolate the results of tests made on basic material, specifically on compounds, to devices. Moreover, suitable test procedures have not been set up yet, aging being a very complex phenomenon.

A reasonable prediction of the variations of the mechanical properties of an isolator in the long run is an open question so far, as the technical literature on the argument clearly shows (1, 2).

In order to give a contribution to the resolution of the problem, some isolators have been subjected to a process of accelerated aging, in accordance with the ISO/TC 45 N 5846. The aim of the test is to estimate the useful lifetime of elastomeric bearings, i.e. the time interval during which the device keeps its characteristics fit to use at the service temperature. Since the laboratory tests have to be performed within a reasonable time interval, the ISO standard suggests the use of the Arrhenius law.

This law, according to the development of the chemical reactions in organic compounds, establishes a direct proportionality between the logarithm of the time t expressed in days ($\ln(t)$) and the inverse of the absolute temperature expressed in Kelvin degrees ($1/T$), resulting in the following equation

$$\ln(t) = \frac{E}{RT} + B$$

where E is the activation energy of the aging reaction, R is the gas constant or the Boltzmann constant (depending on the units) and B is an integration constant. The representation of $ln(t)$ versus $1/T$ is better known as "***Arrhenius plot***" and it coincides with a straight line, under the hypothesis, to be confirmed, that the E/R ratio is constant.

As the standard ISO/TC 45 N 5846 requires, the variations of one or more selected properties must be determined as a function of time, for some prefixed values of temperature. In this case, 3 values of temperature and 2 mechanical properties, namely the axial and shear stiffness of the isolators, were considered. Theoretically, the duration of the test should be as long as the selected properties achieve a prefixed threshold value, chosen to suit the conditions of use. Actually, as the application of the above described procedure would be very expensive, due to its duration, the variations of properties are typically evaluated after a prefixed interval of time, generally rather limited (from 1 to 3 weeks). By suitably extrapolating the results, the time in which the selected properties would achieve the prefixed threshold value is estimated.

This simplified approach has the advantage of being not much expensive, but it frequently asks for strong extrapolations that are applied to variation laws, which result to be significantly non linear. Consequently, inaccurate and maybe optimistic estimations of the aging time could be obtained, whose errors increase as the ratio between the adopted test duration and the necessary time to achieve the threshold value decreases.

However, as the simplified approach is usual in the current practice (3) and, moreover, it was also used to estimate the behavior of the aged compound, it seemed appropriate also for the prediction of the lifetime of the devices.

In order to make a better extrapolation of the results, a test duration ranging from 4 weeks up to a maximum time of 18 weeks was used in the present experimental program. In Table 6 the complete program of accelerated aging performed on the bearing N. 15 is shortly summarized. Tests B1 and B3 have been performed before and after the aging, and the behavior of the specimens has been evaluated and compared in terms of axial and shear stiffness.

	Group A (Bearing N. 15)			Groups B÷C (Bearing N. 15)		
TEST	Specimens number	Temperature (°C)	TIME (weeks)	Specimens number	Temperature (°C)	TIME (weeks)
B1	6	100	4-8-12-14-16-18	6	80	4-8-12-14-16-18
	6	80	4-8-12-14-16-18	6	70	4-8-12-14-16-18
	4	60	4-8-12-16	4	60	4-8-12-16
B3	8	100	8-12-14-16	8	80	8-12-14-16
	8	80	4-8-12-16	8	70	4-8-12-16
	8	60	4-8-12-16	8	60	4-8-12-16

Tab.6. Accelerated aging program performed on the bearing N. 15.

Preliminary results

As said before, two diagrams are plotted (one for the compression stiffness and one for the shear stiffness). Each diagram has three curves, relevant to the three aging temperatures considered (60°C, 80°C and 100°C). Each curve shows (see fig. 11 and 12):

- the ratio between compression (or shear) stiffness after and before aging procedure, on the vertical axis,
- the aging elapsed time, expressed in days, on the horizontal axis.

The points of the Arrhenius plot are obtained from the above said two diagrams.

On each diagram a straight horizontal line must be traced, identifying a value of the ratio between the stiffness after and before the aging procedure. This line crosses the three curves corresponding to the three examined aging temperatures (60°C, 80°C and 100°C). in three points; to each point corresponds a value of the aging temperature (constant for each curve) and a value of the aging elapsed time.

The so obtained three points are positioned on an Arrhenius plot (as said before a plot of ln(t) versus 1/T). A straight line is traced, best fitting the three points via a least squares algorithm; this line crosses in a point the horizontal straight line corresponding to the assumed medium value (20°C) of ambient temperature.

The cross point identifies the time requested by the bearing to reach, with a natural aging, the stiffness ratio relevant to the three considered points. The procedure described above is followed, obviously, for each considered stiffness, obtaining two Arrhenius plots (see fig.13, 14).

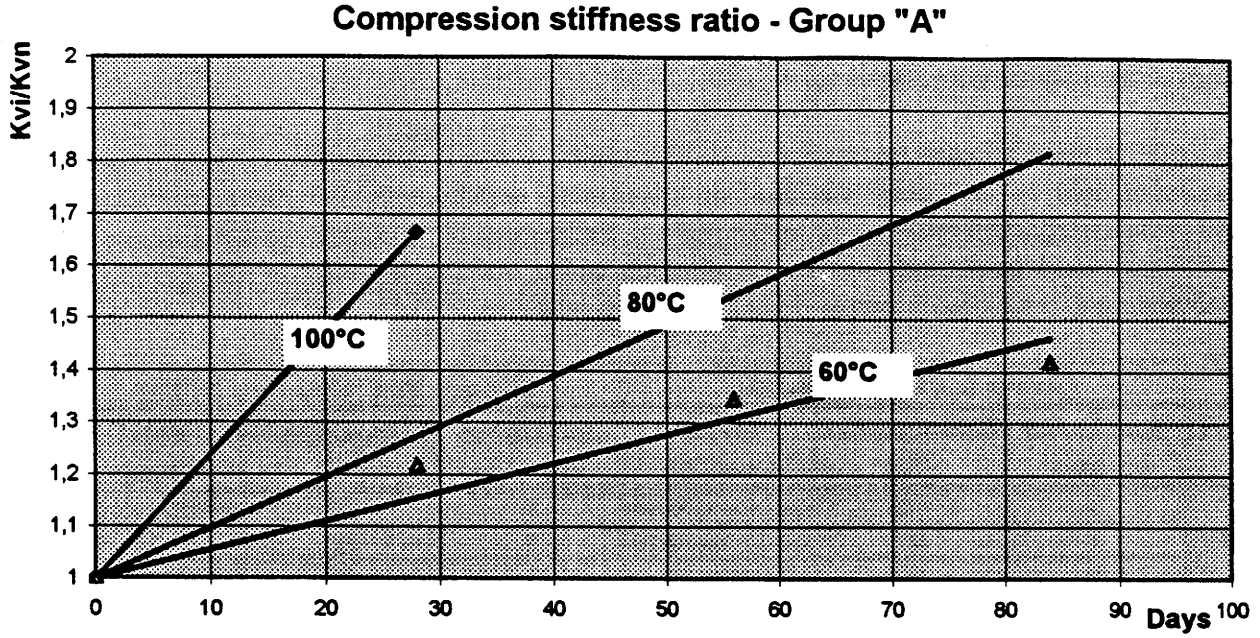


Fig.11- Ratio between the compression stiffness after (**Kvi**) and before (**Kvn**) the aging procedure, vs. elapsed time in days

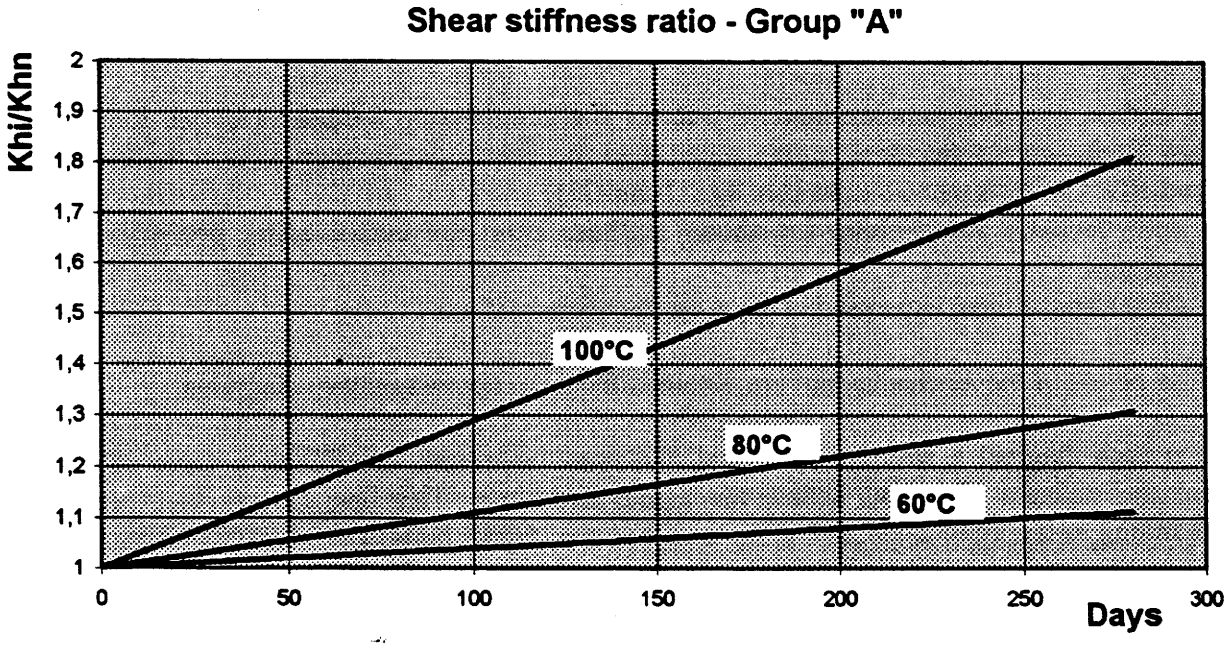


Fig.12- Ratio between the shear stiffness after (**Khi**) and before (**Khn**) the aging procedure, vs elapsed time in days

In the Arrhenius plot relevant to compression stiffness, five groups of points have been represented. Each group corresponds to an increment equal to 5%, 10%, 20% 50% and 400% respectively, of the ratio between compression stiffness after (Kvi) and before (Kvn) aging procedure. Each group has a number of points (three) equal to the number of accelerated aging temperatures.

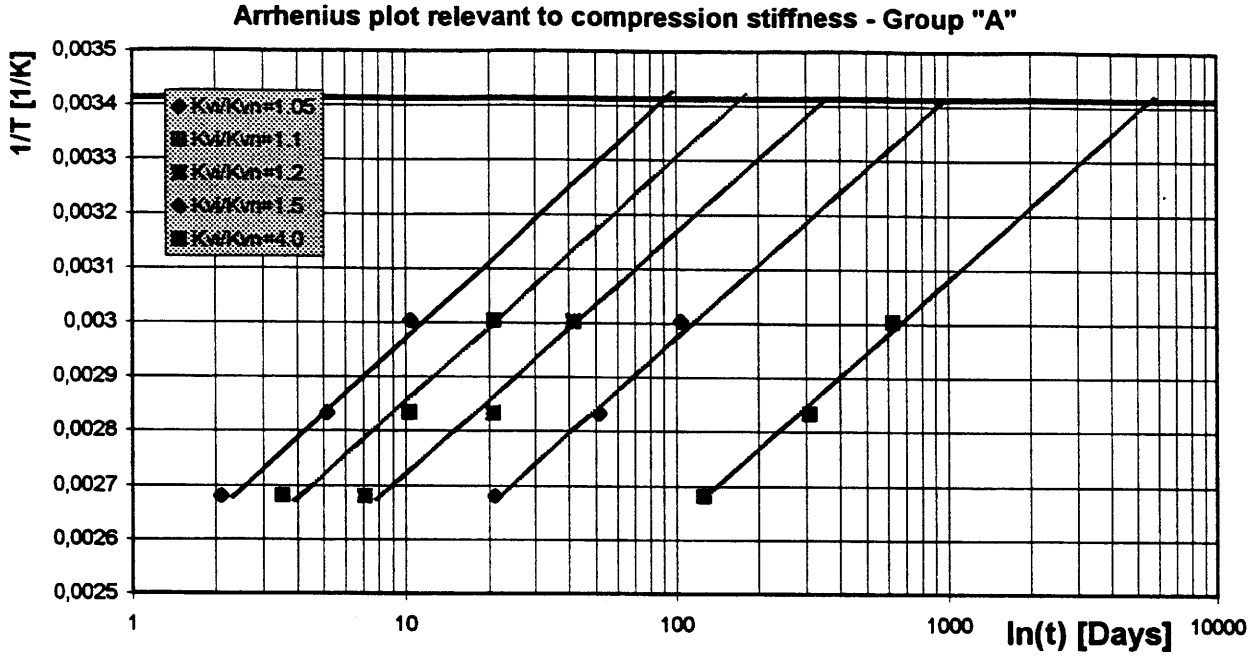


Fig. 13.- Arrhenius plot of the ratio between the compression stiffness after (**Kvi**) and before (**Kvn**) the aging procedure, vs. the elapsed time in days.

In the Arrhenius plot relevant to shear stiffness, four groups of points have been represented. Each group corresponds to an increment equal to 5%, 10%, 20% and 50% respectively, of the ratio between shear stiffness after (Khi) and before (Khn) aging procedure. Each group has a number of points (three) equal to the number of accelerated aging temperatures.

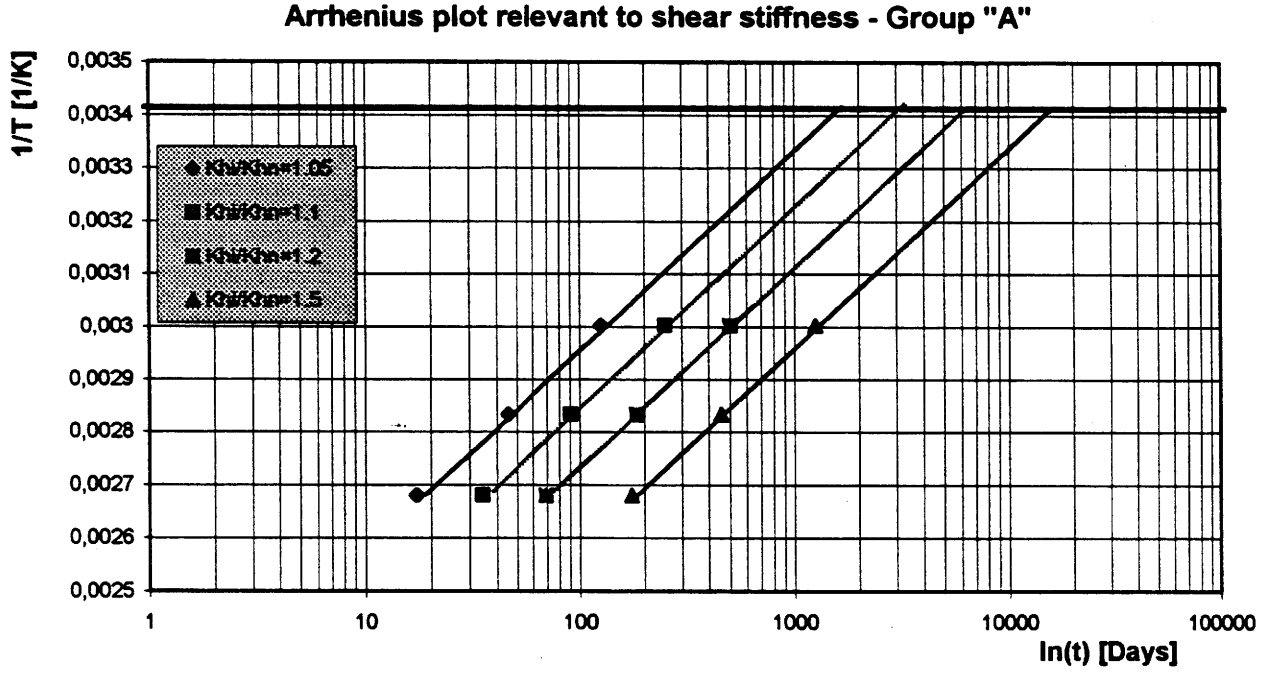


Fig. 14.- Arrhenius plot of the ratio between the shear stiffness after (**Khi**) and before (**Khn**) the aging procedure, vs. the elapsed time in days.

The Arrhenius plot relevant to the compression stiffness shows that, for an increment of the stiffness equal to 5%, 10%, 20%, 50% and 400% respectively, the requested elapsed time under an ambient temperature of 20°C is equal to about 3 months, 6 months, 1 year, 3 years and 16 years.

The Arrhenius plot relevant to the shear stiffness shows that, for an increment of the stiffness equal to 5%, 10%, 20% and 50% respectively, the requested elapsed time under an ambient temperature of 20°C is equal to about 4 years, 8 years, 16 years and 40 years.

The different sensitivity of the compression stiffness and shear stiffness to the elapsed time is well-known and confirmed by the preliminary results shown above.

It must be underlined that, at present time, the Arrhenius plot is usually not traced at all. The effects of elapsed time are evaluated after an aging of seven days at 70°C (3). If the value of the considered characteristic has been changed of less than 15%, the aging effects are considered allowable. The results obtained show that this criterion is probably safe, but more work on this subject is necessary.

REFERENCES

1. Barker, L. R., 1991, "Accelerated long-term ageing of natural rubber vulcanizates. Part 2: Results from ageing tests at 40°C" , Rubber Developments, vol. 44, no 2/3.

2. Fuller, K. N. G., Pond, T. J., 1995, "The long term performance of high damping natural rubber seismic bearings", European Seismic Design Practice, Balkema, Rotterdam.

3. CEN –TC 167/SC1 WG 15 N 26 "Elastomeric Laminated Bearings used as isolators"

Optimal Design of Isolated Bridges and Isolation Systems for Existing Bridges

Gian Michele Calvi and Alberto Pavese

Dipartimento di Meccanica Strutturale, Università di Pavia, Italy

Abstract

Designing new isolated bridges, the selection of optimal characteristics for strength, stiffness and displacement capacity for both piers and isolators is not at all obvious. When designing an isolation system for an existing bridge, the variable parameters are less, but it should not be assumed as a principle that all piers have to be isolated.

A study on this subject has been recently presented by the same authors (1) where an optimization procedure was outlined, even if it was more an idea to be developed and verified than a reliable design tool. Since then, the idea has become a proposal for a design method, and the method has been implemented in an efficient software program and applied to a large number of cases which confirmed the soundness of the principles adopted in the design philosophy.

The design approach assumes that a displacement profile predicted using a linear equivalent model, will be reproduced by the envelope of the maximum displacement obtained from a series of non-linear analyses, considered to be representative of the real response.

A displacement reduction factor is proposed in analogy with the force reduction factor commonly used in force-based approaches, and a response index is used to predict whether the non-linear response is likely to be similar to the response predicted by the linear equivalent model. The response index is then used as the main parameter to be optimized, to design an appropriate isolation system, keeping the appropriate boundary conditions to assure a capacity protection of the foundation-pier systems.

The procedure has been applied to several cases, comparing the results with those obtained from non-linear analysis, showing that the design approach seems to be efficient and reliable.

Introduction

There is little merit in discussing when and why an isolation system should be considered to design a new bridge or to increase the seismic protection of an existing bridge. Actually the answer may simply be: "anytime some bearing system is being considered to support the deck".

However, it is well known that different objectives may coexist and have different relevance when conceiving an isolation system:

- A capacity design protection of undesired collapse modes for piers, foundation and soil;
- A concentration of the expected damage where repair is easy and not expensive;
- A regularization of the bridge response, in terms of stiffness, strength and expected displacement of different piers;
- An increase of the energy dissipation capacity, to reduce strength and displacement demand;
- A period elongation of the main response modes, to reduce the spectral acceleration.

The first two objectives are automatically reached when each isolator strength is set at a lower level with respect to all possible damage modes of the corresponding soil-foundation-pier system.

On the contrary, the last three objectives pose difficult problems on the most appropriate set of parameters to be selected for each isolator, in terms of strength, stiffness, displacement and ductility capacity. While it is obviously possible to design an isolation system and to perform a non-linear analysis to check the acceptability of the response, it is certainly more desirable to develop some criterion to design an optimum system, possibly using a linear model capable to predict the expected results of a non-linear analysis with a known reliability.

In this paper a displacement-based design approach is proposed, defining a *response index* which allows to design an efficient isolation system. The index is defined in such a way that the bridge will respond non linearly as expected from a linear analysis, with a given coefficient of variation, function of the difference between design spectrum and actual input ground motions.

A *displacement reduction factor* is also proposed in the paper, in analogy with the force reduction factor (or behavior factor) traditionally used in forced-based design approaches.

Modeling, analysis and design of isolated bridges

Only bridges constituted by vertical piers connected by a horizontal deck will be considered in this paper. Their response is therefore very simple in principle, being constituted by a series of soil-foundation-pier-isolator systems more or less coupled by the deck. As an alternative to a full non-linear analysis, each soil-foundation-pier system can be modeled with a single non-linear spring, defined on the base of some event-to-event (pushover) analysis. Using the force-displacement monotonic curve as the envelope curve, the actual hysteretic response can be represented adopting one of the two following options:

- A non-linear dynamic model can be produced, where the hysteresis cycles will be defined as a function of the assessed damage and failure modes.
- A linear-equivalent model can be produced, with secant stiffness to the appropriate limit state. A viscous damping equivalent to the effective energy dissipation capacity, again dependent on the assessed damage and failure modes has been proposed in this case (2,3).

If the coupling offered by the deck is small, each pier can be regarded as an independent system, to be analyzed separately. This is often not the case for isolated bridges, where the deck can be continuous and the global pier stiffness have been reduced by the isolators. It may be then necessary to study the response of the bridge as a multi-degrees-of-freedom system, even if each pier

has been condensed into a single-degree-of-freedom system. The attention will be here concentrated on the transversal response, which is in most cases more critical than the longitudinal response. The procedure that will be outlined will be anyway applicable to a global 3-dimensional evaluation of the bridge response.

Provided that the model is made with linear equivalent elements, a modal analysis can be performed. In this case a problem may be constituted by the appropriate definition of the equivalent damping, which is required to be a single value by most analysis program, and cannot therefore be different for different piers.

The design approach proposed here is based on a linear equivalent structure, on the assumption of a set of maximum displacements for isolators, piers and decks, and on the definition of a *displacement reduction factor* and of a *response index*, as defined in the following section.

Definition of a "displacement reduction factor"

Displacement based design approaches

It is well known that the approach presently adopted in all modern seismic design codes is based on the comparison of strength demand and strength capacity, considering the elastic response of the structure, possibly based on some cracked stiffness evaluation, and a *strength demand reduction factor*. This strength reduction factor (also defined "behavior factor", q in Europe) should account for ductility capacity, energy dissipation capacity, strength reserves, structural redundancy. Obviously, it may as well be considered a *strength capacity enhancement* factor.

The implications of this approach are that the elastic response of the structure represents well also the post-elastic response and that strength is a good measure of damage, i.e., since this is clearly not the case, that there is a reasonable proportionality between strength and displacement. These assumptions may be acceptable, even if not at all rational, provided that the application of capacity design principles forces a reasonably uniform distribution of damage.

It has been discussed in several recent papers (4) how more rational it is to shift to direct displacement based approaches, where displacement capacity and displacement demand are compared to define the limit state that will be attained by the structures excited by the design earthquake. In this case, obviously, displacement spectra should be used, the structure period of vibration should be calculated in terms of some secant stiffness, and *some displacement demand reduction factor* should be defined (5), to account for dissipation capacity etc.

Acceleration and displacement spectra

Acceleration response spectra are perfectly adequate when a linear response is assumed and are relatively easy to define, showing larger values at relatively low periods of vibration, where the spectral values are easier to be derived from accelerograms. Even significant errors at large period values are not important, since the spectral accelerations are anyway low.

Displacement spectra have been traditionally considered essentially linearly increasing with period, since periods larger than 2-3 seconds have never been of interest. At large periods it is difficult to obtain accurate values from the integration of recorded accelerograms, especially from analogical signals, but it is conceptually well known that the spectral values should tend to the ground peak displacement. Recent studies based on digital recording have confirmed the conceptual shape of displacement spectra shown in Figure 1.

Spectra for non linear response

As previously discussed, acceleration spectra have been traditionally corrected using some force reduction factor, it is then natural to discuss whether displacement spectra may be similarly corrected to include non linear response. It is immediate to observe that a period of vibration somehow related to the global response would be more representative of the real response, and consequently to adopt an equivalent period (6) related to the secant stiffness to the displacement defining the LS of interest. A correction of the spectral ordinates is then required to include a measure of the energy dissipation capacity of the structure, possibly function of the target displacement, of the structural response and of the characteristics of the input motion. Families of spectral curves may be generated, based on expected ductility demand or equivalent viscous damping, when the hysteretic structural response and the equivalent number of large cycles of the earthquake motion have been estimated.

Linear equivalent damped spectra

Design spectra will assume the shape shown in Figure 1, where ductility demand and equivalent viscous damping are considered somehow equivalent. In earlier studies on displacement based design (2,3) a relation suggested in EC8 (7) for damping values different from 5%, was adopted to calculate the correction factor (η) for displacement spectra as a function of equivalent viscous damping:

$$\eta = \left(\frac{7}{2+\xi}\right)^{1/2} \tag{1}$$

The relation between equivalent damping (ξ_e) and ductility (μ) may be of the form:

$$\xi_e = \alpha\left(1-\frac{1}{\mu^{\beta}}\right)+\xi_v \tag{2}$$

where α is a factor that depends on the energy dissipation capacity of the structure (of the order of 20–30 for RC structures, of the order of 40-50 for an artificial dissipating element), β is a factor between 0.5 and 1 (again depending on the hysteretic properties of the structure), and ξ_v is assumed to be the damping ratio characterizing the linear response.

It has to be noted that η has a tendency to an asymptotic value, so that larger dissipation (or larger ductility) tends to have no further significant effect on the response at increasing values. Recent parametric studies (not published) seem to confirm that the effects tend to become negligible at ductility values larger than 4 or 5, or at equivalent damping values larger than 15 or 20 %. This would imply that an error in the evaluation of the effective damping is not crucial, provided that damping is not too small. It is suggested that the factor resulting from equations 1 and 2 is kept for period values shorter than the period corresponding to maximum spectral displacement (T_0, probably in the range 1.5-2.5 s), while for larger period it is corrected according to the following equation:

$$\eta' = \eta + \frac{4}{\pi}(1-\eta)\left(Tan^{-1}\left(1-\frac{T_0}{T}\right)^3\right) \tag{3}$$

For isolated bridges it has been proposed (10) that the effective global ductility of the pier-isolator system is calculated using the following expression:

$$\mu_G = 1+(\mu_D - 1)\frac{\Delta_{DE}}{\Delta_S + \Delta_{DE}} \tag{4}$$

where μ_G is the global ductility the system pier-isolator, μ_D is the ductility of the isolator, Δ_S is the pier yield displacement and Δ_{DE} is the maximum isolator displacement.

A flexible pier therefore reduces the equivalent global ductility, and consequently the global equivalent damping, since the pier displacement does not increase after yielding of the isolator. It has also been proposed that the global effective damping of the structure can be approximately computed from the following equation, which expresses a weighted average of the different damping ratios (M_i is the tributary mass of pier i and M_d is the total mass of the deck).

$$\xi_b = \frac{\sum \xi_i M_i}{M_d} \tag{5}$$

Equations 1 to 5 allow the calculation of a correction factor to be applied to the elastic displacement response spectrum.

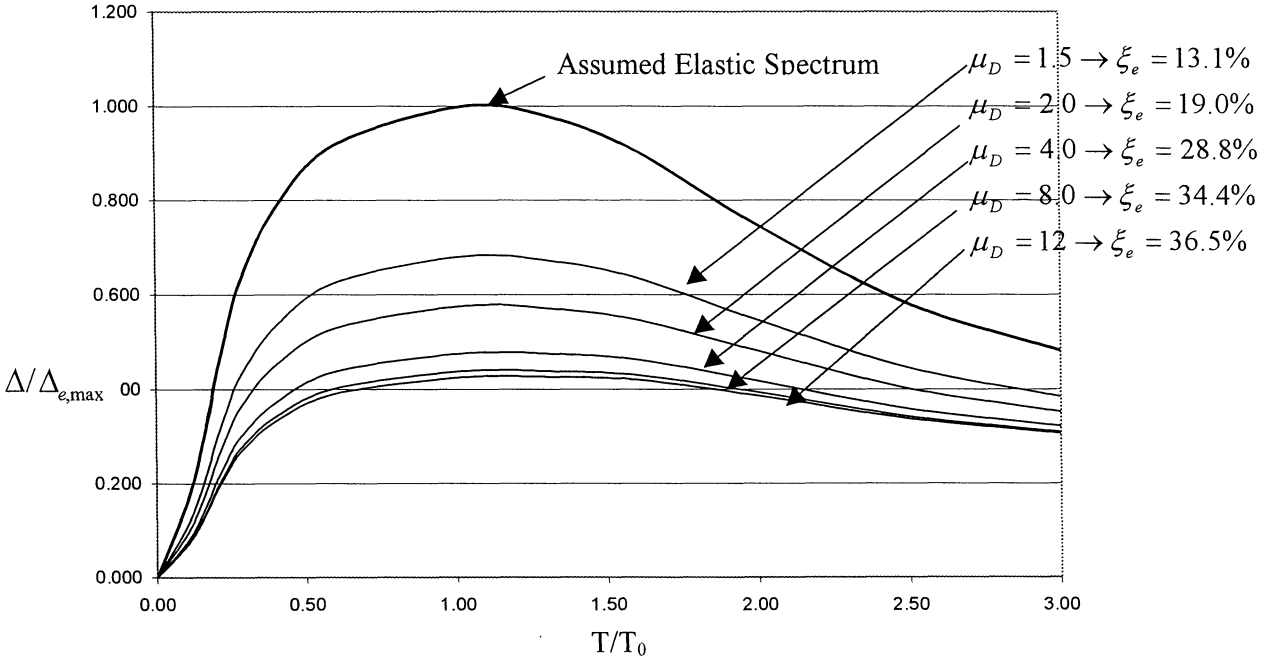


Figure 1: Displacement response spectra as function of energy dissipation, obtained correcting an assumed elastic spectrum using equations 1, 2 and 3 (with $\alpha = 0.40$, $\beta = 0.80$, and $\xi_v = 2$).

Definition of a "displacement reduction factor"

Conceptually, the factor η is similar to the force reduction factor used in traditional force approaches, it could be defined *displacement reduction factor*, and there is no more reason for it to be strictly derived from ductility or energy dissipation properties of the structure, than *for a force reduction factor*. The displacement reduction factor can therefore be considered a free design parameter, where a number of structural variables can be condensed. Its value may then be set as a function of expected structural response, limit state of interest, duration or energy content of the design motion. Considering force and displacement based approach from this point of view, the main conceptual differences are: the consideration of a secant stiffness, and therefore of a more

appropriate equivalent period of vibration, and a much easier tuning of the behavior factor related to energy aspects only. Displacement capacity aspects are obviously explicitly considered.

If a number of different bridges are considered and reasonable values are assumed for the parameters required in equations 1 to 5 it is easy to verify that η is likely to result around 0.5 – 0.6, with a lower limit around 0.40 and an upper limit around 0.75.

Definition of a "response index"

The displacement based design approach adopted in this paper implies that a target displacement shape of the bridge is defined. The displacement shape of the bridge ($\underline{v}$) deck can be expressed as a linear combination of the eigenvector matrix of the equivalent structure ($\underline{\underline{\Phi}}$) and a vector $\underline{y}$, as expressed by the following equations:

$$\underline{v} = \underline{\underline{\Phi}}\,\underline{y} \tag{6}$$

$$y_i = \frac{\underline{\Phi}_i^t \underline{\underline{M}}\,\underline{v}}{\underline{\Phi}_i^t \underline{\underline{M}}\,\underline{\Phi}_i} \tag{7}$$

The displaced shape produced by the earthquake motion can be expressed in terms of the modal components as:

$$\underline{v} = \underline{\underline{\Phi}}\,\underline{z} \tag{8}$$

$$\underline{z}_i = \beta_i S_{Di} \tag{9}$$

where β_i are the modal participating factor and S_{di} are the spectral displacements obtained from the response spectra scaled to the design values of the peak ground acceleration.
In case of linear response it is then trivial to observe that the target displacement shape will be obtained when the vector $\underline{y}$ is equal to the vector $\underline{z}$. According to their definition the component z_i are positive but their sign during a seismic excitation depends on how the earthquake 'activates' the initial phase of the shapes. For the case of a 2 d.o.f system the possible combinations of the signs of z_1 and z_2 identify 4 vectors $\underline{z}$.

The comparison between the two vectors can be performed calculating the modulus of the difference vector $\left|\underline{y} - \underline{z}^y\right|$ in the quadrant in which lies the vector $\underline{y}$ and is expressed as.

$$R_D = \left|\underline{y} - \underline{z}^y\right| = \frac{\sqrt{\sum_{i=1}^{m} \left(|y_i| - z_i\right)^2}}{\sqrt{\sum_{i=1}^{m} (y_i)^2} + \sqrt{\sum_{i=1}^{m} (z_i)^2}} \tag{10}$$

In case of non-linear response of the structure this index will not work properly, since the strengths of the piers have not been considered and it is well possible that a pier will still be elastic when another has penetrated significantly into the non-linear range. If an "equivalent linear structure" is being used a different displacement implies a different force, while in a non-linear simulation the forces will remain constant after yielding.

To overcome the problem it is necessary to include a measure of the difference between the yield strength of each pier and the force that would be reached with a hypothetical elastic response, possibly introducing a second index, as follows:

$$R_F = \frac{\left(\sqrt{\sum_{i=1}^{n}(V_i - k_{ei}\Delta_{ei})^2}\right)}{\sqrt{\sum_{j=1}^{n} V_j^2}} \tag{11}$$

where V_i are the strengths of the isolators, k_{ei} are the equivalent stiffness of the pier-isolator systems and Δ_{ei} are the assumed target displacements.

A single index has been finally obtained combining R_D and R_F, possibly as follows:

$$R = 1 - \frac{1}{2}(R_D + R_F) \tag{12}$$

i.e.:

$$R = 1 - \frac{1}{2}\left(\frac{\sqrt{\sum_{i=1}^{m}(|y_i| - z_i)^2}}{\sqrt{\sum_{i=1}^{m}(y_i)^2} + \sqrt{\sum_{i=1}^{m}(z_i)^2}} + \frac{\left(\sqrt{\sum_{i=1}^{n}(V_i - k_{ei}\Delta_{ei})^2}\right)}{\sqrt{\sum_{j=1}^{n} V_j^2}}\right) \tag{13}$$

To summarize, the first term of the index is a measure of the difference between a vector containing the product of modal mass and spectral amplification and a vector containing the coefficients producing the target deformed shape, when applied to the modes. The second term is a measure of the difference between the yield strength of each pier and the force that would be reached with an hypothetical elastic response.

Design of isolation systems for existing bridges

When an isolation system for an existing bridge has to be designed, strength and stiffness of the piers are known. A few principles will guide the selection of the appropriate isolation devices:

- the strength of each one of them should be lower than the yielding strength of the corresponding pier;
- the strength and deformation capacity of each isolator should be selected to minimize the deck absolute displacements and the deck deformation (i.e. the relative displacements at the pier tops).

It is also desirable that the displacements predicted in the design phase are not too different from the actual displacements.

An approach proposed to design isolating systems for existing bridges (1) can be summarized as follows:

1. Choice of a deformed shape, based on maximum and minimum drifts, on symmetry considerations, on the first mode of vibration of the deck.
2. Computation of the contribution of each pier displacement to the corresponding deck displacement, assuming in the first trial a complete exploitation of the pier strength (with an appropriate safety factor, here taken as 0.85).
3. Computation of the displacement reduction factor (equations 1 – 5)
4. Computation of eigenvalues and eigenvectors of the linear equivalent structure (using the secant stiffness to the target displacement of each pier-isolator system).
5. Computation of the response index (equation 10)

6. Computation of the regularity index. As discussed, if R is close to 1 the bridge is likely to be able to produce the deformed shape assumed, the displacement demand of each pier-isolator system will be therefore similar to the displacement assumed in the preliminary design phase. In case of a low value of the index the procedure will be repeated selecting a different displacement shape and/or different yield strengths for the isolators. In principle the strength of the isolator will be kept as high as possible to reduce the displacements.

Clearly, this last step contains the essence of the design, particularly because no precise guidance is given to select appropriate revisions for displacement shapes and isolators strengths. This last variable is the real crucial parameter for an optimal design.

The set of displacements, strength and stiffness assumed for the piers should, in principle, be so that the response index becomes close to 1, when calculated with the assessment spectrum corrected with the assumed value of displacement reduction factor. In this case it is likely that the results of a non-linear analysis will be similar to the results obtained from the static, linear equivalent, design approach.

The procedure is based on an algorithm that searches the extreme values of implicit functions which select in each step a tentative displacement shape and check whether the value of R is close to 1. The procedure outlined above has been implemented into a computer program, whose structure is summarized in Figure 2.

Design of new bridges using isolation system

A procedure to design new bridges using isolation systems has been proposed by Priestley et al (10) and will not be repeated here. It is worth noticing, however, that the philosophy of this procedure is such that a very different design of the pier reinforcement will result, if compared with the case of standard non-isolated bridge. Actually the fundamental assumption consists in imposing a rigid deformation of the deck, obtained by forcing each pier-isolator system to respond with the same peak force. This implies that taller piers should be capable to resist higher bending moments, and therefore they will require larger reinforcement percentage than shorter piers. Clearly this is exactly the opposite of what usually happens for non-isolated bridges, where shorter piers are stiffer, tend to attract larger forces and therefore require larger reinforcement percentages. On the contrary this is consistent with the standard requirement of a gravity (non-seismic) design, in which case higher piers normally require larger strength, and therefore larger reinforcement for the case of similar sections.

The assumption of having a rigid deformation of the deck allows a very good estimation of the expected response, since a SDOF model will be accurate in describing the structure response. On the other side, clearly, this will inhibit to take any advantage of significant "low cost" strength when it is available, for example when strong abutments are easy to be constructed.

The method described above can be applied to new bridges, as well. In this case, the initial strengths of piers and abutments will serve as a starting condition, but the response index will be optimized on the displacement shape only, accepting large variations in the required strengths.

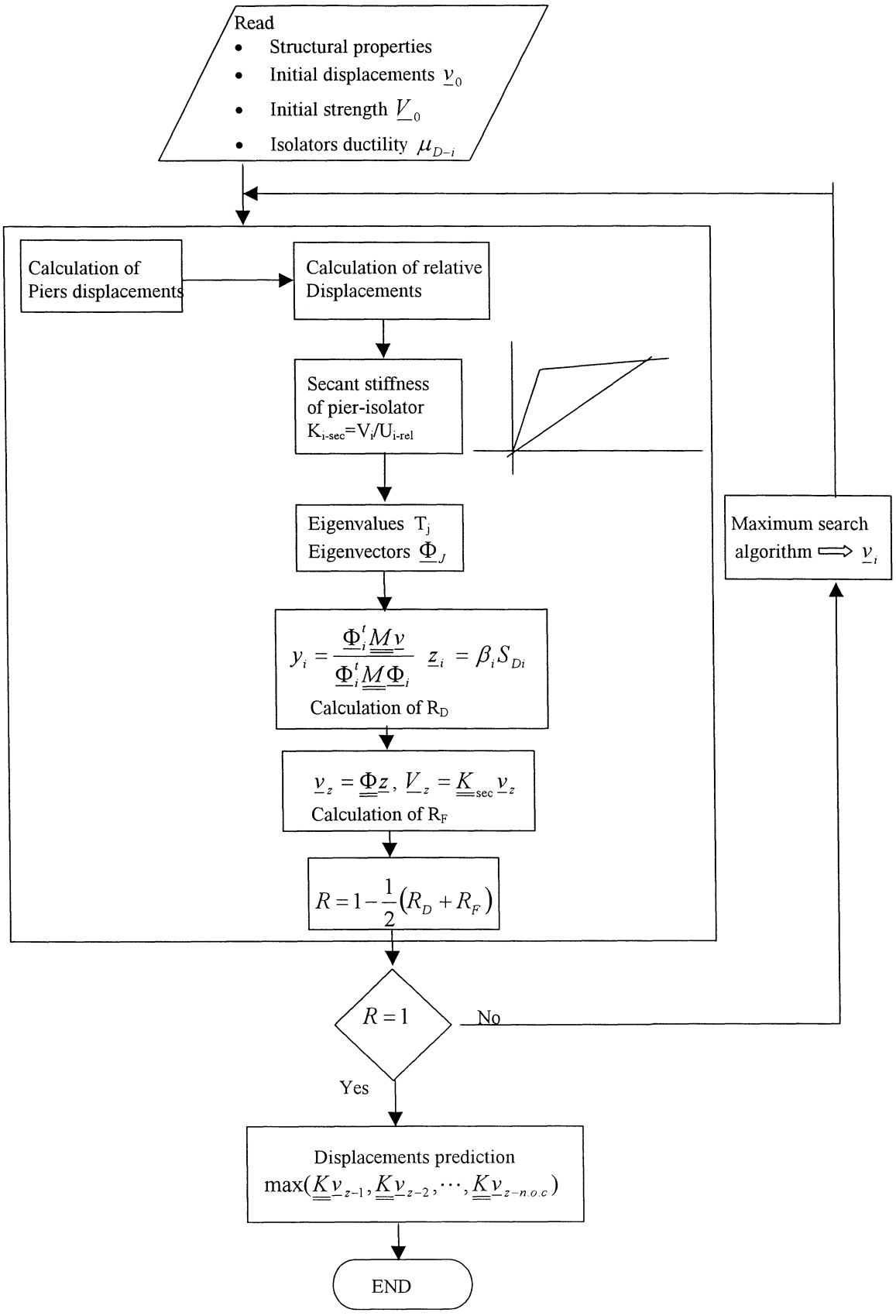


Figure 2: Flow chart of the computer program used to design "optimal" isolation systems

Results of design examples

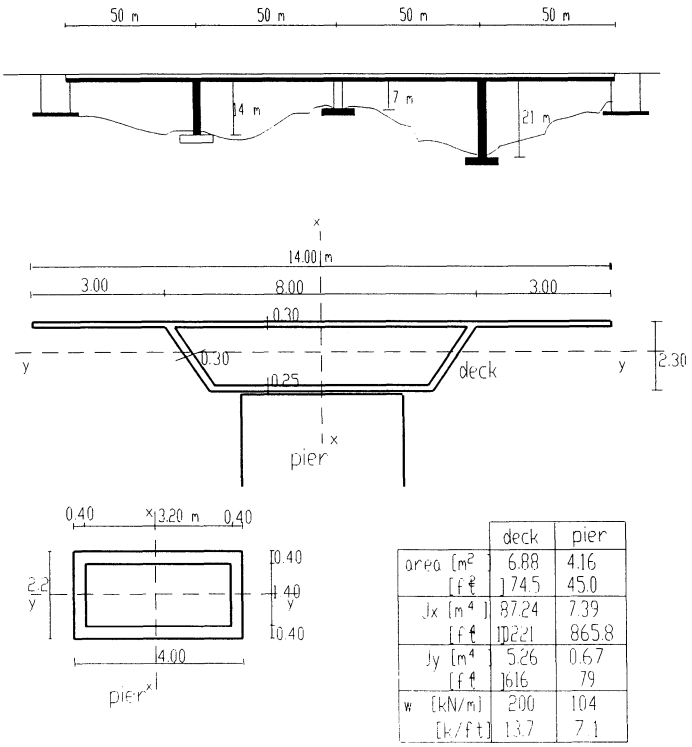
A few design examples are presented in Figure 4 to Figure 15 for the case of existing bridges, comparing the results predicted by the design approach with the results of full non-linear analyses. All bridges are similar to the bridge depicted in Figure 3, with variable pier lengths and constant reinforcement percentage equal to 1%. In Figure 4 to Figure 15 the number in the captions (e.g. B113) indicates the length of the piers, 1 means 7meters, 2 means 14 meters, etc. In each one of figures three bridges are depicted, showing the results obtained for weaker abutments, stronger abutments and applying a "minimum strength approach" (1).

It is evident that the optimal approach, i.e. the use of the response index, results in significantly improved design:

- In most cases the elimination of one or more isolator is recommended;
- The deck displacements are in general significantly smaller, particularly when some higher resistance is available at the abutments;
- The displacement profiles resulting from the non-linear analyses are closer to those predicted and less dispersed.

The importance of stronger abutments results clearly from the plots, but it is also possible to note that the algorithm does not always allow the exploitation of stronger abutments when a weak pier is next to them, unless a strong pier on the other side offers a retention. In this last case the weak, possibly flexible pier is somehow excluded from the seismic response.

The cases considered for the case of new bridges (not reported here), where the piers and abutments strength essentially becomes a free parameter, confirms the indications given above. The main noticeable effect, with respect to the geometrically similar bridges, is the considerable increment of strength recommended for taller and more flexible pier. This last result points towards the same direction intuitively suggested by Priestley et al. (10), i.e. to try to design bridges with piers of similar shear strengths (i.e. with flexural strength somehow proportional to the height of the pier).



	deck	pier
area [m²]	6.88	4.16
[ft²]	74.5	45.0
Jx [m⁴]	87.24	7.39
[ft⁴]	2221	865.8
Jy [m⁴]	5.26	0.67
[ft⁴]	616	79
w [kN/m]	200	104
[k/ft]	13.7	7.1

Figure 3: The bridge type used for the examples

Acknowledgments

The research presented in this paper has been funded by the Italian "Gruppo Nazionale per la Difesa dai Terremoti" (GNDT) and by the European Union, contract number ERBFMRXCT96-0022

References

1. Calvi, G. M. and A. Pavese, Conceptual design of isolation systems for bridge structures, *Journal of Earthquake Engineering*, 1997, 1, 1: 193-218
2. Kowalski M.J. and Priestley M.J.N., Displacement-Based Design of RC Bridge Columns in Seismic Regions, *Earthquake Engineering and Structural Dynamics*, 24: 1995
3. Calvi, G. M. and G. R. Kingsley, Displacement based design of multi-degree-of-freedom bridge structures, *Earthquake Engineering and Structural Dynamics*, 1995, Vol. 24, 1247-1266
4. Priestley M.J.N. and Calvi G.M., Concepts and procedures for direct displacement-based deisgn and assessment, *Proc. of Workshop on Seismic Design Methodologies for the Next generation of Codes*, Bled, Slovenia, 24-27 June, 1997, pp.171-181
5. Calvi, G. M., Performance-based approaches for seismic assessment of existing bridges, *Proc. of the XI ECEE*, Paris, 1998
6. Shibata, A. and M. A. Sozen, Substitute-structure method for seismic design in reinforced concrete, *J. Str. Div. ASCE*, 102: 1-18, 1976
7. "*Eurocode 8 - Design provisions for earthquake resistance of structures - Part 2: Bridges*", ENV 1998-2, CEN, Brussels, 1994
8. Calvi, G.M., , Performance based assessment procedures for reinforced concrete bridges, *Proc. of the Structural Engineers World Congress*, San Francisco, 1998
9. Priestley, M.J.N. and G.M. Calvi, Concepts and procedures for direct displacement-based design and assessment, in: *Seismic design meth. for the next generation of codes*, Balkema, 1997
10. Priestley, M. J. N., F. Seible and G. M. Calvi, "*Seismic design and retrofit of bridges*", John Wiley, New York, 1996

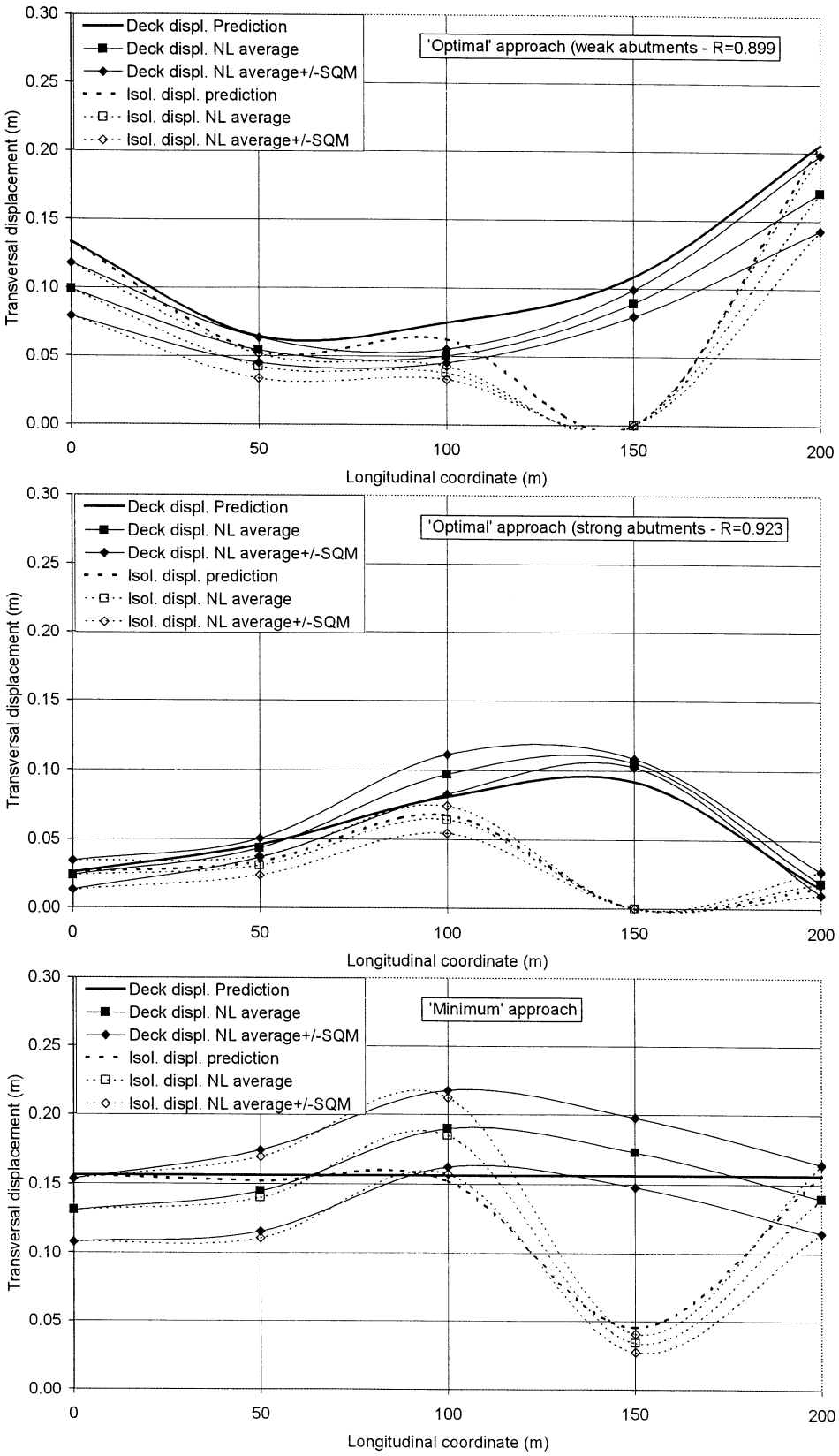
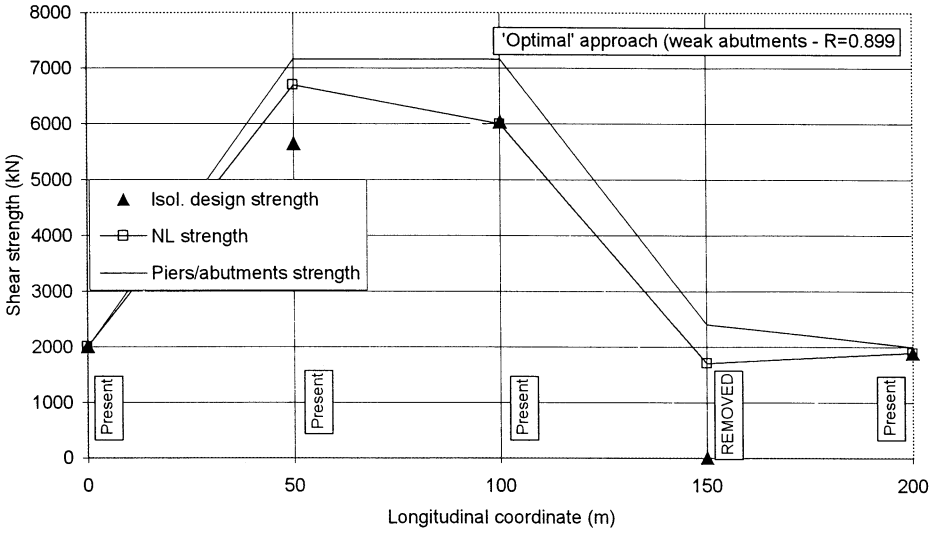
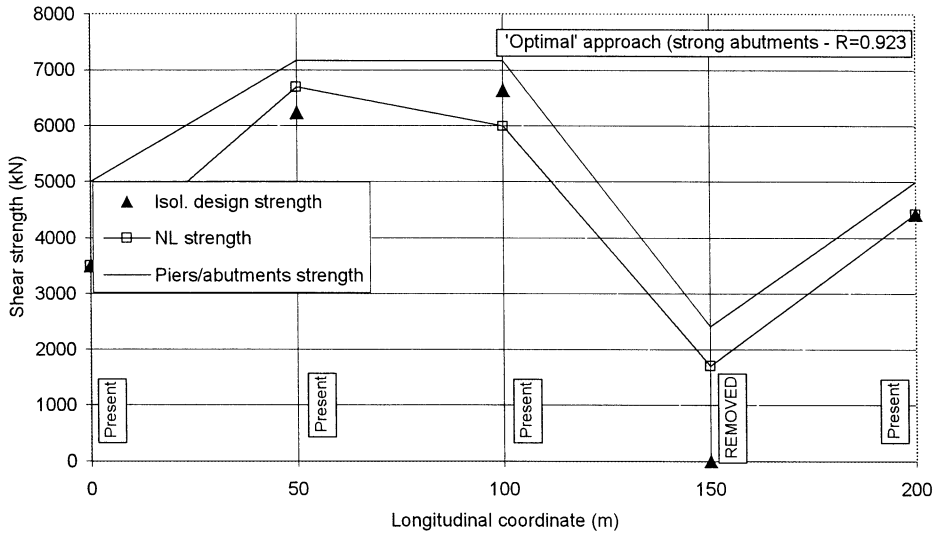


Figure 4: Bridge B113 transversal displacements





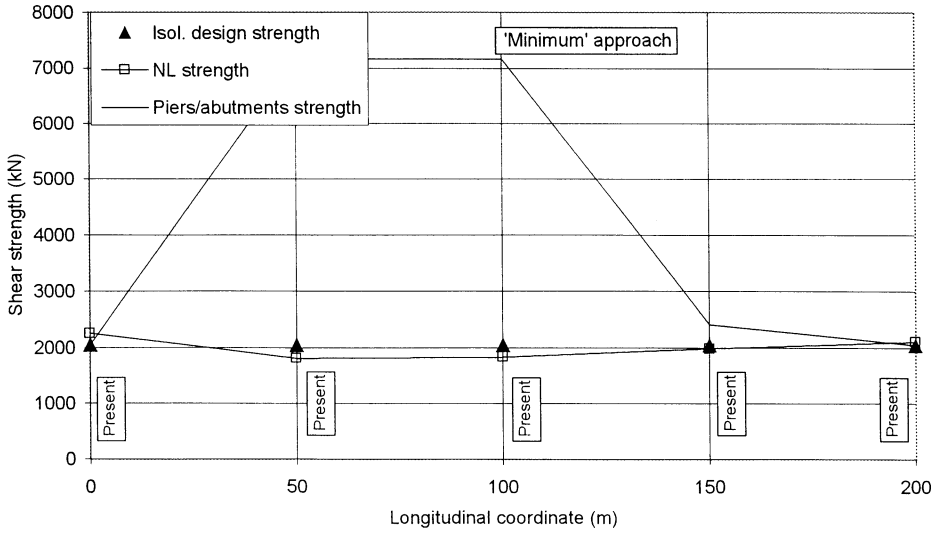


Figure 5: Bridge B113 shear strength

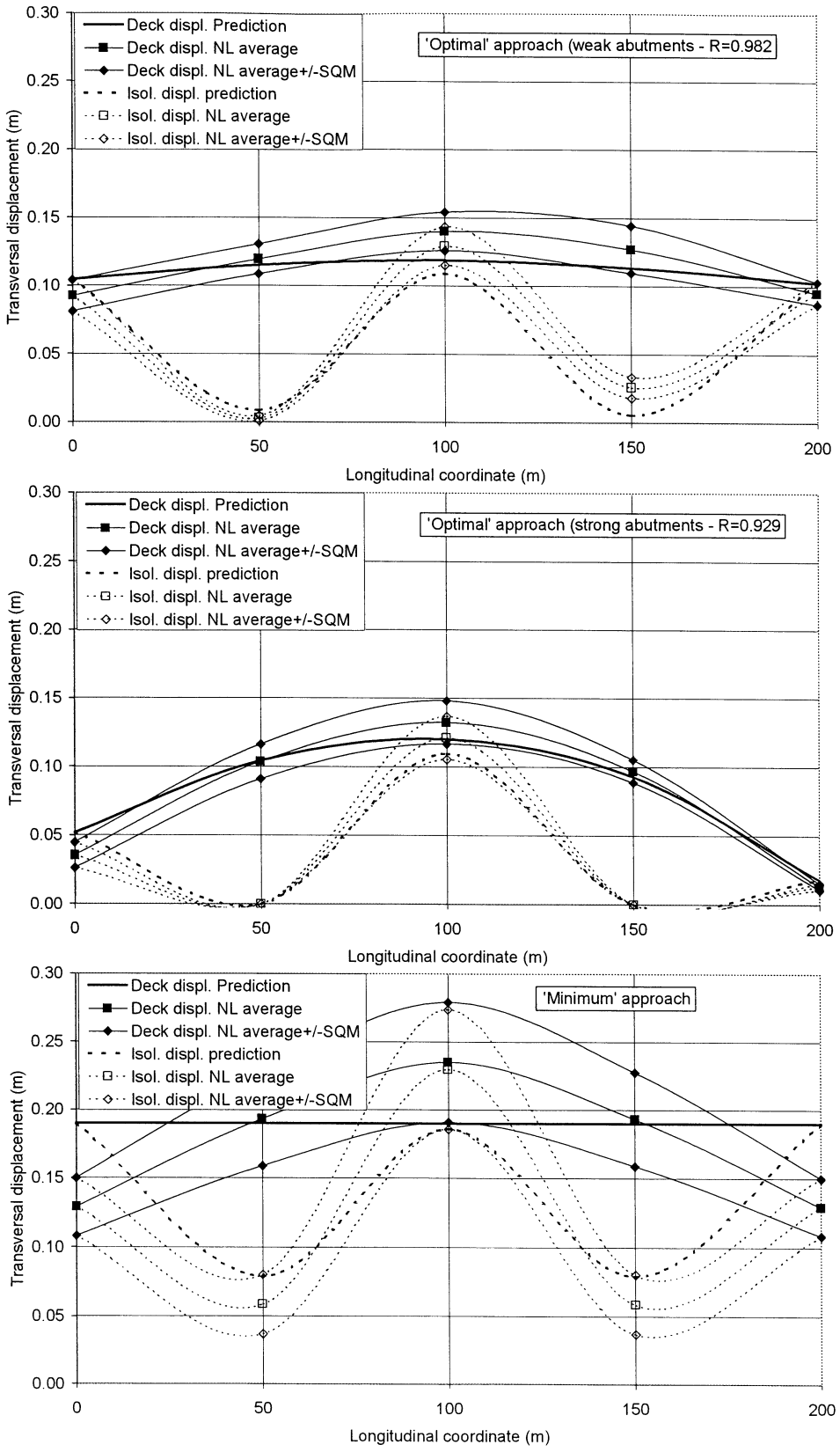


Figure 6: Bridge B313 transversal displacements

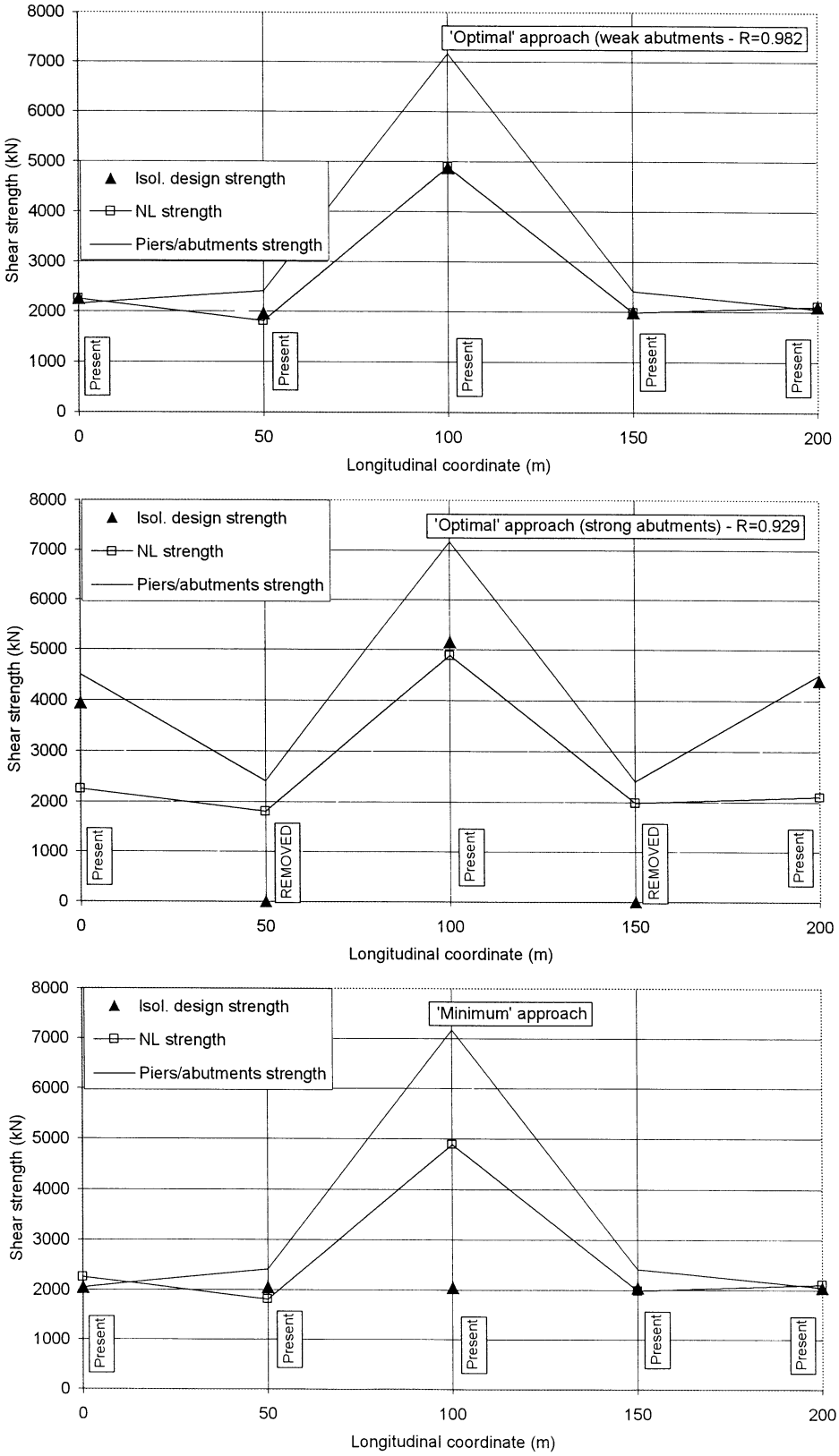


Figure 7: Bridge B313 shear strength

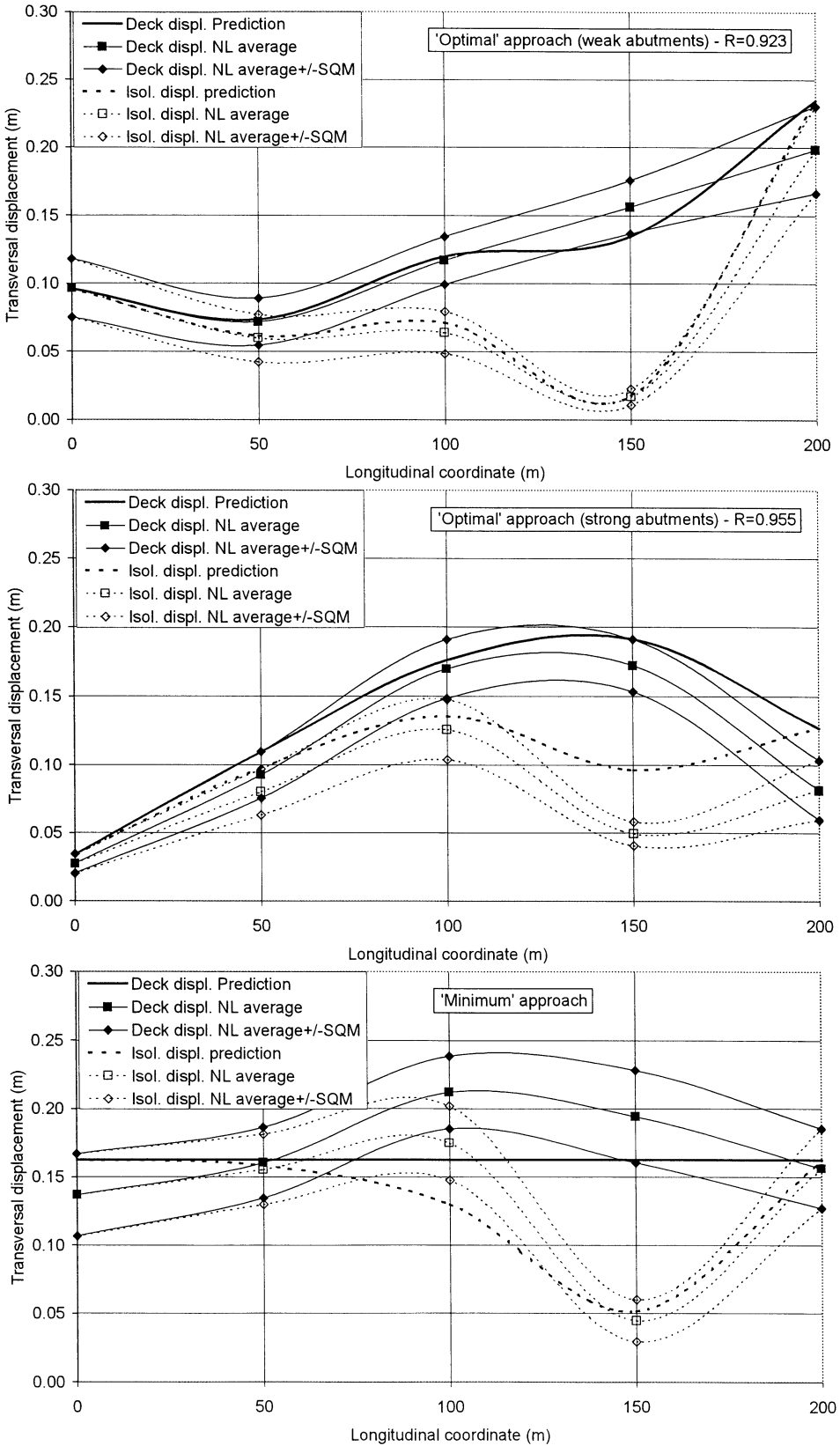
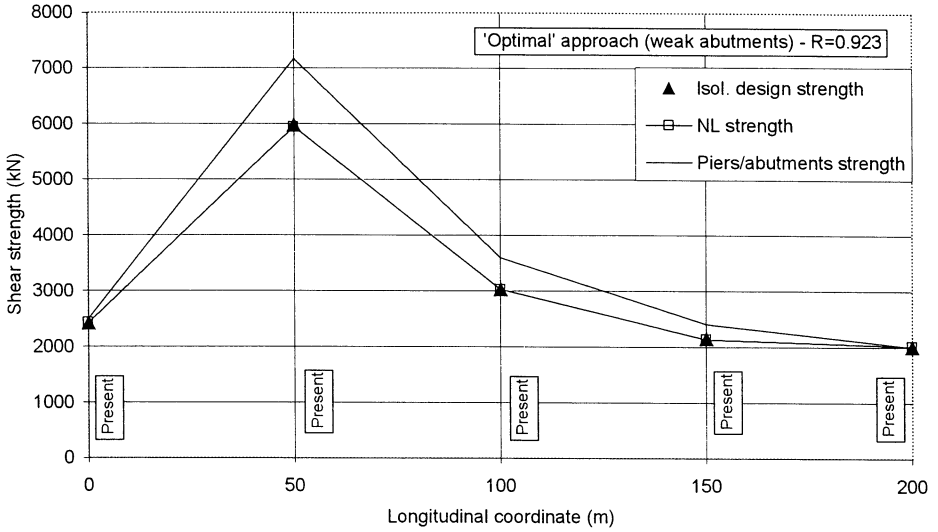
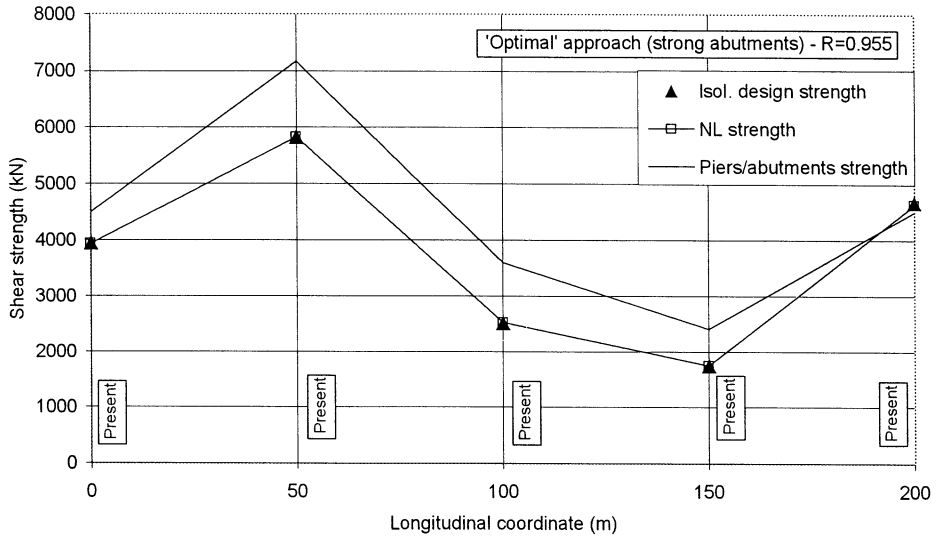


Figure 8: Bridge B123 transversal displacements





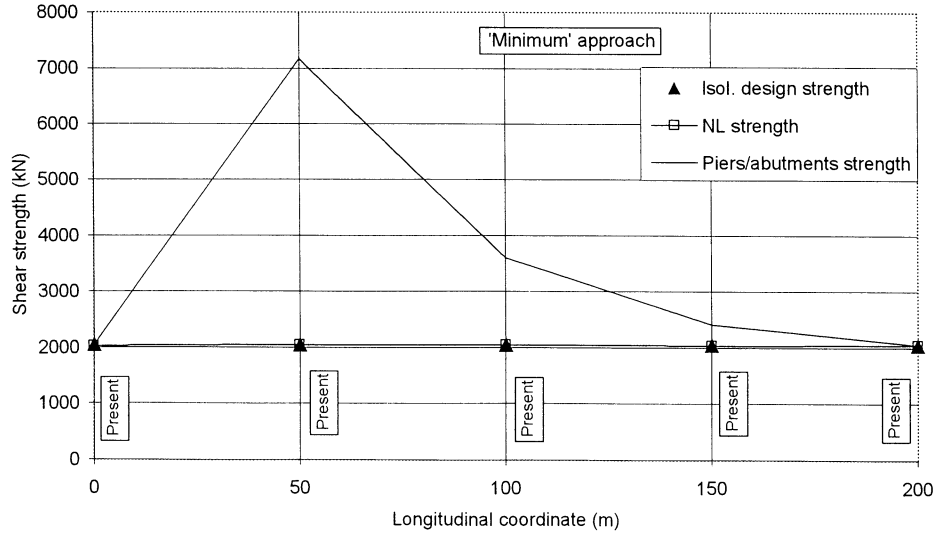


Figure 9: Bridge B123 shear strength

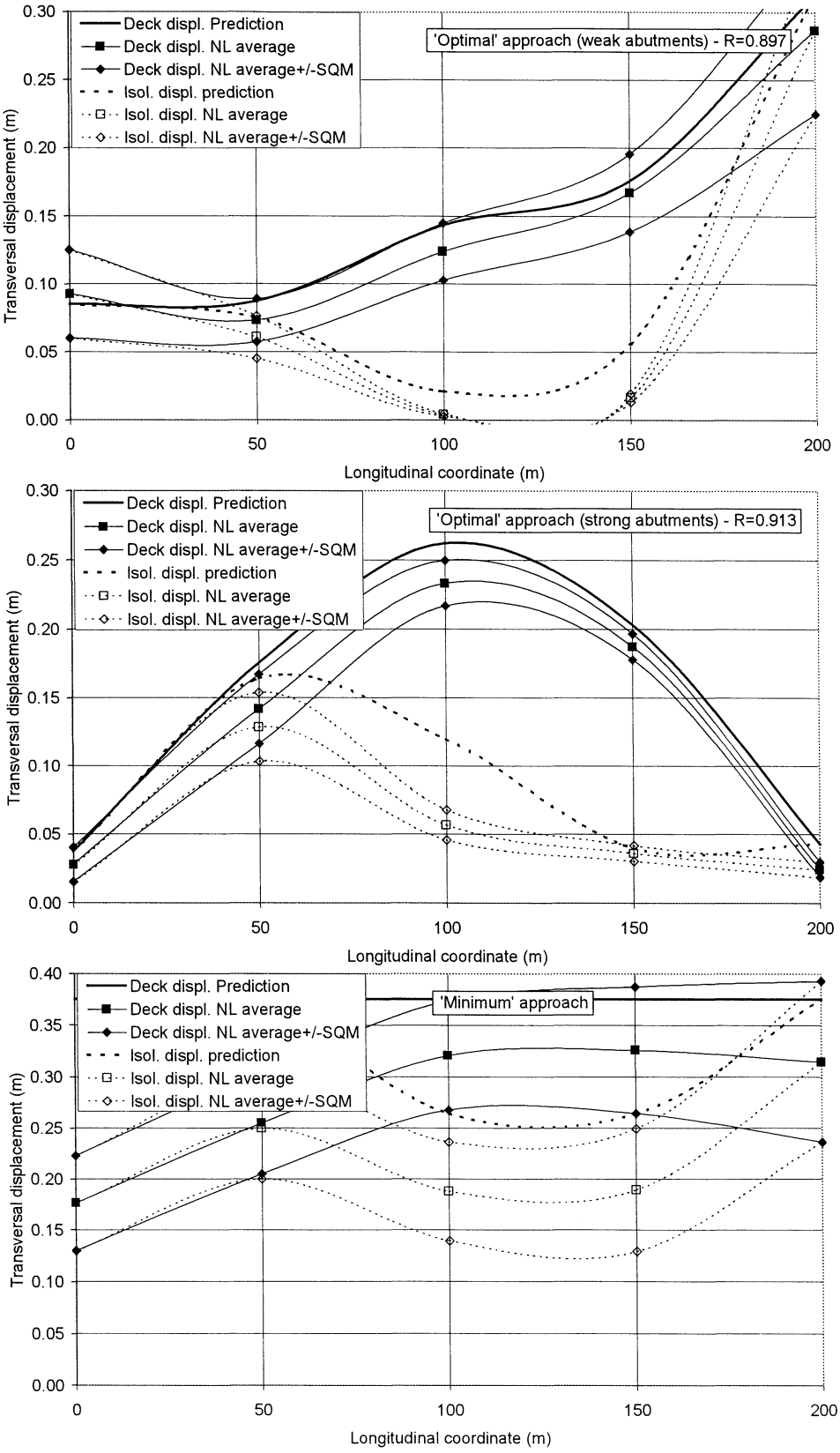
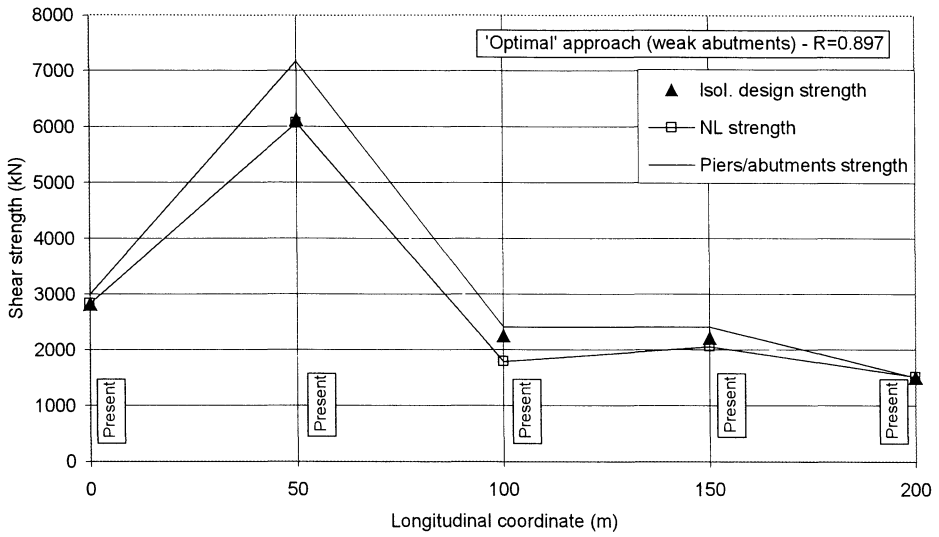
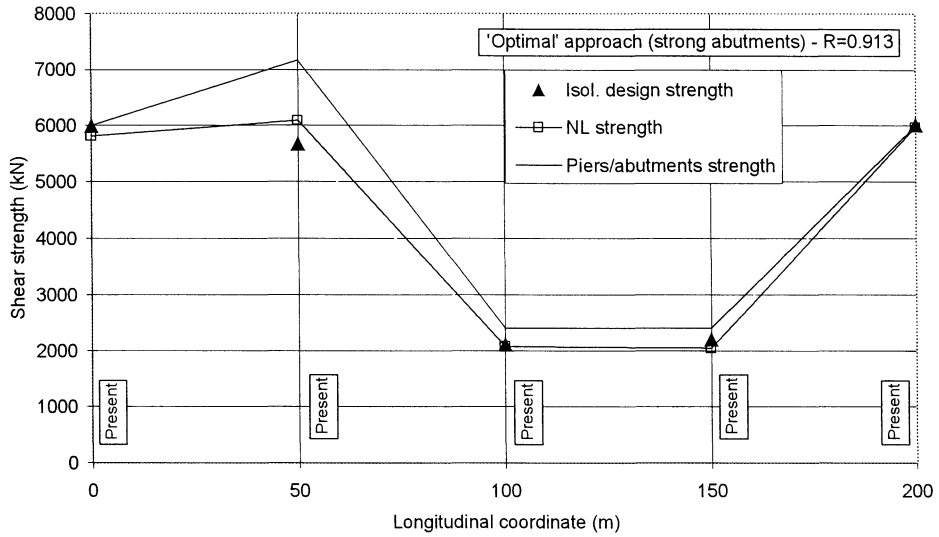


Figure 10: Bridge B133 transversal displacements





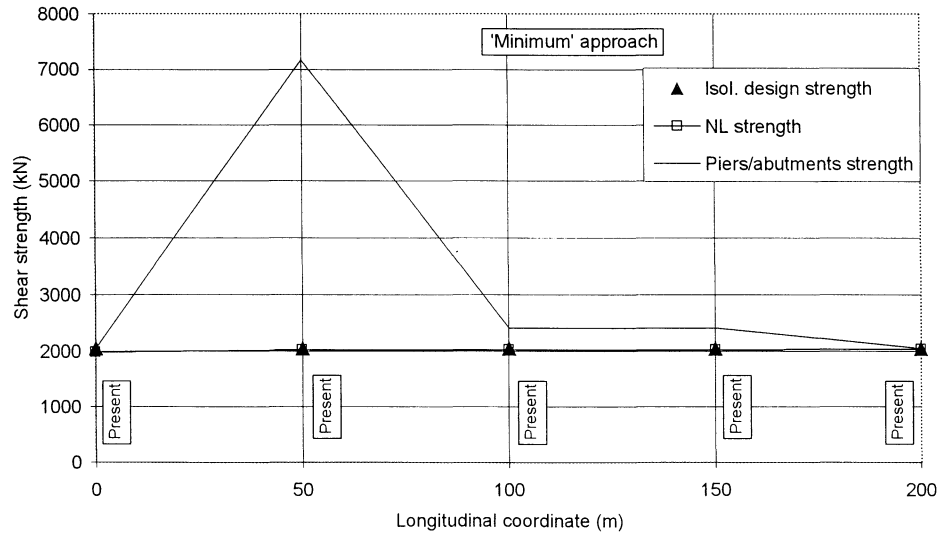


Figure 11: Bridge B133 shear strength

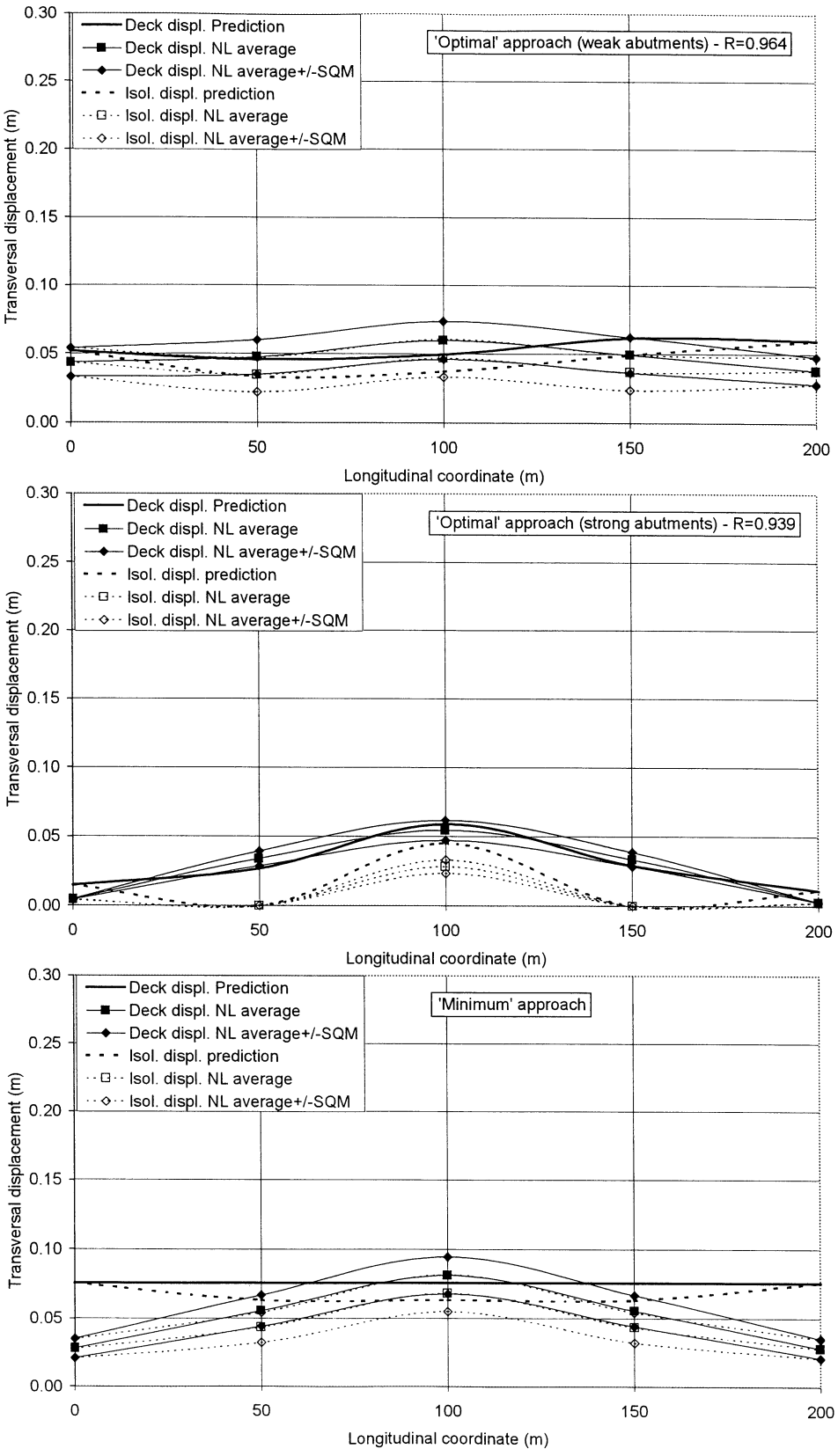
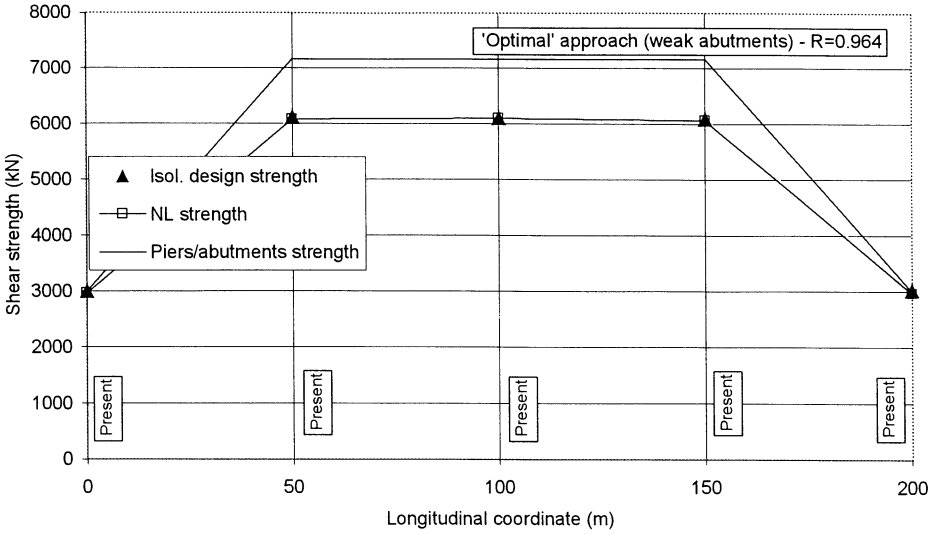
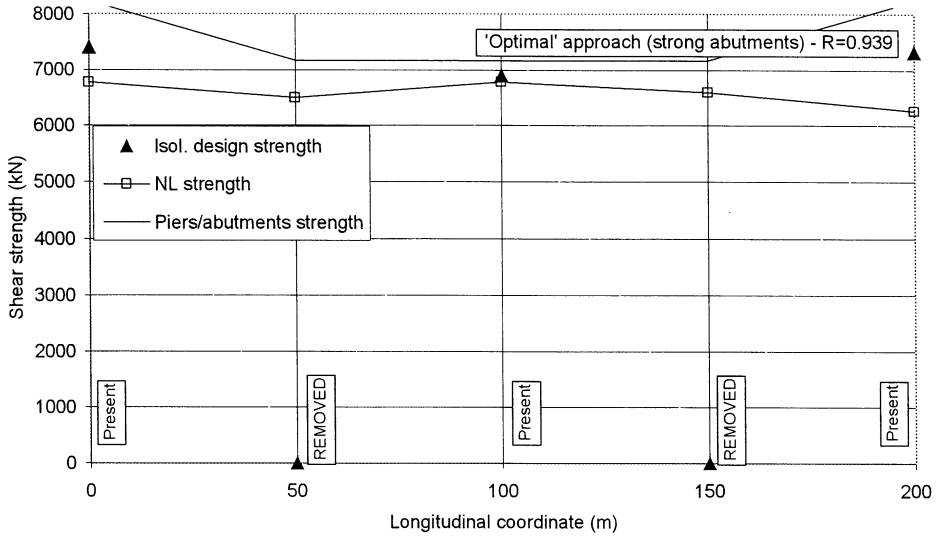


Figure 12: Bridge B111 transversal displacements





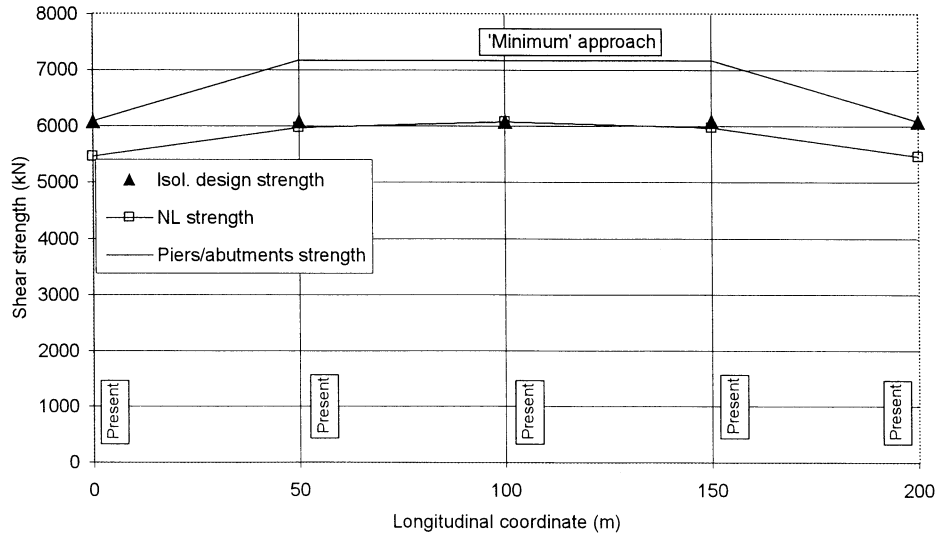
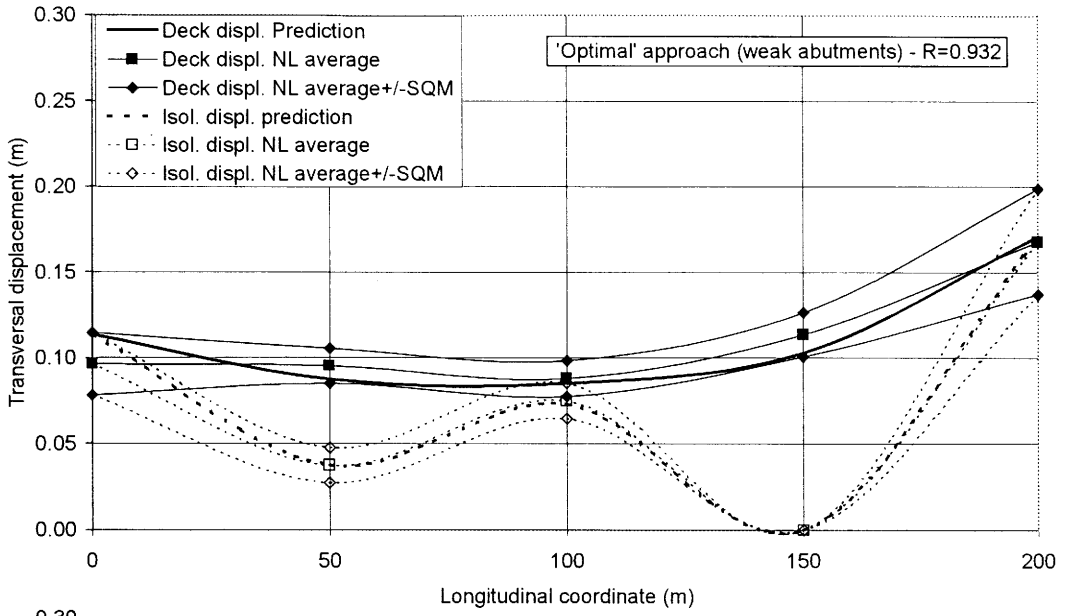
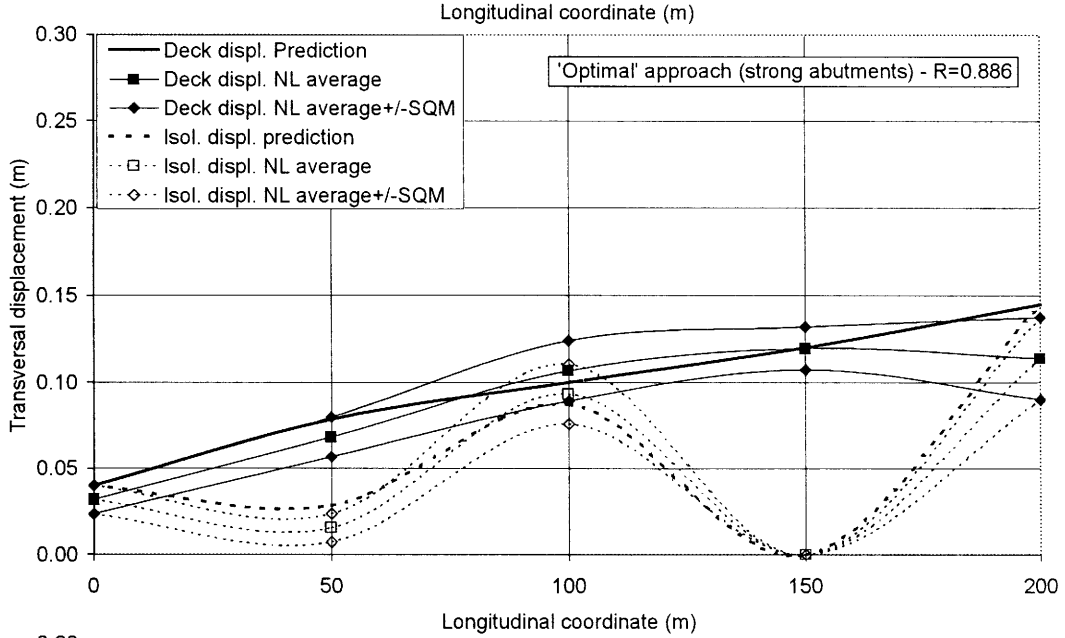


Figure 13: Bridge B111 shear strength





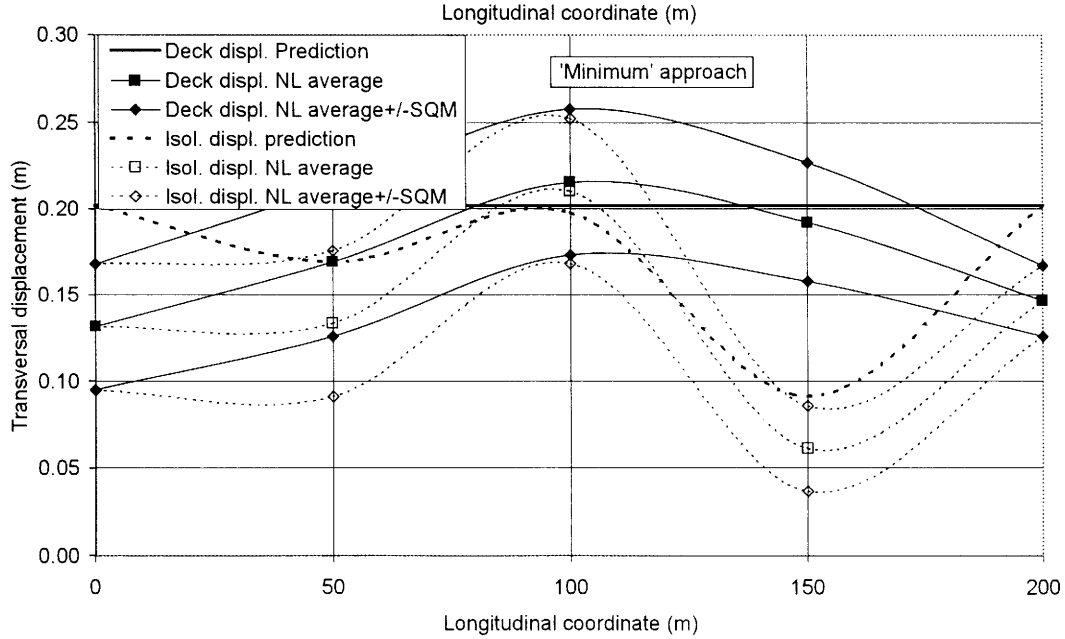


Figure 14: Bridge B213 transversal displacements

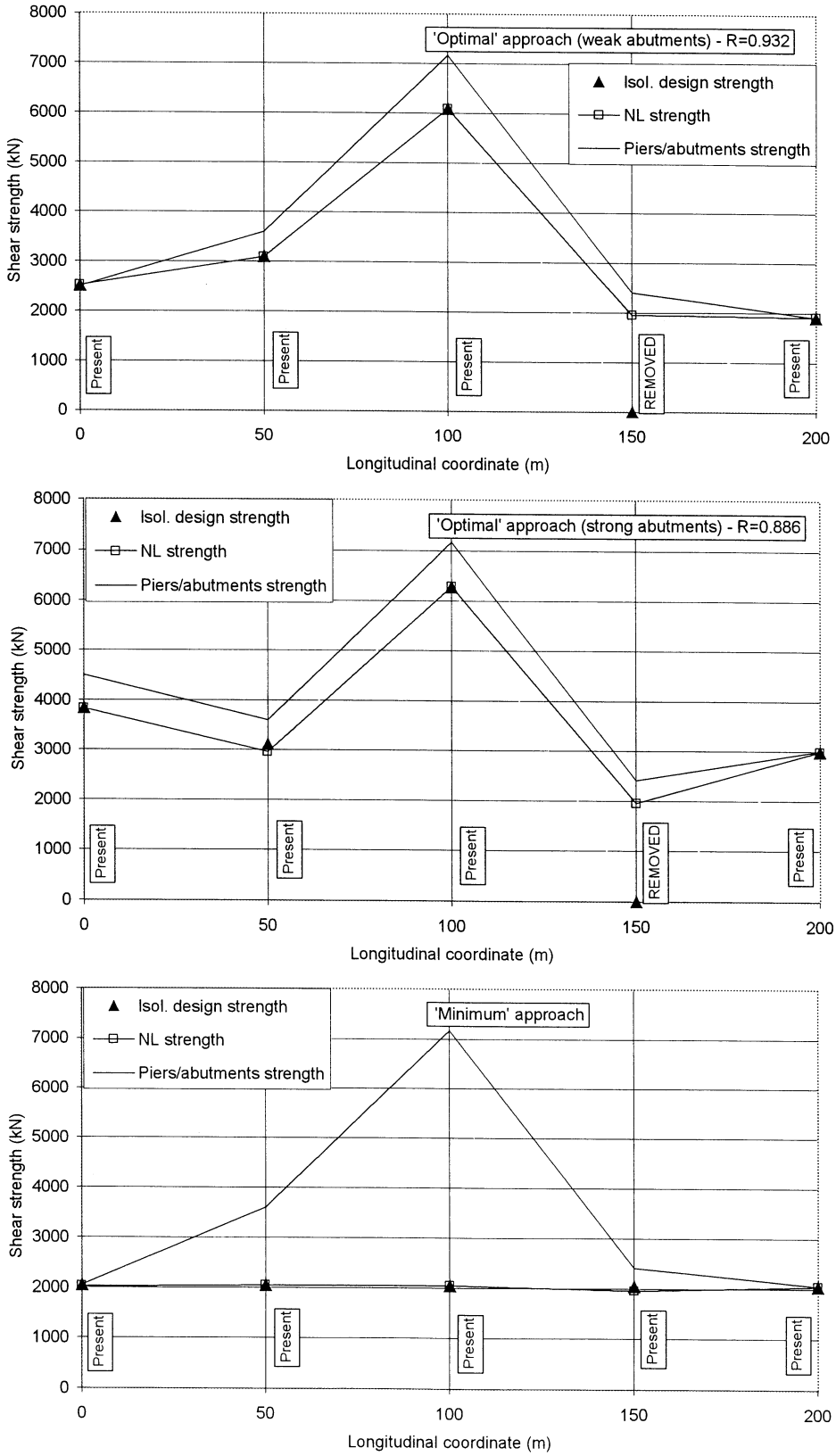
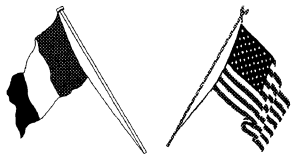


Figure 15: Bridge B213 shear strength



Appendix A

Workshop Agenda

U.S. Participants List

Italian Participants List

US-Italy Workshop on Seismic Protective Systems For Bridges
April 26 - 28, 1998
New York City, NY

AGENDA

SUNDAY, APRIL 26

10:00 am - 3:00 pm	New York City Bridge Tour - hosted by Dr. Bojidar Yanev, Assistant Commissioner, New York City Department of Transportation
7:00 pm	Dinner Hosted by U.S. Side: **Charlotte Restaurant**, Millennium Broadway Hotel

MONDAY, APRIL 27 — **Columbia University, Hecker West Seminar Room #415, Schapiro Center for Engineering and Physical Science Research (CEPSR)**

8:30 am - 9:00 am	Coffee and Gathering (outside meeting room)
9:00 am - 9:15 am	Opening Session - Welcome, Introduction, Announcements
9:15 am - 10:15 am	Session I - State of Practice in Italy and the U.S.
	Italian and European Guidelines for Seismic Design of Isolated Bridges, Franco Braga, Gian Michele Calvi, and Paolo E. Pinto
	Seismic Protective Systems for Bridges in the United States: State-of-the-Art and State-of-Practice, Michael C. Constantinou and Andrew S. Whittaker
10:15 am - 10:45 am	Break
10:45 am –12:00 pm	Session II - G.M. Calvi and F. Seible, session chairs
	The 1997 AASHTO Seismic Isolation Guide Specification, John F. Stanton
	Development of the European Standard on Antiseismic Devices, Agostino Marioni and Renzo Medeot

	Caltrans Bridge Research and Applications of New Technologies, Dorie E. Mellon and Thomas J. Post
	The Analysis and Design of Elastomeric Bearings for Application in Bridges, James M. Kelly
	A Methodology for the Design of Energy Dissipation Devices for the Seismic Protection of Bridges, Vincenzo Ciampi
12:00 pm - 1:30 pm	Lunch: Columbia University, Faculty House, Harison Room (Luncheon Speaker: Professor Raimondo Betti, Columbia University)
1:45 pm - 3:00 pm	Session III - A. De Luca and T. Post, session chairs
	Energy Dissipation as a Technological Answer to Highly Demanding Design Problems, Renzo Medeot
	Seismic Isolation of Railway Bridges, Mauro Dolce, Domenico Liberatore, Corrado Bonuccelli, and Giuseppe Traini
	Applications of Isolation Bearings to Bridges, Manouchehr Karshenas and Iraj I. Kaspar
	Seismic Bearings for Large Span Bridges, Roy A. Imbsen
	Design of the Caltrans Seismic Response Modification Device (SRMD) Test Facility, Gianmario Benzoni Frieder Seible
3:00 pm - 3:30 pm	Break
3:30 pm - 5:00 pm	Discussion on Design Practices/Testing/Specifications in U.S. and Italy
8:00 pm	Dinner Hosted by the Italian Side: **Carmine's Restaurant**, 200 West 44th Street
TUESDAY, APRIL 28	**Columbia University, Hecker West Seminar Room #415, Schapiro Center for Engineering and Physical Science Research (CEPSR)**
8:30 am - 9:00 am	Coffee and Gathering (outside the meeting room)

9:00 am - 10:15 am	Session IV - M. Dolce and H. Capers, session chairs
	Design Criteria for Seismic Isolation Devices, Rosario Ceravolo, Alessandro De Stefano, and Giuseppe Mancini
	Sensitivity of Response of Isolated Bridges to Modeling and Design Parameters - A Case Study, Andrei M. Reinhorn, Vassil K. Simeonov, Grant DeRue, and Michael C. Constantinou
	Effects of Multi-support Excitation on Isolated Bridges, Giorgio Monti and Paolo E. Pinto
	Development of Bridge Fragility Curves, Masanobu Shinozuka
	Testing of Bridges with Isolation/Dissipation Devices at the ELSA Laboratory, Artur V. Pinto, Paolo Negro and Fabio Taucer
10:15 am - 10:45 am	Break
10:45 am – 12:00 pm	Session V - V. Ciampi and M. Lwin, session chairs
	The Use of Advanced Composites in Seismic Retrofitting, Frieder Seible
	Stress Reduction System of Medium Span Bridges Using Semiactive Controls, William Neff Patten, Jinghui Sun and Guangjun Li
	SMA Devices for Seismic Isolation of Bridges: Design and Experimental Behaviour, Mauro Dolce and Roberto Marnetto
	Rocking Columns: An Effective Means of Seismically Isolating a Bridge, John B. Mander R. Contreras and R. Garcia
12:00 pm - 1:30 pm	Lunch: Columbia University, Faculty House, Harison Room
1:30 pm - 2:30 pm	Session VI - F. Braga and M. Karshenas, session chairs
	Modeling of Elastomeric Devices in the Dynamic Linear and Non-linear Range, Antonello De Luca and Giuseppe Faella
	Modeling and Characterization of Seismic Isolation Bearings, Gregory L. Fenves, Wei-Hsi Huang, Andrew S. Whittaker, Peter W. Clark and Stephen A. Mahin

	High Damping Elastomeric Bearings (HDEB): Experimental Tests and Preliminary Results, Franco Braga
	Optimal Design of Isolated Bridges and Isolation Systems for Existing Bridges, Gian Michele Calvi and Alberto Pavese
2:30 pm - 3:15 pm	Discussion on Research Needs: Standardization of Practice/ Codes
3:15 pm - 3:30 pm	Closing Remarks

U.S. – Italy Workshop on Seismic Protective Systems for Bridges
U.S. Participants List

Serafim G. Arzoumanidis
Steinman Boynton Gronquist & Birdsall
110 William Street
New York, NY 10038
212-266-8370 / 212-266-8540
serafim_g_arzoumanidis@parsons.com

Gianmario Benzoni
University of California, San Diego
Division of Structural Engineering
Mail Code 0085
La Jolla, CA 92093-0085
619-534-1432 / 619-534-6373

Raimondo Betti
Columbia University
Dept. of Civil Engrg. and Engrg. Mechanics
610 S.W. Mudd Building
New York, NY 10027
212-854-6388 / 212-854-6267
betti@cucers1.civil.columbia.edu

James N. Bollman
Oregon Department of Transportation
Room 301 Transportation Building
Salem, OR 97310
503-986-3341 / 503-986-3407
james.n.bollman@odot.state.or.us

Harry A. Capers, Jr.
Manager - Structural Engineering
New Jersey Dept. of Transportation
1035 Parkway Avenue, CN 615
Trenton, NJ 08625-0615
609-530-2557 / 609-530-5777
hcapers@cpm.dot.state.nj.us

George Christian
New York State Dept. of Transportation
Building 5, Room 600
1220 Washington Avenue
Albany, NY 12232
518-457-4453 / 518-485-5165
gchristian@gw.dot.state.ny.us

Michael C. Constantinou
State University of New York at Buffalo
Dept. of Civil and Environ. Engrg.
132 Ketter Hall
Buffalo, NY 14260
716-645-2114 x2404 / 716-645-3733
constan1@eng.buffalo.edu

Gregory Fenves
University of California, Berkeley
Department of Civil and Environ. Engineering
729 Davis Hall
Berkeley, CA 94720
510-643-8543 / 510-643-8928
fenves@ce.berkeley.edu

Ian M. Friedland
National Center for Earthquake Engrg. Research
State University of New York at Buffalo
102 Red Jacket Quadrangle
Buffalo, NY 14261-0025
716-645-3391 / 716-645-3399
imf@acsu.buffalo.edu

Hamid Ghasemi
Federal Highway Administration, HNR-10
Turner-Fairbank Highway Research Center
6300 Georgetown Pike
McLean, VA 22101
703-285-2447 / 703-285-2766
hamid.ghasemi@fhwa.dot.gov

Chia Hung
Bureau of Bridge
New York City Dept. of Transportation
2 Rector Street, 7th Floor
New York, NY 10006
212-788-9016

Roy A. Imbsen
Imbsen & Associates, Inc.
9912 Business Park Drive
Suite 130
Sacramento, CA 95827
916-366-0632 / 916-366-1501
raimbsen@imbsen.com

Manouchehr Karshenas
Illinois Department of Transportation
Bureau of Bridges and Structures
2300 Dirksen Parkway
Springfield, IL 62764
217-785-3054 / 217-782-7960

James M. Kelly
Earthquake Engineering Research Center
1301 South 46th Street
Richmond, CA 94804
510-231-9480 / 510-231-5696
jmkelly@eerc.berkeley.edu

M. Myint Lwin
Washington State Dept. of Transportation
Transportation Building
P.O. Box 47340
Olympia, WA 98504-7340
360-705-7207 /360-705-6814
lwinm@wsdot.wa.gov

John B. Mander
State University of New York at Buffalo
Dept. of Civil, Structural and Environ. Engrg.
230 Ketter Hall
Buffalo, NY 14260
716-645-2114 x2418 / 716-645-3733
jmander@acsu.buffalo.edu

Dorie Mellon
California Dept. of Transportation
Engineering Service Center, MS9
1801 30th Street, West Building
Sacramento, CA 95816
916-227-8850 / 916-227-8089
dmellon@trmx3.dot.ca.gov

William N. Patten
Center for Structural Control
University of Oklahoma
865 Asp Avenue, Felgar Hall
Norman, OK 73019
405-325-1749 / 405-325-1088
wpatten@ou.edu

Tom Post
California Dept. of Transportation
Office of Earthquake Engineering
Division of Structures, MS-9
P.O. Box 942874
Sacramento, CA 94274-0001
916-227-8728 / 916-227-8898
tpost@trmx3.dot.ca.gov

Andrei Reinhorn
State University of New York at Buffalo
Dept. of Civil and Environ. Engrg.
232 Ketter Hall
Buffalo, NY 14260
716-645-2114 x2419 / 716-645-3733
reinhorn@civil.eng.buffalo.edu

Frieder Seible
Powell Structural Research Laboratories
University of California, San Diego
Mail Code 0085
La Jolla, CA 92093-0085
619-534-4640 / 619-534-6373
seible@ucsd.edu

Masanobu Shinozuka
University of Southern California
Department of Civil Engineering
3620 S. Vermont Avenue, KAP 254
Los Angeles, CA 90089-2531
213-740-9528 / 213-740-9529
shinozuk@usc.edu

Glenn Smith
Federal Highway Administration
400 Seventh Street, SW
Washington, DC 20590
202-366-8795 / 202-366-3077

John F. Stanton
University of Washington
Department of Civil Engineering
More Hall, FX-10
Seattle, WA 98195
206-543-6057 / 206-543-1543
stanton@u.washington.edu

Andrew S. Whittaker
Earthquake Engineering Research Center
University of California, Berkeley
1301 South 46th Street
Richmond, CA 94804-4698
510-231-9554 / 510-231-9471
asw@eerc.berkeley.edu

Bojidar Yanev
New York City Dept. of Transportation
2 Rector Street
New York, NY 10006
212-788-2030 / 212-788-2027

W. Phillip Yen
Federal Highway Administration, HNR-10
Turner-Fairbank Highway Research Center
6300 Georgetown Pike
McLean, VA 22101
703-285-2315 / 703-285-2766
pyen@cais.com

Ray J. Zelinski
California Dept. of Transportation
Office of Earthquake Engineering, MS-9
P.O. Box 942874
Sacramento, CA 94274-0001
916-227-8806 / 916-227-8898
rzelins1@trmx2.dot.ca.gov

U.S. - Italy Workshop on Seismic Protective Systems for Bridges
Italian Participants List

Franco Braga
Dipartimento di Strutture
Geotecnica e Geologia Applicata (DiSGG)
Università della Basilicata
Via della Tecnica 3
85100 Potenza
Italy
39-971-474-607 or 609 / 39-971-57477
braga@unibas.it

Gian Michele Calvi
Dipartimento di Meccanica Strutturale
Università degli Studi di Pavia
Via Ferrata 1
27100, Pavia
Italy
39-382-505461 / 39-382-528422
calvi@gndt.unipv.it

Vincenzo Ciampi
Dipartimento di Ingegneria Strutturale e Geotecnica
Università di Roma "La Sapienza"
Via Eudossiana, 18
00184, Roma
Italy
39-6-44585299 / 39-6-4884852
ciampi@scilla.ing.uniroma1.it

Antonello De Luca
Università di Napoli "Federico II"
Istituto di Tecnica delle Costruzioni
P.le V. Tecchio,
80125 Napoli
Italy
39-81-7682442 / 39-81-5934792
adeluca@cds.unina.it

Alessandro De Stefano
Dipartimento di Ingegneria Strutturale
Politecnico di Torino
Corso Duca degli Abruzzi, 24
10129 Torino
Italy
39-11-5644847 / 39-11-5644899

Mauro Dolce
Dipartimento di Strutture
Geotecnica e Geologia Applicata (DiSGG)
Università della Basilicata
Via della Tecnica 3
85100 Potenza
Italy
39-971-474-607 or 609 / 39-971-57477
dolce@unibas.it

Agostino Marioni
Alga S.p.a.
Via Olona 12
20123 Milano
Italy
39-2-48569-1 / 39-2-48569-245
alga_spa@pointest.com

Roberto Marnetto
TIS Spa
Roma
Italy
39-6-508-24-59 / 39-06-508-12-92
tis_ste@pronet.it

Renzo Medeot
Managing Director
FIP Industriale Spa
Via Scapacchio, 41
1-35030 Selvazzano - PD
Italy
39-49-8225511 / 39-49-638567
medeot@protec.it

Giorgio Monti
Dipartimento di Ingegneria Strutturale e
Geotecnica
Università di Roma "La Sapienza"
Via Gramsci, 53
Roma
Italy
39-6-49919197 / 39-6-3221449
giorgio@dsg.uniroma1.it

Alberto Pavese
Dipartimento di Meccanica Strutturale
Università degli Studi di Pavia
Via Ferrata 1
27100, Pavia
Italy
39-382-505402 / 39-382-528422
pavese@gndt.unipv.it

Paolo Emilio Pinto
Dipartimento di Ingegneria Strutturale e
Geotecnica
Università di Roma "La Sapienza"
Via Gramsci, 53
00197, Roma
Italy
39-6-49919156 / 39-6-3221449
pinto@uniroma1.it

Fabio Taucer
European Commission
Joint Research Centre, TP480
Via Enrico Fermi
21020 Ispra (VA)
Italy
39-332-78-62-11 / 39-332-78-90-49
fabio.taucer@jrc.it



MULTIDISCIPLINARY CENTER FOR EARTHQUAKE ENGINEERING RESEARCH

A National Center of Excellence in Advanced Technology Applications

University at Buffalo, State University of New York
Red Jacket Quadrangle ■ Buffalo, New York 14261-0025
Phone: 716/645-3391 ■ Fax: 716/645-3399
E-mail: mceer@acsu.buffalo.edu ■ WWW Site: http://mceer.buffalo.edu